



**Syntheses and evaluation of novel histamine H₃
receptor ligands and multi-target-directed ligands
as neuroprotective agents**

Inaugural-Dissertation

zur Erlangung des Doktorgrades
der Mathematisch-Naturwissenschaftlichen Fakultät
der Heinrich-Heine-Universität Düsseldorf

vorgelegt von

Sicheng Zhong

aus Guiyang

Düsseldorf, September 2021

Aus dem Institut für Pharmazeutische und Medizinische Chemie
der Heinrich-Heine-Universität Düsseldorf

Gedruckt mit der Genehmigung der
Mathematisch-Naturwissenschaftlichen Fakultät der
Heinrich-Heine-Universität Düsseldorf

Berichtersteller:

1. Univ.-Prof. Dr. Dr. h.c. Holger Stark

2. Univ.-Prof. Dr. Thomas Kurz

Tag der mündlichen Prüfung: 24.Aug.2021

Meine Familie

Dankesagung

Die vorliegende Arbeit wurde zwischen Januar 2016 und Juni 2021 im Institut für Pharmazeutische und Medizinische Chemie der Heinrich-Heine-Universität Düsseldorf im Arbeitskreis von Prof. Dr. Dr. h.c. Holger Stark angefertigt.

Ich möchte mich sehr herzlich bei Herrn Prof. Dr. Dr. h.c. Holger Stark für die interessanten Aufgabenstellungen bedanken. Zudem bedanke ich mich für die zahlreichen wissenschaftlichen Anregungen und Ideen sowie das Korrekturlesen der Artikel und dieser Arbeit. Ich habe mich stets gut betreut gefühlt.

Ich bedanke mich des Weiteren bei Herrn Prof. Dr. Thomas Kurz für die Begutachtung der vorliegenden Dissertation. Zudem bedanke ich mich für den wissenschaftlichen Austausch mit seinem Arbeitskreis an der Heinrich-Heine-Universität.

Für die pharmakologische Testung der synthetisierten Substanzen danke ich Dr. Stefanie Hagenow, Dr. Annika Frank, Dr. David Reiner-Link, Frau Mariam Dubiel, Frau Luisa Leitzbach, und Frau Kathrin Grau aus unserem Arbeitskreis an der Heinrich-Heine-Universität in Düsseldorf, Herrn Professor Bassem Sadek und seinem Arbeitskreis an der United Arab Emirates University in Al-Ain, Vereinigten Arabischen Emiraten, Herrn Professor Andrzej Borjaski und seinem Arbeitskreis an der Polish Academy of Science in Krakau, Polen.

Ein großer Dank gilt allen aktuellen und ehemaligen Mitgliedern des Arbeitskreises für kollegiale Zusammenarbeit und den wissenschaftlichen Austausch. Besonders bedanken möchte ich mich bei Dr. Aleksandra Živković für die wissenschaftliche und persönliche Hilfestellung sowie das Korrekturlesen dieser Arbeit. Auch meinen Laborkollegen Dr. Hjördis Brückmann, Dr. Kiril Lutsenko, und Frau Milica Elek, danke ich für die Unterstützung in den verschiedenen Phasen meiner Promotion und die schöne Zeit während und außerhalb der Arbeit. Ich danke zusätzlich Dr. Leandro Alves Avelar, Dr. Kiril Lutsenko, und Frau Mariam Dubiel für das Korrekturlesen meiner Arbeit.

Ich bedanke mich vor allem bei meiner Familie für die bedingungslose Unterstützung, die mir das Studium und die Promotionsarbeit in Deutschland ermöglicht und mich weitergebracht hat.

TABLE OF CONTENTS

1	Introduction.....	- 1 -
1.1	Histamine	- 1 -
1.1.1	Chemistry	- 1 -
1.1.2	Biosynthesis, distribution and degradation.....	- 1 -
1.2	Histamine H ₁ , H ₂ , and H ₄ receptors.....	- 3 -
1.2.1	Histamine H ₁ receptor	- 3 -
1.2.2	Histamine H ₂ receptor	- 4 -
1.2.3	Histamine H ₄ receptor	- 5 -
1.3	Histamine H ₃ receptor	- 6 -
1.3.1	Functions of H ₃ R	- 7 -
1.3.2	Computational modeling of H ₃ R binding site.....	- 9 -
1.4	Receptor ligands of H ₃ R.....	- 11 -
1.4.1	H ₃ R agonists	- 11 -
1.4.2	Imidazole-containing H ₃ R antagonists and inverse agonists	- 12 -
1.4.3	Non-imidazole H ₃ R antagonists/inverse agonists	- 13 -
1.5	Indications and potential therapeutical use of H ₃ R antagonists	- 16 -
1.5.1	Excessive sleepiness	- 16 -
1.5.2	Cognitive impairment and dementia.....	- 17 -
1.5.3	Parkinson's disease	- 18 -
1.5.4	Schizophrenia	- 19 -
1.5.5	Attention deficit hyperactivity disorder.....	- 20 -
1.5.6	Autism spectrum disorder	- 21 -
1.5.7	Tourette's syndrome	- 22 -
1.5.8	Epilepsy.....	- 23 -
1.5.9	Neuropathic pain	- 23 -
1.5.10	Multiple sclerosis.....	- 24 -
1.5.11	Obesity	- 24 -
1.5.12	Alcohol use disorders.....	- 25 -
1.5.13	Allergic rhinitis	- 26 -

Table of contents

1.6	Multi-target-directed ligands	26 -
1.6.1	Neurodegeneration – multifactorial mechanisms	28 -
1.6.2	Neuroprotective effects targeting H ₃ R	29 -
1.6.3	MAO-B inhibition	29 -
1.6.4	Voltage-gated calcium channel blockade	31 -
1.6.5	<i>N</i> -Methyl-D-aspartate receptor modulation	34 -
2	Aims and objectives	37 -
3	Chemistry	41 -
3.1	General notes for synthesis	41 -
3.2	Preparation of the intermediates	41 -
3.2.1	Preparation of the building blocks.	41 -
3.2.2	Preparation of primary amines	43 -
3.2.3	Preparation of aldehydes from corresponding alcohols	44 -
3.2.4	Preparation of carboxylic acids	46 -
3.2.5	Preparation intermediates with <i>N</i> -acylated piperazine scaffold	46 -
3.3	Synthesis of H ₃ R ligands with organo-fluoride and -chloride	47 -
3.4	Synthesis of H ₃ R ligands with benzylidene structure	48 -
3.4.1	Benzylidene malononitrile derivatives and their modifications	49 -
3.4.2	Benzylidene (thioxo-)imidazolidinone derivatives and their modifications	50 -
3.5	Synthesis of H ₃ R ligands with guanidine structure	52 -
3.6	Synthesis of H ₃ R ligand with phenyl pyrazole structure	54 -
3.7	Synthesis of Spin-labeled H ₃ R ligands	55 -
3.8	Synthesis of hybrid ligand comprising two H ₃ R-antagonist scaffolds	55 -
3.9	Synthesis of hybrid ligands potentially targeting H ₃ R and Calcium channels	56 -
3.9.1	Dihydropyridine derivatives	56 -
3.9.2	Dihydropyrimidine derivatives	58 -
3.9.3	Barbiturate derivatives	59 -
3.10	Synthesis of hybrid ligands with propargyl amine structure	62 -
3.11	Synthesis of hybrid ligands with D-cycloserine structure	62 -
3.12	Synthesis of a hybrid ligand comprising the pimavanserin structure	65 -

Table of contents

3.13	Synthesis of an A _{2A} R/H ₃ R dual-antagonist.....	- 66 -
4	Pharmacology.....	- 69 -
4.1	Overview of in-vitro assays in the present work.....	- 69 -
4.2	H ₃ R ligands with organo-fluoride and -chloride substituents.....	- 70 -
4.3	H ₃ R ligands with aromatic malononitrile structures.....	- 74 -
4.4	Benzylidene (thio)hydantoin derivatives.....	- 76 -
4.5	H ₃ R ligands with <i>N,N'</i> -disubstituted urea and carbamate structures.....	- 79 -
4.6	H ₃ R ligands with guanidine structure.....	- 81 -
4.7	H ₃ R ligand with phenyl pyrazole structure.....	- 83 -
4.8	Spin-labeled H ₃ R ligands.....	- 84 -
4.9	Hybrid ligands comprising two different H ₃ R antagonist pharmacophores.....	- 86 -
4.10	Hybrid ligands of H ₃ R antagonists and calcium channel blockers.....	- 86 -
4.10.1	Hybrid H ₃ R ligands with 1,4-dihydropyridine structure.....	- 86 -
4.10.2	Hybrid H ₃ R ligands with dihydropyrimidine structure.....	- 89 -
4.10.3	Hybrid H ₃ R ligands with barbituric acid structure.....	- 90 -
4.11	H ₃ R ligands with propargyl amine structure.....	- 92 -
4.12	H ₃ R ligands with D-cycloserine structure.....	- 93 -
4.13	Hybrid H ₃ R ligand with pimavanserin structure.....	- 94 -
4.14	Hybrid H ₃ R ligand with a novel PD treatment strategy.....	- 95 -
4.15	Conclusion.....	- 95 -
5	Summary & Zusammenfassung.....	- 97 -
5.1	Summary.....	- 97 -
5.2	Zusammenfassung.....	- 103 -
6	Experiment.....	- 109 -
6.1	Equipment and materials for the synthesis.....	- 109 -
6.2	General claims for the chemistry experiments.....	- 112 -
6.3	Not commercially procured chemicals.....	- 112 -
6.4	Synthesis and analytic.....	- 113 -
6.4.1	Intermediates.....	- 113 -
6.4.2	Compounds with organochloride and organofluoride.....	- 143 -

Table of contents

6.4.3	Benzylidene malononitrile derivatives	152 -
6.4.4	Benzylidene thiohydantoin and hydantoin derivatives.....	155 -
6.4.5	Guanidine derivatives	161 -
6.4.6	H ₃ R ligand with Phenyl pyrazole structure	165 -
6.4.7	Spin-labeled H ₃ R ligands.....	166 -
6.4.8	Hybrid ligand with two H ₃ R pharmacophores	167 -
6.4.9	Dihydropyridine derivatives	168 -
6.4.10	Dihydropyrimidine derivatives	175 -
6.4.11	5,5-Substituted barbituric acid derivatives.....	179 -
6.4.12	Urea derivatives	180 -
6.4.13	<i>N,N'</i> -Disubstituted barbituric acid derivatives.....	185 -
6.4.14	Propargyl amine derivatives	187 -
6.4.15	D-Cycloserine derivatives	189 -
6.4.16	Carbamate derivative	193 -
6.4.17	Pimavanserin analog with H ₃ R pharmacophore.....	194 -
6.4.18	Adenosine A _{2A} receptor antagonist derivative	195 -
6.5	Selected NMR, LC-MS, and HPLC spectra.....	197 -
6.6	General procedures for pharmacological experiments.....	208 -
6.6.1	Human histamine H ₃ receptor radioligand displacement assay	208 -
6.6.2	Human histamine H ₁ receptor binding assay	209 -
6.6.3	Human histamine H ₄ receptor radioligand displacement assay	209 -
6.6.4	Inhibition studies with human monoamine oxidases A and B	210 -
6.6.5	Cell viability assay	211 -
6.6.6	Oxygen-radical absorbance capacity assay.....	212 -
7	Reference	213 -
8	Annex.....	241 -
8.1	List of Abbreviations	241 -
8.2	Publications	246 -
8.3	Curriculum vitae.....	245 -
8.4	Eidesstattliche Erklärung	247 -

1 Introduction

1.1 Histamine

1.1.1 Chemistry

Histamine is a biogenic amine consisting of an imidazole ring and an ethanamine side chain (Figure 1-1). According to the International Union of Pure and Applied Chemistry (IUPAC) nomenclature, histamine is named 2-(1*H*-imidazol-4-yl)ethanamine. Black and Ganellin have suggested a widely used, straightforward terminology to describe both nitrogens in the imidazole ring of histamine half-century ago (Black and Ganellin, 1974): The imidazole nitrogen, which is near to the aliphatic ethanamine chain, is termed π (pros. ancient Greek: near to), and the other one is named τ (tele. ancient Greek: far from), while the primary aliphatic amine is termed α . The name histamine indicates the relationship with tissues and the nature of an amine with biological activities. Sir Henry Dale and colleagues first described histamine over a century ago. Histamine is a hygroscopic colorless crystalline solid at ambient temperature, which has a melting point of 84 °C.

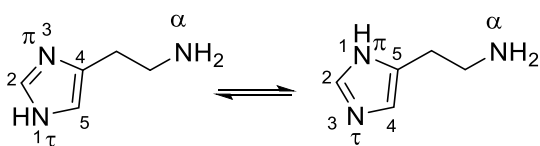


Figure 1-1: Tautomerism of histamine.

Histamine has two basic functional groups. The imidazole ring can be considered as a cyclic aromatic amidine, which can be protonated to 50% at pH 6.04, while the much stronger base, the primary amine, has a pK_a value of 9.75 at 25 °C (Paiva *et al.*, 1970). Thus, under the physiological condition, the α -nitrogen is presented in the protonated form.

1.1.2 Biosynthesis, distribution and degradation

Histamine is biosynthesized by decarboxylation of L-histidine by histidine decarboxylase (HDC). Peripheral degradation in extracellular is catalyzed mainly by diamine oxidase (DAO) and in the cytosol by histamine *N*-methyltransferase (HMT) (Maintz and Novak, 2007), while the inactivation of histamine in CNS is mainly catalyzed by HMT in the extracellular space (Haas *et al.*, 2008). In the body, histamine distributes ubiquitously. Most abundant is found in the lung, skin, and gastrointestinal tract. The most important location for its synthesis and storage are basophils and mast cells, where histamine is associated with heparin. The non-mast cell histamine can be found in the stomach, lymph nodes and thymus in high concentration, while less abundant in the heart, spleen, and kidney and clearly lower but still modest in liver, lung,

intestine and histaminergic neurons (Zimmermann *et al.*, 2011). In humans and rodents, the histaminergic neurons localize in a specific part of the posterior hypothalamus, termed tuberomammillary nucleus, with projections all over the central nervous system (CNS) (Haas and Panula, 2003; Haas *et al.*, 2008).

In neurons, the histamine precursor L-histidine is taken up by the L-amino-acid transporter and converted into histamine by intracellular HDC, which is a pyridoxal-5'-phosphate-dependent enzyme and can be inhibited by (S)- α -fluoromethylhistidine, an irreversible inhibitor of HDC. The synthesized histamine is taken by vesicular monoamine transporter 2 (VMAT-2) into vesicles in cell bodies and axonal varicosities for storage. Histamine is released when the action potential of the cell membrane is reached. After the release in the synaptic cleft, histamine is promptly metabolized by postsynaptic localized HMT. The resulting *N*⁷-methylhistamine does not display any histaminergic activities. HMT uses S-adenosyl-methionine as the methyl donor. In the brain, *N*⁷-methylhistamine is further degraded by monoamine oxidase type-B (MAO-B) to *N*⁷-methyl imidazole acetic aldehyde, which is subsequently oxidized to *N*⁷-methyl imidazole acetic acid (MIMA) by aldehyde dehydrogenase (ADH). (Figure 1-2)

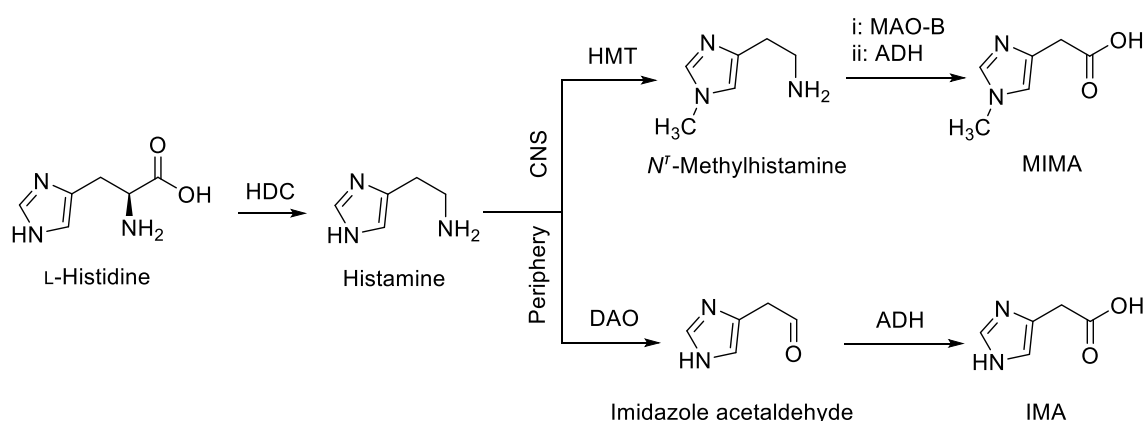


Figure 1-2: The synthesis and inactivation of histamine.

HDC: Histidine decarboxylase; HMT: Histamine *N*-methyltransferase; MAO-B: Monoamine oxidase isoform B; DAO: Diamine oxidase; ADH: Aldehyde dehydrogenase; IMA: Imidazole methyl acetic acid; MIMA: *N*⁷-Methyl imidazole acetic acid.

In peripheric tissues, histamine is mainly metabolized by DAO and followed by ADH to imidazole acetic acid (IMA), which can bind to the γ -aminobutyric acid (GABA) binding site on GABA receptor isoform A (GABA_A) and acts as an effective agonist (Tunnicliff, 1998; Haas and Panula, 2003). IMA could be further conjugated with phosphoribosyl pyrophosphate to IMA-ribotide, which can be dephosphorylated by phosphatases and 5'-nucleotidases to produce IMA-riboside. However, IMA, IMA-ribotide as well as IMA-riboside could also be found in the brain. Their regulatory functions in the CNS and periphery have been identified (Prell *et al.*,

2004). Histamine and all metabolites mentioned above are found in urine, indicating that renal excretion is the primary elimination route.

1.2 Histamine H₁, H₂, and H₄ receptors

The four known histamine receptor subtypes (H₁R-H₄R) are class A guanine nucleotide-binding protein-coupled receptors (GPCRs), which form the most abundant human membrane protein superfamily. Class A or rhodopsin-like receptors comprise the largest subclass. All GPCRs consist of seven transmembrane helices, which form seven transmembrane domains (TM), three intracellular and three extracellular loops (ICL and ECL, respectively) with extracellular *N*-terminus and intracellular *C*-terminus.

Almost all known physiological effects of histamine can be attributed to the activation of the four histamine receptors. In the brain, histamine acts as a neurotransmitter; in the immune cells, it promotes inflammation and the production of chemotaxis and cytokine; in the bronchus, it causes contraction of smooth muscle; in the vascular system, it induces dilatation of capillaries; in the stomach, it leads to gastric acid secretion (Panula *et al.*, 2015).

1.2.1 Histamine H₁ receptor

The H₁ receptor (H₁R) is coupled to G_{q/11} protein and is expressed in various human tissues, including epithelial, vascular, smooth muscle, glial, neuronal, and immune cells. To date, the H₁ receptor is the only histamine receptor, of which detailed structural information has been revealed via crystal structure (Shimamura *et al.*, 2011). H₁R is a 487-amino acid long protein encoded by an intron-free gene mapped on chromosome 3p25 (Fukui *et al.*, 1994). Activation of the G_{q/11} coupled H₁R promotes the activation of phospholipase C (PLC), which triggers the production of 1,2-diacylglycerol (DAC) and inositol-1,4,5-trisphosphate (IP₃). DAC and IP₃ induce protein kinase C (PKC) activation, leading to phosphorylation of downstream mediators and Ca²⁺ influx from endoplasmic reticulum Ca²⁺ storage and acidic organelle such as lysosome (Hill *et al.*, 1997; Panula *et al.*, 2015). Additionally, alternative signaling paths have been reported, e.g., the activation of H₁R mediates the production of arachidonic acid, nitric oxide, and cyclic GMP via G_{i/o} associated conduction (Richelson, 1978; Snider *et al.*, 1984; Panula *et al.*, 2015); H₁R activation also promotes Ca²⁺ influx and therefore induces cell depolarization and contraction of smooth muscle cells; G proteins of H₁R can activate nuclear factor -κB (NF-κB), which plays a crucial role in inflammation (Bakker *et al.*, 2001). Furthermore, the allergic responses triggered by the activation of H₁R are related to a series of occurrences, such as contraction of the smooth muscle in the respiratory tract, increased vascular permeability, and enhanced prostacyclin production and platelet-activating factor. Studies also suggested that H₁R activation may also enhance immune responses mediated by T-helper

cells (Thangam *et al.*, 2018). Furthermore, neurons in most brain regions can be excited upon the activation of H₁R, affecting wakefulness, memory, and mood. This process is associated with the release of Ca²⁺ from intracellular storage.

H₁R displays constitutive activity in the absence of agonists (Bakker *et al.*, 2000). The discovery of receptor constitutive activity has led to an evolution in the research of ligand-receptor interaction. According to the modern concept, ligands can be characterized and described as full agonists, partial agonists, neutral antagonists, partial inverse agonists, or full inverse agonists in a specified system (Kenakin, 2001; Seifert and Wenzel-Seifert, 2002).

Most of the classical H₁R antagonists have been later identified as inverse agonists (Bakker *et al.*, 2007). There are first- and second-generation antihistaminics according to their physicochemical and pharmacological properties. The first-generation such as diphenhydramine, doxylamine, pyrilamine, and doxepin, can easily cross the blood-brain barrier (BBB) and induce sedative and often anticholinergic effects. To overcome such unwanted effects in the treatment of allergic disorders, second-generation antihistamines have been developed. Diverse strategies have been employed to depress the BBB penetration, including the design of prodrugs, the introduction of polar ionic functional groups and zwitterionic structures, the establishment of recognition sites for ATP-dependent P-glycoprotein or organic anion transport polypeptide efflux pumps (Broccatelli *et al.*, 2010; Panula *et al.*, 2015; Sadek and Stark, 2016). The efforts led to numerous non-CNS permeable second-generation antihistamines, such as cetirizine, loratadine, levocabastin, fexofenadine, and mizolastine.

1.2.2 Histamine H₂ receptor

The histamine H₂ receptor (H₂R) is coupled to G_s protein, abundantly expressed in the stomach and CNS, but could also be found in smooth muscle cells, chondrocytes, skin, and immune cells (Jutel *et al.*, 2009). The human H₂R is a 359-amino acid long protein, which is encoded by an intron-free gene mapped on the q-arm of chromosome 5 (Traiffort *et al.*, 1995; Kobayashi *et al.*, 1996; HUGO Gene Nomenclature Committee, 2021). H₂R activation stimulates adenylyl cyclase promoted cyclic adenosine monophosphate (cAMP) production, PKA, and transcription factor cAMP response element-binding (CREB) protein, which is crucial regulators in neuronal physiology and plasticity (Haas and Konnerth, 1983; McCormick *et al.*, 1991; Panula *et al.*, 2015). Interestingly, in gastric parietal cells and some transfected systems, H₂R is coupled with G_{q/11} proteins and promotes an elevation of cytosolic calcium level (Hill, 1990; Hill *et al.*, 1997). Like H₁R, also H₂R displays the constitutive activation of adenylyl cyclase both in rats and humans (Smit *et al.*, 1996a; Monczor *et al.*, 2003). Physiological activation of H₂R stimulates gastric acid secretion, increases the heart rate. Additionally, the activation of the H₂ receptor leads to the inhibition of phospholipase A₂ and reduces the release

of arachidonic acid, while stimulation of H₁R promotes the release of arachidonic acid. These divergent physiological responses elicited by H₁R and the H₂R may be of importance in regulating the release of arachidonic acid in many tissues (Traiffort *et al.*, 1992). Furthermore, H₂R knock-out mice displayed cognitive deficits, suggesting the importance of H₂R in CNS. H₂R antagonists, more precisely inverse agonists (Smit *et al.*, 1996a) such as cimetidine, famotidine, and ranitidine are well-established therapeutic agents for the treatments of dyspepsia, gastric ulcers, or gastroesophageal reflux. Most of the H₂R antihistaminics have a poor capability to cross the BBB, except zolantidine, a benzothiazole derivative. Despite their efficacy, the later discovered proton pump inhibitors are to date a more preferred first-line treatment.

Despite less relevant as therapeutical agents, H₂R agonists are helpful pharmacological tools. Interestingly, (*R*)-sopromidine acts as a potent H₂R agonist in the guinea pig atrium, while the (*S*)-enantiomer demonstrates an antagonism activity in the same system (Elz and Schunack, 1988; Panula *et al.*, 2015). Moreover, prolonged receptor binding with inverse agonists could induce receptor upregulation, while agonists could stimulate desensitization and internalization of canine H₂R (Smit *et al.*, 1996a; Fukushima *et al.*, 1997).

1.2.3 Histamine H₄ receptor

The most recently discovered member of the histamine receptor family, the histamine H₄ receptor (H₄R), was cloned and reported almost simultaneous by a handful of independent research groups (Nakamura *et al.*, 2000; Oda *et al.*, 2000; Liu *et al.*, 2001; Morse *et al.*, 2001; Nguyen *et al.*, 2001; Zhu *et al.*, 2001). Since its discovery, studies on H₄R have focused on its impact on inflammatory processes and immune response involvement. H₄R is localized mainly on hematopoietic and immune cells. This subtype of histamine receptor is found to mediate chemotaxis, modulate mast cells' functions, eosinophile, basophile, dendritic cells, and T-lymph cells (Hofstra *et al.*, 2003). H₄R is involved in the release of cytokines (Gantner *et al.*, 2002; Gutzmer *et al.*, 2005; Cowden *et al.*, 2014) and is, together with H₁R responsible for the migration of T-helper immune cells (Mahapatra *et al.*, 2014). H₄R is expressed most strongly in bone marrow at the mRNA level but could also be detected in peripheral blood, spleen, thymus, lung, gut, and heart (Oda *et al.*, 2000; Liu *et al.*, 2001; Zhu *et al.*, 2001). Although approved drugs that selectively target H₄R are still not available, H₄R antagonists have been investigated in clinical trials for the treatment of histamine-induced itch (JNJ39758979), bronchial allergen challenge (ZPL-3893787), allergic rhinitis (UR63325), atopic dermatitis (JNJ39758979 and ZPL-3893787), rheumatoid arthritis (Toreforant and JNJ39758979), asthma (Toreforant and JNJ39758979) and psoriasis (ZPL-383787 and Toreforant) (Verweij *et al.*, 2020). An overview of the clinical trials is presented in table 1-1.

Table 1-1: An overview of the clinical tested H₄R antagonists.

H ₄ R antagonists	Tested indications	ClinicalTrials.gov Identifier
JNJ39758979	Asthma	NCT00946569
	Atopic dermatitis	NCT01497119
	Histamine induced itch	NCT01068223
	Rheumatoid arthritis	NCT01442545
ZPL-3893787 (ZPL-389, PF-03893787)	Atopic dermatitis	NCT02424253
	Bronchial allergen challenge	NCT00856687
	Psoriasis	NCT02618616
Toreforant (JNJ-38518168)	Asthma	NCT01823016
	Psoriasis	NCT02295865
	Rheumatoid arthritis	NCT00941707

The H₄R gene is mapped on chromosome 18q11.2 (Cogé *et al.*, 2001b), encoding a 390-amino acid long, G_{i/o} protein-coupled transmembrane receptor. Notably, the H₄R gene consists of three exons and two introns and therefore likely to form isomers. Indeed, two non-functional isoforms (H₄R₃₀₂ with 302 amino acids and H₄R₆₇ comprising only 67 amino acids) have been identified (van Rijn *et al.*, 2008). Interestingly, human H₄R shares high gene sequence homology to H₃R, especially in the membrane domain. Therefore numerous H₃R ligands also demonstrate a high affinity to H₄R (Lim *et al.*, 2005). Furthermore, H₄R exhibits high constitutive activity in recombinant systems. H₄R agonists reduce the cAMP accumulation as a result of inhibition of adenylyl cyclase (Oda *et al.*, 2000), activation of extracellular-signal-regulated kinase (ERK), phosphatidylinositol 3-kinase (PI3K), the inflammation associated p38 mitogen-activated protein kinases (MAPKs) (Zhu *et al.*, 2001) and the transcription factor activating protein with Ca²⁺ mobilization (Morse *et al.*, 2001; Hofstra *et al.*, 2003; Panula *et al.*, 2015).

1.3 Histamine H₃ receptor

The first description of histamine H₃ receptor (H₃R) emerged in 1983. Based on the pharmacological evidence, that histamine could auto-inhibit its release in CNS (Arrang *et al.*, 1983). Also, the capability of modulating noradrenaline, acetylcholine, dopamine, serotonin, GABA, and glutamate as a presynaptic heteroreceptor at non-histaminergic neurons in the central nervous system as well as in the peripheral neurons, such as bronchial and gastrointestinal tract was described (Schlicker *et al.*, 1994; Endou *et al.*, 1994). For two decades, the interest in this type of novel identified receptor has been grown notably.

Lovenberg and colleagues reported the first clone of H₃R (Lovenberg *et al.*, 1999). The gene sequence, which encodes the 445 amino acid long protein (Figure 1-3), has been mapped to the q-arm of chromosome 20 (Tardivel-Lacombe *et al.*, 2001). Unlike most GPCRs, including H₁ and H₂ receptors, the gene encoding H₃R consisted of either four exons and three introns or three exons interrupted by two introns, leading to multiple isoforms (Tardivel-Lacombe *et al.*, 2001; Cogé *et al.*, 2001a). Approximately 20 shorter human isoforms have been reported to date with deletions at the N-terminus, the second transmembrane domain, the first extracellular loop, the third intracellular loop, or the C-terminus (Leurs *et al.*, 2005).

H₃R localizes mainly and abundantly in various CNS regions: cerebral cortex, thalamus, hippocampus, amygdaloid complex, basal ganglia, hypothalamus, cerebellum, and lower brainstem (Lovenberg *et al.*, 1999; Pillot *et al.*, 2002). Besides the CNS expression, H₃R mRNA was also detectable on peripheric tissues such as skin, stomach, intestine, thymus, kidney, heart, liver, and respiratory epithelia in adult rats or the development phase (Héron *et al.*, 2001).

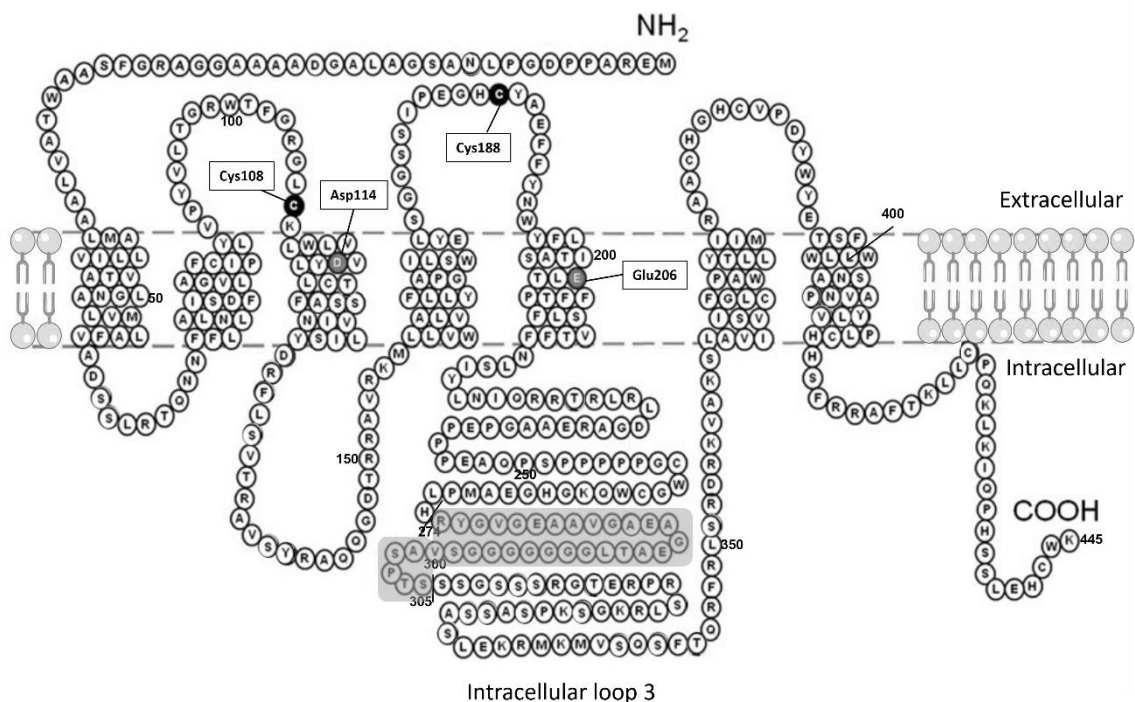


Figure 1-3: Membrane topology of H₃R (modified from Nieto-Alamilla *et al.*, 2016). The H₃R isoform 1 (in full length with 445 amino acids) has an extraordinary long intracellular loop 3. The cysteine residues in extracellular loops 2 and 3 (Cys108 and 188) putatively form a disulfide bond. The amino acid residues Asp114 and Glu206 may play crucial roles in the interaction with the basic moieties of H₃R ligands. Deleting the residues from 274 to 305 (highlighted area) in intracellular loop 3 resulted in a shorter isoform with 413 amino acids.

1.3.1 Functions of H₃R

H₃R is a G_{i/o} protein coupled-receptor with highly constitutive activity (Morisset *et al.*, 2000; Rouleau *et al.*, 2002), which inhibits forskolin-stimulated cAMP accumulation, whereas agonists demonstrate decreasing and inverse-agonists increasing effects in cAMP

accumulation. The high constitutive activity demonstrates a species, isoform, cell type, and signal transduction route-dependent differences. Therefore, some ligands, such as proxyfan, displayed the property of agonism or inverse agonism in a cell system-dependent manner (Gbahou *et al.*, 2003). Activation of H₃R stimulates MAPK phosphorylation, which can be associated with memory enhancement (Hill *et al.*, 1997). H₃R also activates PI3K, leading to the subsequent activation and phosphorylation of protein kinase B (PKB, also known as Akt), which in turn inhibits glycogen synthase kinase 3 isoform β (GSK-3 β) (Bongers *et al.*, 2007). GSK-3 β is a major tau-protein kinase in the brain and is involved in several neurodegenerative diseases, including Alzheimer's disease. The PI3K/Akt/GSK-3 β pathway plays a crucial role in cell survival, indicating that targeting H₃R may be a promising neuroprotection strategy (Li *et al.*, 2002; Rickle *et al.*, 2004; Bongers *et al.*, 2007). Interestingly, the H₃R in full length with 445 amino acids demonstrated superiority in the quality of coupling to MAPK phosphorylation in comparison to a few shorter variations (Drutel *et al.*, 2001), while a shorter isoform with 413 amino acid with a deletion in the third intracellular domain (Figure 1-3), was identified predominant expressed in rat brain and functions as autoreceptor (Gbahou *et al.*, 2012). Activation of H₃R autoreceptor inhibits histamine synthesis and release through Ca²⁺/calmodulin and cAMP-dependent protein kinase pathways (Torrent *et al.*, 2005). Furthermore, H₃R activation decreases the cytosolic Ca²⁺ concentration in sympathetic nerve endings, therefore inhibits the noradrenaline exocytosis (Silver *et al.*, 2002) and inhibits Na⁺/H⁺ exchange activity (Silver *et al.*, 2001). The observation suggested a novel mechanism of cardioprotection by H₃R agonists (Silver *et al.*, 2001).

H₃R is mainly localized on histaminergic neuron somata, dendrites, and axons to control firing, histamine synthesis, and release. The function as autoreceptor is based on a blockage of Ca²⁺ current, which is part of histaminergic neurons' pacemaker function (Stevens *et al.*, 2001). As heteroreceptors, H₃R controls transmitter release from GABAergic, glutamatergic, serotonergic, noradrenergic, cholinergic, and dopaminergic neurons in the mammalian brain. Furthermore, activation of H₃R inhibits neurotransmission in peripheral autonomous and sensory systems (Panula *et al.*, 2015). Many research groups observed sympathetic neurotransmitter release regulation by H₃R on diverse animal tissues, such as guinea pig mesenteric artery (Ishikawa and Sperelakis, 1987) and atria (Endou *et al.*, 1994), human saphenous vein (Molderings *et al.*, 1992) and heart (Imamura *et al.*, 1996), rat tail artery (Godlewski *et al.*, 1997), and dog kidney (Yamasaki *et al.*, 2001). H₃R also controls the release of tachykinins and calcitonin gene-related peptides from sensory C fibers (Ichinose and Barnes, 1990; Matsubara *et al.*, 1992; Ohkubo and Shibata, 1995; Imamura *et al.*, 1996; Sun *et al.*, 2011).

H₃R is involved in many physiological brain functions, including sleep-wake rhythms, food intake behavior, cognitive process, behavioral states, and locomotor activity (Haas and Panula,

2003). The versatile pharmacological and physiological properties led to an intense growth of interest in the H₃R for potential therapeutic exploitation for the treatment of sleep disorders (Lin *et al.*, 2011), disease of the cardiovascular system (Silver *et al.*, 2001), obesity (Yoshimoto *et al.*, 2006), cognitive deficits in Alzheimer's disease, epilepsy (Alachkar *et al.*, 2019), attention deficit hyperactivity disorder or schizophrenia (Leurs *et al.*, 1998), as well as alcohol use disorder (Panula, 2020).

Furthermore, there is evidence for the existence of homo- and hetero-dimers of H₃R, though their relevance and function require further investigation. Evidence for a functional dimer of H₃R and dopamine D₁ receptor (D₁R) was reported based on a few observations: Activation of H₃R inhibits D₁R agonist-induced cAMP accumulation (Sánchez-Lemus and Arias-Montaño, 2004), H₃R activation inhibits D₁R dependent release of GABA (Arias-Montão *et al.*, 2001) and the cross-antagonism of H₃R/D₁R (Moreno *et al.*, 2011). Recently, H₃R agonist (*R*)- α -methylhistamine induced Ca²⁺ mobilization at a heterodimer of H₃R and adenosine A_{2A} receptor (A_{2A}R) have supported the hypothesis of the existence of functional H₃R/A_{2A}R heterodimer (Márquez-Gómez *et al.*, 2018).

In addition to investigating dual- or multi-acting ligands on separated systems, the dimer- or oligomer-systems assessment should also draw more attention. Such approaches may be attractive alternatives in the treatment of multiple factors-associated diseases.

1.3.2 Computational modeling of H₃R binding site

To date, detailed receptor structure information of H₃R from X-ray crystallography or cryogenic electron microscopy (cryo-EM) is still missing. Ligand-based structure-activity relationship (SAR) study and drug design have evolved independently from but supported by the computer-assisted receptor assessment and mutation studies. An early SAR (Figure 1-4 A) described exclusive imidazole-containing H₃R ligands (Stark *et al.*, 1998).

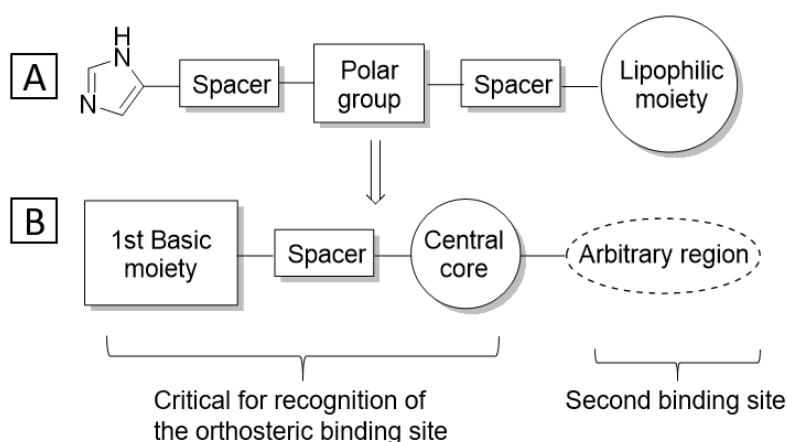


Figure 1-4: Evolution of SAR description (modified from Stark *et al.* 1998 and Celanire *et al.* 2005).

With the development of numerous highly affine non-imidazole H₃R ligands, the SAR has been refined from a large amount of given data (Celanire *et al.*, 2005; Wingen and Stark, 2013) and has been successfully extended (Figure 1-4 B) to be applicable in multi-targeting ligands (von Coburg *et al.*, 2009).

The 1st basic moiety, often a tertiary amine such as piperidine or pyrrolidine, is linked to a usually aromatic central core via an alky spacer, presents the orthosteric binding site recognition area. A great diversity of different structural elements is allowed in the arbitrary region, including a 2nd basic moiety, lipophilic moiety, polar group, acidic group, electron-withdrawing, and electron-donating group or a further pharmacophore. The arbitrary region's modifications play a crucial role in receptor binding affinity (von Coburg *et al.*, 2009; Sander *et al.*, 2010a; b; Sadek and Stark, 2016).

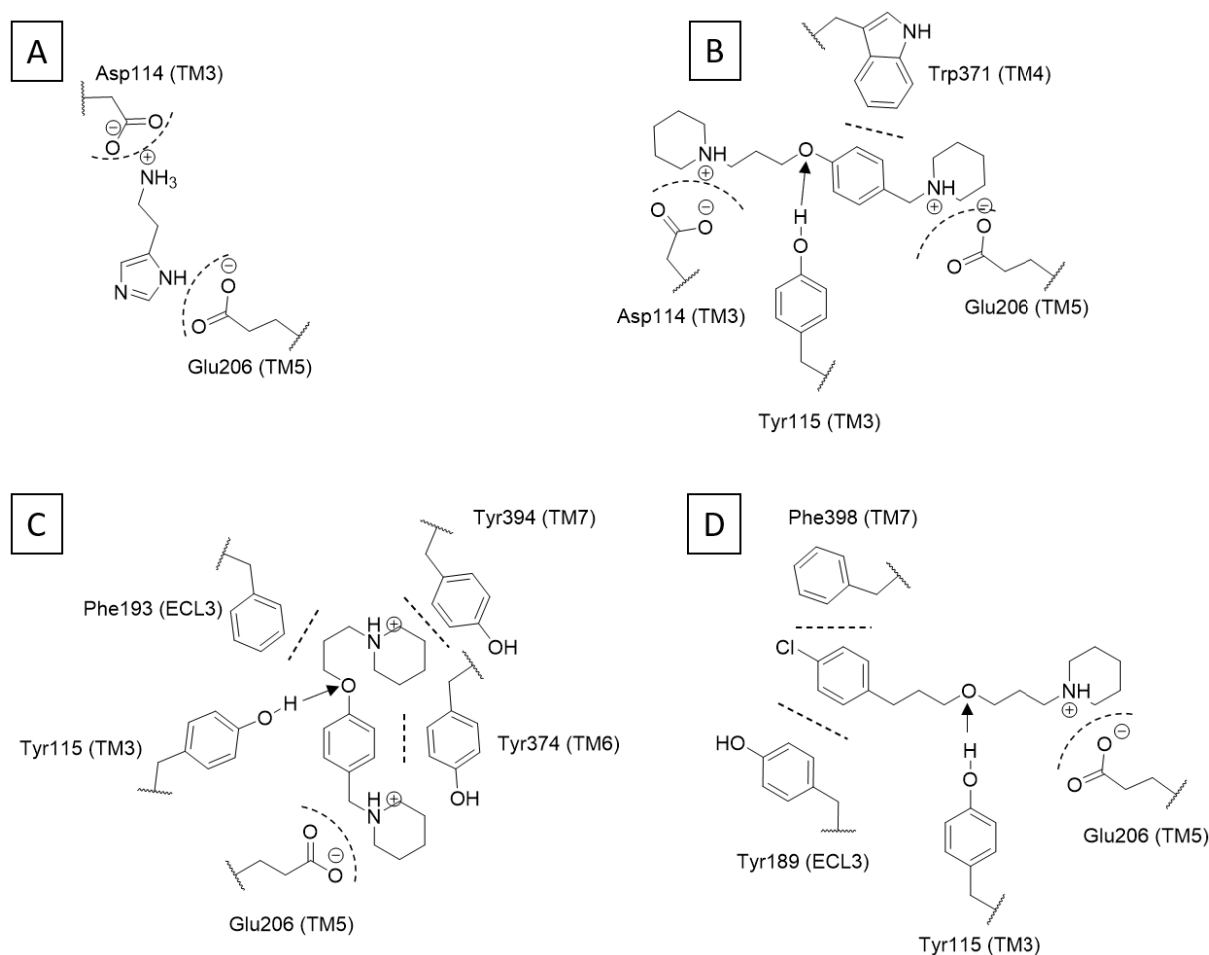


Figure 1-5: Ligand interaction from selected *in-silico* docking studies are simplified and illustrated in 2D. Linearly dashed lines indicate hydrophobic interactions, while the curved ones indicate ionic interactions. Arrows suggest possible interactions between hydrogen donor and acceptor. (A: histamine, modified from Nieto-Alamilla *et al.* 2016; B: JNJ-5207852, modified from Axe *et al.* 2006; C: JNJ-5207852, modified from Jończyk *et al.* 2017; D: pitolisant, modified from Ghamari *et al.* 2019b)

Many *in-silico* assessments support the general structural pattern of H₃R antagonists. Since the crystal structure is not available, homology modeling has been the mainstream in the structural investigation of H₃R. Several well-studied crystal structures or *in-silico* developed

models were used as templates, such as bovine rhodopsin (Axe *et al.*, 2006; Schlegel *et al.*, 2007), H₁R (Harusawa *et al.*, 2013), and the previously *in-silico* developed model for endothelin receptor (Yao *et al.*, 2003). Additionally, hybrid approaches were employed, in which two model systems refined each other (Jończyk *et al.*, 2017; Ghamari *et al.*, 2019b).

Independent of the methods and templates used in the docking studies, the results have many in common. The residues Asp114 and Glu206 may be crucial for the interaction with either 1st basic structure or the 2nd basic moiety if presented. The observation provided a reasonable explanation for the high affinities of H₃R ligands with two tertiary amines. Furthermore, the residue Tyr115 acts as a hydrogen bond donator, which may be responsible for the high affinities of many H₃R ligands with an ether function. A few selected *in-silico* docking studies are presented here (Figure 1-5). Discrepancies between the individual *in-silico* studies can often be observed in predicting the hydrophobic interactions and molecule orientation in the binding pocket (Figure 1-5, B and C).

Furthermore, the predicted information about the receptor conformation and dynamics could provide insight into how a ligand-induced receptor motion affects the signal transduction and the receptor efficacy. The gained knowledge is valuable for the further development of novel selective and potent compounds.

1.4 Receptor ligands of H₃R

The initial development of H₃R ligands was derived from the endogen ligand histamine and focused on imidazole derivatives. Numerous imidazole-containing ligands display excellent potencies and are established as useful pharmacological tools. However, similarly to theazole antifungals such as ketoconazole and fluconazole or H₂R inverse agonist cimetidine (Aymard *et al.*, 1988), the imidazole moiety was attached to lipophilic structures, such as thioperamide, clobenpropit, and ciproxifan, which displayed an inhibitory effect on cytochrome P450 enzymes via coordination with the heme iron (Yang *et al.*, 2002). This feature impacts the metabolism of various substances, including H₃R ligands themselves. Furthermore, the hydrophilic imidazole ring is an excellent hydrogen-acceptor and donator at the same time, which negatively impacts the oral bioavailability and BBB penetration (Chadha *et al.*, 1994). Hence, compounds with better drug-likeness and reduced potential interactions to other drugs devoid of imidazole moiety have been intensively developed (Berlin *et al.*, 2006) and represent, to date, the most important trend.

1.4.1 H₃R agonists

Compared to H₃R antagonists, the agonists are valuable pharmacological tools rather than therapeutic agents. Histamine and its methylated derivatives *N*^α-methylhistamine (NAMH) and

(*R*)- α -methylhistamine (RAMH) are highly potent agonists, the tritiated [^3H]-*N* $^{\alpha}$ -methylhistamine and [^3H]-(*R*)- α -methylhistamine are widely used radioligands for in-vitro assessments. Histamine, NAMH, and RAMH also display affinities at other histamine receptors, especially at H_4R , due to the high receptor homology between H_3R and H_4R (Lim *et al.*, 2005). Like most other aminergic compounds, the high basicity and hydrophilicity result in an extensive first-pass effect and low bioavailability, limiting their application in in-vivo conditions. BP2-94, a prodrug of RAMH (Figure 1-6), bears an imine function with a lipophilic structure, which led to an improved pharmacokinetic property (Krause *et al.*, 2001). Replacement of the primary amino group of histamine with an isothioureia function resulted in the highly effective agonist imetit. Its side chain's steric restriction to a piperidine ring yielded the potent agonist immepip, which has an interestingly high permeability of blood-brain-barrier (BBB) (Jansen *et al.*, 1998). *N*-Methylation of the piperidine ring in immepip resulted in methimmepip, which could also penetrate the BBB and, importantly, has a high selectivity toward H_3R over H_4R (Kitbunnadaj *et al.*, 2005; Sadek and Stark, 2016). Moreover, depending on the constitutive activity from different species, test systems, and receptor isoforms, proxyfan acts as a partial agonist, antagonist, or inverse agonist (Gbahou *et al.*, 2003). The aforementioned H_3R agonists are listed below (Figure 1-6).

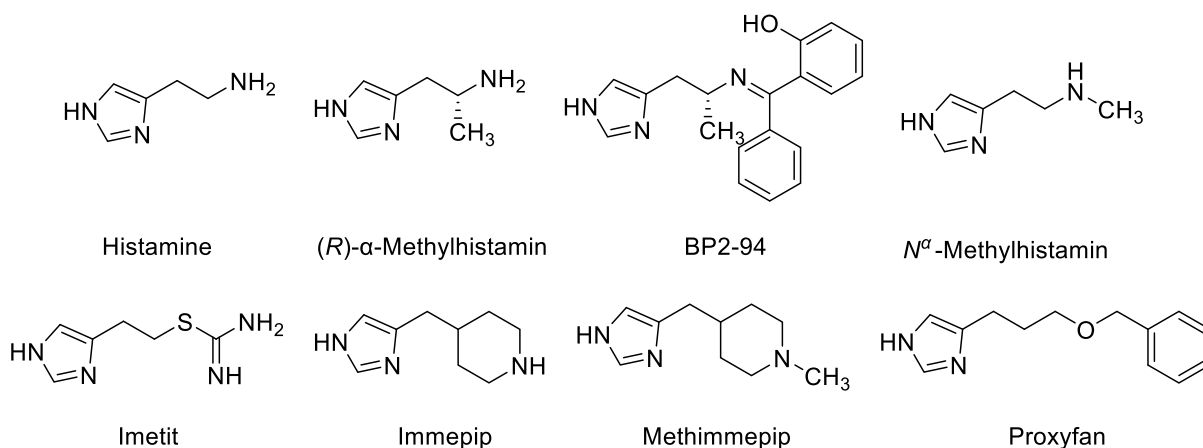


Figure 1-6: Selected examples of H_3R antagonists.

1.4.2 Imidazole-containing H_3R antagonists and inverse agonists

H_3R displays high constitutive activity. Many H_3R antagonists have been identified as inverse agonists. The first reported selective H_3R antagonist was the thiourea derivative thioperamide (Figure 1-7). It is a well-established reference substance and played an essential role in the history of the discovery of H_3R (Arrang *et al.*, 1987). Further prominent imidazole-containing H_3R antagonists or inverse agonists are clobenpropit and ciproxifan (Figure 1-7). Clobenpropit is an isothioureia derivative and an analog of the H_3R agonist imetit. Ciproxifan is a widely used pharmacological tool. It represents the core scaffold for developing a series of well-established

non-imidazole phenoxy alkyl H₃R ligands. Due to the high homology of H₃R to H₄R, a few compounds of this class also displayed significant affinity at H₄R (Ligneau *et al.*, 2000; Lim *et al.*, 2005; Gbahou *et al.*, 2006).

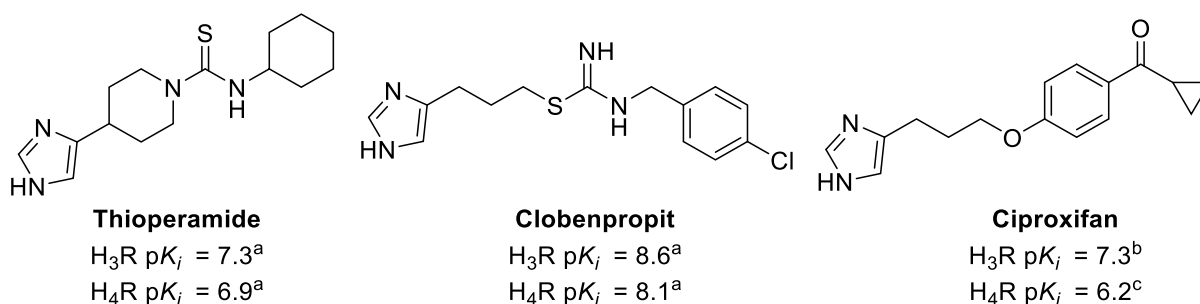


Figure 1-7: Representative imidazole-containing H₃R ligands. (^aLim *et al.*, 2005; ^bLigneau *et al.*, 2000; ^cGbahou *et al.*, 2006)

1.4.3 Non-imidazole H₃R antagonists/inverse agonists

Sir James Black Foundation has reported one of the earliest series of highly potent non-imidazole H₃R antagonists (Linney *et al.*, 2000). The highly effective guanidine derivatives could be considered an improvement of their imidazole analogs that are previously reported by Stark and colleagues (Stark *et al.*, 1994), whereas the imidazole ring was replaced by azacycles such as pyrrolidine, piperazine, or homopiperidine ring. Similar strategies have been applied to many different imidazole-containing lead structures and indeed obtained a large number of valuable novel compounds in only several years, such as alkylamines and aromatic ether derivatives (Ganellin *et al.*, 1998; Schwartz *et al.*, 2000; Meier *et al.*, 2001). The novel non-imidazole H₃R ligands have gained more interest in developing drugs for clinical use, especially with the introduction of piperidine as a basic ring system.

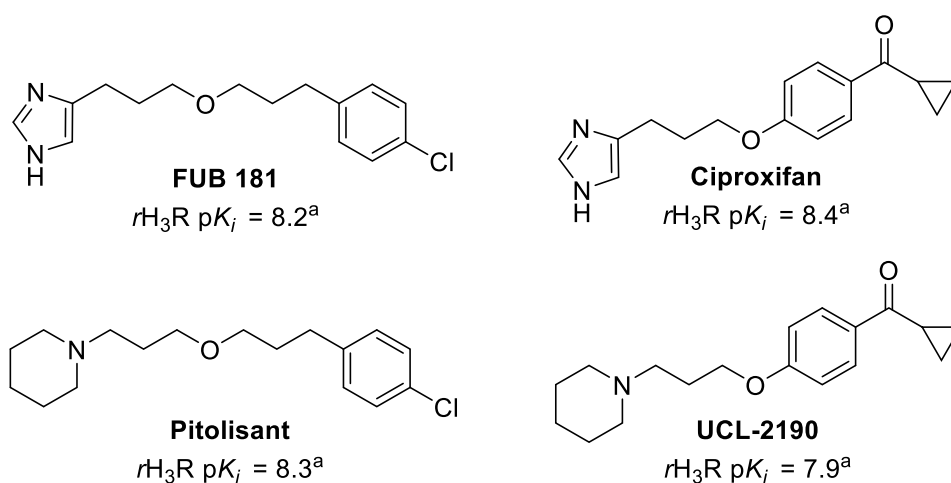


Figure 1-8: Representative examples of ligands with a piperidine-imidazole exchange. (^aMeier *et al.*, 2001)

One most prominent piperidine-containing H₃R antagonist is pitolisant, a piperidine analog of FUB 181 (Figure 1-8). The latter is also a potent H₃R antagonist (Stark *et al.*, 1998) with an aliphatic ether structure. Pitolisant (Wakix®) is an inverse agonist and, to date, the only selective H₃R targeting drug on the market. Pitolisant was approved by the European Medicines Agency (EMA) in 2016 and by the U.S. Food and Drug Administration (FDA) in 2019, with orphan drug status for the treatment for narcolepsy with or without cataplexy in adults. Narcolepsy is a chronic neurologic disorder of hypersomnolence and characterized by excessive daytime sleepiness (EDS). Cataplexy is an abrupt and reversible loss of muscle tone during wakefulness. Frequent triggers are emotional events (Scammell, 2015). Multiple assessments aiming for extending the indication were aspired, including the pediatric application ([ClinicalTrials.gov](https://clinicaltrials.gov/ct2/show/study/NCT02611687) identifier: NCT02611687), the treatment of EDS in patients with obstructive sleep apnea ([ClinicalTrials.gov](https://clinicaltrials.gov/ct2/show/study/NCT02739568) identifier: NCT02739568), epilepsy (Kuder *et al.*, 2016), alcohol use disorder ([ClinicalTrials.gov](https://clinicaltrials.gov/ct2/show/study/NCT02800083) identifier: NCT02800083), Prader-Willi syndrome ([ClinicalTrials.gov](https://clinicaltrials.gov/ct2/show/study/NCT04257929) identifier: NCT04257929) and other neurodegenerative progressions like Parkinson's disease and Alzheimer's dementia (Harwell and Fasinu, 2020). A recent after-approval report revealed that pitolisant demonstrated low abuse potential with a similar overall profile to that of placebo (Setnik *et al.*, 2020).

UCL-2190 is the piperidine-containing ciproxifan analog (Figure 1-8) with a high affinity to H₃R (Meier *et al.*, 2001). The *N*-(3-phenoxypropyl)piperidine structural pattern in UCL-2190 can be found in numerous excellent H₃R ligands. It is used as a lead structure for many compounds in this work.

With similar structural features as UCL-2190, JNJ-5207852 (Figure 1-9) has a second piperidine ring, which is supposed to interact with the residue Glu206 in the TM5 and provide a "boost effect" in the receptor binding affinity. Despite the excellent in-vitro and in-vivo pharmacological feature of JNJ-5207852 (Barbier *et al.*, 2004), a significant drawback prevent its clinic use. This compound can induce phospholipidosis (Bonaventure *et al.*, 2007). Phospholipidosis is an excessive accumulation of intracellular phospholipids. The induction of phospholipidosis by cationic amphiphilic drugs (CADs) has been well documented (Halliwell, 1997; Vater *et al.*, 2017). CADs are defined by a few common features, such as hydrophobic ring structure and hydrophilic chain with a charged cationic amine group. These characteristics comprise a wide variety of substance classes such as antidepressants, antipsychotics, and antiarrhythmics. Similar reports about H₃R ligands bearing diverse structures have been published. Structural modification aiming at reduced lipophilicity and basicity indicates a solution of this problem (Rodríguez Sarmiento *et al.*, 2009; Singh and Jadhav, 2013).

The *N*-alkyl piperidine structural pattern has been extensively investigated. Many potent H₃R ligands with similar structural features were characterized (Apelt *et al.*, 2002; Łazewska *et al.*, 2006; Levoine *et al.*, 2011).

Additionally, a few *N*-(3-phenoxypropyl)piperidine H₃R antagonists such as FUB2.922 (Figure 1-9) can lead to potential cardiovascular safety issues, including the inhibition of the hERG (human Ether-a-go-go Related Gene) channels, preventing further clinical development. As for FUB2.922, despite being a potent H₃R antagonist with $K_i = 3$ nM, it inhibits 70% of hERG activity at a concentration of 1 μ M (Levoine *et al.*, 2011). Further issues to be overcome are potential mutagenicity, low oral availability, and intensive metabolism. Thus, modifications in the *N*-(3-phenoxypropyl)piperidine structure, and the development of alternative pharmacophores, have been pursued (Black *et al.*, 2008; Letavic *et al.*, 2015).

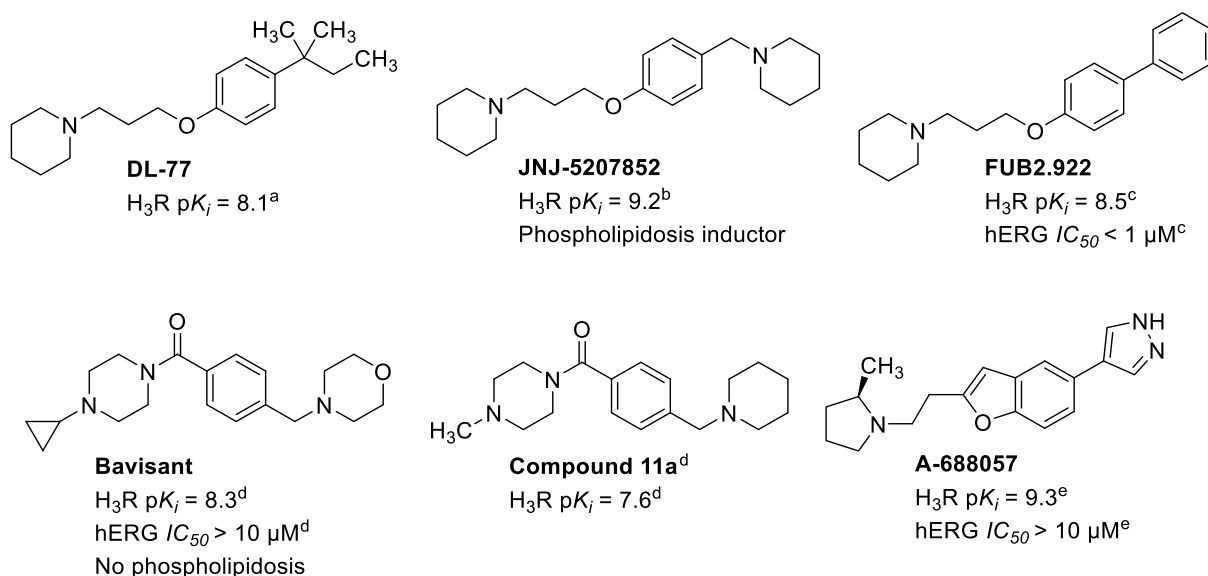


Figure 1-9: Selected examples of H₃R ligands. (^aŁazewska *et al.*, 2006; ^bBarbier *et al.*, 2004; ^cLevoine *et al.*, 2011; ^dLetavic *et al.*, 2015; ^eBlack *et al.*, 2008)

DL-77 was developed by Łazewska and colleagues, exhibiting ameliorated alcohol-intake behavior, anticonvulsant and memory-enhancing properties in animal models (Bahi *et al.*, 2015; Sadek *et al.*, 2016c). Bavisant has shown effectiveness in different animal models to promote wakefulness and attention and improve cognitive performance (Weisler *et al.*, 2012; Letavic *et al.*, 2015). However, the development was withdrawn after a series of phase-I studies and one phase-II study on attention deficit hyperactivity disorder (ADHD) in adults, where bavisant did not differ from placebo (Weisler *et al.*, 2012).

1.5 Indications and potential therapeutical use of H₃R antagonists

1.5.1 Excessive sleepiness

H₃R antagonist/inverse agonist pitolisant (Wakix[®], structure see Figure 1-8), is used in the EU since 2016 and the US since 2019 to treat narcolepsy with or without cataplexy in adults. Narcolepsy is spontaneously excessive sleepiness and the irregular onset of rapid eye movement sleep during the daytime that affects life quality. Episodes of a sudden loss of muscle control, termed cataplexy, are accompanying most narcoleptic patients (Calik, 2017). Hypothalamus is the most critical control center of the autonomic nervous system and is responsible for regulating sleep and wakefulness. Histamine plays a crucial role in regulating the sleep-wake rhythm, affecting the general state of arousal. Histamine release follows a circadian rhythm in rodents and humans. The researchers observed a low level of histamine release during sleep while a high level during wakefulness (Tuomisto and Tuomisto, 1982; Mochizuki *et al.*, 1992; Tuomisto *et al.*, 2001). Suppressing the constitutive activity of presynaptic H₃ autoreceptor by an antagonist/inverse agonist leads to an increase of the neurotransmission in histaminergic neurons and consequently activation of postsynaptic H₁R, which in turn promotes wakefulness and vigilance. The wake-promoting effect of H₃R antagonism has been well documented. H₃R antagonists ciproxifan and thioperamide (Structure see Figure 1-7) increased wakefulness and cortical EEG fast rhythms in mice, while ciproxifan failed to induce corresponding wakefulness in HDC or H₁R or H₃R knock-out mice, respectively (Parmentier *et al.*, 2002, 2007). Pitolisant provided significant improvement in reducing excessive daily sleepiness in adult patients with narcolepsy with or without cataplexy, though not superior to modafinil. The unique wake-promoting feature by increasing histamine transmission is advantageous compared to classical psychostimulants such as caffeine and amphetamine. This novel therapeutical strategy causes no locomotor activity, behavioral excitation, and sleep rebound. (Parmentier *et al.*, 2007; Berlin *et al.*, 2011; Broderick and Masri, 2011; Lin *et al.*, 2011). Furthermore, pitolisant has low abuse potential (Setnik *et al.*, 2020).

Obstructive sleep apnea (OSA) is a common disorder characterized by repetitive nocturnal breathing pauses due to upper airway collapse. Affecting 2-4% of the adult population (Young *et al.*, 1993), OSA causes severe symptoms, such as excessive daytime sleepiness, and is associated with significant cardiovascular morbidity and mortality (Spicuzza *et al.*, 2015). In a recent phase-III clinical study, pitolisant significantly reduced self-reported daytime sleepiness and fatigue and improved patient-reported outcomes and physician disease severity assessment in sleepy patients with obstructive sleep apnea refusing or nonadherent to continuous positive airway pressure (Dauvilliers *et al.*, 2020). The promising result suggests a further indication for ligands targeting H₃R.

1.5.2 Cognitive impairment and dementia

Alzheimer's disease (AD) is the most common reason for cognitive and memory impairment. Its prevalence increases in advanced age. AD affects around 40 million people worldwide today. The highest prevalence was found in the population over 65 years of age. In most cases, AD appears sporadically. Only a minor population (1%-2%) are of the familial form, which is featured by early-onset and more severe pathogenesis (Selkoe and Hardy, 2016; Long and Holtzman, 2019). The amyloid hypothesis has become the dominant AD pathogenesis model (Beyreuther and Masters, 1991; Hardy and Higgins, 1992). The misfolded proteins exert significant effects on the viability of neuronal cells in-vitro and facilitating multiple toxic downstream mechanisms.

Cholinesterase inhibitors (e.g., donepezil, rivastigmine, and galantamine) and *N*-methyl-D-aspartate (NMDA) receptor antagonist (e.g., memantine) are often used symptomatic therapeutics. Aiming at searching disease-modifying treatments, the dominant β -amyloid pathogenesis hypothesis has driven the mainstream of AD drug development in the past decade. The monoclonal antibody aducanumab (Aduhelm[®]), which gained accelerated approval from the FDA in June 2021, demonstrated promising β -amyloid elimination and, therefore, a reduction of clinical declination in AD patients (FDA, 2021). However, aducanumab and other drugs targeting β -amyloid failed to ameliorate the cognitive impairment in recent clinical trials, suggesting that the downstream factors, such as the glucose hypometabolism and toxic Ca^{2+} burden, may play crucial roles in the progression of AD in the clinical phase (Nimmrich and Eckert, 2013; Hammond *et al.*, 2020). Meanwhile, the Ca^{2+} hypothesis of AD has been updated and attracted increased attention (Berridge, 2011; Khachaturian, 2017).

In preclinical studies, various H_3R antagonists such as ABT-288 (Esbenshade *et al.*, 2012) and GSK239512 (Wilson *et al.*, 2013) have increased acetylcholine and dopamine levels in the rat prefrontal cortex and demonstrated pro-cognitive abilities. ABT-288 (Figure 1-10) showed behavioral improvement in social recognition memory, spatial learning, and the water maze test. GSK239512 (Figure 1-10) provided enhanced working memory in the novel object recognition paradigm and reversed the scopolamine-induced amnesia in the passive avoidance task of learning.

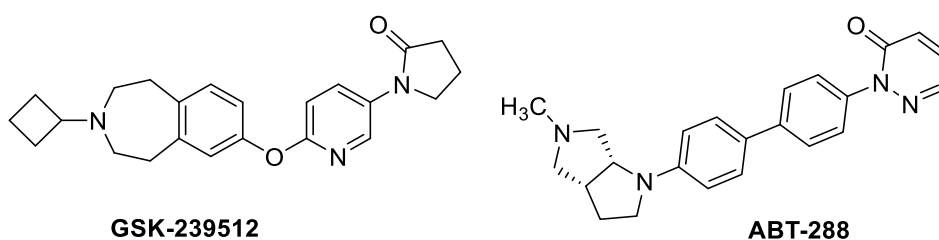


Figure 1-10: H_3R antagonists exhibit cognitive-enhancing effects in animal models.

However, in phase-II clinical trials, none of both drugs have demonstrated cognitive-enhancing effects in patients with mild to moderate AD, suggesting that the “one drug, one target” criterion might meet its limit in treating diseases with multifactorial origins. Multi-target-directed ligands (MTDLs) simultaneously addressing several pathomechanisms may be helpful novel therapeutic strategies in AD treatment (Gauthier *et al.*, 2019; Long and Holtzman, 2019). MTDLs will be discussed in section 1.6.

Contilisant (see Figure 1-11), an H₃R/Cholinesterase/MAO/sigma 1 receptor (S₁R) tetratargeting ligand, has shown promising effect against cognitive impairment in an AD mouse model induced by β -amyloid oligopeptide (Bautista-Aguilera *et al.*, 2018). Further development remains necessary to prove this multi-targeting concept. Furthermore, the unique pharmacological features of contilisant are also interesting for the treatment of Parkinson’s disease, which will be discussed in the next section.

1.5.3 Parkinson’s disease

Parkinson’s disease (PD) is the second most common neurodegenerative disorder that affects 2-3% of the elderly population (Poewe *et al.*, 2017). Muscular rigidity, bradykinesia, rest tremor, and postural instability are common clinical motor symptoms (Ghamari *et al.*, 2019a). Non-motor symptoms include rapid eye movement sleep behavior disorder, cognitive impairment, depression, orthostatic hypotension, and sialorrhea (Connolly and Lang, 2014). Furthermore, with a prevalence higher than 20%, the psychosis spectrum increases with the PD duration (Ffytche *et al.*, 2017). PD is pathologically characterized by degeneration of the dopaminergic cells in the substantia nigra (SN), which causes striatal dopamine deficiency and consequently reduced excitatory activity via dopamine D₁R and inhibitory effects via dopamine D₂R, respectively (Ellenbroek and Ghiabi, 2014). Aggregation of α -synuclein, mitochondrial dysfunction, oxidative stress, dysregulation in the Ca²⁺ homeostasis, and neuroinflammation are involved in PD’s pathogenesis (Poewe *et al.*, 2017).

To date, a disease-modifying therapy is still not available. The most widely applied treatments are based on replacing (e.g., levodopa with a DOPA carboxylase inhibitor), prolonging (e.g., selegiline and rasagiline), or imitating (e.g., pramipexole, ropinirole, and rotigotine) the biogenic amine dopamine as symptomatic therapies. Levodopa-induced dyskinesia represents a pronounced complication of the treatment of PD in standard therapy (Connolly and Lang, 2014).

A novel target for PD treatment is the adenosine A_{2A} receptor (A_{2A}R), which distributes abundantly in the dopaminergic neuron-rich striatal area (Schiffmann *et al.*, 1990), and played an important role in regulating dopamine receptor function. Recently, the A_{2A}R antagonist istradefylline became available in Japan and the U.S. as add-on therapy to levodopa (Dungo and Deeks, 2013; Chen and Cunha, 2020), introducing a novel strategy in the PD treatment.

H₃R has a high expression level in the striatum and modulates striatal GABAergic, glutamatergic and dopaminergic transmission. Postmortem analysis of PD patients showed increased histaminergic innervation in substantia nigra (SN), elevated histamine levels in caudate putamen, globus pallidus, and SN, indicating a possible application of H₃R ligands (Ryu *et al.*, 1994; Anichtchik *et al.*, 2000). Furthermore, H₃Rs form heterodimers with the dopamine D₁R and the dopamine D₂R. Dimerized H₃R/D₁R couples to G_i protein, the activation of which exerts an inhibitory effect (Ferrada *et al.*, 2009), while dimerized H₃R/D₂R displays a decreased affinity to D₂R agonist in the presence of H₃R agonists (Ferrada *et al.*, 2008). In an animal experiment, co-administration of H₃R agonists immapip or imetit and levodopa can alleviate levodopa-induced dyskinesia without affecting the antiparkinsonian effects (Gomez-Ramirez *et al.*, 2006). Furthermore, functional heterodimer H₃R/A_{2A}R was recently described. H₃R activation decreased A_{2A}R affinity for the agonist in membranes from rat striatal synaptosomes (Márquez-Gómez *et al.*, 2018). The features of histaminergic neurons and heterodimerized H₃R mentioned above indicate the application of H₃R ligands as potential PD treatments. The clinical studies with pitolisant and bavisant in PD treatment have focused on associated excessive sleepiness ([ClinicalTrials.gov](https://clinicaltrials.gov/ct2/show/study/NCT01036139) identifier: NCT01036139, NCT03194217). The direct involvement of H₃R in PD remains to be understood.

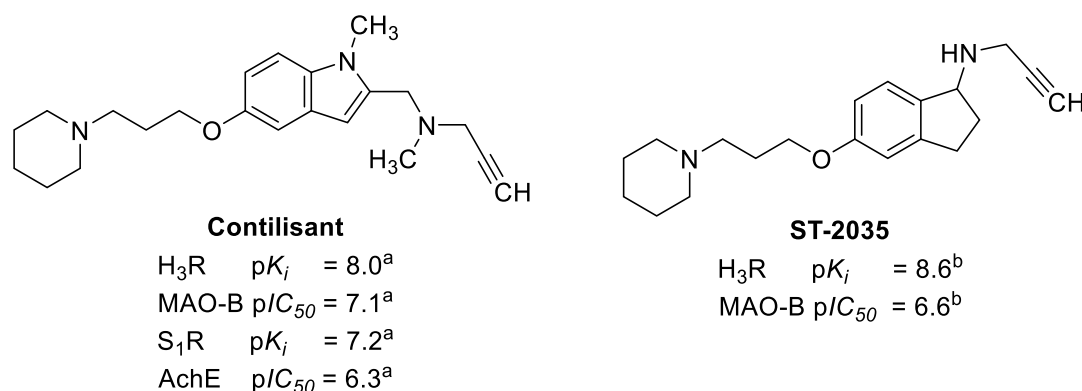


Figure 1-11: H₃R/MAO dual-active ligand ST-2035. (^aBautista-Aguilera *et al.*, 2018; ^bLutsenko *et al.*, 2019)

As a multifactorial disease, many novel strategies as PD treatment are reported in the last decade, such as MAO inhibition, iron chelation, A_{2A}R antagonism, dopamine agonism, H₃R antagonism, cholinesterase inhibition, and antioxidation (Cheong *et al.*, 2019). Ligands simultaneously targeting H₃R/MAO such as contilisant and ST-2035 (Figure 1-11) displayed excellent in-vitro activities at both proteins (Affini *et al.*, 2018; Bautista-Aguilera *et al.*, 2018; Lutsenko *et al.*, 2019). However, their in-vivo effect as PD treatment is still insufficient studied.

1.5.4 Schizophrenia

Schizophrenia is a chronic debilitating neurological syndrome characterized by positive symptoms such as hallucination and delusion, negative symptoms such as emotionlessness and lack of motivation, and impaired cognitive symptoms. Besides the well-recognized role of

D₂R in schizophrenia, dysregulation of the neurotransmitter systems of dopamine, serotonin, GABA, and glutamate are mainly discussed in the pathogenesis of schizophrenia and other psychotic disorders. The current therapy strategies are focused on the use of typical and atypical antipsychotics, whose effects are mainly based on negative modulation of dopamine receptors (Mainly D₂R) and serotonin receptors [Mainly serotonin receptor subtype-2A, (5-HT_{2A})] (Kondej *et al.*, 2018). However, antagonism at D₂R is frequently associated with Parkinson-like extrapyramidal symptoms such as rigor, tremor, akinesia, dystonia, and dyskinesia. Some atypical antipsychotic agents often have weight gain as a common adverse effect, which may affect therapy compliance (Sadek *et al.*, 2016b). Many antipsychotics are “dirty drugs”, simultaneously targeting a broad spectrum of proteins, including dopaminergic, serotonergic, muscarinic, adrenergic, and histaminergic receptors, leading to eventual severe adverse effects (Kondej *et al.*, 2018).

Some adverse effects, including weight gain and drowsiness of risperidone and quetiapine, can be ascribed to H₁R antagonism. However, evidence for the involvement of the histaminergic system in schizophrenia is emerging. An elevated level of *N*^ε-methylhistamine was found in the cerebrospinal fluid of patients suffering from schizophrenia (Prell *et al.*, 1995), while high-level expression of H₃R has been shown in the prefrontal in a *post-mortem* assessment of schizophrenia patients (Jin *et al.*, 2009). H₃R became a potential target for schizophrenia. The available knowledge suggests that H₃R antagonists may not be primarily effective in treating positive symptoms but might be beneficial as add-on therapy (Sadek *et al.*, 2016b). However, the H₃R antagonists ABT-288 and GSK239512 (see Figure 1-10), displaying in preclinical studies promising cognitive-enhancing effects (Esbenshade *et al.*, 2012; Wilson *et al.*, 2013), failed to ameliorate the cognitive deficits in schizophrenia patients in phase-II clinical trials (Haig *et al.*, 2014; Jarskog *et al.*, 2015), respectively. The unsuccess of selective H₃R ligands needs further investigation. Rationally designed drugs selectively targeting several proteins became a promising strategy, which has been pursuing by many research groups (Chen *et al.*, 2013; Yang *et al.*, 2016; Xiamuxi *et al.*, 2017).

1.5.5 Attention deficit hyperactivity disorder

Attention deficit hyperactivity disorder (ADHD) is a neurobehavioral disorder with high prevalence in children. The most common symptoms are hyperactivity, lack of attention, impulsivity, agitation, and disorganized behaviors. The symptoms may persist with varying severity into adulthood. The exact mechanism is still not fully understood. A dysregulation in the dopaminergic and noradrenergic systems is postulated (Singh, 2008).

Clinically often used drugs are the noradrenaline reuptake inhibitor atomoxetine and the noradrenaline and dopamine reuptake inhibitor methylphenidate. However, both drugs have considerable abuse potential (Setlik *et al.*, 2009; Chang *et al.*, 2014). In neonatal habenula

lesion-induced ADHD animal models, H₃R antagonists thioperamide (see Figure 1-7), carcinine, and conessine (Figure 1-12), attenuated the ADHD-like behavioral hyperlocomotion, impulsivity, and attention deficits in a dose-dependent manner. (Kim *et al.*, 2018).

Furthermore, thioperamide, ABT-239, GT-2331 (Figure 1-12), and ciproxifan (see Figure 1-8) have demonstrated pro-attentional effects in various ADHD animal models (Fox *et al.*, 2002; Komater *et al.*, 2003; Bardgett *et al.*, 2011). A preliminary, single-blind trial with pitolisant (see Figure 1-8) in 20 adult patients resulted in a progressive improvement in the Conners' adult ADHD rating scale (Schwartz, 2011). However, bavisant (see Figure 1-9) (Weisler *et al.*, 2012), MK-0249 (Herring *et al.*, 2012), and PF-03654746 ([ClinicalTrials.gov](https://clinicaltrials.gov/ct2/show/study/NCT00531752) identifier: NCT00531752, Structure Figure 1-12) could not reproduce the benefit in their completed phase-II clinical studies.

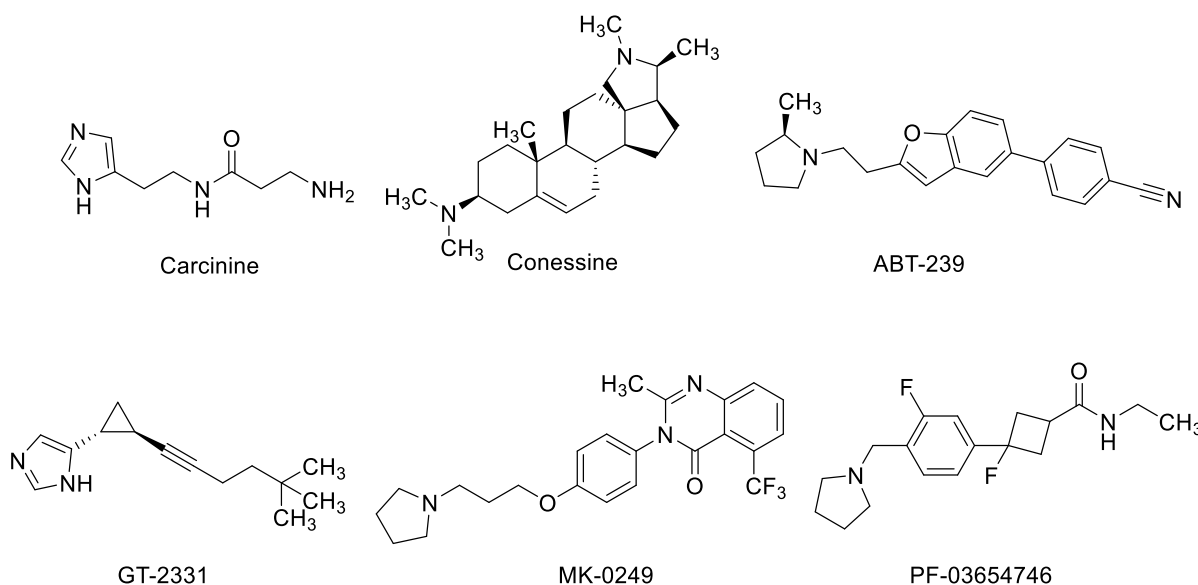


Figure 1-12: H₃R antagonists investigated as treatments of ADHD.

The observations suggest that drugs indirectly regulate neurotransmitters via H₃R may not provide sufficient therapeutic effect. ADHD may be more directly associated with noradrenaline and dopamine levels, where H₃R ligands may provide helpful add-on features.

1.5.6 Autism spectrum disorder

Autism spectrum disorder (ASD) is a neurodevelopmental disorder characterized by impairment in social communication and repetitive behavior patterns. Similar to its most common comorbid ADHD (Simonoff *et al.*, 2008), ASD frequently manifests at a young age and could persist into adolescence and adulthood. The prevalence has been estimated to be as high as 1 in 160 children worldwide (World-Health-Organization, 2019). Many genetic and environmental factors are involved in ASD. The histaminergic system is implicated in many neurological disorders, some of which, such as neuroinflammation and microglial regulation, share comorbidity with ASD (Wright *et al.*, 2017). Benefits have been reported by using H₃R

antagonists in preclinical studies in various animal models for AD, schizophrenia, narcolepsy and epilepsy (Schwartz *et al.*, 2000; Sadek and Stark, 2016; Sadek *et al.*, 2016a).

Investigations with H₃R antagonist DL-77 (see Figure 1-9) have demonstrated promising effects in behavior assessment in mice exposed to valproic acid (Eissa *et al.*, 2018, 2019). Recently, the MTDL ST-713 (Figure 1-13), simultaneously targeting H₃R, D₂R, and D₃R, developed in Stark-Lab (von Coburg *et al.*, 2009), has shown ameliorating effect in autism-like behavior regarding multiple parameters in a mouse model with a specific gene defect (Venkatachalam *et al.*, 2021). Further studies are necessary to estimate the clinical relevance of H₃R ligands in ASD.

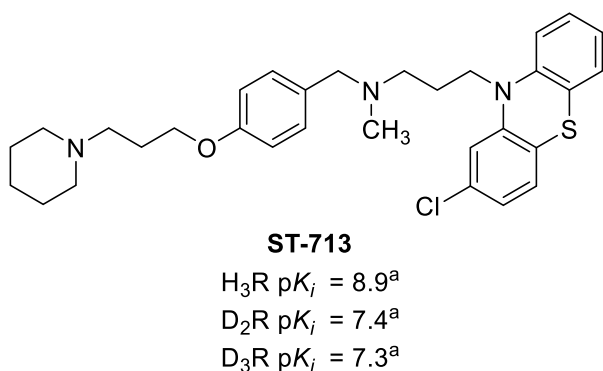


Figure 1-13: ST-713 simultaneously targets H₃R, D₂R, and D₃R. (^avon Coburg *et al.*, 2009)

1.5.7 Tourette's syndrome

Tourette's syndrome is a neurodevelopmental disorder characterized by chronic motor and vocal tics, expressing repetitive, involuntary movements and vocalizations. Many cases tend to be most severe in children and adolescents. As a common comorbid of ASD, Tourette's syndrome and ASD share some genetic risk factors. Frequently used pharmacological treatments of tics are neuroleptics such as risperidone, aripiprazole, or haloperidol. Though appreciable effectiveness can be achieved, the treatments are accompanied by numerous adverse effects (Eddy *et al.*, 2011). A rare mutation in the HDC gene has revealed the relationship between histamine and Tourette's syndrome. Thus H₃R antagonists became attractive options for novel treatment (Ercan-Sencicek *et al.*, 2010; Rapanelli and Pittenger, 2016). However, the H₃R antagonist AZD5213 (Figure 1-14) has failed in a phase-II study to reduce the tics after a three-week therapy in adolescents ([ClinicalTrials.gov](https://clinicaltrials.gov/ct2/show/study/NCT01904773) identifier: NCT01904773).

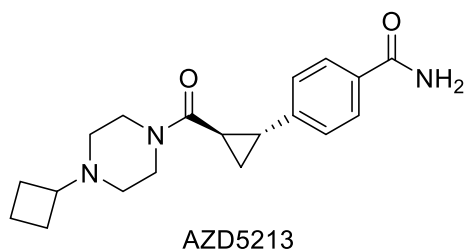


Figure 1-14: Clinical candidate for the treatment of Tourette's syndrome.

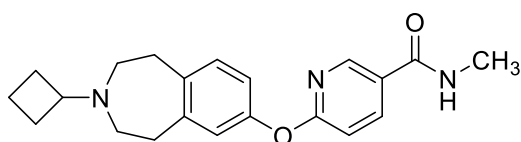
1.5.8 Epilepsy

Epilepsy is a frequent debilitating disease with a prevalence of 0.6-0.7% worldwide (Fiest *et al.*, 2017), characterized by recurrent, spontaneous seizures due to hyperactivity in the central neurons. A dysregulation of excitatory glutamate and inhibitory GABA in the neurotransmitter system is commonly postulated (Naylor, 2010). Seizures have also been associated with a paucity of histamine (Tuomisto and Tacke, 1986). The modulation of histaminergic transmission became a novel strategy for the treatment of epilepsy. Furthermore, the H₃R heteroreceptor regulates the neurotransmitter systems, including GABA and glutamate release. In preclinical experiments, a few H₃R antagonists, including DL-77 (see Figure 1-9), have demonstrated dose-dependent anticonvulsive effects (Sadek *et al.*, 2016c; a). Furthermore, pitolisant (see Figure 1-8) significantly abolished the response to intermittent photic stimulation in an early phase-II study (Kasteleijn-Nolst Trenité *et al.*, 2013). However, in a following open-labeled phase-II study, only one-third of subjects have experienced a decreased seizure rate by more than 50%. Thus, no evidence for the efficacy of pitolisant use could be confirmed (Dutilleul *et al.*, 2016). Notably, the study had included only a small number of test persons and was not placebo-controlled. Further clinical investigations are still necessary to get a comprehensive conclusion.

1.5.9 Neuropathic pain

Neuropathic pain is a severe and debilitating disease that arises from a lesion or disease in the central and periphery somatosensory nervous system. It is estimated that the prevalence lies between 7%-10% worldwide (van Hecke *et al.*, 2014). Clinically, neuropathic pain is characterized by spontaneous persistent and pulsating pain and induces an amplified pain response following noxious or harmless stimuli (Baron *et al.*, 2010). Apart from manifested nerve lesions, numerous pathophysiological and biochemical changes, including increases of excitatory neurotransmitters and neuropeptides, such as histamine, bradykinin, serotonin, and glutamate, cause morphological and functional adaptations in the nervous system (Baron *et al.*, 2010). H₃Rs may involve in the nociceptive transmission. Many studies revealed controversial effects introduced by H₃R agonists or antagonists on the nociceptive threshold. Several

experiments reported pain releasing effect by using agonist (Cannon *et al.*, 2003; Hasanein, 2011), while H₃R antagonists, including pitolisant in a high dose, led to reduced mechanical or thermal hypersensitivity associated neuropathic pain (Hsieh *et al.*, 2010; Zhang *et al.*, 2012; Popiolek-Barczyk *et al.*, 2018). Furthermore, preclinical studies have shown that repeated oral administration of H₃R antagonists demonstrated significantly analgetic effects in several animal models. The effects were comparable to first-line therapeutics pregabalin or gabapentin (Medhurst *et al.*, 2008; Cowart *et al.*, 2012; Chaumette *et al.*, 2018; Obara *et al.*, 2020). A phase-I study of H₃R antagonist GSK189254 (Figure 1-15) was conducted in the electrical hyperalgesia model of healthy volunteers. However, no results have been published since the study completed in 2007 ([ClinicalTrials.gov](https://clinicaltrials.gov/ct2/show/study/NCT00387413) identifier: NCT00387413). The involvement of H₃R in neuropathic pain and the clinical benefit of using H₃R ligands for this indication still need further investigation.



GSK189254

Figure 1-15: The H₃R antagonist GSK189254, a clinical candidate for the treatment of neuropathic pain.

1.5.10 Multiple sclerosis

Multiple sclerosis is a chronic progressive neurologic autoimmune disorder characterized by inflammatory-demyelinating lesions in the CNS and associated with axonal loss. Its pathogenesis is complex and heterogenic and still not fully understood. H₃R activation leads to the release of arachidonic acid and lipid mediators, subsequently induces neuronal apoptosis that might be associated with a few neurodegenerative diseases (Farooqui and Horrocks, 2006; Sander *et al.*, 2008). Furthermore, mice with a disrupted H₃R can develop more severe disease and neuroinflammation (Teuscher *et al.*, 2007). The observation suggests that H₃R may play a role in forming and developing lesions in multiple sclerosis (Jadidi-Niaragh and Mirshafiey, 2010). A phase-II trial demonstrated that the H₃R antagonist GSK239512 (see Figure 1-10) provided a positive effect on lesion remyelination. However, the benefits seemed insufficient to achieve clinical amelioration (Schwartzbach *et al.*, 2017).

1.5.11 Obesity

According to the World Health Organization, obesity is defined as abnormal or excessive fat accumulation in the body with a body mass index of 30 or more (World-Health-Organization, 2017). Obesity increases the risk of cardiovascular disease, type-2 diabetes, and cancer (Berlin *et al.*, 2011). The key to losing body weight appears to be a restoration of food intake

and expenditure homeostasis. Appetite and satiety are regulated by a complex interplay of central neurotransmitter systems, peripheral endocrine stimuli, the circadian rhythm, and environmental cues (Passani *et al.*, 2011). Several studies revealed that H₁ and H₃ receptors were involved in feeding behaviors. Loss of appetite has been observed in response to elevated hypothalamic histamine levels in rodent models following the blockade of the H₃ autoreceptor (Ookuma *et al.*, 1993; Passani *et al.*, 2011). However, controversial results have been reported. Both H₃R agonist imetit and antagonist could reduce the food intake behavior in animals (Yoshimoto *et al.*, 2006; Rao *et al.*, 2012). Thus, more clarification in this area is needed. A few preclinical studies reported weight reduction in rodents by applying selective H₃R antagonists (Hancock *et al.*, 2004; Malmjöf *et al.*, 2005). However, in a phase-I clinical trial, H₃R antagonist SCH-497079, whose structure is not published yet, displayed no significant difference to placebo in plasma glucose reduction in type-2 diabetes patients. Additionally, in a phase-II study, SCH-497079 failed to provide significant weight reduction against placebo ([ClinicalTrials.gov](https://clinicaltrials.gov) identifier: NCT00673465 and NCT00642993). The effect discrepancy between preclinical and clinical studies needs further investigation to guide future drug development. Recently, in a phase-I trial, pitolisant (see Figure 1-8) exhibited though not significant, but a tendentious reduction of hypoglycemia-induced glucagon in five type-1 diabetes patients ([ClinicalTrials.gov](https://clinicaltrials.gov) identifier: NCT04026750). Also here, more comprehensive experiments with a larger number of test persons are required.

1.5.12 Alcohol use disorders

Excessive alcohol consumption produces serious physical, psychological, and social problems and contributes to the pathogenesis of many diseases (Edenberg and Foroud, 2013). Many efforts, including behavioral therapy, medical intervention (mainly targeting the dopaminergic, serotonergic, glutamatergic, and GABAergic systems), and social support, have been made to combat alcoholism (Huebner and Kantor, 2010). Nuutinen and co-workers suggest a role for H₃R in modulating ethanol stimulation and reward (Nuutinen *et al.*, 2010). Many experiments in rodents revealed that H₃R antagonists could reduce alcohol drinking and alcohol-induced place preference (Galici *et al.*, 2011; Bahi *et al.*, 2013, 2015). These findings indicate a promising novel pharmacological strategy for alcoholism treatment. Bioprojet and Johnson&Johnson have planned phase-II clinical trials with pitolisant (see Figure 1-8) and bavisant (see Figure 1-9), respectively, to investigate the effect in alcohol use disorders. However, both trials have been withdrawn before the recruitment. Recently, Boston Medical Center had announced a phase-I trial with pitolisant for this indication. The results would be valuable for further understanding and evaluating the role of H₃R in alcoholism.

1.5.13 Allergic rhinitis

Allergic rhinitis is characterized by inflammation of the nasal mucosa caused by an abnormal activated immune response, which often causes sneezing, pruritus, snuff, and nasal congestion. Histamine is a critical mediator in the allergic response, where H₁R antagonists are the most common treatments. Furthermore, α -adrenergic receptor agonists have often been co-administrated to alleviate nasal congestion. However, the possibly cardiovascular and CNS excitatory adverse effects may not be neglect. Varty and colleagues have identified a high level of H₃R distribution in the human nasal mucosa and observed the effect of H₃R agonist (*R*)- α -methylhistamine (see Figure 1-6) and antagonist clobenpropit (see Figure 1-7) in the modulation of sympathetic nasal vascular tone (Varty *et al.*, 2004). H₃R blockade on nasal mucosa promotes the release of noradrenaline and also histamine. Thus, a combination of H₁/H₃R with minimized BBB penetration could be helpful (Berlin *et al.*, 2011). However, a series of clinical studies made by GlaxoSmithKline with H₁/H₃ dual-antagonism are not more effective than H₁ antagonism alone in reducing total nasal symptoms or nasal blockage (Daley-Yates *et al.*, 2012).

1.6 Multi-target-directed ligands

The “One molecule-one target” paradigm is a milestone in drug discovery, leading to the development of many successful drugs. However, highly selective ligands for given targets may confront its limit (Cavalli *et al.*, 2008). Many cardiovascular diseases, diabetes, cancer, and neurodegenerative diseases such as Alzheimer’s disease and Parkinson’s disease have well-documented multifactorial pathogenesis (Cavalli *et al.*, 2008). One single target might not be sufficient for adequate treatment. Multiple drug regimens for diseases with or without comorbidities may be applied to overcome such problems. Like the so-called cocktail treatment, two or more active ingredients targeting different proteins are administered as multiple drugs, or they can be comprised in one pill as a multi-component formulation.

Multiple-drugs administration frequently has drawbacks on therapy compliance and drug-drug interactions. The multi-component formulation is advantageous in patient compliance compared to the permanent use of several medicines. However, the pharmacokinetics difference resulted in the limited possibility of combination, and the drug-drug interaction remains unimproved. Hence, multi-target-directed ligands (MTDLs) may provide multiple advantages such as better patient compliance, less complicated metabolism pattern, and reduced potential of drug interactions (Morphy *et al.*, 2004; Cavalli *et al.*, 2008; Oset-Gasque and Marco-Contelles, 2018; Proschak *et al.*, 2019).

Morphy and Rankovic have described different strategies to engineer MTDLs. Two pharmacophores could be hybridized by linking, fusing, or merging (Morphy and Rankovic, 2006). The resulting MTDLs via linking have considerable molecular weight and negligible modification in the parent compounds, while the merged compounds often have smaller sizes, but more modifications are necessary (Figure 1-16A). In this work, if not state otherwise, hybrid ligands are referred to as MTDLs, which are designed based on two selected pharmacophores.

The molecular linker (Figure 1-16 A) can be designed to be metabolic stable or cleavable, such as disulfide bonds (Morphy *et al.*, 2004). To develop a fused ligand, functional groups whose modification could be tolerated by the binding site are directly coupled to each other without introducing an additional group. For a merged ligand, similar patterns are overlapped. In this way, two ligands are integrated into each other to obtain a small molecule.

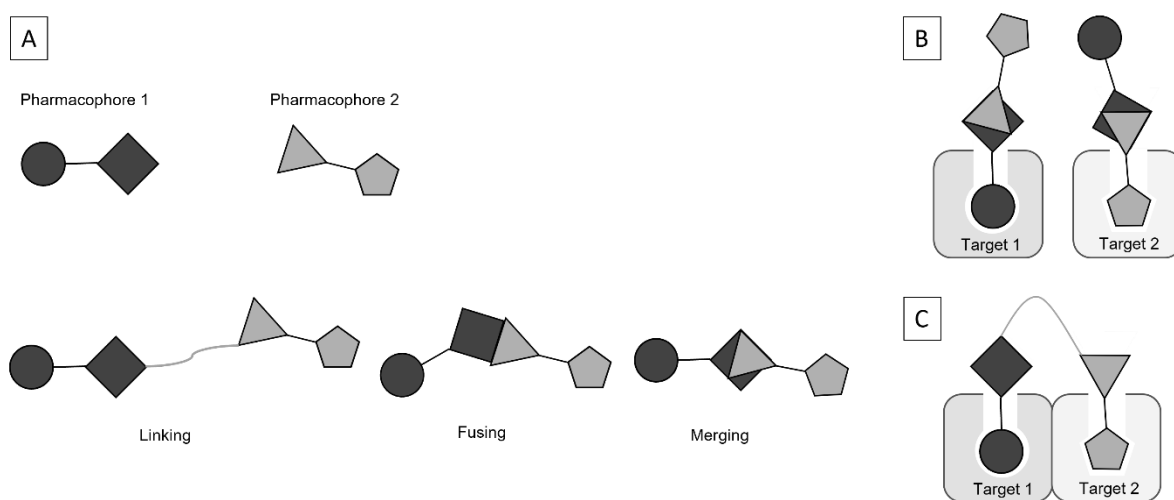


Figure 1-16: **A:** Design of MTDLs, modified according to Proschak *et al.*, 2019; **B:** MTDL interacts with two isolated targets; **C:** An MTDL interacts with two geometrically related targets at the same time. (**B** and **C** are modified according to Meunier, 2008.)

A few interaction models of hybrid ligands have been proposed by Meunier (Meunier, 2008). The author's initial intent was to develop an efficient treatment for drug-resistant malaria strain, with two different “weapons” in one drug. The “double-edged sword” had shown a promising effect in preclinical development. One hybrid molecule could interact either with two independent targets, in the case of linked, fused, or merged ligands (Figure 1-16 B), or simultaneously with two related targets, as linked ligands (Figure 1-16 C) (Meunier, 2008).

Simultaneously addressing several pathomechanisms may facilitate effective treatment for neurodegenerative diseases. However, the development of MTDLs is challenging. On the one hand, the selectivity at chosen targets should be rationalized. On the other hand, the effectiveness at different targets should be cautiously adjusted to make an efficient dose for all targets possible.

1.6.1 Neurodegeneration – multifactorial mechanisms

Alzheimer's disease (AD) and Parkinson's disease (PD) are neurodegenerative diseases with high prevalence. Due to their complex molecular mechanisms, rationally developed MTDLs may significantly improve the medical care in AD and PD patients.

The hallmarks of AD include senile plaques, mainly composed of β -amyloid peptide, neurofibrillary tangled tau protein, and selective synaptic and neuronal loss in brain regions involved in learning and memory, particularly the hippocampus and the cerebral cortex (Pereira *et al.*, 2005). The soluble oligomeric β -amyloid peptides are potent neurotoxins that inhibit a key process for memory formation, namely hippocampal long-term potentiation (LTP), and disrupt synaptic plasticity, resulting in cognitive impairment (Pereira *et al.*, 2005; Selkoe and Hardy, 2016). Moreover, evidence indicates that not only β -amyloid and its impaired clearance but also genetic and environmental factors may initialize and drive many cellular and molecular pathological events, including abnormal neuronal activities, vascular alterations, glial responses, inflammation, oxidative stress (Palop and Mucke, 2010; Long and Holtzman, 2019). Furthermore, the presynaptic protein α -synuclein, which is mainly associated with synucleinopathies like PD, is involved in the pathophysiology of AD (Twohig and Nielsen, 2019). Notably, some less prominent hypotheses of AD pathogenesis, such as the Ca^{2+} hypothesis (Khachaturian, 2017; Pchitskaya *et al.*, 2018) and the neurovascular hypothesis (Zlokovic, 2011; De Strooper and Karran, 2016), should not be neglected in the research of this highly complex and multifactorial diseases.

Neuronal loss in the substantia nigra, striatal dopamine deficiency, and intracellular inclusions of α -synuclein aggregates are the neuropathological hallmarks of PD (Poewe *et al.*, 2017). However, the cellular and molecular mechanism of neuronal loss in PD remain to be fully understood. Disturbed α -synuclein proteostasis, mitochondrial dysfunction, oxidative stress, impaired Ca^{2+} homeostasis, neuro-, as well as environmental toxins, and neuroinflammation are believed to be involved in PD's pathogenesis (Poewe *et al.*, 2017; Cheong *et al.*, 2019).

As disease-modifying therapies to slow or even reverse the disease progression are still poorly available, novel drugs simultaneously providing multiple neuroprotective effects may become promising therapeutic strategies for neurodegenerative diseases. Antioxidant therapy, neurotransmission regulation, hormonal replacement therapy, misfolded protein elimination, apoptosis prevention via kinase inhibition, and Ca^{2+} homeostasis restoration are conceivable therapeutical approaches (Pereira *et al.*, 2005; Pchitskaya *et al.*, 2018). A few strategies involved in this work will be introduced here.

1.6.2 Neuroprotective effects targeting H₃R

As discussed previously in section 1.3.1, targeting H₃R may provide promising cell protection. In preclinical studies, H₃R ligands have demonstrated promising neuroprotective effects in various animal models. H₃R antagonists clobenpropit and pitolisant have shown neuroprotective effects in pathology induced by β -amyloid peptide (Patnaik *et al.*, 2018). Thioperamide, another H₃R antagonist, has demonstrated protective effects in primary neurons against injury induced by oxygen-glucose deprivation and in cerebral ischemia (Yan *et al.*, 2014). Furthermore, thioperamide promoted neurogenesis and thereby ameliorated cognitive deficit (Wang *et al.*, 2020). However, many clinical studies suggest that selective H₃R ligands might not significantly benefit diseases with high complexity in the etiology. The knowledge encourages the development of multi-targeting H₃R ligands as adjuvant or standalone therapeutic strategies.

The *N*-(3-phenoxypropyl)piperidine scaffold has been proven as a suitable component for the development of hybrid ligands by numerous previous studies (Figure. 1-17) such as the tacrine derivative FUB 833 [H₃R, HMT, acetyl, and butyryl-cholinesterase (AChE, BuChE)] (Apelt *et al.*, 2002; Petroianu *et al.*, 2006), chlorpromazine derivative ST-713 [H₃R, dopamine D₂, and D₃ receptor (D₂R, D₃R)] (von Coburg *et al.*, 2009) and the rasagiline derivative ST-2035 (H₃R/MAO-B) (Lutsenko *et al.*, 2019).

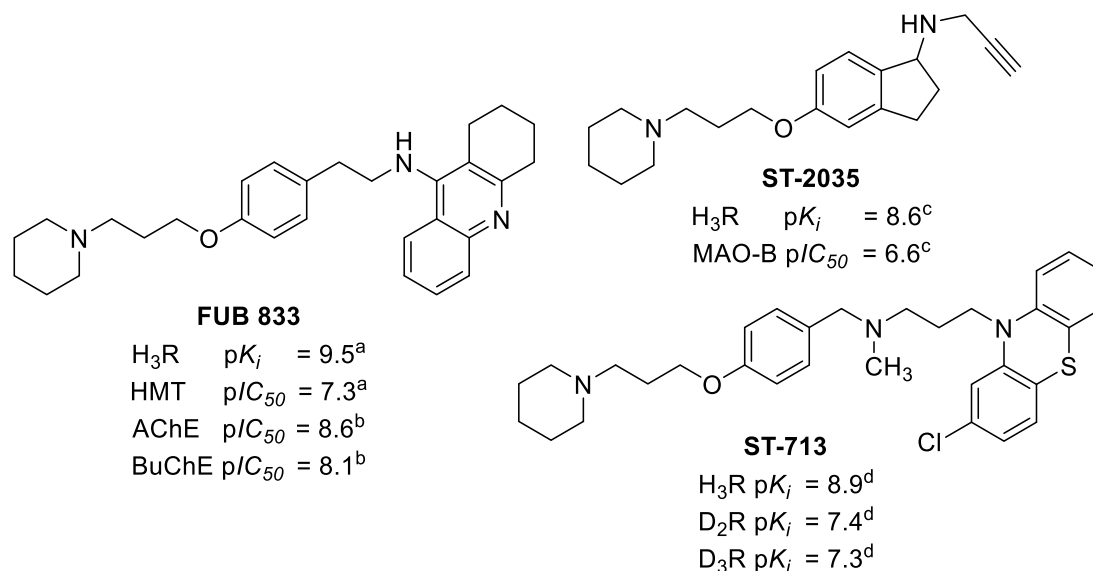


Figure 1-17: Selected hybrid ligands including *N*-(3-phenoxypropyl)piperidine structure as H₃R pharmacophore. (^aApelt *et al.*, 2002; ^bPetroianu *et al.*, 2006; ^cLutsenko *et al.*, 2019; ^dvon Coburg *et al.*, 2009)

1.6.3 MAO-B inhibition

Both isoenzymes MAO-A and MAO-B are tethered to the mitochondrial membrane. The activity and distribution of the two isoenzymes are tissue-dependent. MAO-B represents the main form in the basal ganglia in the human brain. The selective substrate of MAO-A is serotonin, while MAO-B demonstrates high activity toward 2-phenylethylamine. Dopamine, noradrenaline,

adrenaline, tryptamine, and tyramine are equally metabolized by both isoenzymes (Youdim *et al.*, 2006). The products created from the enzyme activity are cytotoxic H_2O_2 , aldehyde, and ammonia (or primary amine) (Youdim *et al.*, 2006; Manzoor and Hoda, 2020). An accumulation of these cytotoxic products in the brain is believed to be related to neurodegeneration (Manzoor and Hoda, 2020). A recent study revealed that instead of generating H_2O_2 , electrons emerged by MAO deamination of dopamine are transferred to the electron transporter chain, contributing to inner membrane polarization and helping sustain dopamine release (Graves *et al.*, 2020). An abnormality of MAO is involved in many neurodegenerative diseases, including AD and PD (Emilsson *et al.*, 2002; Tong *et al.*, 2017).

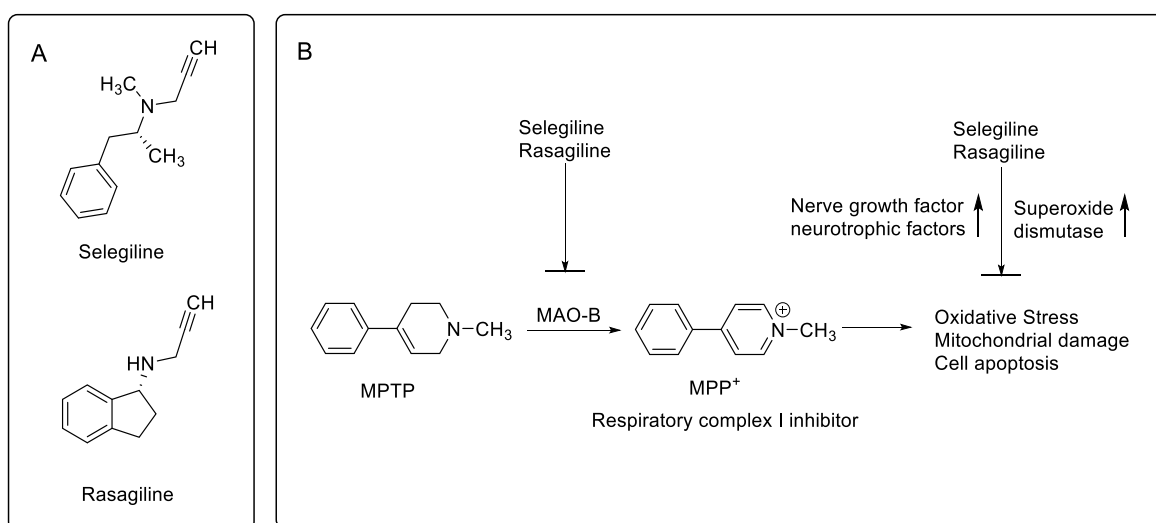


Figure 1-18: Cell-protective effect provided by Selegiline and Rasagiline against the neurotoxin MPTP and MPP⁺. (Figure B is modified from Szökő *et al.*, 2018.)

Selegiline and rasagiline (Figure 1-18 A) are widely used drugs for PD treatment, either as adjuvants to L-DOPA or monotherapies. Elevation of central dopamine levels by inhibiting its degradation has been proposed to be a major effect against PD. Furthermore, selegiline and rasagiline can prevent the activation of 1-methyl-4-phenyl-1,2,3,6-tetrahydropyridine (MPTP) to the neurotoxin 1-methyl-4-phenyl-pyridinium (MPP⁺) by MAO-B (Figure 1-18 B) (Chiba *et al.*, 1984; Cohen *et al.*, 1984). MPP⁺ is a potent inhibitor of mitochondrial respiratory complex I, whose dysregulation often associates with oxidative stress and cell death (Nicklas *et al.*, 1987). In addition to their selective MAO-B inhibition, numerous studies also indicated that both drugs displayed neuroprotective properties in MAO-independent mechanisms, including direct antioxidative property (Cohen and Spina, 1989), induction of superoxide dismutase (Li *et al.*, 1998). antiapoptotic and neurorescue effects after neurotoxin insulting have been reported (Tatton and Greenwood, 1991). The neurorescue effects may be associated with the increase of a series of nerve growth factors and neurotrophic factors (Mizuta *et al.*, 2000). Furthermore, selegiline prevents neurodegeneration induced by *N*-(2-chloroethyl)-*N*-ethyl-2-bromobenzylamine (Structure not shown), which is a selective neurotoxin for adrenergic

neurons (Ross, 1976). Similar neuroprotective effects are also observed for rasagiline (Szökő *et al.*, 2018). Moreover, Bar-Am and colleagues have shown that rasagiline regulates the β -amyloid precursor by a protein kinase C-dependent mechanism (Bar-Am *et al.*, 2004). The unique pharmacological properties made selegiline and rasagiline attractive neuroprotective agents and potential therapeutics for a wide range of neuronal impairments (Youdim *et al.*, 2006).

Despite the success as PD therapeutic, selegiline failed to slow the progression of the disease (Turnbull *et al.*, 2005), while rasagiline demonstrated limited disease-modifying effects (Rascol *et al.*, 2011; Poewe *et al.*, 2015), suggesting additional neuroprotective mechanisms are required for an effective cure for neurodegenerative diseases.

1.6.4 Voltage-gated calcium channel blockade

Ca^{2+} plays an essential role in cell vitality as it contributes to membrane potential and serves intracellular as a signal messenger, which is involved in gene transcription, muscle contraction, as well as the release of neurotransmitters and hormones (Zamponi, 2017). The transmembrane voltage-gated calcium channels (VGCCs), which respond to cell membrane depolarization and allow the entry of calcium ions along its gradient, are crucial for maintaining vital processes in cells.

According to the central pore-forming subunits, ten VGCC subtypes have been characterized in mammals (Table 1-2). $\text{Ca}_v1.1$, $\text{Ca}_v1.2$, $\text{Ca}_v1.3$ and $\text{Ca}_v1.4$ are designated as L-type calcium channels (LTCCs) due to their long-lasting (thus L-type) channel opening time. The LTCCs are primary targets of clinically used calcium channel blockers (CCBs), including dihydropyridines (DHPs), phenylalkylamines, and benzothiazepines. DHPs are the most widely used CCBs. They induce the closed states of the channel, bind to which in higher affinity, and stabilize their closed states (Bean *et al.*, 1986; Zamponi *et al.*, 2015). $\text{Ca}_v2.1$, $\text{Ca}_v2.2$ and $\text{Ca}_v2.3$, also termed P/Q (auxiliary subunits consisting dependent), N, and R-type, respectively, are expressed primarily in neuron cells. They regulate neurotransmission in most fast synapses (Takemura *et al.*, 1989; Takeshita *et al.*, 1998). The members of the Ca_v2 subfamily, similar to the LTCCs, respond to strong depolarization. However, they are generally not sensitive to CCBs, with only few exceptions (e.g., cilnidipine), but could be blocked by spider or snake venoms. The $\text{Ca}_v3.1$, $\text{Ca}_v3.2$, and $\text{Ca}_v3.3$ channels were designated as T-type calcium channels due to the short opening time (Transit). The T-type calcium channels respond to weak membrane depolarization and are thus also termed low-voltage calcium channels. Each of the ten subtypes can undergo tissue- and age-dependent alternative splices that lead to various functionalities (Catterall *et al.*, 2005; Zamponi *et al.*, 2015; Schampel and Kuerten, 2017; Zamponi, 2017).

Table 1-2: Localization and function of VGCCs

Channel	Type	Localization	Cellular functions
Ca_v1.1	L	Skeletal muscle; transverse tubules	Excitation-contraction coupling
Ca_v1.2	L	Cardiac and smooth muscle myocytes; endocrine cells; neuronal cell bodies; proximal dendrites	Excitation-contraction coupling; hormone release; regulation of transcription; synaptic integration
Ca_v1.3	L	Endocrine cells; neuronal cell bodies and dendrites; cardiac atrial myocytes and pacemaker cells; cochlear hair cells	Hormone release; regulation of transcription; synaptic regulation; cardiac pacemaking; hearing; neurotransmitter release from sensory cells
Ca_v1.4	L	Retinal rod and bipolar cells; spinal cord; adrenal gland; mast cells	Neurotransmitter release from photoreceptors
Ca_v2.1	P/Q	Nerve terminals and dendrites; neuroendocrine cells	Neurotransmitter release; dendritic Ca ²⁺ transients; hormone release
Ca_v2.2	N	Nerve terminals and dendrites; neuroendocrine cells	Neurotransmitter release; dendritic Ca ²⁺ transients; hormone release
Ca_v2.3	R	Neuronal cell bodies and dendrites	Repetitive firing; dendritic Ca ²⁺ transients
Ca_v3.1	T	Neuronal cell bodies and dendrites; cardiac and smooth muscle myocytes	Pacemaking; repetitive firing
Ca_v3.2	T	Neuronal cell bodies and dendrites; cardiac and smooth muscle myocytes	Pacemaking; repetitive firing
Ca_v3.3	T	Neuronal cell bodies and dendrites	Pacemaking; repetitive firing

(Table is modified according to Catterall *et al.*, 2005).

The pathological increase of intracellular Ca²⁺ level is cytotoxic (Stanika *et al.*, 2012; Simms and Zamponi, 2014). Dysregulation of calcium channels in neuronal cells has been linked to a broad spectrum of neurological disorders, including epilepsy, anxiety, multiple sclerosis, schizophrenia, migraine, autism, neuropathic pain, PD, and AD (Cain and Snutch, 2011; Schampel and Kuerten, 2017).

Despite controversial observations (Marras *et al.*, 2012), evidence suggests that inhibition of calcium channels in the CNS could be beneficial for different neuronal disorders (Ritz *et al.*, 2010; Pasternak *et al.*, 2012; Lee *et al.*, 2014). To be highlighted here are the roles LTCCs played in AD and PD. In AD, the formation of neurotoxic peptide β -amyloid was related to increased $\text{Ca}_v1.2$ subtype and elevated intracellular Ca^{2+} level, which is believed to induce cell death and impairment in the hippocampus and cerebral cortex (Anekonda *et al.*, 2011). In PD, the pacemaker activity of substantia nigra (SN) neurons is regulated by neuronal LTCCs (mainly by $\text{Ca}_v1.3$), pathological activation of LTCCs induced elevation of Ca^{2+} level in the cytoplasm and mitochondrial lead to increased production of reactive oxygen species (ROS), inducing cell death and loss of dopaminergic neurons in Parkinson's disease. Notably, LTCCs are also abundantly expressed in skeletal muscle, arterial smooth muscle and cardiac myocytes, where the CCBs exhibit their antihypertensive or antianginal effects. Despite the excellent safety profiles of many CCBs, novel drugs with CNS preference or selective block the $\text{Ca}_v1.3$ subtype to minimize the effect in vascular and cardio systems would be advantageous (Ortner and Striessnig, 2016; Zamponi, 2016).

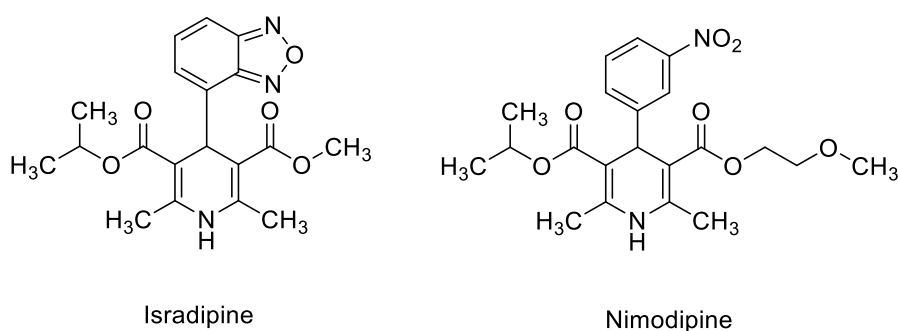


Figure 1-19: DHPs tested in clinical trials for the treatment of CNS disorders.

The antihypertension drug Isradipine (Vascal[®], Figure 1-19) has displayed in-vitro and in-vivo neuroprotective effects. However, it has failed to provide benefit in early PD ([ClinicalTrials.gov](https://clinicaltrials.gov/ct2/show/study/NCT02168842) identifier: NCT02168842). Nimodipine (Nimotrop[®], Figure 1-19) is a clinically used drug to ameliorate the ischemic deficits in patients with subarachnoid hemorrhage and the cognitive impairment in aging-related dementia. The outcomes of clinical trials using nimodipine in patients with dementia were heterogeneous. The improvements in a few clinical parameters seemed insufficient to ameliorate patients' daily lives (Birks and López-Arrieta, 2002; Nimmrich and Eckert, 2013).

The promising cellular mechanism but unconvincing clinical benefits of CCBs suggest that simultaneously involving multiple neuroprotective mechanisms, improved subtype selectivity, and CNS preference may provide adequate protection from neurodegeneration.

1.6.5 N-Methyl-D-aspartate receptor modulation

The amino acid L-glutamate is the most important excitatory neurotransmitter in the CNS, the effects of which are mediated by a large family of metabotropic and ionotropic receptors. The ionotropic glutamate receptors include N-methyl-D-aspartate (NMDA) receptor, α -amino-3-hydroxy-5-methyl-4-isoxazole propionic acid (AMPA) receptor and kainate receptor. NMDA receptors form one major subclass of the glutamate receptor family and localize abundant in the CNS. NMDA receptors are ligand-gated heteromeric transmembrane ion channels consisting of four subunits. To date, seven subunits of NMDA receptors have been identified, namely GluN1, four GluN2s (GluN2A-D), and two GluN3s (GluN3A-B). At least one GluN1 and one of the GluN2 subunits are necessary for a functional receptor, which typically consists of two GluN1 and two GluN2 subunits.

The pore opening of NMDA receptors needs two simultaneous signals (Figure 1-20). First, the postsynaptic membrane's depolarization removes Mg^{2+} from the binding site in the channel pore. Second, the agonist glutamate (or its name-giver, the selective ligand NMDA) and co-agonist glycine bind simultaneously to their binding sites at GluN2 and GluN1, respectively (Temme *et al.*, 2018).

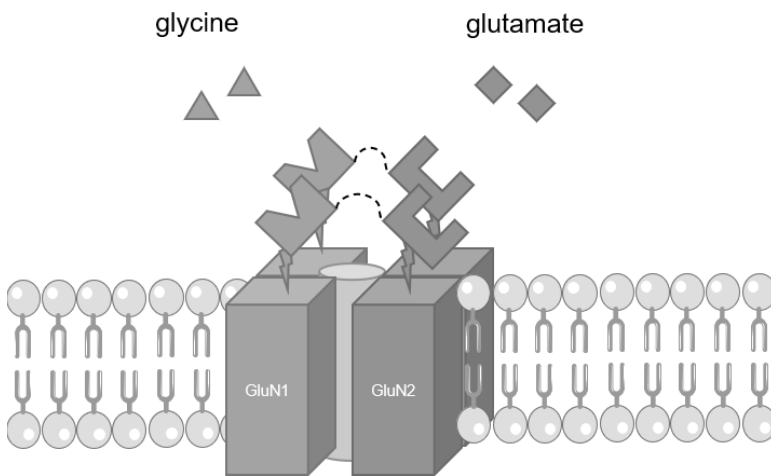


Figure 1-20: Tetrameric channels comprise two GluN1 and two GluN2 subunits in GluN1-GluN1-GluN2-GluN2 arrangement. Dashed wave lines indicate heterodimer interfaces. The central cylinder illustrates a transmembrane channel pore. For a channel opening, simultaneously binding of glycine and glutamate to the respective extracellular binding domain is necessary. (Graphic is modified after Furukawa *et al.*, 2005).

NMDA receptors mediate the efflux of K^+ and influxes of Na^+ and Ca^{2+} . Its high permeability to Ca^{2+} and its voltage-dependent blocking by Mg^{2+} enable this kind of receptor as a coincidence detector of presynaptic and postsynaptic firing, triggering use-dependent changes in synaptic activity, such as long-term potentiation (LTP) or long-term depression (LTD), which is essential for synaptic plasticity and cognitive function (Collingridge *et al.*, 2010; Benarroch, 2011; Hasan *et al.*, 2013).

Pathological enhanced NMDA receptor activity can cause a Ca^{2+} overload, which is excitotoxic and associated with neurodegenerative diseases such as AD and PD and can even trigger neuronal death in acute brain injury conditions (Choi, 1992). Furthermore, the Ca^{2+} influx mediated by NMDA receptors is believed to be more toxic than that mediated by VGCCs (Stanika *et al.*, 2012). Therefore, NMDA receptors are attractive targets in the treatment of some neurodegenerative diseases. However, most non-selective antagonists such as phencyclidine and ketamine were unsuccessful as neuroprotective agents. In contrast, psychomimetic side effects and cognitive disorders are well documented for those NMDA channel blockers (Chaffey and Chazot, 2008). The subtype pharmacology and subtype-selective compounds were intensively investigated. GluN2B-containing receptors displayed slow desensitization, longer recovery time, and increased channel opening duration than GluN2A-containing receptors. These subtypes consisting of the GluN2B subunit are believed to be primarily involved in the etiology of some neurodegenerative disorders. Thus, GluN2B selective agents were considered as promising drug candidates (Menniti *et al.*, 2000; Schreiber *et al.*, 2019). Moreover, NMDA receptor blocker-induced neuronal degeneration is reversible when applied in low to moderate doses and irreversible when applied in high doses (Jevtovic-Todorovic *et al.*, 2001). Thus, both hypo- and hyperactivity of the glutamatergic system lead to dysfunction.

Although the involvement of excessive-activated NMDA receptors in numerous neurodegenerative diseases is widely accepted, the advance in drug development was relatively slow. Memantine (Figure 1-21) is one of few NMDA targeting drugs approved for use in neurodegenerative diseases. It is a moderate affine, open-channel blocker at NMDA receptor with fast on/off kinetics. Furthermore, memantine preferentially inhibits the excessively, usually extrasynaptic NMDA receptor activity (Lipton, 2007; Xia *et al.*, 2010). Interestingly, as a channel blocker, memantine enhances the LTP (Parsons *et al.*, 2007). The unique pharmacological property made memantine a successful neuroprotective drug, which is often used to treat AD. Amantadine (Figure 1-21) is another NMDA blocker with an adamantane structure. It is a widely used drug in treating early symptomatic PD and dyskinesia (Hubsher *et al.*, 2012). However, its mechanism of action is still poorly understood.

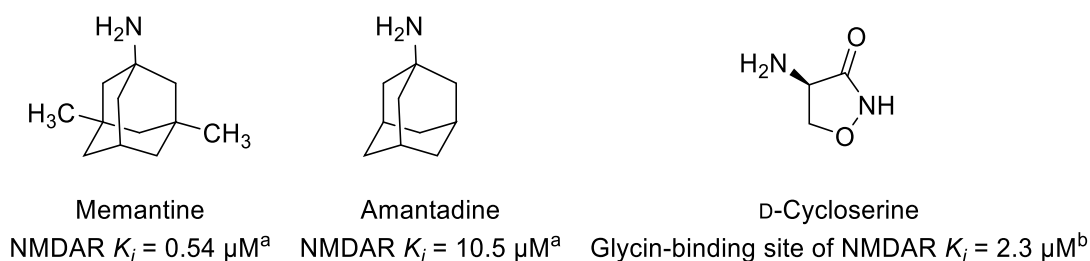


Figure 1-21: Potential neuroprotective drugs targeting NMDA receptors: Memantine, amantadine, and DCS. (^aKornhuber *et al.*, 1991; ^bLeeson and Iversen, 1994).

Another interesting drug targeting the NMDA receptor is D-cycloserine (DCS, Figure 1-21). It is a potent broadband antibiotic on the model list of essential medicines of the World Health Organization for the treatment of multi-drug resistant tuberculosis (WHO, 2015). DCS effectively inhibits alanine racemase and D-alanine-D-alanine ligase and, therefore, the cell wall synthesis (Neuhaus and Lynch, 1964; Lambert and Neuhaus, 1972). However, the use of DCS is frequently accompanied by severe psychotic adverse effects, which are related to a high daily dose (1-2 g/day) required to maintain proper antimicrobial blood levels (Crane, 1961).

The neuropsychiatric adverse effects evoked the study on the central effects of DCS. It acts as a partial agonist at the glycine binding site (Watson *et al.*, 1990) with a K_i value of 2.3 μM , while the endogenous ligand glycine itself has a K_i value of 0.2 μM (Leeson and Iversen, 1994). Furthermore, DCS increases the extracellular level of D-serine, which is another endogenous NMDA receptor co-agonist for the glycine binding site with a K_i value of 0.3 μM (Leeson and Iversen, 1994; Fujihira *et al.*, 2007). DCS impacts cognitive functions, mainly through the LTP-associated mechanism, a neuronal mechanism relevant to the learning process. Interestingly, DCS demonstrated higher efficacy in GluN2C-containing NMDA receptors than in GluN2A and GluN2B-containing ones (Sheinin *et al.*, 2001).

The weak and subtype-selective NMDAR activating unique property made DCS a potential therapeutical agent for various CNS disorders. DCS displayed more effectiveness in low dose and acute administration than in high dose and chronic use in treating AD and anxiety (Schwartz *et al.*, 1996; Tsai *et al.*, 1999; Hofmann *et al.*, 2006). In studies with small patient numbers, DCS demonstrated benefits in autism, depression, and spinocerebellar ataxia (Ogawa *et al.*, 2003; Posey *et al.*, 2004; Heresco-Levy *et al.*, 2013), but not schizophrenia (Goff *et al.*, 2005). The miscellaneous outcomes suggest that DCS may provide some neuroprotective effect. A rational drug regimen and as an add-on therapy strategy may establish its use in neuronal diseases.

2 Aims and objectives

Despite the devotion of several generations of scientists, neurodegenerative diseases remain incurable, cost-intensive, disabling disorders. Disease-modifying treatments and novel strategies for treating such impairments are urgently required. The H₃R plays a crucial role in regulating various neurotransmitters, including histamine, dopamine, noradrenaline, serotonin, acetylcholine, GABA, and glutamate. This unique property enables H₃R as an attractive drug target for a wide range of neuropsychiatric disorders (Discussed in section 1.5).

The establishment of the structure-activity-relationship of H₃R antagonists was a ligand-guided development. Despite numerous high-quality computational models, the exact spatial structure of the binding pocket is still unknown. This work aimed to present potent H₃R ligands with novel structural elements as pharmacological tools. To further understand the ligand-receptor interaction, different modifications will be applied to selected scaffolds as H₃R pharmacophores. The *N*-(3-phenoxypropyl)piperidine scaffold and the *N*-benzoyl piperazine scaffold (Figure 2-1) are presented in many excellent H₃R ligands. JNJ-5207852 and bavisant are prominent examples of the selected scaffold, respectively.

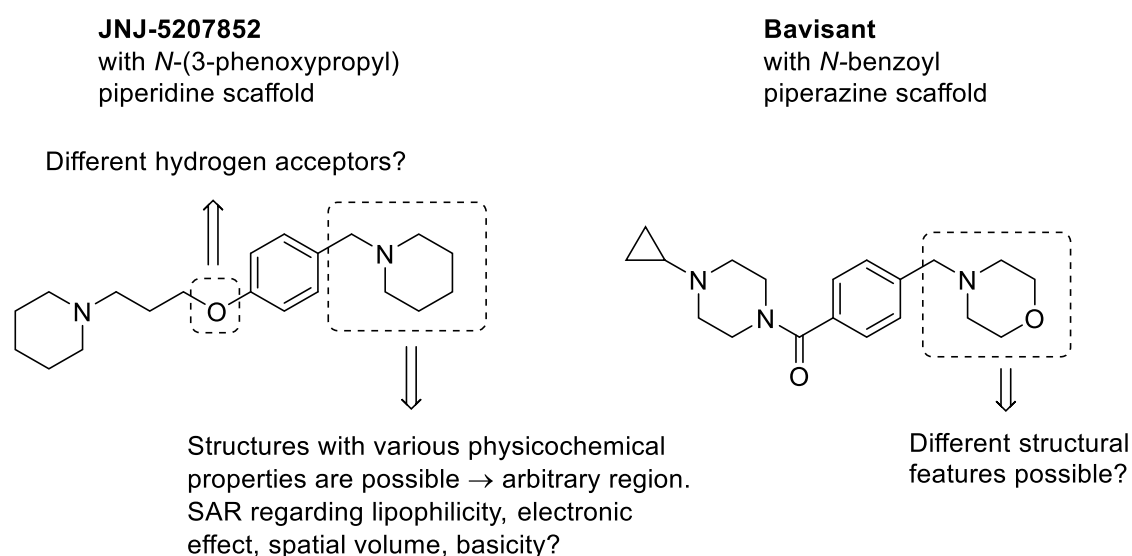


Figure 2-1: Designed modification in lead structures of H₃R ligands.

Many researchers have reported highly affine H₃R ligands derived from the *N*-(3-phenoxypropyl)piperidine structure. Modifications at the piperidine ring (Isensee *et al.*, 2009; Łażewska *et al.*, 2020), the aliphatic spacer (Łażewska *et al.*, 2020), the phenyl ring (Swanson *et al.*, 2009; Sander *et al.*, 2010c), and its substituents were reported. However, many details, including the hydrophobic interactions, which may have essential contributions to binding affinities, need further investigation. Also, a quantitative structure-activity relationship is still

missing. To gain more understanding of ligand-receptor interaction and spatial receptor structure, modifications in the *N*-(3-phenoxypropyl)piperidine structure will be focused on the substituents at the phenyl ring. Furthermore, the ether function is believed to be crucial for the binding affinity and may be involved in hydrogen bond formation (Axe *et al.*, 2006; Ghamari *et al.*, 2019b), while there are a few potent H₃R ligands without an ether function (e.g., bavisant, histamine). Therefore, studying the polar interaction of ether function is an exciting project.

Modifications in the *N*-benzoyl piperazine scaffold will be focused on the phenyl ring's substituents (Figure 2-1). In contrast to the *N*-(3-phenoxypropyl)piperidine scaffold, the structural diversity of substituents at phenyl ring in the *N*-benzoyl piperazine scaffold were rarely reported. The most known H₃R ligands with this scaffold comprise a second tertiary amine structure (e.g., *N*-benzyl morpholine in bavisant). Presenting H₃R ligands with this scaffold containing more structural variations will be an exciting project.

A significant part of this work aims to present multi-functional or multi-target-directed ligands (MTDLs) with H₃R pharmacophores as pharmacological tools and neuroprotective agents. The employment of MTDLs with H₃R antagonism property stands as a promising neuroprotective strategy. A few rational selected neuroprotective strategies, including blockade of L-type calcium channels (LTCC), regulation of *N*-methyl-D-aspartate (NMDA) receptors, and inhibition of monoamine oxidases, were discussed previously in section 1.6.

Dihydropyridines (DHPs) are widely used calcium channel blockers in the treatment of hypertension and cardiovascular events. Several studies suggested the neuroprotective effects of this class of drugs. A few drawbacks prevent the use of the most DHPs as neuroprotective agents, including limited blood-brain barrier (BBB) permeability (Uchida *et al.*, 1997), oxidative instability of the DHP ring, hydrolytic volatility of the ester group in the side chain, and lack of selectivity, resulting in cardiovascular events.

Combining the H₃R pharmacophore will increase the lipophilicity of the DHPs and probably enhance the BBB permeability. Furthermore, hydrolytic-stable alternatives in the side chains and the oxidative-stable alternative of the 1,4-dihydropyridine ring will be employed to synthesize the calcium channel blockers in this work (Figure 2-2).

To facilitate the Ca_v1.3 subtype-selectivity, the novel *N,N*-disubstituted barbituric acid structures (Figure 2-2, **compounds 3** and **8**) (Kang *et al.*, 2012; Cooper *et al.*, 2020) will be used in the development of MTDLs targeting H₃R and LTCCs. The miscellaneous structures of hybrid ligands presented in this work will provide an overview of a few applicable combinations and may inspire the further rational design of ligands simultaneously targeting H₃R and calcium channels.

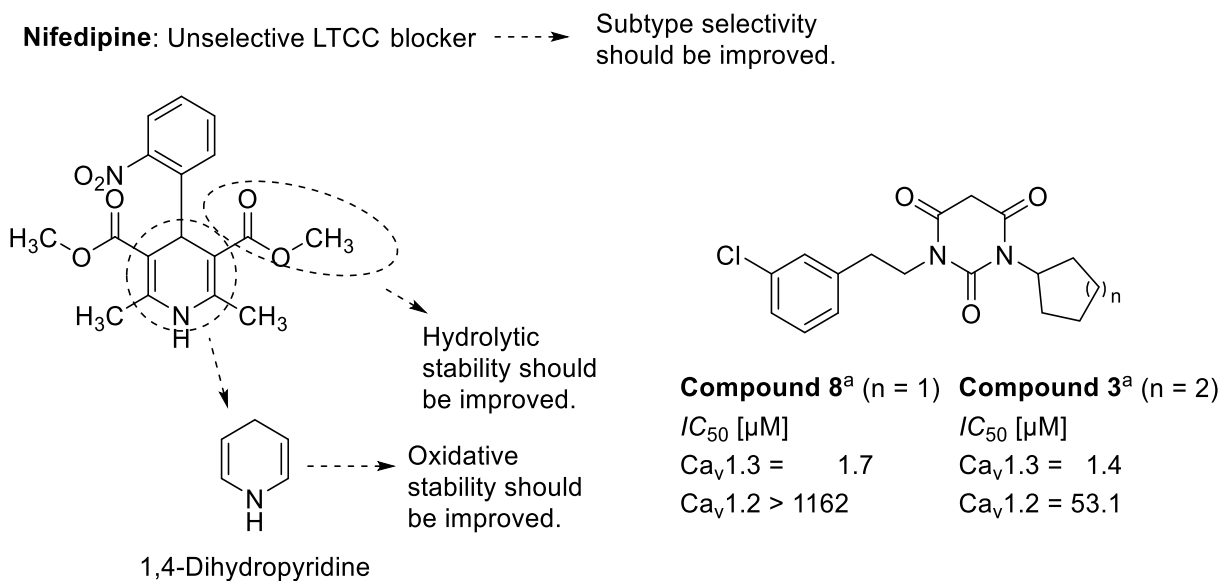


Figure 2-2: The design of hybrid ligands targeting H₃R and calcium channels. (^aKang *et al.*, 2012)

NMDA receptors have even higher Ca²⁺ permeability than the LTCCs. Pharmacological interventions in NMDA receptors need particular cautions. Both abnormal blockade or activation of NMDA receptors can lead to neuronal death. Simultaneously modulating H₃R and the NMDA receptor may present helpful neuroprotective or cognitive-enhancing strategies.

The cation channels stand as promising targets for neurodegenerative disorders. However, only a few candidates have reached clinical trials, and even fewer displayed convincing therapeutical results. In contrast, selective MAO-B inhibitors are widely used drugs for the symptomatic treatment of Parkinson's disease (PD). Several studies have revealed that selegiline and rasagiline displayed neuroprotective properties in MAO-dependent and -independent mechanisms (Cohen *et al.*, 1984; Cohen and Spina, 1989; Szökő *et al.*, 2018). Propargylamine is a common structural feature in both drugs (Figure 2-3). Potent H₃R/MAO-B dual-acting ligands have been synthesized and reported by the Stark-Lab (Affini *et al.*, 2018; Lutsenko *et al.*, 2019). This work aims to present H₃R ligands with the propargylamine structure and investigate their neuroprotective effects.

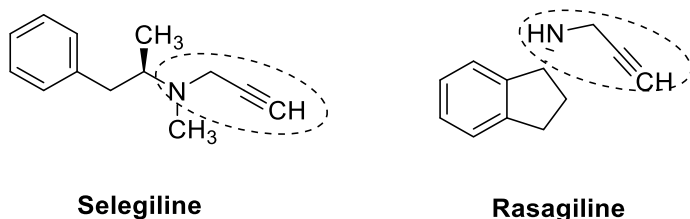


Figure 2-3: Propargylamine moiety (marked with dashed circles) is a common structural element of selegiline and rasagiline.

The brain is a fascinating and highly complex organ. The development of central active compounds is challenging, whereas great caution should be taken. The novel compounds synthesized in this work should help gain a deeper understanding of the structure-activity relationship of H₃R ligands, strategies in the multi-target-directed ligands development, and novel approaches in neuroprotection.

3 Chemistry

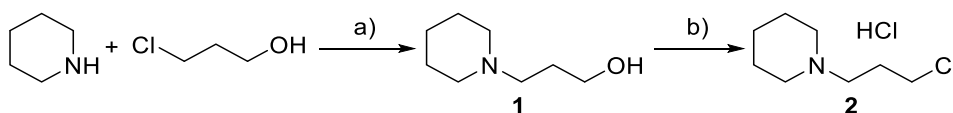
3.1 General notes for synthesis.

Various synthetic strategies may be applied to prepare compounds, intermediates, and synthons with similar structural features within this thesis. The selected synthetic routes were determined according to the feasibility of the reaction, availability, costs, reactivity, and stability of starting material and intermediates. Thus, this section is structured according to chemical structures rather than chemical reactions. In designing dual- or multi-targeting ligands, to keep a smaller molecular weight (Lipinski *et al.*, 2012), both pharmacophores have been fused or merged rather than linked, if applicable. The prepared intermediates and building blocks were assigned with consecutive numbers, while the compounds for pharmacological tests were designated with the prefix P to the consecutive numbers. A yield of over 95% will be concerned as quantitative.

3.2 Preparation of the intermediates

3.2.1 Preparation of the building blocks.

The central part of the synthesized compounds in this work contains the structure of *N*-(3-hydroxypropyl)piperidine (compound **1**, Scheme 3-1). This rudimentary building block was prepared via the *N*-alkylation of piperidine by using 3-chloropropan-1-ol in acetone under reflux. Potassium iodide was used as a catalyst to enable the exchange of chloride to iodide for an increased reactivity (Finkelstein, 1910). The obtained alkyl alcohol **1** was treated with thionyl chloride at room temperature (r.t.) to prepare the corresponding alkyl chloride **2** as the hydrochloride salt (Meier *et al.*, 2001).



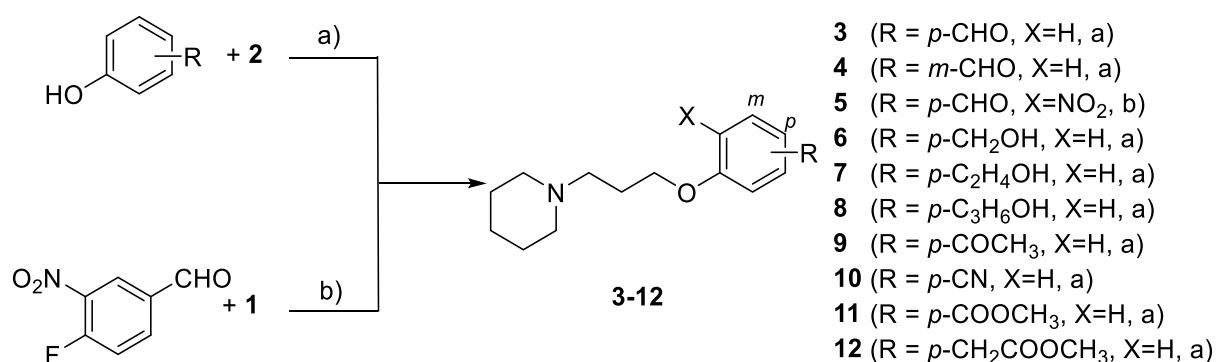
Scheme 3-1: Synthesis of the rudimentary building blocks.

a) K_2CO_3 , KI (cat.), acetone, reflux, 60 h, 80%; b) i: HCl in dioxane, ii: $SOCl_2$, DCM, r.t., 18 h, 90%.

Further intermediates comprising the 3-(piperidin-1-yl)propan-1-ol structure have been prepared by two types of nucleophilic substitution: Aromatic nucleophilic substitution at fluorobenzene derivatives with a corresponding alcoholate (Affini *et al.*, 2018) or Williamson ether synthesis from corresponding phenols and an appropriate alkyl chloride (Apelt *et al.*, 2005) (Scheme. 3-2).

The substitution groups in the aromatic ring of fluorobenzene had a significant influence on starting material's reactivity. For substrates with electron-withdrawing groups, a shorter reaction time is needed, and the yield is often higher than that with an electron-donating group (Rodriguez *et al.*, 2006).

In this work, the Williamson ether syntheses are S_N2 reactions, where primary alkyl halides were attacked by the nucleophilic alcoholates or phenolates (Williamson, 1851). This reaction can usually be conducted under mild conditions and acquire high yields. In this work, acetone was the solvent of choice due to its volatility and the Finkelstein reaction-promoting property.



Scheme 3-2: Preparation of intermediates with an *N*-(3-phenoxypropyl)piperidine structure.

a) K₂CO₃, KI (cat.), acetone, reflux, 18-48 h; b) NaH, THF, 0 °C- reflux, 5 h.

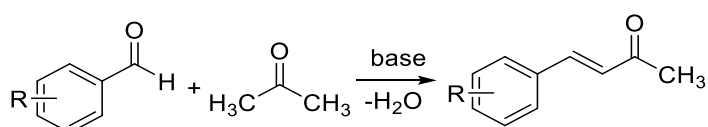
The intermediates **3**, **4**, and **6-12** were obtained from Williamson ether syntheses, where the alkyl chloride **2** reacted with the corresponding phenol derivatives.

Table 3-1: Intermediates obtained from ether synthesis

Intermediate	method	X	R ^a	Time (h)	Yield
3	a	-H	<i>p</i> -CHO	44	92%
4	a	-H	<i>m</i> -CHO	16	41%
5	b	-NO ₂	<i>p</i> -CHO	5	21%
6	a	-H	<i>p</i> -CH ₂ OH	48	59%
7	a	-H	<i>p</i> -CH ₂ CH ₂ OH	18	76%
8	a	-H	<i>p</i> -CH ₂ CH ₂ CH ₂ OH	18	Quantitative
9	a	-H	<i>p</i> -COCH ₃	15	Quantitative
10	a	-H	<i>p</i> -C≡N	18	93%
11	a	-H	<i>p</i> -COOCH ₃	48	94%
12	a	-H	<i>p</i> -CH ₂ COOCH ₃	48	79%

Compound **5** was prepared from 4-fluoro-3-nitrobenzaldehyde and the *in-situ* generated alcoholate from the alkyl alcohol **1**. The methods and yields of etherification were summarized in table 3-1.

The stated yields were calculated according to the amount after purification. The yields of products from Williamson ether synthesis were modest to quantitative. During the preparation of compounds **3** and **4**, traces of condensation products from benzaldehyde and acetone were observed (Scheme. 3-3), which could be avoided by changing the solvent system. For compound **5**, the chromatographic monitoring suggested a possible degradation of the product, which indicates a reason for the low yield of the reaction. The low solubility of 4-hydroxybenzyl alcohol in acetone may explain the low yield for compound **6**.

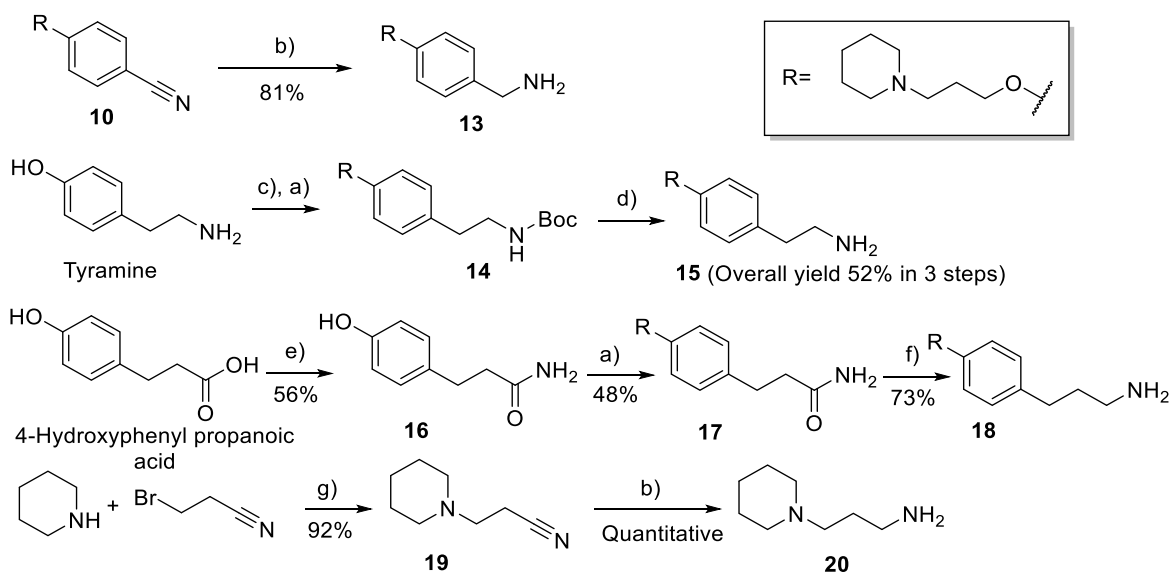


Scheme 3-3: The Aldol-condensation between aldehyde and acetone.

Intermediate **3-6** were used directly in the synthesis of compounds for pharmacological tests, while compounds **7-12** were used to prepare further intermediates, including amines, aldehydes, and carboxylic acids.

3.2.2 Preparation of primary amines

Various approaches were used for the preparation of the primary amines in this work (Scheme 3-4). Amines **13** and **20** have been obtained by Raney-Nickel catalyzed hydrogenation from the corresponding cyano derivatives **10** and **19** in an autoclave reactor (Sander *et al.*, 2010b).



Scheme 3-4: Preparation of primary amines.

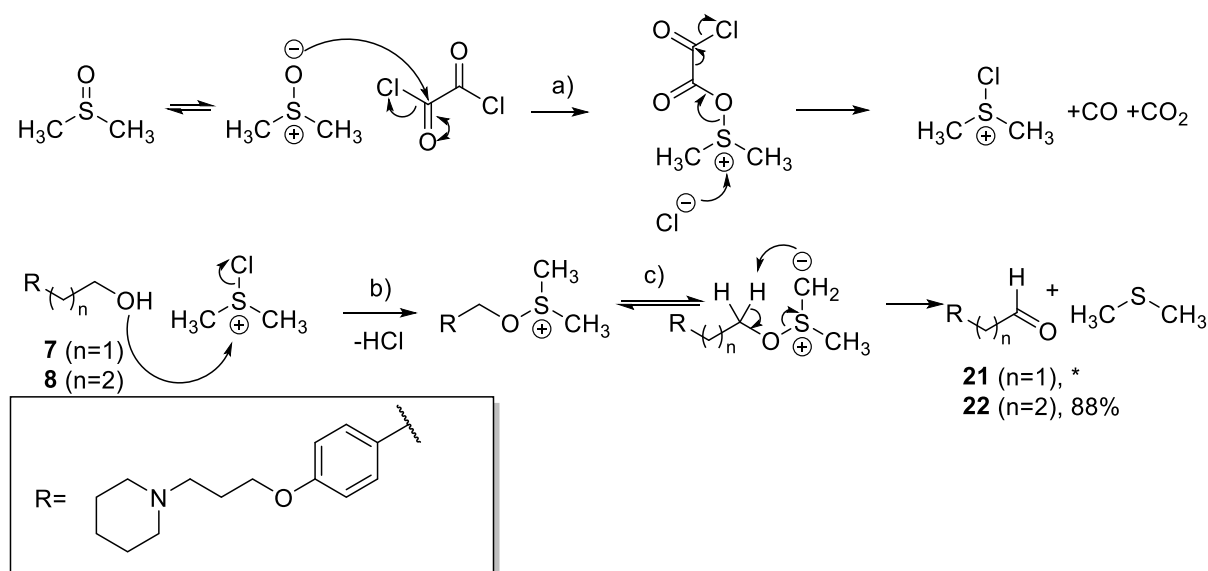
a) Alkyl chloride **2**, K_2CO_3 , KI (cat.), acetone, reflux, 18-64 h; b) Raney-Nickel, NH_3 (sat. in MeOH), H_2 , 5 bar, 40 °C, 18 h; c) sulfamic acid, di-Boc (di-tert-butyl dicarbonate), DCM, ultrasonic power level 9, 15 min; d) HCl in dioxane,

r.t. 18 h; e) *i*: Thionyl chloride, *n*-hexane, reflux, 18 h, ii: NH_3 (sat. in MeOH); f) LiAlH_4 , THF, reflux, 2 h; g) K_2CO_3 , acetone, r.t., 48 h.

The phenyl cyanide derivative **10** was obtained as described previously via Williamson ether synthesis (see scheme 3-2). The compound **19** was prepared according to the method reported by Amon and co-workers (Amon *et al.*, 2006): Piperidine reacts with 3-bromopropanenitrile in acetone under reflux in the presence of K_2CO_3 . Compound **16** was prepared from the *tert*-butyloxycarbonyl group (Boc) protected tyramine derivative **14** (Upadhyaya *et al.*, 2007). The Boc-group removed under acidic conditions, yielding the corresponding primary amine **16** in an overall yield of 52% over three steps. For compound **18**, ammonia was first acylated by phenyl propanoic acid chloride to carboxamide **16**, which was further etherified to compound **17**. Reduction of the carboxamide **17** with LiAlH_4 resulted in the corresponding primary amine **18** in 73% yield (Bullock *et al.*, 1970).

3.2.3 Preparation of aldehydes from corresponding alcohols

The benzaldehyde derivatives **3-5** were prepared by etherification of appropriate commercially available benzaldehyde derivatives. For the preparation of phenylacetaldehyde and phenyl propanal, additional oxidation or reduction was necessary. Swern-oxidation is a mild method to prepare aldehydes by oxidating the corresponding alcohols in the presence of dimethyl sulfoxide (DMSO), oxalyl chloride, and triethylamine (TEA) (Omura and Swern, 1978). The side products are easily removable volatile compounds. The mechanism of Swern-oxidation is illustrated in scheme 3-5 with examples for preparing the corresponding aldehydes **21** and **22**.



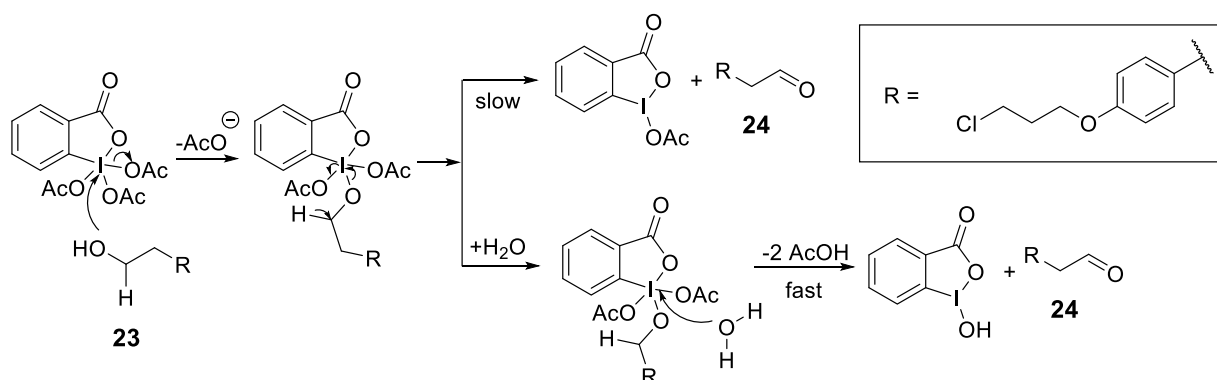
Scheme 3-5: Mechanism of Swern-oxidation.

a): DMSO, oxalyl chloride, 1 h, -60 °C; b) corresponding alcohol, DCM, -60 °C, 2 h; c) TEA, -60 °C - r.t., 30 min.
*: Product was detected by TLC and mass spectrometer but cannot be isolated.

The phenyl propanal derivative **22** was prepared in 88% yield, while the phenylacetaldehyde derivative **21** underwent further spontaneous reactions, probably in the manner of Aldol

condensation, catalyzed by the basic *N*-alkylated piperidine. Neither oxidizing the corresponding alcohol **7** by Dess-Martin periodinane nor reducing the carboxylic ester **12** by di-isobutyl aluminum hydride (DIBAH) nor workup in buffer solution could avoid this unwanted reaction. This observation indicated that the spontaneous reaction is independent of the preparation process. The putative Aldol reaction product could be observed via nuclear magnetic resonance (NMR) spectrum and mass spectrometry (MS). However, they were not isolated and fully characterized.

Despite many efforts, purifications of compound **21** and further reactions with it were unsuccessful. Hence, an alternative synthetic route was applied. Instead of preparing compound **21** as an intermediate, the non-basic phenylacetaldehyde **24** was synthesized for further use. For this purpose, the phenyl ethanol derivative **23**, which was obtained from the reaction of 4-hydroxyphenyl ethanol and 1-bromo-3-chloropropane under reflux in acetone (reaction not shown), was oxidized by Dess-Martin periodinane. The mechanism is shown in scheme 3-6 with the preparation of compound **24** as an example.

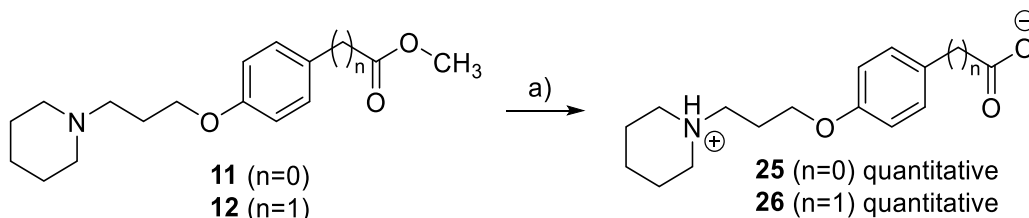


Scheme 3-6: The mechanism of oxidation with Dess-Martin-Periodinane. Aldehyde **24** was obtained in 88% yield.

Dess-Martin periodinane (1,1-dihydro-1,1,1-triacetoxy-1,2-benziodoxol-3(1*H*)-on) is a ready-to-use, commercially available mild oxidizing agent for the preparation of aldehydes or ketones from the corresponding primary or secondary alcohols, respectively (Scheme 3-6). This reagent was firstly developed by its name-givers (Dess and Martin, 1983). Similar to Swern-oxidation, the reaction using Dess-Martin periodinane is usually performed in chlorinated solvents, such as chloroform or dichloromethane. A few advantages of Dess-Martin periodinane made it a popular oxidation reagent: A small amount of water present in the reaction can accelerate the oxidizing process (Meyer and Schreiber, 1994), circumventing the water-free condition obliged by the Swern-oxidation; The reaction is applicable at room temperature, avoiding the strict low temperature (< -60 °C) required by Swern-oxidation. However, the byproduct is not volatile compounds like Swern-oxidation, and purification via column chromatography is often required.

3.2.4 Preparation of carboxylic acids

The corresponding carboxylic acids **25** and **26** with H₃R antagonists scaffold (Scheme. 3-7) were prepared by hydrolyzing the corresponding methyl ester **11** and **12** in NaOH solution. Both compounds could be obtained in quantitative yields.



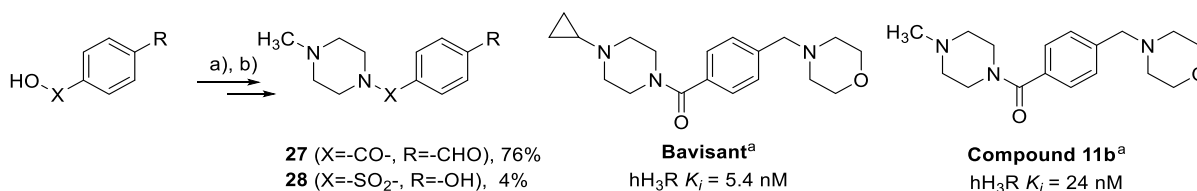
Scheme 3-7: Preparation of carboxylic acid.

Chemical and condition: a) NaOH, H₂O, MeOH, r.t. 20 h.

The obtained zwitterionic compounds **25** and **26** have been treated with conc. HCl (37%, aq.) and converted into corresponding hydrochloride salts.

3.2.5 Preparation intermediates with N-acylated piperazine scaffold

The second class of H₃R ligand involved in this work bear N-benzoyl piperazine or N-sulfonyl piperazine structure. This scaffold can be found in the clinical candidate bavisant and a series of its derivatives (Scheme 3-8) developed by Johnson&Johnson (Letavic *et al.*, 2015). N-Methylpiperazine was acylated by the appropriate benzoyl or sulfonyl chloride, which were prepared by the reaction of the corresponding benzoic or sulfonic acids with thionyl chloride in an aprotic solvent or neat. For a strong aromatic carboxylic acid with an electron-withdrawing effect or sulfonic acid, catalytic amounts of DMF were used (Koroleva *et al.*, 2011). The mechanism of DMF catalyzed preparation of acyl chloride was described elsewhere (Bosshard *et al.*, 1959).



Scheme 3-8: Preparation of synthons with N-acylated piperazine structure. (^aLetavic *et al.*, 2015)

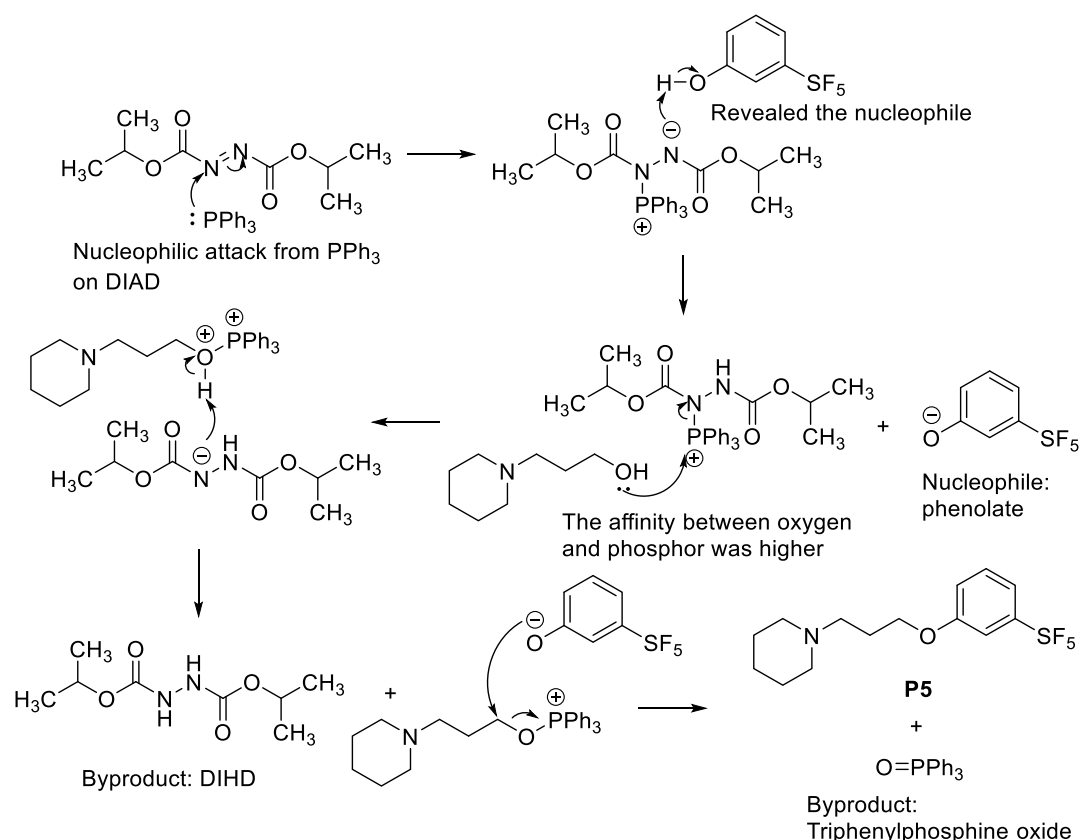
a): SOCl₂, toluene (**27**) or neat (**28**), DMF 4-18 h, reflux; b): N-Methylpiperazine, pyridine or TEA, DCM, 18 h, r.t.

The carboxamide derivative **27** was obtained in 76% yield, while only 4% could be achieved for compound **28**. The reason for the poor yield may be attributed to the limited solubility of 4-hydroxybenzenesulfonic acid in thionyl chloride or an intermolecular ester formation.

3.3 Synthesis of H₃R ligands with organo-fluoride and -chloride

In this project, modifications were focused on the substitution at the phenyl ring of both previously described scaffolds: The *N*-(3-phenoxypropyl)piperidine and *N*-acylated piperazine structures. The following substitutes were involved in this project: Fluoride, chloride, pentafluorosulfanyl (SF₅) group, and trifluoromethyl (CF₃) group. The substitutes exhibit different strengths of negative inductive effects and various atomic volumes. The substitutions were in *para* or *meta* position to the corresponding carboxamide or ether groups. Three synthetic routes were applied for the ether formation of compounds bearing *N*-(3-phenoxypropyl)piperidine structure. In addition to Williamson ether synthesis and the aromatic nucleophilic substitution of fluorobenzene described previously (see section 3.2.1), the Mitsunobu reaction was also employed for ether synthesis.

In 1967 Mitsunobu introduced an esterification method with alcohols and carboxylic acids in the presence of triphenylphosphine (PPh₃) and diethyl azodicarboxylate at ambient temperature (Mitsunobu *et al.*, 1967). Besides esterification, this reaction was also extended to etherification, *N*-alkylation, and epoxide formation (Hughes, 1996).



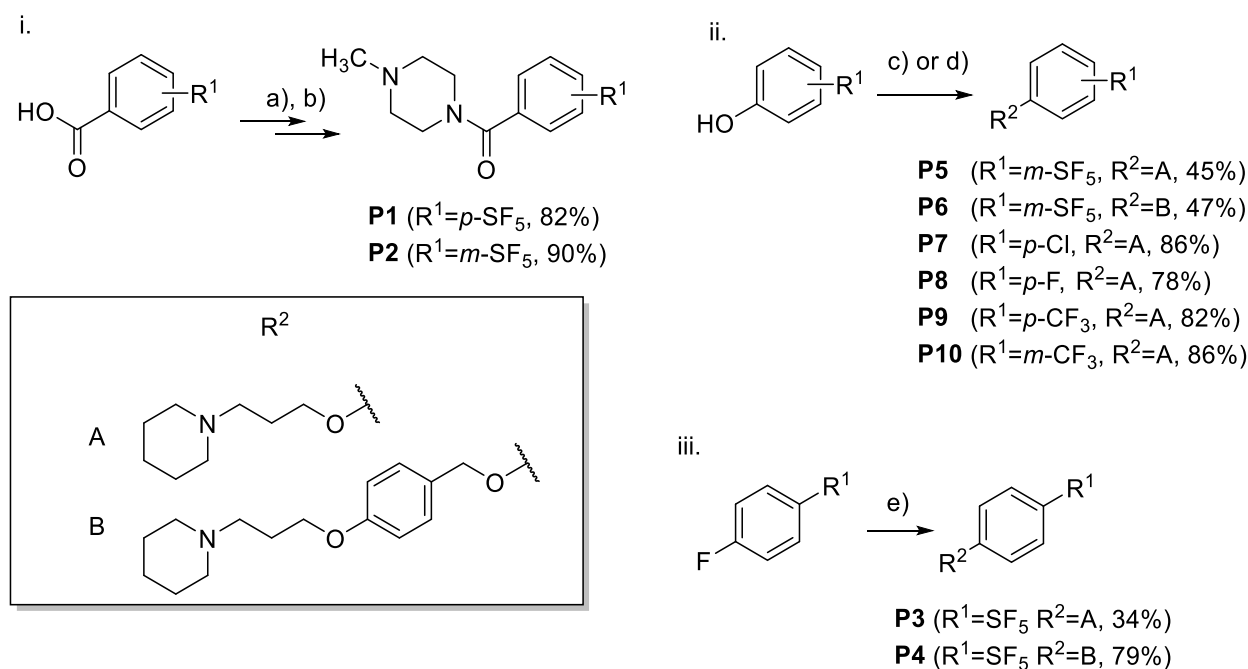
Scheme 3-9: Mechanism of Mitsunobu-Reaction.

The Mitsunobu reaction was implemented to prepare the compounds **P5** and **P6** from the corresponding alcohols and phenols in the presence of PPh₃ and diisopropyl azodicarboxylate (DIAD). In the first step, PPh₃ attacked DIAD nucleophilic. The generated positively charged

phosphor owned a higher affinity to the oxygen of the alcohol, so that in the end diisopropyl hydrazine dicarboxylate (DIHD), a reduced form of DIAD was obtained as a by-product. On the other hand, the quaternary phosphonium salt acted as an excellent leaving group, facilitating the formation of the desired ether and the other by-product triphenylphosphine oxide. The schematic mechanism is shown with the formation of compound **P5** as an example (Scheme 3-9).

Similar to the intermediate **27** with *N*-benzoyl piperazine structure, compounds **P1** and **P2** were prepared from the corresponding acyl chlorides intermediates and *N*-methyl piperazine.

Furthermore, the compounds **P4** and **P6** bearing the *N*-(3-phenoxypropyl)piperidine scaffold were extended by one more methoxybenzene group. This extension may provide additional information about the structure-activity relationship of H₃R. An overview of the synthetic routes and the products is illustrated (Scheme 3-10).



Scheme 3-10: Syntheses of H₃R ligands with halide or halide-containing-group in the aromatic ring.

a): SOCl₂, DCM, 4 h, reflux; b): *N*-Methylpiperazine, TEA, DCM, r.t. 18 h; c): Alkyl chloride **2**, K₂CO₃, KI, acetone, reflux (**P7-P10**); d): Alcohols **1** or **6**, PPh₃, DIAD, THF, 0 °C - r.t., 18-24 h (**P5** and **P6**); e): Alcohols **1** or **6**, NaH, DMF, 0 °C - r.t., 6-18 h.

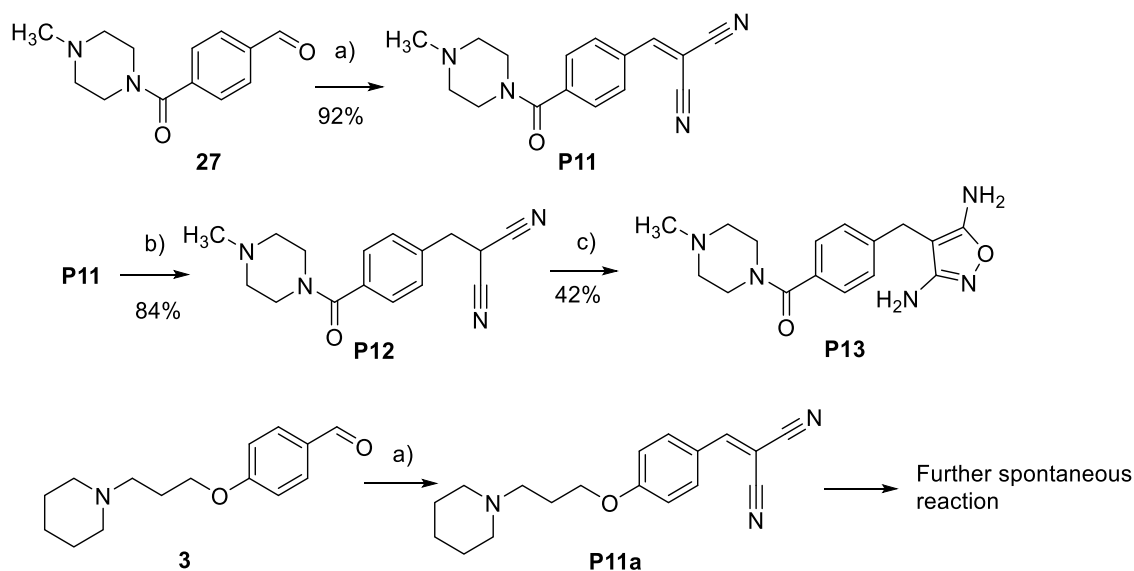
3.4 Synthesis of H₃R ligands with benzylidene structure

Similar to the substitutions with organo-fluoride and -chloride, modifications in this project focused on substitutes at phenyl ring of the *N*-(3-phenoxypropyl)piperidine and *N*-acylated piperazine structures. In contrast to the previous project, the substituents exhibit different negative mesomeric effects in conjugated systems.

The compounds with benzylidene structures were synthesized via Knoevenagel condensation. The original Knoevenagel reaction was carried out using benzaldehyde and ethyl acetoacetate in the presence of piperidine as a basic catalyst at $-5\text{ }^{\circ}\text{C}$ (Knoevenagel, 1896). The starting materials used in this work demonstrated various physicochemical properties and reactivities, requiring accordingly modified conditions. The reactions were performed in different solvents such as toluene, ethanol (EtOH), ethyl acetate (EtOAc), acetic acid (AcOH), with catalysts like ammonium salts, Lewis acid AlCl_3 (Li *et al.*, 2012), or catalyst-free. The reaction conditions varied from r.t. to $200\text{ }^{\circ}\text{C}$ in the microwave reactor (Freeman, 1981; Mendgen *et al.*, 2012).

3.4.1 Benzylidene malononitrile derivatives and their modifications

The benzylidene malononitriles **P11** and **P11a** were synthesized by corresponding benzaldehyde and malononitrile (Scheme 3-11). Malononitrile is an active methylene reagent with a $\text{p}K_{\text{a}} \approx 11$. The reaction between malononitrile and aldehydes or ketones usually are base-catalyzed reactions (Jones, 1972). The aldehydes **3** and **27** in this work contained basic tertiary amines, namely *N*-methylpiperazine in compound **27** and *N*-propylpiperidine in compound **3** with approximately $\text{p}K_{\text{a}}$ values of 8 and 10 (estimated via Chemdraw professional, version 19, 2019, PerkinElmer, Waltham, USA), respectively. Therefore additional bases were not necessary. Furthermore, one equivalent of anhydrous MgSO_4 was given to the reaction to absorb the leaving water molecules from the condensation.



Scheme 3-11: Preparation of benzylidene malononitrile derivatives and their further modifications.

a): EtOAc, MgSO_4 , r.t., 1 h; b): NaBH_4 , EtOH, $0\text{ }^{\circ}\text{C}$, 2 h; c): $\text{NH}_2\text{-OH} \times \text{HCl}$, TEA, MeOH, r.t., 48 h.

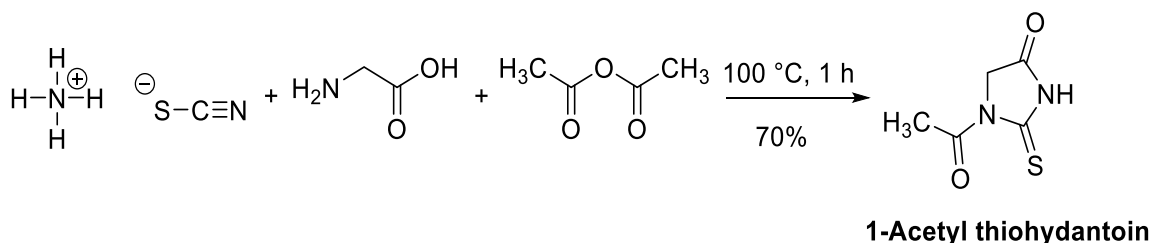
Compound **P11** was obtained as yellowish crystals from the reaction solution in a high yield. However, compound **P11a** underwent further spontaneous reactions under the same condition, resulting in a black-colored, viscid, hardly in methanol soluble mass. Despite many efforts, including the application of different solvents, temperature, catalysts in the reaction, and

various work-up- and purification methods, the synthesis of compound **P11a** was not successful. The product from the spontaneous reaction was not further characterized. A few reaction mechanisms have been proposed elsewhere (Jones, 1972; Freeman, 1980).

The benzylidene malononitrile derivative **P11** was further reduced to benzyl malononitrile **P12** with sodium borohydride (NaBH_4). Compound **P12** further reacted with hydroxylamine to obtain an isoxazole derivative **P13** (Scheme 3-11).

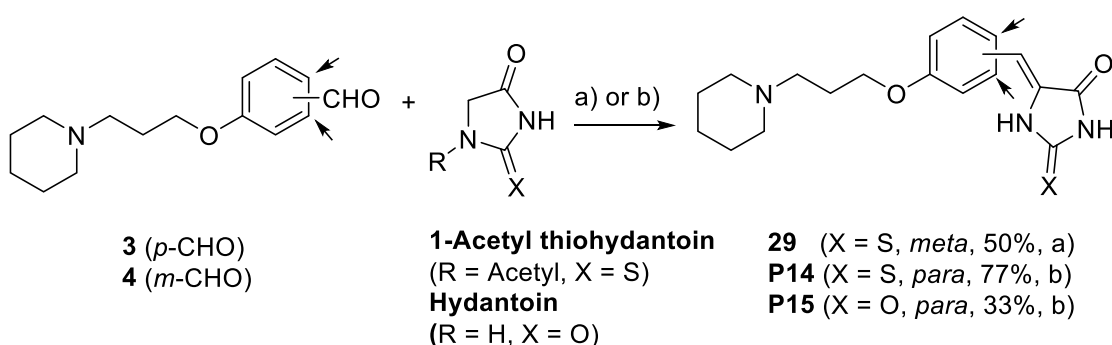
3.4.2 Benzylidene (thioxo-)imidazolidinone derivatives and their modifications

Compounds for this project were synthesized from aldehyde **3** or **4** with hydantoin or acetyl thiohydantoin in glacial acetic acid, catalyzed by ammonium acetate (NH_4OAc). Hydantoin is commercially available, while 1-acetyl thiohydantoin (Scheme 3-12) was obtained from the reaction between NH_4SCN and glycine in acetic acid anhydride (Ac_2O) at 100°C (Johnson and Nicolet, 1911).



Scheme 3-12: The synthesis of acetyl thiohydantoin.

The following condensation reactions were carried out either in the microwave reactor or by heating in an oil bath. Both methods gave products as (*Z*)-isomers in moderate yields, but the reaction time of the microwave reaction was drastically reduced (Scheme 3-13).



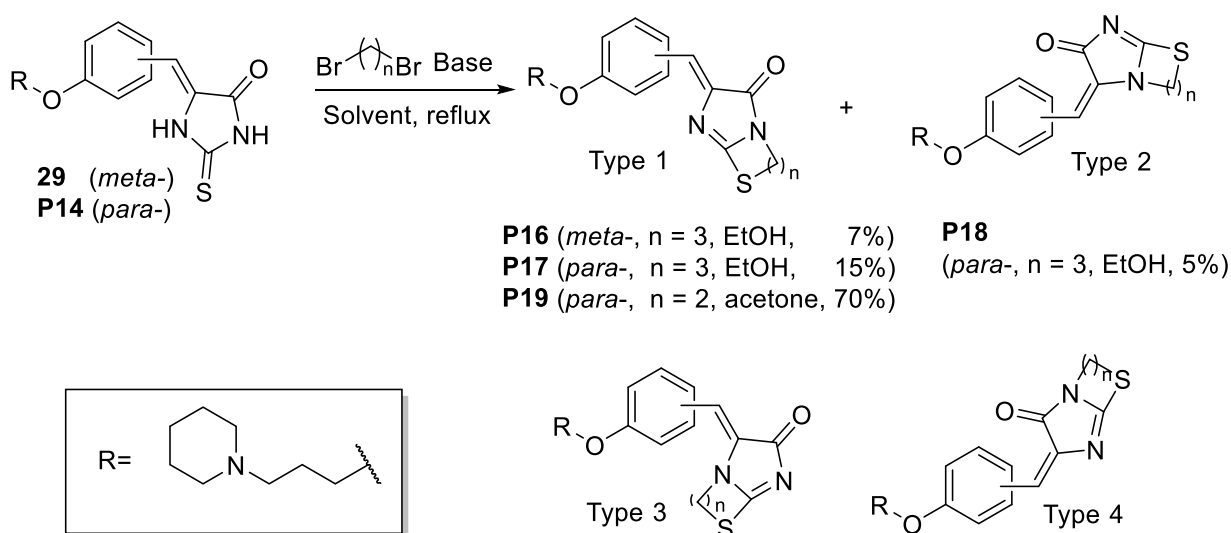
Scheme 3-13: Preparation of benzylidene (thioxo)imidazolidinone.

a): NH_4OAc , AcOH , reflux, 6 h; b): NH_4OAc , MW, $180\text{--}200^\circ\text{C}$, 15 min.

Further alkylation of **P14** and **29** with 1,2-dibromoethane or 1,3-dibromopropane generated annulated five- or six-membered rings in the thiohydantoin structure. The obtained imidazo[2,1-*b*]thiazolidinone or an imidazo[2,1-*b*][1,3]thiazinane annulated ring system

increase the size as well as the lipophilicity of the molecule. The benzylidene thiohydantoin structure has three nucleophilic sites: sulfur, *N1*, and *N3* (Scheme 3-14).

Unexpectedly, a conversion of (*Z*)- to (*E*)- configuration was observed when the alkylation reaction was carried out in EtOH, but not in acetone. The reason might be the higher boiling point of ethanol (78 °C) than acetone (56 °C). Due to the *E/Z*-conversion, theoretically, there could be four products from one single reaction (Scheme 3-14).



Scheme 3-14: Establishment of annulated ring system in compounds **29** and **P14**.

The base used for compounds **P16-P18** was Na₂CO₃, while for compound **P19**, K₂CO₃ was used.

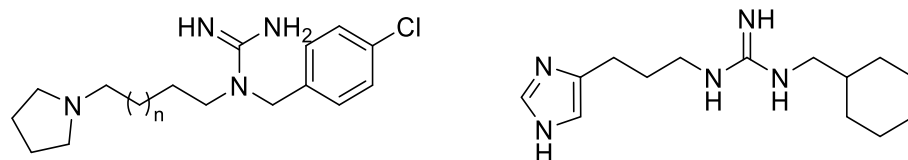
Type 1 product with *Z*-configuration and substitution at *N3* was the dominant or exclusive product. Type 2 product with *E*-configuration and substitution at *N1* was the minor product. Type 3 and Type 4 products have not been observed in this work. The configurations and alkylated positions were investigated via the ROESY-NMR technique (Spectra see section 6.5). The results were in agreement with the observation made by X-ray analyses with structurally related compounds (Kieć-Kononowicz and Karolak-wojciechowska, 1992). The poor yields of **P16-P18** were probably due to the use of ethanol, an inadequate solvent choice for S_N2-type reactions.

Additionally, the reactivity of **P19** as a potential Michael acceptor was investigated, where **P19** was dissolved in the potassium phosphate buffer solution (pH 7.4) and incubated with acetylcysteine for up to 7 days at 37 °C. Several samples were taken in planned time points and examined with liquid chromatography coupled with mass spectrometry (LC-MS) (Spectra see section 6.5). The thiol group of acetylcysteine was expected to react with an active α,β-unsaturated carbonyl compound to form a Michael addition product. This property can cause nonspecifically binding behavior to different target proteins. Ligands that exhibit unspecific interaction to numerous proteins and give false-positive results in pharmacological experiments are termed Pan-assay interference compounds (PAINS). In the present

investigation with **P19**, no Michael product was detected, suggesting that **P19** is unlikely to react chemically as a Michael acceptor in a physiological environment.

3.5 Synthesis of H₃R ligands with guanidine structure

The ether structure in the *N*-3-(phenoxypropyl)piperidine scaffold was replaced by *N,N'*-disubstituted and *N,N',N''*-trisubstituted guanidines in this project. Several excellent H₃R antagonists with guanidine structures (Figure 3-1) have been described in the past, including the imidazole-containing (Stark *et al.*, 1994) and non-imidazole derivatives (Linney *et al.*, 2000). However, the known compounds are not suitable to directly compare to the *N*-3-(phenoxypropyl)piperidine structure due to their significantly structural discrepancies. Notably, compound **P23** was included in a patent document of the company Bioprojet (Schwartz and Lecomte, 2006), but no biological activity was reported.



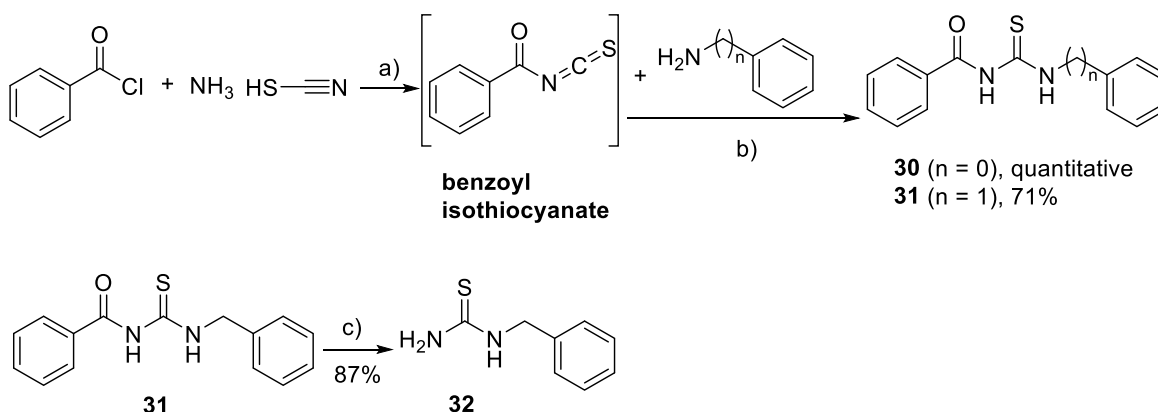
Compound **30**^a: $n = 3$, H₃R $pK_i = 8.4$

Compound **31**^a: $n = 4$, H₃R $pK_i = 8.7$

Compound **7**^b: H₃R $pK_i = 9.1$

Figure 3-1: Known H₃R ligands with guanidine structures. (^aLinney *et al.*, 2000; ^bStark *et al.*, 1994)

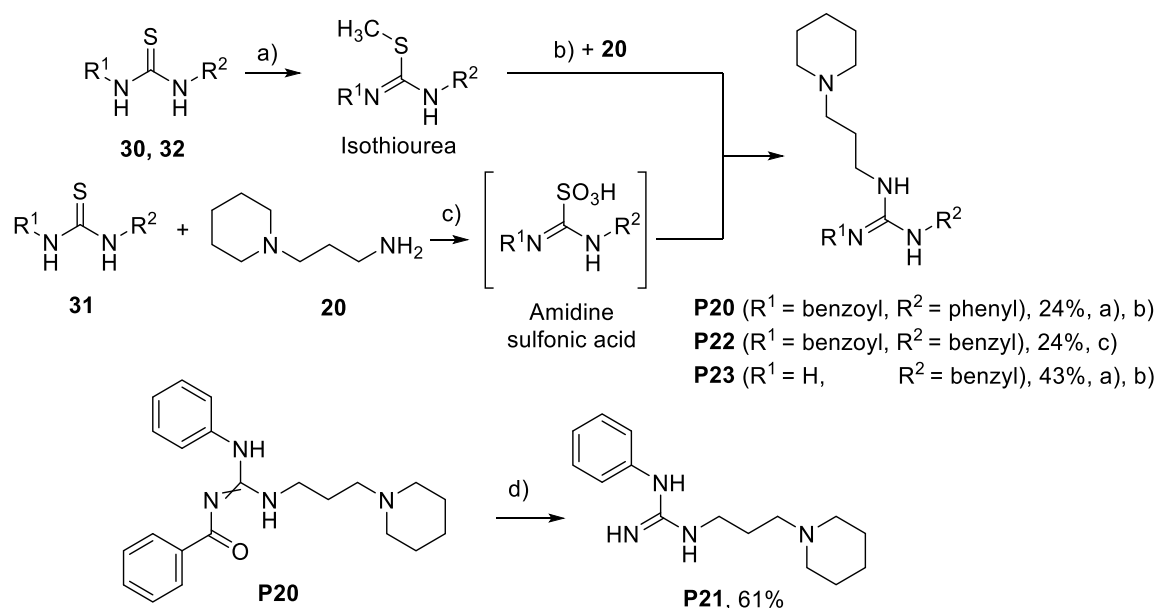
Guanidine synthesis in this work started from the preparation of benzoyl-protected thioureas **30** and **31**, which were obtained from the reaction between benzoyl isothiocyanate and aniline or benzylamine. The benzoyl isothiocyanate was synthesized from benzoyl chloride and ammonium thiocyanate under reflux (Scheme 3-15).



Scheme 3-15: Preparation of thiourea-derivatives.

a): Acetone, reflux, 30 min; b): Acetone, r.t. 2 h; c): NaOH (4 M, aq.), 90 °C, 1 h.

Without work-up, the intermediate benzoyl isothiocyanate reacted with aniline or benzylamine consequently to give the corresponding thioureas (Singh *et al.*, 2011). The benzoyl group could be removed either by acidic or basic hydrolysis.



Scheme 3-16: Preparation of guanidines from thioureas.

a): Iodomethane, K_2CO_3 , EtOH, r.t.; b): THF, r.t., 18 h; c): TEA, *t*-BuOOH, MeCN, 0 °C-r.t., 48 h; d) 7M HCl, 90 °C, 48 h.

Two different synthetic approaches were applied to convert the thiourea derivatives into corresponding guanidines. Accordingly, two intermediates were prepared: S-methyl isothiurea derivatives and amidine sulfonic acids (Scheme 3-16). Oxidation of thiourea **31** to corresponding amidine sulfonic acid was carried out with a mild oxidizing agent *tert*-butyl hydroperoxide (*t*-BuOOH). The corresponding guanidine **P22** was obtained in the presence of the primary amine **20** (Scheme 3-16) (Esteves *et al.*, 2015).

The yields of both methods were similar. The latter method could be carried out as a one-pot reaction and avoid the volatile and toxic methanethiol. However, side products, which were putatively associated with the oxidative process, have similar adsorption and desorption behaviors with silica gel as the product, which made the purification by a normal phase column chromatography challenging. Therefore, only **P22** was synthesized using amidine sulfonic acid as an intermediate and purified successfully from side products. Compounds **P20** and **P23** were prepared by using S-methyl isothiureas as intermediates.

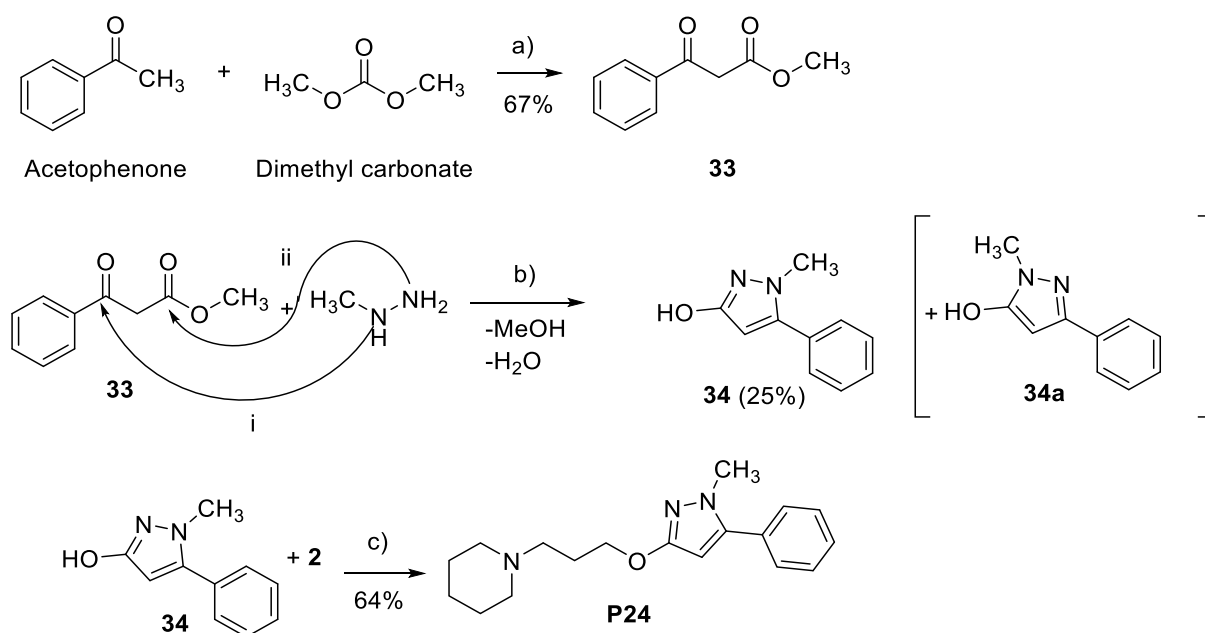
S-Methyl isothiurea-derivatives were prepared by methylating the corresponding thiourea **30** and **32** with iodomethane (MeI). The obtained isothiureas were subsequently nucleophilically attacked by 3-(piperidin-1-yl)propan-1-amine (compound **20**). Accompanied by the leaving of methanethiol, guanidines **P20** and **P23** have been obtained in 24% and 43% yields,

respectively (Linney *et al.*, 2000). The benzoyl group in the compound **P20** was removed in the acidic condition to obtain guanidine derivative **P21** in 61% of yield (Durant *et al.*, 1985).

3.6 Synthesis of H₃R ligand with phenyl pyrazole structure

In this project, the phenyl ring in *N*-(3-phenoxypropyl)piperidine structure was replaced through the pyrazole structure. Compound **34** is a condensation product from methyl hydrazine and β -diketone **33**, which was prepared via Claisen condensation from acetophenone and dimethyl carbonate (Scheme 3-17).

The formation of the pyrazine ring from β -ketoester **33** and methylhydrazine proceeded in two reaction steps (Scheme 3-17). In the first step, the more nucleophilic secondary amine in methylhydrazine reacted with the stronger electrophilic ketone group in compound **33**. The obtained Schiff's base underwent in the second step an intramolecular S_N2t reaction between the primary amine and the ester carbonyl group to give the phenyl pyrazolol derivative **34**. However, Yan and colleagues have reported the exclusive formation of **34a** under the same reaction condition. Notably, instead of the methyl β -ketoester **33**, Yan had used the ethyl analog of **33**, namely ethyl 3-oxo-3-phenylpropanoate (Yan *et al.*, 2016). In the present study, the ROESY-NMR investigation of **P24** (Spectrum see section 6.5) displayed that the methyl group was near to the phenyl ring, not the aliphatic chain, confirming the structure of **34**.

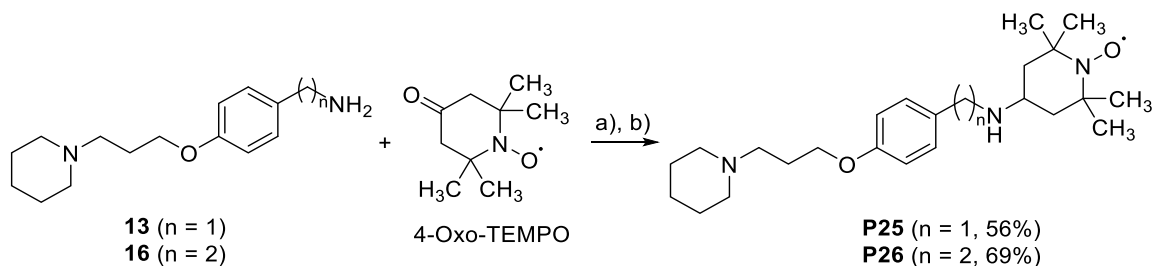


Scheme 3-17: The synthesis of H₃R ligand with phenyl pyrazole structure.

a): NaH, toluene, reflux, 20h; b): Ethanol, reflux, 2.5 h; c): K₂CO₃, KI, acetone, reflux, 60 °C.

3.7 Synthesis of Spin-labeled H₃R ligands

Nitroxide spin-labels are widely used in the EPR technique in studying protein structures. Spin-labeled ligands **P25** and **P26** were synthesized from 4-oxo-2,2,6,6-tetramethyl-1-piperidinyloxy free radical (4-oxo-TEMPO) and the amines **13** and **16** via Borch reductive amination. The reactions have been performed in the presence of the mild reductive agent sodium triacetoxyborohydride (NaBH(OAc)₃) in 1,2-dichloroethane (DCE). Both products were obtained as reddish viscous liquids in modest yields (Scheme 3-18).



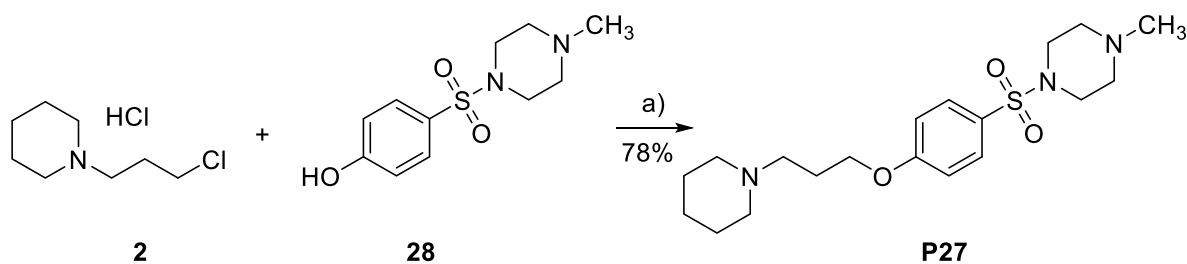
Scheme 3-18: The synthesis of spin-labeled H₃R ligands.

a): AcOH, DCE, r.t. 1 h; b): NaBH(OAc)₃, r.t., 18 h.

The presence of free radical after the reaction could be confirmed indirectly by ¹H- and ¹³C-NMR spectra, in which the signal of TEMPO structure was significantly suppressed while the complete piperidinyl propoxy-structure and a part of benzyl-structure were still well recognizable (Spectra see section 6.5).

3.8 Synthesis of hybrid ligand comprising two H₃R-antagonist scaffolds

In this project, the *N*-(3-phenoxypropyl)piperidine and the *N*-acyl piperazine scaffolds were merged into one molecule. A sulfonyl moiety replaced the carbonyl structure of the *N*-acyl piperazine scaffold. The previously described intermediate **28** was etherified by the alkyl chloride **2** via a Williamson synthesis to obtain the hybrid bivalent H₃R ligand **P27** (Scheme 3-19).



Scheme 3-19: The preparation of the hybrid bivalent H₃R ligand.

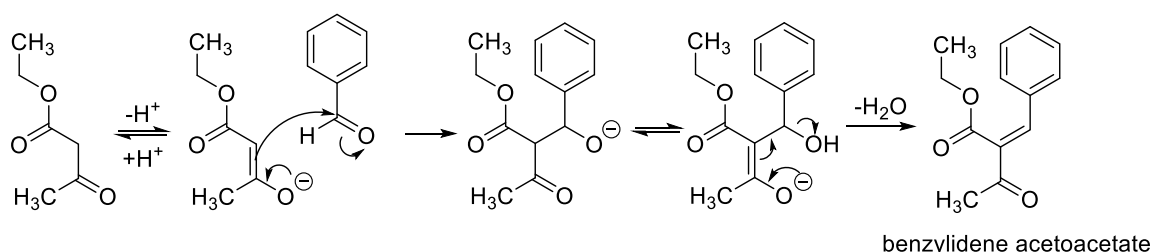
a): K₂CO₃, KI, acetone, reflux, 18 h.

3.9 Synthesis of hybrid ligands potentially targeting H₃R and Calcium channels

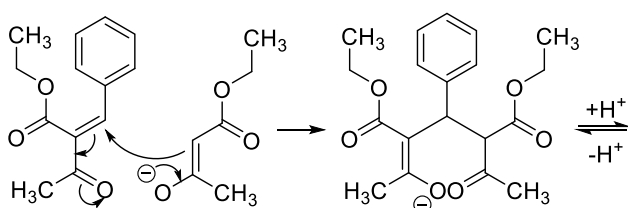
3.9.1 Dihydropyridine derivatives

The dihydropyridine derivatives in the present project have been synthesized by Hantzsch dihydropyridine synthesis. Hantzsch reported in 1881 a type of condensation reaction from acetaldehyde, ammonia, and ethyl acetoacetate to a dihydropyridine derivative (Hantzsch, 1881). The course of this one-pot reaction can be divided into three steps (Scheme 3-20). The product of the first step is benzylidene acetoacetate ethyl ester, a product of Knoevenagel condensation. This intermediate is a reactive Michael acceptor and readily undergoes an addition reaction with another molecule of ethyl acetoacetate. In the end, ammonia attacks the carbonyl groups nucleophilically and leads to a ring closure with subsequent cleavage of two molecules of water.

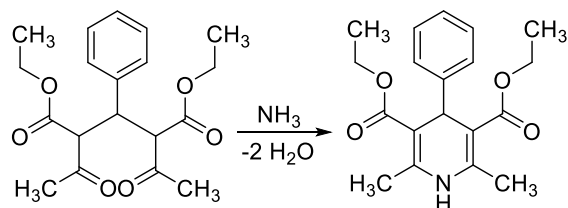
Step 1: Knoevenagel Condensation



Step 2: Michael Addition



Step 3: Nucleophilic attack and ring closure



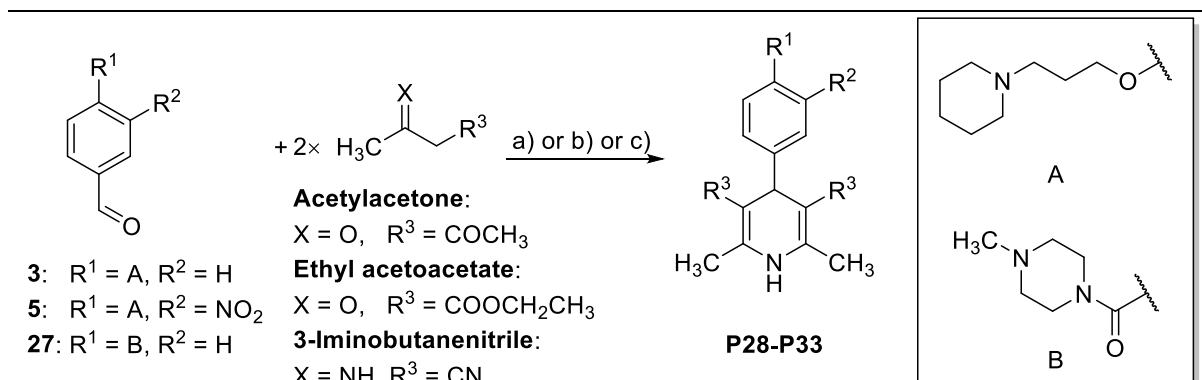
Scheme 3-20: Mechanism of Knoevenagel condensation and Hantzsch dihydropyridine synthesis.

The symmetric dihydropyridines **P28-P33** have been prepared from appropriate benzaldehyde, two molecules of corresponding β -diketones or iminobutanenitrile, and ammonia or ammonium carbonate (not necessary for reaction with iminobutanenitrile) (Table. 3-2).

The reactivities of corresponding aldehydes and β -diketones, as well as the products' oxidative stabilities play crucial roles in the yield of accordingly products. Compared to the aldehyde **25** with the *para*-substituted carbonyl group, the aldehydes **3** and **5** were less reactive due to the electron-donating effect of the *para*-localized alkoxy group. Aldehyde **5** with a nitro substituent was slightly more reactive than compound **3** due to the electron-withdrawing effect. The difference in reactant activity is reflected in the yield of **P30**, **P31** and **P32**. Moreover, ethyl acetoacetate is notably more reactive than acetylacetone, which could be observed in the comparison between the yields of **P28** and **P30** (11% to 33%), as well as between **P29** and

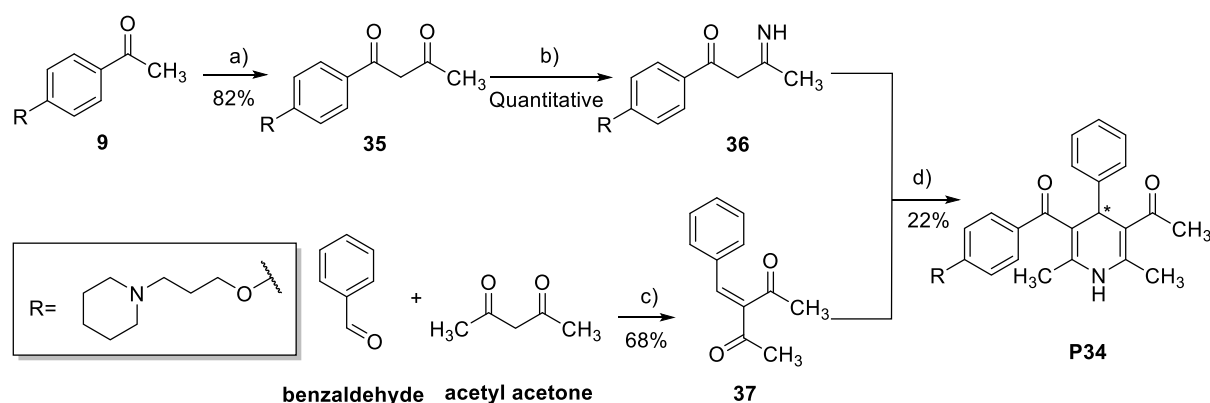
P31 (14% to 41%), respectively. Despite the higher reactivity of the carbonyl group than that of an ester, the strong basic piperidine can stabilize acetylacetone in a six-membered enolization form (Bartoli *et al.*, 2008; Clayden *et al.*, 2012). Furthermore, in the synthesis with iminobutanenitrile, even though the quantitative consumption of starting material was observed, the expected product **P33** was partly aerobic oxidized to the corresponding pyridine derivative under acidic conditions. The pyridine derivative was observed in LC-MS, but not further purified and fully characterized.

Table 3-2 Preparation of symmetric dihydropyridines



Aldehyde	X	R ¹	R ²	R ³	Method	Products	Yield
3	O	A	-H	-COCH ₃	a)	P28	11%
5	O	A	-NO ₂	-COCH ₃	a)	P29	14%
3	O	A	-H	-COOCH ₂ CH ₃	a)	P30	33%
5	O	A	-NO ₂	-COOCH ₂ CH ₃	a)	P31	41%
25	O	B	-H	-COOCH ₂ CH ₃	a)	P32	60%
3	N	A	-H	-C≡N	a)	P33	19%

Chemicals and conditions: a): (NH₄)₂CO₃, corresponding α,β-diketone, H₂O, EtOH, 55 °C-60 °C, 4 h; b): Ammonia solution (25 %, aq.), EtOH, reflux, 20 h; c): AcOH, 120 °C, MW, 10 min.



Scheme 3-21: The preparation of asymmetric dihydropyridine.

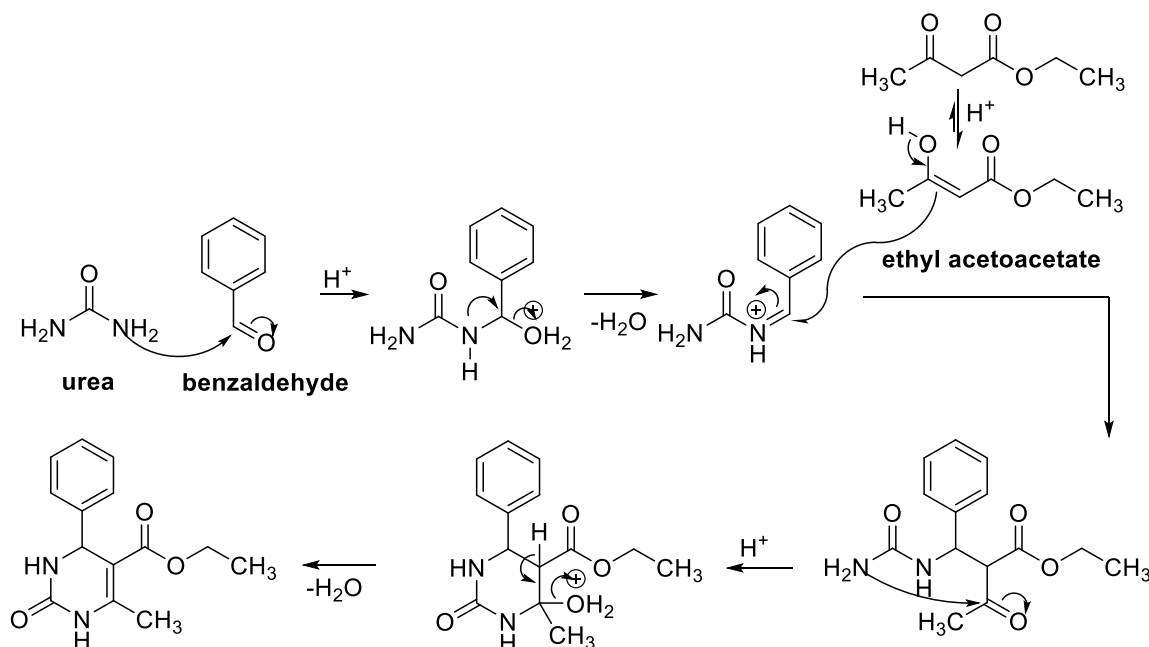
a): NaH, EtOAc, 18-crown-6-ether, THF, reflux, 3 h; b): NH₄OAc, MeOH, reflux, 2 h; c): AlCl₃, DCM, r.t. 3 h; d): EtOH, MW, 160 °C, 15 min.

The one-pot Hantzsch dihydropyridine synthesis is not applicable for the preparation of asymmetric dihydropyridine. Compound **P34** was obtained from several convergent synthetic steps (Scheme 3-21).

First, the β -diketone **35** was prepared by crossed Claisen condensation from acetophenone derivative **9** and EtOAc in the presence of NaH and 18-crown-6-ether in THF. The Claisen product reacted further with NH_4OAc in MeOH to obtain the corresponding iminophenylbutanone derivative **36**. Meanwhile, the Knoevenagel condensation product **37** was prepared from benzaldehyde and acetylacetone with AlCl_3 as a catalyst. In the end, compounds **36** and **37** were radiated in MW to produce the desired asymmetric, racemized dihydropyridine **P34** in 22% yield. The low yield of the last step may be caused by the low reactivity of compound **37** as a Michael acceptor.

3.9.2 Dihydropyrimidine derivatives

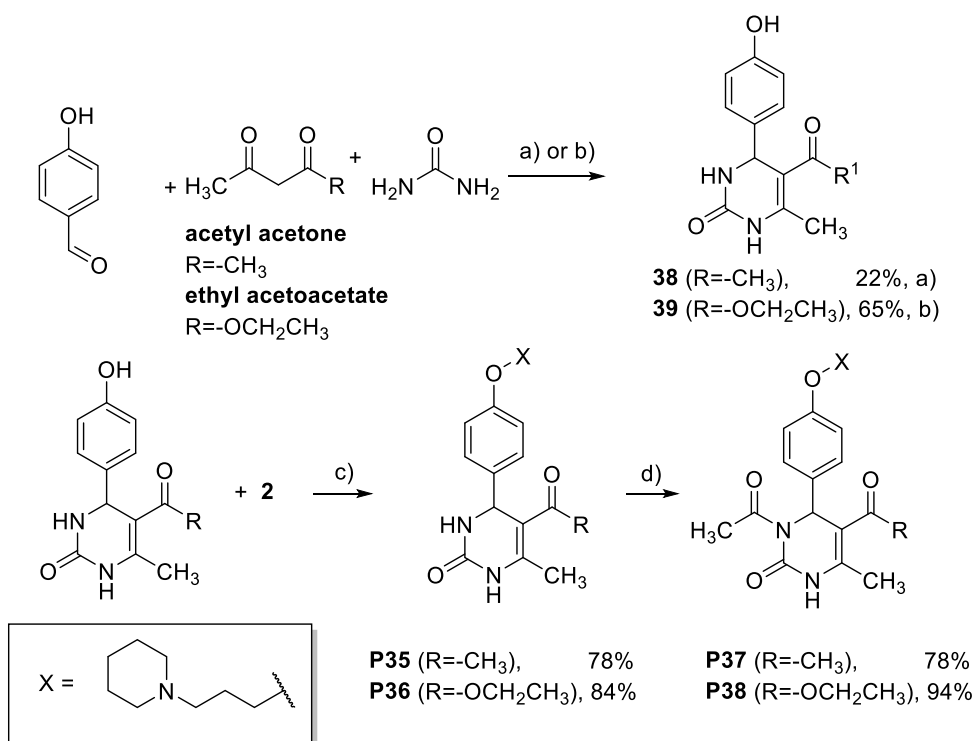
Biginelli reported in 1891 the synthesis of 3,4-dihydropyrimidin-2-one (DHPM) from benzaldehyde, urea, and ethyl acetoacetate as a multi-component one-pot reaction (Scheme 3-22) (Biginelli, 1891). The DHPMs are structurally similar to the DHPs but more resistant against metabolic oxidation to form inactive pyridine derivatives. Numerous DHPMs have displayed only slightly lower effectivity than the classic DHPs. Therefore, the DHPMs are interesting pharmacological tools.



Scheme 3-22: Mechanism of acid-catalyzed Biginelli Reaction.

With different aldehyde, urea, and β -ketoesters or β -diketones, Biginelli products with large diversity can be synthesized. The DHPMs in this work were prepared from 4-hydroxy benzaldehyde, urea, and acetylacetone or ethyl acetoacetate, catalyzed by HCl or ZrCl_4

(Reddy *et al.*, 2002; Kiyani and Ghiasi, 2015). Besides, in the present work, the free *N3* positions of DHPMs have been acetylated. An overview of the synthesis route for DHPMs in this work is shown in the scheme 3-23. The attempt to synthesize compound **38** with acetylacetone using $ZrCl_4$ as the catalyst has failed to give the corresponding product, where no reaction was observed. Under the same condition, the reaction with ethyl acetoacetate succeeded modestly in giving the DHPM derivative **39** in a 65% yield. Phenols in the Biginelli products **38** and **39** have been etherified with alkyl chloride **2** via Williamson ether syntheses to obtain the hybrid ligands **P35** and **P36**. The unsubstituted *N3* positions of the DHPM derivatives have been further acylated by acetic anhydride in the presence of 4-dimethyl aminopyridine (DMAP) and TEA in a microwave reactor (Dallinger *et al.*, 2003) to give the compound **P37** and **P38** (Scheme 3-23).



Scheme 3-23: Syntheses of Biginelli dihydropyrimidines.

a): EtOH, HCl (37%, aq., catalytic amount), reflux, 18 h; b): EtOH, $ZrCl_4$ (catalytic amount), reflux, 15 h; c): Acetone, K_2CO_3 , KI, reflux, 18 h; d): Ac_2O , TEA, DMAP, MeCN, 130 °C, MW, 10 min.

3.9.3 Barbiturate derivatives

Classical barbiturates such as phenobarbital and thiopental are 5,5-disubstituted barbituric acid derivatives (Figure 3-2). Besides their effects on $GABA_A$ receptors, they also act as weak channel blockers at several VGCCs and ionotropic glutamate receptors (Hirota *et al.*, 2000; Löscher and Rogawski, 2012).

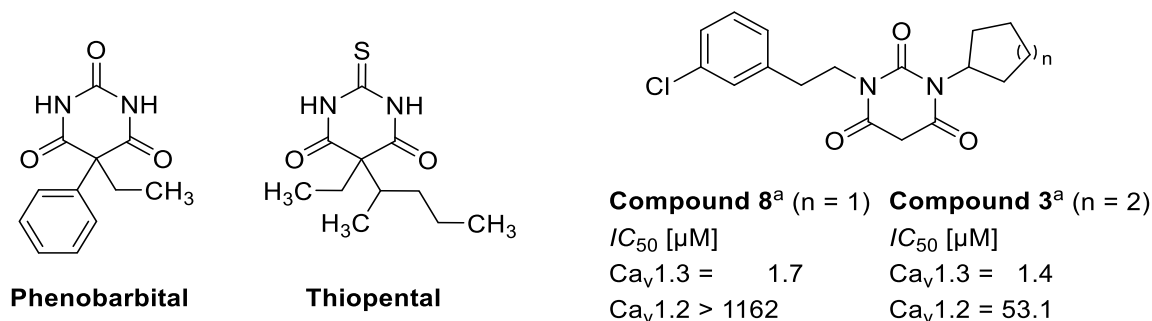
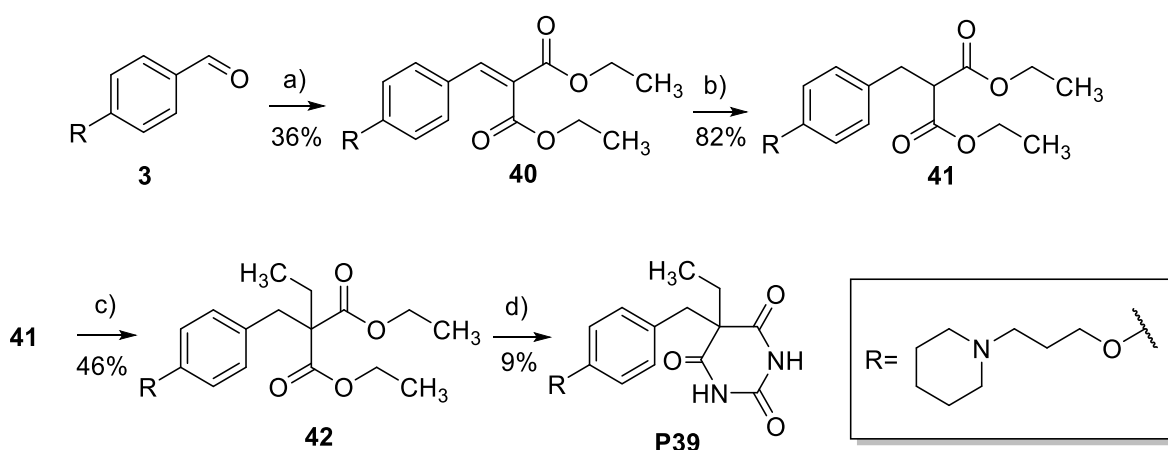


Figure 3-2: Barbituric acid derivatives: The 5,5-substituted examples are used as antiepileptics and anesthetics, while the *N,N*-substituted derivatives are potent, selective calcium channel blockers. (^aKang *et al.*, 2012)

The hybrid ligand comprising the structures of H₃R antagonists and the 5,5-disubstituted barbituric acid was obtained from a condensation reaction between urea and corresponding ethyl malonate derivative **42** (Scheme 3-24).



Scheme 3-24: Synthesis of 5,5-substituted barbituric acid derivative.

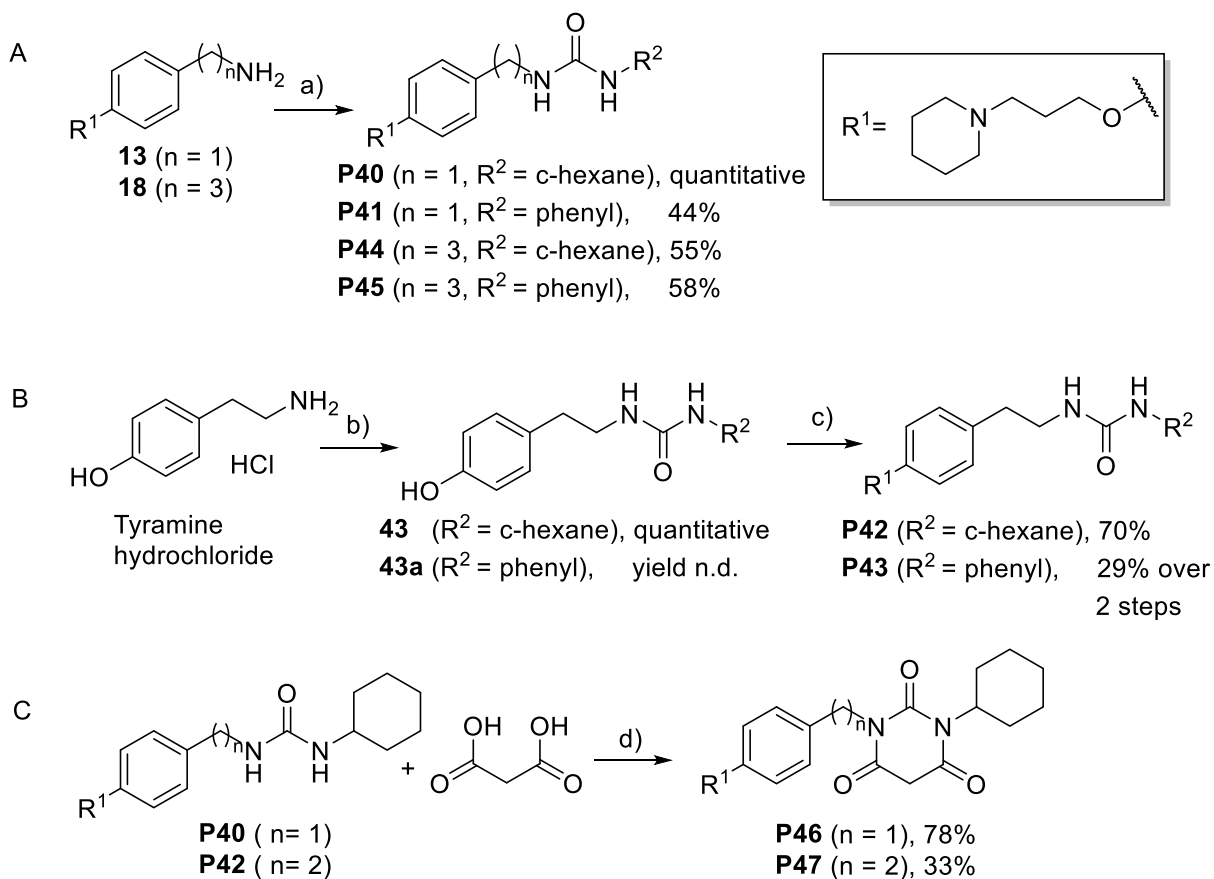
a): Diethyl malonate, piperidine, AcOH, EtOH, reflux, 18 h; b): NaBH₄, EtOH, 0 °C, 30 min; c): Bromoethane, NaH, DMF, r.t., 72 h, 46%; d): Urea, NaH, DMF, r.t., 18 h.

For the first step, the Knoevenagel condensation product benzylidene malonate **40** was prepared from aldehyde **3** and diethyl malonate in EtOH in the presence of piperidine and acetic acid as catalysts and buffer. Compound **40** was subsequently reduced by NaBH₄ and alkylated with bromoethane to obtain the 2,2-substituted diethyl malonate **42**, which reacted with urea in the presence of NaH to give the 5,5-disubstituted barbituric acid derivative **P39**.

A series of *N,N*-substituted barbiturate derivatives has been synthesized and characterized as selective Ca_v1.3 subtype calcium channel blockers (Kang *et al.*, 2013; Cooper *et al.*, 2020) (Figure 3-2). The compounds synthesized in this work comprised both substitution patterns of the PYT derivative.

The potential calcium channel blockers, *N,N*-substituted barbituric acid derivatives **P46** and **P47** were synthesized by acylating *N,N*-substituted ureas by malonic acid in acetic acid anhydride (Scheme 3-25 C) (Milite *et al.*, 2015). The corresponding urea derivatives have been

prepared from commercially available cyclohexyl isocyanate or phenyl isocyanate and appropriate amines in THF at ambient temperature in moderate to good yields. The benzylamine and phenyl propylamine derivatives **13** and **18** were prepared as described previously in section 3.2.2 and could be used directly for the synthesis of ureas with H₃R pharmacophore (Scheme 3-25 A). In contrast, the phenyl ethyl urea derivatives were prepared from tyramine hydrochloride in several subsequent steps without work-up. The etherification of phenol was performed after the urea synthesis (Scheme 3-25 B). The primary amine of tyramine was a more reactive nucleophile than phenol in the given reaction conditions. No significant side product formation was observed.



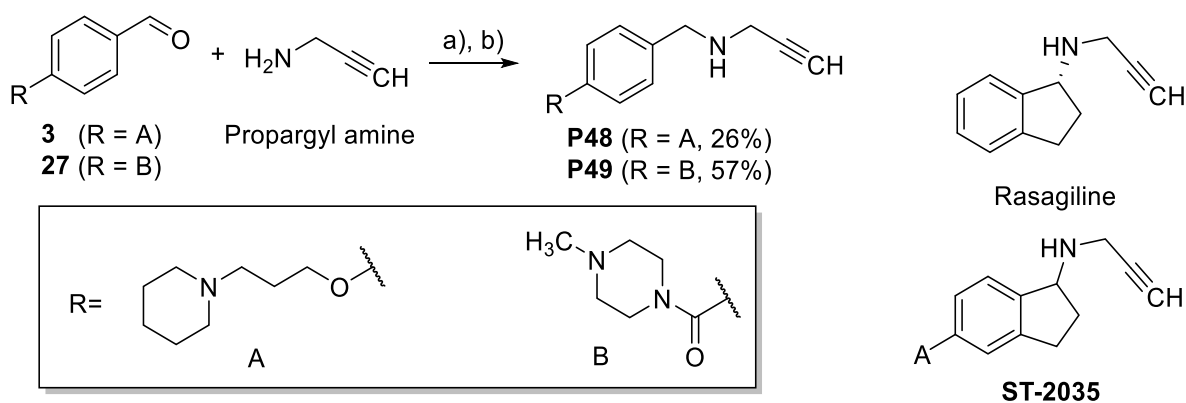
Scheme 3-25: Synthesis of ureas and corresponding barbituric acid derivatives.

a): *c*-Hexyl or phenyl isocyanates, THF, r.t. 2 h); b): *c*-Hexyl or phenyl isocyanates, TEA, THF (**43**) or MeCN (**44**), r.t.; c): Alkyl chloride **2**, K₂CO₃, KI, acetone (**43**) or MeCN (**43a**), reflux, 18 h; d): Ac₂O, MW, 60 °C, 10 min.

The yields of reactions with phenyl isocyanate were lower than that of cyclohexyl isocyanate. One possible reason is the higher reactivity and moisture sensitivity of phenyl isocyanate. Working in an inert atmosphere and using dried solvent may improve the yield.

3.10 Synthesis of hybrid ligands with propargyl amine structure

The hybrid ligands comprising the H₃R pharmacophore and rasagiline structure with annulated indane ring (e.g., ST-2035, Scheme 3-26) were synthesized and reported by Dr. Affini and Dr. Lutsenko (Affini *et al.*, 2018; Lutsenko *et al.*, 2019). In contrast, the hybrid ligands in this project focused on unrestricted, open-chain benzylamine derivatives. Both propargyl amine derivatives **P48** and **P49** were obtained via Borch reductive amination (Abdel-Magid *et al.*, 1996) from propargyl amine and appropriate benzaldehydes **3** or **27** in the presence of NaBH(OAc)₃ (Scheme 3-26). To increase the reactivity of aldehyde **3**, three equivalents of acetic acid were used for preparing compound **P48**. Compound **27** was a more reactive aldehyde than **3**. Therefore, the preparation of compound **P49** proceeded without additional acid in a modest yield.

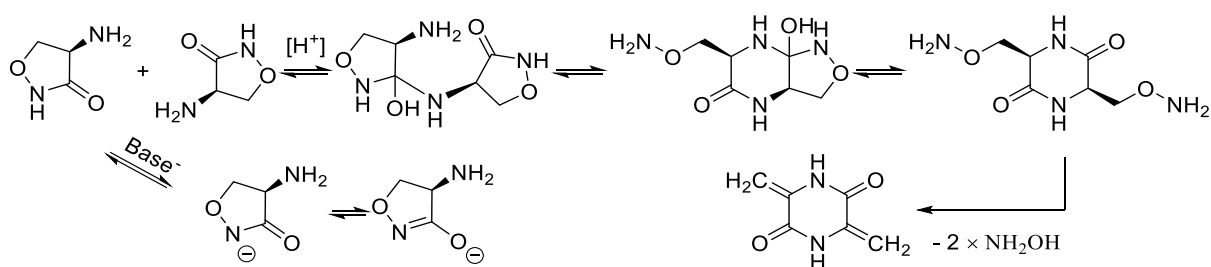


Scheme 3-26: Synthesis of propargylamine derivatives comprising H₃R pharmacophores.

a): AcOH, DCE, 1 h; b): NaBH(OAc)₃, DCE, 18 h.

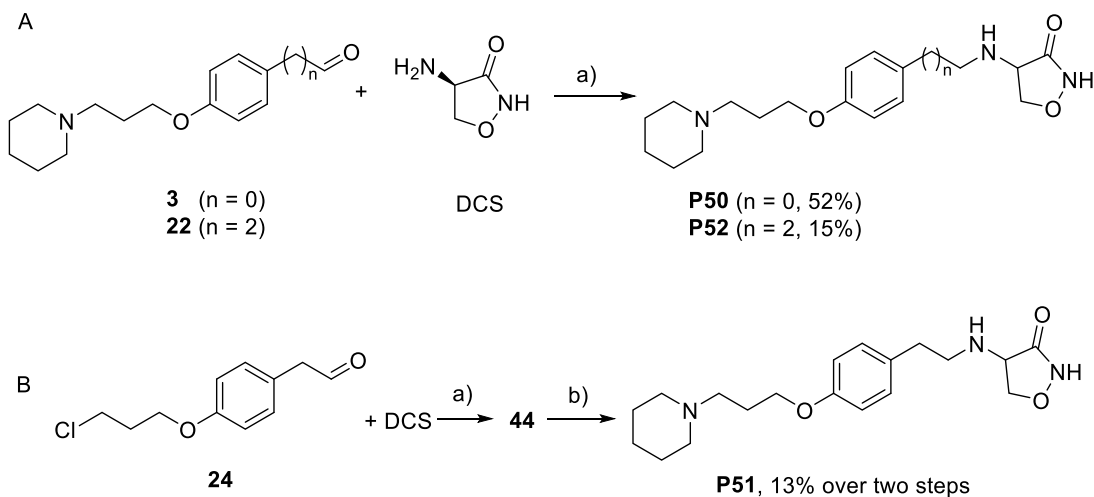
3.11 Synthesis of hybrid ligands with D-cycloserine structure

D-Cycloserine (DCS) is a natural compound produced by *Streptomyces garyphalus* from L-serine via the intermediates O-acetyl-L-serine and hydroxyurea (Svensson and Gatenbeck, 1982). Like most amino acids, the solubility of DCS is limited in many organic solvents but excellent in water. While relatively stable in an alkaline solution, DCS is unstable at low pH values or under high temperatures. DCS can be acidic hydrolyzed in an aqueous solution, where serine and hydroxylamine are degradation products (Malspeis and Gold, 1964). Furthermore, The five-membered isoxazolidinone ring could be opened, dimerize to a six-membered diketopiperazine structure via an acidic catalyzed mechanism, and followed by hydroxylamine cleavage (Scheme 3-27) (Lassen and Stammer, 1971; Lee *et al.*, 1998; Awasthi *et al.*, 2017).



Scheme 3-27: DCS is stable under alkaline conditions but readily dimerized at a lower pH value.

The solubility of DCS is insufficient in the most commonly used solvents for Borch reductive amination. Therefore, instead of using this aforementioned facile method, the secondary amine linkers in H₃R-DCS hybrid ligands **P50-P52** were prepared in two subsequent, separated synthetic steps described by Stamm and colleagues (Stammer *et al.*, 1970). The corresponding imine derivatives were first prepared from an appropriate aldehyde and DCS in a mixed solvent of EtOH and MeOH. The poor solubility of DCS in EtOH could be used as a reaction monitor. The disappearance of the DCS residue in EtOH indicates the completion of the reaction. The obtained imine derivative was separated and subsequently reduced by NaBH₄. Both steps had moderate yields at approximately 50%. An excessive amount of aldehydes was used in the first step to force the chemical equilibrium toward the formation of the acquired Schiff's base. Compounds **P50** and **P52** have been successfully prepared from the corresponding aldehydes **3** and **22** (Scheme 3-28 A).

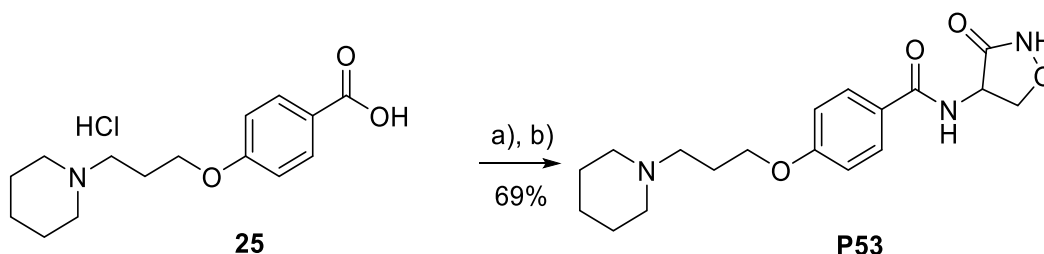


Scheme 3-28: Syntheses of DCS derivatives with secondary amines as linkers.

a) i: EtOH, MeOH, r.t. 2 h; ii: EtOH, NaBH₄, 0 °C-r.t., 30 min-90 min.; b): Piperidine, neat, 72 h, r.t..

As discussed in section 3.2.3, the presence of piperidine caused a spontaneous reaction of phenylacetaldehyde, probably in an Aldol-like manner. Therefore, aldehyde **24** was used to synthesize compound **P51**. Piperidine moiety was attached to the intermediate **44** in a later stage (Scheme 3-28 B).

Furthermore, the carboxylic acid derivative **25** was used to synthesize the H₃R-DCS hybrid ligand with a carboxamide structure as the linker. Benzoic acid derivative **25** was first converted to the corresponding acid chloride, which subsequently reacted with DCS in a solvent mixture of H₂O and MeOH (Scheme 3-29). The benzamide derivative **P53** was obtained in a yield of 69%.

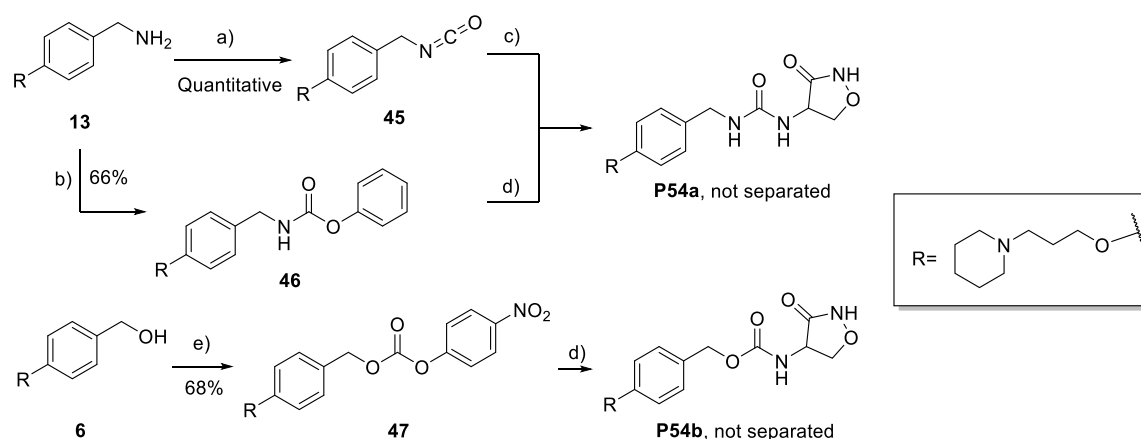


Scheme 3-29: Preparation of acylated DCS derivatives.

a): Thionyl chloride, DCM, reflux, 3 h; b): DCS, TEA, H₂O, MeOH, 0 °C - r.t., 18 h.

The stereochemistry of compounds **P50-P53** was studied via HPLC equipped with a chiral column. For the benzylamine derivative **P50**, only one peak was observed in the HPLC (Spectrum see section 6.5). Furthermore, its specific rotation ($[\alpha]_D^{25} = +234$) was determined via a polarimeter, indicating its enantiomeric purity. However, compounds **P51**, **P52**, and **P53** have shown two enantiomers in the investigation via HPLC with the ratio of 87:13, 40:60 (peaks are not sharply separated), and 89:11, respectively (Spectra see section 6.5). The differed enantiomeric purities may be due to the qualities of the starting materials (DCS) purchased from different lots.

Moreover, many efforts have been made to synthesize DCS derivatives comprising H₃R pharmacophore with more linker variations, including urea and carbamate structures. Two method variations have been applied for the synthesis of DCS with the urea linker. Two intermediates have been prepared accordingly: The phenyl carbamate derivative **46** was obtained from the reaction between benzylamine derivative **13** and phenyl chloroformate and followed by purification via column chromatography. The isocyanate derivative **45** was prepared from compound **13** and diphosgene (Scheme 3-30). In contrast to the preparation of compound **46**, the yield of isocyanate **45** was quantitative. After the work-up, no further purification was necessary. Both intermediates reacted with DCS respectively to afford the urea derivative **P54a**. However, in both reactions, DCS was not quantitatively consumed. Though the product could be detected via LC-MS, its separation from the reaction mixture was not successful.



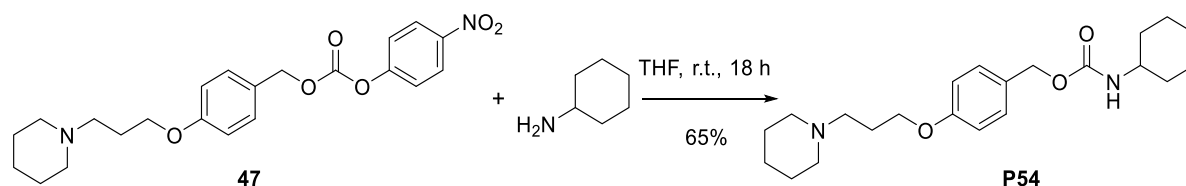
Scheme 3-30: Synthesis of DCS derivatives with urea or carbamate linkers.

a): Dipphosgene, TEA, DCM, 0 °C - r.t., 2 h; b): Phenyl chloroformate, DCM, TEA, r.t., 4 h; c): DCS, various solvent (MeOH, EtOH, H₂O, DMF or THF), r.t., 2 h - 72 h; d): DCS, DMF, r.t. 72 h; e): 4-Nitrophenyl chloroformate, DCM, pyridine, r.t., 18 h.

For synthesizing the DCS derivative **P54b** with carbamate linker, the phenyl carbonate derivative intermediate **47** was prepared from benzyl alcohol derivative **6** and 4-nitrophenyl chloroformate. However, similar to the urea derivative **P54a**, the carbamate derivative **P54b** was not successfully purified after the reaction between DCS and intermediate **47**.

Additionally, cyclohexylamine has been used to react with the phenyl carbonate derivative **47**, obtaining the carbamate derivative **P54** in a modest yield (Scheme 3-31). Performing this experiment was helpful in understanding and practicing this kind of reaction. Furthermore, the product is a valuable supplement to structurally related substituted urea derivatives **P40-P45**.

The thermal and acidic vulnerabilities of DCS made the work with DCS challenging. The highly hydrophilic property of the urea and carbamate derivatives further hampered the purification. Strategies for developing the related compounds need to be further rationalized.

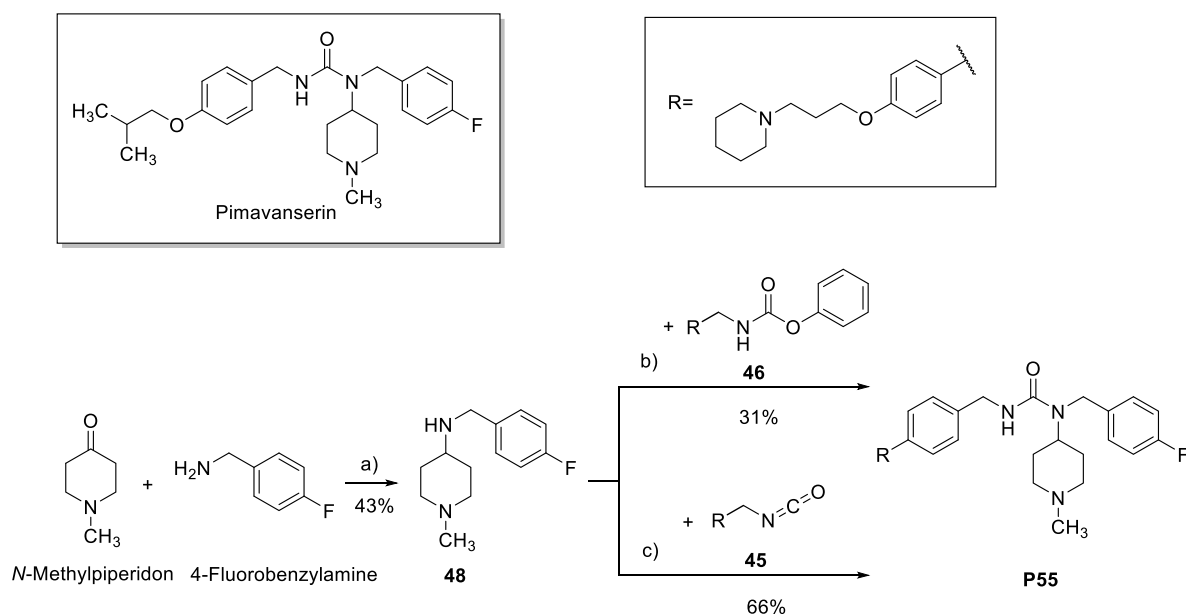


Scheme 3-31: Synthesis of the carbamate derivative **P54**.

3.12 Synthesis of a hybrid ligand comprising the pimavanserin structure

The substituted urea structure is a crucial structural element of the antipsychotic drug pimavanserin, which was merged with the *N*-(3-phenoxypropyl)piperidine scaffold in this project. The urea structure of the hybrid ligand **P55** was synthesized via two methods described by the inventor of pimavanserin Acadia pharmaceuticals (Burstein *et al.*, 2019). The

common reactant for both methods – the secondary amine derivative **48** was synthesized via Borch reductive amination from *N*-methyl piperidone and 4-fluorobenzylamine in the presence of $\text{NaBH}(\text{OAc})_3$ (Scheme 3-32).



Scheme 3-32: Synthesis of pimavanserin derivative.

a): AcOH , $\text{NaBH}(\text{OAc})_3$, DCE , r.t. 18 h; b): K_2CO_3 , toluene, 90 °C, 16 h; c): THF , r.t., 18 h.

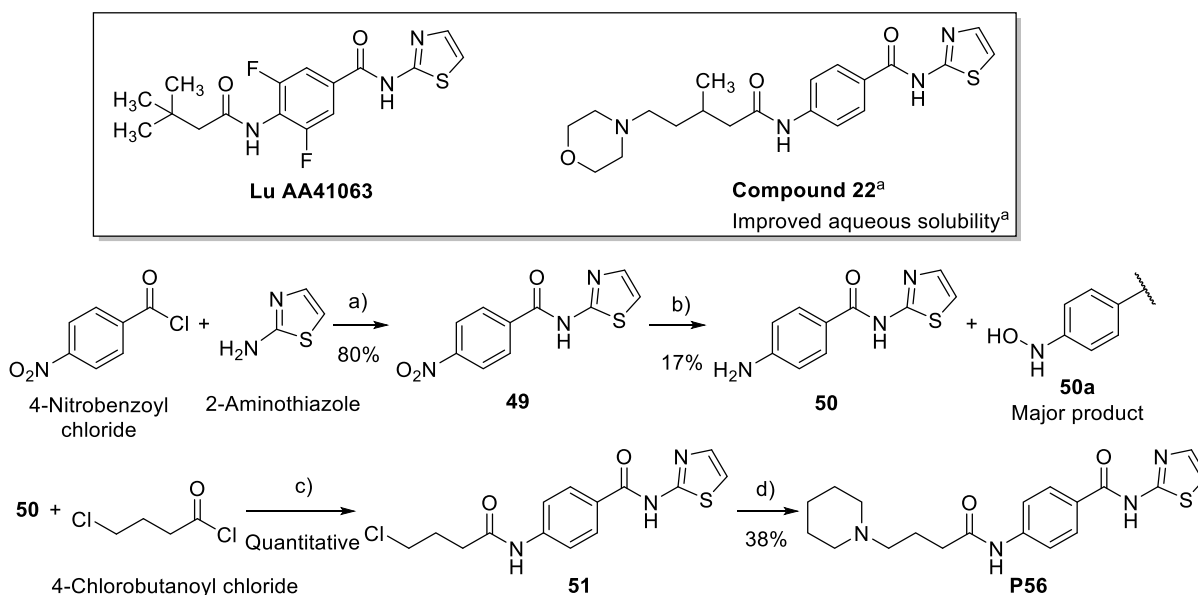
The first method of urea synthesis used phenyl carbamate derivative as an intermediate, obtaining the product **P55** in a yield of 31%. The second method yielded hybrid ligand **P55** from the reaction between amine **48** and isocyanate **45** at a rate of 66% (Scheme 3-32). The use of isocyanate to synthesize this compound is advantageous: Milder condition and higher yield.

Furthermore, the preparation of isocyanate intermediate **45** was more efficient and convenient than the preparation of phenyl carbamate intermediate **46**, making this method an overall more attractive synthetic route for preparing the pimavanserin derivative **P55**.

3.13 Synthesis of an $\text{A}_{2\text{A}}\text{R}/\text{H}_3\text{R}$ dual-antagonist

The adenosine $\text{A}_{2\text{A}}$ receptor ($\text{A}_{2\text{A}}\text{R}$) is a novel target for PD therapy. The xanthine-derivative Istradefylline is the first-in-class drug (Structure not shown). However, its highly hydrophobic structure limited its aqueous solubility. Lu AA41063 (Scheme 3-33) is a lead structure for a series of non-xanthine-like $\text{A}_{2\text{A}}$ receptor antagonists with improved aqueous solubility, including the **compound 22** (Scheme 3-33) with a morpholine ring (Mikkelsen *et al.*, 2015). Two *para*-positioned amide structures at the phenyl ring are crucial for the high affinity to $\text{A}_{2\text{A}}\text{R}$. Hence,

in this project, the ether structure of *N*-(3-phenoxypropyl)piperidine structure – the H₃R antagonist pharmacophore, was replaced by an amide group.



Scheme 3-33: The lead compound Lu AA41063 and the preparation of its hybrid derivative **P56**.

a): Pyridine, DCE, 60 °C, 18 h, 80%; b): H₂, Pd/C, MeOH, r.t., 144 h, 17%; c): Pyridine, DCE, r.t., 18 h, quantitative; d): Piperidine, neat, 72 h, r.t., 38%. (^aMikkelsen et al., 2015)

The A_{2A}R-H₃R hybrid ligand **P56** was obtained from a multiple-step synthetic route (Scheme 2-33). 2-Aminothiazole was acylated by 4-nitrobenzoyl chloride to obtain the intermediate **49**. Its nitro group was reduced by palladium-catalyzed hydrogenation. However, the sulfur-containing compounds, including thiazole, can deactivate several metal-catalysts (Rodriguez and Hrbek, 1999). The major product was the not completely reduced hydroxylamine derivative **50a**. The minor product **50** was obtained by adding further portions of the palladium catalyst and prolonging the reaction time. The obtained aniline derivative **50** was acylated by 4-chlorobutanoyl chloride to obtain the intermediate **51**, where the alkyl chloride was less prone to react than the acyl chloride. The compound **51** was further treated with piperidine to afford the product **P56** in a yield of 38%.

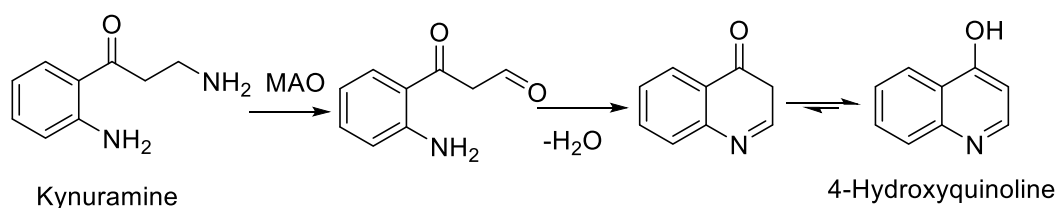
4 Pharmacology

4.1 Overview of in-vitro assays in the present work

The pharmacological assessments of the histamine receptors, monoamine oxidases, oxygen-radical absorbance capacity, and cell viability have been kindly conducted in the working group of Prof. Dr. Dr. h.c. Holger Stark of Institute for pharmaceutical and medicinal chemistry in the Heinrich-Heine-University, by Ms. M.Sc. Mariam Dubiel, Ms. Dr. Annika Frank, Ms. Dr. Stefanie Hagenow, Mr. Dr. David Reiner-Link, and Ms. B.Sc. Frauke Stölting with the kind assistant by Ms. Kathrin Grau. The screening of serotonin receptors was performed in the working group of Prof. Andrzej Borjaski from the Polish Academy of Science in Kraków, Poland. The in-vivo study was performed in the working group of Prof. Bassem Sadek from United Arab Emirates University in Al Ain, United Arab Emirates.

The binding affinities of the synthesized compounds for human histamine H₃ receptor (hH₃R) were characterized by radioligand displacement study with the membrane preparation from transfected HEK293 cells, whereby [³H]-N^α-methylhistamine was used as a radioligand (Kottke *et al.*, 2011; Affini *et al.*, 2018). The H₁R displacement assay has been performed on membrane preparation from CHO-K1 cells stably expressing hH₁R using [³H]-pyrilamine as radioligand (Smit *et al.*, 1996b). The displacement assay on hH₄R has been conducted on membrane preparation from Sf9 insect cells transient co-expressing hH₄R with Gα_{i2} and Gβ₁γ₂ by employing [³H]-histamine dihydrochloride as radioligand (Łazewska *et al.*, 2014). The results are presented as mean binding affinity *K_i* values and the confidence interval at 95% level (95% CI).

The inhibition studies on recombinant human monoamine oxidase isoform A (hMAO-A) and B (hMAO-B) have been carried out, as reported previously, by using kynuramine as substrate (Scheme 4-1), where clorgyline and safinamide were used as positive references for MAO-A and MAO-B inhibitions, respectively. The measurement was either carried out via the continuous spectrophotometric method or the discontinuous fluorometric method (Hagenow *et al.*, 2017; Affini *et al.*, 2018). The results are presented as inhibition (%) at a concentration of 10 μM.



Scheme 4-1: MAO enzymes convert kynuramine to fluorescent 4-hydroxyquinoline.

Additionally, oxygen-radical absorbance capacity assay (ORAC) has been performed by using free radical generating 2,2'-azobis(2-amidinopropane) dihydrochloride (AAPH) (Masood *et al.*, 2014) and fluorescein as an indicator of oxidative stress. The results are presented as mean \pm standard deviation (SD) in the ORAC unit, which equals the protective effect provided by 1 μ M of the water-soluble tocopherol analog 6-hydroxy-2,5,7,8-tetramethylchroman-2-carboxylic acid (Trolox) (Figure 4-1).

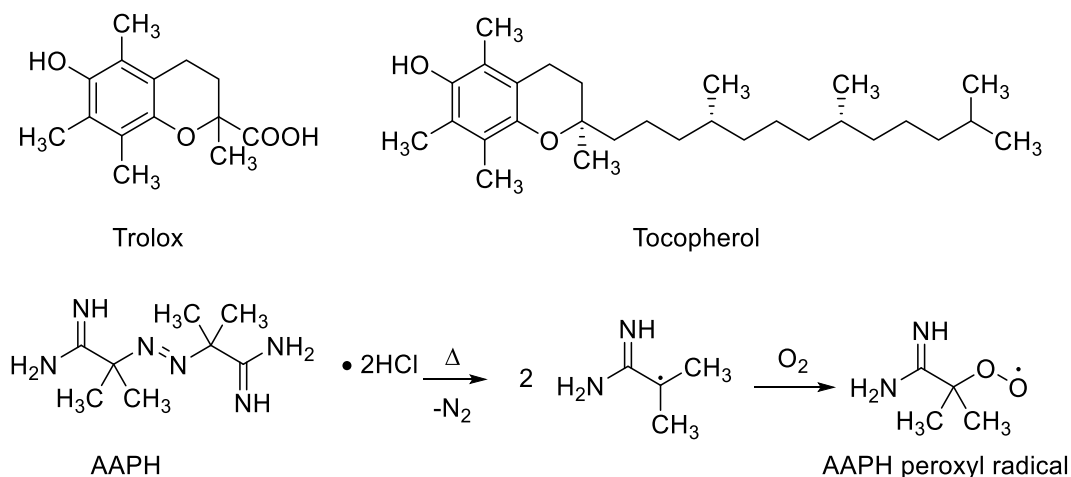


Figure 4-1: The antioxidative substance Trolox and tocopherol; The mechanism of AAPH induced oxidative stress.

Moreover, the cell viability assay was conducted in SH-SY5Y neuroblastoma cells using the blue-colored, nonfluorescent dye resazurin (O'Brien *et al.*, 2000), which can be reduced to pink-colored, fluorescent substance resorufin by living cells. 1-Methyl-4-phenylpyridinium (MPP⁺, structure see Figure 1-18), a neurotoxin, was used as the positive control in this study. The results are expressed as percentages of decreased cell viability.

4.2 H₃R ligands with organo-fluoride and -chloride substituents

Oranohalide substituents can be found in the structure of pitolisant. The chloride substituent made pitolisant a successful drug in comparison to a structurally related compound FUB 637 (Figure 4-2). Both compounds share comparable in-vitro affinities at the H₃R of guinea pig ileum and rat cerebral cortex. Interestingly, pitolisant displayed a 2-fold higher in-vivo effect than FUB 637 when administered per oral (Meier *et al.*, 2001). UCL-2138 (Schwartz *et al.*, 2000) is a potent H₃R ligand with the cyano substituent, a pseudo halide, at the phenyl ring (Figure 4-2). Like most compounds synthesized in this work, UCL-2138 has an *N*-(3-phenoxypropyl)piperidine structure.

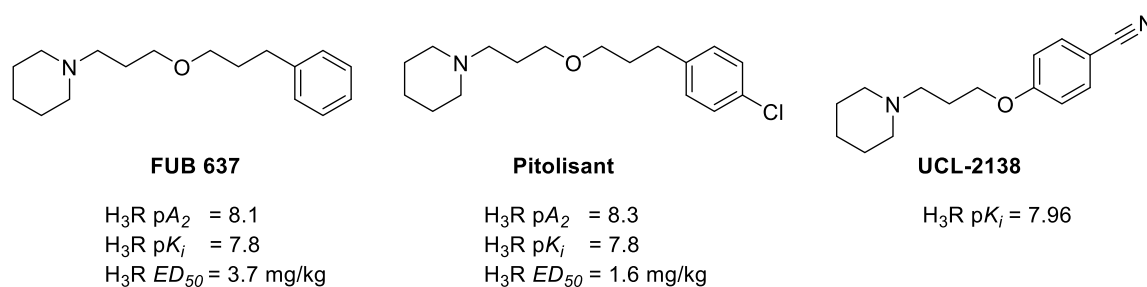


Figure 4-2: Examples of the introduction of organohalide and pseudohalide groups in H_3R ligands.

Fluorine is a widely used element in medicinal chemistry. Over 20% of pharmaceuticals in use are fluorinated compounds. The introduction of fluoride or fluoride-containing groups often has a significant impact on physicochemical properties, conformation, metabolic stability, lipophilicity, and bioavailability (Purser *et al.*, 2008; Meanwell, 2018). A former researcher from the Stark-Lab Isensee introduced a series of potent fluorinated non-imidazole H_3R ligands comprising the *N*-(3-phenoxypropyl)piperidine structure (Isensee *et al.*, 2009). The substitution exclusively taken place in the aliphatic part of the molecules and was limited to hydrogen-fluorine exchange.

In this project, chloride, fluoride, trifluoromethyl (CF_3), and pentafluorosulfanyl (SF_5) groups were introduced directly to the phenyl ring. Notably, the 4-Cl substituted derivative **P7** was previously synthesized and reported by Beasley and Stephenson alongside a few other compounds, where this compound displayed a weak analgesic effect (Beasley *et al.*, 1958). The 4-F derivative **P8** was previously prepared and assayed at the 5-HT_{5A} receptor by Khorana and colleagues, where no binding affinity was observed (Khorana *et al.*, 2003a; b). In this study, both compounds were re-evaluated for their pharmacological property at hH_3R . Moreover, the introduction of SF_5 and CF_3 groups enabled a direct comparison between both groups in their physicochemical and pharmacological properties.

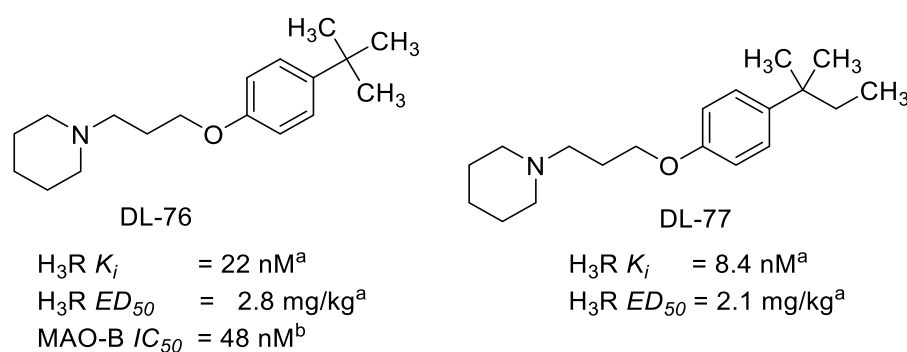


Figure 4-3: DL-76 and DL-77 present lead structures for bioisosteric exchange in **P3** and **P10**. (^aŁazewska *et al.* 2006, ^bŁazewska 2020).

Additionally, SF_5 and CF_3 groups present interesting bioisosteres for the *tert*-butyl group, which could be found in a potent lead structure DL-76 (Figure 4-3) with good H_3R affinity and appreciable MAO-B inhibition (Łazewska *et al.*, 2006, 2020). DL-77 (Figure 4-3), a structurally

close derivative of DL-76, has shown significant benefit in a series of in-vivo studies, including anti-autistic, anticonvulsive, procognitive effects, and ameliorated alcohol-intake behavior (Bahi *et al.*, 2015; Sadek *et al.*, 2016c; Eissa *et al.*, 2018).

William A. Sheppard prepared the first aryl-SF₅ derivatives in the 1960s from AgF₂ and hydrolysis vulnerable phenyl sulfur trifluoride. Unexpectedly, the obtained phenyl-SF₅ derivatives were stable at high temperatures and inert against various acids and bases (Sheppard, 1960, 1962). Similar to the CF₃ group, the SF₅ group could be degraded via photolysis under mild environmental-like conditions (Figure 4-4) (Jackson and Mabury, 2009).

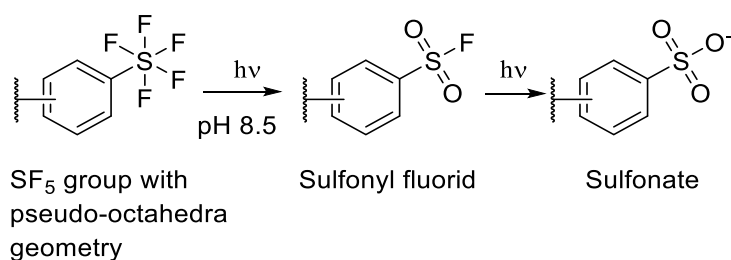


Figure 4-4: Photolysis of aryl-SF₅ structure. (Figure is modified from Jackson and Mabury 2009).

More building blocks containing the SF₅ group have been made commercially available in the last two decades. This evolution encouraged their introductions to medicinal chemistry (Kirsch, 2013). Notably, the accessibility to the aliphatic SF₅ groups is still limited and challenging (Penger *et al.*, 2013). Compared to CF₃, the SF₅ group displayed a similar electron-withdrawing effect but higher electronegativity and negative inductive effect. The SF₅ group owns a pseudo-octahedra geometry around the sulfur atom. It is slightly less voluminous than the *tert*-butyl group but bulkier than CF₃ (Savoie and Welch, 2015). The observed lipophilicities of SF₅ containing compounds were on average 0.6 log units higher than those of their CF₃ containing derivatives (Jackson and Mabury, 2009). All these unique characteristics made the SF₅ group an interesting alternative to the CF₃ group.

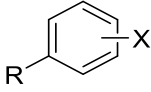
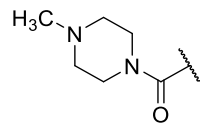
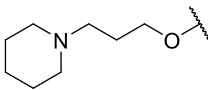
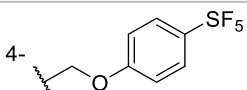
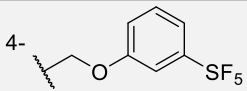
Several research groups conducted head-to-head comparisons between CF₃ and SF₅ groups. For fluoxetine, fenfluramine, and norfenfluramine, the replacements of the CF₃ groups via SF₅ groups led to enhanced selectivities or potencies (Welch and Lim, 2007). Furthermore, a few SF₅ containing compounds demonstrated prolonged half-lives compared to their analogs comprising CF₃ groups (Micheli *et al.*, 2010; Moraski *et al.*, 2017).

In this study, in addition to the H₃R assay, the logarithm of octanol/water partition coefficient under physiological pH ($\log D_{7.4}$) of the compounds have been calculated by MarvinSketch (ChemAxon, v21, 2021, Budapest, Hungary). Furthermore, the Pauling scale (Pauling, 1960) and the group negativities calculated via the method proposed by Bratsch (Bratsch, 1985) are presented (Table 4-1). The additional information about the ligands' physicochemical

properties may help to examine if the electronegativities of the introduced substituents play a role in the binding affinity to H₃R.

The in-vitro results were in agreement with that reported by Welch and Lim. The SF₅ group enhanced the affinities of the ligands substantially on hH₃R when compared to the compounds substituted with the CF₃ group or fluoride. Among the investigated compounds, the 4-Cl substituted compound **P7** has shown the best affinity, followed by the 4-SF₅ substituted **P3**, 4-methoxy phenyl SF₅ substituted **P4** and **P6** in the two-digit nanomolar concentration range.

Table 4-1: In-vitro test results and calculated logD_{7.4} value of H₃R ligands with organo-fluoride and -chloride.

						
Compounds	R	X	hH ₃ R K _i [nM] (95% CI)	logD _{7.4} ^{a)}	Electro-negativities [Pauling Unit]	
P1		4-SF ₅	4520 (376-54296)	2.79	3.65 ^{b)}	
P2		3-SF ₅	12440 (1355-114246)	2.80	3.65 ^{b)}	
P3		4-SF ₅	75.1 (32.2-176)	2.72	3.65 ^{b)}	
P5		3-SF ₅	273 (140-532)	2.78	3.65 ^{b)}	
P7		4-Cl	63.1 (32.5 ± 123)	1.51	3.16 ^{c)}	
P8		4-F	276 (86.9-874)	1.05	3.98 ^{c)}	
P9		4-CF ₃	134 (70.2-256)	1.78	3.49 ^{b)}	
P10		3-CF ₃	473 (68.9-3249)	1.80	3.49 ^{b)}	
P4			4-SF ₅	84.6 (27.2-263)	4.09	2.51 ^{b), d)}
P6			4-SF ₅	80.3 (32.0-201)	4.09	2.51 ^{b), d)}

^{a)}: Calculated with Marvin Sketch in consensus mode; ^{b)}: Bratsch et al., 1985; ^{c)}: Pauling, 1960; ^{d)}: Calculated for -CH₂O-.

Moreover, *para*-substitutions to the ether function in *N*-(3-phenoxypropyl)piperidine scaffold or to the carboxamide function in *N*-benzoyl piperazine scaffold resulted in ligands with higher affinities than the *meta*-substitutions when compared **P1** to **P2** (4520 nM to 12440 nM), **P3** to **P5** (75.1 nM to 273 nM), and **P9** to **P10** (134 nM to 473 nM), respectively. The observation is also in agreement with numerous previous studies.

A ranking of the receptor binding affinities and physicochemical properties of ligands with *para*-substituted *N*-(3-phenoxypropyl)piperidine structures indicates that the electronegativities and lipophilicities seemed not to be directly correlated with the ligand affinities (Table 4-2).

Table 4-2: Analyses of the relationships between physicochemical properties and the receptor binding affinities.

Ranking	4-Cl	4-SF ₅	4-Methoxy phenyl-SF ₅	4-CF ₃	4-F
Binding affinities	Highest	High	Medium	Low	Lowest
Electronegativities	Low	High	Lowest	Medium	Highest
Lipophilicities	Low	High	Highest	Medium	Lowest

Unexpectedly, the compounds **P1** and **P2** with the *N*-benzoyl piperazine scaffold did not display the expected high affinities at H₃R. The observation showed that the lipophilic, electron-withdrawing SF₅ substituent was not an ideal replacement for the tertiary amines in the *N*-benzoyl piperazine scaffold presented in bavisant and its derivatives. More substitution variations will provide further insight into the SAR of the *N*-acylated piperazine scaffold.

4.3 H₃R ligands with aromatic malononitrile structures

Benzylidene malononitrile derivatives were characterized as potent tyrosine kinase inhibitor three decades ago (Gazit *et al.*, 1989). More recently, Turpaev and colleagues reported a series of cell-protective effects of approximately 50 benzylidene malononitrile compounds. Several mechanisms were postulated, including up-regulating the human heme oxygenase 1 gene expression, protecting cells from menadione-caused oxidative stress, the inhibition of cytokine-dependent induction of nitric oxide synthase, the blockade of the intracellular generation of ROS, and antagonizing the effect of pro-inflammatory cytokines in some species of insulin-secreting cells (Turpaev *et al.*, 2011; Turpaev and Welsh, 2016).

The pyrogallol derivative AG82 (Figure 4-5) acted in-vitro as a direct antioxidant and protected the cell from ROS induced by glutamate and hydrogen peroxide, while AG17 and AG126 are identified as mitochondrial uncouplers (Sagara *et al.*, 2002; Soltoff, 2004).

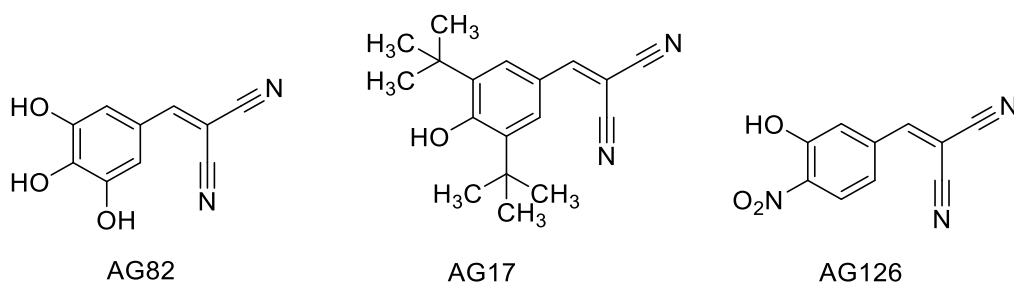


Figure 4-5: Lead structure of aromatic malononitrile.

Compounds synthesized within this project contain the *N*-benzoyl piperazine scaffold as the H₃R pharmacophore element. Benzylidene malononitrile derivative **P11** and its reduced derivative benzyl malononitrile **P12** have been assessed regarding the affinities at hH₃R and their inhibitory effects on MAO enzymes.

However, similar to **P1** and **P2**, compounds **P11** and **P12** bearing *N*-benzoyl piperazine structure displayed affinities to hH₃R in the micromolar concentration range. Furthermore, compounds **P11** and **P12** showed weak inhibitory effects on both MAO enzymes. Notably, the benzylidene malononitrile derivative **P11** has an approximately 25-fold higher selectivity for MAO-B over MAO-A, while the compound **P12** showed only a slight MAO-B preference. (Table 4-3). Due to the unconvincing pharmacological test results at H₃R and MAO, the postulated cell protection effects were not performed.

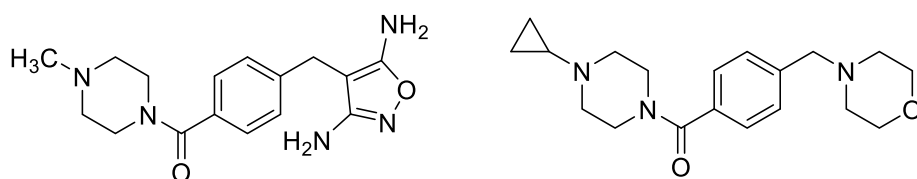
Table 4-3: Aromatic malononitrile derivatives.

	R	hH ₃ R <i>K_i</i> [μM] (95% CI)	hMAO-A Inh. at 10 μM (%)	hMAO-B Inh. at 10 μM (%)	Selectivity MAO-B/A
P11		5.17 (0.78-38.22)	1.0 ± 15.3	24.6 ± 15.2	24.6
P12		7.78 (4.79-12.65)	5.8 ± 5.6	27.0 ± 24.2	4.6

The inhibition studies on recombinant hMAO-A and hMAO-B have been carried out in one-point screening via the spectrophotometric method. The percentage of inhibition was presented as mean ± standard deviation at 10 μM.

Malononitrile conjugated or not conjugated with the phenyl ring seemed not to be ideal substitutions at phenyl ring for the *N*-acylated piperazine scaffold as the H₃R pharmacophore.

Therefore, the benzyl malononitrile structure of compound **P12** was further modified to a diamino isoxazole ring, introducing a second basic moiety with a pK_a value of approximately 12 (Zvilichovsky and David, 1983). This modification led to compound **P13** (Figure 4-6).

**P13**

$hH_3R K_i [\mu M] = 2.71$
(95% CI) (1.40 – 5.24)

Enzyme inhibition at
10 μM (%)
hMAO-A = 6.9 ± 11.6
hMAO-B = 24.5 ± 33.1

Bavisant

$hH_3R K_i [\mu M] = 0.005^a$

Figure 4-6: The second basic moiety improved the binding affinity at H3R substantially. (^aLetavic *et al.*, 2015).

Though still in the micromolar concentration range, the H₃R affinity of compound **P13** was substantially improved when compared to **P12**. The experiment indicated the essential role of a second basic function in the *N*-acylated piperazine scaffold as an H₃R pharmacophore. A benzylic, cyclic tertiary amine seemed to be a crucial structural feature for the *N*-acylated piperazine scaffold. The modification in this structure has confronted more limitations than expected.

4.4 Benzylidene (thio)hydantoin derivatives

A few five-membered heterocyclic compounds, including hydantoin and thiohydantoin, are well-known structures that can interact with numerous biological targets and frequently enhance ligands' affinities to their respective binding sites. Hence structures with these features were described as "privileged scaffolds" (Mendgen *et al.*, 2012). This strategy of improving the ligand affinity was employed in compounds developed for various targets such as anticonvulsant (Habib *et al.*, 2015), antipsychotic (Kucwaj-Brysz *et al.*, 2016), and compounds with anti-cancer and anti-inflammatory activities (Cho *et al.*, 2019). However, this specific capability was recognized by other researchers as a problem, a "promiscuous binder": The acquired selectivity might be missing, the interaction is based on unspecific reactivity toward nucleophile of the target (Powers *et al.*, 2006) or the physicochemical properties of these compounds might impact the assay and leads to false positive in the screening. Ligands with such features are termed "Pan-assay interference compounds" (PAINS) (Baell and Holloway, 2010; Baell and Nissink, 2018). Mendgen and colleagues had screened 163 compounds bearing rhodanine, hydantoin, thiohydantoin and thiazolidinedione structures on

four different enzymatic targets and confirmed that a part of these compounds had promiscuous behaviors, but not via unspecific ways. Interestingly, both the potency and the promiscuous behavior were more distinct if the heterocycles are involved in conjugated systems, e.g., by bonding to benzylidene-structure (Mendgen *et al.*, 2012).

A few highly affine H₃R ligands bearing benzylidene rhodanine structure (Figure 4-7, **compound 10**) were synthesized by Dr. von Coburg from the Stark-Lab (Sander *et al.*, 2010a). The reduction of the double bond of benzylidene rhodanine derivative to its benzyl analog led to a decrease of the affinity of 7-fold, but still displayed modest affinity (Figure 4-7, **compound 12**).

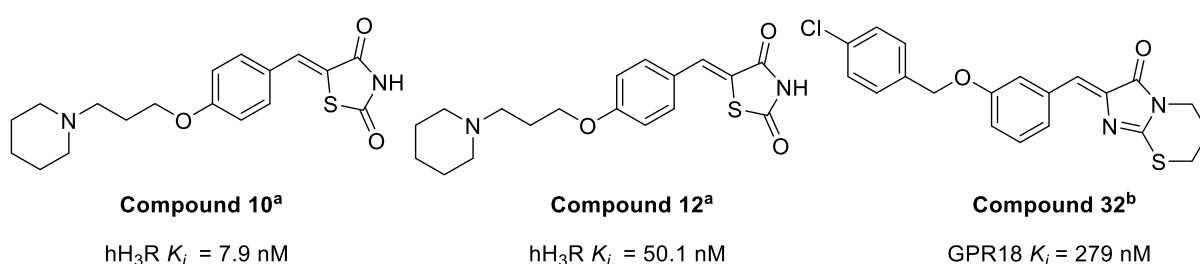


Figure 4-7: Ligands with heterocycles inspired this work. (^aSander *et al.*, 2010a; ^bRempel *et al.*, 2014).

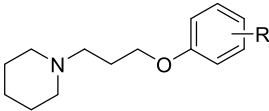
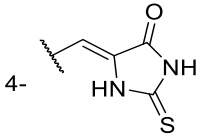
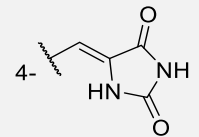
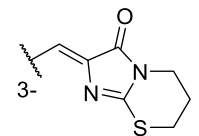
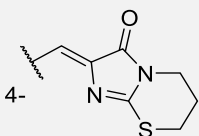
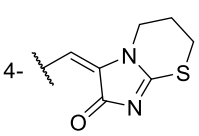
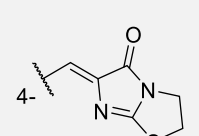
Furthermore, a series of fused arylidene thiohydantoin derivatives have displayed interesting anticonvulsive, anxiolytic, antidepressive, and analgesic activities (Kieć-Kononowicz and Karolak-wojciechowska, 1992). One compound with this structure feature (Figure 4-7, **compound 32**) demonstrated a high affinity to an orphan receptor GPR18 (Rempel *et al.*, 2014), whose endogenous ligand is still unknown.

Compounds **P14-P19** were screened in the H₃R displacement assay. As expected, similar to the H₃R ligands with rhodanine structure, all compounds within this project displayed excellent affinities to hH₃R (Table 4-4). Compounds **P17** and **P18**, characterized as ligands with the highest affinities to H₃R in this work, have shown K_i values in the sub-nanomolar concentration range.

The thiohydantoin derivative **P14** and the hydantoin derivative **P15** demonstrated similar affinities to hH₃R, suggesting that here sulfur and oxygen may interact with the receptor in a similar manner. Though not significantly, compound **P18** with *E*-configuration displayed substantially higher hH₃R affinity than **P17** with *Z*-configuration. Notably, fusing a six-membered thiazinane ring to the thiohydantoin derivative **P14** led to compounds **P17** and **P18** with significantly increased affinities to H₃R. However, the imidazothiazolidine derivative **P19** with the condensed five-membered thiazolidine ring showed no improvement in affinity at H₃R

compared to that of **P14**. This observation suggested that a larger ring size and more flexibility in the ring structure might be crucial for hydrophobic interactions with the receptor.

Table 4-4: Benzylidene (thio)hydantoin derivatives.

						
	R	K_i (hH ₃ R) [nM] (95% CI)	K_i (hH ₁ R) [nM] (95% CI)	K_i (hH ₄ R)	K_i (GPR18) K_i (GPR55)	ORAC ^a [Trolox equivalent]
P14		18.6 (5.96-58.1)	n.d.	n.d.		n.d.
P15		21.5 (9.54-48.5)	n.d.	n.d.		n.d.
P16		44 (11-184)	n.d.	n.d.	> 10 μM > 10 μM	n.d.
P17		0.96 (0.32-2.90)	1079 (0-10 ⁷)	> 10 μM	> 10 μM > 10 μM	0.95 ± 0.92
P18		0.17 (0.03-0.96)	2449 (0.1-10 ⁸)	> 10 μM	> 10 μM > 10 μM	-0.60 ± 0.79
P19		18.8 (7.52-47.0)	n.d.	n.d.	n.d.	n.d.

n.d.: not determined. ^a: Data are presented as mean ± standard deviation. A high value suggests a good antioxidative capacity

Furthermore, for selected compounds, the receptor binding affinities at H₁R, H₄R, and two orphan receptors GPR18 and GPR55, have been studied to identify their potential

promiscuous binding behavior as PAINS. Compounds **P17** and **P18** displayed low affinities to the hH₁R, while no significant binding behavior to hH₄R, GPR18, and GPR55 could be observed.

An acetylcysteine binding study was performed to examine the potential property as a Michael-acceptor and exclude the unspecific binding to the target protein. The compound **P19** was dissolved in buffer solution ($pH = 7.4$) and incubated with excessive acetylcysteine at 37 °C. Five probes have been taken at the planned time and investigated in LC-MS (Spectra see section 6.5). No adduct with acetylcysteine could be detected in this study. However, an impurity with twice the molecular weight of compound **P19** was detected. The amount of this impurity increased significantly (up to 30%) in the group treated with acetylcysteine. In the control group without acetylcysteine, only a trace of this impurity, whose amount did not increase during the time (up to 3%), was observed, indicating that acetylcysteine may contribute to the probable dimerization reaction. However, the putative dimer of **P19** was not further characterized, and the mechanism needs further investigation.

Moreover, the ORAC assay was carried out for the compounds **P17** and **P18** to identify their antioxidative property. Interestingly, **P17** with *Z*-configuration displayed a modest antioxidative capacity with 0.95 ORAC unit, which is comparable to that of the reference substance Trolox, while **P18** with *E*-configuration failed to neutralize the free radical produced in this experiment.

In this project, highly affine H₃R ligands with hydantoin and thiohydantoin structures have been developed. Setting up the condensed imidazothiazinane ring system from the thiohydantoin structure led to ligands with excellent selectivity to H₃R and further significant affinity enhancement.

4.5 H₃R ligands with *N,N'*-disubstituted urea and carbamate structures

Substituted ureas can be found in a wide range of drugs, such as the antipsychotic cariprazine, the antiviral drug ritonavir, kinase inhibitor sorafenib, and the sulfonylurea antidiabetic drugs glimepiride and glibenclamide.

The company Sanofi reported a series of highly effective H₃R antagonists comprising aryl ureas as a crucial structural feature (Gao *et al.*, 2013). The structural variation focused mainly on the substitution at the periphery phenyl ring (Figure 4-8) and the basic amine moiety (Structures not shown here).

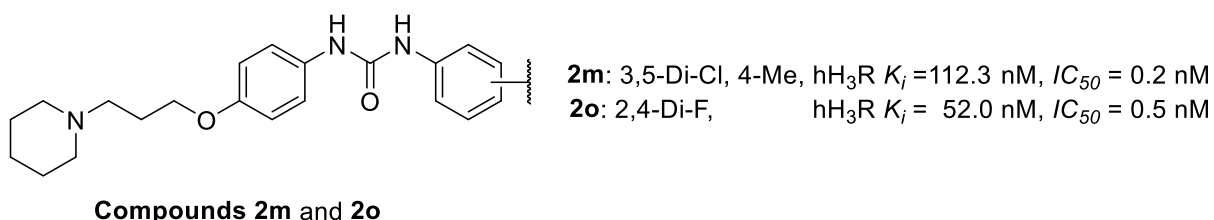


Figure 4-8: H₃R antagonists bearing substituted ureas as a crucial structural feature.

The structural modification focused on the chain length between the central phenyl and the urea functionality in this work. Furthermore, the periphery phenyl ring was replaced by a cyclohexyl ring to reduce the molecule's rigidity. Carbamate is a related structure of urea but has only one hydrogen bond donor. A comparison of their pharmacological property could obtain valuable information about the ligand-binding site.

All the substituted urea derivatives have displayed modest to good binding affinities at H₃R (Table 4-5). The chain length between the central phenyl ring and the urea structure played a crucial role. A pronounced linker length-affinity relationship could be observed in the phenyl urea derivatives. For the methyl- (**P41**), ethyl- (**P43**), and propyl- (**P45**) derivatives, affinities to hH₃R were determined as 125 nM, 21 nM, and 15.4 nM, respectively. A similar trend was observed for the cyclohexyl urea derivatives, where the compound **P44** with a propyl linker bond to H₃R with the highest affinity (8.41 nM) within this project.

Table 4-5: H₃R ligands comprising substituted urea and carbamate structures.

	R ¹	R ²	R ³	X	n	hH ₃ R K _i (95% CI) [nM]
P40	Cyclohexyl	H	H	N	1	18.6 (7.13-48.5)
P41	Phenyl	H	H	N	1	125 (82.5-191)
P54	Cyclohexyl	-	H	O	1	86.9 (42.3-178)
P42	Cyclohexyl	H	H	N	2	29.2 (7.6-112)
P43	Phenyl	H	H	N	2	21.0 (1.92-229)
P44	Cyclohexyl	H	H	N	3	8.41 (5.96-11.9)
P45	Phenyl	H	H	N	3	15.4 (2.30-103)

Furthermore, the rigidity of the peripheric ring structure affected the affinities at H₃R as well. A significant distinct in binding affinity was observed when a comparison was made between **P40** (cyclohexyl, hH₃R affinity: 18.6 nM) and **P41** (phenyl, hH₃R affinity: 125 nM) with the same methyl linker between the central phenyl ring and the urea functional group. However, the superiority of cyclohexyl in the H₃R binding affinity over the phenyl ring was not significant in

the compounds with a propyl linker (i.e., **P44** and **P45**) and was not observed in the compounds with an ethyl linker (i.e., **P42** and **P43**).

Additionally, **P54**, the carbamate analog of **P40**, displayed a notable but not significant decrease in affinity when compared to **P40**. The observation indicated that the hydrogen bond donor function of urea derivatives might play a role in the interaction with the binding site of H₃R.

Taken together, the urea derivative **P44**, substituted with a propyl linker and the non-rigid cyclohexyl structures, was identified as a lead structure. Its hydrogen bond donor function may contribute to its high binding affinity at H₃R. For a more comprehensive view, different linker types and lengths between the central phenyl and the urea structure as well as different structural elements as replacement of cyclohexyl will be needed.

4.6 H₃R ligands with guanidine structure

The ether structure of the *N*-(3-phenoxypropyl)piperidine scaffold with its hydrogen bond acceptor function plays a crucial role in the binding affinity at H₃R. Guanidines are strong organic bases and highly polar structures. It can act as a hydrogen bond acceptor as well as a hydrogen bond donor if not fully substituted. Substituted non-basic guanidines are presented in H₂R antagonists such as the gastric ulcer therapeutics famotidine, ranitidine, and cimetidine. The clinical used H₂R antagonists have poor blood-brain-barrier (BBB) permeabilities, which may attribute to their properties as P-glycoprotein (P-gp) substrates (Kim, 2002). P-gp acts as an efflux pump, translocating the substrate from intracellular to the extracellular space. P-gp is abundantly localized in cells with barrier function, including the BBB (Seelig and Landwojtowicz, 2000). The hydrogen bond acceptor property of the guanidine structures in H₂R antagonists is believed to be essential for the P-gp to recognize its substrate (Seelig and Landwojtowicz, 2000).

H₃R antagonists designed as P-gp substrates may allow the study of the exclusive pharmacological property of H₃R in the periphery, such as the role of H₃R in diabetes. Contradictory results regarding the role of H₃R in diabetes have been published in the past. Yoshimoto et al. reported a reduction of the food-intake behavior in mice and thus an ameliorated obesity and hyperinsulinemia by chronic administration of an H₃R agonist imetit (Yoshimoto *et al.*, 2006), while Rao and colleagues have achieved an improvement in glycemic control in a diabetic mouse model when treated with an H₃R antagonist of thiazole type (Rao *et al.*, 2012).

One of the earliest series of H₃R ligands with guanidine structure was synthesized and published by Stark and colleagues. Ten highly potent imidazole-containing H₃R ligands were

reported (see Figure 3-1, compound 7) (Stark *et al.*, 1994). Linney and colleagues from the James Black foundation reported a series of non-imidazole H₃R antagonists bearing *N,N*- and *N,N'*-disubstituted guanidine structures. The reported lead structures compound **30** and **31** (Figure 4-9) displayed interestingly high affinities to H₃R with excellent selectivity over H₁R and H₂R (Linney *et al.*, 2000). Notably, the structures of compounds **P21** and **P23** were included in a patent of the company Bioprojet (Schwartz and Lecomte, 2006). However, no bioactivities were reported.

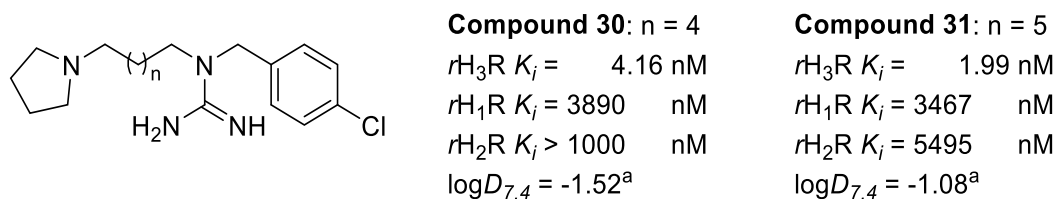
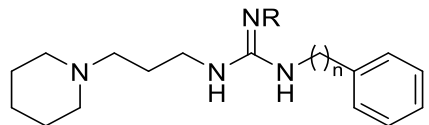


Figure 4-9: H₃R ligands with *N,N*-substituted guanidine structure. (Linney *et al.*, 2000). ^a: The log*D*_{7.4} values were calculated by ChemAxon Marvin Sketch v21 with the consensus method

In this project, H₃R screenings were performed for *N,N'*-disubstituted, and *N,N',N''*-trisubstituted guanidines **P20-P23**. Lipophilicity plays a crucial role in the permeability of the blood-brain barrier. Therefore, the log*D*_{7.4} values were calculated and presented alongside the pharmacological data (Table 4-6). Norinder and Haerberlein have suggested a rule of thumb to predict the BBB permeability: if the count of nitrogen and oxygen atoms is bigger than its log*P* or log*D*_{7.4} value, one compound is unlikely to cross the BBB (Norinder and Haerberlein, 2002). According to this prediction, the lead structures **compounds 30, 31**, and compounds synthesized in this work **P20-P23** might not be BBB permeable.

Table 4-6: H₃R ligand with guanidine structure.

					
	R	n	<i>K_i</i> (hH ₃ R) [nM] (95% CI)	log <i>D</i> _{7.4} ^a	BBB permeability ^b
P20	Benzoyl-	0	3560 (791-16023)	1.63	unlikely
P21	H-	0	391 (208-734)	-2.00	unlikely
P22	Benzoyl-	1	2687 (767-9419)	0.61	unlikely
P23	H	1	233 (174-310)	-2.23	unlikely

^a: log*D*_{7.4} values were calculated by ChemAxon Marvin Sketch v21 with the consensus method; ^b: The compounds are unlikely to cross the BBB (Norinder and Haerberlein, 2002) if the Count (N+O)-log*D*_{7.4}>0.

The trisubstituted guanidines **P20** and **P22** displayed low affinities to H₃R with *K_i* values in the micromolar concentration range, while the 1,3-disubstituted derivatives **P21** and **P23** showed about 10-fold higher affinities to H₃R. The higher lipophilicities of **P20** and **P22** did not positively

contribute to the receptor binding affinities. These observations suggest that the voluminous benzoyl substitution may be a steric hindrance, preventing the crucial hydrogen bond formation. Furthermore, compound **P23** has displayed a slightly higher affinity at H₃R than that of **P21**, suggesting that the increase of lipophilicity or a more flexible substitution leads to improved affinity. This observation was also in agreement with the results reported by Linney *et al.*, where compound **31** with a chain length of seven carbons at the guanidine structure displayed higher affinity than compound **30** with a shorter chain length instead (Figure 4-9).

In this project, the replacement of the ether function of the *N*-(3-phenoxypropyl)piperidine scaffold with substituted guanidine structure yielded moderate affine H₃R ligands. Further modification in the chain length and substitution at the phenyl ring may further improve the affinity at H₃R.

4.7 H₃R ligand with phenyl pyrazole structure

In the previous projects, the modification of the ether structure and the substitution at phenyl ring in the *N*-(3-phenoxypropyl)piperidine scaffold resulted in several H₃R ligands with moderate to very high affinities.

A study focused on replacing the phenyl ring through aromatic heterocycles has been reported by Swanson and colleagues, where a series of highly effective H₃R antagonists have been identified (Swanson *et al.*, 2009). However, the choices of heteroaromatics were limited to pyridine and isoxazole. Like their lead structure **JNJ-5207852**, all compounds reported in the literature comprised a second basic moiety, such as piperidine (Figure 4-10).

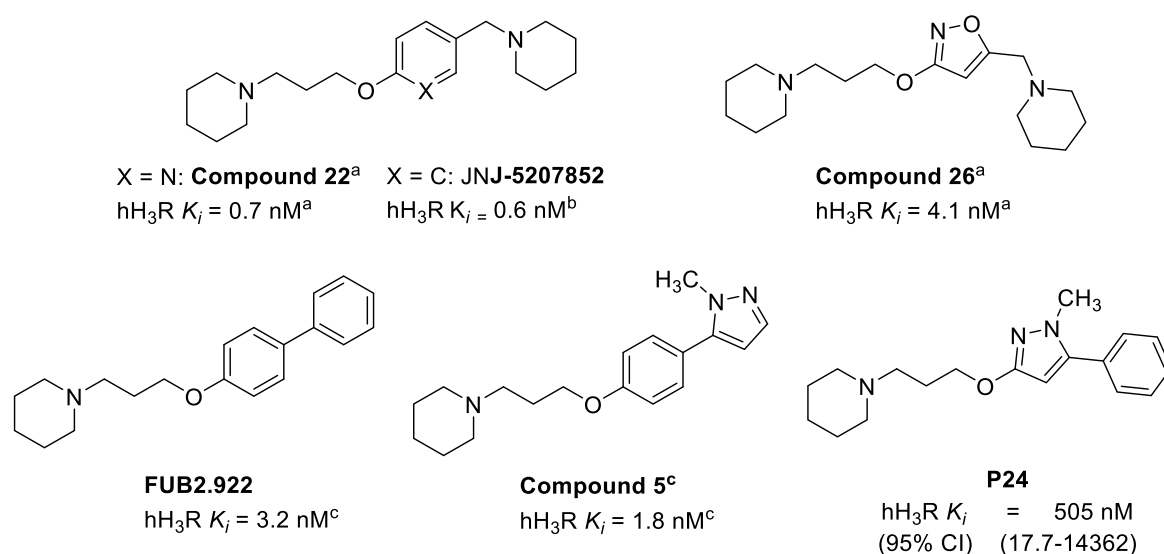


Figure 4-10: The replacement of the phenyl ring with a heteroaromatic. (^a Swanson *et al.*, 2009; ^b Barbier *et al.*, 2004; ^c Levoin *et al.*, 2011).

Notably, in the literature **compound 22**, a replacement with pyridine led to no loss of affinity at H₃R compared to that of **JNJ-5207852**, while an isoxazole – phenyl exchange resulted in a significant decrease in the affinity. The non-linear molecular geometry of **compound 26** may contribute to the loss of affinity.

The biphenyl derivative **FUB2.922** (Figure 4-10) is a potent H₃R antagonist with only one basic moiety. A replacement of the peripheric phenyl ring with a methyl pyrazole structure resulted in the literature **compound 5** (Figure 4-10) with increased H₃R affinity compared to that of **FUB2.922** (Levain *et al.*, 2011).

In this work, a replacement of the central phenyl ring of **FUB2.922** with a methyl pyrazole structure resulted in **P24** (Figure 4-10), which demonstrated a moderate affinity at H₃R. The drastic loss of affinity compared to that of the lead structures suggested that for H₃R ligands with one basic moiety, a linear molecular geometry of the central aromatic ring plays a significant role in the binding affinity. Six-membered heteroaromatics may be more promising replacements for the phenyl ring in the *N*-(3-phenoxypropyl)piperidine scaffold.

4.8 Spin-labeled H₃R ligands

In addition to crystallography, cryo-EM, and NMR spectroscopy, the electron paramagnetic resonance (EPR) spectroscopy study combined with spin-labeling became a powerful tool in studying the structure and conformational dynamics of biomolecules under physiologic-like conditions (Schweiger, 1993; Hendricks *et al.*, 2012). The EPR technique can detect and analyze the paramagnetic field created by the spin of an unpaired electron, revealing information about the mobility of the spin-labeled side chain, solvent accessibility, the polarity of the real-time environment, and intra- or intermolecular distances up to 80 Å between two or more spin-labels. The spin-labels can be free radicals or paramagnetic metal atoms such as Ni²⁺ and Gd³⁺.

Typical site-direct spin labeling experiment introduced spin-labels at selected sites within proteins, usually by site-directed mutagenesis followed by a click reaction with the -SH group of cysteine with a nitroxide free radical reagent such as MTSSL and M-TETPO (Figure 4-11). In the so-called “nitrox scanning” study, a series of at different sites spin-labeled proteins are prepared. The analyses of their EPR data with the assistant of computational modeling can reveal reliable protein structures with spatial details (Klare, 2013; Karthikeyan *et al.*, 2018).

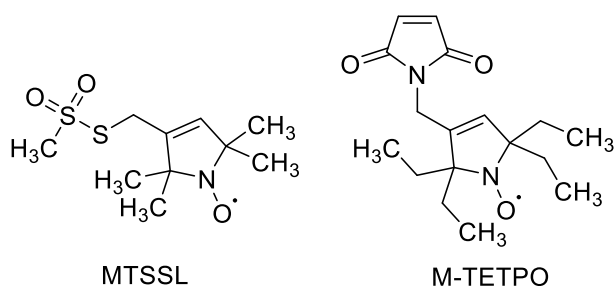


Figure 4-11: Frequently used reagents for site-directed spin-labeling of proteins.

Besides the methodology of site-direct spin-labeling for distance measurement, the hyperfine spectroscopy presented another powerful application of the EPR technique, which could provide information about the microenvironment of the spin through analyses of the data of hyperfine interactions. However, numerous parameters can have a contribution to the generated information. The analyses can be compared to the work with a “black box” (Goldfarb, 2019).

The compounds **P25** and **P26** have a 2,2,6,6-tetramethyl-1-piperidinyloxy (TEMPO) structure with a free radical shielded from both sides through the *gem*-dimethyl groups. This kind of protected radical is stable in laboratory conditions against mild reductive agents (e.g., sodium triacetoxyborohydride). For initial characterization of the spin-labeled ligands **P25** and **P26**, the H₃R assay has been conducted (Table 4-7).

Table 4-7: Spin-labeled H₃R ligands.

	Compounds	n	hH ₃ R K _i [nM] (95% CI)
	P25		1
P26		2	4.39 (2.64-7.32)

Compound **P26** demonstrated more than 20-fold higher affinity at H₃R than compound **P25** with a methylamine linker, indicating that the ethylamine linker significantly contributes to the high affinity at H₃R. Furthermore, the stability of the nitroxide free radicals in **P25** and **P26** under physiological conditions needs further investigation, though they overcame mild reductive reagents during the synthesis. A few strategies further enhancing the radical stability have been reported, including replacing the piperidine ring with a pyrrolidine ring and enlarging the tetramethyl to tetraethyl such as in M-TETPO (Jagtap *et al.*, 2015; Karthikeyan *et al.*, 2018).

4.9 Hybrid ligands comprising two different H₃R antagonist pharmacophores

Many GPCRs form homo- or hetero-dimerized or -oligomerized receptors. This kind of protein-protein interaction may lead to distinctions in receptor functions from their monomer (Pfleger and Eidne, 2005). Evidence of dimerization and oligomerization of H₃R have been reported (Shenton *et al.*, 2005; Bongers *et al.*, 2007). However, their pharmacological meaning was hardly studied. For this purpose, the bivalent compounds, which comprise two pharmacophores targeting the orthosteric binding site, may be useful pharmacological tools (Pulido *et al.*, 2018).

The compound **P27**, which is composed of the *N*-(3-phenoxypropyl)piperidine and *N*-acylated piperazine scaffolds as H₃R antagonist pharmacophores (Figure 4-12), was investigated in this work regarding its affinity at hH₃R. This compound displayed a modest affinity in the investigation. Notably, **P27** is a fused hybrid ligand with a small molecular weight, unlikely to simultaneously binding at two binding sites within a dimerized receptor. In contrast, bivalent ligands, whose pharmacophores are attached with a long, flexible linker, may be helpful pharmacological tools in studying the dimerized receptors.

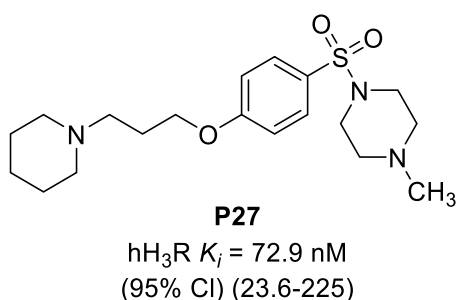


Figure 4-12: The bivalent ligand **P27** is composed of two H₃R antagonist pharmacophores.

4.10 Hybrid ligands of H₃R antagonists and calcium channel blockers

As discussed in section 1.6, calcium channel blockers (CCBs) may be useful neuroprotective agents. The most investigated CCBs are 1,4-dihydropyridine (DHP) derivatives. However, the DHPs, such as the hypertension drugs nilvadipine and isradipine, still have limited success in clinical trials against several neurodegenerative diseases. An improved permeability of the blood-brain barrier, subtype-selective blockade to minimize the cardiovascular side effects, and metabolic stability, including the hydrolysis in the ester structure and oxidation in the DHP structure, should be considered as desired features for the drug candidates.

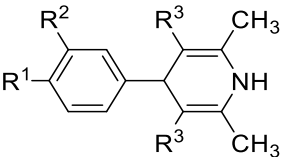
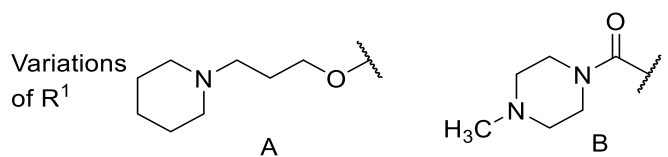
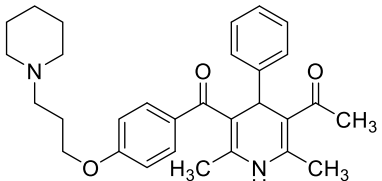
4.10.1 Hybrid H₃R ligands with 1,4-dihydropyridine structure

Many studies have focused on the phenyl substitutions in the DHP structures. One or two substitutions at *ortho*- or/and *meta*-position to the DHP moiety are crucial for the effectivity on

the calcium channels (Costa *et al.*, 1997; Yao *et al.*, 2005). However, only few discussion about the impact of the side chains was reported (Carosati *et al.*, 2012). Hence, it is exciting to study the pharmacological properties of DHPs bearing different side chains other than the classic esters. In this work, the hydrolysis-stable ketones and cyano group were introduced to the side chain.

Compounds **P28-P34** having a DHP structure were assayed on hH₃R. Their effectiveness as calcium channel blockers has been currently investigating. Additionally, DHPs are widely accepted antioxidants. Therefore, compounds **P28**, **P30**, and **P34** with the highest binding affinities at H₃R were investigated in the ORAC assay. The potential cytotoxicity properties were also of interest and have been conducted for compounds **P28**, **P30**, and **P34**. The results of the pharmacological assessment are summarized in table 4-8.

Table 4-8: Hybrid H₃R ligands with dihydropyridine structure.

						
	R ¹	R ²	R ³	hH ₃ R K _i [nM] (95% CI)	ORAC ^a [Trolox equivalence]	Cytotoxicity ^b (% at 1 and 10 μM)
P28	A	-H	-COCH ₃	3.09 (0.77-12.5)	4.21 ± 1.24	Non-toxic
P29	A	-NO ₂	-COCH ₃	70.9 (29.0-174)	n.d.	n.d.
P30	A	-H	-COOC ₂ H ₅	11.4 (5.21-24.8)	-0.18 ± 0.54	Non-toxic
P31	A	-NO ₂	-COOC ₂ H ₅	222 (89-554)	n.d.	n.d.
P32	B	-H	-COOC ₂ H ₅	2394 (850-6745)	n.d.	n.d.
P33	A	-H	-C≡N	29.1 (3.12-271)	n.d.	n.d.
P34				1.56 (0.68-3.60)	2.59 ± 1.34	34.27 ± 58.52 (1 μM) 9.66 ± 30.79 (10 μM)

^a: Data are presented as mean ± standard deviation. A high value suggests a good antioxidative capacity; ^b: Decreased cell viability in percent. A high value indicates high toxicity.

Compounds **P30** and **P31** preserved ester structure in the side chain, which is a common structural feature of the clinical used DHP calcium channel blockers. The replacement of the ester groups in the side chain with hydrolytic-stable ketones resulted in compounds **P28** and **P29**, which demonstrated approximately 3-fold higher receptor binding affinity at the H₃R with K_i values of 3.09 and 70.9 nM than **P30** and **P31** with the K_i values of 11.4 and 222 nM, respectively. Compounds **P29** and **P31** have a nitro substituent at the phenyl ring. An electron-withdrawing substituent at the *ortho*- or *meta*-position is crucial for the calcium channels' inhibitory activity. However, the additional nitro substituent led to approximately 20-fold declines in the affinity at H₃R. The significant loss of affinities can be observed from comparing the compounds **P28** to **P29** with K_i values of 3.09 to 70.9 nM and **P30** to **P31** with K_i values of 11.4 to 222 nM.

The observation suggested that the typical DHP structural features, including *meta*- or *ortho*-site substituted aromatic moiety and the ester structure in the side chains, were not optimized structural features for H₃R. However, these structures were well tolerated by the receptor.

The ligand with the highest binding affinity at H₃R within this project is the compound **P34**, with the H₃R pharmacophore in one of the hydrolytic stable side chains. Using **P34** as a lead structure may allow further modifications at the DHP structure to favor the CCB effectiveness without significant loss of the H₃R affinity. However, this speculation needs to be investigated. Furthermore, though inferior to compounds **P28** and **P30** comprising ketone or ester structures in the side chains, compound **P33** with cyano groups in the side chains is a modest H₃R ligand with a K_i value of 29.1 nM.

Notably, the compound **P32** with the *N*-benzoyl piperazine structure had an improved binding affinity at H₃R with a K_i value of 2.4 μ M, compared to other ligands in this work comprising the same scaffold as H₃R pharmacophore (i.e., **P1**, **P2**, **P11**, **P12**, and **P13** with K_i values of 4.5, 12, 5.2, 7.8, and 2.7 μ M, respectively). The comparatively high affinity of **P32** suggested that the DHP structure may have an affinity-enhancing effect for H₃R ligands.

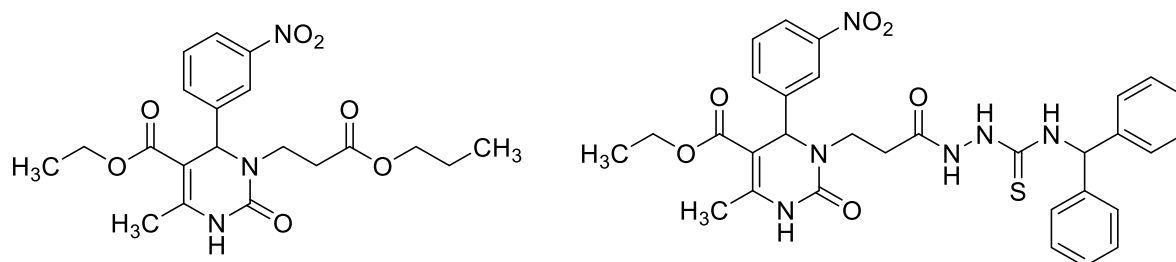
Additionally, compounds **P28** and **P30** were found to be non-toxic in the cell viability assay, while compound **P34** demonstrated dose-independent toxicity. The reason for a higher cell death rate in a lower dose requires further investigation. Furthermore, the compounds **P28** and **P34**, which demonstrated the highest affinities at H₃R within this project, displayed strong antioxidative properties with 4.21 and 2.59 folds of that of the reference substance Trolox, respectively. Unexpectedly, the compound **P30** with ester structure in the side chains did not show any antioxidative capacity. Notably, Malek and colleagues reported a series of hybrid ligands targeting H₃R and calcium channels (Malek *et al.*, 2019) during the time this work was performed. The compound **P30** shared the same structure as the literature compound **3j**, which has shown a good antioxidative property in the ORAC assay with 2.3 folds of that of Trolox

(Malek *et al.*, 2019). The discrepancy between **P30** and literature substance **3j** regarding antioxidative capacity needs further clarification.

However, according to Malek *et al.*, compound **3j** has demonstrated a low inhibitory effect at calcium channels with only 28% of inhibition at a concentration of 10 μM . As discussed before, the result is expected due to the absence of the essential electron-withdrawing substituents at the phenyl ring. The screening of the compounds from this work on calcium channels will provide a wide-ranging overview of the pharmacological properties of this series of hybrid ligands.

4.10.2 Hybrid H₃R ligands with dihydropyrimidine structure

Biginelli dihydropyrimidines (DHPMs) are DHP structure mimics but less vulnerable to form biological inactive oxidation products. Many DHPMs have displayed modest calcium channel inhibition. However, despite their success in the preclinical studies, the major drawback of DHPMs is the extensive first-pass effect with the removal of *N*³ substitution and accompanied short half-life (Atwal *et al.*, 1991).



2d: Ca_v1.2 *IC*₅₀ > 70%, Ca_v3.2 *IC*₅₀ > 90%

9c: Ca_v1.2 *IC*₅₀ < 20%, Ca_v3.2 *IC*₅₀ > 75%

Figure 4-13: DHPM derivatives developed as subtype-selective calcium channel blockers. (Data presented refer to as Inhibition at 10 μM . Teleb *et al.*, 2017b, 2017a).

Similar to the DHPs, the presence of lipophilic side chains at positions 3 and 5 of the DHPM ring and the substitution at *ortho*- or *meta*-position at the phenyl ring are essential for the CCB activity (Cho *et al.*, 1989; Atwal *et al.*, 1990a; b, 1991; Atwal and Moreland, 1991; Rovnyak *et al.*, 1992, 1995; Yarım *et al.*, 1999).

Recently, selective DHPMs toward the L-type channel Ca_v1.2 or the T-type channel Ca_v3.2 (Figure 4-13) have been reported (Teleb *et al.*, 2017b; a). The literature compound **9c** has demonstrated antinociceptive effects in an animal model. Furthermore, both Ca_v1.2 and Ca_v3.2 channels are of great interest in the perspective of neurodegenerative disorders.

Table 4-9: H₃R ligands with 2-oxo-DHPM structure.

				hH ₃ R K _i Cl (95%) [nM]
P35	-CH ₃	-H	61.5 (19.8-191)	
P36	-OCH ₂ CH ₃	-H	45.2 (13.6-151)	
P37	-CH ₃	-COCH ₃	83.9 (38.5-183)	
P38	-OCH ₂ CH ₃	-COCH ₃	77.3 (57.1-105)	

In the radioligand displacement assay at hH₃R, all DHPM derivatives demonstrated modest affinities at H₃R (Table 4-9), where the compounds **P37** and **P38** with an acetyl group in N³-position tended to display slightly lower affinities at H₃R when compared to compounds **P35** and **P36**. Also, for the DHPM derivatives, the calcium channel assay is currently under investigation.

4.10.3 Hybrid H₃R ligands with barbituric acid structure

Aiming to develop a novel treatment for Parkinson's disease, Kang and co-workers synthesized a series of N,N'-disubstituted barbituric acid derivatives and reported their selective blockade at subtype Ca_v1.3 over the Ca_v1.2 (Kang *et al.*, 2012, 2013). The literature **compound 8** (Figure 4-14) demonstrated the best selectivity toward the Ca_v1.3 subtype and was identified as a lead structure. However, independent research groups have reported contradictory results regarding the CCB effect of **compound 8**. Ortner and colleagues reported that **compound 8** had an activating rather than an inhibitory effect at the Ca_v1.3 channel (Ortner *et al.*, 2014), while Huang and colleagues could not confirm the results of Kang *et al.* in their study. The claimed selectivity and effectiveness of **compound 8** might depend on a specific β-subunit of calcium channel (Huang *et al.*, 2014). A possible explanation was made recently by the original reporter of **compound 8** (Cooper *et al.*, 2020). A single amino acid mutagenesis or differed test conditions might responsible for the contradictory results. Furthermore, they revealed that the N,N'-disubstituted barbituric acids bind to the DHP binding

pocket of the Ca_v1.3 subtype calcium channel. Much work is still required in developing potent and selective compounds targeting this interesting target.

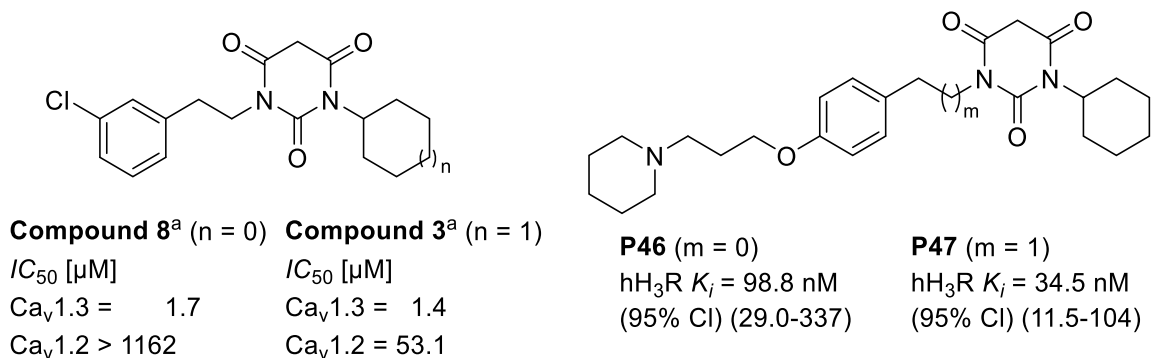


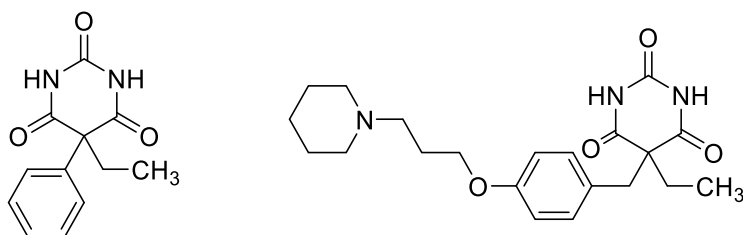
Figure 4-14: H₃R ligands with *N,N'*-disubstituted barbituric acid structure and their lead structures. (^a Kang *et al.*, 2012).

Unlike the lead structure **compound 3** and **8**, the substitution in the phenyl ring was at the *para*-position to ensure a good H₃R affinity. The compound **P47** with an ethyl linker has shown a substantially higher affinity than the compound **P46** with a methyl linker between the phenyl and barbiturate structures (*K*_i value 34.5 to 98.8 nM). Similar to the H₃R ligands with substituted urea structures (see Table 4-5), a long, flexible chain may be advantageous for the H₃R binding affinity. The investigation of their inhibitory effect on LTCCs will provide a comprehensive view of the pharmacological property of compounds **P46** and **P47**.

In addition to *N,N'*-disubstituted barbiturate derivatives **P46** and **P47**, the 5,5-disubstituted derivative **P39** was investigated regarding its binding affinity at H₃R. The biological activities of 5,5-disubstituted barbiturates were discovered over a century ago. Today, phenobarbital (Figure 4-15) is still an essential drug for combating some epileptic forms. Furthermore, some anesthetics, including the thiobarbituric acid derivative thiopental, have shown neuronal protective effects after ischemic injury and antioxidative properties (Schifilliti *et al.*, 2010). In addition to their pronounced positive GABA_A receptor modulating property, phenobarbital and many other 5,5-disubstituted barbiturate derivatives have been identified as weak blockers at P/Q type VGCCs, AMPA- and kainate receptors (Hirota *et al.*, 2000; Löscher and Rogawski, 2012).

Unlike benzodiazepines, which are safer alternatives and widely used as antiseizure, hypnotic, and anxiolytic drugs, the 5,5-disubstituted barbiturate derivatives could activate the GABA_A receptor in high concentration even without the presence of GABA and lead to fatal occurrences (Macdonald and Olsen, 1994). Therefore, their clinical uses are limited to antiepileptics and narcotics. Compound **P39** comprises barbiturate and H₃R pharmacophore (Figure 4-15). Several H₃R antagonists displayed promising antiseizure activity in animal models (Sadek *et al.*, 2016c; a). A possible synergism may result in highly effective drugs with

improved safety profiles. Furthermore, the wakefulness-promoting effect of the H₃R antagonists may counteract the sleepiness caused by classic antiseizure drugs.



Phenobarbital

P39

hH₃R K_i [nM] : 26.5
(95% CI) (9.68-72.4)

Figure 4-15: Phenobarbital is a lead structure for the 5,5-disubstituted barbiturate derivative P39.

The chimeric H₃R ligand **P39** comprising a 5,5-disubstituted barbiturate structure has displayed in the radioligand displacement assay good affinity at H₃R with a K_i value of 26.5 nM. The determination of the effect on the GABA_A receptor and associated pharmacological properties requires further investigation.

4.11 H₃R ligands with propargyl amine structure

The propargylamine derivatives selegiline and rasagiline demonstrate neuroprotective effects in both MAO inhibition-dependent and -independent manner (see section 1.6.3). For the multi-targeting ligands **P48** and **P49**, the affinity at H₃R and the inhibitory effects on both MAO enzymes have been determined. Moreover, the modest H₃R ligand **P48** was tested in the ORAC assay to examine its antioxidative property (Table 4-10).

Table 4-10: H₃R ligands with a propargyl amine structure.

	R	hH ₃ R K_i [nM] (95% CI)	MAO-A	MAO-B	ORAC [Trolox equivalent] (mean ± SD)
			Inhibition at 10 μM (% ± SD)		
P48		73.3 (37.2-145)	-2.9 ± 5.3^b	33.1 ± 10.2^b	0.95 ± 0.47
P49		>10.000	-1.9 ± 9.0^a	37.6 ± 27.6^a	n.d. ^c

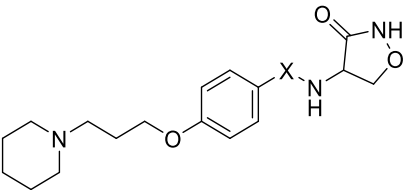
^a: Measured by the spectrophotometric method; ^b: Measured by fluorimetric method; ^c: not determined.

Similar to other structurally related compounds in this work, i.e., **P1**, **P2**, **P11-P13**, and **P32**, the *N*-benzoyl piperazine derivative **P49** displayed low affinity at H₃R. In contrast, **P48** bearing *N*-(3-phenoxypropyl)piperidine structure was a modest H₃R ligand with a *K_i* value of 73.3 nM. Furthermore, both compounds exhibited weak but selective inhibitory effects on the MAO-B. **P48** demonstrated a moderate antioxidative capacity in the ORAC assay, which is comparable to that of the reference substance Trolox. The initial screening of **P48** suggested that this compound may be a potential neuroprotective agent.

4.12 H₃R ligands with D-cycloserine structure

D-Cycloserine (DCS) is a partial agonist at the glycine binding site of the NMDA receptor. Several research groups have reported the therapeutical value of using DCS in various disorders in the CNS, including AD and anxiety (see section 1.6.5). Blood-brain barrier (BBB) permeability is a crucial feature for potential CNS effective agents. Like DCS, compounds **P50-P53** own zwitterionic structures, making these compounds good soluble in water. Despite the high hydrophilicity, DCS crosses the BBB readily. In human intestinal cells and bacteria, several amino acid transporters are involved in DCS transport (Wargel *et al.*, 1970; Ranaldi *et al.*, 1994). The *N*-(3-phenoxypropyl)piperidine scaffold in the chimeric compounds **P50-P53** led to increased lipophilicity than that of DCS, which may positively contribute to BBB permeability.

Table 4-11: H₃R screening of DCS derivatives.

			
Compounds	X	hH ₃ R <i>K_i</i> [nM] (95% CI)	
P50	-CH ₂ -	87.0	(37.1-204)
P51	-CH ₂ -CH ₂ -	17.0	(3.37-85.9)
P52	-CH ₂ -CH ₂ -CH ₂ -	99.0	(17.3-568)
P53	-CO-	190	(127-285)

All cycloserine derivatives displayed modest affinities at H₃R (Table 4-11). The compounds **P50-P52** with a secondary amine linker demonstrated higher affinities than **P53** containing a carboxamide group. The affinity discrepancy between **P51** with an ethylamine and **P53** with a carboxamide linker was significant. The result has again confirmed the previous observation that a second basic function positively contributed to binding affinity (Axe *et al.*, 2006; Schlegel

et al., 2007; Sander *et al.*, 2010a). Similar to the spin-labeled compound **P26**, a phenethylamine structure in **P51** tended to provide a more remarkable affinity enhancement than the benzylamine or phenylpropylamine structure. Further comprehensive investigations, including their impacts on NMDAR and cognitive function, are required to reveal their therapeutic potential.

4.13 Hybrid H₃R ligand with pimavanserin structure

Pimavanserin (Nuplazid®) is an atypical antipsychotic drug approved by the FDA in 2016 for the treatment of hallucinations and delusions associated with Parkinson's disease psychosis. Furthermore, this drug has demonstrated tangible benefits in patients with depressive disorder (Fava *et al.*, 2019). Pimavanserin acts as an inverse agonist at 5-HT_{2A} and 5-HT_{2C}, where the affinity at 5-HT_{2A} is higher than that at 5-HT_{2C}. No striking off-target binding on a series of other GPCRs, including H₃R, ion channels, or transporters, was detected (Vanover *et al.*, 2006). The hybrid ligand **P55** is a merged molecule comprising pimavanserin and the *N*-(3-phenoxypropyl)piperidine scaffold (Figure 4-16). Antagonism at H₃R leads to elevated dopamine release. Hybrid ligands based on this strategy may further improve the treatment of PD-associated psychosis and depression.

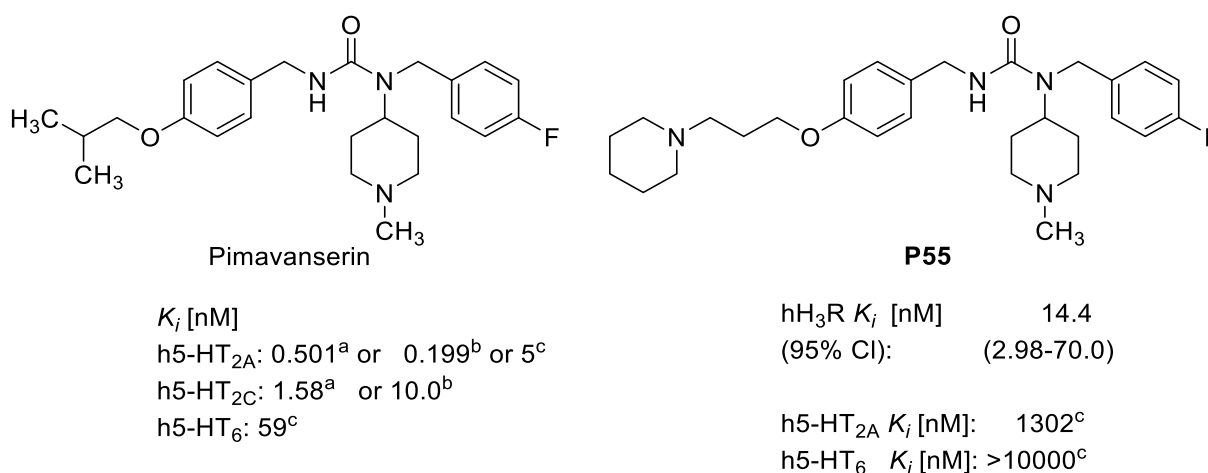


Figure 4-16: The structures and pharmacological data of pimavanserin and the hybrid ligand **P55**. Receptor binding studies were performed using ^a: membrane preparation or using ^b: whole cells (Vanover *et al.*, 2006). ^c: Preliminary screening results from the research group of Prof. Dr. Andrzej Bojarski (*n*=2).

Similar to other urea derivatives **P40-P45** in the present work, compound **P55** has demonstrated an appreciable affinity at H₃R with a K_i value of 14.4 nM. The in-vitro assessment at 5-HT receptors and the in-vivo study in a depressive mouse model are currently performing. An initial report of the in-vivo study has shown that **P55** demonstrated a dose-dependent antidepressive effect. However, the preliminary results from the 5-HT receptor screenings demonstrated that **P55** might be a weak 5-HT_{2A} ligand with a K_i value in the micromolar concentration range.

4.14 Hybrid H₃R ligand with a novel PD treatment strategy

The adenosine A_{2A} receptor (A_{2A}R) plays a vital role in regulating dopamine receptor function. The interplay between the A_{2A}R and dopamine D₂ receptor is especially interesting for PD treatment. Antagonism at A_{2A}R enhances the effects of dopamine agonists (Koga *et al.*, 2000). Furthermore, the A_{2A} receptor also interacts with glutamatergic synapses (Cunha *et al.*, 2008), GABAergic neurons, as well as cholinergic terminals, suggesting a potential therapeutic target in various psychotic disorders, including AD and depression (Svenningsson *et al.*, 1999; El Yacoubi *et al.*, 2001; Franco *et al.*, 2020). More recently, A_{2A}-H₃ receptor heterodimer was identified in rat striatum (Márquez-Gómez *et al.*, 2018). The physiological function of this putative heterodimer needs further clarification. Simultaneous antagonism at H₃R and A_{2A}R could increase the level as well as enhance the effect of dopamine. This strategy might represent an attractive therapeutic alternative to standard therapies. **Compound 22** (Figure 4-17), a non-xanthine-like A_{2A}R antagonist with appreciable aqueous solubility (Mikkelsen *et al.*, 2015), is used as a lead structure to design the hybrid ligand **P56**.

The replacement of the ether function of the *N*-(phenoxyalkyl)piperidine scaffold with an amide function, maintaining the di-amide structure in the lead **compound 22**, caused a drastic loss of the affinity to H₃R. Compound **P56** has displayed a weak binding affinity at H₃R in the micromolar concentration range. Thus, further structural optimization is required.

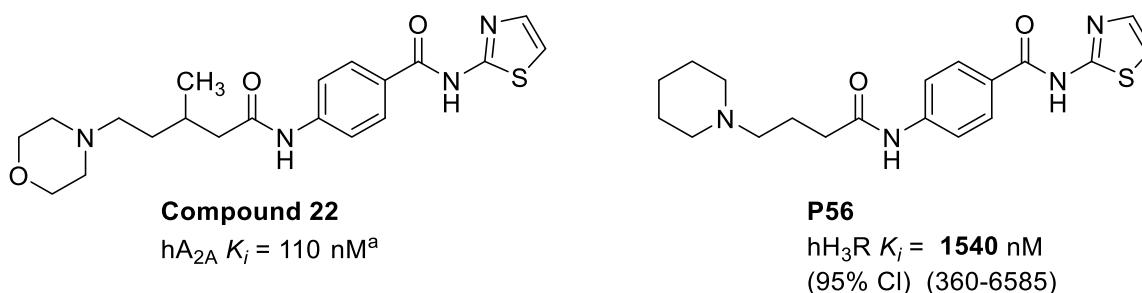


Figure 4-17: The literature **compound 22** was used as the lead structure for the hybrid H₃R ligand **P56**. (a: Mikkelsen *et al.*, 2015).

4.15 Conclusion

In conclusion, the application of *N*-(3-phenoxypropyl)piperidine scaffold as H₃R pharmacophore resulted in many ligands in this work with affinities at H₃R in the low nanomolar concentration range. To be highlighted here are the first SF₅ group-containing H₃R ligands **P3-P6**, the highly affine, selective H₃R ligands **P17** and **P18** with the imidazo[2,1-*b*]thiazinane structures, displaying K_i values in the subnanomolar concentration ranges, the dihydropyridine derivatives **P28** and **P34**, demonstrating excellent H₃R affinities and antioxidative properties,

and the pimavanserin derivative **P55**, presenting in-vivo antidepressive effects in a mouse model.

Furthermore, bulky structures and polar structures as substituents at the benzylic position of the *N*-(3-phenoxypropyl)piperidine scaffold (e.g., the H₃R ligands with TEMPO-spin-label, DCS structure, and *N,N'*-disubstituted barbituric acid) led to decreased H₃R affinity. Prolong the benzylamine structure to phenethylamine resulted in a remarkably improved binding affinity at H₃R.

However, due to the diversities in targets addressed by the MTDLs here, not all the pharmacological screenings can be finished within the limited duration of this dissertation work. A comprehensive overview of the potentials of the MTDLs synthesized in this work will be obtained when more data is available.

5 Summary & Zusammenfassung

5.1 Summary

The major part of this work has focused on presenting highly affine H₃R ligands and multi-target-directed ligands (MTDLs) comprising an H₃R pharmacophore. For this purpose, various modifications (Figure 5-1) have been performed to substituents of the central phenyl ring of the *N*-(3-phenoxypropyl)piperidine scaffold.

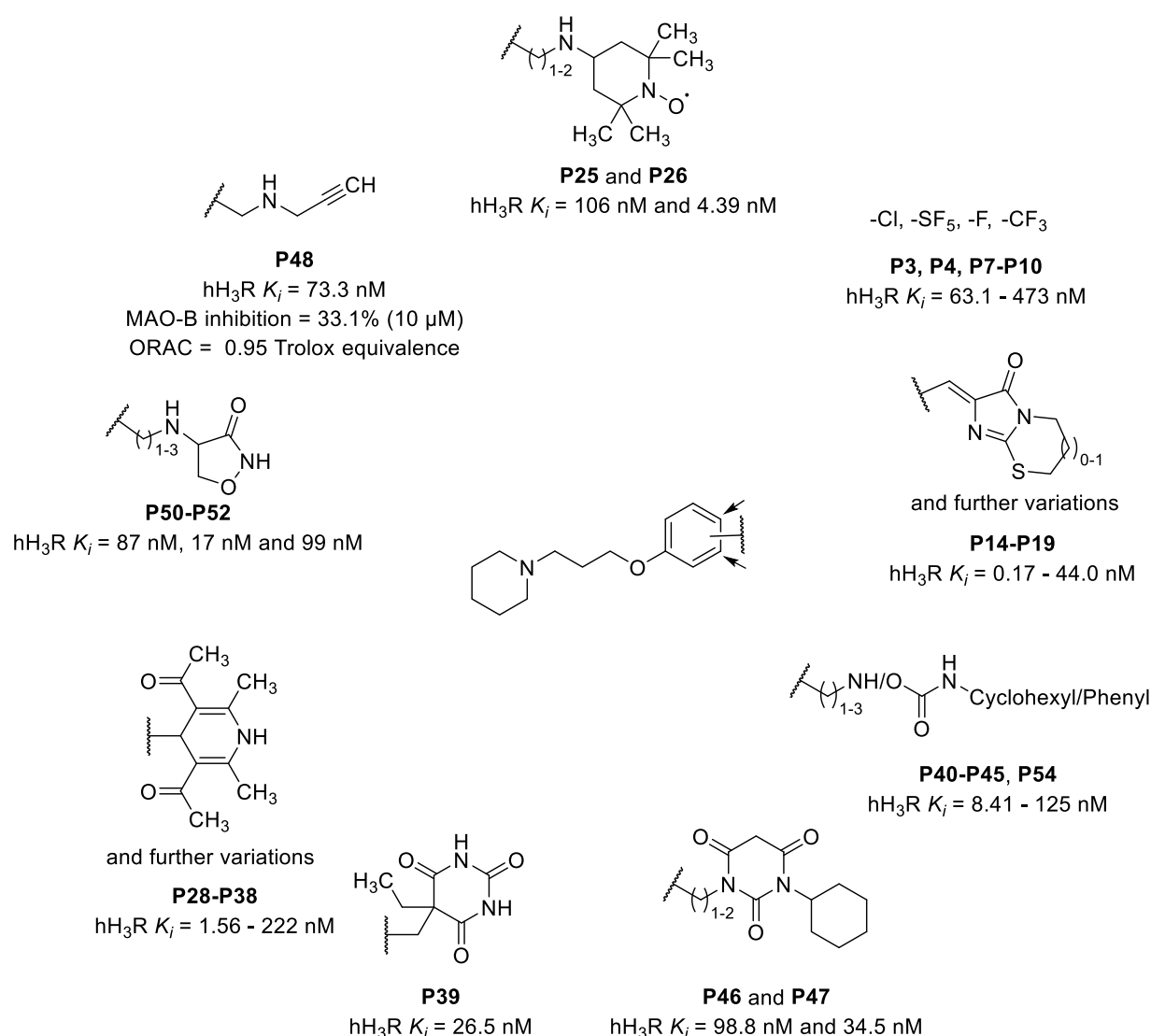


Figure 5-1: Representative H₃R ligands and MTDLs developed in this work, using *N*-(3-phenoxypropyl)piperidine scaffold as the H₃R pharmacophore. ORAC: Oxygen-radical absorbance capacity. Trolox: An antioxidant used as reference.

The synthesized compounds possess vastly varied physicochemical and pharmacological properties. Investigating their H₃R binding affinities has provided valuable structure-activity

relationships, which may be helpful to guide further design and development of H₃R ligands and MTDLs.

Compounds **P3-P6** are, to my knowledge, the first pentafluorosulfanyl (SF₅) group containing H₃R ligands. The SF₅ group is a lipophilic, chemically stable, and strongly electron-withdrawing group. This project confirmed that for the *N*-(3-phenoxypropyl)piperidine scaffold, the phenyl ring's substituents at the *para* position to the ether function have more remarkable affinity enhancing effects than those at the *meta* positions. The 4-SF₅ and 4-Cl substituted compounds (**P3**, hH₃R *K_i* = 75.1 nM and **P7**, hH₃R *K_i* = 63.1 nM, respectively) were determined as the most affine ligands within compounds bearing similar structural features in this work. However, a direct association between receptor affinity and the substitutions' lipophilicity, electronic effect, or spatial volume could not be observed.

Furthermore, ylidene thiohydantoin-derived structures as substituents of the *N*-(3-phenoxypropyl)piperidine scaffold have displayed affinity-enhancing effects at H₃R. The benzylidene thiohydantoin derivative **P14** was a Knoevenagel condensation product. Further reactions between **P14** and 1,2-dibromoethane or 1,3-dibromopropane yielded ligand **P19** with an imidazo[2,1-*b*]thiazolidine structure or **P17** and **P18** with imidazo[2,1-*b*]thiazinane structures, respectively (Figure 5-2). Interestingly, an *E/Z* conversion in the configuration was observed when the reaction was carried out in ethanol. Compound **P17** and **P18** were two products obtained from one reaction with ethanol as the solvent, while **P19** was yielded as the only product from the reaction with acetone as solvent (Figure 5-2).

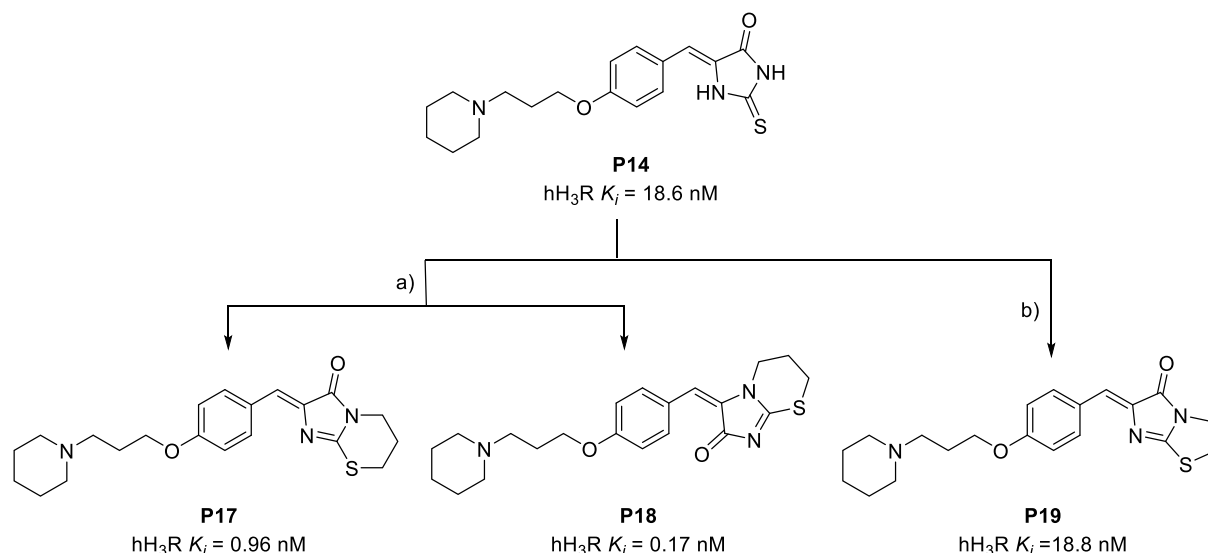


Figure 5-2: H₃R ligands containing conjugated systems in the substituents.

a): 1,3-Dibromopropane, Ethanol; b): 1,2-Dibromoethane, acetone.

Compounds **P14-P19** displayed high affinities at H₃R. Especially the imidazo[2,1-*b*][1,3]thiazinane derivatives **P17** and **P18**, which have shown *K_i* values in the subnanomolar

concentration range (Figure 5-2). Moreover, **P17** and **P18** demonstrated no significant affinities at H₁R, H₄R, and the orphan receptors GPR18 and GPR55, indicating that the ligands owned high selectivity to H₃R.

Also, for compound **P19**, evidence of reactivity as a Michael acceptor was missing, suggesting that the high H₃R affinity of this class of compounds could be ascribed to specific ligand-protein interaction.

As reported previously (Eissa *et al.*, 2019; Lutsenko *et al.*, 2019; Łażewska *et al.*, 2020; Venkatachalam *et al.*, 2021) and observed in this work, many different structural variations at the phenyl ring of the *N*-(3-phenoxypropyl)piperidine scaffold are well accepted by H₃R. This unique property enables the rational design of multi-functional H₃R ligands or multi-targeting ligands.

Diverse structures have been employed in this work to acquire further functions in addition to the H₃R antagonism, such as spin-labels or pharmacophores for additional target proteins, including voltage-gated calcium channels (VGCC), GABA_A receptors, NMDA receptors, monoamine oxidase isoenzymes A and B (MAO-A and -B), serotonin 5-HT_{2A}, 5-HT_{2C} receptors, and adenosine A_{2A} receptor.

Compound **P48** with the propargylamine structure – a common structural feature of the widely used antiparkinson drugs selegiline and rasagiline, demonstrated modest H₃R affinity and antioxidative property, which is independent of its MAO-B inhibition. The neuroprotective effect of **P48** needs further investigation.

The 2,2,6,6,-tetramethyl piperidinyloxy free radical (TEMPO) structure was used as a spin-label for H₃R ligands in this work. The bulky TEMPO structure at the benzyl position of the *N*-(3-phenoxypropyl)piperidine scaffold has led to a moderate H₃R ligand **P25**. Prolong the benzylamine to phenethylamine structure resulted in **P26** with a significant affinity increase at H₃R. Similar phenomena were also observed for the hydrophilic barbituric acid (Compound **P46** and **P47**) and cycloserine structure (**P50-P52**).

The use of the NMDA receptor partial agonist D-cycloserine (DCS) is intensively researched in various neuronal disorders, including Alzheimer's disease, anxiety, and schizophrenia. Despite having secondary amine as a common structural feature, the hybrid compounds **P50-P52** could not be synthesized from one-pot Borch reductive amination reactions like the spin-labeled compounds **P25** and **P26** and the propargylamine derivative **P48**. The corresponding Schiff's base intermediates have been obtained from reactions in alcoholic solution, and the products **P50-P52** were yielded from subsequent hydrogenation. As mentioned before, the compound **P51** with a phenylethylamine structure displayed a higher affinity at H₃R than **P50**

with a benzylamine structure. However, prolong the linker of **P51** to a phenylpropylamine structure (compound **P52**) failed to further improve the affinity at H₃R.

Like the NMDA receptors, VGCCs are intensively researched ion channels involved in neurodegenerative diseases. Compounds **P28-P34** are H₃R ligands with a 1,4-dihydropyridine (DHP) structure – a common structural feature of a series of widely used calcium channel blockers (CCB). Electron-withdrawing substituents at the phenyl ring and lipophilic substituents at the DHP structure are relevant for their CCB activities.

Compound **P28** (Figure 5-3 A) has shown the highest H₃R affinity within the ligands comprising symmetric DHP structures, while compound **P34** (Figure 5-3 B) with an asymmetric DHP structure was the most affine H₃R ligand with a DHP structure in this work. As expected for DHPs, **P28** and **P34** displayed strong antioxidative properties (4.21 and 2.59 Trolox units, respectively). An additional nitro substituent at the phenyl ring of **P28** led to a more than 20-fold decrease in affinity at H₃R (**P29**), while replacing the ketone structure in the 3,5-position of the DHP ring with the hydrolytic vulnerable ester structure or the cyano group led to 3- or 9-fold decreases in H₃R affinities (**P30** or **P33**, respectively) (Figure 5-3 A). Nonetheless, the compounds **P29-P33** are excellent to modest H₃R ligands.

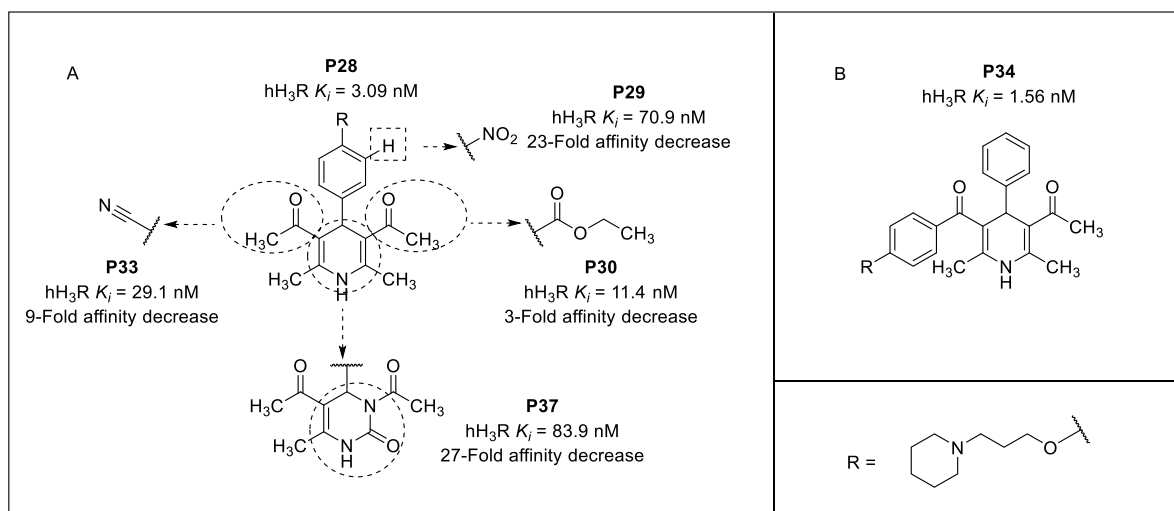


Figure 5-3: A: H₃R ligands with symmetric DHP structures and their DHPM analogs. B: H₃R ligands with an asymmetric DHP structure.

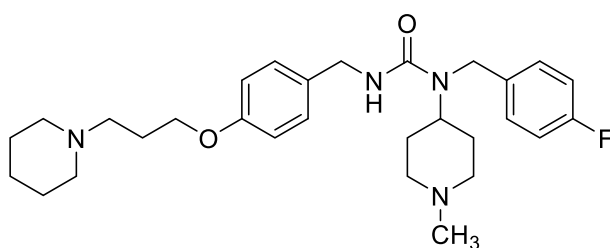
Furthermore, the oxidation-susceptible DHP structure was replaced with the 3,4-dihydropyrimidine (DHPM) structure, leading to compound **P35-P38** (**P37** shown in Figure 5-3 A) with modest affinity at H₃R.

As most CCBs with DHP structures block the L-type calcium channels unselectively, the subtype-selective CCBs may be useful therapeutic agents for neurodegenerative diseases. The H₃R ligands **P46** and **P47** used a series of *N,N'*-disubstituted barbituric acid derivatives,

which displayed selective antagonism at the $\text{Ca}_v1.3$ channel, as lead structures. Modest H_3R affinities were observed for both compounds.

The compounds with DHP, DHPM, and N,N' -substituted barbituric acid structures are currently investigated regarding their VGCC blocking activities. The effort will provide valuable insight into the pharmacological profiles of the multi-targets directed ligands targeting H_3R and calcium channels.

In this work, the design of MTDLs addressing H_3R and further GPCRs have focused on novel strategies in treating psychosis, depression, and Parkinson's disease. The selective $5\text{-HT}_{2A/2C}$ antagonist pimavanserin is an effective drug to treat parkinsonian psychosis. It also displayed a remarkable antidepressive effect. The pimavanserin derivative **P55** (Figure 5-4) has shown a high H_3R affinity with a K_i value of 14.4 nM. However, a preliminary result of screening at the 5-HT_{2A} receptor suggested that **P55** may not be particularly active at the investigated receptor. Interestingly, **P55** ameliorated depressive behavior in an in-vivo study (Publication in preparation).



P55

hH_3R $K_i = 14.4$ nM

h5-HT_{2A} $K_i = 1302$ nM (Preliminary result)

Figure 5-4: Hybrid ligands with potential novel therapeutic strategies against psychosis and Parkinson's disease.

Additionally, the ether function in the spacer and the phenyl ring of the N -(3-phenoxypropyl)piperidine scaffold were modified in this work. The ether structure was replaced by substituted guanidine structures or an amide structure, while a phenyl pyrazole structure was used instead of the phenyl ring. Unexpectedly, the resulting H_3R ligands **P20-P24** and **P56** have displayed only weak to moderate binding affinities at H_3R , while a few literature compounds with similar structural features have shown high affinities in the low nanomolar concentration range (Stark *et al.*, 1994; Linney *et al.*, 2000; Swanson *et al.*, 2009).

The success in applying the N -benzoyl piperazine scaffold as the H_3R pharmacophore was limited. Modifications in the substitution at the phenyl ring with several structure variations (Figure 5-5) have failed to produce highly affine H_3R ligands. The observation suggested that the substituents at phenyl ring in this scaffold may be restricted to a few given structures, e.g., benzylic, cyclic tertiary amines.

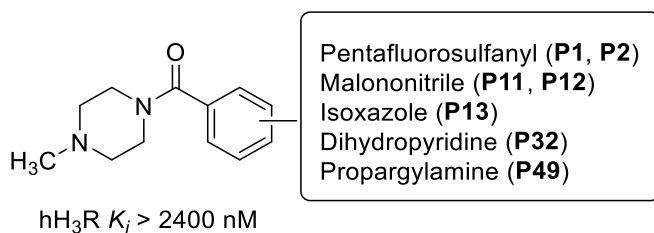


Figure 5-5: Compounds with the *N*-benzoyl piperazine scaffold.

In conclusion, the compounds synthesized in this work have shown a decent diversity in their structures, covering a broad range of spatial volume, lipophilicity, basicity, and blood-brain-barrier permeability. With only few exceptions, the ligands investigated in this work have molecular weights smaller than 500 Da, which is a crucial criterion for an acceptable drug-likeness. Compounds synthesized in this work rationally enlarged the H₃R ligands pool and contributed to further understanding of the SAR of H₃R ligands. Moreover, this work confirmed that hybrid ligands with H₃R antagonist properties provide promising strategies for the development of novel therapeutic options for CNS disorders. The pharmacological tools with potential therapeutical, neuroprotective properties developed in this work may help to gain a deeper understanding of the complex interactions in the CNS.

5.2 Zusammenfassung

Der Hauptteil dieser Arbeit befasste sich mit der Darstellung hochaffiner H₃R-Liganden und Multi-Target-directed Liganden, die ein H₃R-Pharmakophor aufweisen. Zu diesem Zweck wurden verschiedene Modifikationen (Abbildung 5-1) an Substituenten des zentralen Phenylrings des *N*-(3-Phenoxypropyl)piperidin-Grundgerüsts vorgenommen.

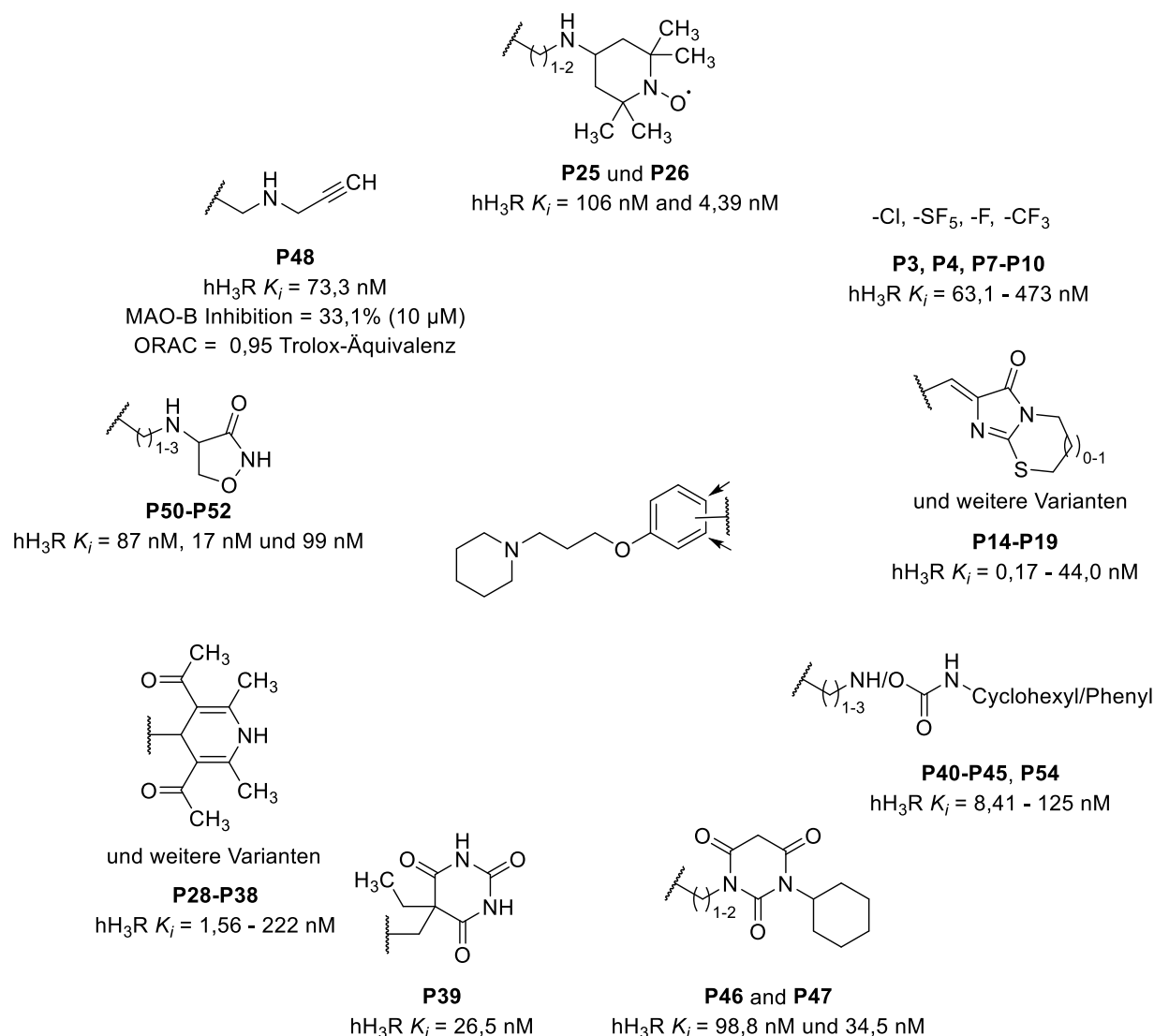


Abbildung 5-1: Repräsentative H₃R-Liganden und MTDL in dieser Arbeit, basierend auf dem *N*-(3-Phenoxypropyl)piperidin-Grundgerüst als H₃R-Pharmakophor. ORAC: Sauerstoff-Radikal-Absorptionskapazität. Trolox: Ein Antioxidans, das als Referenz verwendet wird.

Die synthetisierten Verbindungen weisen sehr unterschiedliche physikochemische und pharmakologische Eigenschaften auf. Die Untersuchung der Bindungsaffinitäten auf dem H₃R lieferte wertvolle Struktur-Aktivitäts-Beziehungen, die für das weitere Design und die Entwicklung von H₃R-Liganden und Multi-Target-directed Liganden hilfreich sein können.

Die Verbindungen **P3-P6** sind meines Wissens nach die ersten Pentafluorsulfanyl (SF_5)-Gruppen enthaltenden H_3R -Liganden. Die SF_5 -Gruppe ist ein lipophiler, chemisch stabiler und stark elektronenziehender Substituent. Dieses Projekt bestätigte, dass für das *N*-(3-Phenoxypropyl)piperidin-Gerüst, die Substituenten des Phenylrings an der *para*-Position zur Etherfunktion zu bemerkenswerteren Affinitätssteigerungen führen als die an den *meta*-Positionen. Die 4- SF_5 und 4-Cl substituierten Verbindungen (**P3**, $\text{hH}_3\text{R } K_i = 75,1 \text{ nM}$ und **P7**, $\text{hH}_3\text{R } K_i = 63,1 \text{ nM}$) weisen die höchste Affinitäten innerhalb dieses Projekts. Ein direkter Zusammenhang zwischen den Affinitäten zum H_3R und der Lipophilie, dem elektronischen Effekt oder der räumlichen Größe der Substitutionen konnte jedoch nicht beobachtet werden.

Darüber hinaus führte Yliden-Thiohydantoin und die verwandte Strukturen als Substituenten des *N*-(3-Phenoxypropyl)piperidin-Gerüsts zu beachtenswerteren Affinitätssteigerung an das H_3R . Das Benzyliden-Thiohydantoin-Derivat **P14** war ein Knoevenagel-Kondensationsprodukt. Weitere Reaktionen zwischen **P14** und 1,2-Dibromethan oder 1,3-Dibrompropan lieferten den Liganden **P19** mit einer Imidazo[2,1-*b*]thiazolidinstruktur bzw. **P17** und **P18** mit Imidazo[2,1-*b*]thiazinanstrukturen (Abbildung 5-2). Interessanterweise wurde eine *E/Z*-Konversion in der Konfiguration beobachtet, wenn die Reaktion in Ethanol durchgeführt wurde. Die Verbindungen **P17** und **P18** waren zwei Produkte, die aus einer Reaktion mit Ethanol als Lösungsmittel erhalten wurden, während **P19** als einziges Produkt aus der Reaktion mit Aceton als Lösungsmittel erhalten wurde (Abbildung 5-2).

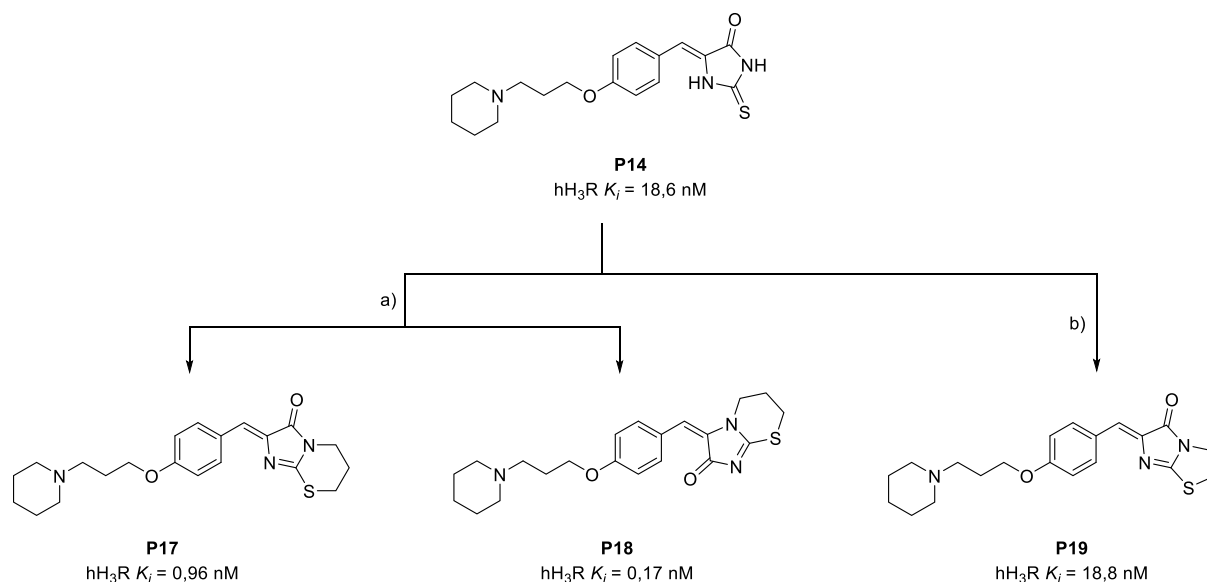


Abbildung 5-2: H_3R -Liganden, die konjugierte Systeme in den Substituenten enthalten.

a): 1,3-Dibromopropan, Ethanol; b): 1,2-Dibromoethan, Aceton.

Die Verbindungen **P14-P19** zeigten hohe Affinitäten an H_3R . Insbesondere die Imidazo[2,1-*b*][1,3]thiazinan-Derivate **P17** und **P18**, die K_i -Werte im subnanomolaren Konzentrationsbereich aufwiesen (Abbildung 5-2). Darüber hinaus zeigten **P17** und **P18** keine

signifikanten Affinitäten zu H₁R, H₄R und den Orphan-Rezeptoren GPR18 und GPR55. Auch für Verbindung **P19** fehlten Hinweise auf eine Reaktivität als Michael-Akzeptor. Die Beobachtungen deutete darauf hin, dass die hohe und selektive H₃R-Affinität dieser Verbindungsklasse auf eine spezifische Ligand-Protein-Wechselwirkung zurückgeführt werden könnte.

Wie bereits woanders berichtet (Eissa *et al.*, 2019; Lutsenko *et al.*, 2019; Łażewska *et al.*, 2020; Venkatachalam *et al.*, 2021) und in dieser Arbeit beobachtet, werden viele verschiedene strukturelle Variationen am Phenylring des *N*-(3-Phenoxypropyl)piperidin-Gerüsts von dem H₃R gut toleriert. Diese Eigenschaft vom H₃R ermöglicht das rationale Design von multifunktionalen Liganden oder Multi-Targeting-Liganden.

Diverse Strukturen wurden in dieser Arbeit eingesetzt, um neben dem H₃R-Antagonismus weitere Funktionen zu erhalten, wie z.B. Spin-Labels oder Pharmakophore für weitere Target-Proteine, darunter spannungsabhängige Calciumkanäle, GABA_A-Rezeptoren, NMDA-Rezeptoren, Monoaminoxidase-Isoenzyme A und B (MAO-A und -B), Serotonin 5-HT_{2A}, 5-HT_{2C}-Rezeptoren, und Adenosin A_{2A} Rezeptor.

Die Propargylamin-Struktur in der Verbindung **P48** ist ein gemeinsames Strukturmerkmal der häufig verwendeten Antiparkinsonmittel Selegilin und Rasagilin. **P48** zeigte eine bescheidene H₃R-Affinität und antioxidative Eigenschaft, während die MAO-Inhibition eher als schwach einzustufen war. Die neuroprotektive Wirkung von **P48** muss weiter untersucht werden.

Die 2,2,6,6,-Tetramethyl-Piperidinyloxy-Radikal (TEMPO) wurde in dieser Arbeit als Spin-Label für H₃R-Liganden verwendet. Die sperrige TEMPO-Struktur an der Benzylposition des *N*-(3-Phenoxypropyl)piperidin hat zu einem moderaten H₃R-Liganden **P25** geführt. Die Verlängerung der Benzylgruppe zu einer Phenylethylgruppe führte zu **P26** mit einer signifikanten Affinitätssteigerung an H₃R. Ähnliche Phänomene wurden auch für die Verbindungen mit den hydrophilen Barbitursäure- (Verbindung **P46** und **P47**) und Cycloserin-Strukturen (**P50-P52**) beobachtet.

Der Einsatz des NMDA-Rezeptor-Partialagonisten D-Cycloserin (DCS) wird intensiv bei verschiedenen neuronalen Erkrankungen erforscht, darunter Alzheimer, Angstzustände und Schizophrenie. Die sekundäre Aminstruktur der Hybridverbindungen **P50-P52** konnte nicht wie die Verbindungen **P25** und **P26** mit Spin-Label und das Propargylamin-Derivat **P48** aus der einfachen Birch reduktiven Aminierung synthetisiert werden. Die entsprechenden Schiff'schen Basen-Zwischenprodukte wurden aus Reaktionen in alkoholischer Lösung gewonnen, und die Produkte **P50-P52** wurden durch anschließende Hydrierung erhalten. Wie bereits erwähnt, zeigte die Verbindung **P51** mit einer Phenylethylaminstruktur eine höhere Affinität an H₃R als **P50** mit einer Benzylaminstruktur. Die Verlängerung des Linkers von **P51** zu einer

Phenylpropylaminstruktur (Verbindung **P52**) führte jedoch zu deutlichen Verschlechterung der Affinität an H₃R.

Wie die NMDA-Rezeptoren sind auch die Calciumkanäle intensiv erforschte Target-Proteine, die bei neurodegenerativen Erkrankungen eine Rolle spielen. Die Verbindungen **P28-P34** sind H₃R-Liganden mit einer 1,4-Dihydropyridin (DHP)-Struktur – ein gemeinsames Strukturmerkmal einer Reihe von klinisch häufig eingesetzten Calciumkanalblockern (CCB). Elektronenziehende Substituenten am Phenylring und lipophile Substituenten an der DHP-Struktur sind relevant für ihre CCB-Aktivitäten.

Verbindung **P28** (Abbildung 5-3 A) zeigte die höchste H₃R-Affinität innerhalb der Liganden mit symmetrischen DHP-Strukturen, während Verbindung **P34** (Abbildung 5-3 B) mit einer asymmetrischen DHP-Struktur der affinste H₃R-Ligand mit einer DHP-Struktur in dieser Arbeit darstellte. Wie für DHPs erwartet, zeigten **P28** und **P34** starke antioxidative Eigenschaften (4,21 bzw. 2,59 Trolox-Einheiten). Ein zusätzlicher Nitro-Substituent am Phenylring von **P28** führte zu der Verbindung **P29** mit einer über 20-fachen Abnahme in der Affinität an H₃R, während das Ersetzen der Ketonstrukturen in der 3,5-Positionen des DHP-Rings durch die hydrolytisch anfällige Esterstruktur oder die Cyanogruppe zu einer 3- bzw. 9-fachen Abnahme der H₃R-Affinitäten führte (**P30** bzw. **P33**) (Abbildung 5-3 A). Nichtsdestotrotz sind die Verbindungen **P29-P33** bescheidene bis moderate H₃R-Liganden.

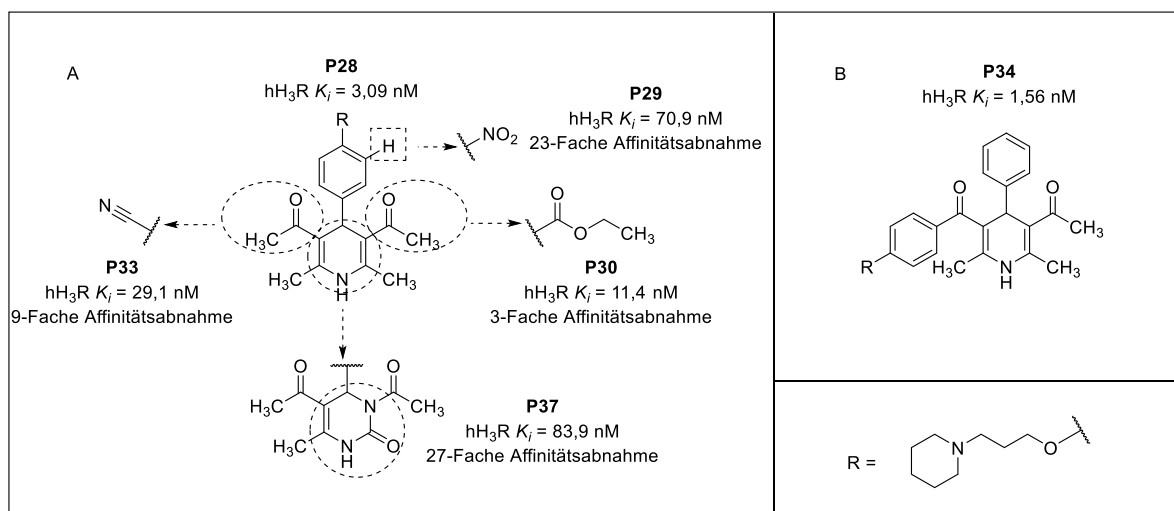


Abbildung 5-3: A: H₃R-Liganden mit symmetrischer DHP-Struktur und ihre DHPM-Analoga; B: H₃R-Ligand mit einer asymmetrischen DHP-Struktur.

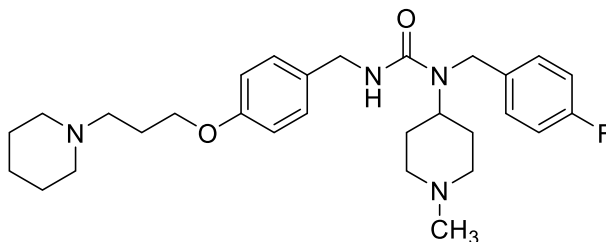
Außerdem wurde die oxidationsanfällige DHP-Struktur durch die 3,4-Dihydropyrimidin (DHPM)-Struktur ersetzt, was zu den Verbindungen **P35-P38** (Struktur von **P37** siehe Abbildung 5-3 A) mit bescheidener Affinität an H₃R führte.

Da die meisten CCBs mit DHP-Strukturen die L-Typ-Calciumkanäle unselektiv blockieren, könnten die subtypselektiven CCBs nützliche therapeutische Strategien für neurodegenerative

Erkrankungen sein. Bei den H₃R-Liganden **P46** und **P47** wurde eine Reihe von *N,N'*-disubstituierten Barbitursäurederivaten, die einen selektiven Antagonismus am Ca_v1.3-Kanal zeigten, als Leitstrukturen verwendet. Beide Verbindungen zeigten bescheidene H₃R-Affinitäten.

Die Verbindungen mit DHP-, DHPM- und *N,N'*-substituierten Barbitursäure-Strukturen werden derzeit hinsichtlich ihrer Calciumkanäle-blockierenden Aktivitäten untersucht. Der Forschungsansatz wird wertvolle Einblicke in die pharmakologischen Profile der Multi-Targets-directed Liganden liefern, die H₃R und Kalziumkanäle gleichzeitig ansprechen sollten.

In dieser Arbeit wurde das Design von Multi-Targets-directed Liganden, die H₃R und weitere GPCRs adressieren, auf neuartige Strategien zur Behandlung von Psychosen, Depressionen und der Parkinson-Krankheit konzentriert. Der selektive 5-HT_{2A/2C}-Antagonist Pimavanserin ist ein Medikament zur Behandlung der mit Parkinson assoziierten Psychose. Es zeigte auch eine beträchtliche antidepressive Wirkung. Das Pimavanserin-Derivat **P55** (Abbildung 5-4) hat eine hohe H₃R-Affinität mit einem *K_i*-Wert von 14,4 nM gezeigt. Ein vorläufiger Bericht deutete jedoch darauf hin, dass **P55** an dem 5-HT_{2A} Rezeptor möglicherweise nicht besonders aktiv ist. Interessanterweise verbesserte **P55** das depressive Verhalten in einer in-vivo-Studie (Publikation in Vorbereitung).



P55

hH₃R *K_i* = 14,4 nM
 h5-HT_{2A} *K_i* = 1302 nM (vorläufiges Ergebnis)

Abbildung 5-4: Hybridliganden mit potenziell neuartigen therapeutischen Strategien gegen Depression, Psychose und Parkinson-Krankheit.

Zusätzlich wurden in dieser Arbeit die Etherfunktion und der Phenylring des *N*-(3-Phenoxypropyl)piperidin-Gerüsts modifiziert. Die Etherstruktur wurde durch substituierte Guanidinstrukturen oder eine Amidstruktur ersetzt. Anstelle des Phenylrings wurde eine Phenylpyrazolstruktur verwendet. Die resultierenden Verbindungen **P20-P24** und **P56** zeigten jedoch nur schwache bis mäßige Bindungsaffinitäten an H₃R.

Der Erfolg bei der Anwendung des *N*-Benzoyl-Piperazin-Gerüsts als H₃R-Pharmakophor war ebenso begrenzt. Modifikationen in der Substitution am Phenylring mit mehreren Strukturvariationen (Abbildung 5-5) haben keine hochaffinen H₃R-Liganden entwickelt. Die Beobachtung deutet darauf hin, dass die Substituenten am Phenylring in dieser Struktur auf

wenige gegebene Strukturen beschränkt sein könnten, z. B. benzyliche, zyklische tertiäre Amine.

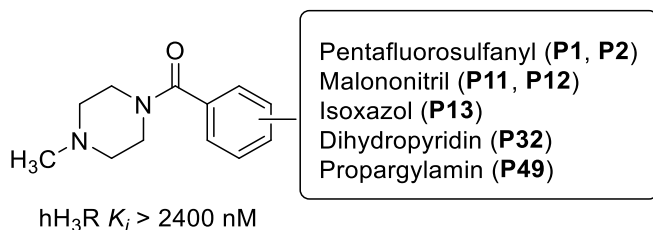


Abbildung 5-5: Verbindungen mit einer N-Benzoyl Piperazin Grundgerüst synthetisiert in dieser Arbeit.

Zusammenfassend lässt sich feststellen, dass die in dieser Arbeit synthetisierten Verbindungen eine anständige Vielfalt in ihren Strukturen gezeigt haben und einen breiten Umfang in der Lipophilie, Basizität und Blut-Hirn-Schranken-Permeabilität abdecken. Bis auf wenige Ausnahmen haben die in dieser Arbeit untersuchten Liganden Molekulargewichte kleiner als 500 Da, was ein wesentliches Kriterium für ein akzeptables Drug-likeness ist. Die in dieser Arbeit synthetisierten Verbindungen haben den Pool der H₃R-Liganden rational vergrößert und zum weiteren Verständnis der Struktur-Wirkungs-Beziehung von H₃R-Liganden beigetragen. Darüber hinaus bestätigte diese Arbeit, dass Hybridliganden mit antagonistischen Eigenschaften an das H₃R vielversprechende Strategien für die Entwicklung neuer therapeutischer Optionen für ZNS-Erkrankungen bieten. Die in dieser Arbeit entwickelten pharmakologischen Werkzeuge mit potenziellen therapeutischen, neuroprotektiven Eigenschaften können dazu beitragen, ein tieferes Verständnis der komplexen Interaktionen im ZNS zu erlangen.

6 Experiment

6.1 Equipment and materials for the synthesis

All commercially available chemicals and solvents in per analysis grade were purchased from ABCR (Karlsruhe, Germany), Acros Organics (Geel, Belgium), Alfa Aesar (Ward Hill, USA), Fluka (Munich, Germany), Apollo Scientific (Bredbury, UK) Merck (Darmstadt, Germany), Sigma-Aldrich (Steinheim, Germany), TCI (Portland, USA), Maybridge (Cornwall, UK), Macherey-Nagel (Düren, Germany) or VWR (Darmstadt, Germany) and used directly without purification in advance. The solvents of technical grade were provided by Zentrales Chemikalienlager of the Heinrich-Heine-University.

Thin-layer chromatography (TLC): Pre-coated 0.20 mm thick layer of silica gel 60 on aluminum foil with fluorescent indicator UV₂₅₄ (Macherey Nagel)

Equipment and reagents for the evaluation of the TLCs: UV-Observer (HP-UVIS, Biostep GmbH, Burkhardtsdorf, Germany). Potassium permanganate solution (1.5 g KMnO₄, 10 g K₂CO₃, 200 mL H₂O). Ninhydrin solution to detect primary and secondary amines (1.0 g ninhydrin, 200 mL ethanol). 2,4-Dinitrophenylhydrazine solution to detect reactive ketones and aldehydes (2,4-dinitrophenylhydrazine 1.0 g, 200 mL 2 M HCl aqueous solution)

Magnetic stirrer: MR Hei- Tec (Heidolph Instrumente GmbH, Schwabach, Germany)

Column chromatography: Silica gel 60 (0.04-0.063 mm) for column chromatography (Macherey-Nagel, Düren, Germany)

Flash chromatography: Isolera™ Spektra Systems with ACI™ and Assist (Biotage, Uppsala, Sweden). The columns used are Snap KP-Sil and Sfaer Silica D (Biotage, Uppsala, Sweden)

Microwave reactor: Biotage Initiator+™ Microwave system EU (Biotage, Uppsala, Sweden)

Autoclave reactor: Model IV 50S (Roth, Karlsruhe, Germany)

Ultrasonic cleaner: Model USC-THD (VWR, Darmstadt, Germany)

Immersion cooler: EK90 (Haake, Karlsruhe, Germany)

Nuclear magnetic resonance spectroscopy: Avance III 300, 500, or 600 MHz (Bruker, Reinstädten, Germany)

Data are reported in the following order: Multiplicity (br, broad; d, doublet; m, multiplet; p, quintet; s, singlet; and t, triplet; q, quartet; p, quintet), approximate coupling constants *J* expressed in Hertz (Hz), and the number of protons.

Mass spectrometry: Atmospheric-pressure chemical ionization (APCI+/-) on Advion Expression L CMS (Advion, Ithaca, USA)

Electrospray ionization (ESI+/-) on Bruker UHR-QTOF maXis 4G (Bruker Daltonics, Billerica, USA)

High-performance liquid chromatography (HPLC): Prostar system (Varian, Palo Alto, U.S.) equipped with a Prostar 410 (autosampler), 210 (pumps), and 330 (UV-detector). Column to evaluate chiral compounds: Phenomenex Lux 5 μ m Cellulose-1 (250 mm x 4.6 mm) (Phenomenex, Aschaffenburg, Germany), supported by Phenomenex Security Guard Cartridge Kit C18 (4.0 mm x 3.0 mm). The UV absorption was detected at 254 nm.

The mobile phase consists of HPLC-grade H₂O + 0.1% trifluoroacetic acid (TFA) (solvent A) and HPLC-grade MeCN + 0.1% TFA (solvent B). A linear gradient of 10% B to 100% B in 30 min was used, where the flow rate was 1 mL/min.

Elemental analysis (CHN-analysis): Vario MICRO cube Elemental Analyzer (Hanau, Germany)

Melting point instrument: M-565 (Büchi, Flawil, Switzerland)

Liquid chromatography coupled with mass spectrometry (LC-MS): LC system: Elute SP (HPG 700) (Bruker Daltonics, Billerica, USA) equipped with vacuum degasser, autosampler, column heater; Column: Intensity Solo 2 C18 RP column (100 mm x 2.1 mm, Bruker Daltonics, Billerica, USA); MS-system: amaZon speed ETD ion trap LC/MSn system (Bruker Daltonics, Billerica, USA), equipped with electrospray; Nebulizer: Nitrogen, 15 Psi; Dry Gas: Nitrogen, 8 l/min, 200 °C; Mass range Mode: Ultrascan. Alternating ion-Polarity has been turned on, scan range: m/z: 80-1200

Sample preparation: The stock solutions in MeOH (approximately 1 mg/mL) have been diluted with MeOH (LC-MS grade), and the concentrations of approximately 0.1-0.2 mg/mL were obtained. The volume of injection was 2 μ L.

The column temperature has been conditioned at 50 °C. The mobile phase consists of gradients (Table 6-1) from MeCN (LC-MS grade, Sigma Aldrich) and H₂O (LC-MS grade, Sigma Aldrich) with 0.1% of formic acid (FA) (v/v) (Merck). The flow rate was 0.2 mL/min, the measurements were only analyzed in positive mode, and the relative purity of the compounds was determined.

Experiment

Table 6-1: Gradients of the mobile phases for LC. Mixing ratios are expressed as H₂O (FA):MeCN.

	Initializing and reconditioning												Gradient																
Time	0	2	4	5	6	9	12	13	14	15	16	17	18	20	21	22	24	25	26	28	30 min.								
Method 1	95:5	To 5:95												To 0:100	To 95:5	95:5													
Method 2	40:60	To 2:98												To 0:100	To 95:5	To 0:100													
Method 3	98:2	To 95:5	95:5	To 5:95												To 0:100	To 98:2	To 40:60											
Method 4	40:60	To 5:95												To 0:100	To 0:100														
Method 5	98:2	To 95:5	95:5	To 5:95												To 99:1	To 99:1												
Method 6	40:60	To 30:70	To 5:95												To 99:1														
Method 7	95:5	To 90:10	To 20:80												To 95:5	95:5	To 95:5												
Method 8	95:5	To 90:10	To 80:20												To 5:95	To 95:5	To 95:5												
Method 9	95:5	To 90:10	To 30:70												30:70	To 95:5													
Method 10	95:5	To 90:10	To 80:20												80:20	To 5:95	To 95:5												
Method 11	98:2	To 95:5	95:5	To 5:95												To 0:100	To 98:2	To 98:2											
Method 12	98:2	To 95:5	95:5	To 5:95												To 0:100	To 98:2	To 98:2											

Rotary evaporator: Rotavapor R II (Büchi, Flawil, Switzerland) equipped with PC 3001 VARIO vacuum pump (Vacuubrand, Wertheim, Germany)

High-performance vacuum pumps: Chemistry hybrid pump RC6 and Rotary-vane pumping unit PC3/RZ2.5 (Vacuubrand, Wertheim, Germany)

Molecule drawing program: Chemdraw Professional 19.1 (PerkinElmer, Waltham, USA)

Estimation of the logarithm of the octanol/water partition coefficient at pH 7.4 ($\log D_{7.4}$): MarvinSketch (Version 21 in consensus mode, ChemAxon, Budapest, Hungary)

6.2 General claims for the chemistry experiments

If not state otherwise, NaHCO₃ solution and brine solution were saturated aqueous solution. HCl, NaOH, and AcOH solution was the aqueous solution with a defined concentration. Completion of the reaction was monitored via TLC. The temperature of the water bath of the rotary evaporator was set at 60 °C. The room temperature ranged from 18 °C to 35 °C. In the analytic data of NMR spectra, the coupling constant *J* referred to the three-bond coupling ³*J*. The melting points presented were uncorrected values. The molecule weight was calculated from the chemical formula (not the exact molecular weight). The yields of **P1-P56** are calculated from the amount after purification and presented as percentages of the theory. A yield of more than 95% was expressed as quantitative. Stereochemical analyses were only performed for the cycloserine derivatives **P50-P53**. A resolution of the enantiomers was not performed. The yields were only improved in single cases. The LC-MS analyses have been kindly performed by Dr. Aleksandra Zivkovic with the assistant of Ms. Kathrin Grau. The HPLC investigations were performed by Dr. Leandro Alves Avelar from the workgroup of Prof. Dr. Thomas Kurz.

6.3 Not commercially procured chemicals

HCl in dioxane and HCl in ethyl acetate have been prepared from concentrated sulfuric acid, which was given dropwise to NaCl (Biltz and Biltz, 1929). The emerged gaseous HCl was driven through dioxane or ethyl acetate for 30 minutes, the final concentration of HCl was not determined.

Ammonia in methanol has been prepared by passing gaseous ammonia (pressure gas) in methanol for 30 minutes at 0 °C. The MeOH solution was saturated with ammonia.

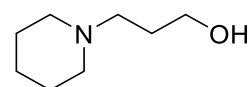
6.4 Synthesis and analytic

6.4.1 Intermediates

3-(Piperidin-1-yl)propan-1-ol (**1**) (Meier *et al.*, 2001)

Intermediate **1** has been synthesized from piperidine (51.1 g, 0.60 mol), 3-chloropropan-1-ol (47.3 g, 0.50 mol), K₂CO₃ (47.3 g, 0.50 mol) and KI (8.3 g, 0.05 mol) in 300 mL of acetone. The reaction mixture was heated at reflux for 60 h. The suspension was filtered, the filtrate was collected, and most of the solvent was removed in a rotary evaporator. The rest of the liquid was obtained via vacuum distillation.

Yield: 70%



Appearance: Colorless transparent viscous liquid

Chemical formula: C₈H₁₇NO

Molecular weight: 143.2 g/mol

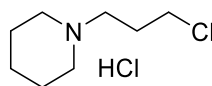
APCI-MS (+): m/z: 144.1 [M+H]⁺

¹H NMR (300 MHz, CDCl₃) δ 5.57 [singlet (s), 1H, -OH], 3.82 – 3.72 [multiplet (m), 2H, CH₂-OH], 2.59 – 2.48 [m, 2H, piperidine (Piperi)-CH₂], 2.43 [broad (br), 4H, Piperi-2,6-H₂], 1.74 – 1.61 (m, 2H, -CH₂-CH₂-OH), 1.55 [quintet (p), J = 5.5 Hz, 4H, Piperi-3,5-H₂], 1.49 – 1.34 (m, 2H, Piperi-4-H₂).

1-(3-Chloropropyl)piperidine hydrochloride (**2**) (Meier *et al.*, 2001)

The alkyl alcohol **1** (3.0 g, 21 mmol) was first treated with HCl solution in dioxane (20 mL). After removing the solvent, the residue was recrystallized in diethyl ether (EtOEt). The HCl salt of compound **1** was dissolved in 60 mL of dichloromethane (DCM). The solution was cooled to 0 °C. Thionyl chloride (3 mL, 41 mmol) was solved in 15 mL of DCM and added to the solution dropwise via a dropping funnel. The mixture was stirred at r.t. for 18 h. Upon completion of the reaction, the solvent and the excessive thionyl chloride were removed subsequently by vacuum distillation equipped with a wash bottle filled with sat. NaHCO₃ solution between condenser and pump. The residue was recrystallized in a solvent mixture of ethanol (EtOH) and EtOEt. The solid was rinsed with toluene and dried in a rotary evaporator.

Yield: 80%



Appearance: White solid

Chemical formula: $C_8H_{17}Cl_2N \times HCl$

Molecular weight: 198.2 g/mol

APCI-MS (+): m/z: 162.1 $[M+H]^+$

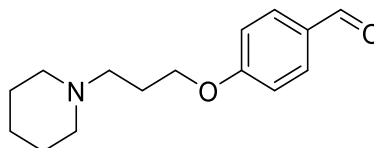
1H NMR (300 MHz, $CDCl_3$) δ 12.27 (s, 1H, Piperi- N^+H), 3.70 – 3.60 (m, 2H, $-CH_2-Cl$), 3.59 – 3.46 [m, 2H, Piperi-2,6- $H_{eqatorial}$ (H_{eq})], 3.16 – 3.03 (m, 2H, Piperi- CH_2-), 2.75 – 2.57 [m, 2H, Piperi-2,6- H_{axial} (H_{ax})], 2.53 – 2.38 (m, 2H, $-CH_2-CH_2-Cl$), 2.38 – 2.12 (m, 2H, Piperi-3,5- H_{eq}), 1.98 – 1.77 (m, 3H, overlap: Piperi-3,5- H_{ax} , Piperi-4- H_{eq}), 1.36 [quartet of triplet [qt], $^{3,4}J = 12.6$, 4.6 Hz, 1H, Piperi-4- H_{ax}].

4-[3-(Piperidin-1-yl)propoxy]benzaldehyde (**3**) (Isensee *et al.*, 2009)

The preparation of compound **3** was performed according to the following process: 4-Hydroxybenzaldehyde (2.9 g, 24 mmol), alkyl chloride **2** (4.0 g, 20 mmol), K_2CO_3 (6.7 g, 50 mmol), and KI (0.33 g, 2 mmol) were suspended in acetone 100 mL. The reaction mixture was heated at reflux for 44 h. Upon the completion of the reaction monitored via TLC, the inorganic residue was removed by filtration. The solution was concentrated and diluted with ethyl acetate (EtOAc) 100 mL and washed with 1M NaOH 60 mL. The wash process was repeated until all phenolic derivative was removed from the organic layer. The organic layer was then washed once with H_2O and once with brine, dried with anhydrous $MgSO_4$, and evaporated in a rotary evaporator. The product was used without further purification in the next steps.

Yield: 92%

Appearance: Light yellowish viscous liquid



Chemical formula: $C_{15}H_{21}NO_2$

Molecular weight: 247.3 g/mol

APCI-MS (+): m/z: 248.2 $[M+H]^+$

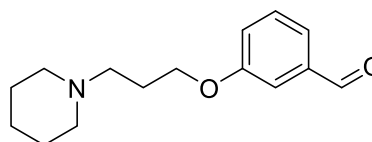
^1H NMR (300 MHz, DMSO- d^6) δ 9.86 (s, 1H, -CHO), 7.85 [doublet (d), J = 8.8 Hz, 2H, phenyl(Ph)-2,6- H], 7.11 (d, J = 8.7 Hz, 2H, Ph-3,5- H), 4.11 (t, J = 6.4 Hz, 2H, -O- CH_2 -), 2.41 – 2.34 (m, 2H, Piperi- CH_2 -), 2.34 – 2.28 (m, 4H, Piperi-2,6- H_2), 1.95 – 1.79 (m, 2H, -O- CH_2 - CH_2 -), 1.53 – 1.43 (m, 4H, Piperi-3,5- H_2), 1.42 – 1.31 (m, 2H, Piperi-4- H_2).

3-[3-(Piperidin-1-yl)propoxy]benzaldehyde (**4**) (Goldberg and Teitel, 1956)

The synthetic process was analogous to that of compound **3**. Compound **4** was prepared from 3-hydroxybenzaldehyde (2.44 g, 20 mmol), alkyl chloride **2** (3.96 g, 20 mmol), K_2CO_3 (6.00 g, 45 mmol), of KI (0.33 g, 2 mmol) in acetone 100 mL refluxed for 16 h. The product was used without further purification in the next step.

Yield: 41%

Appearance: Slightly brownish viscous liquid



Chemical formula: $\text{C}_{15}\text{H}_{21}\text{NO}_2$

Molecular weight: 247.3 g/mol

APCI-MS (+): m/z : 248.2 $[\text{M}+\text{H}^+]^+$

^1H NMR (300 MHz, DMSO- d^6) δ 9.97 (s, 1H, Ph- $\text{CH}=\text{O}$), 7.53 – 7.48 (m, 2H, Ph-5,6- H), 7.44 – 7.38 (m, 1H, Ph-2- H), 7.29 – 7.23 (m, 1H, Ph-4- H), 4.07 [triplet (t), J = 6.4 Hz, 2H, -O- CH_2 -], 2.41 – 2.26 (m, 6H, overlap: Piperi- CH_2 -, Piperi-2,6- H_2), 1.95 – 1.78 (m, 2H, -O- CH_2 - CH_2 -), 1.53 – 1.44 (m, 4H, Piperi-3,5- H_2), 1.42 – 1.32 (m, 2H, Piperi-4- H_2).

3-Nitro-4-[3-(piperidin-1-yl)propoxy]benzaldehyde (**5**)

Compound **5** was synthesized via an adapted method reported previously (Apelt *et al.*, 2005). NaH (0.6 g, 60% in mineral oil, 15mmol) was suspended in 10 mL of tetrahydrofuran (THF) in a dried Schlenk flask equipped with a septum. Alkyl alcohol **1** (1.58 g, 11 mmol) was dissolved in 20 mL of THF and given via cannula to the suspension of NaH. This mixture was stirred at r.t. for 1 h. 4-Fluoro-3-nitro-benzaldehyde (1.69 g, 10 mmol) was dissolved in 10 mL of THF and was added dropwise to the previously prepared reaction mixture via cannula. The resulting mixture was refluxed for 5 h and followed by quenching and dilution with 40 mL of H_2O at 0 °C. The aqueous solution was extracted with EtOAc three times. The organic layers were

Experiment

combined and washed with brine. After drying with anhydrous MgSO_4 , the organic solvent was removed in the rotary evaporator. The residue was purified with column chromatography, whereby the solvent mixture of DCM and methanol (MeOH) in the ratio of 95:5 and 90:10 was used as eluent.

Yield: 21%

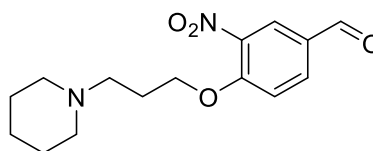
Appearance: Red viscous liquid

Chemical formula: $\text{C}_{15}\text{H}_{20}\text{N}_2\text{O}_4$

Molecular weight: 292.3 g/mol

APCI-MS (+): m/z : 293.2 $[\text{M}+\text{H}^+]^+$

^1H NMR (300 MHz, CDCl_3) δ 9.93 (s, 1H, Ph-CHO), 8.34 (d, $^4J = 2.1$ Hz, 1H, Ph-2-H), 8.06 (dd, $^3,4J = 8.7, 2.1$ Hz, 1H, Ph-6-H), 7.30 – 7.21 (m, 1H, Ph-5-H), 4.32 (t, $J = 6.1$ Hz, 2H, -O- CH_2 -), 2.67 (t, $J = 7.2$ Hz, 2H, Piperi- CH_2 -), 2.57 (s, 4H, Piperi-2,6- H_2), 2.18 (dt, $J = 7.8, 6.3$ Hz, 2H, -O- CH_2 - CH_2 -), 1.69 (p, $J = 5.7$ Hz, 4H, Piperi-3,5- H_2), 1.57 – 1.43 (m, 2H, Piperi-4- H_2).



{4-[3-(Piperidin-1-yl)propoxy]phenyl}methanol (**6**) (Sander *et al.*, 2010b)

Similar to compound **3**, compound **6** was synthesized from 4-hydroxyphenyl ethanol (2.99 g, 12 mmol), alkyl chloride **2** (1.98 g, 10 mmol), K_2CO_3 (4.14 g, 40 mmol), and KI (0.17 g, 1 mmol) in 50 mL of acetone, refluxed for 48 h. The product was used without further purification in the next step.

Yield: 59%

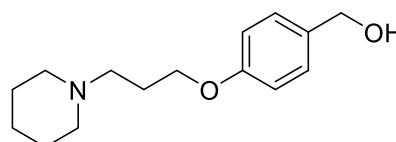
Appearance: Beige solid

Chemical formula: $\text{C}_{15}\text{H}_{23}\text{NO}_2$

Molecular weight: 249.35 g/mol

APCI-MS (+): m/z : 250.2 $[\text{M}+\text{H}^+]^+$

^1H NMR (300 MHz, $\text{DMSO}-d_6$) δ 7.20 (d, $J = 8.6$ Hz, 2H, Ph-2,6-H), 6.86 (d, $J = 8.7$ Hz, 2H, Ph-3,5-H), 5.02 (t, $J = 5.7$ Hz, 1H, -OH), 4.40 (d, $J = 5.5$ Hz, 2H, Ph- CH_2 -), 3.96 (t, $J = 6.4$ Hz,



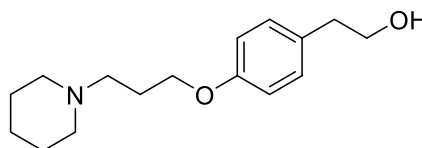
2H, Ph-O-CH₂-), 2.40 – 2.25 (m, 6H, overlap: Piperi-CH₂-, Piperi-2,6-H₂), 1.90 – 1.75 (m, 2H, Piperi-CH₂-CH₂-), 1.48 (p, *J* = 5.4 Hz, 4H, Piperi-3,5-H₂), 1.42 – 1.31 (m, 2H, Piperi-4-H₂).

2-[4-[3-(Piperidin-1-yl)propoxy]phenyl]ethan-1-ol (**7**) (Apelt *et al.*, 2002)

Similar to compound **3**, compound **7** was synthesized from 4-(2-hydroxyethyl)phenol (1.40 g, 10 mmol), alkyl chloride **2** (2.40 g, 12 mmol), K₂CO₃ (6.91 g, 50 mmol), and KI (0.17 g, 1 mmol) in 50 mL of acetone, reflux for 18 h. The product was purified via column chromatography, whereby the solvent mixture of DCM and MeOH in the ratio of 90:10 and 85:15 was used as eluents.

Yield: 76%

Appearance: White solid



Chemical formula: C₁₆H₂₅NO₂

Molecular weight: 263.4 g/mol

APCI-MS (+): *m/z*: 264.3 [M+H]⁺

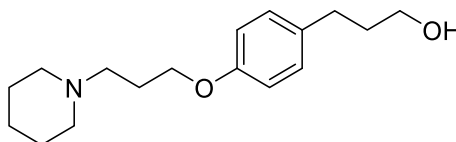
¹H NMR (300 MHz, CDCl₃) δ 7.12 (d, *J* = 8.6 Hz, 2H, Ph-2,6-*H*), 6.83 (d, *J* = 8.6 Hz, 2H, Ph-3,5-*H*), 3.97 (t, *J* = 6.4 Hz, 2H, Ph-O-CH₂-), 3.80 (t, *J* = 6.7 Hz, 2H, Ph-CH₂-CH₂-), 2.79 (t, *J* = 6.6 Hz, 2H, Ph-CH₂-), 2.53 – 2.32 (m, 6H, overlap: Piperi-CH₂-, Piperi-2,6-H₂), 2.03 – 1.91 (m, 2H, Piperi-CH₂-CH₂-), 1.89 (s, 1H, -OH), 1.66 – 1.50 (m, 4H, Piperi-3,5-H₂), 1.50 – 1.36 (m, 2H, Piperi-4-H₂).

3{4-[3-(Piperidin-1-yl)propoxy]phenyl}propan-1-ol (**8**) (Apelt *et al.*, 2002)

Like compound **3**, compound **8** was synthesized from 4-(3-hydroxypropyl)phenol (0.76 g, 5 mmol), alkyl chloride **2** (1.19 g, 6 mmol), K₂CO₃ (2.0 g, 15 mmol), and a catalytic amount of KI in 30 mL of acetone under reflux for 18 h. Compound **8** was purified with column chromatography, whereby the solvent mixture of DCM and MeOH (NH₃) in the ratio of 98:2 and 97:3 was used as eluent.

Yield: quantitative

Appearance: White solid



Chemical formula: $C_{17}H_{27}NO_2$

Molecular weight: 277.4 g/mol

APCI-MS (+): m/z : 278.3 $[M+H]^+$

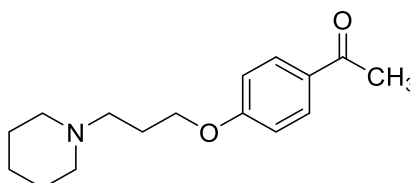
1H NMR (300 MHz, $CDCl_3$) δ 7.09 (d, J = 8.6 Hz, 2H, Ph-2,6- H), 6.82 (d, J = 8.6 Hz, 2H, Ph-3,5- H), 3.98 (t, J = 6.3 Hz, 2H, Ph-O- CH_2 -), 3.66 (td, J = 6.4, 5.2 Hz, 2H, - CH_2 -OH), 2.70 – 2.59 (m, 2H, Ph- CH_2 -), 2.56 – 2.41 (m, 6H, overlap: Piperi- CH_2 -, Piperi-2,6- H_2), 2.08 – 1.93 (m, 2H, Piperi- CH_2 - CH_2 -), 1.93 – 1.78 (m, 2H, Ph- CH_2 - CH_2 -), 1.63 (p, J = 5.6 Hz, 4H, Piperi-3,5- H_2), 1.56 – 1.38 (m, 2H, Piperi-4- H_2).

1-{4-[3-(Piperidin-1-yl)propoxy]phenyl}ethan-1-one (**9**) (Levain *et al.*, 2011)

Compound **9** was prepared analog to compound **3** from 4-Hydroxyacetophenon (1.63 g, 12 mmol), alkyl chloride **2** (1.98 g, 10 mmol), K_2CO_3 (6.91 g, 50 mmol), and KI (0.17 g, 1 mmol) in 50 mL of acetone, heated for 15 h at reflux. The product was used without further purification.

Yield: Quantitative

Appearance: Brown viscous liquid



Chemical formula: $C_{16}H_{23}NO_2$

Molecular weight: 261.4 g/mol

APCI-MS (+): m/z : 262.3 $[M+H]^+$

1H NMR (300 MHz, $CDCl_3$) δ 7.91 (d, J = 8.9 Hz, 2H, Ph-2,6- H), 6.91 (d, J = 8.9 Hz, 2H, Ph-3,5- H), 4.06 (t, J = 6.4 Hz, 2H, -O- CH_2 -), 2.54 (s, 3H, - CH_3), 2.51 – 2.34 (m, 6H, overlap: Piperi- CH_2 -, Piperi-2,6- H_2), 2.06 – 1.89 (m, 2H, -O- CH_2 - CH_2 -), 1.59 (p, J = 5.5 Hz, 4H, Piperi-3,5- H_2), 1.50 – 1.38 (m, 2H, Piperi-4- H_2).

4-[3-(Piperidin-1-yl)propoxy]benzonitrile (**10**) (Sander *et al.*, 2010b)

Similar to compound **3**, compound **10** was synthesized from 4-cyanophenol (2.62 g, 22 mmol), alkyl chloride **2** (3.96 g, 20 mmol), K_2CO_3 (16 g, 119 mmol), and KI (0.70 g, 4.2 mmol) in acetone 100 mL refluxed for 18 h. The product was used in the next step without further purification.

Yield: 93%

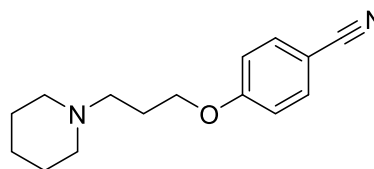
Appearance: Light brownish viscous liquid

Chemical formula: $C_{15}H_{20}N_2O$

Molecular weight: 244.3 g/mol

APCI-MS (+): m/z : 245.2 $[M+H]^+$

1H NMR (300 MHz, $DMSO-d_6$) δ 7.74 (d, $J = 8.9$ Hz, 2H, Ph-2,6-*H*), 7.09 (d, $J = 8.9$ Hz, 2H, Ph-3,5-*H*), 4.07 (t, $J = 6.4$ Hz, 2H, -O- CH_2 -), 2.41 – 2.24 (m, 6H, overlap: Piperi- H_2 , Piperi-2,6- H_2), 1.97 – 1.78 (m, 2H, -O- CH_2-CH_2 -), 1.53 – 1.42 (m, 4H, Piperi-3,5- H_2), 1.41 – 1.31 (m, 2H, Piperi-4- H_2).



Methyl 4-[3-(piperidin-1-yl)propoxy]benzoate (**11**) (Sander *et al.*, 2010c)

Similar to compound **3**, compound **11** was synthesized from methylparaben (0.91 g, 6 mmol), alkyl chloride **2** (0.99 g, 5 mmol), K_2CO_3 (1.34 g, 10 mmol), and a catalytic amount of KI in 30 mL of acetone, heated at 60 °C for 48 h. The product was used without further purification in the next step.

Yield: 94%

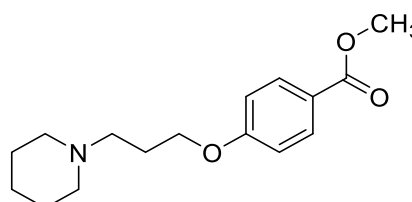
Appearance: Slightly yellow viscous liquid

Chemical formula: $C_{16}H_{23}NO_3$

Molecular weight: 277.4 g/mol

APCI-MS (+): m/z : 278.3 $[M+H]^+$

1H NMR (300 MHz, $CDCl_3$) δ 7.97 (d, $J = 8.9$ Hz, 2H, Ph-2,6-*H*), 6.90 (d, $J = 8.9$ Hz, 2H, Ph-3,5-*H*), 4.06 (t, $J = 6.3$ Hz, 2H, Ph-O- CH_2 -), 3.88 (s, 3H, - CH_3), 2.57 – 2.48 (m, 2H, Piperi- CH_2 -),



2.45 (br, 4H, Piperi-2,6- H_2), 2.10 – 1.95 (m, 2H, -O- CH_2 - CH_2 -), 1.63 (p, J = 5.6 Hz, 4H, Piperi-3,5- H_2), 1.50 – 1.40 (m, 2H, Piperi-4- H_2).

Methyl 2-{4-[3-(piperidin-1-yl)propoxy]phenyl}acetate (**12**) (Bowers *et al.*, 2011)

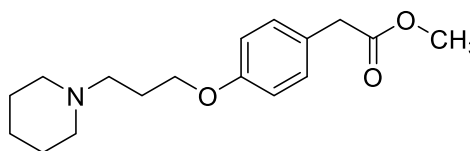
Similar to compound **3**, compound **12** was synthesized from methyl 2-(4-hydroxyphenyl)acetate (1.0 g, 6 mmol), alkyl chloride **2** (0.99 g, 5 mmol), K_2CO_3 (1.34 g, 10 mmol), and a catalytic amount of KI in 30 mL of acetone, heated at 60 °C for 48 h. The product was used without further purification in the next step.

Yield: 79%

Appearance: Slightly yellowish transparent viscous liquid

Chemical formula: $C_{17}H_{25}NO_3$

Molecular weight: 291.4 g/mol



APCI-MS (+): m/z : 292.2 $[M+H]^+$

1H NMR (300 MHz, $CDCl_3$) δ 7.17 (d, J = 8.5 Hz, 2H, Ph-2,6- H), 6.84 (d, J = 8.7 Hz, 2H, Ph-3,5- H), 3.99 (t, J = 6.3 Hz, 2H, Ph-O- CH_2 -), 3.68 (s, 3H, - CH_3), 3.56 (s, 2H, Ph- CH_2 -), 2.57 – 2.38 (m, 6H, overlap: Piperi- CH_2 -, Piperi-2,6- H_2), 2.08 – 1.92 (m, 2H, -O- CH_2 - CH_2 -), 1.63 (p, J = 5.6 Hz, 4H, Piperi-3,5- H_2), 1.52 – 1.38 (m, 2H, Piperi-4- H_2).

{4-[3-(Piperidin-1-yl)propoxy]phenyl}methanamine (**13**) (Sander *et al.*, 2010c)

Preparation of Raney-Nickel: 1.0 g of Nickel-Aluminium alloy was treated with 80 mL of 10% NaOH solution (aq. m/V), the mixture was heated at 90 °C for 60 min, and the colorless solution was decanted. The black-colored nickel particles were washed with H_2O . The wash process was repeated until the pH value of the wash water was neutral. The nickel particles were subsequently washed three times with 20 mL of MeOH to remove the rest of the water and transferred cautiously to an autoclave tube.

Reduction with Raney-Nickel: The cyano-derivative **10** (4.5 g, 18.5 mmol) was dissolved in MeOH (NH_3) 100 mL, and this solution was given to the activated nickel particles. The reaction was stirred under 5 bar of hydrogen and heated at 40 °C. After 18 h, the gas pressure was released cautiously, the suspension of the reaction was filtered through kieselgur. The filter

cake was rinsed three times with 20 mL of MeOH. The filtrate was collected and evaporated to dryness. The product was sufficiently pure to use in the following steps without further purification.

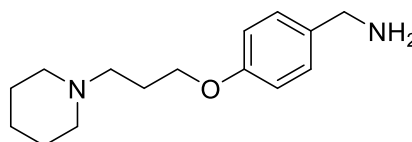
Deactivation and disposal of Raney-Nickel waste: The filter cake, which contains the flammable nickel particles, was stirred in 20 mL of HCl (37%, aq.) for 4 h. According to the local rule, the resulting suspension was filtered, declared as a heavy metal-containing acidic aqueous solution, and discarded via the chemical storage center of HHU.

Yield: 81%

Appearance: Slightly yellowish transparent viscous liquid

Chemical formula: C₁₅H₂₄N₂O

Molecular weight: 248.4 g/mol



APCI-MS (+): m/z: 249.2 [M+H]⁺

¹H NMR (300 MHz, CDCl₃) δ 7.20 (d, *J* = 8.1 Hz, 2H, Ph-2,6-*H*), 6.86 (d, *J* = 8.0 Hz, 2H, Ph-3,5-*H*), 3.99 (t, *J* = 6.4 Hz, 2H, -O-CH₂-), 3.82 (s, 2H, Ph-CH₂-), 2.55 – 2.32 (m, 6H, overlap: Piperi-CH₂-, Piperi-2,6-*H*₂), 1.97 (p, *J* = 6.6 Hz, 2H, -O-CH₂-CH₂-), 1.78 (br, 2H, -NH₂), 1.60 (p, *J* = 5.6 Hz, 4H, Piperi-3,5-*H*₂), 1.50 – 1.37 (m, 2H, Piperi-4-*H*₂).

tert-Butyl {4-[3-(piperidin-1-yl)propoxy]phenethyl}carbamate (**14**)

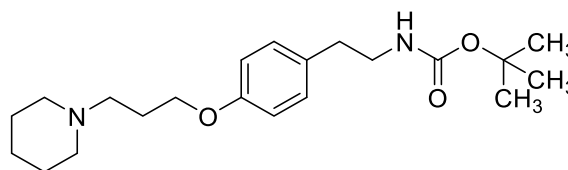
Compound **14** was prepared via an adapted method described previously (Upadhyaya *et al.*, 2007): Tyramine hydrochloride (0.87 g, 5 mmol) was suspended in 15 mL of DCM, triethylamine (TEA) (0.69 mL, 5 mmol), di-*tert*-butyl dicarbonate (1.17 mL, 5.5 mmol), and a catalytic amount of amidosulfonic acid was given, the mixture was sonicated in ultrasonic cleaner at power level 9 for 15 min. The solvent was removed in a rotary evaporator. The residue was directly used in ether synthesis by applying the method for preparing compound **3** with alkyl chloride **2** (1.08 g, 5.5 mmol), K₂CO₃ (1.34 g, 10 mmol), and a catalytic amount of KI in 50 mL of acetone. The reaction was refluxed for 18 h. The product was purified with column chromatography, whereby the solvent mixture of DCM and MeOH in a ratio of 95:5 was used as the eluent.

Experiment

Yield: 66%

Appearance: Beige solid

Chemical formula: $C_{21}H_{34}N_2O_3$



Molecular weight: 362.5 g/mol

APCI-MS (+): m/z : 363.4 $[M+H]^+$

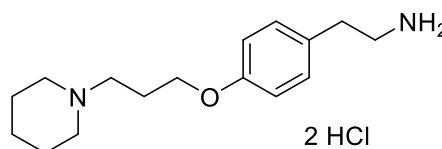
1H NMR (300 MHz, $CDCl_3$) δ 7.08 (d, J = 8.5 Hz, 2H, Ph-2,6- H), 6.83 (d, J = 8.6 Hz, 2H, Ph-3,5- H), 4.53 (s, 1H, -NH-), 3.98 (t, J = 6.3 Hz, 2H, -O- CH_2 - CH_2 -), 3.33 (q, J = 6.8 Hz, 2H, - CH_2 -NH-), 2.72 (t, J = 7.0 Hz, 2H, Ph- CH_2 -), 2.55 – 2.38 (m, 6H, overlap: Piperi- CH_2 -, Piperi-2,6- H_2), 2.06 – 1.90 (m, 2H, -O- CH_2 - CH_2 -), 1.61 (p, J = 5.5 Hz, 4H, Piperi-3,5- H_2), 1.50 – 1.35 (m, 11H, overlap: Piperi-4- H_2 -, - CH_3).

2-{4-[3-(Piperidin-1-yl)propoxy]phenyl}ethan-1-amine dihydrochloride (**15**)

The *Boc*-protected tyramine derivative **14** (1.2 g, 3.3 mmol) was dissolved in 20 mL of HCl in dioxane. The solution was stirred at r.t. for 18 h. Upon completion of the reaction monitored via TLC, the solvent was removed in a rotary evaporator. The residue was washed with acetone. The product was used without further purification.

Yield: 52%

Appearance: White solid



Chemical formula: $C_{16}H_{26}N_2O \times 2HCl$

Molecular weight: 335.3 g/mol

APCI-MS (+): m/z : 263.2 $[M+H]^+$

1H NMR (300 MHz, $DMSO-d_6$) δ 10.81 (s, 1H, Piperi- N^+H), 8.18 (s, 3H, - CH_2 - N^+H_3), 7.18 (d, J = 8.6 Hz, 2H, Ph-2,6- H), 6.90 (d, J = 8.6 Hz, 2H, Ph-3,5- H), 4.02 (t, J = 6.1 Hz, 2H, -O- CH_2 -), 3.41 (d, J = 13.2 Hz, 2H, Piperi-2,6- H_{eq}), 3.19 – 3.07 (m, 2H, Piperi- CH_2 -), 3.03 – 2.90 (m, 2H, Ph- CH_2 - CH_2 -), 2.89 – 2.76 (m, 4H, overlap: Piperi-2,6- H_{ax} , Ph- CH_2 -), 2.27 – 2.11 (m, 2H, -O- CH_2 - CH_2 -), 1.96 – 1.63 (m, 5H, overlap: Piperi-3,5- H_2 , Piperi-4- H_{eq}), 1.48 – 1.27 (m, 1H, Piperi-4- H_{ax}).

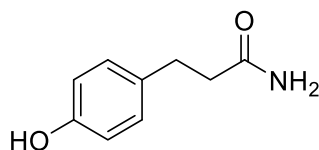
3-(4-Hydroxyphenyl)propanamide (16) (Eliahu, 2004)

Compound **16** was synthesized according to the method reported by Eliahu et al. 4-Hydroxypropionic acid (1.66 g, 10 mmol) was suspended in 30 mL of cyclohexane, the mixture was cooled in an ice-water bath and stirred vigorously while excessive thionyl chloride (3 mL, 41.3 mmol) was given dropwise. The reaction was heated in an oil bath at 80 °C for 18 h. The solvent inclusive excessive thionyl chloride was removed subsequently by vacuum distillation equipped with a wash bottle filled with NaHCO₃ solution between condenser and pump. The residue was treated with toluene, and the solution was removed by vacuum evaporation in a rotary evaporator. The prepared acid chloride was dissolved in 30 mL of MeCN and given dropwise to 20 mL of NH₃ in MeOH. The reaction was stirred at r.t. for 4 h. After completion of the reaction monitored via TLC, the solvent was removed in a rotary evaporator. The residue was purified via column chromatography. EtOAc was used as the eluent.

Yield: 56%

Appearance: White solid

Chemical formula: C₉H₁₁NO₂



Molecular weight: 165.2 g/mol

APCI-MS (+): m/z: 166.0 [M+H]⁺

¹H NMR (300 MHz, DMSO-*d*⁶) δ 9.12 (s, 1H, -OH), 7.24 (s, 1H, -CO-NH), 6.98 (d, *J* = 8.4 Hz, 2H, Ph-2,6-*H*), 6.72 (s, 1H, -CO-NH'), 6.64 (d, *J* = 8.5 Hz, 2H, Ph-3,5-*H*), 2.73 – 2.61 (m, 2H, Ph-CH₂-CH₂-), 2.33 – 2.21 (m, 2H, Ph-CH₂-CH₂-).

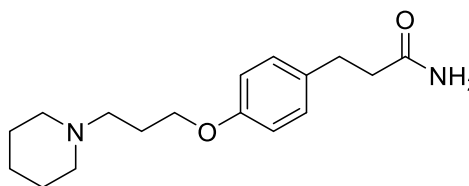
3-{4-[3-(Piperidin-1-yl)propoxy]phenyl}propanamide (17)

Analogous to compound **3**, compound **17** was synthesized from the phenol derivative **16** (0.47 g, 2.8 mmol), alkyl chloride **2** (0.59 g, 3.0 mmol), K₂CO₃ (0.81 g, 6 mmol), a catalytic amount of KI, acetone 20 mL, refluxed for 18 h. The product was purified with column chromatography, whereby a solvent mixture of DCM and MeOH in a ratio of 90:10 was used as an eluent.

Yield: 48%

Appearance: White solid

Chemical formula: $C_{17}H_{26}N_2O_2$



Molecular weight: 290.4 g/mol

APCI-MS (+): m/z : 291.2 $[M+H]^+$

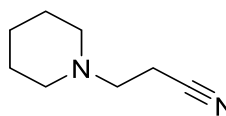
1H NMR (300 MHz, $CDCl_3$) δ 7.10 (d, J = 8.6 Hz, 2H, Ph-2,6- H), 6.81 (d, J = 8.6 Hz, 2H, Ph-3,5- H), 5.47 (d, J = 20.5 Hz, 2H, -CO-NH₂), 3.96 (t, J = 6.4 Hz, 2H, -O-CH₂-), 2.95 – 2.83 (m, 2H, Ph-CH₂-CH₂-), 2.59 – 2.29 (m, 8H, overlap: Ph-CH₂-CH₂-, Piperi-CH₂-, Piperi-2,6- H_2), 2.04 – 1.89 (m, 2H, -O-CH₂-CH₂-), 1.60 (p, J = 5.6 Hz, 4H, Piperi-3,5- H_2), 1.50 – 1.36 (m, 2H, Piperi-4- H_2).

3-(Piperidin-1-yl)propanenitrile (**19**) (Amon *et al.*, 2006)

The synthesis was carried out analogous to the method described by Amon and colleagues: piperidine (10 mL, 100 mmol), 3-bromopropanenitrile (6.5 mL, 78 mmol), and K_2CO_3 (13.8 g, 100 mmol) were stirred in 90 mL of acetone in r.t. for 48 h. The suspension was filtered, the volume of the filtrate was reduced in rotary evaporation to about 20 mL. The product was obtained by vacuum distillation.

Yield: 92%

Appearance: Brownish liquid



Chemical formula: $C_8H_{14}N_2$

Molecular weight: 138.2 g/mol

APCI-MS (+): m/z : 139.3 $[M+H]^+$

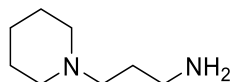
1H NMR (300 MHz, $DMSO-d_6$) δ 2.70 – 2.59 (m, 2H, -CH₂-CN), 2.58 – 2.46 (m, 2H, Piperi-CH₂-), 2.36 (t, J = 5.2 Hz, 4H, Piperi-2,6- H_2), 1.56 – 1.43 (m, 4H, Piperi-3,5- H_2), 1.43 – 1.34 (m, 2H, Piperi-4- H_2).

3-(Piperidin-1-yl)propan-1-amine (**20**) (Amon *et al.*, 2006)

The primary amine **20** was obtained similar to the process to prepare compound **13** via Raney-Nickel catalyzed hydrogenation. 2 g Ni-Al-alloy was activated by 120 mL of 10% NaOH solution. The compound **19** (9.89 g, 78.2 mmol) was hydrogenated under 5 bar of H₂ in 50 mL of MeOH and 50 mL of NH₃ (MeOH) at 40 °C for 24 h. The product was used without further purification in the following steps.

Yield: Quantitative

Appearance: Brownish liquid



Chemical formula: C₈H₁₈N₂

Molecular weight: 142.3 g/mol

APCI-MS (+): m/z: 143.2 [M+H]⁺

¹H NMR (300 MHz, CDCl₃) δ 2.70 (t, *J* = 6.8 Hz, 2H, NH₂-CH₂-), 2.43 – 2.19 (m, 6H, overlap: Piperi-CH₂-, Piperi-2,6-H₂), 1.71 – 1.48 (m, 8H, overlap: NH₂-CH₂-CH₂-, Piperi-3,5-H₂), 1.46 – 1.33 (m, 2H, Piperi-4-H₂).

3-{4-[3-(Piperidin-1-yl)propoxy]phenyl}propanal (**22**)

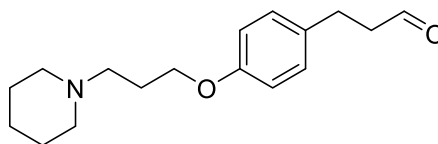
Aldehyde **22** was prepared via Swern oxidation: To a moisture-free Schlenk flask, which was filled with argon and equipped with magnet bar and silicon septum, 0.75 mL of oxalyl chloride in 12 mL of DCM was given via a cannula. The reaction was cooled to -60 °C with an immersion cooler. 1.3 mL of DMSO in 3 mL of DCM was given dropwise through a cannula, and the reaction was kept at -60 °C for 1 h. A solution of alcohol **8** (1.4 g, 5 mmol) in 5 mL of DCM was added to the reaction mixture via cannula dropwise over 2 min. The mixture was kept at -60 °C for another 2 h, and 5.3 mL of TEA in 4 mL of DCM was given dropwise. The reaction was kept at -60 °C for a further 30 min and then allowed to warm up to r.t. and diluted with 50 mL of DCM. The reaction mixture was washed with 20 mL of sat. NaHCO₃ and 20 mL of brine, respectively. The obtained product was purified by column chromatography. Solvent mixtures of DCM and MeOH in ratios 95:5 and 90:10 were used as the eluents.

Yield: 88%

Appearance: Yellowish viscous liquid

Chemical formula: C₁₇H₂₅NO₂

Molecular weight: 275.4 g/mol



APCI-MS (+): m/z: 276.3 [M+H]⁺

¹H NMR (300 MHz, CDCl₃) δ 9.80 (t, *J* = 1.5 Hz, 1H, -CHO), 7.08 (d, *J* = 8.8 Hz, 2H, Ph-2,6-*H*), 6.81 (d, *J* = 8.7 Hz, 2H, Ph-3,5-*H*), 3.97 (t, *J* = 6.3 Hz, 2H, -O-CH₂-), 2.89 (t, *J* = 7.2 Hz, 2H, Ph-CH₂-), 2.78 – 2.68 (m, 2H, Ph-CH₂-CH₂-), 2.54 – 2.39 (m, 6H, overlap: Piperi-CH₂-, Piperi-2,6-*H*₂), 2.07 – 1.91 (m, 2H, -O-CH₂-CH₂-), 1.62 (p, *J* = 5.6 Hz, 4H, Piperi-3,5-*H*₂), 1.51 – 1.42 (m, 2H, Piperi-4-*H*₂).

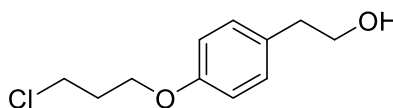
2-[4-(3-Chloropropoxy)phenyl]ethanol (**23**) (Tao *et al.*, 2012)

Analogous to compound **3**, compound **23** was synthesized from tyrosol (1.40 g, 10 mmol), 1-bromo-3-chloropropane (1.5 mL, 15 mmol), and K₂CO₃ (3 g, 22 mmol). The suspension was heated in 60 mL of acetone at reflux temperature for 100 h. After the workup, the excessive 1-bromo-3-chloropropane was removed via the high vacuum pump. The residue was used without further purification.

Yield: Quantitative

Appearance: Wax-like white solid

Chemical formula: C₁₁H₁₅ClO₂



Molecular weight: 214.7 g/mol

APCI-MS (+): m/z: 215.5 [M+H]⁺

¹H NMR (300 MHz, CDCl₃) δ 7.15 (d, *J* = 8.7 Hz, 2H, Ph-2,6-*H*), 6.86 (d, *J* = 8.6 Hz, 2H, Ph-3,5-*H*), 4.10 (t, *J* = 5.8 Hz, 2H, Ph-O-CH₂-), 3.83 (t, *J* = 6.5 Hz, 2H, -CH₂-OH), 3.75 (t, *J* = 6.4 Hz, 2H, Cl-CH₂-), 2.81 (t, *J* = 6.5 Hz, 2H, Ph-CH₂-), 2.30 – 2.15 (m, 2H, Cl-CH₂-CH₂-), 1.47 (s, 1H, -OH).

2-[4-(3-Chloropropoxy)phenyl]acetaldehyde (**24**) (Tao *et al.*, 2011)

The synthesis of compound **24** was performed according to the method reported previously by Tao *et al.* A solution of **23** (0.43 g, 2 mmol) in 5 mL DCM was added dropwise to a suspension

of Dess-Martin periodinane (1.02 g, 2.4 mmol) in 10 mL DCM at 0 °C. The mixture was stirred for 1 h at r.t. and followed by dilution with 50 mL of EtOEt. This solution was washed with one portion of 50 mL of 1 N NaOH(aq.) and three times 50 mL of H₂O and once 50 mL of brine, consecutively. The product was further purified via flash column chromatography. Gradients from *n*-hexane and EtOAc in the ratio of 2:1 to 1:2 were used as the mobile phase.

Yield: 55%

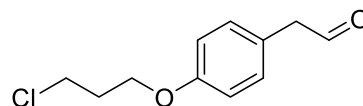
Appearance: Colorless liquid

Chemical formula: C₁₁H₁₃ClO₂

Molecular weight: 212.7 g/mol

APCI-MS (+): m/z: 213.5 [M+H]⁺

¹H NMR (300 MHz, CDCl₃) δ 9.72 (t, *J* = 2.4 Hz, 1H, -CHO), 7.13 (d, *J* = 8.6 Hz, 2H, Ph-2,6-*H*), 6.91 (d, *J* = 8.6 Hz, 2H, Ph-3,5-*H*), 4.12 (t, *J* = 5.8 Hz, 2H, Ph-O-CH₂-), 3.75 (t, *J* = 6.3 Hz, 2H, Cl-CH₂-), 3.63 (d, *J* = 2.4 Hz, 2H, Ph-CH₂-), 2.24 (p, *J* = 6.1 Hz, 2H, Cl-CH₂-CH₂-).



4-[3-(Piperidin-1-yl)propoxy]benzoic acid hydrochloride (**25**) (Tomasch *et al.*, 2013)

The hydrolysis procedure of carboxylic ester has been employed according to the description by Collman and co-workers (Collman *et al.*, 2006). The methyl ester **11** (1.31 g, 4.7 mmol) and NaOH (1.50 g, 37.5 mmol) were dissolved in a solvent mixture of 20 mL of MeOH and 10 mL of H₂O. The reaction was stirred at r.t. for 20 h, and the pH was adjusted to approximately 1 with conc. HCl. After removing the solvent in the rotary evaporator. The residue was treated in EtOH and filtered. The filtrate was cooled and crystallized from a solvent mixture from EtOH and EtOEt.

Yield: Quantitative

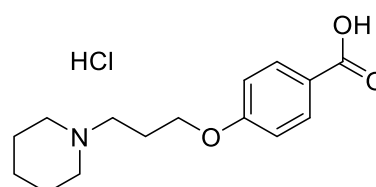
Appearance: White solid

Chemical formula: C₁₅H₂₁NO₃ × HCl

Molecular weight: 299.8 g/mol

APCI-MS (+): m/z: 264.1 [M+H]⁺

¹H NMR (300 MHz, DMSO-*d*⁶) δ 12.65 (s, 1H, -CO-OH), 10.45 (s, 1H, Piperi-N⁺H), 7.89 (d, *J* = 8.9 Hz, 2H, Ph-2,6-*H*), 7.02 (d, *J* = 8.9 Hz, 2H, Ph-3,5-*H*), 4.14 (t, *J* = 6.1 Hz, 2H, -O-CH₂-),



3.43 (br, 2H, Piperi-2,6- H_{eq}), 3.21 – 3.10 (m, 2H, Piperi- CH_2 -), 2.87 (br, 2H, Piperi-2,6- H_{ax}), 2.29 – 2.14 (m, 2H, -O- CH_2 - CH_2 -), 1.88 – 1.60 (m, 5H, overlap: Piperi-3,5- H_2 , Piperi-4- H_{eq}), 1.39 (br, 1H, Piperi-4- H_{ax}).

4-(4-Methylpiperazine-1-carbonyl)benzaldehyde (**26**) (Koroleva *et al.*, 2011)

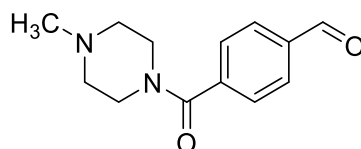
Compound **26** was synthesized analogous to the method reported by Koroleva and colleagues. 4-Formylbenzoic acid (1.0 g, 6.47 mmol) was suspended in 30 mL of toluene. Thionyl chloride (2 mL, 27 mmol) was added to the mixture dropwise at 0 °C. The reaction mixture was subsequently heated for 10 h at 60 °C. The solvent and excess thionyl chloride were removed via vacuum distillation with subsequent co-evaporation with toluene. The prepared acid chloride was dissolved in 10 mL of DCM and given to a solution of *N*-methylpiperazine (1 mL, 10 mmol) and pyridine (1 mL, 12 mmol) in 10 mL of DCM. The reaction was stirred at ambient temperature for 2 hours. Upon completing the reaction monitored via TLC, the solution was diluted with 20 mL of DCM and washed twice with 30 mL of sat. NaHCO_3 solution. The organic layer was collected and dried with anhydrous MgSO_4 . After removing the solvent in a rotary evaporator, the product was obtained as a brownish viscous liquid (1.15 g, 4.95 mmol), which was used in the next step without further purification.

Yield: 76.5%

Appearance: Brownish viscous liquid

Chemical formula: $\text{C}_{13}\text{H}_{16}\text{N}_2\text{O}_2$

Molecular weight: 232.3 g/mol



ESI-MS (+): m/z : 233.2 $[\text{M}+\text{H}]^+$

^1H NMR (300 MHz, CDCl_3) δ 9.98 (s, 1H, Ph- $\text{CH}=\text{O}$), 7.87 (d, J = 8.3 Hz, 2H, Ph-3,5- H), 7.49 (d, J = 8.2 Hz, 2H, Ph-2,6- H), 3.75 [br, 2H, 4-Me-piperazine (Pipera)-2,6- H_{eq}], 3.33 (br, 2H, Pipera-2,6- H_{ax}), 2.43 (br, 2H, Pipera-3,5- H_{eq}), 2.35 – 2.22 (m, 5H, overlap: Pipera-3,5- H_{ax} , - CH_3).

4-[(4-Methylpiperazin-1-yl)sulfonyl]phenol (**27**)

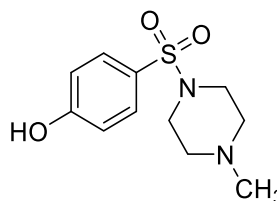
Sodium 4-hydroxybenzenesulfonate dihydrate (2.5 g, 10.7 mmol) was treated with 25 mL of toluene, and the suspension was heated to reflux for 2 h with a Dean-Stark apparatus to remove

the crystal water. Toluene was removed in a rotary evaporator. The residue was treated with 7 mL of thionyl chloride at 0 °C, and 0.2 mL of DMF was given as a catalyst. The reaction mixture was heated at 60 °C for 4 h. The solvent and excess thionyl chloride were removed via vacuum distillation with subsequent co-evaporation with toluene. The prepared acid chloride was suspended in 20 mL of MeCN and given to a solution of pyridine (2 mL, 24 mmol) and *N*-methylpiperazine (2 mL, 20 mmol) in 40 mL of MeCN. The reaction was stirred for 18 h at r.t. The solvent was removed in a rotary evaporator, and the residue was purified with column chromatography. Solvent mixtures of DCM and MeOH in ratios of 95:5 and 90:10 were used as eluents.

Yield: 4%

Appearance: White solid

Chemical formula: C₁₁H₁₆N₂O₃S



Molecular weight: 256.3 g/mol

APCI-MS (+): m/z: 257.1 [M+H]⁺

¹H NMR (300 MHz, DMSO-*d*⁶) δ 10.53 (s, 1H, Ph-OH), 7.54 (d, *J* = 8.8 Hz, 2H, Ph-3,5-*H*), 6.95 (d, *J* = 8.8 Hz, 2H, Ph-2,6-*H*), 2.82 (t, *J* = 4.9 Hz, 4H, Pipera-2,6-*H*₂), 2.34 (t, *J* = 4.9 Hz, 4H, Pipera-3,5-*H*₂), 2.13 (s, 3H, -CH₃).

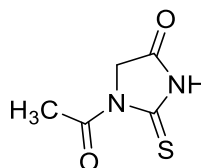
1-Acetyl-2-thioxoimidazolidin-4-one (**28**) (Johnson and Nicolet, 1911)

Compound **28** was synthesized according to the method reported previously: NH₄SCN (3.15 g, 41.4 mmol) and glycine (3.0 g, 39.9 mmol) were suspended in 22.5 mL of Ac₂O, the mixture was heated at 100 °C for 1 h. After cooling down, the suspension was poured into ca. 60 mL of ice water and kept at 4 °C overnight. The yellow precipitate was collected by filtration. The mother liquid was kept at 4 °C for another night and yield a second harvest.

Yield: 70%

Appearance: Yellow solid

Chemical formula: C₅H₆N₂O₂S



Molecular weight: 158.2 g/mol

APCI-MS (+): m/z: 159.1 [M+H]⁺

^1H NMR (300 MHz, DMSO- d^6) δ 12.57 (br, 1H, NH), 4.40 (s, 2H, $-\text{CH}_2-$), 2.67 (s, 3H, $-\text{CH}_3$).

(Z)-5-{3-[3-(Piperidin-1-yl)propoxy]benzylidene}-2-thioxoimidazolidin-4-one (**29**)

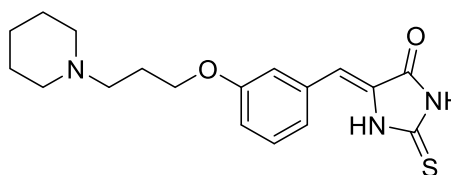
The synthesis process was performed adapted to the method described previously (Mendgen *et al.*, 2012). Aldehyde **4** (0.25 g, 1 mmol), the thiohydantoin derivative **28** (0.16 g, 1 mmol), and NaOAc (0.08 g, 1 mmol) were suspended in 1 mL of AcOH. The mixture was heated at 125 °C for 6 h. Upon completion of the reaction monitored via TLC, the mixture was poured into 10 mL of ice-water, neutralized with 6 N NaOH solution under vigorously stirring to about $\text{pH} = 8$. The aqueous layer was extracted with 20 mL of EtOAc at least three times until no notable amount of product remained in the aqueous phase. The combined organic layers were dried with anhydrous MgSO_4 , and the solvent was removed in a rotary evaporator. The residue was purified via column chromatography. Solvent mixtures of DCM and MeOH in ratios of 95:5 and 90:10 were used as the eluents.

Yield: 50%

Appearance: Yellow solid

Chemical formula: $\text{C}_{18}\text{H}_{23}\text{N}_3\text{O}_2\text{S}$

Molecular weight: 345.5 g/mol



APCI-MS (+): m/z : 346.3 $[\text{M}+\text{H}^+]^+$

^1H NMR (300 MHz, CDCl_3) δ 7.25 (t, $J = 8.0$ Hz, 1H, Ph-5- H), 7.08 (t, $^4J = 2.0$ Hz, 1H, Ph-2- H), 6.89 – 6.77 (m, 2H, overlap: Ph-4,6- H), 6.56 (br, 2H, NH), 6.40 (s, 1H, Ph- $\text{CH}=\text{C}$), 4.05 (t, $J = 5.7$ Hz, 2H, $-\text{O}-\text{CH}_2-$), 2.90 (t, $J = 7.1$ Hz, 2H, Piperi- CH_2-), 2.84 – 2.78 (m, 4H, Piperi-2,6- H_2), 2.16 – 2.01 (m, 2H, $-\text{O}-\text{CH}_2-\text{CH}_2-$), 1.80 (p, $J = 5.5$ Hz, 4H, Piperi-3,5- H_2), 1.58 – 1.48 (m, 2H, Piperi-4- H_2).

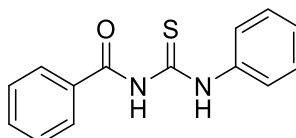
3-Benzoyl-1-phenylthiourea (**30**) (Singh *et al.*, 2011)

The compound **30** was synthesized according to the method published by Singh *et al.*: NH_4SCN (0.91 g, 12 mmol) was dissolved in 15 mL of acetone, benzoyl chloride (1.16 mL, 10 mmol) was added dropwise to the solution to form a white suspension. The suspension was heated at reflux for 30 min, and the color of the suspension turned yellow. The suspension was

allowed to be cool down to ambient temperature. Aniline (1.09 mL, 12 mmol) was given dropwise, and the mixture was stirred at r.t. for a further 2 h. The reaction mixture was poured into ice-water, resulting in white precipitates and yellow solution. The suspension was filtrated. The filter cake was rinsed with cold water and dried in a rotary evaporator. The product was used without further purification in the next step.

Yield: Quantitative

Appearance: White solid



Chemical formula: C₁₄H₁₂N₂OS

Molecular weight: 256.3 g/mol

APCI-MS (+): m/z: 257.2 [M+H]⁺

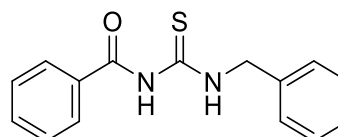
¹H NMR (300 MHz, DMSO-*d*⁶) δ 12.61 (s, 1H, Ph-NH-), 11.56 (s, 1H, -CO-NH-), 8.04 – 7.88 (m, 2H, benzoyl-2,6-*H*), 7.74 – 7.60 (m, 3H, overlap: Ph-2,6-*H*, benzoyl-4-*H*), 7.59 – 7.50 (m, 2H, benzoyl-3,5-*H*), 7.48 – 7.38 (m, 2H, Ph-3,5-*H*), 7.33 – 7.22 (m, 1H, Ph-4-*H*).

3-Benzoyl-1-benzylthiourea (**31**)

Similar to compound **30**, compound **31** was synthesized from NH₄SCN (1.82 g, 24 mmol), benzoyl chloride (2.32 mL, 20 mmol), and benzylamine (2.20 mL, 24 mmol). The product was used without further purification in the next step.

Yield: 71%

Appearance: White solid



Chemical formula: C₁₅H₁₄N₂OS

Molecular weight: 270.4 g/mol

APCI-MS (+): 271.2 [M+H]⁺

¹H NMR (300 MHz, DMSO-*d*⁶) δ 11.41 (s, 1H, -CO-NH-), 11.23 (t, *J* = 5.7 Hz, 1H, Ph-CH₂-NH-), 7.99 – 7.85 (m, 2H, benzoyl-2,6-*H*), 7.69 – 7.58 (m, 1H, benzoyl-4-*H*), 7.57 – 7.44 (m, 2H, benzoyl-3,5-*H*), 7.44 – 7.23 (m, 5H, Ph-2,3,4,5,6-*H*), 4.88 (d, *J* = 5.6 Hz, 2H, Ph-CH₂-).

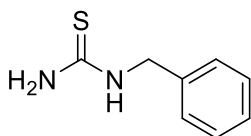
1-Benzylthiourea (**32**) (Thanigaimalai *et al.*, 2010)

Compound **32** was obtained by treating *N*-benzoyl thiourea derivative **31** (1.10 g, 4.07 mmol) with NaOH (50 mL, 4 N, aq.). The mixture was heated at 90 °C for 1 h. The solution was allowed to cool down and poured into crushed ice. White precipitate emerged was collected by filtration. The product was used without further purification in the following steps.

Yield: 87%

Appearance: White solid

Chemical formula: C₈H₁₀N₂S



Molecular weight: 166.2 g/mol

APCI-MS (+): 167.1 [M+H]⁺

¹H NMR (300 MHz, DMSO-*d*⁶) δ 7.98 (br, 1H, -NH-), 7.39 – 7.19 (m, 5H, Ph-2,3,4,5,6-H), 7.07 (br, 2H, -NH₂), 4.62 (s, 2H, Ph-CH₂-).

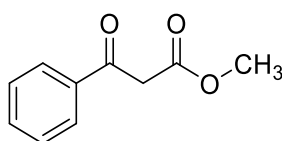
Methyl 3-oxo-3-phenylpropanoate (**33**) (Borowiecki and Bretner, 2013)

The synthesis was carried out according to the procedure reported by Borowiecki and Bretner: Acetophenone (2.40 g, 20 mmol), dimethyl carbonate (5 mL, 59 mmol), and sodium hydride (3.21 g, 80 mmol) were heated in toluene (100 mL) at refluxing temperature for 20 h. The pH value was subsequently adjusted to about 2-3 with conc. HCl (aq.) at 0 °C. The mixture was diluted with EtOAc. The organic layer was separated, and the aqueous layer was extracted twice with 50 mL of EtOAc. The organic layers were combined and dried with anhydrous MgSO₄. The product was obtained by vacuum distillation.

Yield: 67%

Appearance: Colorless transparent liquid

Chemical formula: C₁₀H₁₀O₃



Molecular weight: 178.2 g/mol

APCI-MS (+): 179.0 [M+H]⁺

¹H NMR (300 MHz, DMSO-*d*⁶) δ 8.01 – 7.82 (m, 2H, Ph-2,6-*H*), 7.74 – 7.62 (m, 1H, Ph-4-*H*), 7.61 – 7.47 (m, 2H, Ph-3,5-*H*), 4.22 (s, 2H, -CH₂-), 3.65 (s, 3H, -CH₃).

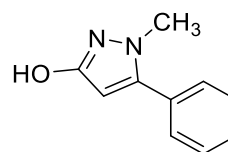
1-Methyl-5-phenyl-1*H*-pyrazol-3-ol (**34**) (Zimmermann *et al.*, 1998)

The synthesis proceeded according to the method reported previously (Yan *et al.*, 2016). A solution of the β-ketoester **33** (0.45 g, 2.5 mmol) in 5 mL of EtOH was given to methylhydrazine (0.26 mL, 5 mmol) at 0 °C. The mixture was heated at reflux for 150 min. The solvent of the reaction was removed in a rotary evaporator. The residue was recrystallized in a mixed solvent of EtOAc and *n*-hexane.

Yield: 25%

Appearance: White solid

Chemical formula: C₁₀H₁₀N₂O



Molecular weight: 174.2 g/mol

APCI-MS (+): 175.1 [M+H]⁺

¹H NMR (300 MHz, DMSO-*d*⁶) δ 9.66 (s, 1H, -OH), 7.53 – 7.35 (m, 5H, Ph-2,3,4,5,6-*H*), 5.61 (s, 1H, -CH=), 3.61 (s, 3H, -CH₃).

4-Hydroxy-4-{4-[3-(piperidin-1-yl)propoxy]phenyl}but-3-en-2-one (**35**) (Hudkins *et al.*, 2008)

Compound **35** was synthesized according to the method reported by Hudkins and colleagues. A solution of acetophenone **9** (4.6 g, 17.6 mmol) and 18-crown-6-ether (100 mg, 0.38 mmol) in 30 mL of THF was given to a suspension of NaH (1.41 g, 60% in mineral oil, 35 mmol) and ethyl acetate (3.1 g, 35 mmol) in 30 mL of THF at ambient temperature. The reaction mixture was heated at reflux. After about 90 min, 20 mL of THF was given to reduce the reaction mixture's viscosity. After 3 h, the mixture was allowed to cool down to r.t. and diluted with 60 mL of H₂O, neutralized with 2 M HCl, buffered with 40 mL of sat. NaHCO₃ and extracted three times with 50 mL EtOAc. The combined organic layer was dried with anhydrous MgSO₄ and concentrated in a rotary evaporator. The residue was purified via column chromatography,

where the solvent mixture of DCM and MeOH in ratios of 95:5 and 90:10 were used as eluents. NMR-spectrum suggested that enol tautomer was dominating.

Yield: 82%

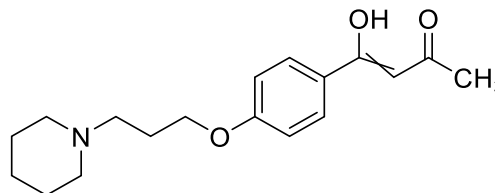
Appearance: Beige solid

Chemical formula: C₁₈H₂₅NO₃

Molecular weight: 303.4 g/mol

APCI-MS (+): m/z: 304.2 [M+H]⁺

¹H NMR (300 MHz, CDCl₃) δ 16.30 (s, 1H, -OH), 7.84 (d, *J* = 8.9 Hz, 2H, Ph-2,6-*H*), 6.93 (d, *J* = 8.8 Hz, 2H, Ph-3,5-*H*), 6.10 (s, 1H, -CO-CH=C), 4.06 (t, *J* = 6.4 Hz, 2H, -O-CH₂-), 2.53 – 2.44 (m, 2H, Piperi-CH₂-), 2.44 – 2.33 (m, 4H, Piperi-2,6-*H*₂), 2.16 (s, 3H, -CH₃), 2.07 – 1.89 (m, 2H, -O-CH₂-CH₂-), 1.60 (p, *J* = 5.6 Hz, 4H, Piperi-3,5-*H*₂), 1.51 – 1.39 (m, 2H, Piperi-4-*H*₂).



3-Imino-1-{4-[3-(piperidin-1-yl)propoxy]phenyl}but-1-en-1-ol (**36**)

Compound **36** was synthesized via a method adapted from a previous report (Sugiura *et al.*, 2009). The β-diketone **35** (0.52 g, 1.7 mmol) and NH₄OAc (0.84 g, 11 mmol) were dissolved in 20 mL of MeOH and heated at reflux for 2 h. MeOH was removed in the rotary evaporator. The residue was dissolved in 50 mL of EtOAc and washed with 50 mL of 1 M NaOH and 50 mL of brine, respectively. The EtOAc layer was dried with anhydrous MgSO₄ and concentrated in the rotary evaporator. The resulting brownish solid was used in the next step without further purification.

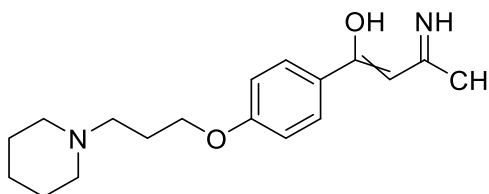
Yield: Quantitative

Appearance: Yellow solid

Chemical formula: C₁₈H₂₆N₂O₂

Molecular weight: 302.4 g/mol

APCI-MS (+): m/z: 303.2 [M+H]⁺



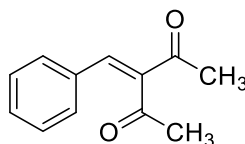
^1H NMR (300 MHz, $\text{DMSO-}d^6$) δ 9.93 (d, $J = 5.4$ Hz, 1H, -OH), 7.79 (d, $J = 8.8$ Hz, 2H, Ph-2,6-H), 7.64 (d, $J = 5.8$ Hz, 1H, NH), 6.92 (d, $J = 8.9$ Hz, 2H, Ph-3,5-H), 5.65 (d, $J = 1.5$ Hz, 1H, -CH=), 4.02 (t, $J = 6.4$ Hz, 2H, -O-CH₂-), 2.41 – 2.26 (m, 6H, overlap: Piperi-CH₂-, Piperi-2,6-H₂), 1.96 (s, 3H, -CH₃), 1.92 – 1.79 (m, 2H, -O-CH₂-CH₂-), 1.48 (p, $J = 5.4$ Hz, 4H, Piperi-3,5-H₂), 1.42 – 1.32 (m, 2H, Piperi-4-H₂).

3-Benzylidenepentane-2,4-dione (**37**) (Li *et al.*, 2012)

The Knoevenagel condensation product **37** was synthesized according to the method reported by Li and colleagues: Benzaldehyde (1.06 g, 10 mmol), acetylacetone (1.0 g, 10 mmol) were dissolved in 30 mL of DCM. Anhydrous AlCl_3 (0.27 g, 2 mmol) was subsequently added to this solution at r.t. The reaction was stirred at r.t. for 3 h and quenched with 30 mL of NaHCO_3 solution. The organic phase was separated, the aqueous layer was extracted with two portions of 30 mL of EtOEt. The combined organic layer was dried with anhydrous MgSO_4 and concentrated in a rotary evaporator. The residue was rinsed with *n*-hexane, the viscous, transparent liquid was used for the next step without further purification.

Yield: 68%

Appearance: Slightly yellow viscous liquid



Chemical formula: $\text{C}_{12}\text{H}_{12}\text{O}_2$

Molecular weight: 188.2 g/mol

APCI-MS (+): m/z : 189.1 $[\text{M}+\text{H}]^+$

^1H NMR (300 MHz, $\text{DMSO-}d^6$) δ 7.69 (s, 1H, Ph-CH=C), 7.46 (s, 5H, Ph-H), 2.44 (s, 3H, *E*-CH₃), 2.25 (s, 3H, *Z*-CH₃).

5-Acetyl-4-(4-hydroxyphenyl)-6-methyl-3,4-dihydropyrimidin-2(1H)-one (**38**) (Kaoukabi *et al.*, 2018)

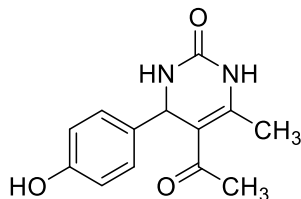
The Biginelli product was synthesized according to the method reported by Kaoukabi and colleagues. 4-Hydroxybenzaldehyde (0.92 g, 7.5 mmol), acetylacetone (0.75 mL, 7.5 mmol), urea (0.45 g, 7.5 mmol), and two drops of conc. HCl (37%, aq.) were dissolved in 10 mL of EtOH. The mixture was heated in MW at 100 °C for 12 min. The suspension was concentrated

in the rotary evaporator. The residue was purified by flash column chromatography, where the solvent mixture of DCM and MeOH in a gradient from 100:0 to 95:5 was used as eluent. The stereochemistry was not characterized.

Yield: 22%

Appearance: Yellow solid

Chemical formula: $C_{13}H_{14}N_2O_3$



Molecular weight: 246.3 g/mol

APCI-MS (+): m/z: 247.1 $[M+H]^+$

1H NMR (300 MHz, DMSO- d_6) δ 9.36 (s, 1H, -OH), 9.09 [d, J = 1.3 Hz, 1H, dihydropyrimidine (DHPM)-3- H], 7.69 (dd, J = 3.6, 1.8 Hz, 1H, DHPM-1- H), 7.04 (d, J = 8.5 Hz, 2H, Ph-3,5- H), 6.69 (d, J = 8.5 Hz, 2H, Ph-2,6- H), 5.14 (d, J = 3.4 Hz, 1H, DHPM-6- H), 2.26 (s, 3H, CH_3 -CO-), 2.05 (s, 3H, DHPM-4- CH_3).

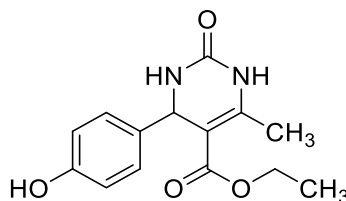
Ethyl 4-(4-hydroxyphenyl)-6-methyl-2-oxo-1,2,3,4-tetrahydropyrimidine-5-carboxylate (39)
(Reddy *et al.*, 2002)

Compound **39** has been synthesized according to the method described by Reddy *et al.* 4-Hydroxy benzaldehyde (0.61 g, 5 mmol), urea (0.30 g, 5 mmol), ethyl acetoacetate (0.63 mL, 5 mmol) and $ZrCl_4$ (0.12 g, 0.5 mmol) were dissolved in 15 mL of EtOH. The mixture was heated at reflux for 15 h. The solvent was removed in the rotary evaporator, and the residue was purified with flash column chromatography, where the solvent mixture of DCM and MeOH in a gradient from 100:0 to 95:5 was used as eluent. The stereochemistry was not determined.

Yield: 65%

Appearance: White solid

Chemical formula: $C_{14}H_{16}N_2O_4$



Molecular weight: 276.3 g/mol

APCI-MS (+): m/z: 277.1 $[M+H]^+$

^1H NMR (300 MHz, $\text{DMSO-}d^6$) δ 7.60 (d, $J = 3.3$ Hz, 1H, DHPM-3-NH), 7.02 (d, $J = 8.5$ Hz, 2H, Ph-2,6-H), 6.68 (d, $J = 8.5$ Hz, 2H, Ph-3,5-H), 5.04 (d, $J = 3.0$ Hz, 1H, DHPM-4-H), 3.97 (q, $J = 7.1$ Hz, 2H, $-\text{CH}_2-\text{CH}_3$), 2.23 (s, 3H, DHPM-6- CH_3), 1.09 (t, $J = 7.1$ Hz, 3H, $-\text{CH}_2-\text{CH}_3$).

Diethyl 2-{4-[3-(piperidin-1-yl)propoxy]benzylidene}malonate (**40**)

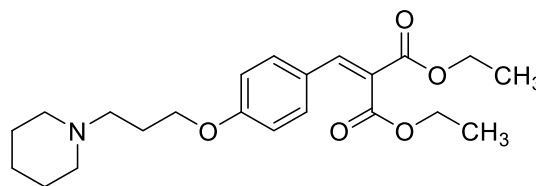
The compound **40** was synthesized via a Knoevenagel condensation. Aldehyde **3** (1.48 g, 6 mmol), diethyl malonate (0.91 mL, 6 mmol), and piperidinium acetate (0.87 g, 6 mmol) were dissolved in 15 mL of EtOH. The mixture was refluxed for 18 h. The solvent was subsequently removed in a rotary evaporator. The residue was purified with flash column chromatography, where a solvent mixture consisting of DCM and MeOH in the gradient from 100:0 to 95:5 was used as the eluent.

Yield: 36%

Appearance: Light yellow transparent viscous liquid

Chemical formula: $\text{C}_{22}\text{H}_{31}\text{NO}_5$

Molecular weight: 389.5 g/mol



APCI-MS (+): m/z : 390.3 $[\text{M}+\text{H}]^+$

^1H NMR (300 MHz, $\text{DMSO-}d^6$) δ 7.63 (s, 1H, Ph-CH=), 7.46 (d, $J = 8.9$ Hz, 2H, Ph-2,6-H), 7.00 (d, $J = 8.9$ Hz, 2H, Ph-3,5-H), 4.35 – 4.12 (m, 4H, overlap: E/Z $-\text{CH}_2-\text{CH}_3$), 4.04 (t, $J = 6.4$ Hz, 2H, Ph-O- CH_2), 2.40 – 2.26 (m, 6H, overlap: Piperi- CH_2 , Piperi-2,6- H_2), 1.85 (p, $J = 6.7$ Hz, 2H, Piperi- CH_2-CH_2), 1.48 (p, $J = 5.4$ Hz, 4H, Piperi-3,5- H_2), 1.42 – 1.32 (m, 2H, Piperi-4- H_2), 1.29 – 1.19 (m, 6H, overlap: E/Z- CH_3).

Diethyl 2-{4-[3-(piperidin-1-yl)propoxy]benzyl}malonate (**41**)

Compound **40** (0.84 g, 2.15 mmol) was dissolved in 15 mL of EtOH, NaBH_4 (0.08 g, 2.15 mmol) was added to the solution at 0 °C, and the reaction was kept at this temperature for 30 min. 2.5 mL of acetic acid was added to the mixture to adjust the pH value to 4-5, and the reaction was stirred for another 10 min. The pH was subsequently adjusted to 9-10 with 1 N NaOH, and the solution was extracted with three portions of 30 mL DCM. The combined organic layer

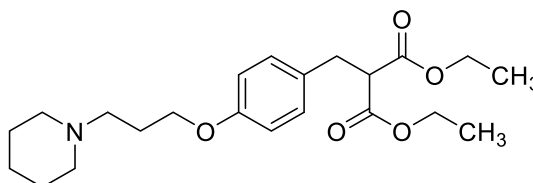
was dried with anhydrous MgSO_4 and consequently concentrated in a rotary evaporator. The residue was used without further purification in the next step.

Yield: 86%

Appearance: Slightly yellow viscous liquid

Chemical formula: $\text{C}_{22}\text{H}_{33}\text{NO}_5$

Molecular weight: 391.5 g/mol



APCI-MS (+): m/z : 392.3 $[\text{M}+\text{H}]^+$

^1H NMR (300 MHz, CDCl_3) δ 7.09 (d, $J = 8.6$ Hz, 2H, Ph-2,6- H), 6.77 (d, $J = 8.7$ Hz, 2H, Ph-3,5- H), 4.14 (qd, $^3,^5J = 7.2$, 2.3 Hz, 4H, $-\text{CH}_2-\text{CH}_3$), 3.95 (t, $J = 6.2$ Hz, 2H, $-\text{O}-\text{CH}_2-$), 3.57 (t, $J = 7.8$ Hz, 1H, Ph- $\text{CH}_2-\text{CH}(\text{CO}-)_2$), 3.13 (d, $J = 7.8$ Hz, 2H, Ph- CH_2-), 2.68 – 2.52 (m, 6H, overlap: Piperi- CH_2- , Piperi-2,6- H_2), 2.08 – 1.99 (m, 2H, $-\text{O}-\text{CH}_2-\text{CH}_2-$), 1.67 (p, $J = 5.6$ Hz, 5H, Piperi-3,5- H_2), 1.54 – 1.41 (m, 2H, Piperi-4- H_2), 1.20 (t, $J = 7.1$ Hz, 6H, $-\text{CH}_3$).

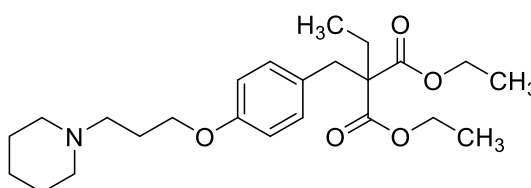
Diethyl 2-ethyl-2-(4-[3-(piperidin-1-yl)propoxy]benzyl)malonate (**42**)

Compound **42** was prepared via an adapted method reported previously (Yoshioka *et al.*, 2015). Compound **41** (0.20 g, 0.51 mmol) was dissolved in 5 mL of DMF in a one-neck Schlenk flask, NaH (40 mg, 60% in mineral oil, 1 mmol) was given to the reaction in one portion, Bromoethane (0.04 mL, 0.54 mmol) was subsequently added to the reaction. The reaction was stirred at ambient temperature under the nitrogen atmosphere. 20 mL of water was given to quench the reaction after 72 h. The aqueous solution was washed with three portions of 20 mL DCM. The combined organic layer was dried with anhydrous MgSO_4 and concentrated in the rotary evaporator. The residue was purified via column chromatography. The solvent mixtures of DCM and MeOH in ratios of 95:5 and 90:10 were used as eluents.

Yield: 46%

Appearance: Colorless viscous liquid

Chemical formula: $\text{C}_{24}\text{H}_{37}\text{NO}_5$



Molecular weight: 419.6 g/mol

APCI-MS (+): m/z: 420.4 [M+H]⁺

¹H NMR (300 MHz, CDCl₃) δ 6.97 (d, *J* = 8.6 Hz, 2H, Ph-2,6-*H*), 6.76 (d, *J* = 8.6 Hz, 2H, Ph-3,5-*H*), 4.17 (qd, *J* = 7.2, 2.6 Hz, 4H, -O-CH₂-CH₃), 3.96 (t, *J* = 6.3 Hz, 2H, Ph-O-CH₂-), 3.16 (s, 2H, Ph-CH₂-), 2.61 – 2.40 (m, 6H, overlap: Piperi-CH₂-, Piperi-2,6-*H*₂), 2.08 – 1.93 (m, 2H, Piperi-CH₂-CH₂-), 1.81 (q, *J* = 7.5 Hz, 2H, CH₃-CH₂-C), 1.64 (p, *J* = 5.6 Hz, 4H, Piperi-3,5-*H*₂), 1.52 – 1.39 (m, 2H, Piperi-4-*H*₂), 1.24 (t, *J* = 7.1 Hz, 6H, -O-CH₂-CH₃), 0.90 (t, *J* = 7.6 Hz, 3H, CH₃-CH₂-C).

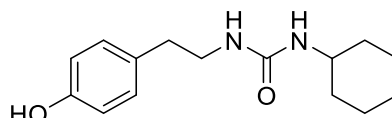
1-Cyclohexyl-3-(4-hydroxyphenethyl)urea (**43**)

Tyramine hydrochloride (0.87 g, 5 mmol) and TEA (0.83 mL, 6 mmol) were stirred in 10 mL of THF for 1 h before cyclohexyl isocyanate (0.63 g, 5 mmol) was given to the mixture. The reaction was stirred for a further 2 h. at r.t. The mixture was evaporated in a rotary evaporator to dryness. The residue was used without further purification in the next step.

Yield: Quantitative

Appearance: White solid

Chemical formula: C₁₅H₂₂N₂O₂



Molecular weight: 262.4 g/mol

APCI-MS (+): m/z: 263.2 [M+H]⁺

¹H NMR (300 MHz, DMSO-*d*⁶) δ 9.13 (s, 1H, -OH), 6.97 (d, *J* = 8.4 Hz, 2H, Ph-2,6-*H*), 6.67 (d, *J* = 8.4 Hz, 2H, Ph-3,5-*H*), 5.73 [d, *J* = 8.1 Hz, 1H, cyclohexane (c-Hex)-NH-], 5.60 (t, *J* = 5.7 Hz, 1H, -CH₂-NH-), 3.41 – 3.26 (m, 1H, c-Hex-1-*H*), 3.14 (td, *J* = 7.3, 4.0 Hz, 2H, -CH₂-NH-), 2.57 – 2.51 (m, 2H, Ph-CH₂-), 1.79 – 1.43 (m, 5H, c-Hex-2,3,4,5,6-*H*_{eq}), 1.34 – 0.94 (m, 5H, c-Hex-2,3,4,5,6-*H*_{ax}).

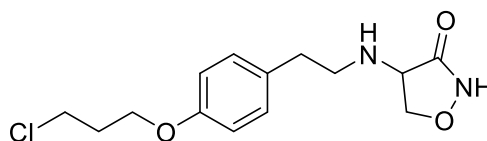
4-[[4-(3-Chloropropoxy)phenethyl]amino]isoxazolidin-3-one (**44**)

Similar to **P50**, compound **44** was synthesized from aldehyde **24** (0.23 g, 1.1 mmol), DCS (0.10 g, 1 mmol) and NaBH₄ (0.10 g, 2.6 mmol). The product was purified with column chromatography, where the solvent mixtures of DCM and MeOH in ratios of 98:2 and 95:5 were used as eluents. The temperature of the water bath for the rotary evaporator was set at approximately 30 °C.

Yield: 36%

Appearance: White solid

Chemical formula: C₁₄H₁₉ClN₂O₃



Molecular weight: 298.8 g/mol

APCI-MS (+): m/z: 299.6 [M+H]⁺

¹H NMR (300 MHz, DMSO-*d*⁶) δ 7.12 (d, *J* = 8.6 Hz, 2H, Ph-2,6-*H*), 6.86 (d, *J* = 8.6 Hz, 2H, Ph-3,5-*H*), 4.45 (dd, *J* = 8.4, 7.7 Hz, 1H, Oxa-5-*H*_{eq}), 4.05 (t, *J* = 6.0 Hz, 2H, Ph-O-CH₂-), 3.87 (t, *J* = 8.6 Hz, 1H, Oxa-6-*H*), 3.78 (t, *J* = 6.5 Hz, 2H, Cl-CH₂-), 3.70 (dd, *J* = 8.7, 7.7 Hz, 1H, Oxa-5-*H*_{ax}), 2.94 – 2.84 (m, 1H, Ph-CH₂-CH-), 2.78 – 2.69 (m, 1H, Ph-CH₂-CH'-), 2.69 – 2.59 (m, 2H, Ph-CH₂-CH₂-), 2.14 (p, *J* = 6.3 Hz, 2H, Cl-CH₂-CH₂-).

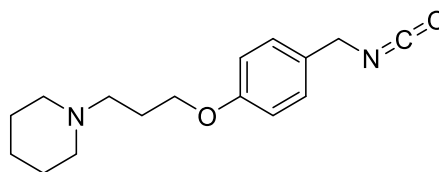
1-{3-[4-(Isocyanatomethyl)phenoxy]propyl}piperidine (**45**)

The isocyanate derivative **45** was synthesized via an adapted method described previously (Burstein *et al.*, 2019). A solution of the benzylamine derivative **13** (0.28 g, 1.12 mmol) and TEA (0.56 mL, 4 mmol) in 5 mL of DCM was given to a solution of diphosgene (0.12 mL, 1 mmol) in 5 mL of DCM at 0 °C. The mixture was allowed to reach r.t. and further stirred for 1.5 h. The solvent was subsequently removed in the rotary evaporator. The crude product was used in the next step without further purification.

Yield: Method A: 65%; Method B: Quantitative

Appearance: White solid

Chemical formula: C₁₆H₂₂N₂O₂



Molecular weight: 274.4 g/mol

APCI-MS (+): m/z: 275.2 [M+H]⁺

¹H NMR (300 MHz, CDCl₃) δ 7.19 (d, *J* = 8.6 Hz, 2H, Ph-2,6-*H*), 6.83 (d, *J* = 8.7 Hz, 2H, Ph-3,5-*H*), 4.33 (d, *J* = 5.9 Hz, 2H, Ph-CH₂-), 4.01 (t, *J* = 5.9 Hz, 2H, -O-CH₂-), 2.89 – 2.71 (m, 6H, overlap, Piperi-CH₂-, Piperi-2,6-*H*₂), 2.29 – 2.14 (m, 2H, -O-CH₂-CH₂-), 1.86 (p, *J* = 5.7 Hz, 4H, Piperi-3,5-*H*₂), 1.63 – 1.51 (m, 2H, Piperi-4-*H*₂).

Phenyl {4-[3-(piperidin-1-yl)propoxy]benzyl}carbamate (**46**)

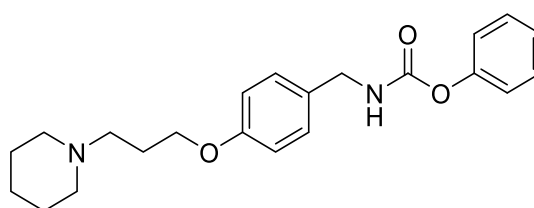
Compound **46** was synthesized via an adapted method reported previously (Stephens *et al.*, 2016). Benzylamine derivative **13** (0.49 g, 2 mmol) and TEA (0.83 mL, 6 mmol) were dissolved in 10 mL of DCM. The solution was cooled to 0 °C. Phenyl chloroformate (0.31 g, 2 mmol) was given in small portions, and the mixture was stirred at ambient temperature for 4 h. After completion of the reaction monitored via TLC, the solvent was concentrated in the rotary evaporator. The residue was treated with acetone. The resulting suspension was filtered off. The filtrate was collected and concentrated. The residue was purified with column chromatography by using the solvent mixture of DCM and MeOH in a ratio of 95:5.

Yield: 66%

Appearance: Light yellowish viscous liquid

Chemical formula: C₂₂H₂₈N₂O₃

Molecular weight: 368.5 g/mol



APCI-MS (+): m/z: 369.2 [M+H]⁺

¹H NMR (300 MHz, CDCl₃) δ 7.40 – 7.32 (m, 2H, Ph-3,5-*H*), 7.26 (d, *J* = 8.7 Hz, 2H, Benzyl-2,6-*H*), 7.23 – 7.16 (m, 1H, Ph-4-*H*), 7.16 – 7.11 (m, 2H, Ph-2,6-*H*), 6.87 (d, *J* = 8.6 Hz, 2H, Benzyl-3,5-*H*), 5.30 (s, 1H, -NH-), 4.38 (d, *J* = 5.8 Hz, 2H, Benzyl-CH₂-), 4.02 (t, *J* = 6.1 Hz, 2H, -O-CH₂-), 2.73 – 2.53 (m, 6H, overlap: Piperi-CH₂-, Piperi-2,6-*H*₂), 2.20 – 2.07 (m, 2H, -O-CH₂-CH₂-), 1.82 – 1.66 (m, 4H, Piperi-3,5-*H*₂), 1.57 – 1.45 (m, 2H, Piperi-4-*H*₂).

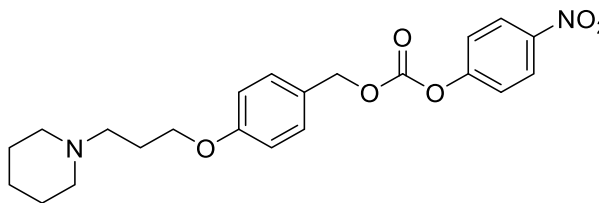
4-Nitrophenyl {4-[3-(piperidin-1-yl)propoxy]benzyl} carbonate (**47**)

The synthesis of compound **47** was performed via a modified method reported previously (Kunai *et al.*, 2006; Burstein *et al.*, 2019). The benzyl alcohol **6** (0.50 g, 2 mmol) was dissolved in 8 mL of DCM. Pyridine (0.3 mL, 3.7 mmol) and 4-nitrophenyl chloroformate (0.60 g, 2.97 mmol) were given to the solution mentioned above at 0 °C. The reaction was stirred at r.t. for 18 h and diluted with 50 mL of DCM. The resulting solution was washed with 50 mL of sat. NaHCO₃ and 50 mL of brine, respectively. The organic layer was dried over anhydrous MgSO₄ and concentrated in the rotary evaporator. The obtained residue was purified with column chromatography, whereby the solvent mixture of DCM and MeOH in ratios of 95:5 and 90:10 were used as eluents.

Yield: 68%

Appearance: Yellow viscous liquid

Chemical formula: $C_{22}H_{26}N_2O_6$



Molecular weight: 414.5 g/mol

APCI-MS (+): m/z : 415.3 $[M+H]^+$

1H NMR (300 MHz, $CDCl_3$) δ 8.26 (d, $J = 9.2$ Hz, 2H, 4-Nitro-Ph-2,6-*H*), 7.41 – 7.32 (m, 4H, overlap: 4-Nitro-Ph-3,5-*H*, Ph-2,6-*H*), 6.90 (d, $J = 8.7$ Hz, 2H, Ph-3,5-*H*), 5.22 (s, 2H, Ph- CH_2 -), 4.02 (t, $J = 6.3$ Hz, 2H, Ph-O- CH_2 -), 2.61 – 2.43 (m, 6H, overlap: Piperi- CH_2 -, Piperi-2,6- H_2), 2.09 – 1.94 (m, 2H, Piperi- CH_2-CH_2 -), 1.63 (p, $J = 5.6$ Hz, 4H, Piperi-3,5- H_2), 1.53 – 1.41 (m, 2H, Piperi-4- H_2).

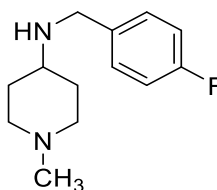
N-(4-Fluorobenzyl)-1-methylpiperidin-4-amine (Burstein *et al.*, 2019) (**48**)

Compound **48** was synthesized analogous to compound **P25** from 4-fluorobenzylamine (0.50 g, 4 mmol), 1-methylpiperidin-4-one (0.45 g, 4 mmol), glacial acetic acid (0.34 mL, 6 mmol), and sodium triacetoxyborohydride (1.00 g, 4.7 mmol) in 20 mL of DCE. The reaction was stirred at r.t. for 18 h. The product was purified with column chromatography, where the solvent mixtures of DCM and MeOH (NH_3) in ratios of 98:2 and 95:5 were used as eluents.

Yield: 43%

Appearance: Yellow liquid

Chemical formula: $C_{13}H_{19}FN_2$



Molecular weight: 222.3 g/mol

APCI-MS (+): m/z : 223.0 $[M+H]^+$

1H NMR (300 MHz, $CDCl_3$) δ 7.34 – 7.22 (m, 2H, Ph-2,6-*H*), 7.07 – 6.93 (m, 2H, Ph-3,5-*H*), 3.78 (s, 2H, Ph- CH_2 -), 2.87 – 2.74 (m, 2H, Piperi-2,6- H_{eq}), 2.58 – 2.40 (m, 1H, Piperi-4-*H*), 2.26 (s, 3H, - CH_3), 2.06 – 1.82 (m, 4H, Piperi-2,6- H_{ax} , Piperi-3,5- H_{eq}), 1.53 – 1.34 (m, 2H, Piperi-3,5- H_{ax}).

4-Nitro-*N*-(thiazol-2-yl)benzamide (Sams *et al.*, 2011) (**49**)

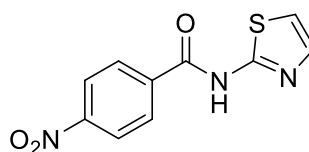
4-Nitro benzoyl chloride (2.78 g, 15 mmol) was added dropwise to a solution of 2-aminothiazole (1.00 g, 10 mmol) and pyridine (0.81 mL, 10 mmol) in 20 mL of DCE at 0 °C. The reaction was heated at 60 °C for 18h. The resulting suspension was filtered off. The filter cake was rinsed with 10 mL of DCE. The filter cake was collected and dried in a rotary evaporator. The crude product was used without further purification in the next step.

Yield: 80%

Appearance: Yellow solid

Chemical formula: C₁₀H₇N₃O₃S

Molecular weight: 249.2 g/mol



APCI-MS (+): m/z: 250.0 [M+H]⁺

¹H NMR (600 MHz, DMSO-*d*⁶) δ 13.02 (s, 1H, -CO-NH-), 8.36 (d, *J* = 8.9 Hz, 2H, Ph-3,5-*H*), 8.30 (d, *J* = 8.9 Hz, 2H, Ph-2,6-*H*), 7.59 (d, *J* = 3.6 Hz, 1H, Thiazole-4-*H*), 7.32 (d, *J* = 3.6 Hz, 1H, Thiazole-5-*H*).

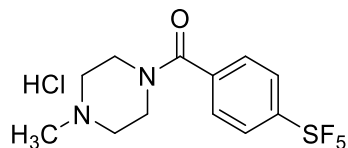
6.4.2 Compounds with organochloride and organofluoride

1-Methyl-4-[4-(pentafluoro- λ⁶-sulfanyl)benzoyl]piperazine hydrochloride (**P1**, ST-2268)

4-(Pentafluoro- λ⁶-sulfanyl)benzoic acid (100 mg, 0.4 mmol) was dissolved in 2 mL of DCM. To this solution, thionyl chloride (0.06 mL, 0.8 mmol) was added dropwise at 0 °C. The reaction was refluxed for 4 h. The excess of thionyl chloride was removed via vacuum distillation with subsequent co-evaporation with toluene. The prepared acid chloride was given to a solution of TEA (0.14 mL, 1 mmol) and *N*-methylpiperazine (0.2 mL, 2 mmol) in 2 mL DCM at 0 °C and the reaction was stirred at r.t. for 18 h. The solvent of the mixture was removed in a rotary evaporator. The residue was purified via column chromatography. The solvent mixture of DCM and MeOH in a ratio of 95:5 was used as an eluent. The product was converted to HCl salt with HCl in dioxane.

Yield: 82%

Appearance: White solid

Chemical formula: $C_{12}H_{15}F_5N_2OS \times HCl$

Molecular weight: 366.8 g/mol

Melting point: 276.8 °C

LC-MS: 98.45%, m/z: 330.92 $[M+H]^+$, with gradient LC-Method 9

1H NMR (300 MHz, DMSO- d_6) δ 11.60 (s, 1H, Pipera- N^+H), 8.02 (d, $J = 8.9$ Hz, 2H, 4-S-Ph-3,5- H), 7.70 (d, $J = 8.3$ Hz, 2H, 4-S-Ph-2,6- H), 3.61 (br, 2H, Pipera-2,6- H_{eq}), 3.35 (br, 4H, Pipera-2,6- H_{ax} , -3,5- H_{eq}), 3.11 (br, 2H, Pipera-3,5- H_{ax}), 2.74 (s, 3H, - CH_3).

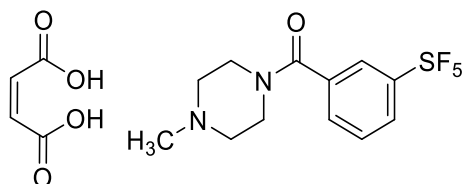
^{13}C NMR (75 MHz, DMSO- d_6) δ 167.25 (-CO-), 153.36 (t, $^2J(C,F) = 16.4$ Hz, 4-S-Ph-4-C), 138.86 (4-S-Ph-1-C), 128.19 (4-S-Ph-2,6-C), 126.26 (p, $^3J(C,F) = 4.8$ Hz, 4-S-Ph-3,5-C), 51.75 (4-Me-Pipera-3,5-C), 43.80 (- CH_3), 42.00 (Pipera-2,6-C).

1-Methyl-4-[3-(pentafluoro- λ^6 -sulfanyl)benzoyl]piperazine hydrogen maleate (**P2**, ST-2269)

Similar to compound **P1**, compound **P2** was synthesized from 3-(pentafluoro- λ^6 -sulfanyl)benzoic acid (100 mg, 0.4 mmol) and thionyl chloride (0.06 mL, 0.8 mmol) in 2 mL of DCM, refluxed for 4 h. The acid chloride was given to a solution of TEA (0.14 mL, 1 mmol) and *N*-methylpiperazine (0.2 mL, 2 mmol) in 2 mL DCM at 0 °C and then stirred at r.t. for 18 h. The product was purified via column chromatography with the solvent mixture from DCM and MeOH in a ratio of 95:5 as an eluent. The product was converted to its hydrogen maleate salt in EtOEt.

Yield: 90%

Appearance: White to light beige solid

Chemical formula: $C_{12}H_{15}F_5N_2OS \times C_4H_4O_4$

Molecular weight: 446.4 g/mol

Melting point: 202.4 °C

LC-MS: 97.13%, $m/z = 330.92$ $[M+H]^+$, with gradient LC-Method 6

^1H NMR (300 MHz, $\text{DMSO-}d^6$) δ 8.04 (dt, $^3J = 6.8, 2.4$ Hz, 1H, 3-S-Ph-6-H), 8.00 – 7.95 (m, 1H, 3-S-Ph-4-H), 7.81 – 7.67 (m, overlap: 2H, Ph-2,5-H), 6.06 (s, 2H, Maleinic acid-CH=CH-), 4.02 – 3.40 (m, 4H, Pipera-2,6- H_2), 3.18 (s, 4H, Pipera-3,5- H_2), 2.77 (s, 3H, - CH_3).

^{13}C NMR (75 MHz, $\text{DMSO-}d^6$) δ 167.19 (Maleinic acid-CO-), 167.04 (Ph-CO-), 152.78 (t, $^2J(\text{C},\text{F}) = 16.7$ Hz, Ph-3-C), 136.22 (Ph-1-C), 135.34 (Maleinic acid-CH=CH-), 131.00 (Ph-5-C), 130.07 (Ph-6-C), 127.22 (t, $^3J(\text{C},\text{F}) = 4.3$ Hz, Ph-2-C), 124.55 (t, $^3J(\text{C},\text{F}) = 4.5$ Hz, Ph-4-C), 52.24 (Pipera-3,5-C), 44.32 (- CH_3), 42.67 (Pipera-2,6-C).

1-{3-[4-(Pentafluoro- λ^6 -sulfanyl)phenoxy]propyl}piperidine (**P3**, ST-2215)

Analogous to compound **5**, compound **P3** was synthesized from alkyl alcohol **1** (0.18 g, 1.25 mmol), 4-fluoro(pentafluoro- λ^6 -sulfanyl)benzene (0.25 g, 1.13 mmol), 0.10 g of NaH (0.10 g, 2.5 mmol) in 2 mL of DMF in a nitrogen atmosphere in a one-neck Schlenk flask. The reaction was stirred at r.t. for 6 h. The product was purified with column chromatography, whereby the solvent mixtures of DCM and MeOH in ratios of 95:5 and 90:10 were used as eluents.

Yield: 34%

Appearance: Reddish viscous liquid

Chemical formula: $\text{C}_{14}\text{H}_{20}\text{F}_5\text{NOS}$

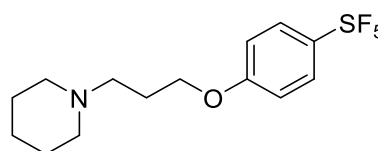
Molecular weight: 345.4 g/mol

APCI-MS (+): m/z : 346.2 $[M+H]^+$

Elemental Analysis: calculated.: C, 48.69%; H, 5.84%; N, 4.06%; S, 9.28%

found: C, 48.87%; H, 5.92%; N, 3.99%; S, 8.99%

^1H NMR (300 MHz, CDCl_3) δ 7.66 (d, $J = 9.2$ Hz, 1H, 4-SF₅-Ph-3,5-H), 6.90 (d, $J = 8.8$ Hz, 2H, 4-SF₅-Ph-2,6-H), 4.06 (t, $J = 6.3$ Hz, 2H, -O- CH_2 -), 2.57 – 2.39 (m, 6H, overlap: Piperi- CH_2 -, Piperi-2,6- H_2), 2.10 – 1.95 (m, 2H, -O- CH_2 - CH_2 -), 1.63 (p, $J = 5.7$ Hz, 4H, Piperi-3,5- H_2), 1.53 – 1.39 (m, 2H, Piperi-4- H_2).



Experiment

^{13}C NMR (75 MHz, CDCl_3) δ 160.94 (4-SF₅-Ph-1-C), 127.92 – 127.51 (m, 4-SF₅-Ph-3,5-C), 114.12 (4-SF₅-Ph-2,6-C), 66.96 (-O-CH₂-), 55.81 (Piperi-CH₂-), 54.73 (Piperi-2,6-C), 26.54 (-O-CH₂-CH₂-), 25.84 (Piperi-3,5-C), 24.37 (Piperi-4-C).

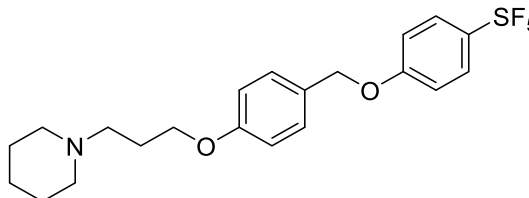
1-[3-(4-{[4-(Pentafluoro- λ^6 -sulfanyl)phenoxy]methyl}phenoxy)propyl]piperidine (**P4**, ST-2216)

Analogous to compound **5**, compound **P4** was synthesized from benzyl alcohol derivative **6** (0.31 g, 1.25 mmol), 4-fluoro(pentafluoro- λ^6 -sulfanyl)benzene (0.25 g, 1.13 mmol), and NaH (0.10 g, 2.5 mmol) in 3 mL of DMF in argon atmosphere in a one-neck Schlenk flask. The reaction was stirred at r.t. for 22 h. The product was purified with column chromatography, whereby the solvent mixture of DCM and MeOH in a ratio of 95:5 was used as an eluent.

Yield: 79%

Appearance: White solid

Chemical formula: C₂₁H₂₆F₅NO₂S



Molecular weight: 451.5 g/mol

APCI-MS (+):m/z: 452.3 [M+H]⁺

Melting point: 112.4 °C

Elemental Analysis: calculated.: C, 55.87%; H, 5.80%; N, 3.10%; S, 7.10%

found: C, 55.66%; H, 5.81%; N, 3.02%; S, 7.00%

^1H NMR (300 MHz, CDCl_3) δ 7.67 (d, J = 9.3 Hz, 2H, 4-Methoxy-Ph-3,5-H), 7.32 (d, J = 8.7 Hz, 2H, 4-SF₅-Ph-3,5-H), 6.96 (d, J = 9.4 Hz, 2H, 4-Methoxy-Ph-2,6-H), 6.92 (d, J = 8.7 Hz, 2H, 4-SF₅-Ph-2,6-H), 5.02 (s, 2H, Ph-CH₂-), 4.02 (t, J = 6.4 Hz, 2H, -O-CH₂-CH₂-), 2.53 – 2.46 (m, 2H, Piperi-CH₂-), 2.46 – 2.39 (m, 4H, Piperi-2,6-H₂), 2.07 – 1.92 (m, 2H, -O-CH₂-CH₂-), 1.61 (p, J = 5.6 Hz, 4H, Piperi-3,5-H₂), 1.51 – 1.38 (m, 2H, Piperi-4-H₂).

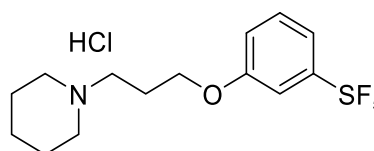
^{13}C NMR (75 MHz, CDCl_3) δ 160.56 (4-SF₅-Ph-1-C), 159.21 (4-Methoxy-Ph-1-C), 146.68 (t, $^2J(\text{C},\text{F})$ = 17.7 Hz, 4-SF₅-Ph-4-C), 129.23 (4-Methoxy-Ph-3,5-C), 127.75 (4-Methoxy-Ph-4-C), 127.61 (p, $^3J(\text{C},\text{F})$ = 4.6 Hz), 4-SF₅-Ph-3,5-C), 114.75 (4-Methoxy-Ph-2,6-C), 114.37 (4-SF₅-Ph-2,6-C), 70.20 (Ph-CH₂-O-), 66.56 (-O-CH₂-CH₂-), 55.94 (Piperi-CH₂-), 54.64 (Piperi-2,6-C), 26.75 (-O-CH₂-CH₂-), 25.90 (Piperi-3,5-C), 24.38 (Piperi-4-C).

1-{3-[3-(Pentafluoro- λ^6 -sulfanyl)phenoxy]propyl}piperidine hydrochloride (**P5**, ST-2217)

Compound **P5** was synthesized via Mitsunobu reaction according to a modified method reported previously (Łażewska *et al.*, 2006): Alkyl alcohol **1** (0.20 g, 1.40 mmol), 3-(pentafluoro- λ^6 -sulfanyl)phenol (0.25 g, 1.14 mmol), and PPh_3 (0.37 g, 1.4 mmol) were dissolved in 10 mL of THF under an argon atmosphere in a one-neck Schlenk flask. The mixture was cooled at 0 °C, and diisopropyl azodicarboxylate (DIAD) (0.28 mL, 1.4 mmol) was added to the solution dropwise. The reaction was kept at 0 °C for 30 min and allowed to stir at r.t. for 24 h. Upon the completion of the reaction monitored via TLC, the solvent was removed in a rotary evaporator. The residue was purified via column chromatography. The solvent mixtures of DCM and MeOH in ratios of 98:2 and 95:5 were used as eluents. The product was treated with HCl in dioxane to obtain the HCl salt.

Yield: 45%

Appearance: White to light beige solid



Chemical formula: $\text{C}_{14}\text{H}_{20}\text{F}_5\text{NOS} \times \text{HCl}$

Molecular weight: 381.8 g/mol

APCI-MS (+): m/z : 346.3 $[\text{M}+\text{H}]^+$

Melting point: 140.0 °C

Elemental Analysis: calculated.: C, 44.04%; H, 5.54%; N, 3.67%; S, 8.40%

found: C, 44.07%; H, 5.26%; N, 3.65%; S, 8.62%

^1H NMR (300 MHz, CDCl_3) δ 12.17 (br, 1H, Piperi- N^+H), 7.41 – 7.30 (m, 2H, overlap: Ph-4,5- H), 7.22 (s, 1H, Ph-2- H), 7.00 (d, $J = 6.8$ Hz, 1H, 3-S-Ph-6- H), 4.11 (br, 2H, -O- CH_2 -), 3.58 (br, 2H, Piperi-2,6- H_{eq}), 3.17 (br, 2H, Piperi- CH_2 -), 2.68 (br, 2H, Piperi-2,6- H_{ax}), 2.48 (br, 2H, -O- CH_2 - CH_2 -), 2.37 – 2.20 (m, 2H, Piperi-3,5- H_{eq}), 1.97 – 1.77 (m, 3H, overlap: Piperi-3,5- H_{ax} , -4- H_{eq}), 1.54 – 1.32 (m, 1H, Piperi-4- H_{ax}).

^{13}C NMR (75 MHz, CDCl_3) δ 158.06 (3-SF₅-Ph-1-C), 154.74 (sextett, $^2J(\text{C},\text{F}) = 17.9$ Hz, 3-SF₅-Ph-3-C), 129.77 (3-SF₅-Ph-5-C), 118.77 (t, $^3J(\text{C},\text{F}) = 4.8$ Hz, 3-SF₅-Ph-4-C), 117.11 (3-SF₅-Ph-6-C), 113.18 (p, $^3J(\text{C},\text{F}) = 4.7$ Hz, 3-SF₅-Ph-2-C), 65.79 (-O- CH_2 -), 55.31 (Piperi- CH_2 -), 53.72 (Piperi-2,6-C), 23.91 (-O- CH_2 - CH_2 -), 22.68 (Piperi-3,5-C), 22.22 (Piperi-4-C).

1-[3-(4-[[3-(Pentafluoro- λ^6 -sulfanyl)phenoxy]methyl]phenoxy)propyl]piperidine (**P6**, ST-2218)

Similar to compound **P5**, compound **P6** was synthesized from benzyl alcohol **6** (0.30 g, 1.20 mmol), 3-(pentafluoro- λ^6 -sulfanyl)phenol (0.25 g, 1.14 mmol), PPh_3 (0.37 g, 1.4 mmol), and DIAD (0.28 mL, 1.4 mmol) in 10 mL of THF under an argon atmosphere. The mixture was stirred at r.t. for 18 h. The product was purified via column chromatography, where the solvent mixture of DCM and MeOH in a ratio of 95:5 was used as an eluent.

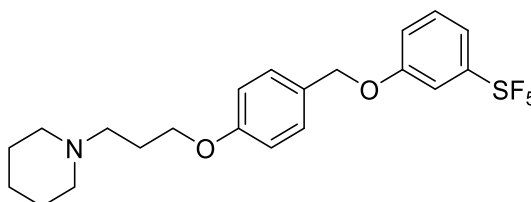
Yield: 47%

Appearance: White to light yellowish solid

Chemical formula: $\text{C}_{21}\text{H}_{26}\text{F}_5\text{NO}_2\text{S}$

Molecular weight: 451.5 g/mol

APCI-MS (+):m/z: 452. $[\text{M}+\text{H}]^+$



Melting point: 46.6 °C

Elemental Analysis: calculated.: C, 55.87%; H, 5.80%; N, 3.10%; S, 7.10%

found: C, 55.89%; H, 5.71%; N, 3.34%; S, 6.80%

^1H NMR (300 MHz, CDCl_3) δ 7.40 – 7.29 (m, 5H, 4-Methoxy-Ph-3,5-*H*, 3-SF₅-Ph-2,4,5-*H*), 7.07 (dt, $^3J = 7.0, 2.5$ Hz, 1H, 3-SF₅-Ph-6-*H*), 6.89 (d, $J = 8.7$ Hz, 2H, 4-Methoxy-Ph-2,6-*H*), 4.99 (s, 2H, Ph- CH_2 -), 4.04 (t, $J = 6.0$ Hz, 2H, -O- CH_2 - CH_2 -), 2.88 – 2.70 (m, 6H, Piperi- CH_2 -, Piperi-2,6-*H*₂), 2.28 – 2.13 (m, 2H, -O- CH_2 - CH_2 -), 1.83 (p, $J = 5.6$ Hz, 4H, Piperi-3,5-*H*₂), 1.56 (p, $J = 6.2$ Hz, 2H, Piperi-4-*H*₂).

^{13}C NMR (75 MHz, CDCl_3) δ 158.86 (3-SF₅-Ph-1-C), 158.57 (4-Methoxy-Ph-1-C), 154.75 (p, $^2J(\text{C},\text{F}) = 17.3$ Hz, 3-SF₅-Ph-3-C), 129.49 (4-Methoxy-Ph-3,5-C), 128.29 (4-Methoxy-Ph-4-C), 118.38 (hept, $^3J(\text{C},\text{F}) = 4.8$ Hz, 3-SF₅-Ph-4-C), 117.93 (3-SF₅-Ph-6-C), 114.75 (4-Methoxy-Ph-2,6-C), 113.32 (hept, $^3J(\text{C},\text{F}) = 4.8$ Hz, 3-SF₅-Ph-2-C), 70.41 (Ph- CH_2 -), 65.93 (-O- CH_2 - CH_2 -), 55.77 (Piperi- CH_2 -), 54.21 (Piperi-2,6-C), 25.54 (-O- CH_2 - CH_2 -), 24.43 (Piperi-3,5-C), 23.36 (Piperi-4-C).

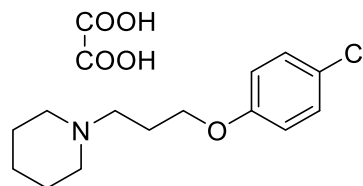
1-[3-(4-Chlorophenoxy)propyl]piperidine hydrogen oxalate (Beasley *et al.*, 1958) (**P7**, ST-2361)

Similar to compound **3**, compound **P7** was synthesized from 4-chlorophenol (0.82 g, 6.4 mmol), alkyl chloride **2** (0.78 g, 3.9 mmol), K₂CO₃ (1.93 g, 14.4 mmol), and KI (0.08 g, 0.5 mmol) in 40 mL of acetone. The reaction was refluxed for 18 h. The product was converted to hydrogen oxalate salt in acetone and recrystallized in acetone.

Yield: 86%

Appearance: White solid

Chemical formula: C₁₄H₂₀ClNO × C₂H₂O₄



Molecular weight: 343.8 g/mol

Melting point: 168.3 °C

LC-MS: 98.38%, m/z: 253.98 [M+H]⁺, with gradient LC-Method 1

¹H NMR (300 MHz, DMSO-*d*⁶) δ 7.33 (d, *J* = 9.0 Hz, 2H, Ph-3,5-*H*), 6.96 (d, *J* = 9.0 Hz, 2H, Ph-2,6-*H*), 4.02 (t, *J* = 6.1 Hz, 2H, -O-CH₂-), 3.22 – 2.96 (m, 6H, Piperi-CH₂-, Piperi-2,6-*H*₂), 2.18 – 2.03 (m, 2H, -O-CH₂-CH₂-), 1.73 (p, *J* = 5.8 Hz, 4H, Piperi-3,5-*H*₂), 1.59 – 1.46 (m, 2H, Piperi-4-*H*₂).

¹³C NMR (75 MHz, DMSO-*d*⁶) δ 164.85 (-CO-), 157.13 (Ph-1-C), 129.26 (Ph-3,5-C), 124.43 (Ph-4-C), 116.26 (Ph-2,6-C), 65.42 (-O-CH₂-), 53.34 (Piperi-CH₂-), 52.06 (Piperi-2,6-C), 23.37 (-O-CH₂-CH₂-), 22.56 (Piperi-3,5-C), 21.49 (Piperi-4-C).

Beasley and colleagues had reported 1-[3-(4-chlorophenoxy)propyl]piperidine as the free base, where the boiling point was 114-116 °C at 0.1 mmHg.

1-[3-(4-Fluorophenoxy)propyl]piperidine hydrogen oxalate (Khorana *et al.*, 2003b) (**P8**, ST-2362)

Analogous to compound **3**, compound **P8** was synthesized from 4-fluorophenol (0.57 g, 5.09 mmol), alkyl chloride **2** (0.83 g, 4.19 mmol), K₂CO₃ (1.72 g, 12.84 mmol), and KI (0.07 g, 0.42 mmol) in 40 mL of acetone. The reaction was refluxed for 18 h. The product was converted to hydrogen oxalate salt in acetone and recrystallized in acetone.

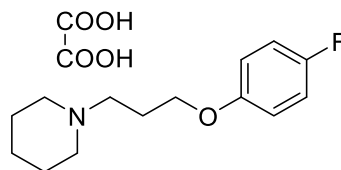
Yield: 78%

Appearance: White solid

Chemical formula: $C_{16}H_{22}FNO_5 \times C_2H_2O_4$

Molecular weight: 327.4 g/mol

Melting point: 156.5 °C



LC-MS: 99.66%, max. m/z: 237.98 $[M+H]^+$, with gradient LC-Method 1

1H NMR (300 MHz, DMSO- d_6) δ 7.12 (t, $^{3,3}J(H,H;H,F) = 8.8$ Hz, 2H, Ph-3,5-*H*), 6.94 (dd, $^{3,4}J(H,H;H,F) = 9.2, 4.4$ Hz, 2H, Ph-2,6-*H*), 4.00 (t, $J = 6.0$ Hz, 2H, -O- CH_2 -), 3.17 – 3.05 (m, 6H, overlap: Piperi- CH_2 -, Piperi-2,6-*H*₂), 2.17 – 2.02 (m, 2H, -O- CH_2 - CH_2 -), 1.73 (p, $J = 5.8$ Hz, 4H, Piperi-3,5-*H*₂), 1.57 – 1.49 (m, 2H, Piperi-4-*H*₂).

^{13}C NMR (75 MHz, DMSO- d_6) δ 164.74 (-CO-), 156.54 (d, $^1J(C,F) = 235.8$ Hz, Ph-4-C), 154.56 (d, $^4J(C,F) = 1.9$ Hz, Ph-1-C), 115.80 (d, $^2J(C,F) = 22.9$ Hz, Ph-3,5-C), 115.73 (d, $^3J(C,F) = 8.2$ Hz, Ph-2,6-C), 65.58 (-O- CH_2 -), 53.37 (Piperi- CH_2 -), 52.03 (Piperi-2,6-C), 23.41 (-O- CH_2 - CH_2 -), 22.53 (Piperi-3,5-C), 21.45 (Piperi-4-C).

Khorana and colleagues had reported 1-[3-(4-fluorophenoxy)propyl]piperidine hydrochloride with a melting point of 136-138 °C.

1-{3-[4-(Trifluoromethyl)phenoxy]propyl}piperidine hydrogen oxalate (**P9**, ST-2359)

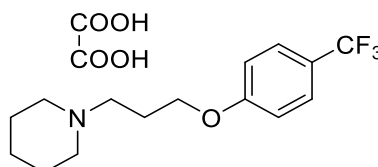
Analogous to compound **3**, compound **P9** was synthesized from 4-trifluoromethyl phenol (0.68 g, 4.18 mmol), alkyl chloride **2** (0.69 g, 3.48 mmol), K_2CO_3 (1.37 g, 10.2 mmol), and KI (0.06 g, 0.34 mmol) in 40 mL of acetone, refluxed for 18 h. The product was converted to hydrogen oxalate salt in acetone and recrystallized from acetone.

Yield: 82%

Appearance: White solid

Chemical formula: $C_{15}H_{20}F_3NO \times C_2H_2O_4$

Molecular weight: 377.4 g/mol



Melting point: 159.5 °C

LC-MS: 100%, m/z: 288.05 [M+H]⁺, with gradient LC-Method 2

¹H NMR (300 MHz, DMSO-*d*⁶) δ 7.66 (d, *J* = 8.7 Hz, 2H, Ph-3,5-*H*), 7.12 (d, *J* = 8.5 Hz, 2H, Ph-2,6-*H*), 4.12 (t, *J* = 6.1 Hz, 2H, -O-CH₂-), 3.30 – 2.93 (m, 6H, overlap: Piperi-CH₂-, Piperi-2,6-*H*₂), 2.22 – 2.05 (m, 2H, -O-CH₂-CH₂-), 1.73 (p, *J* = 5.8 Hz, 4H, Piperi-3,5-*H*₂), 1.58 – 1.45 (br, 2H, Piperi-4-*H*₂).

¹³C NMR (75 MHz, DMSO-*d*⁶) δ 164.75 (-CO-), 161.10 (Ph-1-C), 126.90 (q, ³*J*(C,F) = 3.7 Hz, Ph-3-C, -5-C), 124.52 (q, ¹*J*(C,F) = 271.4 Hz, -CF₃), 121.25 (q, ²*J*(C,F) = 32.1 Hz, Ph-4-C), 114.94 (Ph-2-C, -6-C), 65.44 (-O-CH₂-), 53.23 (Piperi-CH₂-), 52.05 (Piperi-2-C, -6-C), 23.26 (-O-CH₂-CH₂-), 22.53 (Piperi-3-C, -5-C), 21.45 (Piperi-4-C).

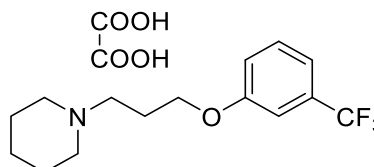
1-{3-[3-(Trifluoromethyl)phenoxy]propyl}piperidine hydrogen oxalate (**P10**, ST-2358)

Analogous to compound **3**, compound **P10** was synthesized from 3-trifluoromethyl phenol (0.68 g, 4.18 mmol), alkyl chloride **2** (0.69 g, 3.48 mmol), K₂CO₃ (1.37 g, 10.2 mmol), and KI (0.06 g, 0.34 mmol) in 40 mL of acetone. The reaction was refluxed for 18 h. The product was converted to hydrogen oxalate salt in acetone and recrystallized from acetone.

Yield: 86%

Appearance: White solid

Chemical formula: C₁₅H₂₀F₃NO × C₂H₂O₄



Molecular weight: 377.4 g/mol

Melting point: 171.2 °C

LC-MS: 100%, max. m/z: 288.05 [M+H]⁺, with gradient LC-Method 2

¹H NMR (300 MHz, DMSO-*d*⁶) δ 7.54 (t, *J* = 7.9 Hz, 1H, Ph-5-*H*), 7.34 – 7.20 (m, 3H, Ph-2,4,6-*H*), 4.12 (t, *J* = 6.0 Hz, 2H, -O-CH₂-), 3.24 – 2.96 (m, 6H, Piperi-CH₂-, Piperi-2,6-*H*₂), 2.20 – 2.05 (m, 2H, -O-CH₂-CH₂-), 1.73 (p, *J* = 5.9 Hz, 4H, Piperi-3,5-*H*₂), 1.58 – 1.44 (m, 2H, Piperi-4-*H*₂).

^{13}C NMR (75 MHz, $\text{DMSO-}d^6$) δ 164.70 (-CO-), 158.59 (Ph-1-C), 130.77 (Ph-5-C), 130.31 [quartet (q), $^2J(\text{C},\text{F}) = 31.6$ Hz, Ph-3-C], 124.00 (q, $^1J(\text{C},\text{F}) = 272.6$ Hz, -CF₃), 118.74 (Ph-6-C), 117.29 (q, $J = 3.9$ Hz, Phenoxy-4-C), 111.04 (q, $J = 3.9$ Hz, Phenoxy-2-C), 65.54 (-O-CH₂-), 53.31 (Piperi-CH₂-), 52.11 (Piperi-2,6-C), 23.37 (-O-CH₂-CH₂-), 22.60 (Piperi-3,5-C), 21.50 (Piperi-4-C).

6.4.3 Benzylidene malononitrile derivatives

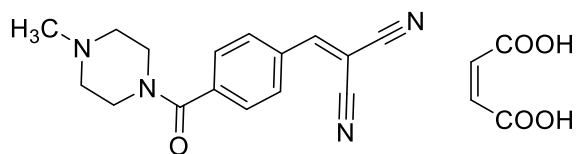
2-[4-(4-Methylpiperazine-1-carbonyl)benzylidene]malononitrile hydrogen maleate (**P11**, ST-2003)

Compound **P11** was synthesized via Knoevenagel condensation. A solution of malononitrile (66 mg, 1 mmol) in 2 mL of EtOAc was added to a solution of aldehyde **25** (232 mg, 1 mmol) in 1 mL EtOAc. Anhydrous MgSO_4 (240 mg, 2 mmol) was given to the solution. The product began to crystallize during the reaction and formed a thick mass. Therefore, 5 mL of EtOAc was given to reduce the viscosity. after 1 h, the reaction was completed, the suspension was filtered, and the residue was washed with warm EtOAc until the filtrate became colorless. The solvent was removed with a rotary evaporator, and the product was recrystallized in EtOAc and subsequently converted into hydrogen maleate salt in EtOAc.

Yield: 92%

Appearance: White solid

Chemical formula: $\text{C}_{16}\text{H}_{16}\text{N}_4\text{O} \times \text{C}_4\text{H}_4\text{O}_4$



Molecular weight: 396.4 g/mol

ESI-MS (+): m/z : 281.1 $[\text{M}+\text{H}]^+$

Melting point: 160.2 °C

CHN Analysis: calculated: C: 60.60%, H: 5.09%, N: 14.13%

found: C: 60.32%, H: 5.24%, N: 13.90%

^1H NMR (300 MHz, $\text{DMSO-}d^6$) δ 8.61 (s, 1H, Ph-CH=), 8.02 (d, $J = 8.2$ Hz, 2H, Ph-3,5-H), 7.68 (d, $J = 8.3$ Hz, 2H, Ph-2,6-H), 6.06 (s, 2H, Maleinic acid-CH=CH-), 3.78 (br, 2H, 4-Me-Pipera-

2,6-*H_{eq}*), 3.54 (br, 2H, 4-Me-Pipera-2,6-*H_{ax}*), 3.15 (br, 4H, 4-Me-Pipera-3,5-*H₂*), 2.75 (s, 3H, -*CH₃*).

¹³C NMR (75 MHz, DMSO-*d*⁶) δ 167.73 (-CO-N-), 167.23 (Maleinic acid-COOH), 160.58 (Ph-CH=), 139.81 (Ph-1-C), 135.47 (Maleinic acid-C=C-), 132.35 (Ph-4-C), 130.61 (Ph-3,5-C), 128.09 (Ph-2,6-C), 114.04 (-CN, E), 113.04 (-CN, Z), 82.97 (-CH=C(-CN)₂), 52.40 (Pipera-3,5-C), 44.35 (br, -CH₃), 42.71 (Pipera-2,6-C).

2-[4-(4-Methylpiperazine-1-carbonyl)benzyl]malononitrile (**P12**, ST-2004)

A solution of malononitrile (66 mg, 1 mmol) in 1.5 mL EtOH was given to a solution of aldehyde **26** (232 mg, 1 mmol) in 10 mL EtOH. The reaction mixture was stirred for 2 h at r.t. and cooled to 0 °C. NaBH₄ (19 mg, 0.5 mmol) was added to this solution. The mixture was kept stirring at 0 °C for 30 min. Upon completion of the reaction, the mixture was quenched with 5 mL of 1 M HCl and neutralized with NaHCO₃ solution. The aqueous solution was extracted with three portions of 20 mL of DCM. The organic layers were combined, dried with anhydrous MgSO₄, and concentrated in a rotary evaporator. The residue was purified via column chromatography. A solvent mixture of DCM and MeOH in a ratio of 95:5 was used as the eluent.

Yield: 84%

Appearance: White Solid

Chemical formula: C₁₆H₁₈N₄O

Molecular weight: 282.3 g/mol

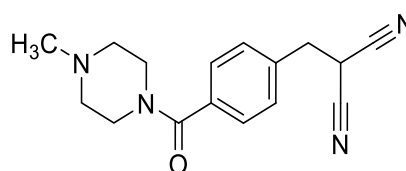
ESI-MS (+): m/z: 283.2 [M+H]⁺

Melting point: 131.3 °C

CHN Analysis: calculated: C, 68.06%; H, 6.43%; N, 19.84%

found: C, 67.87%; H, 6.72%; N, 19.57%

¹H NMR (300 MHz, CDCl₃) δ 7.44 (d, *J* = 8.4 Hz, 2H, Ph-3,5-*H*), 7.37 (d, *J* = 8.3 Hz, 2H, Ph-2,6-*H*), 4.01 (t, *J* = 6.8 Hz, 1H, -CH(-CN)₂), 3.81 (br, 2H, 4-Me-Pipera-2,6-*H_{eq}*), 3.47 (br, 2H, 4-Me-Pipera-2,6-*H_{ax}*), 3.30 (d, *J* = 6.8 Hz, 2H, Ph-CH₂-CH-), 2.51 (br, 2H, 4-Me-Pipera-3,5-*H_{eq}*), 2.41 (br, 2H, 4-Me-Pipera-3,5-*H_{ax}*), 2.35 (s, 3H, -*CH₃*).



Experiment

^{13}C NMR (75 MHz, DMSO- d^6) δ 168.60 (-CO-), 136.10 (Ph-1-C), 135.52 (Ph-4-C), 129.46 (Ph-2,6-C), 127.24 (Ph-3,5-C), 114.09 (-CN), 54.45 (4-Me-Pipera-3,5-C), 47.01 (br, -CH₃), 45.60 (4-Me-Pipera-2,6-C), 34.22 (Ph-CH₂-), 24.10 (-CH(-CN)₂).

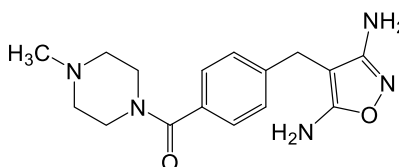
4-[[4-(4-Methylpiperazine-1-carbonyl)phenyl]methyl]-1,2-oxazole-3,5-diamine (**P13**, ST-2185)

Compound **P13** was synthesized via an adapted method reported previously (Vaquero *et al.*, 1987): **P12** (120 mg, 0.42 mmol), hydroxylamine hydrochloride (30 mg, 0.43 mmol), and TEA (0.12 mL, 0.84 mmol) were stirred in 2 mL of MeOH at r.t. for 48 h. The solvent was removed with a rotary evaporator, and the residue was purified via column chromatography. A solvent mixture of DCM and MeOH in a ratio of 90:10 was used as the eluent. The product was recrystallized in MeCN.

Yield: 42%

Appearance: White solid

Chemical formula: C₁₆H₂₁N₅O₂



Molecular weight: 315.4 g/mol

ESI-MS (+): 316.2 [M+H]⁺

Melting point: 151.5 °C

CHN-Analyse: calculated: C, 60.94%; H, 6.71%; N, 22.21%.

Found: C, 60.70%; H, 7.00%; N, 21.99%.

^1H NMR (300 MHz, DMSO- d^6) δ 7.27 (s, 4H, Ph-2,3,5,6-H), 6.10 (s, 2H, Isoxazole-3-NH₂), 5.01 (s, 2H, Isoxazole-5-NH₂), 3.51 (s, 2H, Ph-CH₂-), 3.74 – 3.20 (m, 4H, 4-Me-Pipera-2,6-H₂), 2.29 (br, 4H, 4-Me-Pipera-3,5-H₂), 2.18 (s, 3H, -CH₃).

^{13}C NMR (75 MHz, DMSO- d^6) δ 169.07 (-CO-), 165.57 (isoxazole-5-C), 163.92 (isoxazole-3-C), 142.92 (4-Me-Ph-1-C), 133.19 (4-Me-Ph-4-C), 127.90 (4-Me-Ph-3,5-C), 126.77 (4-Me-Ph-2,6-C), 79.73 (isoxazole-4-C), 54.46 (4-Me-Pipera-3,5-C), 47.06 (br, -CH₃), 45.58 (4-Me-Pipera-2,6-C), 25.36 (Ph-CH₂-).

6.4.4 Benzylidene thiohydantoin and hydantoin derivatives

(Z)-5-{4-[3-(Piperidin-1-yl)propoxy]benzylidene}-2-thioxoimidazolidin-4-one (**P14**, ST-2457)

The compound **P14** was synthesized with a microwave reactor. Aldehyde **3** (0.72 g, 2.9 mmol), compound **28** (0.48 g, 3 mmol), and NH₄OAc (0.46 g, 6 mmol) were dissolved in 15 mL of acetic acid in a microwave reaction tube. The mixture was radiated in MW at 180 °C for 15 min. The workup was analogous to that for compound **29**. The product was purified via column chromatography. Solvent mixtures of DCM and MeOH in ratios of 95:5 and 90:10 were used as the eluents.

Yield 77%

Appearance: Yellow solid

Chemical formula: C₁₈H₂₃N₃O₂S

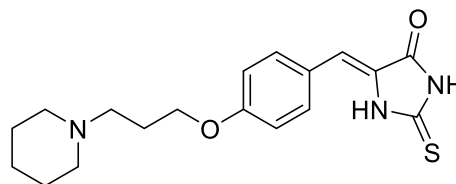
Molecular weight: 345.5 g/mol

Melting point: 166.4 °C

LC-MS: 100%, m/z: 346.15 [M+H]⁺, with gradient LC-Method 1

¹H NMR (300 MHz, DMSO-*d*⁶) δ 11.96 (s, 2H, NH), 7.73 (d, *J* = 8.6 Hz, 2H, Ph-2,6-*H*), 6.95 (d, *J* = 8.8 Hz, 2H, Ph-3,5-*H*), 6.42 (s, 1H, Ph-CH=), 4.05 (t, *J* = 6.3 Hz, 2H, -O-CH₂-), 2.47 – 2.30 (m, 6H, overlap: Piperi-CH₂-, Piperi-2,6-*H*₂), 1.87 (p, *J* = 6.6 Hz, 2H, -O-CH₂-CH₂-), 1.50 (p, *J* = 5.4 Hz, 4H, Piperi-3,5-*H*₂), 1.44 – 1.32 (m, 2H, Piperi-4-*H*₂).

¹³C NMR (75 MHz, DMSO-*d*⁶) δ 178.71 (-C=S), 166.25 (-CO-), 159.50 (Ph-4-C), 132.10 (Ph-2,6-C), 126.79 (Ph-CH=C), 125.06 (Ph-1-C), 114.78 (Ph-3,5-C), 111.87 (Ph-CH=C), 66.05 (-O-CH₂-), 54.94 (Piperi-CH₂-), 53.98 (Piperi-2,6-C), 26.04 (-O-CH₂-CH₂-), 25.41 (Piperi-3,5-C), 23.96 (Piperi-4-C).

(Z)-5-{4-[3-(Piperidin-1-yl)propoxy]benzylidene}imidazolidine-2,4-dione (**P15**, ST-2408)

Similar to **P14**, compound **P15** was synthesized from the corresponding aldehyde **3** (0.50 g, 2 mmol), hydantoin (0.20 g, 2 mmol), and NH₄OAc (0.15 g, 2 mmol) in 4 mL of AcOH. The mixture was heated at 200 °C in a sealed tube in MW for 20 min. The product was purified via

column chromatography. Solvent mixtures of DCM and MeOH in ratios of 95:5 and 90:10 were used as the eluents.

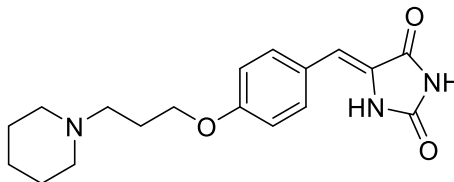
Yield: 33%

Appearance: Light yellowish solid

Chemical formula: C₁₈H₂₃N₃O₃

Molecular weight: 329.4 g/mol

Melting point: 199.1 °C



LC-MS: 100%, m/z: 330.23 [M+H]⁺, with gradient LC-Method 1

¹H NMR (300 MHz, DMSO-*d*⁶) δ 10.70 (s, 2H, -CO-NH), 7.57 (d, *J* = 8.8 Hz, 2H, Ph-2,6-*H*), 6.94 (d, *J* = 8.8 Hz, 2H, Ph-3,5-*H*), 6.37 (s, 1H, Ph-CH=), 4.03 (t, *J* = 6.4 Hz, 2H, -O-CH₂-), 2.42 – 2.21 (m, 6H, overlap: Piperi-CH₂-, Piperi-2,6-*H*₂), 1.85 (p, *J* = 6.6 Hz, 2H, -O-CH₂-CH₂-), 1.48 (p, *J* = 5.4 Hz, 4H, Piperi-3,5-*H*₂), 1.42 – 1.29 (m, 2H, Piperi-4-*H*₂).

¹³C NMR (75 MHz, DMSO-*d*⁶) δ 165.67 (Hyd-4-*C*), 158.87 (Ph-4-*C*), 155.70 (Hyd-2-*C*), 131.10 (Ph-2,6-*C*), 126.07 (Hyd-5-*C*), 125.34 (Ph-1-*C*), 114.77 (Ph-3,5-*C*), 108.67 (Ph-CH=), 66.07 (-O-CH₂-), 55.09 (Piperi-CH₂-), 54.12 (Piperi-2,6-*C*), 26.24 (-O-CH₂-CH₂-), 25.62 (Piperi-3,5-*C*), 24.16 (Piperi-4-*C*).

ROESY ¹H NMR (300 MHz, DMSO-*d*⁶) δ 7.57, 6.94 (Ph-2,6-*H*, Ph-3,5-*H*), 7.57, 6.37 (Ph-2,6-*H*, Ph-CH=), 6.94, 4.03 (Ph-3,5-*H*, -O-CH₂-), 4.03, 1.85 (-O-CH₂-, -O-CH₂-CH₂-), 2.37, 1.85 (Piperi-CH₂-, -O-CH₂-CH₂-)

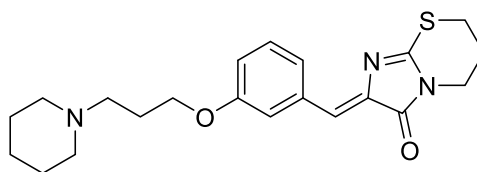
(*Z*)-2-{3-[3-(Piperidin-1-yl)propoxy]benzylidene}-6,7-dihydro-5*H*-imidazo[2,1-*b*][1,3]thiazin-3(2*H*)-one (**P16**, ST-2187)

The synthesis of compound **P16** was performed as described below: Compound **29** (1.03 g, 2.98 mmol), 1,3-dibromopropane (0.31 mL, 2.98 mmol), and Na₂CO₃ (0.64 g, 6 mmol) were suspended in 20 mL of EtOH. The mixture was refluxed for 16 h. After the completion of the reaction, the solvent was removed in a rotary evaporator, and the residue was purified with column chromatography. Solvent mixtures of DCM and MeOH in ratios of 95:5 and 90:10 were used as the eluents.

Yield: 7%

Appearance: Light yellow solid

Chemical formula: C₂₁H₂₇N₃O₂S



Molecular weight: 385.5 g/mol

APCI-MS (+): m/z: 386.3 [M+H]⁺

Melting point: 127.4 °C

Elemental Analysis: calculated: C, 65.43%; H, 7.06%; N, 10.90%; S, 8.32%

found: C, 65.68%; H, 7.08%; N, 10.70%; S, 8.12%

¹H NMR (300 MHz, CDCl₃) δ 7.70 (dd, ^{4,4}J = 2.6, 1.5 Hz, 1H, Ph-2-*H*), 7.62 (dt, ^{3,4}J = 7.8, 1.1 Hz, 1H, Ph-6-*H*), 7.27 (t, *J* = 8.0 Hz, 1H, Ph-5-*H*), 6.92 – 6.86 (m, 2H, overlap: Ph-4-*H*, Ph-*CH*=), 4.03 (t, *J* = 6.4 Hz, 2H, -O-*CH*₂-), 3.72 (t, *J* = 5.9 Hz, 2H, Thiazin-N-*CH*₂-), 3.17 – 3.04 (m, 2H, -S-*CH*₂-), 2.54 – 2.40 (m, 2H, Piperi-*CH*₂-), 2.40 (t, *J* = 5.3 Hz, 4H, Piperi-2,6-*H*₂), 2.32 – 2.18 (m, 2H, -S-*CH*₂-*CH*₂-), 2.07 – 1.90 (m, 2H, -O-*CH*₂-*CH*₂-), 1.58 (p, *J* = 5.5 Hz, 4H, Piperi-3,5-*H*₂), 1.51 – 1.35 (m, 2H, Piperi-4-*H*₂).

¹³C NMR (75 MHz, CDCl₃) δ 169.16 (-S-C(-N)=N-), 159.92 (-CO-), 159.19 (Ph-3-C), 137.77 (Ph-*CH*=C), 135.56 (Ph-1-C), 129.59 (Ph-5-C), 124.72, 124.29 (Ph-2,6-C), 117.18, 116.81 (Ph-4-C, Ph-*CH*=), 66.69 (-O-*CH*₂-), 56.14 (Piperi-*CH*₂-), 54.75 (Piperi-2,6-C), 39.95 (Thiazin-N-*CH*₂-), 26.93 (-O-*CH*₂-*CH*₂-), 26.21 (-S-*CH*₂-), 26.11 (Piperi-3,5-C), 24.57 (Piperi-4-C), 23.07 (-S-*CH*₂-*CH*₂-).

ROESY ¹H NMR (300 MHz, CDCl₃) δ 7.70, 6.94 (Ph-2-*H*, Ph-*CH*=), 7.62, 6.93 (Ph-4-*H*, Ph-6-*H*), 7.62, 7.27 (Ph-5-*H*, Ph-6-*H*), 7.27, 6.93 (Ph-4-*H*, Ph-5-*H*), 7.70, 4.03 (Ph-2-*H*, -O-*CH*₂-), 6.90, 4.03 (Ph-4-*H*, -O-*CH*₂-), 4.03, 2.01 (-O-*CH*₂-, -*CH*₂-*CH*₂-), 3.72, 2.28 (Thiazin-N-*CH*₂-, -S-*CH*₂-*CH*₂-), 3.14, 2.28 (-S-*CH*₂-, -S-*CH*₂-*CH*₂-), 2.50, 1.99 (Piperi-*CH*₂-, -O-*CH*₂-*CH*₂-), 1.58, 1.45 (Piperi-3,5-*H*₂, Piperi-4-*H*₂). Spectrum see section 6.5 (Figure 6-1).

(*Z*)-2-{4-[3-(Piperidin-1-yl)propoxy]benzylidene}-6,7-dihydro-5*H*-imidazo[2,1-*b*][1,3]thiazin-3(2*H*)-one (**P17**, ST-2188)

Experiment

The synthesis and purification of compound **P17** were analogous to **P16** from compound **P14** (0.50 g, 1.45 mmol), 1,3-dibromopropane (0.15 mL, 1.9 mmol), and Na₂CO₃ (0.32 g, 3 mmol) in 10 mL of EtOH. The mixture was refluxed for 16 h.

Yield: 15%

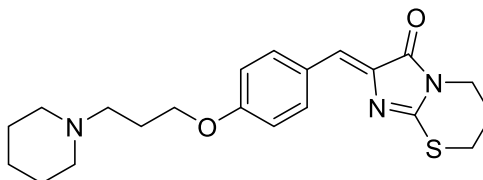
Appearance: Yellow solid

Chemical formula: C₂₁H₂₇N₃O₂S

Molecular weight: 385.5 g/mol

APCI-MS (+): m/z: 386.3 [M+H]⁺

Melting point: 157.9 °C



Elemental Analysis: calculated: C, 65.43%; H, 7.06%; N, 10.90%; S, 8.32%

found: C, 65.29%; H, 7.16%; N, 10.62%; S, 8.08%

¹H NMR (300 MHz, CDCl₃) δ 8.05 (d, *J* = 8.9 Hz, 2H, Ph-2,6-*H*), 6.93 (s, 1H, Ph-CH=), 6.90 (d, *J* = 8.9 Hz, 2H, Ph-3,5-*H*), 4.03 (t, *J* = 6.4 Hz, 2H, -O-CH₂-), 3.72 (t, *J* = 5.9 Hz, 2H, Thiazin-N-CH₂-), 3.11 (t, *J* = 5.7 Hz, 2H, -S-CH₂-), 2.52 – 2.43 (m, 2H, Piperi-CH₂-), 2.39 (t, *J* = 5.3 Hz, 4H, Piperi-2,6-*H*₂), 2.32 – 2.18 (m, 2H, -S-CH₂-CH₂-), 2.06 – 1.89 (m, 2H, -O-CH₂-CH₂-), 1.58 (p, *J* = 5.4 Hz, 4H, Piperi-3,5-*H*₂), 1.51 – 1.35 (m, 2H, Piperi-4-*H*₂).

¹³C NMR (75 MHz, CDCl₃) δ 169.24 (-S-C(=N)-N-), 160.74 (-CO-), 158.14 (Ph-4-C), 135.88 (Ph-CH=C), 133.93 (Ph-2,6-C), 127.18 (Ph-1-C), 124.71 (Ph-CH=C), 114.87 (Ph-3,5-C), 66.71 (-O-CH₂-), 56.00 (Piperi-CH₂-), 54.76 (Piperi-2,6-C), 39.95 (Thiazin-N-CH₂-), 26.86 (-O-CH₂-CH₂-), 26.22 (-S-CH₂-), 26.09 (Piperi-3,5-C), 24.54 (Piperi-4-C), 23.16 (-S-CH₂-CH₂-).

(*E*)-3-{4-[3-(Piperidin-1-yl)propoxy]benzylidene}-6,7-dihydro-5*H*-imidazo[2,1-*b*][1,3]thiazin-2(3*H*)-one (**P18**, ST-2189)

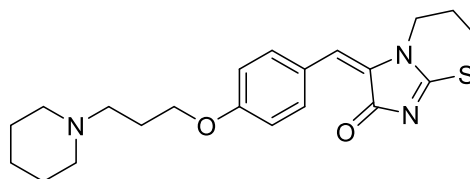
Compound **P18** was the second product isolated from the previously described reaction for compound **P17**.

Yield: 5%

Appearance: Yellow solid

Chemical formula: C₂₁H₂₇N₃O₂S

Molecular weight: 385.5 g/mol



APCI-MS (+): m/z: 386.3 [M+H]⁺

Melting point: 223.8 °C

Elemental Analysis: calculated.: C, 65.43%; H, 7.06%; N, 10.90%; S, 8.32%

found: C, 65.22%; H, 7.20%; N, 10.78%; S, 8.62%

¹H NMR (300 MHz, CDCl₃) δ 8.22 (d, *J* = 8.5 Hz, 2H, Ph-2,6-*H*), 6.88 (d, *J* = 8.6 Hz, 2H, Ph-3,5-*H*), 6.35 (s, 1H, Ph-CH=C), 4.04 (t, *J* = 6.3 Hz, 2H, -O-CH₂-), 3.70 (t, *J* = 5.9 Hz, 2H, Thiazin-N-CH₂-), 3.18 – 3.08 (m, 2H, -S-CH₂-), 2.58 – 2.34 (m, 8H, overlap: Piperi-CH₂-, Piperi-2,6-*H*₂-, -S-CH₂-CH₂-), 2.02 (p, *J* = 6.6 Hz, 2H, -O-CH₂-CH₂-), 1.63 (p, *J* = 5.6 Hz, 4H, Piperi-3,5-*H*₂), 1.52 – 1.42 (m, 2H, Piperi-4-*H*₂).

¹³C NMR (75 MHz, CDCl₃) δ 173.68, 171.11(-S-C(=N)-N-, -CO-), 160.72 (Ph-4-C), 133.42 (Ph-2,6-C), 130.87 (Ph-CH=C), 125.17 (Ph-1-C), 121.16 (Ph-CH=C), 114.43 (Ph-3,5-C), 66.56 (-O-CH₂-), 55.90 (Piperi-CH₂-), 54.64 (Piperi-2,6-C), 41.31 (Thiazin-N-CH₂-), 26.57 (-O-CH₂-CH₂-), 25.77 (Piperi-3,5-C), 25.45 (-S-CH₂-), 24.32 (Piperi-4-C), 22.47 (-S-CH₂-CH₂-).

ROESY ¹H NMR (300 MHz, CDCl₃) δ 8.22, 6.88 (Ph-2,6-*H*, Ph-3,5-*H*), 8.22, 6.35 (Ph-2,6-*H*, Ph-CH=), 6.88, 3.97 (Ph-3,5-*H*, -O-CH₂-), 6.30, 3.65 (Ph-CH=C, Thiazin-N-CH₂-), 4.04, 2.02(-O-CH₂-, -O-CH₂-CH₂-), 3.70, 2.35 (Thiazin-N-CH₂-, -S-CH₂-CH₂-), 2.48, 1.99 (Piperi-CH₂-, -O-CH₂-CH₂-), 1.63, 1.40 (Piperi-3,5-*H*₂, Piperi-4-*H*₂). Spectrum see section 6.5 (Figure 6-2).

(*Z*)-6-{4-[3-(Piperidin-1-yl)propoxy]benzylidene}-2,3-dihydroimidazo[2,1-*b*]thiazol-5(6*H*)-one (**P19**, ST-2395)

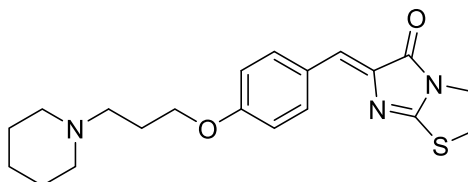
The synthesis of **P19** was analogous to that of **P16** from the compound **P14** (0.40 g, 1.16 mmol) and 1,2-dibromoethane (0.1 mL, 1.16 mmol). Instead of Na₂CO₃ and EtOH, K₂CO₃ (0.54 g, 3 mmol) and 10 mL of acetone were used in the preparation of **P19** (Kieć-Kononowicz and Karolak-wojciechowska, 1992). The reaction was refluxed for 16 h and subsequently filtered.

The filter cake was rinsed with acetone. The filtrate was collected, the solvent was removed in a rotary evaporator, and the residue was purified with column chromatography. Solvent mixtures of DCM and MeOH in ratios of 95:5 and 90:10 were used as the eluents.

Yield: 70%

Appearance: Yellow solid

Chemical formula: $C_{20}H_{25}N_3O_2S$



Molecular weight: 371.5

Melting point: 141.2 °C

LC-MS: 100%, m/z : 372.17 $[M+H]^+$, with gradient LC-Method 1

1H NMR (300 MHz, $CDCl_3$) δ 8.01 (d, J = 8.3 Hz, 2H, Ph-2,6-*H*), 6.94 – 6.84 (m, 3H, overlap: Ph-3,5-*H*, Ph-CH=C), 4.03 (t, J = 6.4 Hz, 2H, -O- CH_2 -), 3.93 (t, J = 7.0 Hz, 2H, -S- CH_2 -), 3.73 (t, J = 6.9 Hz, 2H, -S- CH_2 - CH_2 -), 2.56 – 2.30 (m, 6H, overlap: Piperi- CH_2 -, Piperi-2,6- H_2), 1.98 (p, J = 6.7 Hz, 2H, -O- CH_2 - CH_2 -), 1.59 (p, J = 5.6 Hz, 4H, Piperi-3,5- H_2), 1.50 – 1.36 (m, 2H, Piperi-4- H_2).

^{13}C NMR (151 MHz, $CDCl_3$) δ 168.05, 167.01 (-CO-, -S-C(=N)-N-), 160.83 (Ph-4-C), 142.80 (Ph-CH=C), 133.78 (Ph-2,6-C), 126.84 (Ph-1-C), 125.30 (Ph-CH=C), 114.91 (Ph-3,5-C), 66.70 (-O- CH_2 -), 55.98 (Piperi- CH_2 -), 54.74 (Piperi-2,6-C), 40.93 (-S- CH_2 - CH_2 -), 34.36 (-S- CH_2 -), 26.77 (-O- CH_2 - CH_2 -), 26.00 (Piperi-3,5-C), 24.49 (Piperi-4-C).

ROESY 1H NMR (300 MHz, $CDCl_3$) δ 8.04, 6.93 (Ph-2,6-*H*, Ph-3,5-*H*), 8.04, 6.91 (Ph-2,6-*H*, Ph-CH=C), 6.93, 4.07 (Ph-3,5-*H*, -O- CH_2 -), 4.07, 2.01 (-O- CH_2 -, -O- CH_2 - CH_2 -), 3.96, 3.77 (-S- CH_2 -, -S- CH_2 - CH_2 -), 2.50, 2.01 (Piperi- CH_2 -, -O- CH_2 - CH_2 -), 1.62, 1.47 (Piperi-3,5- H_2 , Piperi-4- H_2). Spectrum see section 6.5 (Figure 6-3).

The unspecific binding of compound **P19** to the thiol functional group was investigated. The following solution of the compound was prepared: The MeOH solution of the compound **P19** at an approximate concentration of 0.1 mg/mL, potassium phosphate buffer (50 mM, pH = 7.4). The solution of the compound **P19** at 0.1 mg/mL by diluting a 2 mg/mL MeOH solution with buffer, and the third solution was prepared in the same manner as the buffer solution with additional acetylcysteine solution (20 mg/mL, 700 μ L). The three mixtures described above were incubated at 37 °C for up to 110 h, samples were taken at 0, 2, 24, 48, and 110 h. 200 μ L of sample solution were promptly diluted with MeOH and investigated with LC-MS.

From the assessment, no signal of the product of Michael-Addition could be observed ($m/z = 534.20$ g/mol), indicating that compound **P19** is not a reactive Michael-acceptor and unlikely to undergo unspecific interaction with the target protein. However, the impurity peak, which displayed M+1 at 743.33, M+2 at 372.11, and M+3 at 248.32 in the solution with the addition of acetylcysteine, increased with time significantly and reached up to 30% AUC at 110 h. In contrast, the impurity peak in the MeOH solution of the compound **P19** remained below 2% and in the buffer solution 3.2%, respectively (Spectra see section 6.5, Figure 6-4 to 6-12). The measured molecular weight indicated a formation of dimer and probably an issue of stability in physiologic conditions. To reveal the mechanism and to identify the structure of this impurity, further investigations are necessary.

6.4.5 Guanidine derivatives

N-{*N*-Phenyl-*N'*-[3-(piperidin-1-yl)propyl]carbamimidoyl}benzamide dihydrochloride (**P20**, ST-2308)

The synthesis process for compound **P20** was adapted from the method described previously (Linney *et al.*, 2000): The thiourea derivative **30** (1.23 g, 4.8 mmol), K_2CO_3 (1.34 g, 10 mmol), and MeI (0.5 mL, 8 mmol) were added to 50 mL of EtOH. The reaction mixture was stirred at ambient temperature for 30 min. Upon the completion of the reaction, the solvent was removed in a rotary evaporator. The residue was taken in 50 mL of THF. Amine **20** (0.75 g, 5.24 mmol) was given to the solution mentioned above, and the reaction was stirred at r.t. for 18 h. The solvent was removed in a rotary evaporator, and the residue was purified with column chromatography. A solvent mixture from DCM and MeOH with a ratio of 95:5 was used as the eluent. The product was converted to HCl salt in dioxane.

Yield: 43%

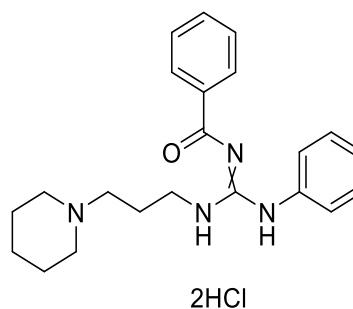
Appearance: White solid

Chemical formula: $C_{22}H_{28}N_4O \times 2xHCl$

Molecular weight: 437.4 g/mol

Melting point: 205.7 °C

LC-MS: 96.98%, m/z : 365.17 $[M+H]^+$, with gradient LC-Method 7



Experiment

^1H NMR (300 MHz, CDCl_3) δ 12.31 (s, 1H), 11.93 (s, 1H), 11.78 (s, 1H), 10.66 (s, 1H), (Piperi- N^+H , Guanidine-NH, N^+H), 8.32 (d, $J = 7.7$ Hz, 2H, Benzoyl-2,6-H), 7.72 – 7.39 (m, 5H, overlap: Benzoyl-3,4,5-H, Ph-3,5-H), 7.37 – 7.26 (m, 3H, overlap: Ph-2,4,6-H), 3.46 (d, $J = 11.8$ Hz, 2H, Piperi-2,6- H_{eq}), 3.25 (dt, $J = 11.0, 5.7$ Hz, 2H, Piperi- CH_2^-), 2.96 (s, 2H, Gua- CH_2^-), 2.79 (q, $J = 11.5$ Hz, 2H, Piperi-2,6- H_{ax}), 2.28 (s, 2H, Gua- $\text{CH}_2\text{-CH}_2^-$), 2.19 – 2.08 (m, 2H, Piperi-3,5- H_{eq}), 1.93 – 1.76 (m, 3H, overlap: Piperi-3,5- H_{ax} , -4- H_{eq}), 1.49 – 1.35 (m, 1H, Piperi-4- H_{ax}).

^{13}C NMR (75 MHz, CDCl_3) δ 169.42 (-CO-), 153.73 (Gua-C), 134.79 (Ph-1-C), 133.51 (Benzoyl-1-C), 130.19 (Ph-3,5-C), 130.06 (Benzoyl-4-C), 129.33 (Ph-4-C), 129.24 (Benzoyl-2,6-C), 129.06 (Benzoyl-3,5-C), 125.95 (Ph-2,6-C), 54.66 (Piperi- CH_2^-), 53.37 (Piperi-2,6-C), 43.03 (Gua- CH_2^-), 22.91 (Gua- $\text{CH}_2\text{-CH}_2^-$), 22.64 (Piperi-3,5-C), 21.99 (Piperi-4-C).

1-Phenyl-3-[3-(piperidin-1-yl)propyl]guanidine dihydrochloride (**P21**, ST-2297)

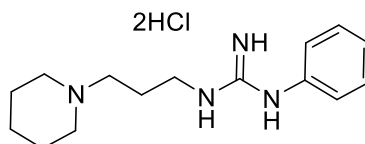
The compound **P21** was obtained by treating **P20** (0.92 g, 2.1 mmol) with 50 mL of 7M HCl (aq.) (Durant *et al.*, 1985). The solution was heated at 90 °C for 48 h and subsequently cooled down to 0 °C. The pH was adjusted with NaOH pellets to 10-11. The aqueous layer was extracted with three portions of 50 mL DCM. The organic layer was combined and dried with anhydrous MgSO_4 and subsequently concentrated in a rotary evaporator. The residue was purified via column chromatography, where solvent mixtures of DCM and MeOH (NH_3) in ratios of 90:10 and 80:20 were used as eluents. The product was converted to HCl salt in dioxane and recrystallized in acetone.

Yield: 61%

Appearance: White solid

Chemical formula: $\text{C}_{15}\text{H}_{24}\text{N}_4 \times 2\text{HCl}$

Molecular weight: 333.3 g/mol



Melting point: 187.5 °C

LC-MS: 96.03% (45.89%+49.14% with identical pattern in MS-spectra),. m/z: 261.08 $[\text{M}+\text{H}]^+$, with gradient LC-Method 8

Elemental Analysis: Calculated.: C, 54.05%; H, 7.86%; N, 16.81%

found: C, 53.71%; H, 8.20%; N, 16.69%

^1H NMR (600 MHz, $\text{DMSO-}d^6$ at 60 °C) δ 10.89 (s, 1H), 10.16 (s, 1H), 8.25 (s, 1H), 7.84 (s, 2H), (Piperi- N^+H , Gua-NH, N^+H_2), 7.44 (t, $J = 8.0$ Hz, 2H, Ph-3,5-H), 7.31 – 7.23 (m, 3H, Ph-2,4,6-H), 3.43 (q, $J = 6.5$ Hz, 2H, Piperi-2,6- H_{eq}), 3.22 (br, 2H, Piperi- CH_2 -), 3.11 – 3.06 (m, 2H, Piperi-2,6- H_{ax}), 2.88 (br, 2H, Gua- CH_2 -), 2.03 (p, $J = 7.2$ Hz, 2H, Gua- $\text{CH}_2\text{-CH}_2$ -), 1.82 (br, 4H, Piperi-3,5- H_2), 1.68 (br, 1H, Piperi-4- H_{eq}), 1.44 (br, 1H, Piperi-4- H_{ax}).

^{13}C NMR (151 MHz, $\text{DMSO-}d^6$) δ 154.90 (Gua-C), 135.56 (Ph-1-C), 129.63 (Ph-3,5-C), 126.20 (Ph-4-C), 124.36 (Ph-2,6-C), 53.21 (Piperi- CH_2 -), 51.99 (Piperi-2,6-C), 38.82 (Gua- CH_2 -), 23.03 (Gua- $\text{CH}_2\text{-CH}_2$ -), 22.19 (Piperi-3,5-C), 21.38 (Piperi-4-C).

N-{*N*-Benzyl-*N'*-[3-(piperidin-1-yl)propyl]carbamimidoyl}benzamide dihydrochloride (**P22**, ST-2298)

The guanidine derivative **P22** was synthesized via an adapted method reported previously (Esteves *et al.*, 2015). Compound **31** (0.54 g, 2 mmol) was dissolved in 20 mL of MeCN. The solution was cooled down to 0 °C. Amine **20** (0.28 g, 2 mmol), TEA (0.28 mL, 2 mmol), and *tert*-butyl hydroperoxide solution (*t*-BuOOH) (1 mL, 5-6 M in decane) were given successively. The reaction was allowed to reach the ambient temperature without removing the ice bath. After 48 h, the mixture was diluted with 60 mL of DCM, and the organic solution was washed with 60 mL of NaOH (1 N, aq.). The organic layer was collected and concentrated in a rotary evaporator, the obtained viscous liquid was dissolved in dioxane and converted to HCl salt. The attained white solid was recrystallized in 2-propanol and washed with acetone.

Yield: 24%

Appearance: White solid

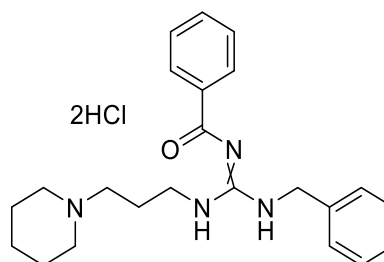
Chemical formula: $\text{C}_{23}\text{H}_{30}\text{N}_4\text{O} \times 2\text{HCl}$

Molecular weight: 451.4 g/mol

Melting point: 194.9 °C

LC-MS: 95.40%, m/z : 379.20 [$\text{M}+\text{H}^+$] $^+$, with gradient LC-Method 8

^1H NMR (600 MHz, $\text{DMSO-}d^6$ at 60 °C) δ 11.59 (s, 1H), 10.80 (s, 1H), 10.21 (s, 1H), 9.88 (s, 1H), (Piperi- N^+H , Gua-NH, N^+H), 8.03 (s, 2H, Benzoyl-2,6-H), 7.65 (t, $J = 7.4$ Hz, 1H, Benzoyl-4-H), 7.53 (t, $J = 7.6$ Hz, 2H, Benzoyl-3,5-H), 7.48 – 7.25 (m, 5H, Ph-2,3,4,5,6-H), 4.74 (s, 2H,



Ph-CH₂-), 3.64 (br, 4H, overlap: Gua-CH₂-CH₂-, Piperi-2,6-*H*_{eq}), 3.05 (s, 2H, Piperi-CH₂-), 2.81 (s, 2H, Piperi-2,6-*H*_{ax}), 2.14 – 2.06 (m, 2H, Gua-CH₂-CH₂-), 1.95 – 1.72 (m, 4H, Piperi-3,5-*H*₂), 1.69 (br, 1H, Piperi-4-*H*_{eq}), 1.40 (br, 1H, Piperi-4-*H*_{ax}).

¹³C NMR (151 MHz, DMSO-*d*⁶ at 60 °C) δ 166.98 (-CO-), 153.34 (Gua-C), 136.14 (Ph-1-C), 132.72 (Benzoyl-1-C), 128.41 (Benzoyl-4-C), 128.26 (Benzoyl-3,5-*H*, Ph-3,5-C), 128.18 (Ph-2,6-C), 127.44 (Benzoyl-2,6-C), 127.36 (Ph-4-C), 52.87 (Piperi-CH₂-), 51.81 (Piperi-2,6-C), 45.62 (Ph-CH₂-), 40.06 (Gua-CH₂-CH₂-), 22.44 (Gua-CH₂-CH₂-), 21.86 (Piperi-3,5-C), 21.10 (Piperi-4-C).

1-Benzyl-3-[3-(piperidin-1-yl)propyl]guanidine (**P23**, ST-2299)

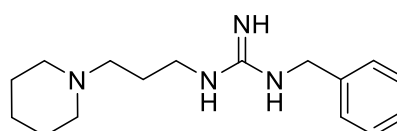
The synthesis of compound **P23** proceeded in analogous to **P20**. Compound **32** (0.56 g, 3.6 mmol) was dissolved in 20 mL of acetone, Mel (0.25 mL, 4 mmol) was given to the well-stirred solution. After 1 h, amine **20** (0.56 g, 4 mmol) was added to the mixture. The reaction was stirred at ambient temperature for 18 h. The solvent was removed in a rotary evaporator subsequently. The residue was purified with column chromatography, where the solvent mixtures of acetone and MeOH in ratios 100:0 and 90:10 were used as eluents.

Yield: 24%

Appearance: White to light yellowish, hygroscopic solid

Chemical formula: C₁₆H₂₆N₄

Molecular weight: 274.4 g/mol



Melting point: 74.5 °C

LC-MS: 97.1%, m/z: 275.12 [M+H]⁺, with gradient LC-Method 3

¹H NMR (300 MHz, CDCl₃) δ 7.26 (s, 2H, Ph-2,6-*H*), 7.20 – 7.05 (m, 3H, Ph-3,4,5-*H*), 4.40 (s, 2H, Ph-CH₂-), 3.07 (s, 2H, Gua-CH₂-), 2.09 (s, 6H, Piperi-CH₂-, Piperi-2,6-*H*₂), 1.51 (s, 2H, Gua-CH₂-CH₂-), 1.22 (s, 6H, Piperi-3,4,5-*H*₂).

¹³C NMR (75 MHz, CDCl₃) δ 157.63 (Gua-C), 137.92 (Ph-1-C), 128.41 (Ph-3,5-C), 127.33 (Ph-2,6-C), 127.09 (Ph-4-C), 53.81 (Piperi-CH₂-), 53.55 (Piperi-2,6-C), 44.81 (Ph-CH₂-), 38.78 (Gua-CH₂-), 25.65 (Gua-CH₂-CH₂-), 25.32 (Piperi-3,5-C), 24.12 (Piperi-4-C).

6.4.6 H₃R ligand with Phenyl pyrazole structure

(P24, ST-2406) 1-{3-[(1-Methyl-5-phenyl-1H-pyrazol-3-yl)oxy]propyl}piperidine

The title compound was synthesized analog to compound **3** from the phenylpyrazolol **34** (0.11 g, 0.63 mmol), alkyl chloride **2** (0.16 g, 0.8 mmol), K₂CO₃ (0.27 g, 2 mmol), and a catalytic amount of KI in 20 mL of acetone, the mixture was heated at 60 °C for 60 h. The product was purified with column chromatography, whereby the solvent mixture of DCM and MeOH with a ratio of 90:10 was used as the eluent.

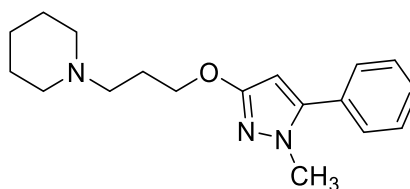
Yield: 64%

Appearance: Beige solid

Chemical formula: C₁₈H₂₅N₃O

Molecular weight: 299.4 g/mol

Melting point: 188.5 °C



LC-MS: 100%, m/z: 300.20 [M+H]⁺, gradient with LC-Method 2

¹H NMR (300 MHz, CDCl₃) δ 7.51 – 7.32 (m, 5H, Ph), 5.70 (s, 1H, -CH=), 4.25 (t, J = 5.5 Hz, 2H, -O-CH₂-), 3.71 (s, 3H, -CH₃), 3.65 (s, 2H, Piperi-2,6-*H*_{eq}), 3.31 – 3.20 (m, 2H, Piperi-CH₂-), 2.77 (s, 2H, Piperi-2,6-*H*_{ax}), 2.48 (dq, J = 11.3, 5.5 Hz, 2H, -O-CH₂-CH₂-), 2.35 (s, 2H, Piperi-3,5-*H*_{eq}), 1.94 (s, 3H, overlap: Piperi-3,5-*H*_{ax}, Piperi-4-*H*_{eq}), 1.57 (s, 1H, Piperi-4-*H*_{ax}).

¹³C NMR (75 MHz, CDCl₃) δ 161.54 (Pyrazol-3-C), 145.27 (Pyrazol-5-C), 130.37 (Ph-1-C), 128.73 (Ph-4-C), 128.71 (Ph-3,5-C), 128.66 (Ph-2,6-C), 90.34 (Pyrazol-4-C), 65.91 (-O-CH₂-), 55.32 (Piperi-CH₂-), 53.44 (Piperi-2,6-C), 37.04 (-CH₃), 23.90 (-O-CH₂-CH₂-), 22.39 (Piperi-3,5-C), 21.88 (Piperi-4-C).

ROESY ¹H NMR (300 MHz, CDCl₃) δ 7.40, 3.71 (Ph-*H*, -CH₃), 7.40, 5.71 (Ph-*H*, -CH=), 5.70, 4.25 (-CH=, -O-CH₂-), 4.26, 3.27 (-O-CH₂-, Piperi-CH₂-), 4.24, 2.47 (-O-CH₂-, -O-CH₂-CH₂-), 3.30, 2.45 (Piperi-CH₂-, -O-CH₂-CH₂-), 2.35, 1.96 (Piperi-3,5-*H*_{eq}, Piperi-4-*H*_{eq}). Spectrum see section 6.5 (Figure 6-13).

6.4.7 Spin-labeled H₃R ligands

2,2,6,6-Tetramethyl-4-({4-[3-(piperidin-1-yl)propoxy]benzyl}amino)-1-piperidinyloxy, free radical (**P25**, ST-2352)

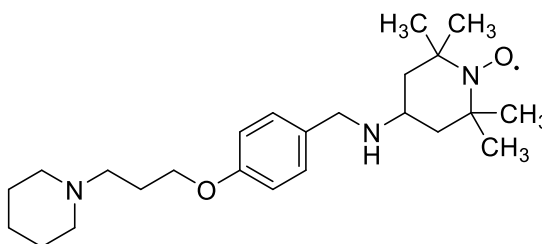
The compound **P25** was synthesized via Borch reductive amination: Amine **13** (0.20 g, 0.80 mmol), 4-oxo-TEMPO (0.10 g, 0.59 mmol), and AcOH (0.03 mL, 0.6 mmol) were dissolved in 5 mL of dichloroethane (DCE). The reaction mixture was stirred in r.t. for 1 h. NaBH(OAc)₃ (0.19 g, 0.9 mmol) was added to the aforementioned solution, and the reaction was further stirred at r.t. for 18 h. Upon the completion of the reaction monitored via TLC, 20 mL of NaHCO₃ solution was given to the mixture. The resulting mixture was extracted three times with 30 mL of DCM. The combined organic layer was dried with anhydrous MgSO₄ and concentrated in a rotary evaporator. The residue was purified with column chromatography, where the solvent mixtures of DCM and MeOH in ratios of 95:5 and 90:10 were used as eluents. The water bath temperature of the rotary evaporator in this experiment was set to approximately 30 °C.

Yield: 56%

Appearance: Red viscous liquid

Chemical formula: C₂₄H₄₀N₃O₂•

Molecular weight: 402.6 g/mol



LC-MS: 96.33%, m/z: 403.31 [M+H]⁺, with gradient LC-Method 11

Due to the presence of the free radical, only the part in the NMR spectrum, which is relatively far from the free radical, could be integrated (Spectra see section 6.5: Figure 6-14).

¹H NMR (300 MHz, CDCl₃) δ 7.31 – 6.99 (m, 2H, Ph-2,6-H), 6.82 (s, 2H, Ph-3,5-H), 3.94 (s, 2H, -O-CH₂-), 3.44 (br, 2H, Ph-CH₂-), 2.52 – 2.21 (m, 6H, Piperi-CH₂-, Piperi-2,6-H₂), 1.91 (s, 2H, -O-CH₂-CH₂-), 1.53 (s, 4H, Piperi-3,5-H₂), 1.38 (s, 2H, Piperi-4-H₂).

¹³C NMR (75 MHz, CDCl₃) δ 158.58 (Ph-4-C), 131.73 (Ph-1-C), 129.53 (Ph-2,6-C), 114.79 (Ph-1,3-C), 66.92 (-O-CH₂-), 56.14 (Piperi-CH₂-), 54.88 (Piperi-2,6-C), 49.30 (Ph-CH₂-), 27.11 (-O-CH₂-CH₂-), 26.23 (Piperi-3,5-C), 24.68 (Piperi-4-C).

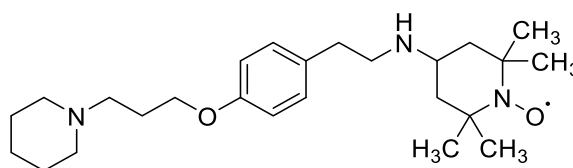
2,2,6,6-Tetramethyl-4-({4-[3-(piperidin-1-yl)propoxy]phenethyl}amino)-1-piperidinyloxy, free radical (**P26**, ST-2405)

Similar to compound **P25**, the compound **P26** was obtained from the tyramine derivative **15** (335 mg, 1 mmol), 4-oxo-TEMPO (170 mg, 1 mmol), AcOH (0.07 mL, 1.2 mmol), and NaBH(OAc)₃ (260 mg, 1.2 mmol) in 10 mL of DCE. The reaction was stirred at r.t. for 18 h. The water bath temperature of the rotary evaporator in this experiment was set to approximately 30 °C.

Yield: 69%

Appearance: Red viscous liquid

Chemical formula: C₂₅H₄₂N₃O₂•



Molecular weight: 416.6 g/mol

LC-MS: 100%, m/z: 417.34 [M+H]⁺, with gradient LC-Method 2

Due to the presence of the free radical, only the part in the NMR spectrum, which is relatively far from the free radical, could be integrated (Spectra see section 6.5: Figure 6-15).

¹H NMR (300 MHz, CDCl₃) δ 7.26 (s, 2H, Ph-2,6-*H*), 6.97 (s, 2H, Ph-3,5-*H*), 4.11 (s, 2H, -O-CH₂-), 3.03 (s, 2H, Ph-CH₂-CH₂-), 2.89 – 2.39 (m, 8H, overlap: Ph-CH₂-, Piperi-2,6-*H*₂, Piperi-CH₂-), 2.11 (t, *J* = 6.9 Hz, 2H, -O-CH₂-CH₂-), 1.73 (t, *J* = 5.4 Hz, 4H, Piperi-3,5-*H*₂), 1.63 – 1.50 (m, 2H, Piperi-4-*H*₂).

¹³C NMR (75 MHz, CDCl₃) δ 155.60 (Ph-4-C), 130.05 (Ph-1-C), 127.57 (Ph-2,6-C), 112.70 (Ph-3,5-C), 64.61 (-O-CH₂-), 54.07 (Piperi-CH₂-), 52.70 (Piperi-2,6-C), 33.22 (Ph-CH₂-), 24.84 (-O-CH₂-CH₂-), 23.95 (Piperi-3,5-C), 22.43 (Piperi-4-C).

6.4.8 Hybrid ligand with two H₃R pharmacophores

1-Methyl-4-({4-[3-(piperidin-1-yl)propoxy]phenyl)sulfonyl)piperazine (**P27**, ST-2360)

Like compound **3**, the title compound was synthesized from the sulfonamide derivative **27** (113 mg, 0.44 mmol), alkyl chloride **2** (105 mg, 0.53 mmol), K₂CO₃ (200 mg, 1.5 mmol), and a catalytic amount of KI in 40 mL of acetone. The reaction was reflux for 18 h. The product was

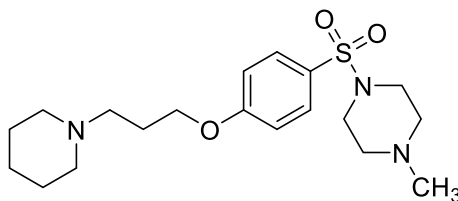
purified via column chromatography, where the solvent mixture of DCM and MeOH (NH₃) in a ratio of 97:3 was used as the eluent.

Yield: 78%

Appearance: Beige solid

Chemical formula: C₁₉H₃₁N₃O₃S

Molecular weight: 381.5 g/mol



Melting point: 78.7 °C

LC-MS: 97.42%, m/z: 191.46 [(M+2H⁺)/2]⁺, 382.16 [M+H⁺]⁺, with gradient LC-Method 2

¹H NMR (300 MHz, CDCl₃) δ 7.65 (d, *J* = 8.9 Hz, 2H, Ph-2,6-*H*), 6.96 (d, *J* = 8.9 Hz, 2H, Ph-3,5-*H*), 4.05 (t, *J* = 6.3 Hz, 2H, -CH₂-O-), 2.99 (t, *J* = 5.0 Hz, 4H, 1-Me-Pipera-3,5-*H*₂), 2.51 – 2.43 (m, 6H, overlap: Piperi-CH₂-, Piperi-2,6-*H*₂), 2.43 – 2.37 (m, 4H, 1-Me-Pipera-2,6-*H*₂), 2.24 (s, 3H, -CH₃), 1.98 (dq, *J* = 8.3, 6.4 Hz, 2H, -O-CH₂-CH₂-), 1.59 (p, *J* = 5.5 Hz, 4H, Piperi-3,5-*H*₂), 1.50 – 1.36 (m, 2H, Piperi-4-*H*₂).

¹³C NMR (75 MHz, CDCl₃) δ 162.62 (Ph-4-C), 129.90 (Ph-2,6-C), 126.64 (Ph-1-C), 114.63 (Ph-3,5-C), 66.93 (-O-CH₂-), 55.66 (Piperi-CH₂-), 54.64 (Piperi-2,6-C), 54.05 (1-Me-Pipera-2,6-C), 45.95 (1-Me-Pipera-3,5-C), 45.71 (-CH₃), 26.57 (-O-CH₂-CH₂-), 25.92 (Piperi-3,5-C), 24.37 (Piperi-4-C).

6.4.9 Dihydropyridine derivatives

3,5-Diacetyl-2,6-dimethyl-4-{4-[3-(piperidin-1-yl)propoxy]phenyl}-1,4-dihydropyridine (**P28**, ST-2186)

The dihydropyridine derivative **P28** was prepared via a modified method reported previously (Tamaddon *et al.*, 2010). The aldehyde **3** (0.5 g, 2.04 mmol) was dissolved in 1 mL of EtOH. This solution was added to a solution of acetylacetone (0.4 mL, 4 mmol) and (NH₄)₂CO₃ (0.31 g, 2 mmol) in 5 mL of H₂O. The mixture was heated at 60 °C for 4 h. Upon the completion of the reaction monitored via TLC, the reaction mixture was diluted with 10 mL of H₂O and extracted with three portions of 20 mL of DCM. The combined organic layer was dried with anhydrous MgSO₄ and concentrated in a rotary evaporator. The residue was purified with

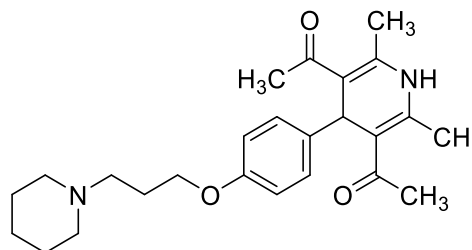
column chromatography using the solvent gradients consisted of DCM and MeOH in ratios from 95:5 to 85:15 as eluents.

Yield: 11%

Appearance: Light yellow solid

Chemical formula: C₂₅H₃₄N₂O₃

Molecular weight: 410.6 g/mol



APCI-MS (+): m/z: 411.4 [M+H]⁺

Melting point: 151.5 °C

Elemental Analysis: Calculated.: C, 73.14%; H, 8.35%; N, 6.82%.

Found: C, 72.99%; H, 8.52%; N, 6.52%.

¹H NMR (300 MHz, CDCl₃) δ 7.12 (d, *J* = 8.3 Hz, 2H, Ph-2,6-*H*), 6.74 (d, *J* = 8.2 Hz, 2H, Ph-3,5-*H*), 6.06 [s, 1H, dihydropyridine (DHP)-NH], 5.02 (s, 1H, DHP-4-*H*), 3.93 (t, *J* = 6.4 Hz, 2H, -O-CH₂-), 2.50 – 2.33 (m, 6H, overlap: Piperi-CH₂-, Piperi-2,6-*H*₂), 2.30 (s, 6H, DHP-2,6-CH₃), 2.25 (s, 6H, CH₃-CO-), 1.92 (p, *J* = 6.5 Hz, 2H, -O-CH₂-CH₂-), 1.57 (p, *J* = 5.5 Hz, 4H, Piperi-3,5-*H*₂), 1.48 – 1.36 (m, 2H, Piperi-4-*H*₂).

¹³C NMR (75 MHz, CDCl₃) δ 198.24 (-CO-), 157.83 (Ph-4-C), 142.91 (DHP-2,6-C), 138.42 (Ph-1-C), 128.58 (Ph-2,6-C), 114.53 (Ph-3,5-C), 114.09 (DHP-3,5-C), 66.53 (-O-CH₂-), 56.13 (Piperi-CH₂-), 54.75 (Piperi-2,6-C), 39.40 (DHP-4-C), 30.22 (CH₃-CO-), 26.97 (-O-CH₂-CH₂-), 26.10 (Piperi-3,5-C), 24.56 (Piperi-4-C), 20.54 (DHP-2,6-CH₃).

3,5-Diacetyl-2,6-dimethyl-4-{3-nitro-4-[3-(piperidin-1-yl)propoxy]phenyl}-1,4-dihydropyridine (**P29**, ST-2146)

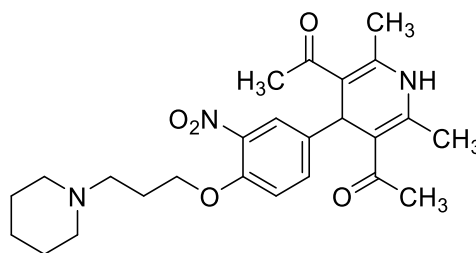
The synthesis and purification succeeded in analogous to that of compound **P28**. Aldehyde **5** (0.54 g, 1.85 mmol), acetylacetone (0.4 mL, 4 mmol), (NH₄)₂CO₃ (0.31 g, 2 mmol) were heated in 5 mL of H₂O and 1 mL of EtOH at 55 °C for 18 h.

Experiment

Yield: 14%

Appearance: Yellow solid

Chemical formula: C₂₅H₃₃N₃O₅



Molecular weight: 455.6 g/mol

APCI-MS (+): m/z: 456.4 [M+H]⁺

Melting point: 139.6 °C

Elemental Analysis: Calculated: C, 65.91%; H, 7.30%; N, 9.22%.

found: C, 65.93%; H, 7.55%; N, 8.84%.

¹H NMR (300 MHz, DMSO-*d*⁶) δ 9.01 (s, 1H, DHP-NH), 7.52 (d, ⁴J = 2.3 Hz, 1H, Ph-2-H), 7.37 (dd, ^{3,4}J = 8.7, 2.4 Hz, 1H, Ph-6-H), 7.19 (d, J = 8.8 Hz, 1H, Ph-5-H), 5.04 (s, 1H, DHP-4-H), 4.09 (t, J = 6.1 Hz, 2H, -O-CH₂-), 2.37 – 2.23 (m, 12H, overlap: Piperi-CH₂-, Piperi-2,6-H₂, DHP-2,6-CH₃), 2.20 (s, 6H, DHP-3,5-CH₃), 1.80 (p, J = 6.5 Hz, 2H, -O-CH₂-CH₂-), 1.45 (p, J = 5.3 Hz, 4H, Piperi-3,5-H₂), 1.39 – 1.31 (m, 2H, Piperi-4-H₂).

¹³C NMR (75 MHz, DMSO-*d*⁶) δ 195.96 (-CO-), 149.83 (Ph-4-C), 145.34 (DHP-2,6-C), 139.43 (Ph-1-C), 139.04 (Ph-3-C), 133.11 (Ph-6-C), 123.13 (Ph-2-C), 115.01 (Ph-5-C), 112.29 (DHP-3,5-C), 67.53 (-O-CH₂-), 54.79 (Piperi-CH₂-), 54.10 (Piperi-2,6-C), 37.23 (DHP-4-C), 30.44 (CH₃-CO-), 26.01 (-O-CH₂-CH₂-), 25.60 (Piperi-2,6-C), 24.14 (Piperi-4-C), 19.21 (DHP-2,6-CH₃).

3,5-Diethyl 2,6-dimethyl-4-{4-[3-(piperidin-1-yl)propoxy]phenyl}-1,4-dihydropyridine-3,5-dicarboxylate (**P30**, ST-2147)

The synthesis and purification were performed in analogous to compound **P28** from aldehyde **3** (0.50 g, 2 mmol), ethyl acetoacetate (0.51 mL, 4 mmol), (NH₄)₂CO₃ (0.31 g, 2 mmol) in 5 mL of H₂O, and 1 mL of EtOH. The reaction was heated at 55 °C for 4 h.

Yield: 33%

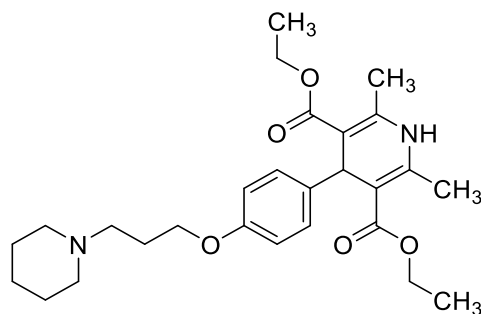
Appearance: Yellowish viscous liquid

Experiment

Chemical formula: $C_{27}H_{38}N_2O_5$

Molecular weight: 470.6 g/mol

APCI-MS: m/z : 471.2 $[M+H]^+$



CHN-Analysis: Calculated.: C, 68.91%; H, 8.14%; N, 5.95%

found: C, 68.82%; H, 8.42%; N, 5.75%

1H NMR (300 MHz, $DMSO-d_6$) δ 8.74 (s, 1H, DHP-1-NH), 7.03 (d, $J = 8.7$ Hz, 2H, Ph-2,6-H), 6.73 (d, $J = 8.7$ Hz, 2H Ph-3,5-H), 4.78 (s, 1H, DHP-4-H), 4.04 – 3.93 (m, 4H, $-CH_2-CH_3$), 3.89 (t, $J = 6.3$ Hz, 2H, Ph-O- CH_2-), 2.37 – 2.26 (m, 6H, overlap: Piperi- CH_2- , Piperi-2,6- H_2), 2.24 (s, 6H, DHP-2,6- CH_3), 1.79 (p, $J = 6.6$ Hz, 2H, $-O-CH_2-CH_2-$), 1.47 (p, $J = 5.4$ Hz, 4H, Piperi-3,5- H_2), 1.40 – 1.31 (m, 2H, Piperi-4- H_2), 1.13 (t, $J = 7.1$ Hz, 6H, CH_3-CH_2-).

^{13}C NMR (75 MHz, $DMSO-d_6$) δ 167.04 ($-CO-$), 156.89 (Ph-4C), 144.97 (DHP-2,6-C), 140.44 (Ph-1-C), 128.33 (Ph-2,6-C), 113.74 (Ph-3,5-C), 102.16 (DHP-3,5-C), 65.74 (Ph-O- CH_2-), 58.95 (DHP-2,6- CH_3), 55.23 (Piperi- CH_2-), 54.13 (Piperi-2,6-C), 37.97 (DHP-4-C), 26.39 ($-O-CH_2-CH_2-$), 25.61 (Piperi-3,5-C), 24.17 (Piperi-4C), 18.22 (DHP-2,6- CH_3), 14.21 ($-CH_2-CH_3$).

3,5-Diethyl 2,6-dimethyl-4-{3-nitro-4-[3-(piperidin-1-yl)propoxy]phenyl}-1,4-dihydropyridine-3,5-dicarboxylate hydrochloride (**P31**, ST-2301)

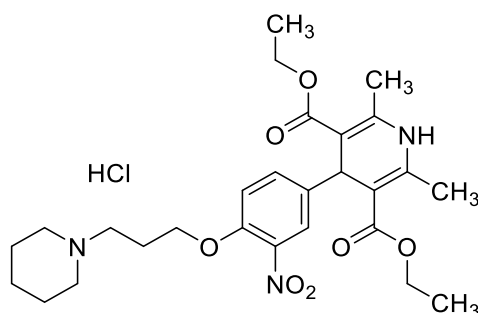
The synthesis and purification were performed in analog to compound **P28**. Aldehyde **5** (0.29 g, 1 mmol), ethyl acetoacetate (0.25 mL, 2 mmol), $(NH_4)_2CO_3$ (0.16 g, 1 mmol) were heated in 5 mL of H_2O and 1 mL of EtOH at 55 °C for 4 h. After purification via column chromatography, the product was converted to the corresponding HCl salt by treating with HCl in 2-propanol.

Yield: 41%

Appearance: Hygroscopic yellow solid

Chemical formula: $C_{27}H_{37}N_3O_7 \times HCl$

Molecular weight: 552.1 g/mol



Melting point: 111.8 °C

LC-MS: 98.5%, m/z: 516.32 [M+H]⁺, with gradient LC-Method 3

¹H NMR (300 MHz, CDCl₃) δ 7.74 (d, ⁴J = 2.2 Hz, 1H, Ph-2-*H*), 7.46 (dd, ^{3,4}J = 8.6, 2.3 Hz, 1H, Ph-6-*H*), 6.87 (d, *J* = 8.6 Hz, 1H, Ph-5-*H*), 6.50 (s, 1H, DHP-NH), 4.96 (s, 1H, DHP-4-*H*), 4.15 (t, *J* = 5.4 Hz, 2H, Ph-O-CH₂-), 4.12 – 4.01 (m, 4H, -CH₂-CH₃), 3.22 – 2.93 (m, 6H, overlap: Piperi-CH₂-, Piperi-2,6-*H*₂), 2.51 – 2.38 (m, 2H, -O-CH₂-CH₂-), 2.35 (s, 6H, DHP-2,6-CH₃), 2.02 (br, 4H, Piperi-3,5-*H*₂), 1.65 (br, 2H, Piperi-4-*H*₂), 1.21 (t, *J* = 7.1 Hz, 6H, CH₃-CH₂-).

¹³C NMR (75 MHz, CDCl₃) δ 167.38 (-CO-), 150.21 (Ph-4-C), 145.16 (DHP-2,6-C), 141.77 (Ph-1-C), 139.00 (Ph-3-C), 134.45 (Ph-6-C), 125.31 (Ph-2-C), 114.16 (Ph-5-C), 103.14 (DHP-3,5-C), 66.72 (Ph-O-CH₂-), 60.00 (CH₃-CH₂-), 55.20 (Piperi-CH₂-), 53.81 (Piperi-2,6-C), 39.06 (DHP-4-C), 24.18 (-O-CH₂-CH₂-), 22.81 (Piperi-3,5-C), 22.31 (Piperi-4-C), 19.56 (DHP-2,6-CH₃), 14.40 (CH₃-CH₂-).

3,5-Diethyl 2,6-dimethyl-4-[4-(4-methylpiperazine-1-carbonyl)phenyl]-1,4-dihydropyridine-3,5-dicarboxylate (**P32**, ST-2302)

The synthesis was performed in analogous to compound **P28** from aldehyde derivative **26** (0.23 g, 1 mmol), ethyl acetoacetate (0.26 g, 2 mmol), and ammonia solution 25%(aq.) (0.15 mL, 2 mmol). The reaction was heated under reflux for 20 h in 5 mL of EtOH. The product was purified via column chromatography, where the solvent mixture of DCM and MeOH in ratios of 95:5 and 90:10 were used as eluents.

Yield: 60%

Appearance: White solid

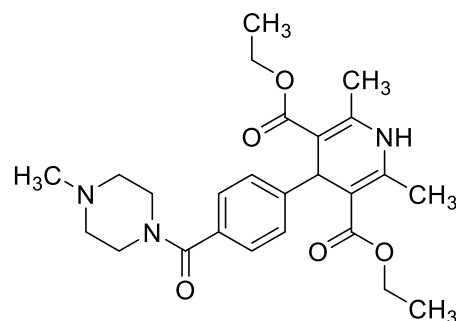
Chemical formula: C₂₅H₃₃N₃O₅

Molecular weight: 455.6 g/mol

Melting point: 194.3 °C

LC-MS: 100%, m/z: 456.27[M+H]⁺, with gradient LC-Method 3

¹H NMR (300 MHz, CDCl₃) δ 7.30 (d, *J* = 8.0 Hz, 2H, Ph-3,5-*H*), 7.19 (d, *J* = 8.5 Hz, 3H, overlap: Ph-2,6-*H*, DHP-NH), 4.89 (s, 1H, Ph-CH), 4.03 (qd, *J* = 7.1, 5.2 Hz, 4H, CH₃-CH₂-O-), 3.75 (br,



2H, Pipera-2,6- H_{eq}), 3.45 (br, 2H, Pipera-2,6- H_{ax}), 2.41 (br, 2H, Pipera-3,5- H_{eq}), 2.32 (br, 2H, Pipera-3,5- H_{ax}), 2.28 (s, 3H, Pipera- CH_3), 2.09 (s, 6H, DHP-2,6- CH_3), 1.17 (t, $J = 7.1$ Hz, 6H, - CH_2-CH_3).

^{13}C NMR (75 MHz, $CDCl_3$) δ 170.96 (Ph-CO-), 167.59 (DHP-CO-O-), 150.66 (Ph-1-C), 145.24 (DHP-2C, -6C), 132.95 (Ph-4-C), 128.19 (Ph-2,6-C), 126.62 (Ph-3,5-C), 103.04 (DHP-3,5-C), 59.65 (-O- CH_2 -), 47.75 (Pipera- CH_3), 46.08 (Pipera-3,5-C), 42.16 (DHP-4-C), 39.74 (Pipera-2,6-C), 18.85 (DHP-2,6- CH_3), 14.33 (CH_3-CH_2 -).

3,5-Dicyano-2,6-dimethyl-4-{4-[3-(piperidin-1-yl)propoxy]phenyl}-1,4-dihydropyridine
(**P33**, ST-2390)

Compound **P33** was synthesized via an adapted method previously reported (Sanad *et al.*, 2016). Aldehyde **3** (0.25 g, 1 mmol), 3-aminocrotonitrile (0.17 g, 2 mmol) were dissolved in 1 mL of AcOH. The mixture was radiated in MW at 120 °C for 10 min. After completion, the reaction mixture was poured into crushed ice. The pH of the resulting solution was adjusted to 9-10 with 6 M NaOH solution (aq.) and the aqueous solution was extracted three times with 30 mL of DCM. The combined organic layer was dried over anhydrous $MgSO_4$ and concentrated in a rotary evaporator. The residue was purified with column chromatography by using the solvent mixture of DCM and MeOH in a ratio of 95:5 as the eluent.

Yield: 19%

Appearance: White solid

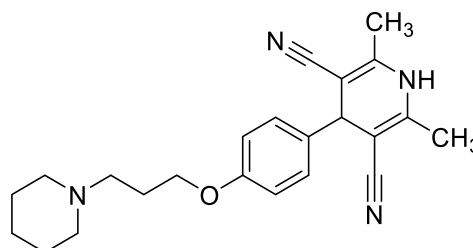
Chemical formula: $C_{23}H_{28}N_4O$

Molecular weight: 376.5 g/mol

Melting point: 131.6 °C

LC-MS: 96.16%, m/z : 377.15 [$M+H^+$] $^+$ with gradient LC-Method 1

1H NMR (300 MHz, $CDCl_3$) δ 7.15 (d, $J = 8.6$ Hz, 2H, Ph-2,6- H), 6.87 (d, $J = 8.6$ Hz, 2H, Ph-3,5- H), 6.71 (br, 1H, DHP-NH), 4.26 (s, 1H, DHP-4- H), 3.99 (t, $J = 6.3$ Hz, 2H, -O- CH_2 -), 2.57 – 2.35 (m, 6H, overlap: Piperi- CH_2 -, Piperi-2,6- H_2), 2.06 (s, 6H, - CH_3), 2.03 – 1.93 (m, 2H, -O- CH_2-CH_2 -), 1.62 (p, $J = 5.6$ Hz, 4H, Piperi-3,5- H_2), 1.52 – 1.40 (m, 2H, Piperi-4- H_2).



^{13}C NMR (75 MHz, CDCl_3) δ 158.92 (Ph-4-C), 145.16 (DHP-2,6-C), 135.11 (Ph-1-C), 128.90 (Ph-2,6-C), 118.99 (-CN), 115.05 (Ph-3,5-C), 85.39 (DHP-3,5-C), 66.52 (-O- CH_2 -), 56.03 (Piperi- CH_2 -), 54.67 (Piperi-2,6-C), 41.42 (DHP-4-C), 26.70 (-O- CH_2 - CH_2 -), 25.81 (Piperi-3,5-C), 24.35 (Piperi-4-C), 18.56 (- CH_3).

3-Acetyl-2,6-dimethyl-4-phenyl-5-{4-[3-(piperidin-1-yl)propoxy]benzoyl}-1,4-dihydropyridin
(**P34**, ST-2267)

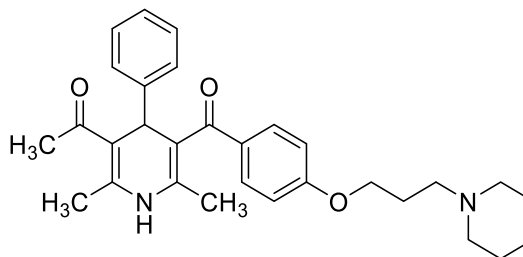
The compounds **37** (0.28 g, 1.5 mmol) and **36** (0.45 g, 1.5 mmol) were dissolved in 2 mL of EtOH in a sealed microwave tube. The reaction mixture was heated in MW at 160 °C for 15 min. The solvent was removed in the rotary evaporator, and the residue was purified via column chromatography. A solvent mixture of DCM and MeOH in the ratio of 85:15 was used as the eluent. The characterization of stereochemistry was not performed.

Yield: 22%

Appearance: Yellow solid

Chemical formula: $\text{C}_{30}\text{H}_{36}\text{N}_2\text{O}_3$

Molecular weight: 472.6 g/mol



Melting point: 74.0 °C

LC-MS: 97.39%, m/z = 473.23 [$\text{M}+\text{H}^+$] $^+$, with gradient LC-Method 4

^1H NMR (300 MHz, CDCl_3) δ 7.52 (d, J = 8.8 Hz, 2H, Benzoyl-2,6- H), 7.22 – 7.13 (m, 2H, Ph-3,5- H), 7.13 – 7.03 (m, 3H, Ph-2,4,6- H , overlap), 6.82 (d, J = 8.8 Hz, 2H, Benzoyl-3,5- H), 6.13 (s, 1H, NH), 5.08 (s, 1H, DHP-4-H), 4.02 (t, J = 6.3 Hz, 2H, -O- CH_2 -), 2.56 – 2.49 (m, 2H, Piperi- CH_2 -), 2.49 – 2.44 (m, 4H, Piperi-2,6- H_2), 2.42 (s, 3H, DHP-2- CH_3), 2.07 (s, 3H, CH_3 -CO-), 2.05 – 1.92 (m, 2H, -O- CH_2 - CH_2 -), 1.73 (s, 3H, DHP-6- CH_3), 1.62 (p, J = 5.6 Hz, 4H, Piperi-3,5- H_2), 1.51 – 1.39 (m, 2H, Piperi-4- H_2).

^{13}C NMR (75 MHz, CDCl_3) δ 198.86 (CH_3 -CO-), 197.56 (Benzoyl-CO-), 162.40 (Benzoyl-4-C), 145.78 (DHP-6-C), 145.64 (DHP-2-C), 136.32 (Ph-1-C), 132.47 (Benzoyl-1-C), 131.02 (Benzoyl-2,6-C), 128.72 (Ph-2,6-C), 127.12 (Ph-3,5-C), 126.68 (Ph-4-C), 115.25 (DHP-3-C), 114.29 (Benzoyl-3,5-C), 109.78 (DHP-5-C), 66.62 (-O- CH_2 -), 55.87 (Piperi- CH_2 -), 54.62

(Piperi-2,6-C), 43.41 (DHP-4-C), 29.60 (CH₃-CO-), 26.46 (-O-CH₂-CH₂-), 25.67 (Piperi-3,5-C), 24.24 (Piperi-4-C), 20.70 (DHP-2-CH₃), 18.39 (DHP-6-CH₃).

ROESY (300 MHz, CDCl₃) Cross peaks: δ 7.52,6.82, (Benzoyl-2,6-*H*, Benzoyl-3,5-*H*), 7.52, 5.08, (Benzoyl-2,6-*H*, DHP-4-*H*), 7.52, 1.73, (Benzoyl-2,6-*H*, DHP-6-CH₃), 7.21, 7.03, (Ph-3,5-*H*, Ph-2,4,6-*H*), 7.07, 5.08, (Ph-2,4,6-*H*, DHP-4-*H*), 7.07, 2.07, (Ph-2,4,6-*H*, CH₃-CO-), 6.82, 4.02, (Benzoyl-3,5-*H*, -O-CH₂-), 6.13, 2.42, (NH, DHP-2-CH₃), {6.13, 1.73, (NH, DHP-6-CH₃), 5.08, 2.07, (DHP-4-*H*, CH₃-CO-), 4.02, 2.52, (-O-CH₂-, Piperi-CH₂-), 4.02, 2.02, (-O-CH₂-, -O-CH₂-CH₂-), 2.51, 2.00, (Piperi-CH₂-, -O-CH₂-CH₂-), 2.07, 2.42, (CH₃-CO-, DHP-2-CH₃), 2.42, 1.73, (DHP-2-CH₃, DHP-6-CH₃), 1.62, 1.45, (Piperi-3,5-*H*₂, Piperi-4-*H*₂). Spectrum see section 6.5 (Figure 6-16).

6.4.10 Dihydropyrimidine derivatives

5-Acetyl-6-methyl-4-{4-[3-(piperidin-1-yl)propoxy]phenyl}-3,4-dihydropyrimidin-2(1*H*)-one hydrochloride (**P35**, ST-2404)

Compound **P35** was synthesized analogous to compound **3**. The Biginelli product **38** (0.47 g, 1.91 mmol), alkyl chloride **2** (0.40 g, 2 mmol), KI (0.17 g, 1 mmol), and K₂CO₃ (0.83 g, 6 mmol) were dissolved in 15 mL of DMF. The reaction was heated at 70 °C for 40 h. The purification was performed via column chromatography, where a solvent mixture of DCM and MeOH in the gradient of 95:5 to 85:15 was used as the eluent. The obtained product was treated with HCl in EtOAc to obtain the corresponding salt.

Yield: 78%

Appearance: Light yellowish solid

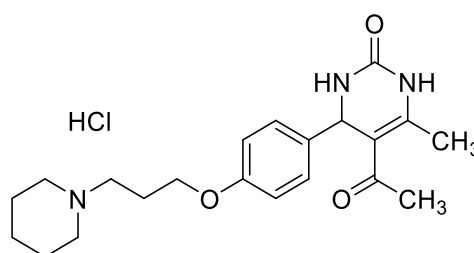
Chemical formula: C₂₁H₂₉N₃O₃ × HCl

Molecular weight: 407.9 g/mol

Melting point: 228.7 °C

LC-MS: 100%, m/z: 372.29 [M+H]⁺, with gradient LC-Method 1

¹H NMR (300 MHz, DMSO-*d*⁶) δ 10.66 (s, 1H, Piperi-NH⁺), 9.15 (d, ⁴J = 2.0 Hz, 1H, DHPM-3-*H*), 7.77 (dd, ^{3,4}J = 3.6, 2.0 Hz, 1H, DHPM-1-*H*), 7.16 (d, J = 8.7 Hz, 2H, Ph-2,6-*H*), 6.89 (d, J



= 8.7 Hz, 2H, Ph-3,5-*H*), 5.20 (d, $J = 3.4$ Hz, 1H, DHPM-6-*H*), 4.02 (t, $J = 6.0$ Hz, 2H, -O-CH₂-), 3.41 (d, $J = 12.3$ Hz, 2H, Piperi-2,6-*H*_{eq}), 3.19 – 3.05 (m, 2H, Piperi-CH₂-), 2.94 – 2.76 (m, 2H, Piperi-2,6-*H*_{ax}), 2.28 (s, 3H, CH₃-CO-), 2.25 – 2.10 (m, 2H, -O-CH₂-CH₂-), 2.07 (s, 3H, DHPM-4-CH₃), 1.89 – 1.64 (m, 5H, overlap: Piperi-3,5-*H*₂, Piperi-4-*H*_{eq}), 1.45 – 1.31 (m, 1H, Piperi-4-*H*_{ax}).

¹³C NMR (75 MHz, DMSO-*d*⁶) δ 194.34 (CH₃-CO-), 157.52 (Ph-4-C), 152.07 (DHPM-2-C), 147.89 (DHPM-4-C), 136.65 (Ph-1-C), 127.67 (Ph-2,6-C), 114.43 (Ph-3,5-C), 109.57 (DHPM-5-C), 65.07 (-O-CH₂-), 53.37, 53.24 (DHPM-6-C, Piperi-CH₂-), 51.93 (Piperi-2,6-C), 30.19 (-O-CH₂-CH₂-), 23.23 (CH₃-CO-), 22.30 (Piperi-3,5-C), 21.41 (Piperi-4-C), 18.85 (DHPM-4-CH₃).

Ethyl 6-methyl-2-oxo-4-{4-[3-(piperidin-1-yl)propoxy]phenyl}-1,2,3,4-tetrahydropyrimidine-5-carboxylate (**P36**, ST-2403)

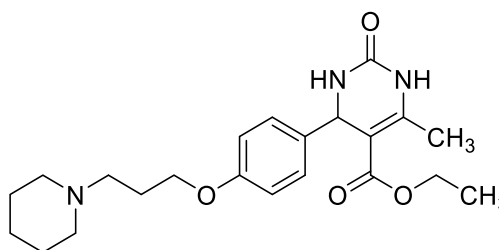
Similar to compound **3**, compound **P36** was obtained from the reaction between intermediate **39** (0.92 g, 3.33 mmol), alkyl chloride **2** (0.68 g, 3.34 mmol), K₂CO₃ (1.0 g, 8 mmol), and a catalytic amount of KI in acetone 30 mL. The reaction mixture was heated at reflux for 40 h. Flash column chromatography was performed to purify the product, where a solvent mixture of DCM and MeOH in the gradient with ratios from 95:5 to 85:15 was used as the eluent.

Yield: 84%

Appearance: White solid

Chemical formula: C₂₂H₃₁N₃O₄

Molecular weight: 401.5 g/mol



Melting point: 147.4 °C

LC-MS: 100%, m/z : 402.28 [M+H]⁺, with gradient LC-Method 2

¹H NMR (300 MHz, DMSO-*d*⁶) δ 9.14 (d, $^4J = 2.0$ Hz, 1H, DHPM-1-NH), 7.65 (dd, $^3J, ^4J = 3.4, 2.1$ Hz, 1H, DHPM-3-NH), 7.13 (d, $J = 8.7$ Hz, 2H, Ph-2,6-*H*), 6.86 (d, $J = 8.7$ Hz, 2H, Ph-3,5-*H*), 5.08 (d, $J = 3.3$ Hz, 1H, DHPM-4-*H*), 4.07 – 3.90 (m, 4H, overlap: Ph-O-CH₂-, CH₃-CH₂-), 2.51 – 2.31 (m, 6H, overlap: Piperi-CH₂-, Piperi-2,6-*H*₂), 2.23 (s, 3H, DHPM-6-CH₃), 1.93 – 1.79 (m, 2H, -O-CH₂-CH₂-), 1.59 – 1.45 (m, 4H, Piperi-3,5-*H*₂), 1.44 – 1.34 (m, 2H, Piperi-4-*H*₂), 1.10 (t, $J = 7.1$ Hz, 3H, -CH₂-CH₃).

^{13}C NMR (75 MHz, $\text{DMSO-}d^6$) δ 165.38 (-CO-O-), 157.79 (Ph-4-C), 152.15 (-NH-CO-NH-), 148.00 (DHPM-6-C), 137.02 (Ph-1-C), 127.40 (Ph-2,6-C), 114.24 (Ph-3,5-C), 99.56 (DHPM-5-C), 65.77 (Ph-O-CH₂-), 59.15 (-O-CH₂-CH₃), 54.94 (Piperi-CH₂-), 53.85 (Piperi-2,6-C), 53.34 (DHPM-4-C), 25.92 (-O-CH₂-CH₂-), 25.20 (Piperi-3,5-C), 23.78 (Piperi-4-C), 17.77 (DHPM-6-CH₃), 14.11 (-CH₂-CH₃).

3,5-Diacetyl-6-methyl-4-{4-[3-(piperidin-1-yl)propoxy]phenyl}-3,4-dihydropyrimidin-2(1H)-one (**P37**, ST-2461)

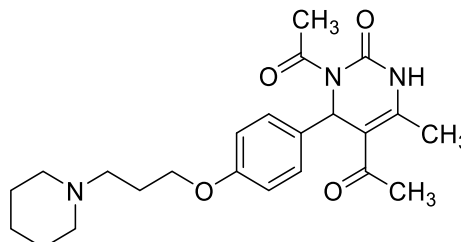
Compound **P37** was synthesized via a modified method reported previously (Dallinger *et al.*, 2003). Compound **P35** (0.52 g, 1.4 mmol), Ac₂O (0.33 mL, 3.5 mmol), TEA (0.49 mL, 3.5 mmol), and DMAP (34 mg, 0.28 mmol) were dissolved in 3 mL of MeCN. The mixture was heated in MW at 130 °C for 10 min. The resulting solution was concentrated in a rotary evaporator, and the residue was purified with column chromatography, where the solvent mixtures consisting of DCM and MeOH in ratios of 95:5 and 90:10 were used as eluents.

Yield: 78%

Appearance: Beige solid

Chemical formula: C₂₃H₃₁N₃O₄

Molecular weight: 413.5 g/mol



Melting point: 163.7 °C

LC-MS: 100%, max. m/z = 414.26 [M+H]⁺, with gradient LC-Method 1

^1H NMR (300 MHz, CDCl_3) δ 8.23 (s, 1H, DHPM-NH), 7.23 (d, J = 8.7 Hz, 2H, Ph-2,6-H), 6.80 (d, J = 8.8 Hz, 2H, Ph-3,5-H), 6.64 (s, 1H, DHPM-6-H), 3.95 (t, J = 6.3 Hz, 2H, -O-CH₂-), 2.54 (s, 3H, DHPM-1-CO-CH₃), 2.50 – 2.34 (m, 9H, overlap: Piperi-CH₂-, Piperi-2,6-H₂, DHPM-5-CO-CH₃), 2.18 (s, 3H, DHPM-4-CH₃), 2.02 – 1.87 (m, 2H, -O-CH₂-CH₂-), 1.58 (p, J = 5.5 Hz, 4H, Piperi-3,5-H₂), 1.49 – 1.36 (m, 2H, Piperi-4-H₂).

^{13}C NMR (75 MHz, CDCl_3) δ 195.68 (DHPM-5-CO-CH₃), 171.63 (DHPM-3-CO-CH₃), 159.20 (Ph-4-C), 151.91(-N-CO-NH-), 144.92 (DHPM-4-C), 130.55 (Ph-1-C), 128.74 (Ph-2,6-C), 114.86 (DHPM-3,5-C), 113.46 (DHPM-5-C), 66.55 (-O-CH₂-), 56.01 (Piperi-CH₂-), 54.71

(Piperi-2,6-C), 53.16 (DHPM-6-C), 29.74 (DHPM-5-CO-CH₃), 26.76, 26.54 (Ph-O-CH₂-CH₂-, DHPM-1-CO-CH₃), 25.95 (Piperi-3,5-C), 24.46 (Piperi-4-C), 18.61.(DHPM-4-CH₃)

Ethyl 3-acetyl-6-methyl-2-oxo-4-{4-[3-(piperidin-1-yl)propoxy]phenyl}-1,2,3,4-tetrahydropyrimidine-5-carboxylate (**P38**, ST-2402)

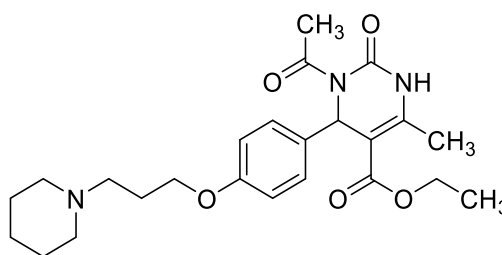
The synthesis and purification of compound **P38** were similar to that of compound **P37**. The starting materials were compound **P36** (0.20 g, 0.5 mmol), Ac₂O (0.12 mL, 1.2 mmol), TEA (0.17 mL, 1.2 mmol), DMAP (12 mg, 0.1 mmol) and 1 mL of MeCN.

Yield: 94%

Appearance: Light yellowish solid

Chemical formula: C₂₄H₃₃N₃O₅

Molecular weight: 443.5 g/mol



Melting point: 159.2 °C

LC-MS: 100%, m/z: 444.29 [M+H]⁺, with gradient LC-Method 2

¹H NMR (300 MHz, CDCl₃) δ 8.04 (s, 1H, DHPM-NH), 7.23 (d, *J* = 8.7 Hz, 2H, Ph-2,6-H), 6.78 (d, *J* = 8.8 Hz, 2H, Ph-3,5-H), 6.56 (s, 1H, DHPM-4-H), 4.15 (q, *J* = 7.1 Hz, 2H, CH₃-CH₂-), 3.95 (t, *J* = 6.3 Hz, 2H, Ph-O-CH₂-), 2.54 (s, 3H, CH₃-CO-), 2.52 – 2.41 (m, 6H, overlap: Piperi-CH₂-, Piperi-2,6-H₂), 2.40 (s, 3H, DHPM-6-CH₃), 2.02 – 1.90 (m, 2H, Ph-O-CH₂-CH₂-), 1.60 (p, *J* = 5.5 Hz, 4H, Piperi-3,5-H₂), 1.49 – 1.39 (m, 2H, Piperi-4-H₂), 1.23 (t, *J* = 7.1 Hz, 3H, CH₃-CH₂-).

¹³C NMR (75 MHz, CDCl₃) δ 171.61 (CH₃-CO-N-), 165.15 (-CO-O-), 158.82 (Ph-4-C), 152.31 (-N-CO-NH-), 145.10 (DHPM-6-C), 132.03 (Ph-1-C), 128.34 (Ph-2,6-C), 114.53 (Ph-3,5-C), 105.90 (DHPM-5-C), 66.48 (Ph-O-CH₂-), 60.61 (-O-CH₂-CH₃), 56.04 (Piperi-CH₂-), 54.68 (Piperi-2,6-C), 53.18 (DHPM-4-C), 26.76, 26.72 (Ph-O-CH₂-CH₂-, CH₃-CO-N-), 25.87 (Piperi-3,5-C), 24.41 (Piperi-4-C), 17.91 (DHPM-6-CH₃), 14.35 (-CH₂-CH₃).

ROESY (300 MHz, CDCl₃) Cross Peaks: δ 8.06, 2.39 (DHPM-NH, DHPM-6-CH₃), 7.24, 6.75 (Ph-2,6-H, Ph-3,5-H), 7.24, 6.56 (Ph-2,6-H, DHPM-4-H), 6.79, 3.96 (Ph-3,5-H, Ph-O-CH₂-), 4.14, 1.29 (CH₃-CH₂-, CH₃-CH₂-), 3.96, 2.48 (Ph-O-CH₂-, Piperi-CH₂-), 3.99, 1.97 (Ph-O-CH₂-,

Ph-O-CH₂-CH₂-), 2.48, 1.96 (Piperi-CH₂-, Ph-O-CH₂-CH₂-). Spectrum see section 6.5 (Figure 6-17).

6.4.11 5,5-Substituted barbituric acid derivatives

5-Ethyl-5-{4-[3-(piperidin-1-yl)propoxy]benzyl}-1,3-diazinane-2,4,6-trione (**P39**, ST-2214)

Compound **P39** was synthesized via an adapted method reported previously (Calamai *et al.*, 2013). NaH (240 mg, 60% in mineral oil, 6 mmol) was given to a solution of urea (0.90 g, 15 mmol) in 9 mL of DMF in a one-neck Schlenk flask. The mixture was kept at 0 °C for 1 h under the N₂-atmosphere. A solution of compound **42** (0.63 g, 1.5 mmol) in 3 mL of DMF was added to the urea solution. The reaction mixture was stirred at ambient temperature for 18 h and evaporated to dryness in the rotary evaporator. The residue was purified via column chromatography, where the solvent mixtures of DCM and MeOH in ratios of 90:10 and 85:15 were used as eluents.

Yield: 9%

Appearance: White solid

Chemical formula: C₂₁H₂₉N₃O₄

Molecular weight: 387.5 g/mol

Melting point: 202 °C

LC-MS: 100%, m/z: 388.07 [M+H]⁺, with gradient LC-Method 6

¹H NMR (300 MHz, DMSO-*d*⁶) δ 6.90 (d, *J* = 8.7 Hz, 2H, Ph-2,6-*H*), 6.79 (d, *J* = 8.7 Hz, 2H, Ph-3,5-*H*), 3.91 (t, *J* = 6.4 Hz, 2H, -O-CH₂-), 3.02 (s, 2H, Ph-CH₂-), 2.40 – 2.22 (m, 6H, overlap: Piperi-CH₂-, Piperi-2,6-*H*₂), 1.96 (q, *J* = 7.3 Hz, 2H, CH₃-CH₂-), 1.88 – 1.73 (m, 2H, -O-CH₂-CH₂-), 1.47 (p, *J* = 5.5 Hz, 4H, Piperi-3,5-*H*₂), 1.42 – 1.30 (m, 2H, Piperi-4-*H*₂), 0.76 (t, *J* = 7.3 Hz, 3H, -CH₃).

¹³C NMR (75 MHz, DMSO-*d*⁶) δ 172.67 (diazinane-4,6-CO), 157.76 (Ph-4-C), 149.47 (diazinane-2-CO), 130.26 (Ph-2,6-C), 127.00 (Ph-1-C), 114.25 (Ph-3,5-C), 65.81 (-O-CH₂-), 57.98 (diazinane-5-C), 55.15 (Piperi-CH₂-), 54.08 (Piperi-2,6-C), 43.19 (Ph-CH₂-), 31.34 (CH₃-CH₂-), 26.29 (-O-CH₂-CH₂-), 25.58 (Piperi-3,5-C), 24.14 (Piperi-4-C), 9.21 (-CH₃).

6.4.12 Urea derivatives

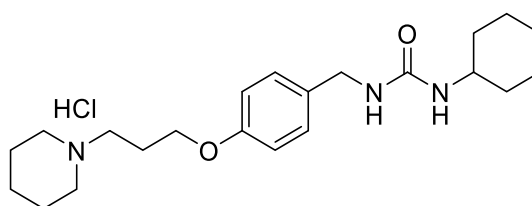
1-Cyclohexyl-3-{4-[3-(piperidin-1-yl)propoxy]benzyl}urea hydrochloride (**P40**, ST-2263)

The benzylamine derivative **13** (2.55 g, 10.2 mmol) and cyclohexyl isocyanate (1.53 mL, 11.9 mmol) were dissolved in 80 mL of THF at r.t. The reaction mixture was stirred at r.t. for 18 h and concentrated in a rotary evaporator. The residue was purified with column chromatography, where the solvent mixtures of DCM and MeOH in ratios of 95:5 and 90:10 were used as eluents. The product was treated with HCl in dioxane to obtain the corresponding salt.

Yield: Quantitative

Appearance: White solid

Chemical formula: $C_{22}H_{35}N_3O_2 \times HCl$



Molecular weight: 410.0 g/mol

Melting point: 189.3 °C

LC-MS: 100.00%, m/z: 374.23 [M+H]⁺, with gradient LC-Method 4

¹H NMR (300 MHz, DMSO-*d*⁶) δ 11.13 (s, 1H, Piperi-N⁺H-), 7.57 (d, *J* = 8.6 Hz, 2H, Ph-3-*H*, -5-*H*), 7.29 (d, *J* = 8.6 Hz, 2H, Ph-2-*H*, -6-*H*), 4.53 (s, 2H, Ph-CH₂-), 4.43 (t, *J* = 6.1 Hz, 2H, -O-CH₂-), 3.92 – 3.70 (m, 3H, overlap: Piperi-2,6-*H*_{eq}, c-Hex-1-*H*), 3.55 (dt, *J* = 10.5, 5.1 Hz, 2H, Piperi-CH₂-), 3.28 (dt, *J* = 12.0, 8.3 Hz, 2H, Piperi-2,6-*H*_{ax}), 2.60 (dq, *J* = 11.7, 6.1 Hz, 2H, -O-CH₂-CH₂-), 2.36 – 1.36 (m, 16H, overlap: Piperi-3,4,5-*H*₂, c-Hex-2,3,4,5,6-*H*₂)

¹³C NMR (75 MHz, DMSO-*d*⁶) δ 157.47 (Ph-1-C), 157.03 (-CO-), 133.25 (Ph-4-C), 128.31 (Ph-3-C, -5-C), 114.26 (Ph-2-C, -6-C), 65.07 (-O-CH₂-), 53.40 (Piperi-CH₂-), 51.94 (Piperi-2,6-C), 47.79 (c-Hex-1-C), 42.22 (Ph-CH₂-), 33.29 (c-Hex-2,6-C), 25.34 (-O-CH₂-CH₂-), 24.46 (c-Hex-3,5-C), 23.28 (c-Hex-4-C), 22.32 (Piperi-3,5-C), 21.43 (Piperi-4-C).

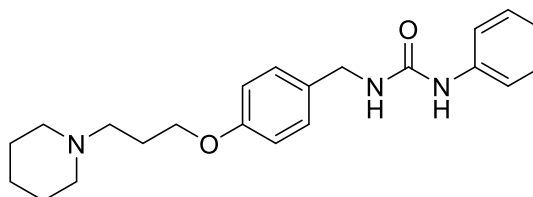
1-Phenyl-3-{4-[3-(piperidin-1-yl)propoxy]benzyl}urea (**P41**, ST-2393)

Analogous to compound **P40**, compound **P41** was synthesized from the hydrochloride salt of benzylamine derivative **13** (0.32 g, 1 mmol), phenyl isocyanate (0.12 g, 1 mmol) in 10 mL of

THF with an additional portion of TEA (0.34 mL, 2.5 mmol) to reveal the primary amine. The product was purified with column chromatography, where the solvent mixtures of DCM and MeOH in ratios of 95:5 and 90:10 were used as eluents.

Yield: 44%

Appearance: White solid



Chemical formula: $C_{22}H_{29}N_3O_2$

Molecular weight: 367.5 g/mol

Melting point: 145.2 °C

LC-MS: 97.90%, m/z: 368.15 $[M+H]^+$, with gradient LC-Method 1

1H NMR (300 MHz, $DMSO-d_6$) δ 8.47 (s, 1H, -NH-Ph), 7.39 (dd, $J = 8.7, 1.1$ Hz, 2H, NH-Ph-2,6-H), 7.27 – 7.15 (m, 4H, overlap: -O-Ph-3,5-H, -NH-Ph-3,5-H), 6.94 – 6.82 (m, 3H, overlap: -O-Ph-2,6-H, -NH-Ph-4-H), 6.49 (t, $J = 5.9$ Hz, 1H, -NH-CH₂-), 4.21 (d, $J = 5.8$ Hz, 2H, -NH-CH₂-), 3.95 (t, $J = 6.4$ Hz, 2H, -O-CH₂-), 2.41 – 2.26 (m, 6H, overlap: Piperi-CH₂-, Piperi-2,6-H₂), 1.83 (p, $J = 6.5$ Hz, 2H, -O-CH₂-CH₂-), 1.48 (p, $J = 5.5$ Hz, 4H, Piperi-3,5-H₂), 1.42 – 1.29 (m, 2H, Piperi-4-H₂).

^{13}C NMR (75 MHz, $DMSO-d_6$) δ 157.59 (-O-Ph-1-C), 155.16 (-CO-), 140.48 (-NH-Ph-1-C), 132.13 (-O-Ph-4-C), 128.64 (-NH-Ph-3,5-C), 128.48 (-O-Ph-3,5-C), 121.04 (-NH-Ph-4-C), 117.64 (-NH-Ph-2,6-C), 114.29 (-O-Ph-2,6-C), 65.93 (-O-CH₂-), 55.18 (Piperi-CH₂), 54.13 (Piperi-2,6-C), 42.20 (-O-Ph-CH₂-), 26.32 (-O-CH₂-CH₂-), 25.62 (Piperi-3,5-C), 24.16 (Piperi-4-C).

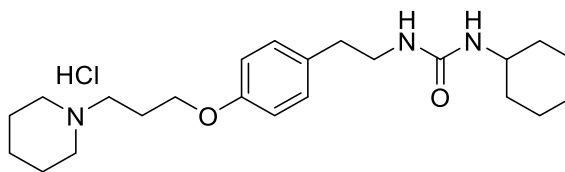
1-Cyclohexyl-3-{4-[3-(piperidin-1-yl)propoxy]phenethyl}urea hydrochloride (**P42**, ST-2265)

Like compound **3**, compound **P42** was synthesized from compound **43** (1.31 g, 5 mmol), alkyl chloride **2** (0.99 g, 5 mmol), K_2CO_3 (2.64 g, 20 mmol), KI (83 mg, 0.5 mmol), and 30 mL of acetone, the reaction was refluxed for 18 h. The product was purified with column chromatography, where the solvent mixtures of DCM and MeOH in ratios of 95:5 and 90:10 were used as eluents. The product was treated with HCl in dioxane to obtain the corresponding salt.

Yield: 70%

Appearance: White to light beige solid

Chemical formula: $C_{23}H_{37}N_3O_2 \times HCl$



Molecular weight: 424.0 g/mol

Melting point: 160.2 °C

LC-MS: 98.71%, m/z: 263.12, 388.27 $[M+H]^+$, with gradient LC-Method 4

1H NMR (300 MHz, DMSO- d_6) δ 10.74 (s, 1H, Piperi- N^+H), 7.10 (d, $J = 8.6$ Hz, 2H, Ph-2,6- H), 6.85 (d, $J = 8.6$ Hz, 2H, Ph-3,5- H), 4.00 (t, $J = 6.1$ Hz, 2H, -O- CH_2 -), 3.46 – 3.36 (m, 2H, Piperi-2,6- H), 3.32 (dt, $J = 10.0, 3.8$ Hz, 1H, c-Hex-1- H), 3.21 – 3.06 (m, 4H, overlap: Piperi- CH_2 -, - CH_2 -NH-CO-), 2.86 (tdd, $J = 12.2, 9.1, 3.7$ Hz, 2H, Piperi-2,6- H_{eq}), 2.58 (t, $J = 7.3$ Hz, 2H, Ph- CH_2 -), 2.18 (dq, $J = 11.6, 6.1$ Hz, 2H, -O- CH_2 - CH_2 -), 1.94 – 0.95 (m, 16H, overlap: Piperi-3,4,5- H_2 , c-Hex-2,3,4,5,6- H_2).

^{13}C NMR (75 MHz, DMSO- d_6) δ 157.40 (Ph-4-C), 156.63 (-CO-), 131.96 (Ph-1-C), 129.62 (Ph-2,6-C), 114.36 (Ph-3,5-C), 65.02 (-O- CH_2 -), 53.41 (Piperi- CH_2 -), 51.94 (Piperi-2,6-C), 47.70 (c-Hex-1-C), 41.14 (- CH_2 -NH-CO-), 35.30 (Ph- CH_2 -), 33.28 (c-Hex-2,6-C), 25.33 (-O- CH_2 - CH_2 -), 24.46 (c-Hex-3,5-C), 23.30 (c-Hex-4-C), 22.31 (Piperi-3,5-C), 21.43 (Piperi-4-C).

1-Phenyl-3-{4-[3-(piperidin-1-yl)propoxy]phenethyl}urea (**P43**, ST-2394)

Compound **P43** was synthesized from subsequently following two steps. Tyramine hydrochloride (0.27 g, 1.5 mmol), TEA (0.3 mL, 1.95 mmol) was stirred in 25 mL of MeCN for 1 h. Phenyl isocyanate (0.16 mL, 1.5 mmol) was given to the solution subsequently, and the reaction was stirred at r.t. for 18 h. Alkyl chloride **2** (0.20 g, 1 mmol), K_2CO_3 (0.40 g, 2.90 mmol), and a catalytic amount of KI were added to the aforementioned reaction mixture, and the mixture was refluxed for 24 h. The suspension was allowed to cool down to r.t. and filtered. The filter cake was rinsed with 20 mL of acetone. The filtrate was combined and concentrated in a rotary evaporator. The residue was purified with column chromatography, where the solvent mixtures of DCM and MeOH in ratios of 95:5 and 90:10 were used as eluents.

Yield: 29%

Appearance: White to light beige solid

Chemical formula: $C_{23}H_{31}N_3O_2$

Molecular weight: 381.5 g/mol

Melting point: 133.0 °C

LC-MS: 100%, m/z: 382.18 $[M+H]^+$, with gradient LC-Method 5

1H NMR (300 MHz, $CDCl_3$) δ 7.34 – 7.22 (m, 4H, -NH-Ph-2,3,5,6-H), 7.14 – 6.98 (m, 3H, overlap: -NH-Ph-4-H, -O-Ph-2,6-H), 6.88 (s, 1H, -NH-Ph), 6.82 (d, J = 8.6 Hz, 2H, -O-Ph-3,5-H), 5.13 (t, J = 5.7 Hz, 1H, -CH₂-NH-CO-), 3.99 (t, J = 6.3 Hz, 2H, -O-CH₂-), 3.44 (q, J = 6.7 Hz, 2H, -CO-NH-CH₂-), 2.75 (t, J = 6.8 Hz, 2H, -O-Ph-CH₂-), 2.60 – 2.44 (m, 6H, overlap: Piperi-2,6-H₂, Piperi-CH₂-), 2.10 – 1.93 (m, 2H, -O-CH₂-CH₂-), 1.66 (p, J = 5.5 Hz, 4H, Piperi-3,5-H₂), 1.55 – 1.43 (m, 2H, Piperi-4-H₂).

^{13}C NMR (75 MHz, $CDCl_3$) δ 157.68 (-O-Ph-4-C), 156.26 (-CO-), 139.22 (-NH-Ph-1-C), 131.31 (-O-Ph-1-C), 129.83 (-O-Ph-2,6-C), 129.18 (-NH-Ph-3,5-C), 123.29 (-NH-Ph-4-C), 120.56 (-NH-Ph-2,6-C), 114.90 (-O-Ph-3,5-C), 66.48 (-O-CH₂-), 55.98 (Piperi-CH₂-), 54.69 (Piperi-2,6-C), 41.72 (-CH₂-NH-), 35.51 (-O-Ph-CH₂-), 26.68 (-O-CH₂-CH₂-), 25.77 (Piperi-3,5-C), 24.33 (Piperi-4-C).

1-Cyclohexyl-3-(3-{4-[3-(piperidin-1-yl)propoxy]phenyl}propyl)urea hydrochloride (**P44**, ST-2392)

4 mL of 1M $LiAlH_4$ in THF was added dropwise to a solution of carboxamide derivative **17** (0.4g, 1.37 mmol) in 20ml of THF at room temperature. The reaction was heated at refluxing temperature. After 2 h, the reaction was allowed to cool down and quenched with H_2O dropwise at 0°C until no more gas developed. The mixture was filtered, and the filtrate was collected and dried in a rotary evaporator. The residue was dissolved in EtOAc and washed with 20 mL H_2O , 20 mL 1M NaOH, and 20 mL brine, respectively. The organic layer was dried with $MgSO_4$ and concentrated in a rotary evaporator. The product was the phenylpropylamine derivative **18**, which was used directly in the next steps.

Experiment

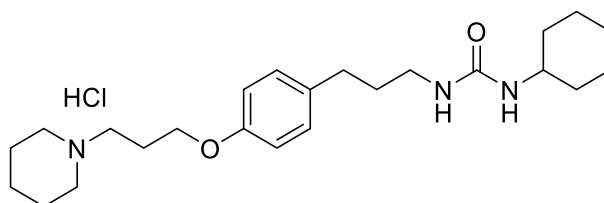
Compound **P44** was subsequently synthesized and purified analogously to compound **P40** from the phenylpropylamine derivative **18** (0.14 g, 0.5 mmol) and cyclohexyl isocyanate (0.1 mL, 0.8 mmol) in 10 mL of THF.

Yield: 55%

Appearance: White solid

Chemical formula: $C_{24}H_{39}N_3O_2 \times HCl$

Molecular weight: 438.1 g/mol



Melting point: 134.9 °C

LC-MS: 95.63%, m/z: 402.27 [M+H]⁺, with gradient LC-Method 5

¹H NMR (300 MHz, DMSO-*d*⁶) δ 10.61 (s, 1H, Piperi-N⁺H-), 7.10 (d, *J* = 8.5 Hz, 2H, Ph-2,6-*H*), 6.84 (d, *J* = 8.6 Hz, 2H, Ph-3,5-*H*), 4.00 (t, *J* = 6.0 Hz, 2H, -O-CH₂-), 3.50 – 3.36 (m, 2H, Piperi-2,6-*H*_{eq}), 3.37 – 3.27 (m, 1H, c-Hex-1-*H*), 3.13 (dt, *J* = 8.3, 5.1 Hz, 2H, Piperi-CH₂-), 2.94 (t, *J* = 6.9 Hz, 2H, -CH₂-NH-CO-), 2.89 – 2.76 (m, 2H, Piperi-2,6-*H*_{ax}), 2.54 – 2.43 (m, 2H, Ph-CH₂-), 2.18 (dq, *J* = 11.7, 6.0 Hz, 2H, -O-CH₂-CH₂-), 1.93 – 0.89 (m, 18H, overlap: Piperi-3,4,5-*H*₂, Ph-CH₂-CH₂-, c-Hex-2,3,4,5,6-*H*₂).

¹³C NMR (75 MHz, DMSO-*d*⁶) δ 157.43 (Ph-4-C), 156.29 (-CO-), 133.98 (Ph-4-C), 129.08 (Ph-2,6-C), 114.30 (Ph-3,5-C), 64.98 (-O-CH₂-), 53.32 (Piperi-CH₂-), 51.88 (Piperi-2,6-C), 47.60 (c-Hex-1-C), 38.57 (-CH₂-NH-CO-), 33.16 (c-Hex-2,6-C), 31.88 (Ph-CH₂-), 31.47 (-O-CH₂-CH₂-), 25.23 (Ph-CH₂-CH₂-), 24.31 (c-Hex-3,5-C), 23.24 (c-Hex-4-C), 22.18 (Piperi-3,5-C), 21.29 (Piperi-4-C).

1-Phenyl-3-(3-{4-[3-(piperidin-1-yl)propoxy]phenyl}propyl)urea hydrochloride (**P45**, ST-2391)

Compound **P45** was synthesized and purified analogously to the compound **P40** with compound **18** (0.14 g, 0.5 mmol) and phenyl isocyanate (0.1 mL, 0.9 mmol) in 10 mL of THF.

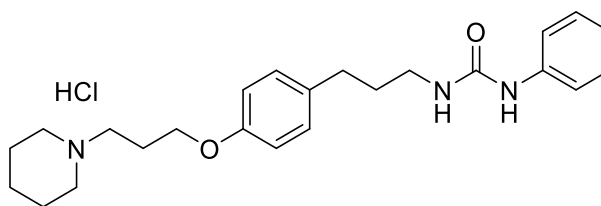
Yield: 58%

Appearance: White solid

Chemical formula: $C_{24}H_{33}N_3O_2 \times HCl$

Molecular weight: 432.0 g/mol

Melting point: 173.2 °C



LC-MS: 95.05%, m/z : 396.20 $[M+H]^+$, with gradient LC-Method 2

1H NMR (600 MHz, $DMSO-d^6$) δ 10.30 (br, 1H, Piperi- NH^+), 8.84 (s, 1H, Ph- NH -), 7.39 (d, J = 8.0 Hz, 2H, N-Ph-2,6- H), 7.19 (t, J = 7.8 Hz, 2H, N-Ph-3,5- H), 7.14 (d, J = 8.1 Hz, 2H, 4-O-Ph-2,6- H), 6.85 (d, J = 8.1 Hz, 3H, 4-O-Ph-3,5- H), 6.52 (t, J = 5.6 Hz, 1H, $-CH_2-NH-CO-$), 4.01 (t, J = 6.0 Hz, 2H, $-O-CH_2-$), 3.45 – 3.40 (m, 2H, Piperi-2,6- H_{eq}), 3.14 (t, J = 7.9 Hz, 2H, $-CH_2-NH-CO-$), 3.05 (q, J = 6.5 Hz, 2H, Piperi- CH_2-), 2.90 – 2.81 (m, 2H, Piperi-2,6- H_{ax}), 2.55 (t, J = 7.6 Hz, 2H, Ph- CH_2-), 2.16 (dq, J = 11.9, 6.1 Hz, 2H, $-O-CH_2-CH_2-$), 1.82 – 1.74 (m, 4H, overlap: Ph- CH_2-CH_2- , Piperi-3,5- H_{eq}), 1.71 – 1.64 (m, 3H, overlap: Piperi-3,5- H_{ax} , $-4-H_{eq}$), 1.42 – 1.34 (m, 1H, Piperi-4- H_{ax}).

^{13}C NMR (75 MHz, $DMSO-d^6$) δ 156.38 (4-O-Ph-4-C), 155.38 ($-CO-$), 140.74 (4-O-Ph-1-C), 133.91 (N-Ph-1-C), 129.28 (4-O-Ph-2,6-C), 128.57 (N-Ph-3,5-C), 120.73 (N-Ph-4-C), 117.38 (N-Ph-2,6-C), 114.33 (4-O-Ph-3,5-C), 64.91 ($-O-CH_2-$), 53.45 (Piperi- CH_2-), 52.00 (Piperi-2,6-C), 38.40 ($-CH_2-NH-CO-$), 31.78 (O-Ph- CH_2-), 31.51 ($-O-CH_2-CH_2-$), 23.35 (O-Ph- CH_2-CH_2-), 22.38 (Piperi-3,5-C), 21.38 (Piperi-4-C).

6.4.13 *N,N'*-Disubstituted barbituric acid derivatives

1-Cyclohexyl-3-{4-[3-(piperidin-1-yl)propoxy]benzyl}-1,3-diazinane-2,4,6-trione hydrochloride (**P46**, ST-2264)

Compound **P46** was synthesized via an adapted method reported previously (Milite *et al.*, 2015). The urea derivative **P40** (0.75 g, 2 mmol) and malonic acid (0.21 g, 2 mmol) were dissolved in 8 mL of $(Ac)_2O$. The mixture was radiated in the microwave at 60 °C for 10 min. Approximately 3 mL of H_2O was given dropwise at 0 °C to quench the reaction, and the solution was concentrated in the rotary evaporator. The residue was purified with column chromatography, where the solvent mixtures of DCM and MeOH in ratios of 90:10 and 85:15 were used as eluents. The product was treated with HCl in EtOAc to obtain the corresponding salt.

Yield: 78%

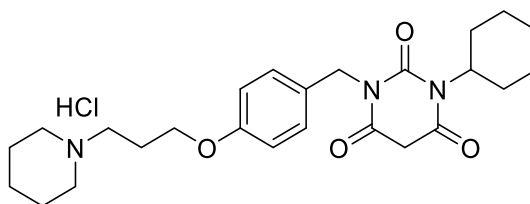
Experiment

Appearance: White solid

Chemical formula: $C_{25}H_{35}N_3O_4 \times HCl$

Molecular weight: 478.0 g/mol

Melting point: 229.2 °C



LC-MS: 99.35%, m/z: 442.23 $[M+H]^+$, with gradient LC-Method 4

1H NMR (300 MHz, $CDCl_3$) δ 12.15 (s, 1H, Piperi- N^+H), 7.34 (d, $J = 8.7$ Hz, 2H, Ph-2,6- H), 6.77 (d, $J = 8.7$ Hz, 2H, Ph-3,5- H), 4.92 (s, 2H, Ph- CH_2 -), 4.56 (tt, $^3J = 12.3, 3.7$ Hz, 1H, c-Hex-1- CH -), 4.03 (t, $J = 5.5$ Hz, 2H, -O- CH_2 -), 3.60 (s, 2H, -CO- CH_2 -CO-), 3.59 – 3.49 (m, 2H, Piperi-2,6- H), 3.12 (dt, $J = 10.5, 5.2$ Hz, 2H, Piperi- CH_2 -), 2.74 – 2.56 (m, 2H, Piperi-2,6- H_{eq}), 2.48 – 2.36 (m, 2H, -O- CH_2 - CH_2 -), 2.34 – 2.12 (m, 4H), 2.00 – 1.73 (m, 4H), 1.68 – 1.51 (m, 2H), 1.50 – 1.07 (m, 6H). (overlap: Piperi-3,4,5- H_2 , c-Hex-2,3,4,5,6- H_2)

^{13}C NMR (75 MHz, $CDCl_3$) δ 164.85, 164.80 (diazinane-4,6-C), 158.03 (Ph-4-C), 151.42 (diazinane-2-C), 130.88 (Ph-2,6-C), 129.22 (Ph-1-C), 114.38 (Ph-3,5-C), 65.05 (-O- CH_2 -), 55.57, 55.40 (c-Hex-1-C, Piperi- CH_2 -), 53.55 (Piperi-2,6-C), 44.39 (Ph- CH_2 -), 40.47 (diazinane-5-C), 29.11 (c-Hex-2,6-C), 26.35 (c-Hex-3,5-C), 25.16 (c-Hex-4-C), 23.91 (-O- CH_2 - CH_2 -), 22.63 (Piperi-3,5-C), 22.21 (Piperi-4-C).

1-Cyclohexyl-3-{4-[3-(piperidin-1-yl)propoxy]phenethyl}-1,3-diazinane-2,4,6-trione hydrochloride (**P47**, ST-2266)

The synthesis and purification processes were analogous to that of the compound **P46** from the urea derivative **P42** (0.85 g, 2 mmol) and malonic acid (0.21 g, 2 mmol) in 8 mL of $(Ac)_2O$.

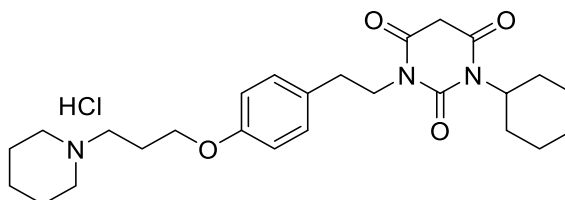
Yield: 33%

Appearance: White to light beige solid

Chemical formula: $C_{26}H_{37}N_3O_4 \times HCl$

Molecular weight: 492.1 g/mol

Melting point: 185.4 °C



LC-MS: 98.62%, m/z: 456.24 [M+H]⁺, with gradient LC-Method 4

¹H NMR (300 MHz, CDCl₃) δ 12.17 (s, 1H, Piperi-N⁺H), 7.12 (d, *J* = 8.5 Hz, 2H, Ph-2,6-*H*), 6.76 (d, *J* = 8.6 Hz, 2H, Ph-3,5-*H*), 4.56 (tt, ^{3,4}*J* = 12.2, 3.7 Hz, 1H, c-Hex-1-CH-), 4.06 – 3.95 (m, 4H, overlap: -O-CH₂-, Ph-CH₂-CH₂-), 3.61 – 3.51 (m, 4H, overlap: Piperi-2,6-*H*_{eq}, diazinane-5-CH₂), 3.20 – 3.07 (m, 2H, Piperi-CH₂-), 2.86 – 2.75 (m, 2H, Ph-CH₂-), 2.74 – 2.58 (m, 2H, Piperi-2,6-*H*_{ax}), 2.50 – 2.37 (m, 2H, -O-CH₂-CH₂-), 2.35 – 2.13 (m, 4H), 1.97 – 1.74 (m, 6H), 1.70 – 1.51 (m, 2H), 1.50 – 1.09 (m, 4H). (Piperi-3,4,5-*H*₂, c-Hex-2,3,4,5,6-*H*₂)

¹³C NMR (75 MHz, CDCl₃) δ 164.91, 164.62, (diazinane-4-CO-, -6-CO-) 157.14 (Ph-4-C), 151.21 (diazinane-2-CO-), 130.69 (Ph-1-C), 130.14 (Ph-2,6-C), 114.49 (Ph-3,5-C), 65.03 (-O-CH₂-), 55.50, 55.41, (Piperi-CH₂-, c-Hex-1-CH), 53.58 (Piperi-2,6-C), 43.14 (Ph-CH₂-CH₂-), 40.34 (diazinane-5-CH₂-), 33.15 (Ph-CH₂-), 29.15 (c-Hex-2,6-C), 26.38 (c-Hex-3,5-C), 25.18 (c-Hex-4-C), 23.97 (-O-CH₂-CH₂-), 22.64 (Piperi-3,5-C), 22.24 (Piperi-4-C).

6.4.14 Propargyl amine derivatives

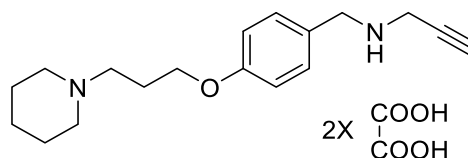
N-{4-[3-(Piperidin-1-yl)propoxy]benzyl}prop-2-yn-1-amine dihydrogenoxalate (**P48**, ST-2367)

The synthesis and workup of compound **P48** were similar to that of compound **P25**, where the starting material aldehyde derivative **3** (247 mg, 1 mmol), propargylamine (0.08 mL, 1.2 mmol), AcOH (0.18 mL, 3 mmol), NaBH(OAc)₃ (311 mg, 1.47 mmol) and 5 mL of DCE were used. The reaction was stirred at r.t for 3 days. The product was purified by column chromatography by using the solvent mixture of DCM and MeOH (NH₃) in a ratio of 98:2 as the eluent. The product was treated with oxalic acid (0.18 g, 2 mmol) in acetone to obtain the corresponding dihydrogen oxalate salt.

Yield: 26%

Appearance: White solid

Chemical formula: C₁₈H₂₆N₂O × 2 C₂H₂O₄



Molecular weight: 466.5 g/mol

Melting point: 187.3 °C

LC-MS: 95.65%, m/z: 287.17 [M+H]⁺, with gradient LC-Method 1

¹H NMR (300 MHz, DMSO-*d*⁶) δ 7.36 (t, *J* = 8.5 Hz, 2H, Ph-2,6-*H*), 6.95 (d, *J* = 8.6 Hz, 2H, Ph-3,5-*H*), 4.09 – 3.99 (m, 4H, overlap: -O-CH₂-, Ph-CH₂-), 3.71 (d, ⁴*J* = 2.6 Hz, 2H, CH≡C-CH₂-), 3.59 (t, ⁴*J* = 2.4 Hz, 1H, CH≡C-CH₂-), 3.28 – 2.97 (m, 6H, overlap: Piperi-CH₂-, Piperi-2,6-*H*₂), 2.20 – 2.04 (m, 2H, -O-CH₂-CH₂-), 1.73 (p, *J* = 5.8 Hz, 4H, Piperi-3,5-*H*₂), 1.59 – 1.45 (m, 2H, Piperi-4-*H*₂).

¹³C NMR (75 MHz, DMSO-*d*⁶) δ 164.13 (Oxa-CO-), 158.31 (Ph-4-C), 130.94 (Ph-2,6-C), 125.51 (Ph-1-C), 114.49 (Ph-3,5-C), 77.99 (CH≡C-CH₂-), 76.69 (CH≡C-CH₂-), 65.06 (-O-CH₂-), 53.31 (Piperi-CH₂-), 52.05 (Piperi-2,6-C), 48.87 (Ph-CH₂-), 35.13 (CH≡C-CH₂-), 23.35 (-O-CH₂-CH₂-), 22.44 (Piperi-3,5-C), 21.33 (Piperi-4-C).

{[4-(4-Methylpiperazine-1-carbonyl)phenyl]methyl}(prop-2-yn-1-yl)amine dihydrogenoxalate (P49, ST-2005)

Compound **P49** was synthesized analogous to compound **P25** from the aldehyde **26** (0.49 g, 2.1 mmol), propargylamine (0.16 mL, 2.1 mmol), and NaBH(OAc)₃ (0.89 g, 4.2 mmol) in 10 mL of DCE. The reaction was stirred for 48 h at r.t. The crude product was purified via column chromatography, where a solvent mixture of DCM, MeOH, and TEA in a ratio of 97:2:1 was used as the eluent. The product was treated with oxalic acid (0.36 g, 4 mmol) in EtOH to obtain the dihydrogen oxalate salt.

Yield: 57%

Appearance: White solid

Chemical formula: C₁₆H₂₁N₃O × 2 C₂H₂O₄

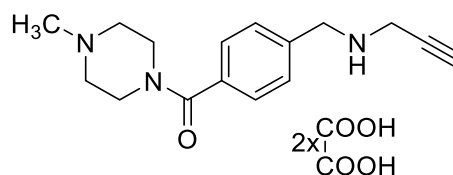
Molecular weight: 451.4 g/mol

ESI-MS (+): m/z: 272.2 [M+H]⁺

Melting point: 181.4 °C

CHN-Analyse: calculated: C, 53.21%; H, 5.58%; N, 9.31%.

found: C, 52.94%; H, 5.60%; N, 9.06%.



^1H NMR (300 MHz, $\text{DMSO-}d^6$) δ 7.53 (d, $J = 8.0$ Hz, 2H, 4-Me-Ph-2,6-*H*), 7.46 (d, $J = 8.0$ Hz, 2H, 4-Me-Ph-3,5-*H*), 4.13 (s, 2H, Ph- CH_2 -), 3.89–3.49 (br, 4H, 4-Me-Pipera-2,6-*H*₂), 3.76 (d, $^4J = 2.6$ Hz, 2H, $\text{CH}\equiv\text{C-CH}_2$), 3.59 (t, $^4J = 2.4$ Hz, 1H, $\text{CH}\equiv\text{C-CH}_2$), 3.02 (s, 4H, 4-Me-Pipera-3,5-*H*₂), 2.64 (s, 3H, - CH_3).

^{13}C NMR (126 MHz, D_2O) δ 172.38 (Ph-CO-), 166.15 (Ox-COOH), 135.11 (4-Me-Ph-4-C), 133.53 (4-Me-Ph-1-C), 131.03 (4-Me-Ph-3,5-C), 128.29 (4-Me-Ph-2,6-C), 79.20 ($\text{CH}\equiv\text{C-CH}_2$ -), 73.61 ($\text{CH}\equiv\text{C-CH}_2$ -), 53.39 (4-Me-Pipera-3,5-C), 50.01 (Ph- CH_2 -), 45.10 (- CH_3), 43.53 (4-Me-Pipera-2,6-C), 36.45 ($\text{CH}\equiv\text{C-CH}_2$ -).

6.4.15 D-Cycloserine derivatives

(*R*)-4-({4-[3-(Piperidin-1-yl)propoxy]benzyl}amino)isoxazolidin-3-one (**P50**, ST-2353)

Compound **P50** was synthesized via a modified method reported previously (Stammer *et al.*, 1970). Benzaldehyde **3** (0.29 g, 1.2 mmol) and D-cycloserine (DCS) (0.10 g, 0.98 mmol) were dissolved in a solvent mixture of 20 mL of EtOH and 2 mL of MeOH. The mixture was stirred at r.t. for 3 h. The disappearance of the sediment indicated the completion of the reaction. The solvent was removed in the rotary evaporator, and the residue was treated and rinsed with EtOEt. The resulting white solid was the corresponding Schiff's base from the reaction above. The obtained white solid was dissolved in 15 mL of EtOH (abs.), the solution was cooled to 0 °C, and NaBH_4 (57 mg, 1.5 mmol) was added subsequently. The reaction was stirred at 0 °C for 90 min, and acetic acid (2 M, aq.) was given to the reaction dropwise to adjust the pH to approximately 5. The mixture was concentrated in a rotary evaporator. The residue was purified with column chromatography. The solvent mixture of DCM and MeOH in the gradient from 90:10 to 75:25 was used as the eluent. The working temperature of the water bath of the rotary evaporator was set to < 40 °C.

Yield: 52%

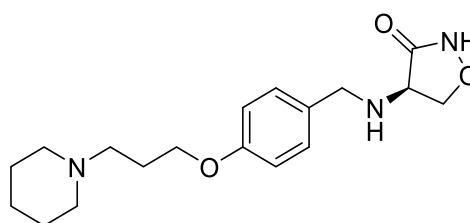
Appearance: White solid

Chemical formula: $\text{C}_{18}\text{H}_{27}\text{N}_3\text{O}_3$

Molecular weight: 333.4 g/mol

Melting point: 120.1 °C

$[\alpha]_D^{25} = +234$, $c = 2$ mg/ml in H_2O



HPLC (equipped with a chiral cellulose column): 100% (Spectrum see section 6.5: Figure 6-18)

LC-MS: 97.89%, m/z: 334.21 [M+H]⁺, with gradient LC-Method 11

¹H NMR (300 MHz, CDCl₃) δ 7.19 (d, *J* = 8.4 Hz, 2H, Ph-2,6-*H*), 6.79 (d, *J* = 8.5 Hz, 2H, Ph-3,5-*H*), 6.73 (br, 2H, -CO-NH-, Ph-CH₂-NH-), 4.24 (t, *J* = 8.0 Hz, 1H, Isoxazole-4-*H*), 3.95 (t, *J* = 6.3 Hz, 2H, Ph-O-CH₂-), 3.92 – 3.68 (m, 4H, overlap: Ph-CH₂-, Oxa-5-*H*₂), 2.72 – 2.51 (m, 6H, Piperi-CH₂-, Piperi-2,6-*H*₂), 2.12 – 1.93 (m, 2H, -O-CH₂-CH₂-), 1.68 (p, *J* = 5.6 Hz, 4H, Piperi-3,5-*H*₂), 1.54 – 1.38 (m, 2H, Piperi-4-*H*₂).

¹³C NMR (75 MHz, CDCl₃) δ 173.08 (-CO-), 158.37 (Ph-4-C), 131.85 (Ph-1-C), 129.60 (Ph-2,6-C), 114.69 (Ph-3,5-C), 75.20 (Isoxazole-5-C), 66.45 (Ph-O-CH₂-), 60.45 (Isoxazole-4-C), 55.58 (Piperi-CH₂-), 54.17 (Piperi-2,6-C), 51.84 (Ph-CH₂-), 26.10 (-O-CH₂-CH₂-), 25.14 (Piperi-3,5-C), 24.05 (Piperi-4-C).

4-({4-[3-(Piperidin-1-yl)propoxy]phenethyl}amino)isoxazolidin-3-one (**P51**, ST-2465)

Compound **P51** was prepared by dissolving **44** (120 mg, 0.4 mmol) in 1 mL of piperidine. The solution was kept at ambient temperature. Needle-like crystals were observed after 24 h, the amount of the crystals increased over time. After 72 h, piperidine was removed with the rotary evaporator. The residue was dissolved in 5 mL of EtOAc and filtered. The solid (piperidinium chloride) was rinsed with 5 mL of EtOAc. The filtrate was collected and concentrated in a rotary evaporator. The crude product was purified with column chromatography. The initial eluent was a mixture of DCM and MeOH (NH₃) in a ratio of 90:10. The initial eluent was used until the fractions containing piperidine ended. The eluents were changed to the mixture of DCM and MeOH in the ratios of 85:15 and 80:20 to obtain the desired product. The temperature of the water bath of the rotary evaporator was set at approximately 30 °C.

Yield: 35%

Appearance: White solid

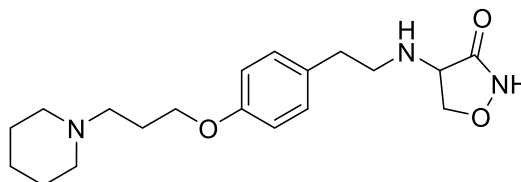
Chemical formula: C₁₉H₂₉N₃O₃

Molecular weight: 347.5 g/mol

Melting point: 87.2 °C

HPLC (equipped with a chiral cellulose column): Two peaks in ratio 87:13 (AUC%, spectrum see section 6.5: Figure 6-19)

LC-MS: 100%, m/z=348.18 [M+H]⁺, with gradient LC-Method 12



^1H NMR (300 MHz, CDCl_3) δ 7.10 (d, $J = 8.6$ Hz, 2H, Ph-2,6-*H*), 6.79 (d, $J = 8.6$ Hz, 2H, Ph-3,5-*H*), 4.44 (dd, $J = 8.6, 7.8$ Hz, 1H, Isoxazole-5-*H*_{eq}), 4.03 (t, $J = 8.5$ Hz, 1H, Isoxazole-6-*H*), 3.96 (t, $J = 6.1$ Hz, 2H, Ph-O-*CH*₂-), 3.77 (t, $J = 8.0$ Hz, 1H, Isoxazole-5-*H*_{ax}), 3.00 (dt, $J = 10.6, 7.1$ Hz, 1H, Ph-*CH*₂-*CH*-), 2.84 (ddd, $J = 10.8, 8.0, 5.7$ Hz, 1H, Ph-*CH*₂-*CH*'-), 2.77 – 2.54 (m, 8H, overlap: Ph-*CH*₂-, Piperi-*CH*₂-, Piperi-2,6-*H*₂), 2.13 – 2.00 (m, 2H, Piperi-*CH*₂-*CH*₂-), 1.71 (p, $J = 5.6$ Hz, 4H, Piperi-3,5-*H*₂), 1.56 – 1.42 (m, 2H, Piperi-4-*H*₂).

^{13}C NMR (151 MHz, CDCl_3) δ 172.70 (Isoxazole-CO-), 157.41 (Ph-4-*C*), 131.79 (Ph-1-*C*), 129.73 (Ph-2,6-*C*), 114.65 (Ph-3,5-*C*), 74.74 (Isoxazole-5-*C*), 66.11 (Ph-O-*CH*₂-), 61.20 (Isoxazole-4-*C*), 55.56 (Piperi-*CH*₂-), 54.01 (Piperi-2,6-*C*), 49.47 (Ph-*CH*₂-*CH*₂-), 35.78 (Ph-*CH*₂-), 25.73 (Piperi-*CH*₂-*CH*₂-), 24.75 (Piperi-3,5-*C*), 23.76 (Piperi-4-*C*).

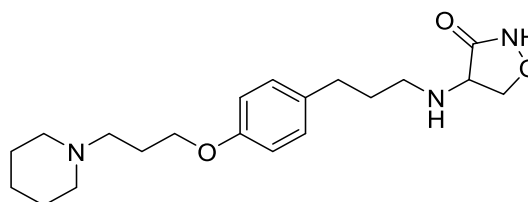
4-[(3-{4-[3-(Piperidin-1-yl)propoxy]phenyl}propyl)amino]isoxazolidin-3-one (**P52**, ST-2407)

Analogous to compound **P50**, compound **P52** was synthesized from the aldehyde **22** (0.35 g, 1.3 mmol), DCS (0.09 g, 0.88 mmol), and NaBH_4 (0.10 g, 2.6 mmol). Additional glacial acetic acid (0.08 mL, 1.4 mmol) was used to prepare the Schiff's base intermediate. The product was purified by column chromatography. The solvent mixture of DCM and MeOH in a gradient of ratios from 85:15 to 75:25 was used as the eluent. The temperature of the water bath of the rotary evaporator was set at approximately 30 °C.

Yield: 15%

Appearance: White to beige solid

Chemical formula: $\text{C}_{20}\text{H}_{31}\text{N}_3\text{O}_3$



Molecular weight: 361.5 g/mol

Melting point: 142.7 °C

HPLC (equipped with a chiral cellulose column): two unseparated peaks (Spectrum see section 6.5: Figure 6-20)

LC-MS: 95.99%, m/z : 362.27 [$\text{M}+\text{H}^+$]⁺, with gradient LC-Method 1

^1H NMR (300 MHz, CDCl_3) δ 7.05 (d, $J = 8.5$ Hz, 2H, Ph-2,6-*H*), 6.79 (d, $J = 8.5$ Hz, 2H, Ph-3,5-*H*), 5.91 (br, 2H, =*NH*), 4.40 (t, $J = 8.2$ Hz, 1H, Oxa-5-*H*_{eq}), 4.07 – 3.92 (m, 3H, overlap: Ph-O-*CH*₂-, Isoxazole-4-*H*), 3.75 (t, $J = 8.1$ Hz, 1H, Isoxazole-5-*H*_{ax}), 2.83 – 2.47 (m, 10H,

overlap: Ph-CH₂-CH₂-CH₂-, Piperi-2,6-H₂, Piperi-CH₂-), 2.11 – 1.95 (m, 2H, -O-CH₂-CH₂-), 1.84 – 1.60 (m, 6H, overlap: Ph-CH₂-CH₂-, Piperi-3,5-H₂), 1.54 – 1.39 (m, 2H, Piperi-4-H₂).

¹³C NMR (75 MHz, CDCl₃) δ 172.75 (-CO-), 157.05 (Ph-4-C), 134.16 (Ph-1-C), 129.38 (Ph-2,6-C), 114.63 (Ph-3,5-C), 74.93 (Isoxazole-5-C), 66.20 (Ph-O-CH₂-), 61.38 (Isoxazole-4-C), 55.51 (Piperi-CH₂-), 54.03 (Piperi-2,6-C), 47.71 (Isoxazole-NH-CH₂-), 32.67 (Ph-CH₂-), 32.07 (Ph-CH₂-CH₂-), 25.81 (-O-CH₂-CH₂-), 24.89 (Piperi-3,5-C), 23.87 (Piperi-4-C).

N-(3-Oxoisoxazolidin-4-yl)-4-[3-(piperidin-1-yl)propoxy]benzamide (**P53**, ST-2458)

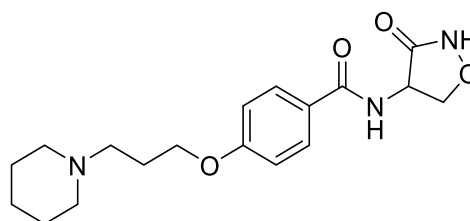
Carboxylic acid derivative **25** (0.17 g, 0.57 mmol, as hydrochloride) was dissolved in 5 mL of DCM, thionyl chloride (0.1 mL, 1.38 mmol) was added to the solution at 0 °C. The reaction was refluxed for 3 h. The solvent inclusive excessive thionyl chloride was removed subsequently by vacuum distillation equipped with a wash bottle filled with NaHCO₃ solution between condenser and pump. The residue was treated with 5 mL toluene, and the solution was removed by vacuum evaporation in a rotary evaporator. The prepared acid chloride was dissolved in 5 mL of DCM and given dropwise to a solution of DCS (55 mg, 0.54 mmol) and TEA (0.5 mL, 3.6 mmol) in 5 mL of MeOH and 1 mL of H₂O at 0 °C. The mixture was stirred at ambient temperature for 18 h. The solvent was removed in the rotary evaporator, and the residue was purified with column chromatography. The solvent mixture of DCM and MeOH in a gradient of ratios of 90:10 to 75:25 was used as the eluent. The water bath of the rotary evaporator was set at approximately 30 °C.

Yield: 69%

Appearance: White solid

Chemical formula: C₁₈H₂₅N₃O₄

Molecular weight: 347.4 g/mol



Melting point: 62.5 °C

HPLC (equipped with a chiral cellulose column): two peaks in ratio 89:11 (AUC%, spectrum see section 6.5: Figure 6-21)

LC-MS: 97.4%, m/z = 348.22 [M+H]⁺, with gradient LC-Method 12

^1H NMR (300 MHz, $\text{DMSO-}d^6$) δ 10.78 (s, 1H, -CO-NH-O-), 8.85 (d, $J = 8.2$ Hz, 1H, Ph-CO-NH-), 7.88 (d, $J = 8.8$ Hz, 2H, Ph-2,6-H), 7.02 (d, $J = 8.8$ Hz, 2H, Ph-3,5-H), 5.02 (dt, $J = 10.4$, 8.5 Hz, 1H, Isoxazole-5- H_{eq}), 4.55 (t, $J = 8.5$ Hz, 1H, Isoxazole-4-H), 4.18 – 4.05 (m, 3H, overlap: Isoxazole-5- H_{ax} , Ph-O- CH_2), 3.18 – 2.97 (m, 6H, overlap: Piperi- CH_2 -, Piperi-2,6- H_2), 2.26 – 2.09 (m, 2H, -O- CH_2 - CH_2 -), 1.76 (p, $J = 5.6$ Hz, 4H, Piperi-3,5- H_2), 1.58 – 1.46 (m, 2H, Piperi-4- H_2).

^{13}C NMR (75 MHz, $\text{DMSO-}d^6$) δ 170.69 (Isoxazole-3-CO-), 165.75 (Ph-CO-), 160.87 (Ph-4-C), 129.30 (Ph-2,6-C), 125.85 (Ph-1-C), 114.00 (Ph-3,5-C), 71.68 (Isoxazole-5-C), 65.35 (Ph-O- CH_2 -), 53.41 (Piperi- CH_2 -), 52.15 (Piperi-2,6-C), 51.38 (Isoxazole-4-C), 23.45 (-O- CH_2 - CH_2 -), 22.62 (Piperi-3,5-C), 21.66 (Piperi-4-C).

6.4.16 Carbamate derivative

4-[3-(Piperidin-1-yl)propoxy]benzyl cyclohexylcarbamate (**P54**, ST-2370)

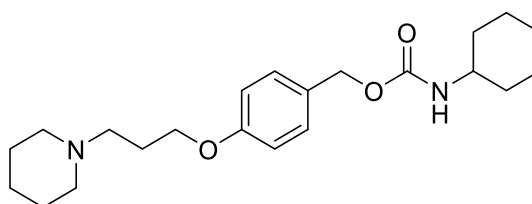
The synthesis process was modified from the previously reported method (Burstein *et al.*, 2019). Cyclohexylamine (0.06 mL, 0.5 mmol) was given to a solution of compound **47** (0.19 g, 0.45 mmol) in 5 mL of THF. The reaction was stirred at r.t. for 18 h. After removing the solvent in the rotary evaporator, the residue was purified with column chromatography, where the solvent mixtures of DCM and MeOH in ratios of 95:5 and 90:10 were used as eluents.

Yield: 65%

Appearance: White solid

Chemical formula: $\text{C}_{22}\text{H}_{34}\text{N}_2\text{O}_3$

Molecular weight: 374.5 g/mol



Melting point: 83.3 °C

LC-MS: 95.82%, m/z : 375.23 [$\text{M}+\text{H}^+$] $^+$, with gradient LC-Method 1

^1H NMR (300 MHz, CDCl_3) δ 7.21 (d, $J = 8.3$ Hz, 2H, Ph-2,6-H), 6.80 (d, $J = 8.6$ Hz, 2H, Ph-3,5-H), 4.93 (s, 2H, Ph- CH_2 -), 4.59 – 4.46 (m, 1H, -CO-NH-), 3.93 (t, $J = 6.4$ Hz, 2H, -O- CH_2 -), 3.51 – 3.32 (m, 1H, c-Hex-1-H-), 2.46 – 2.28 (m, 6H, overlap: Piperi- CH_2 -, Piperi-2,6- H_2), 1.99

– 1.78 (m, 4H), 1.68 – 1.45 (m, 7H), 1.44 – 1.17 (m, 4H), 1.14 – 0.95 (m, 3H), (overlap: -O-CH₂-CH₂-, Piperi-3,4,5-*H*₂-, c-Hex-2,3,4,5,6-*H*₂).

¹³C NMR (75 MHz, CDCl₃) δ 159.23 (Ph-4-C), 155.84 (-CO-O-), 130.02 (Ph-2,6-C), 128.97 (Ph-1-C), 114.76 (Ph-3,5-C), 66.76, 66.46 (-CH₂-O-Ph-CH₂-), 56.07 (Piperi-CH₂-), 54.81 (Piperi-2,6-C), 50.06 (c-Hex-1-C), 33.59 (c-Hex-2,6-C), 26.97 (Ph-O-CH₂-CH₂-), 26.10 (c-Hex-3,5-C), 25.68 (c-Hex-4-C), 24.91 (Piperi-3,5-C), 24.58 (Piperi-4-C).

6.4.17 Pimavanserin analog with H₃R pharmacophore

1-(4-Fluorobenzyl)-1-(1-methylpiperidin-4-yl)-3-{4-[3-(piperidin-1-yl)propoxy]benzyl}urea
(**P55**, ST-2300)

The pimavanserin analog **P55** was synthesized via modified methods described in a patent of ACADIA (Burstein *et al.*, 2019).

Method A: Compounds **48** (0.39 g, 1.73 mmol), **47** (0.48 g, 1.32 mmol), and K₂CO₃ (0.40 g, 3 mmol) were suspended in 10 mL of toluene, and the solution was heated at 90 °C for 16 h. After cooling down, the suspension was diluted with 40 mL of DCM and 40 mL of NaOH (1 N, aq.). The organic layer was separated and dried in a rotary evaporator. The residue was purified by column chromatography, where solvent mixtures of DCM and MeOH (NH₃) in ratios of 98:2 and 95:5 were used as eluents.

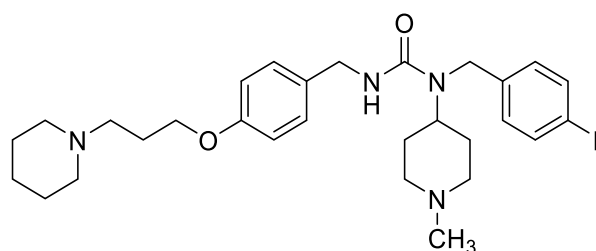
Method B: A solution of the isocyanate derivative **45** (0.31 g, 1.12 mmol) in 10 mL of THF was given to a solution of compound **48** (0.32 g, 1.44 mmol) in 10 mL THF. The reaction mixture was stirred at r.t. for 18 h. The solvent was subsequently reduced in the rotary evaporator. The residue was purified with column chromatography, whereby the solvent mixture of DCM and MeOH in a ratio of 90:10 and the mixture of DCM and MeOH (NH₃) in a ratio of 90:10 were used as eluents.

Yield: Method A: 31%; Method B: 66%

Appearance: White to beige solid

Chemical formula: C₂₉H₄₁FN₄O₂

Molecular weight: 496.7 g/mol



Melting point: 114.0 °C

LC-MS: 96.18%, m/z: 249.08 [(M+2H⁺)/2]⁺ and 497.33 [M+H⁺]⁺, with gradient LC-Method 10

¹H NMR (300 MHz, CDCl₃) δ 7.21 – 7.10 (m, 2H, 4-F-Ph-2,6-*H*), 7.05 – 6.89 (m, 4H, 4-O-Ph-2,6-*H*, 4-F-Ph-3,5-*H*), 6.76 (d, *J* = 8.7 Hz, 2H, 4-O-Ph-3,5-*H*), 4.47 (t, *J* = 5.4 Hz, 1H, -CO-NH-), 4.36 – 4.27 (m, 3H, overlap: 4-F-Ph-CH₂-, 1-Me-Piperi-4-CH-), 4.25 (d, *J* = 5.4 Hz, 2H, 4-O-Ph-CH₂-), 3.94 (t, *J* = 6.4 Hz, 2H, -O-CH₂-), 2.90 – 2.77 (m, 2H, 1-Me-Piperi-2,6-*H*_{eq}), 2.49 – 2.33 (m, 6H, overlap: Piperi-CH₂-, Piperi-2,6-*H*₂), 2.23 (s, 3H, -CH₃), 2.04 (td, ^{3,4}*J* = 11.6, 3.2 Hz, 2H, 1-Me-Piperi-2,6-*H*_{ax}), 1.99 – 1.88 (m, 2H, -O-CH₂-CH₂-), 1.77 – 1.62 (m, 4H, 1-Me-Piperi-3,5-*H*₂), 1.57 (p, *J* = 5.2 Hz, 4H, Piperi-3,5-*H*₂), 1.47 – 1.36 (m, 2H, Piperi-4-*H*₂).

¹³C NMR (75 MHz, CDCl₃) δ 162.06 (d, ¹*J* (C,F) = 245.7 Hz, 4-F-Ph-4-C), 158.29, 158.15 (4-O-Ph-4-C, -CO-), 134.20 (d, ⁴*J* (C,F) = 3.0 Hz, 4-F-Ph-1-C), 131.38 (4-O-Ph-1-C), 128.71 (4-O-Ph-2,6-C), 127.75 (d, ³*J* (C,F) = 8.0 Hz, 4-F-Ph-2,6-C), 115.79 (d, ²*J* (C,F) = 21.6 Hz, 4-F-Ph-3,5-C), 114.59 (4-O-Ph-3,5-C), 66.60 (-O-CH₂-), 56.06 (Piperi-CH₂-), 55.35 (Piperi-2,6-C), 54.71 (1-Me-Piperi-2,6-C), 52.31 (1-Me-Piperi-4-C), 46.17 (4-F-Ph-CH₂-), 45.18 (-CH₃), 44.49 (4-O-Ph-CH₂-), 30.26 (1-Me-Piperi-3,5-C), 26.88 (-O-CH₂-CH₂-), 26.03 (Piperi-3,5-C), 24.49 (Piperi-4-C).

6.4.18 Adenosine A_{2A} receptor antagonist derivative

(P56, ST-2354) 4-[4-(Piperidin-1-yl)butanamido]-*N*-(thiazol-2-yl)benzamide

The title compound was synthesized via a modified method reported previously (Sams *et al.*, 2011). Compound **49** (1.99 g, 8 mmol) and Pd/C (30 mg) were suspended in 100 mL of MeOH. The suspension was treated with H₂ with a balloon. The reaction was stirred at ambient temperature. After 72 h, TLC, APCI-MS, and NMR analyses indicated that the reaction was not completed. The major product was a hydroxylamine derivative. Therefore another portion of Pd/C (30 mg) and 20 mL of MeOH (NH₃) was added to the reaction, and the reaction was stirred at r.t. for a further 72 h. The suspension was filtered, and the filter cake was rinsed with five portions of 50 mL MeOH. The filtrate was concentrated in the rotary evaporator. The resulting product was a mixture of amine and hydroxylamine derivate, which were not separated from each other and used in the next step. The mixture of amine and hydroxylamine (0.5 g, 2 mmol together) was suspended in 15 mL DCE, to which pyridine (0.16 g, 2 mmol) and 4-chlorobutanoyl chloride (0.42 g, 3 mmol) were given at 0 °C. The mixture was stirred at r.t. for 18 h and subsequently diluted with 50 mL of DCM and 50 mL of NaHCO₃ solution. The

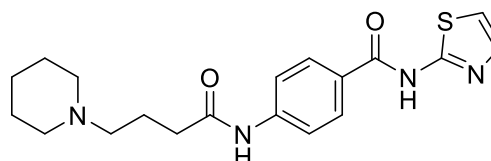
organic layer was collected and evaporated in the rotary evaporator to dryness. The residue was dissolved in 5 mL of piperidine, and the solution was stirred at r.t. for 72 h. The excessive piperidine was removed with the rotary evaporator. The residue was purified with column chromatography, whereby the solvent mixture of DCM and MeOH in ratios of 95:5 and 90:10 were used as eluents. The product was recrystallized in acetone.

Yield: 38%

Appearance: Slightly yellow to white solid

Chemical formula: $C_{19}H_{24}N_4O_2S$

Molecular weight: 372.5 g/mol



Melting point: 166.3 °C

LC-MS: 100%, max. m/z: 373.16 $[M+H]^+$, with gradient LC-Method 1

1H NMR (300 MHz, $CDCl_3$) δ 9.76 (s, 1H, Ph-NH-), 8.00 (d, $J = 8.1$ Hz, 2H, Benzoyl-2,6-H), 7.68 (d, $J = 8.3$ Hz, 2H, Benzoyl-3,5-H), 7.09 (d, $J = 3.8$ Hz, 1H, Thiazol-4-H), 6.90 (d, $J = 3.9$ Hz, 1H, Thiazol-5-H), 2.59 – 2.28 (m, 8H, overlap: Piperi-2,6- H_2 , Piperi- CH_2 -, $-CH_2$ -CO-), 1.90 (p, $J = 6.5$ Hz, 2H, $-CH_2$ - CH_2 -CO-), 1.62 (p, $J = 5.6$ Hz, 4H, Piperi-3,5- H_2), 1.55 – 1.41 (m, 2H, Piperi-4- H_2).

^{13}C NMR (75 MHz, $CDCl_3$) δ 172.27 (Ph-NH-CO-), 165.28 (Ph-CO-), 160.52 (Thiazol-2-C), 142.89 (Benzoyl-4-C), 137.32 (Thiazol-4-C), 129.40 (Benzoyl-2,6-C), 127.60 (Benzoyl-1-C), 119.47 (Benzoyl-3,5-C), 113.51 (Thiazol-5-C), 57.67 (Piperi- CH_2 -), 54.45 (Piperi-2,6-C), 36.36 (Ph-NH-CO- CH_2 -), 26.04 (Piperi-3,5-C), 24.42 (Piperi-4-C), 22.21 (Piperi- CH_2 - CH_2 -).

6.5 Selected NMR, LC-MS, and HPLC spectra

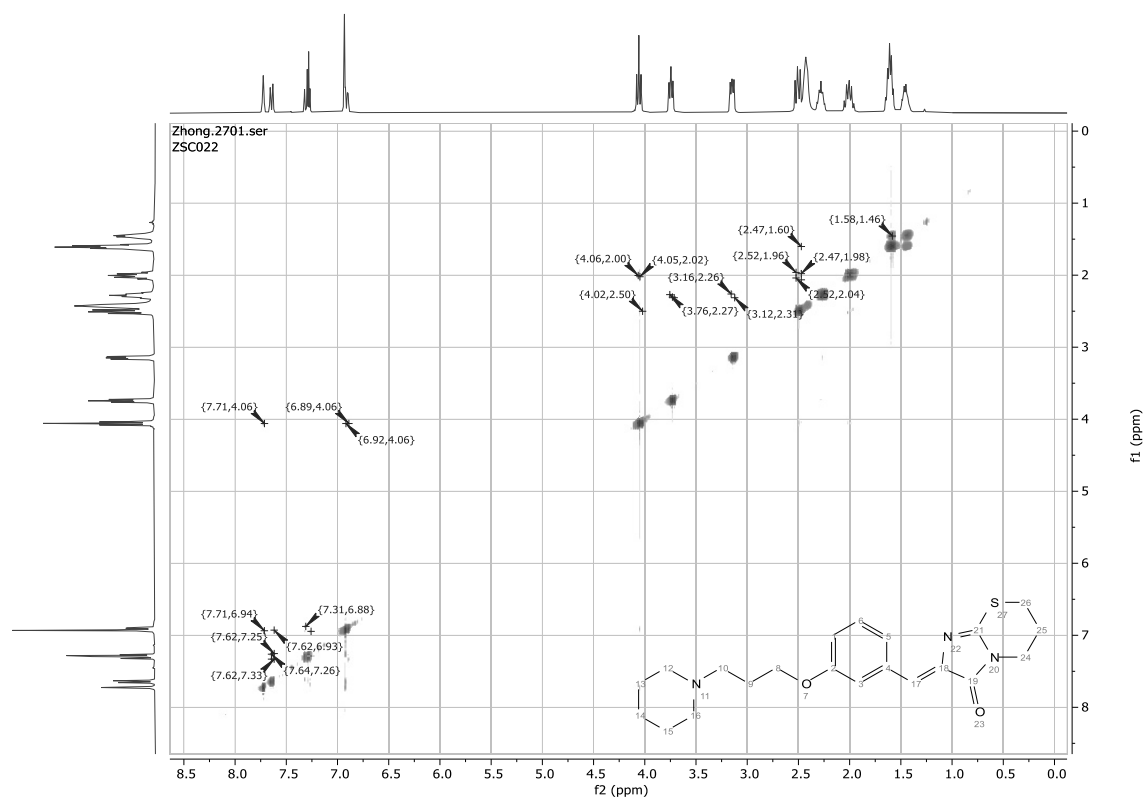


Figure 6-1: ROESY spectrum of P16.

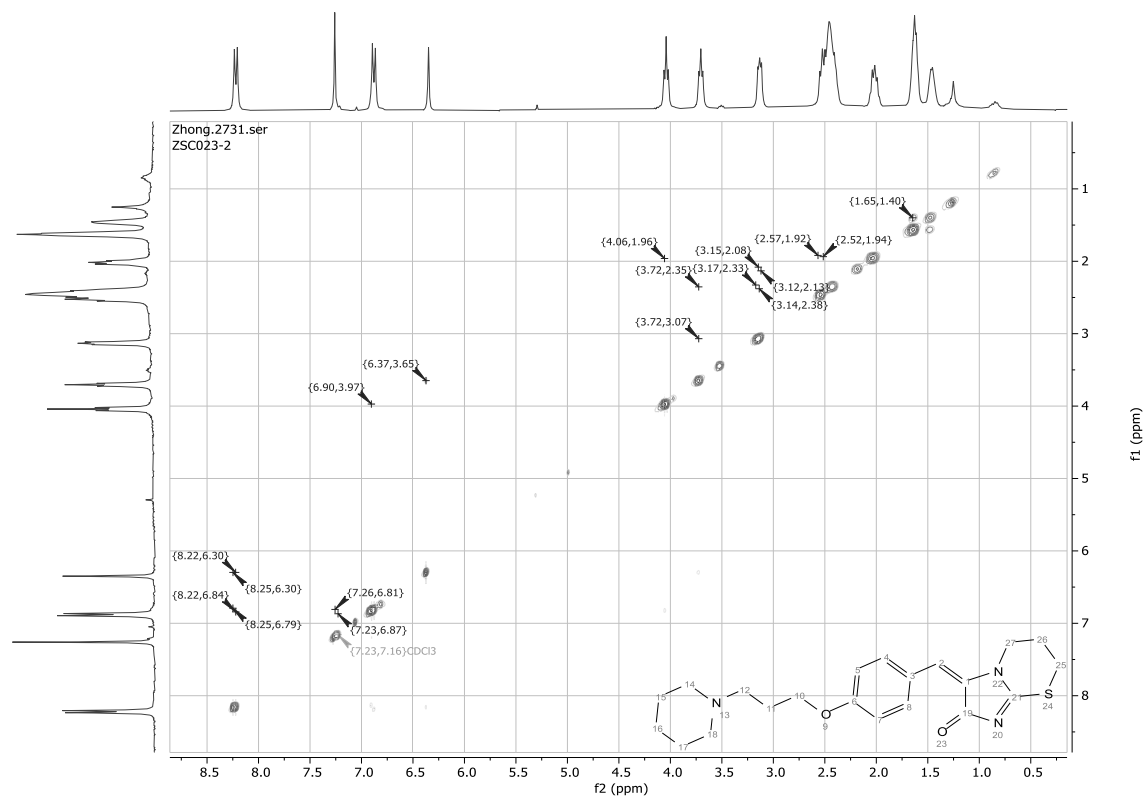


Figure 6-2: ROESY spectrum of P18.

Experiment

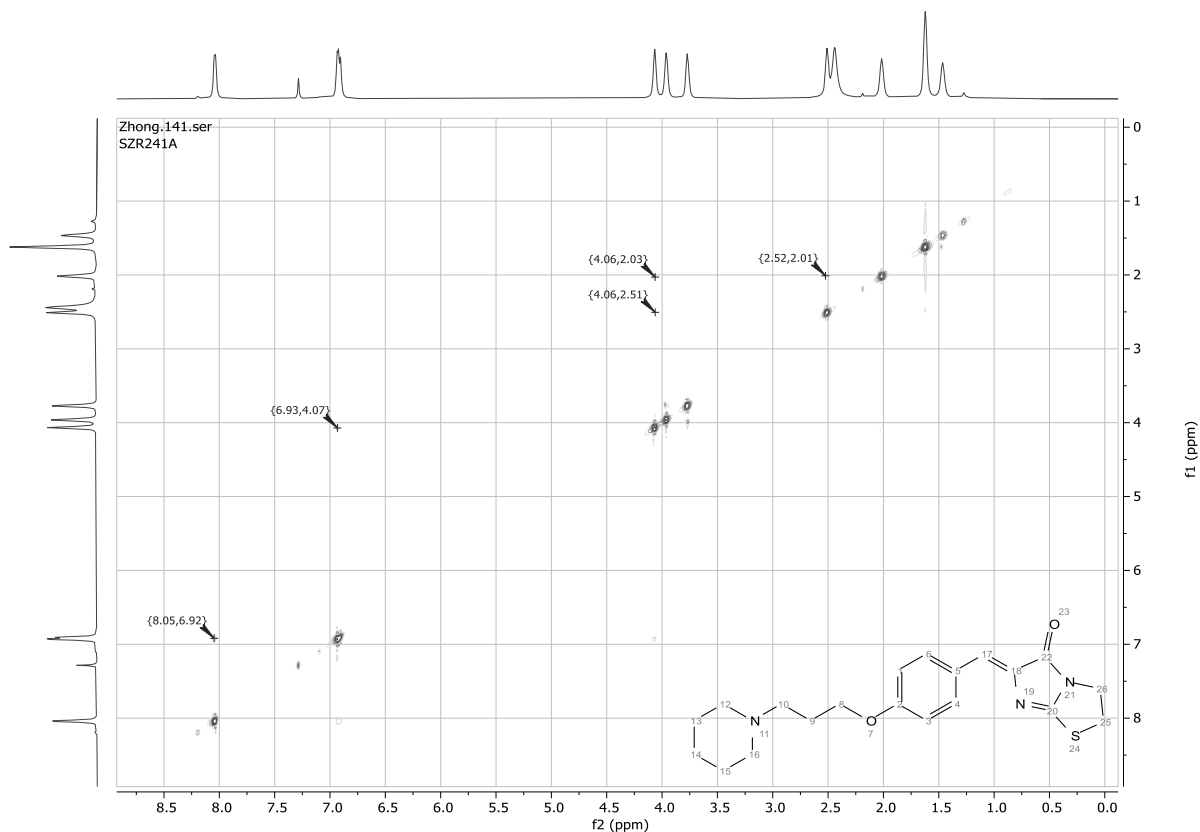
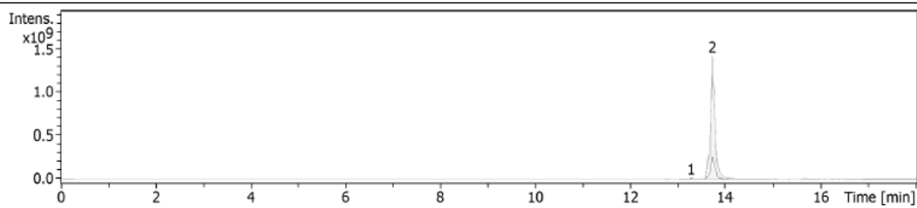


Figure 6-3: ROESY spectrum of P19.

Compound Spectrum List Report

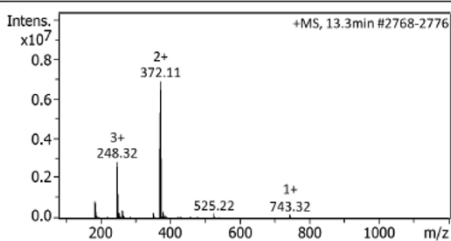
Analysis Info		Acquisition Date	6/12/2019 10:37:24 AM
Analysis Name	D:\Data\Reinheit\2019\12062019\Steven_MAddition\S241A_MeOH_3_01_2259.d	Operator	demo
Method	ab2bis100LONG_50LOOP_PASA_wash5EQ3min_2259.m	Instrument	amaZon speed ETD
Sample Name	S241A_MeOH		
Comment			

Acquisition Parameter			
Ion Source Type	ESI	Ion Polarity	Negative
Mass Range Mode	UltraScan	Scan Begin	80 m/z
Accumulation Time	2000 μ s	RF Level	59 %
SPS Target Mass	350 m/z	Averages	5 Spectra
		Alternating Ion Polarity	on
		Scan End	1200 m/z
		Trap Drive	44.9



#	RT [min]	Area	S/N	Area Frac. %	Max. m/z
1	13.3	18763528	28.4	0.2	372.11
2	13.7	8726447104	4302.4	99.8	372.10

Cmpd 1, 13.3 min



Cmpd 2, 13.7 min

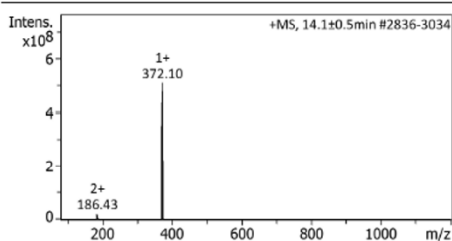


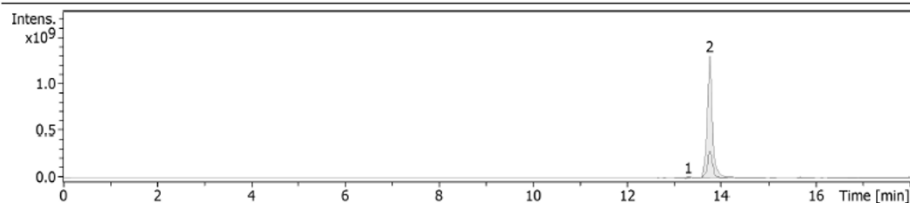
Figure 6-4: Investigation of potential reactivity of P19 as Michael acceptor (MeOH, 0 h).

Compound Spectrum List Report

Analysis Info
 Analysis Name D:\Data\Reinheit\2019\12062019\Steven_MAddition\S241MeOH48h_3_01_2299.d
 Method ab2bis100LONG_50LOOP_PASA_wash5EQ3min_2299.m
 Sample Name S241MeOH48h
 Comment
 Acquisition Date 6/14/2019 1:48:59 PM
 Operator demo
 Instrument amaZon speed ETD

Acquisition Parameter

Ion Source Type ESI Ion Polarity Negative Alternating Ion Polarity on
 Mass Range Mode UltraScan Scan Begin 80 m/z Scan End 1200 m/z
 Accumulation Time 2000 μ s RF Level 59 % Trap Drive 44.9
 SPS Target Mass 350 m/z Averages 5 Spectra



#	RT [min]	Area	S/N	Area Frac. %	Max. m/z
1	13.3	136848944	133.0	1.3	372.11
2	13.8	10006010880	9567.3	98.7	372.11

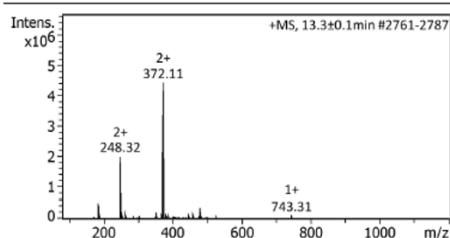
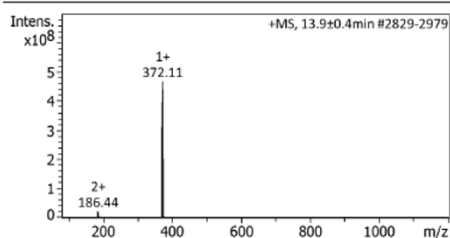
Cmpd 1, 13.3 min**Cmpd 2, 13.8 min**

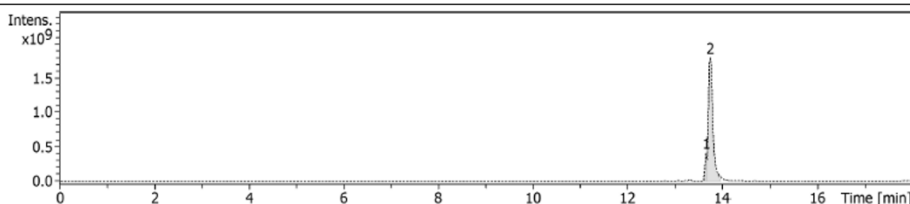
Figure 6-5: Investigation of potential reactivity of P19 as Michael acceptor (MeOH, 48 h).

Compound Spectrum List Report

Analysis Info
 Analysis Name D:\Data\Reinheit\2019\12062019\Steven_MAddition\S241_MeOH110h_3_01_2312.d
 Method ab2bis100LONG_50LOOP_PASA_wash5EQ3min_2312.m
 Sample Name S241_MeOH110h
 Comment
 Acquisition Date 6/17/2019 11:29:47 AM
 Operator demo
 Instrument amaZon speed ETD

Acquisition Parameter

Ion Source Type ESI Ion Polarity Positive Alternating Ion Polarity on
 Mass Range Mode UltraScan Scan Begin 80 m/z Scan End 1200 m/z
 Accumulation Time 2000 μ s RF Level 59 % Trap Drive 47.4
 SPS Target Mass 350 m/z Averages 5 Spectra



#	RT [min]	Area	S/N	Area Frac. %	Max. m/z
1	13.7	1281251328	1547.8	9.7	372.09
2	13.7	11914868736	6639.3	90.3	372.10

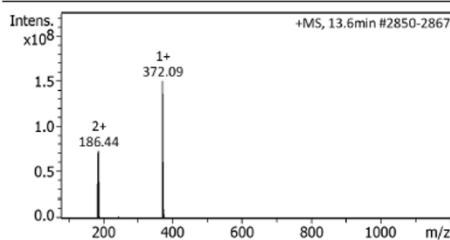
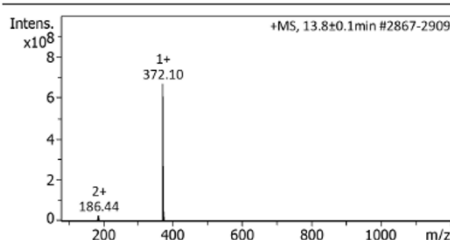
Cmpd 1, 13.7 min**Cmpd 2, 13.7 min**

Figure 6-6: Investigation of potential reactivity of P19 as Michael acceptor (MeOH, 110 h).

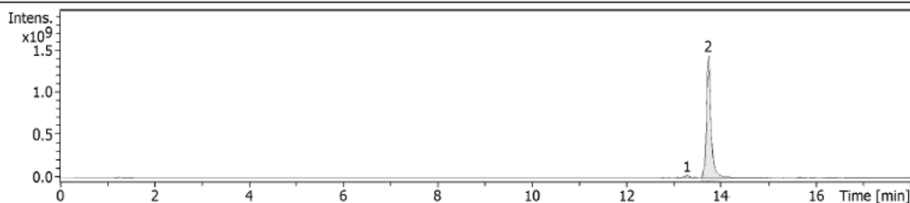
Experiment

Compound Spectrum List Report

Analysis Info Acquisition Date 6/12/2019 11:14:18 AM
 Analysis Name D:\Data\Reinheit\2019\12062019\Steven_MAddition\S241_Puffer60min_4_01_2261.d
 Method ab2bis100LONG_50LOOP_PASA_wash5EQ3min_2261.m Operator demo
 Sample Name S241_Puffer60min Instrument amaZon speed ETD
 Comment

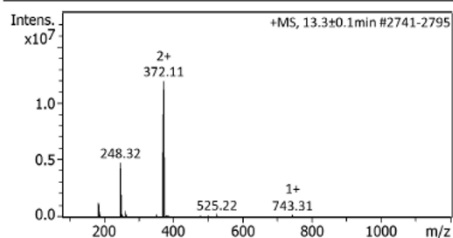
Acquisition Parameter

Ion Source Type	ESI	Ion Polarity	Negative	Alternating Ion Polarity	on
Mass Range Mode	UltraScan	Scan Begin	80 m/z	Scan End	1200 m/z
Accumulation Time	2000 µs	RF Level	59 %	Trap Drive	44.9
SPS Target Mass	350 m/z	Averages	5 Spectra		



#	RT [min]	Area	S/N	Area Frac. %	Max. m/z
1	13.3	166874464	94.9	1.5	372.11
2	13.7	10705802240	4665.8	98.5	372.10

Cmpd 1, 13.3 min



Cmpd 2, 13.7 min

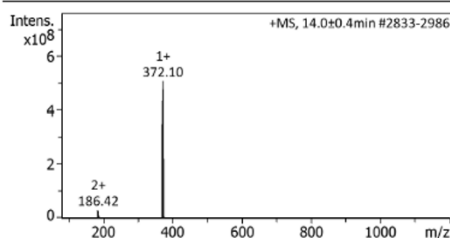


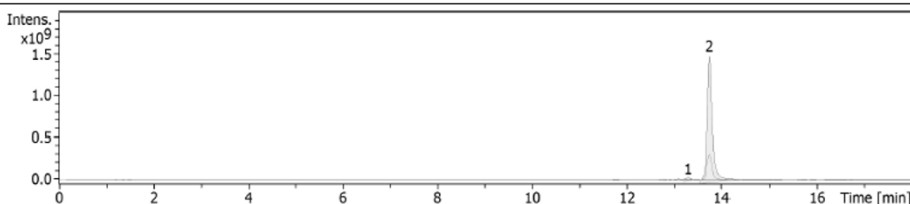
Figure 6-7: Investigation of potential reactivity of P19 as Michael acceptor (Puffer, 1 h).

Compound Spectrum List Report

Analysis Info Acquisition Date 6/14/2019 12:35:11 PM
 Analysis Name D:\Data\Reinheit\2019\12062019\Steven_MAddition\S241_Puffer48h_4_01_2295.d
 Method ab2bis100LONG_50LOOP_PASA_wash5EQ3min_2295.m Operator demo
 Sample Name S241_Puffer48h Instrument amaZon speed ETD
 Comment

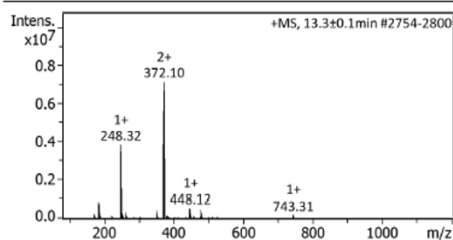
Acquisition Parameter

Ion Source Type	ESI	Ion Polarity	Negative	Alternating Ion Polarity	on
Mass Range Mode	UltraScan	Scan Begin	80 m/z	Scan End	1200 m/z
Accumulation Time	2000 µs	RF Level	59 %	Trap Drive	44.9
SPS Target Mass	350 m/z	Averages	5 Spectra		



#	RT [min]	Area	S/N	Area Frac. %	Max. m/z
1	13.3	378770464	266.6	3.1	372.10
2	13.7	11907806208	9841.6	96.9	372.12

Cmpd 1, 13.3 min



Cmpd 2, 13.7 min

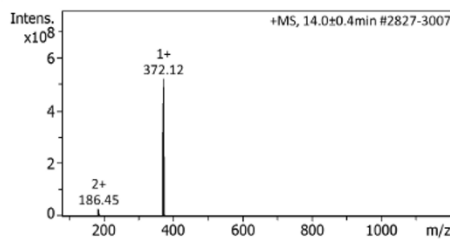


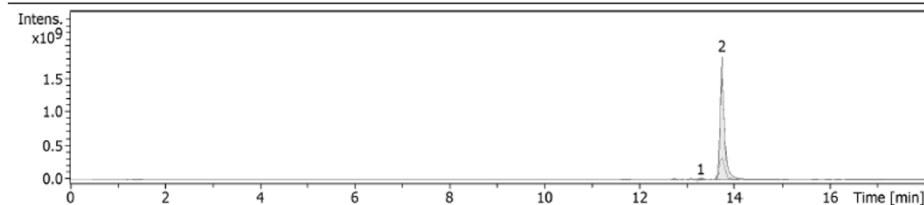
Figure 6-8: Investigation of potential reactivity of P19 as Michael acceptor (Puffer, 48 h).

Experiment

Compound Spectrum List Report

Analysis Info Acquisition Date 6/17/2019 7:52:29 AM
 Analysis Name D:\Data\Reinheit\2019\12062019\Steven_M\Addition\S241_Puffer110h_4_01_2303.d
 Method ab2bis100LONG_50LOOP_PASA_wash5EQ3min_2303.m Operator demo
 Sample Name S241_Puffer110h Instrument amaZon speed ETD
 Comment

Acquisition Parameter
 Ion Source Type ESI Ion Polarity Negative Alternating Ion Polarity on
 Mass Range Mode UltraScan Scan Begin 80 m/z Scan End 1200 m/z
 Accumulation Time 2000 μ s RF Level 59 % Trap Drive 44.9
 SPS Target Mass 350 m/z Averages 5 Spectra



#	RT [min]	Area	S/N	Area Frac. %	Max. m/z
1	13.3	355847008	188.9	3.2	372.11
2	13.7	10732425216	8523.5	96.8	372.09

Cmpd 1, 13.3 min

Cmpd 2, 13.7 min

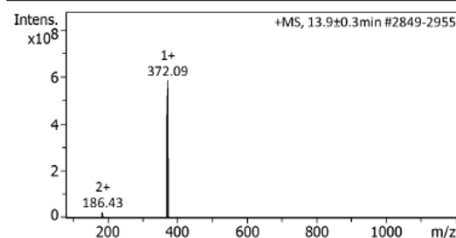
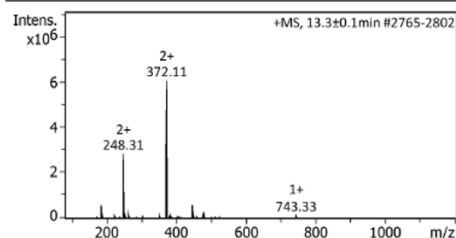
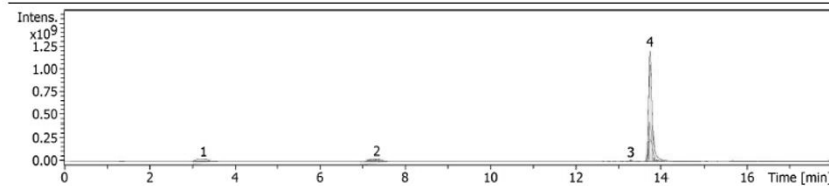


Figure 6-9: Investigation of potential reactivity of P19 as Michael acceptor (Puffer, 48 h).

Compound Spectrum List Report

Analysis Info Acquisition Date 6/12/2019 11:51:11 AM
 Analysis Name D:\Data\Reinheit\2019\12062019\Steven_M\Addition\S241ACC\PUff0min_5_01_2263.d
 Method ab2bis100LONG_50LOOP_PASA_wash5EQ3min_2263.m Operator demo
 Sample Name S241ACC\PUff0min Instrument amaZon speed ETD
 Comment

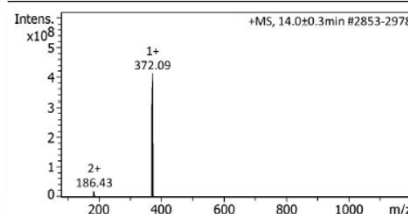
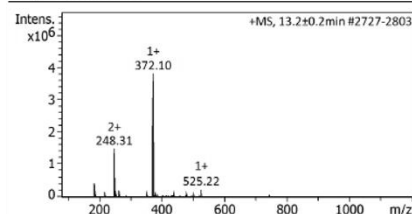
Acquisition Parameter
 Ion Source Type ESI Ion Polarity Negative Alternating Ion Polarity on
 Mass Range Mode UltraScan Scan Begin 80 m/z Scan End 1200 m/z
 Accumulation Time 2000 μ s RF Level 59 % Trap Drive 44.9
 SPS Target Mass 350 m/z Averages 5 Spectra



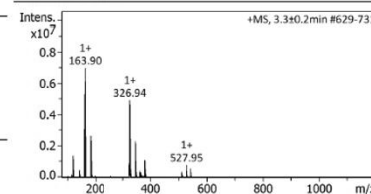
#	RT [min]	Area	S/N	Area Frac. %	Max. m/z
1	3.3	884846528	115.2	9.5	163.90
2	7.3	1508247808	149.6	16.2	324.96
3	13.3	58138096	30.1	0.6	372.10
4	13.7	6837002752	3899.4	73.6	372.09

Cmpd 3, 13.3 min

Cmpd 4, 13.7 min



Cmpd 1, 3.3 min



Cmpd 2, 7.3 min

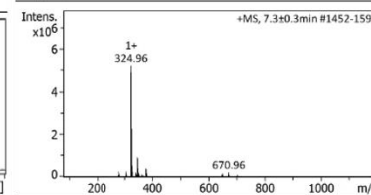


Figure 6-10: Investigation of potential reactivity of P19 as Michael acceptor (ACC, 0 h).

Experiment

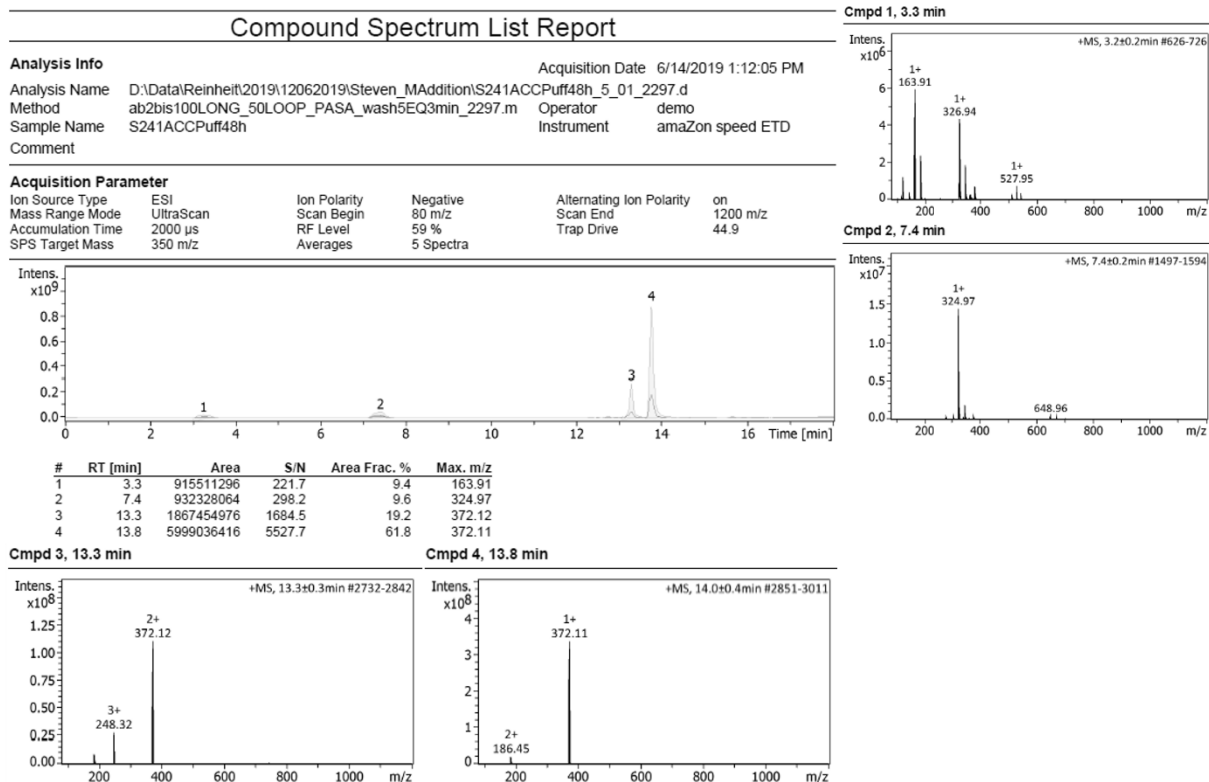


Figure 6-11: Investigation of potential reactivity of **P19** as Michael acceptor (Puffer, 48 h).

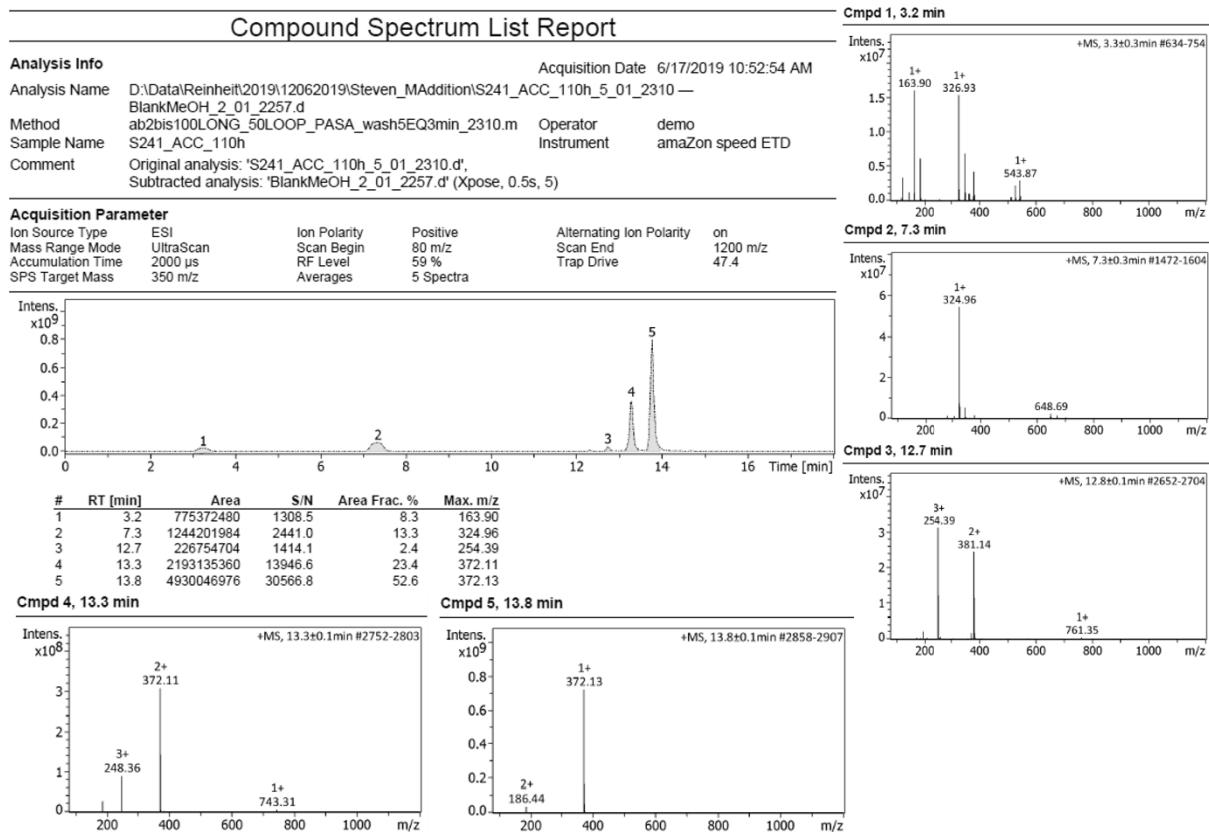


Figure 6-12: Investigation of potential reactivity of **P19** as Michael acceptor (Puffer, 110 h).

Experiment

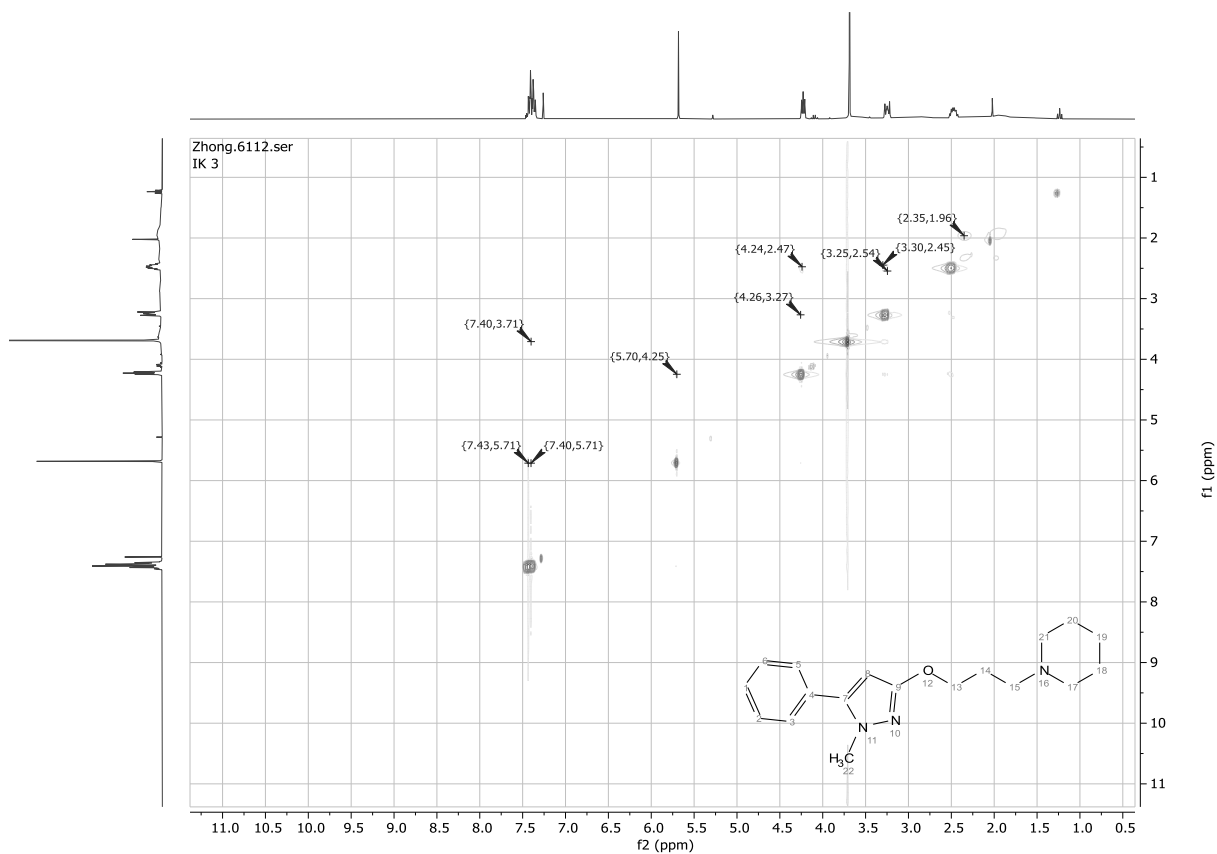
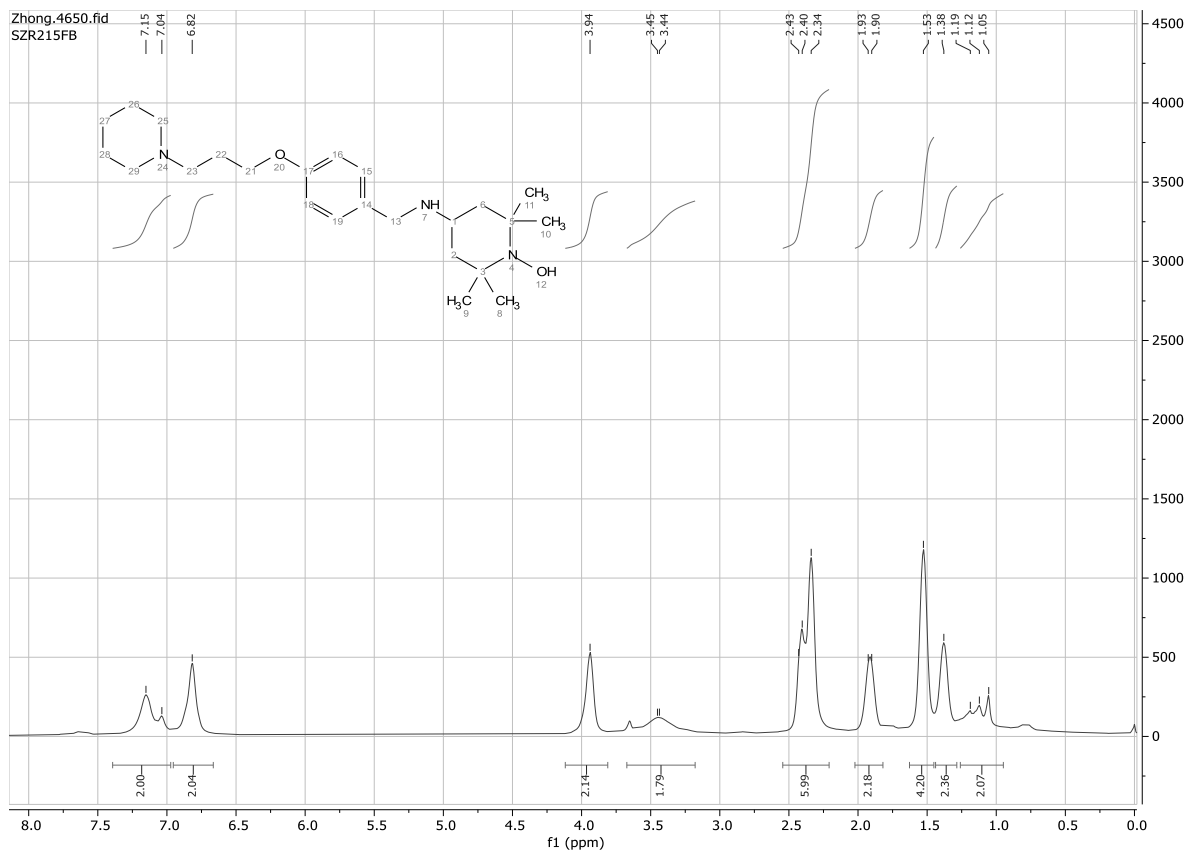


Figure 6-13: ROESY spectrum of P24.



Experiment

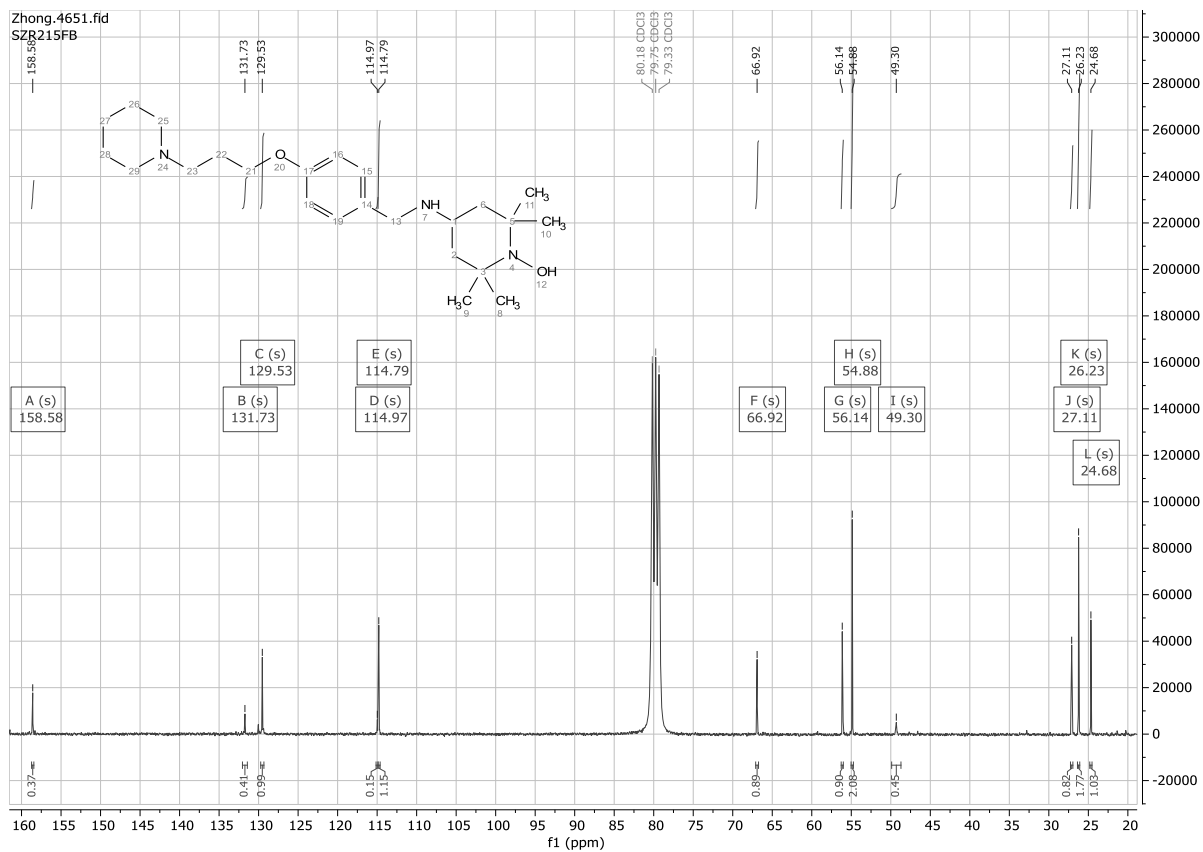
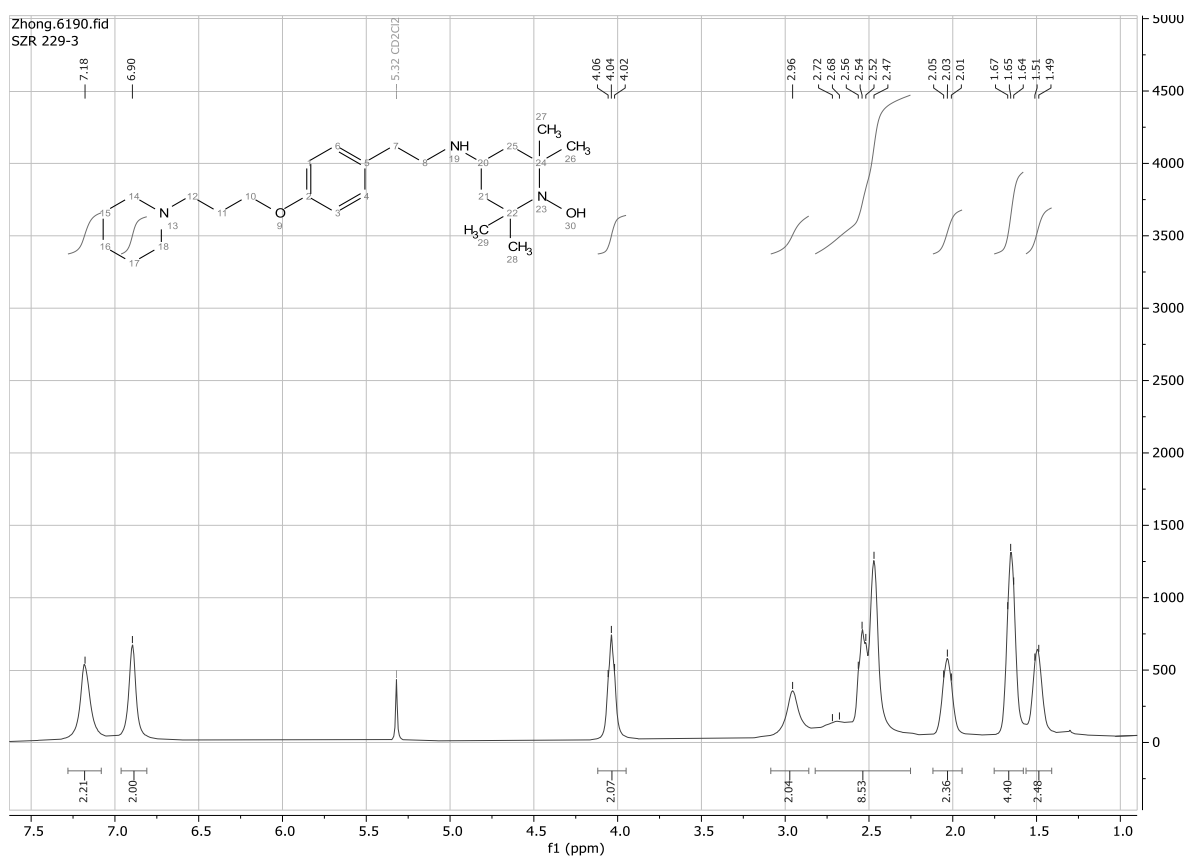


Figure 6-14: NMR spectra of P25.



Experiment

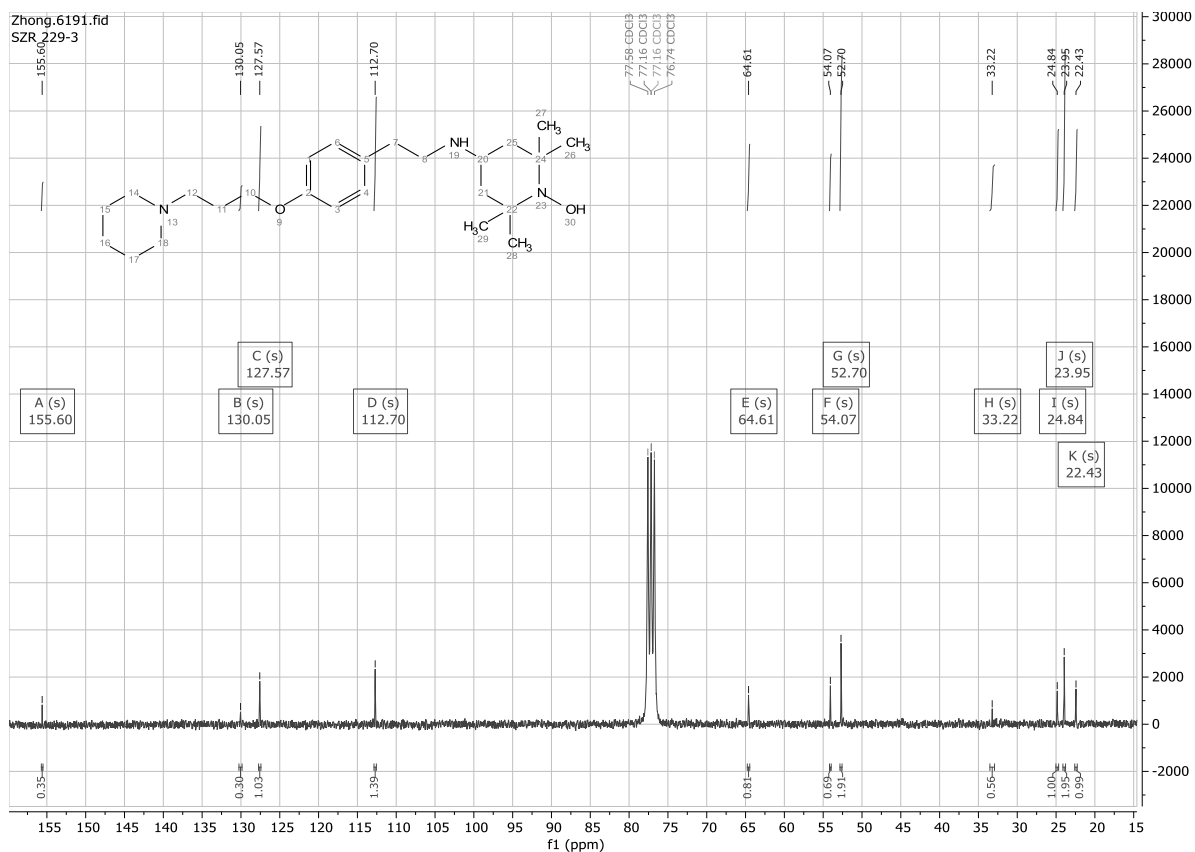


Figure 6-15: NMR spectra of P26.

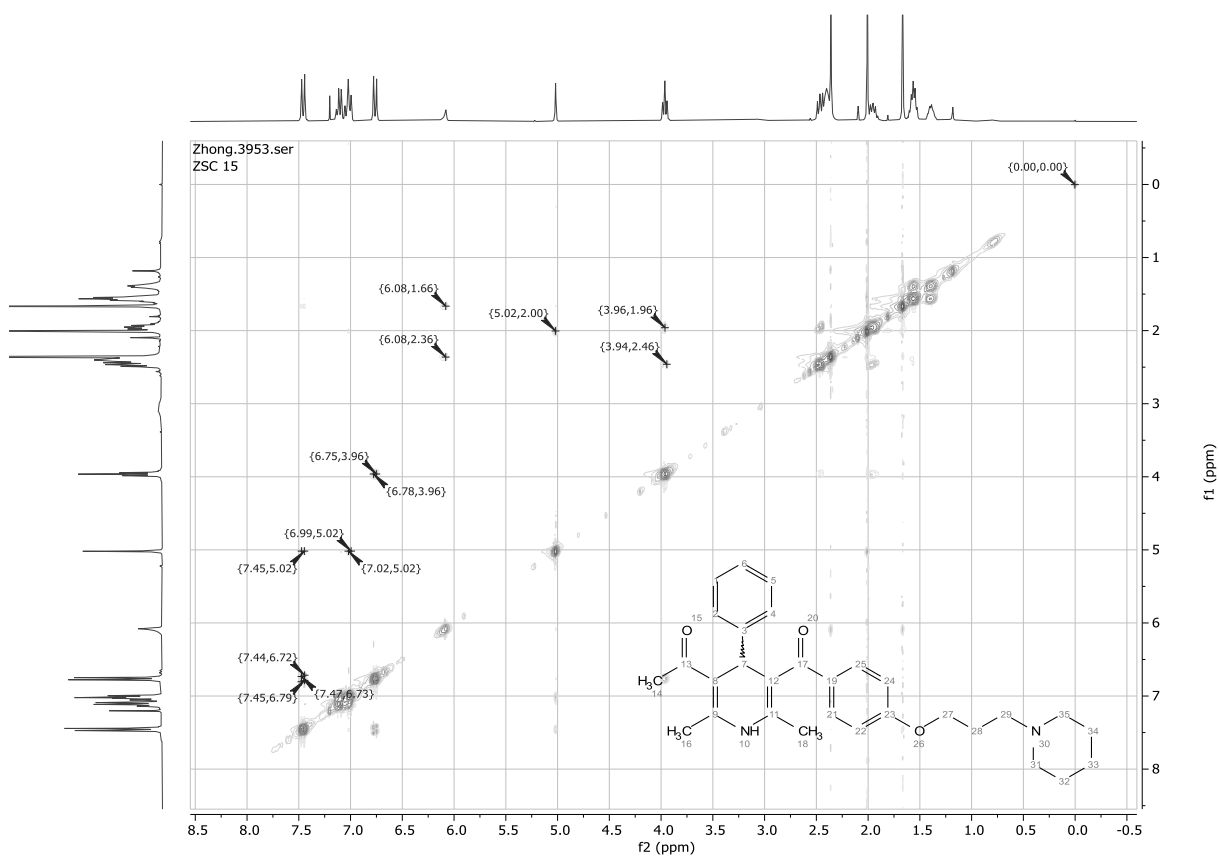


Figure 6-16: ROESY spectrum of compound P34.

Experiment

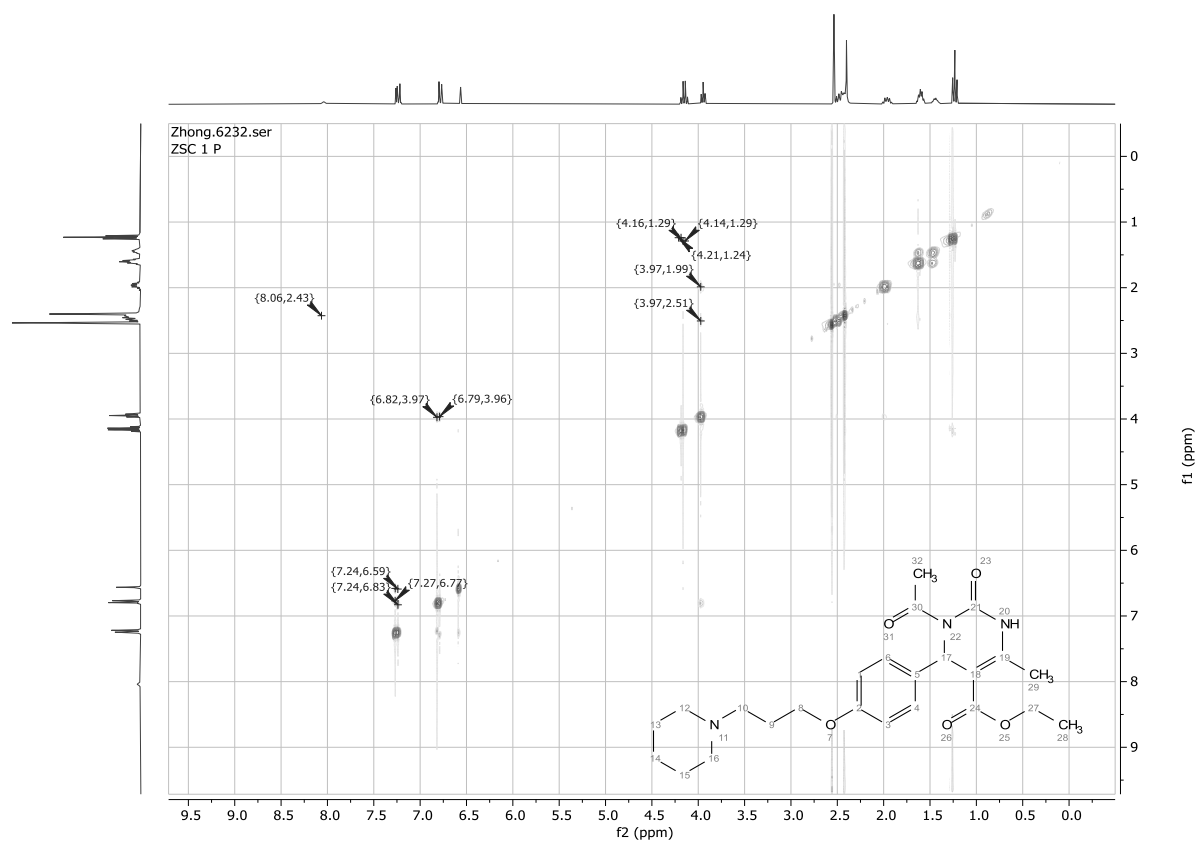
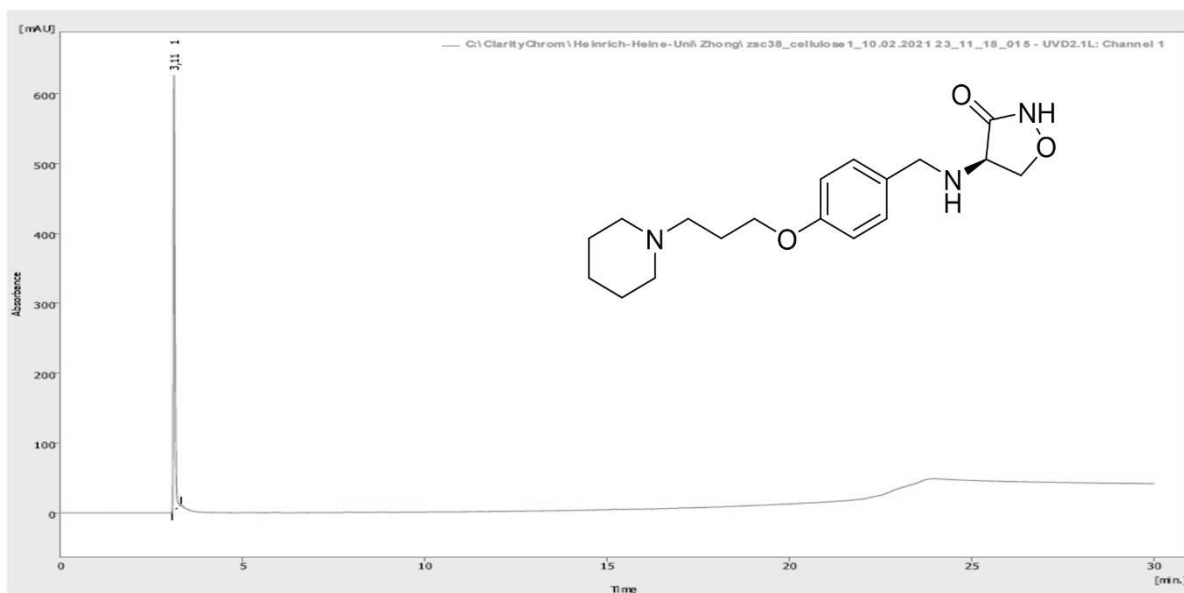


Figure 6-17: ROESY spectrum of P38.



Result Table (Uncal - C:\ClarityChrom\Heinrich-Heine-Uni\Zhong\zsc38_cellulose1_10.02.2021_23_11_18_015 - UVD2.1L: Channel 1)

	Reten. Time [min]	Area [AU.s]	Height [AU]	Area [%]	Height [%]	W05 [min]	Compound Name
1	3,107	1,853	0,623	100,0	100,0	0,04	
	Total	1,853	0,623	100,0	100,0		

Figure 6-18: HPLC spectrum of P50.

Experiment

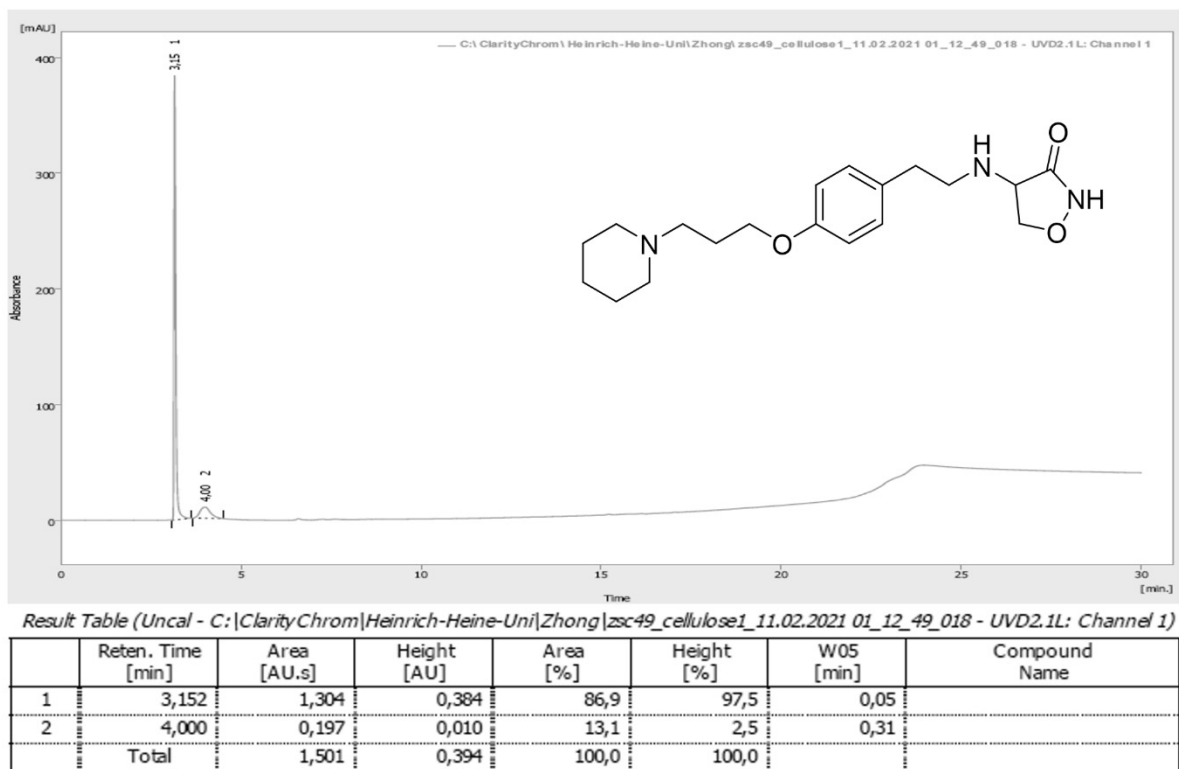


Figure 6-19: HPLC spectrum of P51.

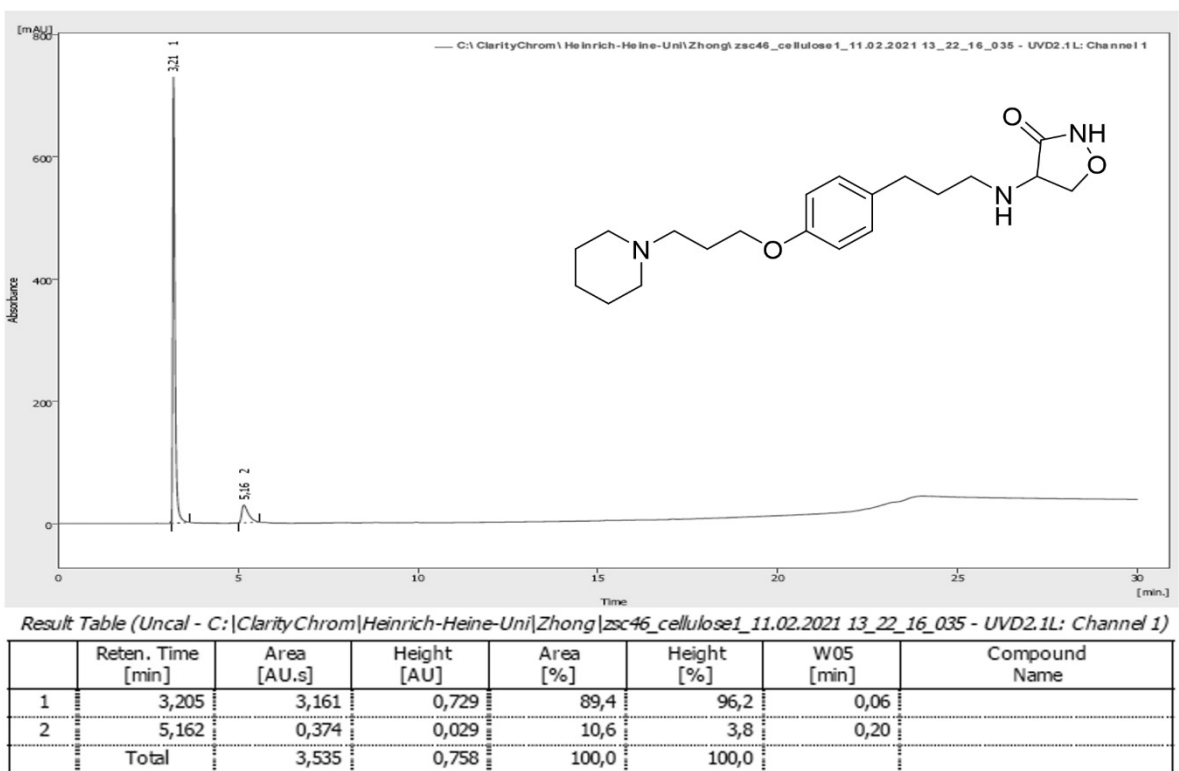


Figure 6-20: HPLC spectrum of P52.

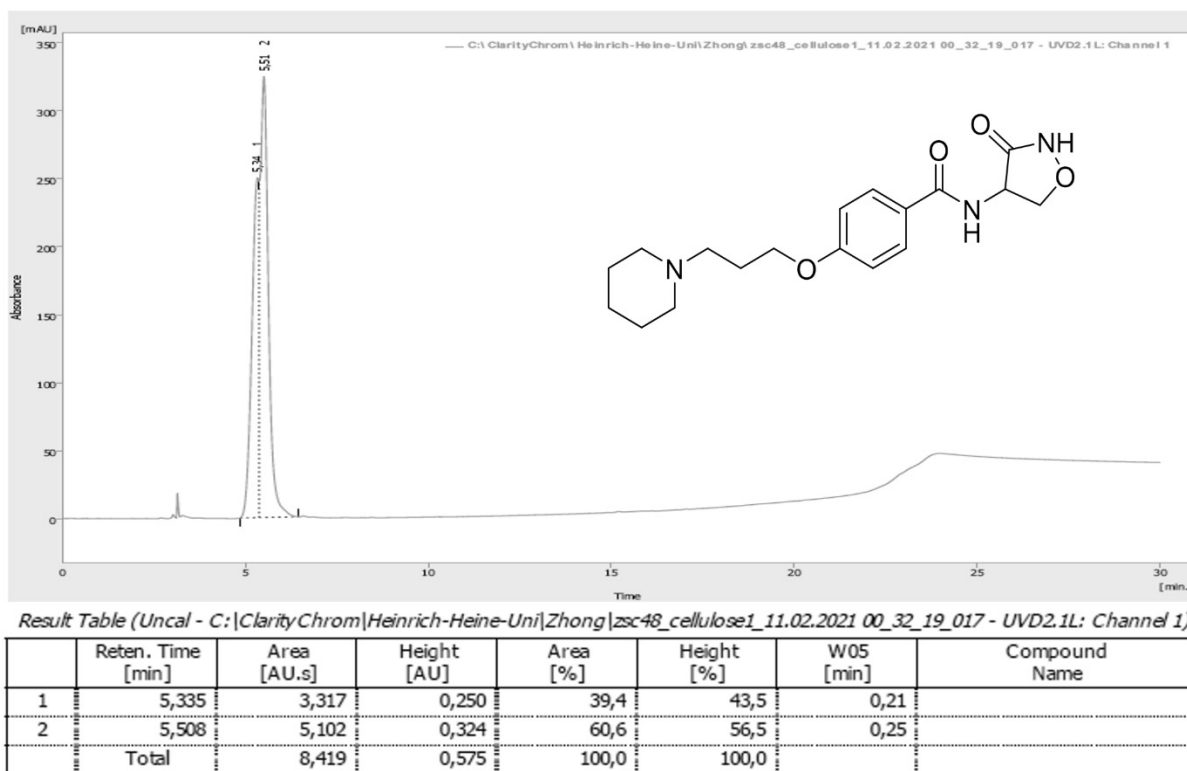


Figure 6-21: HPLC spectrum of P53.

6.6 General procedures for pharmacological experiments

6.6.1 Human histamine H₃ receptor radioligand displacement assay

Radioligand displacement assays were performed as described previously (Kottke *et al.*, 2011; Affini *et al.*, 2018). HEK-293 cells stably expressing the recombinant human histamine H₃ receptor gene (Ligneau *et al.*, 2000) were grown in Dulbecco's modified Eagle's medium supplemented with 2 mM glutamine, 10 mM HEPES, 10% fetal bovine serum, and 10 µl/mL penicillin/streptomycin in an atmosphere of 5% CO₂ at 37 °C. Cells were grown to confluence. The medium was removed, and cells were collected in 15mL ice-cold phosphate-buffered saline (PBS) (140 mM NaCl, 3 mM KCl, 1.5 mM KH₂PO₄, 8 mM Na₂HPO₄, pH 7.4) and centrifuged two times at 3,000×g for 10 min with subsequent aspiration in 20 mL of PBS buffer at 4 °C. After the last centrifugation step, cells were disrupted and homogenized using an ULTRA-TURRAX® T25 digital (IKA, Germany) in ice-cold binding buffer (12.5 mM MgCl₂, 100 mM NaCl, and 75 mM Tris/HCl, pH 7.4). The cell membrane homogenate was centrifuged two times at 20,000×g for 20 min at 4 °C and homogenized again by sonication at 4 °C and kept in ice-cold binding buffer.

Competition binding experiments were carried out as follows briefly: membranes (20 µg/well in a final volume of 0.2 mL binding buffer) were incubated with [³H]-N^α-methylhistamine (2 nM), purchased from PerkinElmer (MA, USA), and different concentrations of the respective test

ligand. Assays were run at least in duplicates with eleven appropriate concentrations between 0.01 nM and 100 μ M of the test compound. Preparation of competitor concentrations was carried out by serial dilution of 10 mM and 3 mM stock solution using a Freedom EVO pipetting instrument (TECAN®, Männergdorf, Switzerland). Incubations were performed for 90 min at r.t. under shaking. Non-specific binding was determined in the presence of selectively acting histamine H₃ receptor inverse agonist/antagonist pitolisant (10 μ M). The bound radioligand was separated from free radioligand by filtration through GF/B filters pretreated with 0.3% (m/v) polyethylenimine using an Inotech cell harvester (Dottikon, Switzerland). Unbound radioligand was removed by three washing steps with approximately 0.25 mL/well of cold deionized water. Liquid scintillation counting using a PerkinElmer MicroBeta Trilux scintillation counter was used to determine the amount of radioactivity collected on the filter used in the current experiment. Competition binding data were analyzed by the software GraphPad Prism™ (2016, version 7.01, San Diego, CA, USA) using non-linear regression fit “one-site competition”. The inhibitory constant (K_i) was calculated from the IC_{50} values according to the Cheng-Prusoff equation (Yung-Chi and Prusoff, 1973) expressed as mean from at least three independent experiments in duplicate with 95% confidence intervals.

6.6.2 Human histamine H₁ receptor binding assay

To determine the hH₁R affinity, compounds and reference substances were tested in a [³H]-pyrilamine competition binding assay. The assay was conducted on membrane preparation of CHO-K1 cells stably expressing hH₁R. Transfection, culture, and membrane preparation were described in detail by Smit and colleagues (Smit *et al.*, 1996b). Briefly, Competition binding experiments were carried out similar to that for hH₃R, where the membranes (40 μ g/well in a final volume of 0.2 mL binding buffer) were incubated with [³H]-pyrilamine (1 nM) and test compounds in different concentration for 120 min at r.t. under shaking. The experimental assays were carried out in duplicates with eleven appropriate concentrations in the concentration range of 100 nM-100 μ M of the test compounds. The resulting nonspecific binding was evaluated in the presence of the standard H₁R antagonist chlorpheniramine hydrogen maleate at a concentration of 10 mM. Competition binding data were analyzed by the software GraphPad Prism™ (2016, version 7.01, San Diego, CA, USA) using non-linear least squares fit.

6.6.3 Human histamine H₄ receptor radioligand displacement assay

To determine the hH₄R affinity, compounds and reference structures were examined in a [³H]-histamine dihydrochloride competition binding assay. Cell culture and membrane preparation of Sf9 cells co-expressing hH₄R-G α_{12} fusion protein with G $\beta_1\gamma_2$ was prepared as described by Schneider and co-workers (Schneider *et al.*, 2009). Membranes were suspended in binding buffer and stored at -80 °C until use.

The competition binding assay has been performed as described previously by Sander, Kottke, and Schwed from the Stark Lab (Sander *et al.*, 2009; Łazewska *et al.*, 2014) and similar to that for hH₃R. Before the experiments, cell membranes were sedimented by 3 min centrifugation at 25 °C and 130 rpm and resuspended in binding buffer. Competition binding experiments were carried out by incubating membranes, 40 µg/well in a final volume of 0.2 mL containing binding buffer and [³H]-histamine dihydrochloride (10 nM). Assays were run in triplicates with four to seven appropriate concentrations between 0.1 nM and 100 µM of the test compound. Incubations were performed for 60 min at room temperature. Non-specific binding was determined in the presence of 10 µM unlabeled JNJ7777120. Competition binding data were analyzed by the software GraphPad Prism™ (2016, version 7.01, San Diego, CA, USA) using non-linear least squares fit.

6.6.4 Inhibition studies with human monoamine oxidases A and B

MAO inhibition assays were carried out using human recombinant membrane-bound MAO-A and MAO-B purchased from Sigma-Aldrich (MO, USA). Kynuramine was used as the substrate, and clorgyline and safinamide were used as positive references for MAO-A and MAO-B inhibitions, respectively. Compounds **P11-13** and **P49** were investigated via one-point screening in both MAO isoenzymes using a continuous spectrophotometric method described previously (Hagenow *et al.*, 2017; Affini *et al.*, 2018). The spectrophotometric one-point measurements were performed in clear, flat-bottom 96-well plates (UV-Star®, No. 655801, Greiner bio-one GmbH, Austria), measuring enzyme activity by spectrophotometrical observation of 4-hydroxyquinoline ($\lambda_{\max} = 316$ nm) formation over time. Initial velocities of substrate conversion (expressed as milli absorption units per minute) were plotted against log inhibitor concentrations and fitted using the implemented nonlinear regression “log inhibitor vs. response (three parameters)”. For one-point measurements, data were calculated as the percentage of control (product formation in the absence of inhibitor) and expressed as mean \pm standard deviation (%) performing at least two independent experiments, each in duplicates.

Compound **P48** was investigated via discontinuous fluorimetric assay, where the IC_{50} value was determined as described previously (Affini *et al.*, 2018). Fluorimetric MAO assays were conducted in a total assay volume of 100 µL (max. 1% DMSO) using black, flat-bottom 96-well plates (No. 655076, Greiner bio-one GmbH, Austria), while pipetting was partly automated using an EVO freedom pipetting robot (Tecan Trading AG, Switzerland). IC_{50} values were obtained by measuring enzyme activity (determined as MAO-dependent product formation) with inhibitor concentrations ranging from 0.001 µM to 100 µM in the presence of 2-fold K_M concentrations of kynuramine ($K_M = 30$ µM for MAO-A and $K_M = 20$ µM for MAO-B). Reactions were started by adding MAO-A (1.25 ng/µL, 900 units/mL) or MAO-B (1.67 ng/µL,

375 units/mL). The shifts of IC_{50} values were also measured after preincubating inhibitors with the enzyme (30 min, 37 °C), while reactions were started by adding substrate. For optimal enzyme activity conditions, reactions were performed in pre-warmed potassium phosphate buffer (50 mM, $pH = 7.4$). After incubation (15 or 20 min, 37 °C with and without preincubation IC_{50} setup, respectively), reactions were stopped by manual addition of 35 μ L sodium hydroxide (2 M), and enzyme activity was determined by detection of 4-hydroxyquinoline ($\lambda_{ex} = 320 \pm 20$ nm, $\lambda_{em} = 405 \pm 20$ nm) using an infinite M1000 Pro microplate reader (Tecan Trading AG, Switzerland). Data were analyzed using GraphPad PRISM 7. Enzyme activity was expressed as relative fluorescence units, were plotted against log inhibitor concentrations, and fitted using the implemented non-linear regression "log inhibitor vs. response (three parameters)". Data were obtained from at least three independent experiments, each performed at least in duplicates. Remained enzyme activity was measured fluorimetrically as described above under substrate saturating ($10 \times K_M$) conditions. Data were expressed as mean values from at least two independent experiments in triplicates within 95% confidence intervals.

6.6.5 Cell viability assay

To test the compounds for cytotoxicity, a resazurin reduction test has been performed on SH-SY5Y cells. The seeding and culture of cells have been detailed described previously (Stölting, 2020). Briefly, resazurin sodium has been diluted in DMF to a stock concentration of 440 mM, which was further diluted with sodium chloride-phosphate-buffer (1.06 mM KH_2PO_4 , 154 mM NaCl, 3.77 mM Na_2HPO_4 , $pH = 7.4$) to obtain a final concentration of 440 μ M (Storage at 4 °C, protected from light). Before use, the resazurin stock solution was freshly diluted with RPMI medium to a working solution with a concentration of 44 μ M. The compounds to test were diluted to 1 mM and 0.1 mM stock concentrations in DMSO. Each compound has been tested in triplicate at final concentrations of 10 μ M and 1 μ M, while 1% DMSO served as a negative control and two empty wells served as blank control. 1-Methyl-4-phenylpyridinium iodide (MPP⁺) 10 mM and 1 mM diluted in PBS served as a positive control for cytotoxicity. For an assay, 90 μ L of the cells seeded with a minimum essential medium eagle at a density of 89,000 cells/mL (8000 cells/well, total volume 100 μ L/well) was preincubated at 37 °C in a 5% CO_2 atmosphere for 24 h. Subsequently, the cells were co-incubated with respective compound dilution and the reference compound for a further 24 h at 37 °C, the liquid phase has been subsequently aspirated. To determine the remained cell vitality, cells were incubated with the resazurin working solution (44 μ M in RPMI medium, 100 μ L) for 2 h. Fluorescence intensity (Excitation: 535 nm, Emission: 590 nm, bandwidth 5 nm) was measured using a Tecan infinite M1000 Pro microplate reader. To analyze the fluorescence intensities, the mean value of the blank control has been subtracted from the values of the compounds. The mean values with standard deviations have been calculated with GraphPad Prism 7.01.

6.6.6 Oxygen-radical absorbance capacity assay

The oxygen-radical absorbance capacity (ORAC) assay was performed using fluorescein and the radical generating compound AAPH (see Figure 4-1) as described previously (Cao *et al.*, 1993; Ou *et al.*, 2001). Briefly, fluorescein (100 nM in KPi buffer) was incubated initially with compounds to be tested in five different concentration (20 μ M, 10 μ M, 5 μ M, 2.5 μ M, and 1.25 μ M, dilution was partly automatized by a Tecan Freedom EVO pipetting instrument) for 15 min and subsequently with AAPH (75 mM in KPi buffer) at 37 °C for 61 min to 91 min in a black, flat-bottom 96-well-plate (final volume 200 μ L). The intensity of fluorescence was reduced when oxidized. Fluorescence intensity (Excitation: 492 nm, Emission: 516 nm, bandwidth 5 nm) was measured using a Tecan infinite M1000 Pro microplate reader. To analyze the fluorescence intensities, the mean value of the blank control has been subtracted from the values of the compounds. After that, a mean value with a standard deviation has been calculated with GraphPad Prism 7.01. The results herein were presented as ORAC units. One ORAC unit equals the net production provided by 1 μ M of 6-hydroxy-2,5,7,8-tetramethylchroman-2-carboxylic acid (Trolox, a water-soluble tocopherol analog). The protocol of execution in detail was described by Stölting (Stölting, 2020).

7 Reference

- Abdel-Magid, A.F., Carson, K.G., Harris, B.D., Maryanoff, C.A. and Shah, R.D. (1996) Reductive Amination of Aldehydes and Ketones with Sodium Triacetoxyborohydride. Studies on Direct and Indirect Reductive Amination Procedures 1. *The Journal of Organic Chemistry*, 61, 3849–3862. <https://doi.org/10.1021/jo960057x>
- Affini, A., Hagenow, S., Zivkovic, A., Marco-Contelles, J. and Stark, H. (2018) Novel indanone derivatives as MAO B/H3R dual-targeting ligands for treatment of Parkinson's disease. *European Journal of Medicinal Chemistry*, 148, 487–497. <https://doi.org/10.1016/j.ejmech.2018.02.015>
- Alachkar, A., Azimullah, S., Ojha, S.K., Beiram, R., Łażewska, D., Kieć-Kononowicz, K. and Sadek, B. (2019) The Neuroprotective Effects of Histamine H3 Receptor Antagonist E177 on Pilocarpine-Induced Status Epilepticus in Rats. *Molecules*, 24, 4106. <https://doi.org/10.3390/molecules24224106>
- Amon, M., Ligneau, X., Schwartz, J.C. and Stark, H. (2006) Fluorescent non-imidazole histamine H3 receptor ligands with nanomolar affinities. *Bioorganic and Medicinal Chemistry Letters*, 16, 1938–1940. <https://doi.org/10.1016/j.bmcl.2005.12.084>
- Anekonda, T.S., Quinn, J.F., Harris, C., Frahler, K., Wadsworth, T.L. and Woltjer, R.L. (2011) L-type voltage-gated calcium channel blockade with isradipine as a therapeutic strategy for Alzheimer's disease. *Neurobiology of Disease*, 41, 62–70. <https://doi.org/10.1016/j.nbd.2010.08.020>
- Anichtchik, O. V., Rinne, J.O., Kalimo, H. and Panula, P. (2000) An altered histaminergic innervation of the substantia nigra in Parkinson's disease. *Experimental Neurology*, 163, 20–30. <https://doi.org/10.1006/exnr.2000.7362>
- Apelt, J., Grassmann, S., Ligneau, X., Pertz, H.H., Ganellin, C.R., Arrang, J.M., Schwartz, J.C., Schunack, W. and Stark, H. (2005) Search for histamine H3 receptor antagonists with combined inhibitory potency at N_T-methyltransferase: Ether derivatives. *Pharmazie*, 60, 97–106. <https://doi.org/10.1002/chin.200522144>
- Apelt, J., Ligneau, X., Pertz, H.H., Arrang, J.-M., Ganellin, C.R., Schwartz, J.-C., Schunack, W. and Stark, H. (2002) Development of a New Class of Nonimidazole Histamine H₃ Receptor Ligands with Combined Inhibitory Histamine N-Methyltransferase Activity. *Journal of Medicinal Chemistry*, 45, 1128–1141. <https://doi.org/10.1021/jm0110845>
- Arias-Montão, J.A., Floran, B., Garcia, M., Aceves, J. and Young, J.M. (2001) Histamine H3 receptor-mediated inhibition of depolarization-induced, dopamine D1 receptor-dependent release of [3H]- γ -aminobutyric acid from rat striatal slices. *British Journal of Pharmacology*, 133, 165–171. <https://doi.org/10.1038/sj.bjp.0704053>
- Arrang, J.-M., Garbarg, M., Lancelo, J.-C., Lecomte, J.-M., Pollard, H., Robba, M., Schunack, W. and Schwartz, J.-C. (1987) Highly potent and selective ligands for histamine H₃-receptors. *Nature*, 327, 117–123. <https://doi.org/10.1038/327117a0>
- Arrang, J.-M., Garbarg, M. and Schwartz, J.-C. (1983) Auto-inhibition of brain histamine release mediated by a novel class (H₃) of histamine receptor. *Nature*, 302, 832–837. <https://doi.org/10.1038/302832a0>
- Atwal, K.S. and Moreland, S. (1991) Dihydropyrimidine calcium channel blockers 51: bicyclic dihydropyrimidines as potent mimics of dihydropyridines. *Bioorganic & Medicinal Chemistry Letters*, 1, 291–294. [https://doi.org/10.1016/S0960-894X\(01\)80810-6](https://doi.org/10.1016/S0960-894X(01)80810-6)
- Atwal, K.S., Rovnyak, G.C., Kimball, S.D., Floyd, D.M., Moreland, S., Swanson, B.N., Gougoutas, J.Z., Schwartz, J., Smillie, K.M. and Malley, M.F. (1990a) Dihydropyrimidine Calcium Channel Blockers. 2.1 3-Substituted-4-aryl-1,4-dihydro-6-methyl-5-pyrimidinecarboxylic Acid Esters as Potent Mimics of Dihydropyridines. *Journal of Medicinal Chemistry*, 33, 2629–2635. <https://doi.org/10.1021/jm00171a044>
- Atwal, K.S., Rovnyak, G.C., Schwartz, J., Moreland, S., Hedberg, A., Gougoutas, J.Z., Malley, M.F. and Floyd, D.M. (1990b) Dihydropyrimidine Calcium Channel Blockers: 2-Heterosubstituted 4-Aryl-1,4-dihydro-6-methyl-5-pyrimidinecarboxylic Acid Esters as Potent Mimics of Dihydropyridines. *Journal of Medicinal Chemistry*, 33, 1510–1515. <https://doi.org/10.1021/jm00167a035>
- Atwal, K.S., Swanson, B.N., Unger, S.E., Floyd, D.M., Moreland, S., Hedberg, A. and O'Reilly, B.C. (1991) Dihydropyrimidine Calcium Channel Blockers. 3. 3-Carbamoyl-4-aryl-1,2,3,4-tetrahydro-6-methyl-5-pyrimidinecarboxylic Acid Esters as Orally Effective Antihypertensive Agents. *Journal of Medicinal Chemistry*, 34, 806–811. <https://doi.org/10.1021/jm00106a048>
- Awasthi, A.K., Kumar, B., Aga, M.A., Tripathi, P., Reddy, C.S. and Kumar, P. (2017) An efficient and facile synthesis of D-cycloserine substantially free from potential impurities. *Chemistry of Heterocyclic Compounds*, 53, 1248–

Reference

1253. <https://doi.org/10.1007/s10593-018-2197-y>

- Axe, F.U., Bembenek, S.D. and Szalma, S. (2006) Three-dimensional models of histamine H3 receptor antagonist complexes and their pharmacophore. *Journal of Molecular Graphics and Modelling*, 24, 456–464. <https://doi.org/10.1016/j.jmgm.2005.10.005>
- Aymard, J.P., Aymard, B., Netter, P., Bannwarth, B., Trechot, P. and Streiff, F. (1988) Haematological Adverse Effects of Histamine H2-Receptor Antagonists. *Medical Toxicology and Adverse Drug Experience*, 3, 430–448. <https://doi.org/10.1007/BF03259895>
- Baell, J.B. and Holloway, G.A. (2010) New substructure filters for removal of pan assay interference compounds (PAINS) from screening libraries and for their exclusion in bioassays. *Journal of Medicinal Chemistry*, 53, 2719–2740. <https://doi.org/10.1021/jm901137j>
- Baell, J.B. and Nissink, J.W.M. (2018) Seven Year Itch: Pan-Assay Interference Compounds (PAINS) in 2017 - Utility and Limitations. *ACS Chemical Biology*, 13, 36–44. <https://doi.org/10.1021/acscchembio.7b00903>
- Bahi, A., Sadek, B., Nurulain, S.M., Łazewska, D. and Kieć-Kononowicz, K. (2015) The novel non-imidazole histamine H3 receptor antagonist DL77 reduces voluntary alcohol intake and ethanol-induced conditioned place preference in mice. *Physiology and Behavior*, 151, 189–197. <https://doi.org/10.1016/j.physbeh.2015.07.012>
- Bahi, A., Sadek, B., Schwed, S.J., Walter, M. and Stark, H. (2013) Influence of the novel histamine H3 receptor antagonist ST1283 on voluntary alcohol consumption and ethanol-induced place preference in mice. *Psychopharmacology*, 228, 85–95. <https://doi.org/10.1007/s00213-013-3019-7>
- Bakker, R.A., Nicholas, M.W., Smith, T.T., Burstein, E.S., Hacksell, U., Timmerman, H., Leurs, R., Brann, M.R. and Weiner, D.M. (2007) In vitro pharmacology of clinically used central nervous system-active drugs as inverse H1 receptor agonists. *Journal of Pharmacology and Experimental Therapeutics*, 322, 172–179. <https://doi.org/10.1124/jpet.106.118869>
- Bakker, R.A., Schoonus, S.B.J., Smit, M.J., Timmerman, H. and Leurs, R. (2001) Histamine H1-receptor activation of nuclear factor- κ B: Roles for G $\beta\gamma$ - and G α q/11-subunits in constitutive and agonist-mediated signaling. *Molecular Pharmacology*, 60, 1133–1142. <https://doi.org/10.1124/mol.60.5.1133>
- Bakker, R.A., Wieland, K., Timmerman, H. and Leurs, R. (2000) Constitutive activity of the histamine H1 receptor reveals inverse agonism of histamine H1 receptor antagonists. *European Journal of Pharmacology*, 387, R5–R7. [https://doi.org/10.1016/S0014-2999\(99\)00803-1](https://doi.org/10.1016/S0014-2999(99)00803-1)
- Bar-Am, O., Yogev-Falach, M., Amit, T., Sagi, Y. and Youdim, M.B.H. (2004) Regulation of protein kinase C by the anti-Parkinson drug, MAO-B inhibitor, rasagiline and its derivatives, in vivo. *Journal of Neurochemistry*, 89, 1119–1125. <https://doi.org/10.1111/j.1471-4159.2004.02425.x>
- Barbier, A.J., Berridge, C., Dugovic, C., Laposky, A.D., Wilson, S.J., Boggs, J., Aluisio, L., Lord, B., Mazur, C., Pudiak, C.M., Langlois, X., Xiao, W., Apodaca, R., Carruthers, N.I. and Lovenberg, T.W. (2004) Acute wake-promoting actions of JNJ-5207852, a novel, diamine-based H 3 antagonist. *British Journal of Pharmacology*, 143, 649–661. <https://doi.org/10.1038/sj.bjp.0705964>
- Bardgett, M.E., Davis, N.N., Schultheis, P.J. and Griffith, M.S. (2011) Ciproxifan, an H3 receptor antagonist, alleviates hyperactivity and cognitive deficits in the APPTg2576 mouse model of Alzheimer's disease. *Neurobiology of Learning and Memory*, 95, 64–72. <https://doi.org/10.1016/j.nlm.2010.10.008>
- Baron, R., Binder, A. and Wasner, G. (2010) Neuropathic pain: Diagnosis, pathophysiological mechanisms, and treatment. *The Lancet Neurology*, 9, 807–819. [https://doi.org/10.1016/S1474-4422\(10\)70143-5](https://doi.org/10.1016/S1474-4422(10)70143-5)
- Bartoli, G., Bosco, M., Carlone, A., Dalpozzo, R., Galzerano, P., Melchiorre, P. and Sambri, L. (2008) Magnesium perchlorate as efficient Lewis acid for the Knoevenagel condensation between β -diketones and aldehydes. *Tetrahedron Letters*, 49, 2555–2557. <https://doi.org/10.1016/j.tetlet.2008.02.093>
- Bautista-Aguilera, Ó.M., Budni, J., Mina, F., Medeiros, E.B., Deuther-Conrad, W., Entrena, J.M., Moreda, I., Iriepa, I., López-Muñoz, F. and Marco-Contelles, J. (2018) Contilisant, a Tetratarget Small Molecule for Alzheimer's Disease Therapy Combining Cholinesterase, Monoamine Oxidase Inhibition, and H3R Antagonism with S1R Agonism Profile. *Journal of medicinal chemistry*, 61, 6937–6943. <https://doi.org/10.1021/acs.jmedchem.8b00848>
- Bean, B.P., Sturek, M., Puga, A. and Hermsmeyer, K. (1986) Calcium channels in muscle cells isolated from rat mesenteric arteries: Modulation by dihydropyridine drugs. *Circulation Research*, 59, 229–235. <https://doi.org/10.1161/01.RES.59.2.229>
- Beasley, Y.M., Petrow, V. and Stephenson, O. (1958) Analgesics. Part I. Some Aryloxypropanolamines. *Journal of Pharmacy and Pharmacology*, 10, 47–59. <https://doi.org/10.1111/j.2042-7158.1958.tb10272.x>

Reference

- Benarroch, E.E. (2011) NMDA receptors: Recent insights and clinical correlations. *Neurology*, 76, 1750–1757. <https://doi.org/10.1212/WNL.0b013e31821b7cc9>
- Berlin, M., Boyce, C.W. and De Lera Ruiz, M. (2011) Histamine H3 receptor as a drug discovery target. *Journal of Medicinal Chemistry*, 54, 26–53. <https://doi.org/10.1021/jm100064d>
- Berlin, M., Ting, P.C., Vaccaro, W.D., Aslanian, R., McCormick, K.D., Lee, J.F., Albanese, M.M., Mutahi, M.W., Piwinski, J.J., Shih, N.Y., Duguma, L., Solomon, D.M., Zhou, W., Sher, R., Favreau, L., Bryant, M., Korfmacher, W.A., Nardo, C., West, R.E., Anthes, J.C., Williams, S.M., Wu, R.L., Susan She, H., Rivelli, M.A., Corboz, M.R. and Hey, J.A. (2006) Reduction of CYP450 inhibition in the 4-[(1H-imidazol-4-yl)methyl] piperidine series of histamine H3 receptor antagonists. *Bioorganic and Medicinal Chemistry Letters*, 16, 989–994. <https://doi.org/10.1016/j.bmcl.2005.10.087>
- Berridge, M.J. (2011) Calcium signalling and Alzheimer's disease. *Neurochemical Research*, 36, 1149–1156.
- Beyreuther, K. and Masters, C.L. (1991) Amyloid Precursor Protein (APP) and BZA4 Amyloid in the Etiology of Alzheimer's Disease: Precursor-Product Relationships in the Derangement of Neuronal Function. *Brain Pathology*, 1, 241–251. <https://doi.org/10.1111/j.1750-3639.1991.tb00667.x>
- Biginelli, P. (1891) Ueber Aldehyduramide des Acetessigäthers. *Berichte der deutschen chemischen Gesellschaft*, 24, 1317–1319. <https://doi.org/10.1002/cber.189102401228>
- Biltz, H. and Biltz, W. (1929) *Laboratory Methods of Inorganic Chemistry 2nd Edition.*, 2nd ed. Chapman & Hall, Ltd., London.
- Birks, J. and López-Arrieta, J. (2002) Nimodipine for primary degenerative, mixed and vascular dementia. *Cochrane Database of Systematic Reviews*. <https://doi.org/10.1002/14651858.CD000147>
- Black, J.W. and Ganellin, C.R. (1974) Naming of substituted histamines. *Experientia*, 30, 111–113. <https://doi.org/10.1007/BF01921632>
- Black, L.A., Liu, H., Diaz, G.J., Fox, G.B., Browman, K.E., Wetter, J., Marsh, K.C., Miller, T.R., Esbenshade, T.A., Brioni, J. and Cowart, M.D. (2008) Minimization of potential hERG liability in histamine H3 receptor antagonists. *Inflammation Research*, 57, 45–46. <https://doi.org/10.1007/s00011-007-0622-2>
- Bonaventure, P., Letavic, M., Dugovic, C., Wilson, S., Aluisio, L., Pudiak, C., Lord, B., Mazur, C., Kamme, F., Nishino, S., Carruthers, N. and Lovenberg, T. (2007) Histamine H3 receptor antagonists: From target identification to drug leads. *Biochemical Pharmacology*, 73, 1084–1096. <https://doi.org/10.1016/j.bcp.2006.10.031>
- Bongers, G., Bakker, R.A. and Leurs, R. (2007) Molecular aspects of the histamine H3 receptor. *Biochemical Pharmacology*, 73, 1195–1204. <https://doi.org/10.1016/j.bcp.2007.01.008>
- Borowiecki, P. and Bretner, M. (2013) Studies on the chemoenzymatic synthesis of (R)- and (S)-methyl 3-aryl-3-hydroxypropionates: The influence of toluene-pretreatment of lipase preparations on enantioselective transesterifications. *Tetrahedron Asymmetry*, 24, 925–936. <https://doi.org/10.1016/j.tetasy.2013.06.004>
- Bosshard, H.H., Mory, R., Schmid, M. and Zollinger, H. (1959) Eine Methode zur katalysierten Herstellung von Carbonsäure- und Sulfosäure-chloriden mit Thionylchlorid. *Helvetica Chimica Acta*, 42, 1653–1658. <https://doi.org/10.1002/hlca.19590420526>
- Bowers, S., Truong, A.P., Neitz, R.J., Neitzel, M., Probst, G.D., Hom, R.K., Peterson, B., Galembo, R.A., Konradi, A.W., Sham, H.L., Tóth, G., Pan, H., Yao, N., Artis, D.R., Brigham, E.F., Quinn, K.P., Sauer, J.M., Powell, K., Ruslim, L., Ren, Z., Bard, F., Yednock, T.A. and Griswold-Prenner, I. (2011) Design and synthesis of a novel, orally active, brain penetrant, tri-substituted thiophene based JNK inhibitor. *Bioorganic and Medicinal Chemistry Letters*, 21, 1838–1843. <https://doi.org/10.1016/j.bmcl.2011.01.046>
- Bratsch, S.G. (1985) A group electronegativity method with Pauling units. *Journal of Chemical Education*, 62, 101. <https://doi.org/10.1021/ed062p101>
- Broccatelli, F., Carosati, E., Cruciani, G. and Oprea, T.I. (2010) Transporter-mediated efflux influences CNS side effects: ABCB1, from antitarget to target. *Molecular Informatics*, 29, 16–26. <https://doi.org/10.1002/minf.200900075>
- Broderick, M. and Masri, T. (2011) Histamine H3 Receptor (H3R) Antagonists and Inverse Agonists in the Treatment of Sleep Disorders. *Current Pharmaceutical Design*, 17, 1426–1429. <https://doi.org/10.2174/138161211796197133>
- Bullock, F.J., Tweedie, J.F., McRitchie, D.D. and Tucker, M.A. (1970) Antiprotozoal quinones. II. Synthesis of 4-amino-1,2-naphthoquinones and related compounds as potential antimalarials. *Journal of Medicinal Chemistry*, 13, 97–103. <https://doi.org/10.1021/jm00295a025>
- Burstein, E., Olsson, R., Jansson, K., Sköld, N., Wahlström, L., Von Wachenfeldt, H., Bergner, M., Dreisch, K.,

Reference

- Popov, K., Kovalenko, O. and Klingstedt, P.T. (2019) Compounds, Salts Thereof And Methods For Treatment Of Diseases. Publication Numer: WO2019/040106A2
- Cain, S.M. and Snutch, T.P. (2011) Voltage-gated calcium channels and disease. *BioFactors*, 37, 197–205. <https://doi.org/10.1002/biof.158>
- Calamai, E., Dall'Angelo, S., Koss, D., Domarkas, J., McCarthy, T.J., Mingarelli, M., Riedel, G., Schweiger, L.F., Welch, A., Platt, B. and Zanda, M. (2013) 18 F-barbiturates are PET tracers with diagnostic potential in Alzheimer's disease. *Chem. Commun.*, 49, 792–794. <https://doi.org/10.1039/C2CC38443D>
- Calik, M.W. (2017) Update on the treatment of narcolepsy: clinical efficacy of pitolisant. *Nature and Science of Sleep*, Volume 9, 127–133. <https://doi.org/10.2147/NSS.S103462>
- Cannon, K.E., Nalwalk, J.W., Stadel, R., Ge, P., Lawson, D., Silos-Santiago, I. and Hough, L.B. (2003) Activation of spinal histamine H3 receptors inhibits mechanical nociception. *European Journal of Pharmacology*, 470, 139–147. [https://doi.org/10.1016/S0014-2999\(03\)01737-0](https://doi.org/10.1016/S0014-2999(03)01737-0)
- Cao, G., Alessio, H.M. and Cutler, R.G. (1993) Oxygen-radical absorbance capacity assay for antioxidants. *Free Radical Biology and Medicine*, 14, 303–311. [https://doi.org/10.1016/0891-5849\(93\)90027-R](https://doi.org/10.1016/0891-5849(93)90027-R)
- Carosati, E., Ioan, P., Micucci, M., Broccatelli, F., Cruciani, G., Zhorov, B.S., Chiarini, A. and Budriesi, R. (2012) 1,4-Dihydropyridine Scaffold in Medicinal Chemistry, The Story So Far And Perspectives (Part 2): Action in Other Targets and Antitargets. *Current Medicinal Chemistry*, 19, 4306–4323. <https://doi.org/10.2174/092986712802884204>
- Catterall, W.A., Perez-Reyes, E., Snutch, T.P. and Striessnig, J. (2005) International Union of Pharmacology. XLVIII. Nomenclature and Structure-Function Relationships of Voltage-Gated Calcium Channels. *Pharmacological Reviews*, 57, 411–425. <https://doi.org/10.1124/pr.57.4.5>
- Cavalli, A., Bolognesi, M.L., Minarini, A., Rosini, M., Tumiatti, V., Recanatini, M. and Melchiorre, C. (2008) Multi-target-Directed Ligands To Combat Neurodegenerative Diseases. *Journal of Medicinal Chemistry*, 51, 347–372. <https://doi.org/10.1021/jm7009364>
- Celanire, S., Wijtmans, M., Talaga, P., Leurs, R. and De Esch, I.J.P. (2005) Keynote review: Histamine H3 receptor antagonists reach out for the clinic. *Drug Discovery Today*, 10, 1613–1627. [https://doi.org/10.1016/S1359-6446\(05\)03625-1](https://doi.org/10.1016/S1359-6446(05)03625-1)
- Chadha, H.S., Abraham, M.H. and Mitchell, R.C. (1994) Physicochemical analysis of the factors governing distribution of solutes between blood and brain. *Bioorganic and Medicinal Chemistry Letters*, 4, 2511–2516. [https://doi.org/10.1016/S0960-894X\(01\)80274-2](https://doi.org/10.1016/S0960-894X(01)80274-2)
- Chaffey, H. and Chazot, P.L. (2008) NMDA receptor subtypes: Structure, function and therapeutics. *Current Anaesthesia and Critical Care*, 19, 183–201. <https://doi.org/10.1016/j.cacc.2008.05.004>
- Chang, Z., Lichtenstein, P., Halldner, L., D'Onofrio, B., Serlachius, E., Fazel, S. and Larsson, H. (2014) Stimulant ADHD medication and risk for substance abuse. *Journal of Child Psychology and Psychiatry and Allied Disciplines*, 55, 878–885. <https://doi.org/10.1111/jcpp.12164>
- Chaumette, T., Chapuy, E., Berrocoso, E., Llorca-Torralba, M., Bravo, L., Mico, J.A., Chalus, M., Eschalier, A., Ardid, D., Marchand, F. and Sors, A. (2018) Effects of S 38093, an antagonist/inverse agonist of histamine H3 receptors, in models of neuropathic pain in rats. *European Journal of Pain (United Kingdom)*, 22, 127–141. <https://doi.org/10.1002/ejp.1097>
- Chen, J.F. and Cunha, R.A. (2020) The belated US FDA approval of the adenosine A2A receptor antagonist istradefylline for treatment of Parkinson's disease. *Purinergic Signalling*, 16, 167–174. <https://doi.org/10.1007/s11302-020-09694-2>
- Chen, Y., Wang, S., Xu, X., Liu, X., Yu, M., Zhao, S., Liu, S., Qiu, Y., Zhang, T., Liu, B.F. and Zhang, G. (2013) Synthesis and biological investigation of coumarin piperazine (piperidine) derivatives as potential multireceptor atypical antipsychotics. *Journal of Medicinal Chemistry*, 56, 4671–4690. <https://doi.org/10.1021/jm400408r>
- Cheong, S.L., Federico, S., Spalluto, G., Klotz, K.N. and Pastorin, G. (2019) The current status of pharmacotherapy for the treatment of Parkinson's disease: transition from single-target to multitarget therapy. *Drug Discovery Today*, 24, 1769–1783. <https://doi.org/10.1016/j.drudis.2019.05.003>
- Chiba, K., Trevor, A. and Castagnoli, N. (1984) Metabolism of the neurotoxic tertiary amine, MPTP, by brain monoamine oxidase. *Biochemical and Biophysical Research Communications*, 120, 574–578. [https://doi.org/10.1016/0006-291X\(84\)91293-2](https://doi.org/10.1016/0006-291X(84)91293-2)
- Cho, S.H., Kim, S.-H.H. and Shin, D. (2019) Recent applications of hydantoin and thiohydantoin in medicinal chemistry. *European Journal of Medicinal Chemistry*, 164, 517–545.

Reference

- <https://doi.org/10.1016/j.ejmech.2018.12.066>
- Cho, H., Ueda, M., Shima, K., Mizuno, A., Havashimatsu, M., Ohnaka, Y., Takeuchi, Y., Hamaguchi, M., Aisaka, K., Hidaka, T., Kawai, M., Takeda, M., Ishihara, T., Funahashi, K., Satoh, F., Morita, M. and Noguchi, T. (1989) Dihydropyrimidines: Novel Calcium Antagonists with Potent and Long-Lasting Vasodilative and Antihypertensive Activity. *Journal of Medicinal Chemistry*, 32, 2399–2406. <https://doi.org/10.1021/jm00130a029>
- Choi, D.W. (1992) Excitotoxic cell death. *Journal of Neurobiology*, 23, 1261–1276. <https://doi.org/10.1002/neu.480230915>
- Clayden, J., Greeves, N. and Warren, S. (2012) *Organic Chemistry*, 2nd ed. Oxford University Press.
- von Coburg, Y., Kottke, T., Weizel, L., Ligneau, X. and Stark, H. (2009) Potential utility of histamine H3 receptor antagonist pharmacophore in antipsychotics. *Bioorganic & Medicinal Chemistry Letters*, 19, 538–542. <https://doi.org/10.1016/J.BMCL.2008.09.012>
- Cogé, F., Guénin, S.-P., Audinot, V., Renouard-Try, A., Beauverger, P., Macia, C., Ouvry, C., NAGEL, N., RIQUE, H., BOUTIN, J.A. and GALIZZI, J.-P. (2001a) Genomic organization and characterization of splice variants of the human histamine H3 receptor. *Biochemical Journal*, 355, 279–288. <https://doi.org/10.1042/bj3550279>
- Cogé, F., Guénin, S.P., Rique, H., Boutin, J.A. and Galizzi, J.P. (2001b) Structure and expression of the human histamine H4-receptor gene. *Biochemical and Biophysical Research Communications*, 284, 301–309. <https://doi.org/10.1006/bbrc.2001.4976>
- Cohen, G., Pasik, P., Cohen, B., Leist, A., Mytilineou, C. and Yahr, M.D. (1984) Pargyline and deprenyl prevent the neurotoxicity of 1-methyl-4-phenyl-1,2,3,6-tetrahydropyridine (MPTP) in monkeys. *European Journal of Pharmacology*, 106, 209–210. [https://doi.org/10.1016/0014-2999\(84\)90700-3](https://doi.org/10.1016/0014-2999(84)90700-3)
- Cohen, G. and Spina, M.B. (1989) Deprenyl suppresses the oxidant stress associated with increased dopamine turnover. *Annals of Neurology*, 26, 689–690. <https://doi.org/10.1002/ana.410260518>
- Collingridge, G.L., Peineau, S., Howland, J.G. and Wang, Y.T. (2010) Long-term depression in the CNS. *Nature Reviews Neuroscience*, 11, 459–473.
- Collman, J.P., Zeng, L., Wang, H.J.H., Lei, A. and Brauman, J.I. (2006) Kinetics of (porphyrin)manganese(III)-catalyzed olefin epoxidation with a soluble iodosylbenzene derivative. *European Journal of Organic Chemistry*, 2707–2714. <https://doi.org/10.1002/ejoc.200600079>
- Connolly, B.S. and Lang, A.E. (2014) Pharmacological treatment of Parkinson disease: A review. *JAMA - Journal of the American Medical Association*, 311, 1670–1683. <https://doi.org/10.1001/jama.2014.3654>
- Cooper, G., Kang, S., Perez-Rosello, T., Guzman, J.N., Galtieri, D., Xie, Z., Kondapalli, J., Mordell, J., Silverman, R.B. and Surmeier, D.J. (2020) A Single Amino Acid Determines the Selectivity and Efficacy of Selective Negative Allosteric Modulators of CaV1.3 L-Type Calcium Channels. *ACS Chemical Biology*, 15, 2539–2550. <https://doi.org/10.1021/acscchembio.0c00577>
- Costa, M.C.A., Gaudio, A.C. and Takahata, Y. (1997) A comparative study of principal component and linear multiple regression analysis in SAR and QSAR applied to 1,4-dihydropyridine calcium channel antagonists (nifedipine analogues). *Journal of Molecular Structure: THEOCHEM*, 394, 291–300. [https://doi.org/10.1016/S0166-1280\(96\)04845-2](https://doi.org/10.1016/S0166-1280(96)04845-2)
- Cowart, M., Hsieh, G., Black, L.A., Zhan, C., Gomez, E.J., Pai, M., Strakhova, M., Manelli, A., Carr, T., Wetter, J., Lee, A., Diaz, G., Garrison, T. and Brioni, J.D. (2012) Pharmacological characterization of A-960656, a histamine H3 receptor antagonist with efficacy in animal models of osteoarthritis and neuropathic pain. *European Journal of Pharmacology*, 684, 87–94. <https://doi.org/10.1016/j.ejphar.2012.03.048>
- Cowden, J.M., Yu, F., Banie, H., Farahani, M., Ling, P., Nguyen, S., Riley, J.P., Zhang, M., Zhu, J., Dunford, P.J. and Thurmond, R.L. (2014) The histamine H4 receptor mediates inflammation and Th17 responses in preclinical models of arthritis. *Annals of the Rheumatic Diseases*, 73, 600–608. <https://doi.org/10.1136/annrheumdis-2013-203832>
- Crane, G.E. (1961) The psychotropic effects of cycloserine: A new use for an antibiotic. *Comprehensive Psychiatry*, 2, 51–59. [https://doi.org/10.1016/S0010-440X\(61\)80007-2](https://doi.org/10.1016/S0010-440X(61)80007-2)
- Cunha, R., Ferre, S., Vaugeois, J.-M. and Chen, J.-F. (2008) Potential Therapeutic Interest of Adenosine A2A Receptors in Psychiatric Disorders. *Current Pharmaceutical Design*, 14, 1512–1524. <https://doi.org/10.2174/138161208784480090>
- Daley-Yates, P., Ambery, C., Sweeney, L., Watson, J., Oliver, A. and McQuade, B. (2012) The efficacy and tolerability of two novel H1/H3 receptor antagonists in seasonal allergic rhinitis. *International Archives of Allergy and Immunology*, 158, 84–98. <https://doi.org/10.1159/000329738>

Reference

- Dallinger, D., Gorobets, N.Y. and Kappe, C.O. (2003) High-Throughput Synthesis of N 3-Acylated Dihydropyrimidines Combining Microwave-Assisted Synthesis and Scavenging Techniques. *Organic Letters*, 5, 1205–1208. <https://doi.org/10.1021/ol034085v>
- Dauvilliers, Y., Verbraecken, J., Partinen, M., Hedner, J., Saaresranta, T., Georgiev, O., Tiholov, R., Lecomte, I., Tamisier, R., Lévy, P., Scart-Gres, C., Lecomte, J.M., Schwartz, J.C., Pépin, J.L., Attali, V., Bourgin, P., Gagnadoux, F., Baharloo, F., Berg, S., Polo, O., Hedner, J.A., Peker, Y., Blau, A., Borreguero, D.G., Cuesta, F.J.P., Belev, G., Ivanov, Y., Metev, H., Petkova, D., Dokic, D., Marku, M.I., Kaeva, B.J., Jankovic, S., Kopitovic, I. and Vukcevic, M. (2020) Pitolisant for daytime sleepiness in patients with obstructive sleep apnea who refuse continuous positive airway pressure treatment a randomized trial. *American Journal of Respiratory and Critical Care Medicine*, 201, 1135–1145. <https://doi.org/10.1164/RCCM.201907-1284OC>
- Dess, D.B. and Martin, J.C. (1983) Readily Accessible 12-I-51 Oxidant for the Conversion of Primary and Secondary Alcohols to Aldehydes and Ketones. *Journal of Organic Chemistry*, 48, 4155–4156. <https://doi.org/10.1021/jo00170a070>
- Drutel, G., Peitsaro, N., Karlstedt, K., Wieland, K., Smit, M.J., Timmerman, H., Panula, P. and Leurs, R. (2001) Identification of rat H3 receptor isoforms with different brain expression and signaling properties. *Molecular Pharmacology*, 59, 1–8. <https://doi.org/10.1124/mol.59.1.1>
- Dungo, R. and Deeks, E.D. (2013) Istradefylline: First global approval. *Drugs*, 73, 875–882. <https://doi.org/10.1007/s40265-013-0066-7>
- Durant, G.J., Ganellin, C.R., Hills, D.W., Miles, P.D., Parsons, M.E., Pepper, E.S. and White, G.R. (1985) The histamine H2-receptor agonist impromidine: synthesis and structure activity considerations. *Journal of Medicinal Chemistry*, 28, 1414–1422. <https://doi.org/10.1021/jm00148a007>
- Dutilleul, P.C., Ryvlin, P., Kahane, P., Vercueil, L., Semah, F., Biraben, A., Schwartz, J.C., De Seze, J., Hirsch, E. and Collongues, N. (2016) Exploratory Phase II trial to evaluate the safety and the antiepileptic effect of pitolisant (BF2.649) in refractory partial seizures, given as adjunctive treatment during 3 months. *Clinical Neuropharmacology*, 39, 188–193. <https://doi.org/10.1097/WNF.000000000000159>
- Eddy, C.M., Rickards, H.E. and Cavanna, A.E. (2011) Treatment strategies for tics in Tourette syndrome. *Therapeutic Advances in Neurological Disorders*, 4, 25–45. <https://doi.org/10.1177/1756285610390261>
- Edenberg, H.J. and Foroud, T. (2013) Genetics and alcoholism. *Nature Reviews Gastroenterology and Hepatology*, 10, 487–494.
- Eissa, N., Azimullah, S., Jayaprakash, P., Jayaraj, R.L., Reiner, D., Ojha, S.K., Beiram, R., Stark, H., Łażewska, D., Kieć-Kononowicz, K. and Sadek, B. (2019) The dual-active histamine H3 receptor antagonist and acetylcholine esterase inhibitor E100 ameliorates stereotyped repetitive behavior and neuroinflammation in sodium valproate induced autism in mice. *Chemico-Biological Interactions*, 312, 108775. <https://doi.org/10.1016/j.cbi.2019.108775>
- Eissa, N., Jayaprakash, P., Azimullah, S., Ojha, S.K., Al-Houqani, M., Jalal, F.Y., Łażewska, D., Kieć-Kononowicz, K. and Sadek, B. (2018) The histamine H3R antagonist DL77 attenuates autistic behaviors in a prenatal valproic acid-induced mouse model of autism. *Scientific Reports*, 8, 1–15. <https://doi.org/10.1038/s41598-018-31385-7>
- Eliahu, K. (2004) Novel compounds for use in the treatment of autoimmune diseases, immuno-allergical diseases and organ or tissue zransplantation rejection. Publication Numer: WO 2004/031129 A2
- Ellenbroek, B.A. and Ghiabi, B. (2014) The other side of the histamine H3 receptor. *Trends in Neurosciences*, 37, 191–199. <https://doi.org/10.1016/j.tins.2014.02.007>
- Elz, S. and Schunack, W. (1988) [Impromidine-analogous guanidines: synthesis and activity at the histamine H2-receptor. 29. Histamine analogs]. *Arzneimittel-Forschung*, 38, 327–32.
- Emilsson, L., Saetre, P., Balciuniene, J., Castensson, A., Cairns, N. and Jazin, E.E. (2002) Increased monoamine oxidase messenger RNA expression levels in frontal cortex of Alzheimer's disease patients. *Neuroscience Letters*, 326, 56–60. [https://doi.org/10.1016/S0304-3940\(02\)00307-5](https://doi.org/10.1016/S0304-3940(02)00307-5)
- Endou, M., Poli, E. and Levi, R. (1994) Histamine H3-receptor signaling in the heart: possible involvement of Gi/Go proteins and N-type Ca²⁺ channels. *The Journal of pharmacology and experimental therapeutics*, 269, 221–9.
- Ercan-Sencicek, A.G., Stillman, A.A., Ghosh, A.K., Bilguvar, K., O'Roak, B.J., Mason, C.E., Abbott, T., Gupta, A., King, R.A., Pauls, D.L., Tischfield, J.A., Heiman, G.A., Singer, H.S., Gilbert, D.L., Hoekstra, P.J., Morgan, T.M., Loring, E., Yasuno, K., Fernandez, T., Sanders, S., Louvi, A., Cho, J.H., Mane, S., Colangelo, C.M., Biederer, T., Lifton, R.P., Gunel, M. and State, M.W. (2010) L-Histidine Decarboxylase and Tourette's Syndrome. *New England Journal of Medicine*, 362, 1901–1908. <https://doi.org/10.1056/nejmoa0907006>

Reference

- Esbenshade, T.A., Browman, K.E., Miller, T.R., Krueger, K.M., Komater-Roderwald, V., Zhang, M., Fox, G.B., Rueter, L., Robb, H.M., Radek, R.J., Drescher, K.U., Fey, T.A., Bitner, R.S., Marsh, K., Polakowski, J.S., Zhao, C., Cowart, M.D., Hancock, A.A., Sullivan, J.P. and Brioni, J.D. (2012) Pharmacological Properties and Procognitive Effects of ABT-288, a Potent and Selective Histamine H₃ Receptor Antagonist. *Journal of Pharmacology and Experimental Therapeutics*, 343, 233–245. <https://doi.org/10.1124/jpet.112.194126>
- Esteves, H., de Fátima, Â., Castro, R.D.P., Sabino, J.R., Macedo, F. and Brito, T.O. (2015) A simple one-pot methodology for the synthesis of substituted benzoylguanidines from benzoylthioureas using tert-butyl hydroperoxide. *Tetrahedron Letters*, 56, 6872–6874. <https://doi.org/10.1016/j.tetlet.2015.10.088>
- Farooqui, A.A. and Horrocks, L.A. (2006) Phospholipase A₂-generated lipid mediators in the brain: The good, the bad, and the ugly. *Neuroscientist*, 12, 245–260. <https://doi.org/10.1177/1073858405285923>
- Fava, M., Dirks, B., Freeman, M.P., Papakostas, G.I., Shelton, R.C., Thase, M.E., Trivedi, M.H., Liu, K. and Stankovic, S. (2019) A Phase 2, Randomized, Double-Blind, Placebo-Controlled Study of Adjunctive Pimavanserin in Patients With Major Depressive Disorder and an Inadequate Response to Therapy (CLARITY). *The Journal of Clinical Psychiatry*, 80. <https://doi.org/10.4088/JCP.19m12928>
- FDA. (2021) FDA's Decision to Approve New Treatment for Alzheimer's Disease. URL <https://www.fda.gov/drugs/news-events-human-drugs/fdas-decision-approve-new-treatment-alzheimers-disease> (Accessed 9 June 2021)
- Ferrada, C., Ferré, S., Casadó, V., Cortés, A., Justinova, Z., Barnes, C., Canela, E.I., Goldberg, S.R., Leurs, R., Lluís, C. and Franco, R. (2008) Interactions between histamine H₃ and dopamine D₂ receptors and the implications for striatal function. *Neuropharmacology*, 55, 190–197. <https://doi.org/10.1016/j.neuropharm.2008.05.008>
- Ferrada, C., Moreno, E., Casadó, V., Bongers, G., Cortés, A., Mallol, J., Canela, E.I., Leurs, R., Ferré, S., Lluís, C. and Franco, R. (2009) Marked changes in signal transduction upon heteromerization of dopamine D₁ and histamine H₃ receptors. *British Journal of Pharmacology*, 157, 64–75. <https://doi.org/10.1111/j.1476-5381.2009.00152.x>
- Ffytche, D.H., Creese, B., Politis, M., Chaudhuri, K.R., Weintraub, D., Ballard, C. and Aarsland, D. (2017) The psychosis spectrum in Parkinson disease. *Nature Reviews Neurology*, 13, 81–95. <https://doi.org/10.1038/nrneurol.2016.200>
- Fiest, K.M., Sauro, K.M., Wiebe, S., Patten, S.B., Kwon, C.-S., Dykeman, J., Pringsheim, T., Lorenzetti, D.L. and Jetté, N. (2017) Prevalence and incidence of epilepsy: A systematic review and meta-analysis of international studies. *Neurology*, 88, 296–303. <https://doi.org/10.1212/WNL.0000000000003509>
- Finkelstein, H. (1910) Darstellung organischer Jodide aus den entsprechenden Bromiden und Chloriden. *Berichte der deutschen chemischen Gesellschaft*, 43, 1528–1532. <https://doi.org/10.1002/cber.19100430257>
- Fox, G.B., Pan, J.B., Esbenshade, T.A., Bennani, Y.L., Black, L.A., Faghieh, R., Hancock, A.A. and Decker, M.W. (2002) Effects of histamine H₃ receptor ligands GT-2331 and ciproxifan in a repeated acquisition avoidance response in the spontaneously hypertensive rat pup. *Behavioural Brain Research*, 131, 151–161. [https://doi.org/10.1016/S0166-4328\(01\)00379-5](https://doi.org/10.1016/S0166-4328(01)00379-5)
- Franco, R., Rivas-Santisteban, R., Casanovas, M., Lillo, A., Saura, C.A. and Navarro, G. (2020) Adenosine A_{2A} Receptor Antagonists Affects NMDA Glutamate Receptor Function. Potential to Address Neurodegeneration in Alzheimer's Disease. *Cells*, 9, 1075. <https://doi.org/10.3390/cells9051075>
- Freeman, F. (1980) Properties and reactions of ylidenemalononitriles. *Chemical Reviews*, 80, 329–350. <https://doi.org/10.1021/cr60326a004>
- Freeman, F. (1981) Reactions of Malononitrile Derivatives. *Synthesis*, 925–954.
- Fujihira, T., Kanematsu, S., Umino, A., Yamamoto, N. and Nishikawa, T. (2007) Selective increase in the extracellular d-serine contents by d-cycloserine in the rat medial frontal cortex. *Neurochemistry International*, 51, 233–236. <https://doi.org/10.1016/j.neuint.2007.06.003>
- Fukui, H., Fujimoto, K., Mizuguchi, H., Sakamoto, K., Horio, Y., Takai, S., Yamada, K. and Ito, S. (1994) Molecular cloning of the human histamine H₁ receptor gene. *Biochemical and Biophysical Research Communications*, 201, 894–901.
- Fukushima, Y., Asano, T., Takata, K., Funaki, M., Ogihara, T., Anai, M., Tsukuda, K., Saitoh, T., Katagiri, H., Aihara, M., Matsushashi, N., Oka, Y., Yazaki, Y. and Sugano, K. (1997) Role of the C terminus in histamine H₂ receptor signaling, desensitization, and agonist-induced internalization. *Journal of Biological Chemistry*, 272, 19464–19470. <https://doi.org/10.1074/jbc.272.31.19464>
- Furukawa, H., Singh, S.K., Mancusso, R. and Gouaux, E. (2005) Subunit arrangement and function in NMDA receptors. *Nature*, 438, 185–192. <https://doi.org/10.1038/nature04089>

Reference

- Galici, R., Rezvani, A.H., Aluisio, L., Lord, B., Levin, E.D., Fraser, I., Boggs, J., Welty, N., Shoblock, J.R., Motley, S.T., Letavic, M.A., Carruthers, N.I., Dugovic, C., Lovenberg, T.W. and Bonaventure, P. (2011) JNJ-39220675, a novel selective histamine H3 receptor antagonist, reduces the abuse-related effects of alcohol in rats. *Psychopharmacology*, 214, 829–841. <https://doi.org/10.1007/s00213-010-2092-4>
- Ganellin, C.R., Leurquin, F., Piripitsi, A., Arrang, J.M., Garbarg, M., Ligneau, X., Schunack, W. and Schwartz, J.C. (1998) Synthesis of potent non-imidazole histamine H3-receptor antagonists. *Archiv der Pharmazie*, 331, 395–404. [https://doi.org/10.1002/\(sici\)1521-4184\(199812\)331:12<395::aid-ardp395>3.0.co;2-7](https://doi.org/10.1002/(sici)1521-4184(199812)331:12<395::aid-ardp395>3.0.co;2-7)
- Gantner, F., Sakai, K., Tusche, M.W., Cruikshank, W.W., Center, D.M. and Bacon, K.B. (2002) Histamine H4 and H2 receptors control histamine-induced interleukin-16 release from human CD8+ T cells. *Journal of Pharmacology and Experimental Therapeutics*, 303, 300–307. <https://doi.org/10.1124/jpet.102.036939>
- Gao, Z., Hurst, W.J., Guillot, E., Czechtizky, W., Lukasczyk, U., Nagorny, R., Pruniaux, M.-P., Schwink, L., Sanchez, J.A., Stengel, S., Tang, L., Winkler, I., Hendrix, J.A. and George, P.G. (2013) Discovery of aryl ureas and aryl amides as potent and selective histamine H3 receptor antagonists for the treatment of obesity (part I). *Bioorganic & medicinal chemistry letters*, 23, 3416–20. <https://doi.org/10.1016/j.bmcl.2013.03.080>
- Gauthier, S., Alam, J., Fillit, H., Iwatsubo, T., Liu-Seifert, H., Sabbagh, M., Salloway, S., Sampaio, C., Sims, J.R., Sperling, B., Sperling, R., Welsh-Bohmer, K.A., Touchon, J., Vellas, B. and Aisen, P. (2019) Combination Therapy for Alzheimer's Disease: Perspectives of the EU/US CTAD Task Force. *The journal of prevention of Alzheimer's disease*, 6, 164–168. <https://doi.org/10.14283/jpad.2019.12>
- Gazit, A., Yaish, P., Gilon, C. and Levitzki, A. (1989) Tyrphostins I: synthesis and biological activity of protein tyrosine kinase inhibitors. *Journal of Medicinal Chemistry*, 32, 2344–2352. <https://doi.org/10.1021/jm00130a020>
- Gbahou, F., Rouleau, A. and Arrang, J.M. (2012) The histamine autoreceptor is a short isoform of the H3 receptor. *British Journal of Pharmacology*, 166, 1860–1871. <https://doi.org/10.1111/j.1476-5381.2012.01913.x>
- Gbahou, F., Rouleau, A., Morisset, S., Parmentier, R., Crochet, S., Lin, J.-S., Ligneau, X., Tardivel-Lacombe, J., Stark, H., Schunack, W., Ganellin, C.R., Schwartz, J.-C. and Arrang, J.-M. (2003) Protean agonism at histamine H3 receptors in vitro and in vivo. *Proceedings of the National Academy of Sciences*, 100, 11086–11091. <https://doi.org/10.1073/pnas.1932276100>
- Gbahou, F., Vincent, L., Humbert-Claude, M., Tardivel-Lacombe, J., Chabret, C. and Arrang, J.M. (2006) Compared pharmacology of human histamine H3 and H4 receptors: Structure-activity relationships of histamine derivatives. *British Journal of Pharmacology*, 147, 744–754. <https://doi.org/10.1038/sj.bjp.0706666>
- Ghamari, N., Zarei, O., Arias-Montaña, J.A., Reiner, D., Dastmalchi, S., Stark, H. and Hamzeh-Mivehroud, M. (2019a) Histamine H3 receptor antagonists/inverse agonists: Where do they go? *Pharmacology and Therapeutics*, 200, 69–84. <https://doi.org/10.1016/j.pharmthera.2019.04.007>
- Ghamari, N., Zarei, O., Reiner, D., Dastmalchi, S., Stark, H. and Hamzeh-Mivehroud, M. (2019b) Histamine H3 receptor ligands by hybrid virtual screening, docking, molecular dynamics simulations, and investigation of their biological effects. *Chemical Biology and Drug Design*, 93, 832–843. <https://doi.org/10.1111/cbdd.13471>
- Godlewski, G., Malinowska, B., Schlicker, E. and Bucher, B. (1997) Identification of histamine H3 receptors in the tail artery from normotensive and spontaneously hypertensive rats. *Journal of Cardiovascular Pharmacology*, 29, 801–807. <https://doi.org/10.1097/00005344-199706000-00014>
- Goff, D.C., Herz, L., Posever, T., Shih, V., Tsai, G., Henderson, D.C., Freudenreich, O., Evins, A.E., Yovel, I., Zhang, H. and Schoenfeld, D. (2005) A six-month, placebo-controlled trial of d-cycloserine co-administered with conventional antipsychotics in schizophrenia patients. *Psychopharmacology*, 179, 144–150. <https://doi.org/10.1007/s00213-004-2032-2>
- Goldberg, M.W. and Teitel, S. (1956) Basic Ethers. Publication Numer: US 2774766 A
- Goldfarb, D. (2019) Pulse EPR in biological systems – Beyond the expert's courtyard. *Journal of Magnetic Resonance*, 306, 102–108. <https://doi.org/10.1016/j.jmr.2019.07.038>
- Gomez-Ramirez, J., Johnston, T.H., Visanji, N.P., Fox, S.H. and Brotchie, J.M. (2006) Histamine H3 receptor agonists reduce L-dopa-induced chorea, but not dystonia, in the MPTP-lesioned nonhuman primate model of Parkinson's disease. *Movement Disorders*, 21, 839–846. <https://doi.org/10.1002/mds.20828>
- Graves, S.M., Xie, Z., Stout, K.A., Zampese, E., Burbulla, L.F., Shih, J.C., Kondapalli, J., Patriarchi, T., Tian, L., Brichta, L., Greengard, P., Krainc, D., Schumacker, P.T. and Surmeier, D.J. (2020) Dopamine metabolism by a monoamine oxidase mitochondrial shuttle activates the electron transport chain. *Nature Neuroscience*, 23, 15–20. <https://doi.org/10.1038/s41593-019-0556-3>
- Gutzmer, R., Diestel, C., Mommert, S., Köther, B., Stark, H., Wittmann, M. and Werfel, T. (2005) Histamine H4 Receptor Stimulation Suppresses IL-12p70 Production and Mediates Chemotaxis in Human Monocyte-

Reference

- Derived Dendritic Cells. *The Journal of Immunology*, 174, 5224–5232. <https://doi.org/10.4049/jimmunol.174.9.5224>
- Haas, H. and Konnerth, A. (1983) Histamine and noradrenaline decrease calcium-activated potassium conductance in hippocampal pyramidal cells. *Nature*, 302, 432–434. <https://doi.org/10.1038/302432a0>
- Haas, H. and Panula, P. (2003) The role of histamine and the tuberomammillary nucleus in the nervous system. *Nature Reviews Neuroscience*, 4, 121–130. <https://doi.org/10.1038/nrn1034>
- Haas, H., Sergeeva, O. and Selbach, O. (2008) Histamine in the nervous system. *Physiological Reviews*, 88, 1183–1241. <https://doi.org/10.1152/physrev.00043.2007>
- Habib, M.M.W., Abdelfattah, M.A.O. and Abadi, A.H. (2015) Design and Synthesis of Novel Phenylpiperazine Derivatives as Potential Anticonvulsant Agents. *Archiv der Pharmazie*, 348, 868–874. <https://doi.org/10.1002/ardp.201500272>
- Hagenow, S., Stasiak, A., Ramsay, R.R. and Stark, H. (2017) Ciproxifan, a histamine H₃ receptor antagonist, reversibly inhibits monoamine oxidase A and B. *Scientific Reports*, 7, 1–6. <https://doi.org/10.1038/srep40541>
- Haig, G.M., Bain, E., Robieson, W., Othman, A.A., Baker, J. and Lenz, R.A. (2014) A randomized trial of the efficacy and safety of the H₃ antagonist ABT-288 in cognitive impairment associated with schizophrenia. *Schizophrenia Bulletin*, 40, 1433–1442. <https://doi.org/10.1093/schbul/sbt240>
- Halliwell, W.H. (1997) Cationic amphiphilic drug-induced phospholipidosis. In *Toxicologic Pathology*, pp. 53–60.
- Hammond, T.C., Xing, X., Wang, C., Ma, D., Nho, K., Crane, P.K., Elahi, F., Ziegler, D.A., Liang, G., Cheng, Q., Yanckello, L.M., Jacobs, N. and Lin, A.L. (2020) β -amyloid and tau drive early Alzheimer's disease decline while glucose hypometabolism drives late decline. *Communications Biology*, 3, 1–13. <https://doi.org/10.1038/s42003-020-1079-x>
- Hancock, A.A., Bennani, Y.L., Bush, E.N., Esbenshade, T.A., Faghieh, R., Fox, G.B., Jacobson, P., Knourek-Segel, V., Krueger, K.M., Nuss, M.E., Pan, J.B., Shapiro, R., Witte, D.G. and Yao, B.B. (2004) Antiobesity effects of A-331440, a novel non-imidazole histamine H₃ receptor antagonist. *European Journal of Pharmacology*, 487, 183–197. <https://doi.org/10.1016/j.ejphar.2004.01.015>
- Hantzsch, A. (1881) Condensationsprodukte aus Aldehydammoniak und ketonartigen Verbindungen. *Berichte der deutschen chemischen Gesellschaft*, 14, 1637–1638. <https://doi.org/10.1002/cber.18810140214>
- Hardy, J.A. and Higgins, G.A. (1992) Alzheimer's disease: The amyloid cascade hypothesis. *Science*, 256, 184–185. <https://doi.org/10.1126/science.1566067>
- Harusawa, S., Sawada, K., Magata, T., Yoneyama, H., Araki, L., Usami, Y., Hatano, K., Yamamoto, K., Yamamoto, D. and Yamatodani, A. (2013) Synthesis and evaluation of N-alkyl-S-[3-(piperidin-1-yl)propyl] isothiourreas: High affinity and human/rat species-selective histamine H₃ receptor antagonists. *Bioorganic and Medicinal Chemistry Letters*, 23, 6415–6420. <https://doi.org/10.1016/j.bmcl.2013.09.052>
- Harwell, V. and Fasinu, P. (2020) Pitolisant and Other Histamine-3 Receptor Antagonists—An Update on Therapeutic Potentials and Clinical Prospects. *Medicines*, 7, 55. <https://doi.org/10.3390/medicines7090055>
- Hasan, M.T., Hernández-González, S., Dogbevia, G., Treviño, M., Bertocchi, I., Gruart, A. and Delgado-García, J.M. (2013) Role of motor cortex NMDA receptors in learning-dependent synaptic plasticity of behaving mice. *Nature Communications*, 4, 1–9. <https://doi.org/10.1038/ncomms3258>
- Hasanein, P. (2011) Histamine H₃ Receptor Modulates Nociception In A Rat Model Of Cholestasis. *European Journal of Pain Supplements*, 5, 24. [https://doi.org/10.1016/S1754-3207\(11\)70078-5](https://doi.org/10.1016/S1754-3207(11)70078-5)
- van Hecke, O., Austin, S.K., Khan, R.A., Smith, B.H. and Torrance, N. (2014) Neuropathic pain in the general population: A systematic review of epidemiological studies. *Pain*, 155, 654–662. <https://doi.org/10.1016/j.pain.2013.11.013>
- Hendricks, J.A., Gullà, S. V., Budil, D.E. and Hanson, R.N. (2012) Synthesis of a spin-labeled anti-estrogen as a dynamic motion probe for the estrogen receptor ligand binding domain. *Bioorganic & Medicinal Chemistry Letters*, 22, 1743–1746. <https://doi.org/10.1016/j.bmcl.2011.12.091>
- Heresco-Levy, U., Gelfin, G., Bloch, B., Levin, R., Edelman, S., Javitt, D.C. and Kremer, I. (2013) A randomized add-on trial of high-dose d-cycloserine for treatment-resistant depression. *International Journal of Neuropsychopharmacology*, 16, 501–506. <https://doi.org/10.1017/S1461145712000910>
- Héron, A., Rouleau, A., Cochois, V., Pillot, C., Schwartz, J.C. and Arrang, J.M. (2001) Expression analysis of the histamine H₃ receptor in developing rat tissues. *Mechanisms of Development*, 105, 167–173. [https://doi.org/10.1016/S0925-4773\(01\)00389-6](https://doi.org/10.1016/S0925-4773(01)00389-6)
- Herring, W.J., Wilens, T.E., Adler, L.A., Baranak, C., Liu, K., Snavelly, D.B., Lines, C.R. and Michelson, D. (2012)

Reference

- Randomized Controlled Study of the Histamine H3 Inverse Agonist MK-0249 in Adult Attention-Deficit/Hyperactivity Disorder. *The Journal of Clinical Psychiatry*, 73, e891–e898. <https://doi.org/10.4088/JCP.11m07178>
- Hill, S. (1990) Distribution, properties, and functional characteristics of three classes of histamine receptor. *Pharmacological Reviews*, 42, 45–83.
- Hill, S., Ganellin, C.R., Timmerman, H., Schwartz, J.C., Shankley, N.P., Young, J.M., Schunack, W., Levi, R. and Haas, H.L. (1997) International Union of Pharmacology. XIII. Classification of Histamine Receptors. *Pharmacological Reviews*, 49, 253 LP – 278.
- Hirota, K., Kudo, M., Kudo, T., Kitayama, M., Kushikata, T., Lambert, D.G. and Matsuki, A. (2000) Barbiturates inhibit K⁺-evoked noradrenaline and dopamine release from rat striatal slices – involvement of voltage sensitive Ca²⁺ channels. *Neuroscience Letters*, 291, 175–178. [https://doi.org/10.1016/S0304-3940\(00\)01408-7](https://doi.org/10.1016/S0304-3940(00)01408-7)
- Hofmann, S.G., Pollack, M.H. and Otto, M.W. (2006) Augmentation Treatment of Psychotherapy for Anxiety Disorders with D-Cycloserine. *CNS Drug Reviews*, 12, 208–217. <https://doi.org/10.1111/j.1527-3458.2006.00208.x>
- Hofstra, C.L., Desai, P.J., Thurmond, R.L. and Fung-Leung, W.-P. (2003) Histamine H₄ Receptor Mediates Chemotaxis and Calcium Mobilization of Mast Cells. *Journal of Pharmacology and Experimental Therapeutics*, 305, 1212–1221. <https://doi.org/10.1124/jpet.102.046581>
- Hsieh, G.C., Honore, P., Pai, M., Wensink, E.J., Chandran, P., Salyers, A.K., Wetter, J.M., Zhao, C., Liu, H., Decker, M.W., Esbenshade, T.A., Cowart, M.D. and Brioni, J.D. (2010) Antinociceptive effects of histamine H₃ receptor antagonist in the preclinical models of pain in rats and the involvement of central noradrenergic systems. *Brain Research*, 1354, 74–84. <https://doi.org/10.1016/j.brainres.2010.07.083>
- Huang, H., Ng, C.Y., Yu, D., Zhai, J., Lam, Y. and Soong, T.W. (2014) Modest CaV1.342-selective inhibition by compound 8 is β -subunit dependent. *Nature Communications*, 5, 4481. <https://doi.org/10.1038/ncomms5481>
- Hubsher, G., Haider, M. and Okun, M.S. (2012) Amantadine: The journey from fighting flu to treating Parkinson disease. *Neurology*, 78, 1096–1099. <https://doi.org/10.1212/WNL.0b013e31824e8f0d>
- Hudkins, R.L., Josef, K.A. and Tao, M. (2008) Pyridazinone Derivatives.
- Huebner, R.B. and Kantor, L.W. (2010) Advances in alcoholism treatment. *Alcohol Research and Health*, 33, 295–299.
- Hughes, D.L. (1996) Progress in the Mitsunobu reaction. A review. *Organic Preparations and Procedures International*, 28, 127–164. <https://doi.org/10.1080/00304949609356516>
- HUGO Gene Nomenclature Committee. (2021) HGNC data for HRH2. URL https://www.genenames.org/data/gene-symbol-report/#!/hgnc_id/HGNC:5183 (Accessed 1 January 2021)
- Ichinose, M. and Barnes, P.J. (1990) A potassium channel activator modulates both excitatory noncholinergic and cholinergic neurotransmission in guinea pig airways. *The Journal of pharmacology and experimental therapeutics*, 252, 1207–12.
- Imamura, M., Smith, N.C.E., Garbarg, M. and Levi, R. (1996) Histamine H₃-receptor-mediated inhibition of calcitonin gene-related peptide release from cardiac C fibers: A regulatory negative-feedback loop. *Circulation Research*, 78, 863–869. <https://doi.org/10.1161/01.RES.78.5.863>
- Isensee, K., Amon, M., Galaparti, A., Ligneau, X., Camelin, J.-C., Capet, M., Schwartz, J.-C. and Stark, H. (2009) Fluorinated non-imidazole histamine H₃ receptor antagonists. *Bioorganic & Medicinal Chemistry Letters*, 19, 2172–2175. <https://doi.org/10.1016/j.bmcl.2009.02.110>
- Ishikawa, S. and Sperelakis, N. (1987) A novel class (H₃) of histamine receptors on perivascular nerve terminals. *Nature*, 327, 158–60. <https://doi.org/10.1038/327158a0>
- Jackson, D.A. and Mabury, S.A. (2009) Environmental properties of pentafluorosulfanyl compounds: Physical properties and photodegradation. *Environmental Toxicology and Chemistry*, 28, 1866–1873. <https://doi.org/10.1897/09-037.1>
- Jadidi-Niaragh, F. and Mirshafiey, A. (2010) Histamine and histamine receptors in pathogenesis and treatment of multiple sclerosis. *Neuropharmacology*, 59, 180–189. <https://doi.org/10.1016/j.neuropharm.2010.05.005>
- Jagtap, A.P., Krstic, I., Kunjir, N.C., Hänsel, R., Prisner, T.F. and Sigurdsson, S.T. (2015) Sterically shielded spin labels for in-cell EPR spectroscopy: Analysis of stability in reducing environment. *Free Radical Research*, 49, 78–85. <https://doi.org/10.3109/10715762.2014.979409>
- Jansen, F.P., Mochizuki, T., Yamamoto, Y., Timmerman, H. and Yamatodani, A. (1998) In vivo modulation of rat

- hypothalamic histamine release by the histamine H3 receptor ligands, immepip and clobenpropit. Effects of intrahypothalamic and peripheral application. *European Journal of Pharmacology*, 362, 149–155. [https://doi.org/10.1016/S0014-2999\(98\)00739-0](https://doi.org/10.1016/S0014-2999(98)00739-0)
- Jarskog, L.F., Lowy, M.T., Grove, R.A., Keefe, R.S.E., Horrigan, J.P., Ball, M.P., Breier, A., Buchanan, R.W., Carter, C.S., Csernansky, J.G., Goff, D.C., Green, M.F., Kantrowitz, J.T., Keshavan, M.S., Laurelle, M., Lieberman, J.A., Marder, S.R., Maruff, P., McMahon, R.P., Seidman, L.J. and Peykamian, M.A. (2015) A Phase II study of a histamine H3 receptor antagonist GSK239512 for cognitive impairment in stable schizophrenia subjects on antipsychotic therapy. *Schizophrenia Research*, 164, 136–142. <https://doi.org/10.1016/j.schres.2015.01.041>
- Jevtovic-Todorovic, V., Wozniak, D.F., Powell, S. and Olney, J.W. (2001) Propofol and sodium thiopental protect against MK-801-induced neuronal necrosis in the posterior cingulate/retrosplenial cortex. *Brain Research*, 913, 185–189. [https://doi.org/10.1016/S0006-8993\(01\)02800-1](https://doi.org/10.1016/S0006-8993(01)02800-1)
- Jin, C.Y., Anichtchik, O. and Panula, P. (2009) Altered histamine H3 receptor radioligand binding in post-mortem brain samples from subjects with psychiatric diseases. *British Journal of Pharmacology*, 157, 118–129. <https://doi.org/10.1111/j.1476-5381.2009.00149.x>
- Johnson, T.B. and Nicolet, B.H. (1911) HYDANTOINS: THE SYNTHESIS OF 2-THIOHYDANTOIN. [SEVENTH PAPER.]. *Journal of the American Chemical Society*, 33, 1973–1978. <https://doi.org/10.1021/ja02225a014>
- Jończyk, J., Malawska, B. and Bajda, M. (2017) Hybrid approach to structure modeling of the histamine H3 receptor: Multi-level assessment as a tool for model verification.(ed A Lodola) *PLOS ONE*, 12, e0186108. <https://doi.org/10.1371/journal.pone.0186108>
- Jones, G.R.N. (1972) CS and its chemical relatives. *Nature*, 235, 257–261. <https://doi.org/10.1038/235257a0>
- Jutel, M., Akdis, M. and Akdis, C.A. (2009) Histamine, histamine receptors and their role in immune pathology. *Clinical and Experimental Allergy*, 39, 1786–1800. <https://doi.org/10.1111/j.1365-2222.2009.03374.x>
- Kang, S., Cooper, G., Dunne, S.F., Dusel, B., Luan, C.-H., Surmeier, D.J. and Silverman, R.B. (2012) CaV1.3-selective L-type calcium channel antagonists as potential new therapeutics for Parkinson's disease. *Nature Communications*, 3, 1146. <https://doi.org/10.1038/ncomms2149>
- Kang, S., Cooper, G., Dunne, S.F., Luan, C.H., Surmeier, D.J. and Silverman, R.B. (2013) Structure-activity relationship of N,N'-disubstituted pyrimidinetriones as CaV1.3 calcium channel-selective antagonists for Parkinson's disease. *Journal of Medicinal Chemistry*, 56, 4786–4797. <https://doi.org/10.1021/jm4005048>
- Kaoukabi, H., Kabri, Y., Curti, C., Taourirte, M., Rodriguez-Ubis, J.C., Snoeck, R., Andrei, G., Vanelle, P. and Lazrek, H.B. (2018) Dihydropyrimidinone/1,2,3-triazole hybrid molecules: Synthesis and anti-varicella-zoster virus (VZV) evaluation. *European Journal of Medicinal Chemistry*, 155, 772–781. <https://doi.org/10.1016/j.ejmech.2018.06.028>
- Karthikeyan, G., Bonucci, A., Casano, G., Gerbaud, G., Abel, S., Thomé, V., Kodjabachian, L., Magalon, A., Guigliarelli, B., Belle, V., Ouari, O. and Mileo, E. (2018) A Bioresistant Nitroxide Spin Label for In-Cell EPR Spectroscopy: In Vitro and In Oocytes Protein Structural Dynamics Studies. *Angewandte Chemie*, 130, 1380–1384. <https://doi.org/10.1002/ange.201710184>
- Kasteleijn-Nolst Trenité, D., Parain, D., Genton, P., Masnou, P., Schwartz, J.C. and Hirsch, E. (2013) Efficacy of the histamine 3 receptor (H3R) antagonist pitolisant (formerly known as tiprolisant; BF2.649) in epilepsy: Dose-dependent effects in the human photosensitivity model. *Epilepsy and Behavior*, 28, 66–70. <https://doi.org/10.1016/j.yebeh.2013.03.018>
- Kenakin, T. (2001) Inverse, protean, and ligand-selective agonism: matters of receptor conformation. *The FASEB Journal*, 15, 598–611. <https://doi.org/10.1096/fj.00-0438rev>
- Khachaturian, Z.S. (2017) Calcium Hypothesis of Alzheimer's disease and brain aging: A framework for integrating new evidence into a comprehensive theory of pathogenesis. *Alzheimer's & Dementia*, 13, 178-182.e17. <https://doi.org/10.1016/j.jalz.2016.12.006>
- Khorana, N., Purohit, A., Herrick-Davis, K., Teitler, M. and Glennon, R.A. (2003a) γ -Carbolines: Binding at 5-HT_{5A} serotonin receptors. *Bioorganic and Medicinal Chemistry*, 11, 717–722. [https://doi.org/10.1016/S0968-0896\(02\)00527-8](https://doi.org/10.1016/S0968-0896(02)00527-8)
- Khorana, N., Smith, C., Herrick-Davis, K., Purohit, A., Teitler, M., Grella, B., Dukat, M. and Glennon, R.A. (2003b) Binding of Tetrahydrocarboline Derivatives at Human 5-HT_{5A} Receptors. *Journal of Medicinal Chemistry*, 46, 3930–3937. <https://doi.org/10.1021/jm030080s>
- Kieć-Kononowicz, K. and Karolak-wojciechowska, J. (1992) SYNTHESIS AND SPECTROSCOPIC PROPERTIES OF FUSED 5-ARYLIDENE-2-THIOHYDANTOIN DERIVATIVES. *Phosphorus, Sulfur, and Silicon and the Related Elements*, 73, 235–248. <https://doi.org/10.1080/10426509208034448>

Reference

- Kim, R.B. (2002) Drugs as P-glycoprotein substrates, inhibitors, and inducers. *Drug metabolism reviews*, 34, 47–54. <https://doi.org/10.1081/dmr-120001389>
- Kim, Y.J., Goto, Y. and Lee, Y.A. (2018) Histamine H3 receptor antagonists ameliorate attention deficit/hyperactivity disorder-like behavioral changes caused by neonatal habenula lesion. *Behavioural Pharmacology*, 29, 71–78. <https://doi.org/10.1097/FBP.0000000000000343>
- Kirsch, P. (2013) Modern Fluoroorganic Chemistry. *Modern Fluoroorganic Chemistry*. <https://doi.org/10.1002/9783527651351>
- Kitbunnadaj, R., Hashimoto, T., Poli, E., Zuiderveld, O.P., Menozzi, A., Hidaka, R., De Esch, I.J.P., Bakker, R.A., Menge, W.M.P.B., Yamatodani, A., Coruzzi, G., Timmerman, H. and Leurs, R. (2005) N-substituted piperidinyll alkyl imidazoles: Discovery of methimepip as a potent and selective histamine H3 receptor agonist. *Journal of Medicinal Chemistry*, 48, 2100–2107. <https://doi.org/10.1021/jm049475h>
- Kiyani, H. and Ghiasi, M. (2015) Solvent-free efficient one-pot synthesis of Biginelli and Hantzsch compounds catalyzed by potassium phthalimide as a green and reusable organocatalyst. *Research on Chemical Intermediates*, 41, 5177–5203. <https://doi.org/10.1007/s11164-014-1621-x>
- Klare, J.P. (2013) Site-directed spin labeling EPR spectroscopy in protein research. *Biological Chemistry*, 394, 1281–1300. <https://doi.org/10.1515/hsz-2013-0155>
- Knoevenagel, E. (1896) Ueber eine Darstellungsweise des Benzylidenacetessigesters. *Berichte der deutschen chemischen Gesellschaft*, 29, 172–174. <https://doi.org/10.1002/cber.18960290133>
- Kobayashi, T., Inoue, I., Jenkins, N.A., Gilbert, D.J., Copeland, N.G. and Watanabe, T. (1996) Cloning, RNA expression, and chromosomal location of a mouse histamine H2 receptor gene. *Genomics*, 37, 390–394. <https://doi.org/10.1006/geno.1996.0575>
- Koga, K., Kurokawa, M., Ochi, M., Nakamura, J. and Kuwana, Y. (2000) Adenosine A(2A) receptor antagonists KF17837 and KW-6002 potentiate rotation induced by dopaminergic drugs in hemi-Parkinsonian rats. *European Journal of Pharmacology*, 408, 249–255. [https://doi.org/10.1016/S0014-2999\(00\)00745-7](https://doi.org/10.1016/S0014-2999(00)00745-7)
- Komater, V.A., Browman, K.E., Curzon, P., Hancock, A.A., Decker, M.W. and Fox, G.B. (2003) H3 receptor blockade by thioperamide enhances cognition in rats without inducing locomotor sensitization. *Psychopharmacology*, 167, 363–372. <https://doi.org/10.1007/s00213-003-1431-0>
- Kondej, M., Stępnicki, P. and Kaczor, A.A. (2018) Multi-target approach for drug discovery against schizophrenia. *International Journal of Molecular Sciences*, 19, 3105.
- Kornhuber, J., Bormann, J., Hübers, M., Rusche, K. and Riederer, P. (1991) Effects of the 1-amino-adamantanes at the MK-801-binding site of the NMDA-receptor-gated ion channel: a human postmortem brain study. *European Journal of Pharmacology: Molecular Pharmacology*, 206, 297–300. [https://doi.org/10.1016/0922-4106\(91\)90113-V](https://doi.org/10.1016/0922-4106(91)90113-V)
- Koroleva, E. V., Gusak, K.N., Ignatovich, Z. V. and Ermolinskaya, a. L. (2011) Synthesis of new amides of the N-methylpiperazine series. *Russian Journal of Organic Chemistry*, 47, 1556–1563. <https://doi.org/10.1134/S1070428011100198>
- Kottke, T., Sander, K., Weizel, L., Schneider, E.H., Seifert, R. and Stark, H. (2011) Receptor-specific functional efficacies of alkyl imidazoles as dual histamine H3/H4 receptor ligands. *European Journal of Pharmacology*, 654, 200–208. <https://doi.org/10.1016/j.ejphar.2010.12.033>
- Krause, M., Stark, H. and Schunack, W. (2001) Azomethine Prodrugs of (R)-alpha-Methylhistamine, a Highly Potent and Selective Histamine H3-Receptor Agonist. *Current Medicinal Chemistry*, 8, 1329–1340. <https://doi.org/10.2174/0929867013372274>
- Kucwaj-Brysz, K., Warszycki, D., Podlewska, S., Witek, J., Witek, K., Izquierdo, A.G., Satała, G., Loza, M.I., Lubelska, A., Latacz, G., Bojarski, A.J., Castro, M., Kieć-Kononowicz, K. and Handzlik, J. (2016) Rational design in search for 5-phenylhydantoin selective 5-HT7R antagonists. Molecular modeling, synthesis and biological evaluation. *European Journal of Medicinal Chemistry*, 112, 258–269. <https://doi.org/10.1016/j.ejmech.2016.02.024>
- Kuder, K., Łażewska, D., Latacz, G., Schwed, J.S., Karcz, T., Stark, H., Karolak-Wojciechowska, J. and Kieć-Kononowicz, K. (2016) Chlorophenoxy aminoalkyl derivatives as histamine H3R ligands and antiseizure agents. *Bioorganic & Medicinal Chemistry*, 24, 53–72. <https://doi.org/10.1016/j.bmc.2015.11.021>
- Kunai, A., Yoshida, H., Nakano, S., Yamaryo, Y., Ohshita, J. and Kunai, A. (2006) Palladium-catalyzed distannylation of ortho-quinodimethanes. *Organic Letters*, 8, 4157–4159. <https://doi.org/10.1021/ol0617345>
- Lambert, M.P. and Neuhaus, F.C. (1972) Mechanism of D-cycloserine action: alanine racemase from *Escherichia coli* W. *Journal of Bacteriology*, 110, 978–987. <https://doi.org/10.1128/jb.110.3.978-987.1972>

- Lassen, F.O. and Stammer, C.H. (1971) Cycloserine dimer hydrolysis and its equilibration with cycloserine. *The Journal of organic chemistry*, 36, 2631–4. <https://doi.org/10.1021/jo00817a015>
- Łażewska, D., Ligneau, X., Schwartz, J.-C., Schunack, W., Stark, H. and Kieć-Kononowicz, K. (2006) Ether derivatives of 3-piperidinopropan-1-ol as non-imidazole histamine H3 receptor antagonists. *Bioorganic & medicinal chemistry*, 14, 3522–9. <https://doi.org/10.1016/j.bmc.2006.01.013>
- Łażewska, D., Olejarz-Maciej, A., Reiner, D., Kaleta, M., Latacz, G., Zygmunt, M., Doroz-Płonka, A., Karcz, T., Frank, A., Stark, H. and Kieć-Kononowicz, K. (2020) Dual Target Ligands with 4-tert-Butylphenoxy Scaffold as Histamine H3 Receptor Antagonists and Monoamine Oxidase B Inhibitors. *International journal of molecular sciences*, 21. <https://doi.org/10.3390/ijms21103411>
- Łażewska, D., Więcek, M., Ner, J., Kamińska, K., Kottke, T., Schwed, J.S., Zygmunt, M., Karcz, T., Olejarz, A., Kuder, K., Latacz, G., Grosicki, M., Sapa, J., Karolak-Wojciechowska, J., Stark, H. and Kieć-Kononowicz, K. (2014) Aryl-1,3,5-triazine derivatives as histamine H4 receptor ligands. *European Journal of Medicinal Chemistry*, 83, 534–546. <https://doi.org/10.1016/j.ejmech.2014.06.032>
- Lee, Y.C., Lin, C.H., Wu, R.M., Lin, J.W., Chang, C.H. and Lai, M.S. (2014) Antihypertensive agents and risk of Parkinson's disease: A nationwide cohort study. *PLoS ONE*, 9, 17–21. <https://doi.org/10.1371/journal.pone.0098961>
- Lee, H.-H., Takeuchi, N., Senda, H., Kuwae, A. and Hanai, K. (1998) Molecular Structure and Dimerization of -Cycloserine in the Solid State. *Spectroscopy Letters*, 31, 1217–1231. <https://doi.org/10.1080/00387019808003297>
- Leeson, P.D. and Iversen, L.L. (1994) The glycine site on the NMDA receptor: structure-activity relationships and therapeutic potential. *Journal of medicinal chemistry*, 37, 4053–67. <https://doi.org/10.1021/jm00050a001>
- Letavic, M.A., Aluisio, L., Apodaca, R., Bajpai, M., Barbier, A.J., Bonneville, A., Bonaventure, P., Carruthers, N.I., Dugovic, C., Fraser, I.C., Kramer, M.L., Lord, B., Lovenberg, T.W., Li, L.Y., Ly, K.S., Mcallister, H., Mani, N.S., Morton, K.L., Ndifor, A., Nepomuceno, S.D., Pandit, C.R., Sands, S.B., Shah, C.R., Shelton, J.E., Snook, S.S., Swanson, D.M. and Xiao, W. (2015) Novel Benzamide-Based Histamine H3 Receptor Antagonists: The Identification of Two Candidates for Clinical Development. *ACS Medicinal Chemistry Letters*, 6, 450–454. <https://doi.org/10.1021/ml5005156>
- Leurs, R., Bakker, R.A., Timmerman, H. and de Esch, I.J.P. (2005) The histamine H3 receptor: from gene cloning to H3 receptor drugs. *Nature Reviews Drug Discovery*, 4, 107–120. <https://doi.org/10.1038/nrd1631>
- Leurs, R., Blandina, P., Tedford, C. and Timmerman, H. (1998) Therapeutic potential of histamine H3 receptor agonists and antagonists. *Trends in Pharmacological Sciences*, 19, 177–184. [https://doi.org/10.1016/S0165-6147\(98\)01201-2](https://doi.org/10.1016/S0165-6147(98)01201-2)
- Levoine, N., Labeeuw, O., Calmels, T., Poupardin-Olivier, O., Berrebi-Bertrand, I., Lecomte, J.-M., Schwartz, J.-C. and Capet, M. (2011) Novel and highly potent histamine H3 receptor ligands. Part 1: withdrawing of hERG activity. *Bioorganic & Medicinal Chemistry Letters*, 21, 5378–5383. <https://doi.org/10.1016/j.bmcl.2011.07.006>
- Li, X., Bijur, G.N. and Jope, R.S. (2002) Glycogen synthase kinase-3 β , mood stabilizers, and neuroprotection. *Bipolar Disorders*, 4, 137–144. <https://doi.org/10.1034/j.1399-5618.2002.40201.x>
- Li, Z.-N., Chen, X.-L., Fu, Y.-J., Wang, W. and Luo, M. (2012) A facile synthesis of trisubstituted alkenes from β -diketones and aldehydes with AlCl₃ as catalyst. *Research on Chemical Intermediates*, 38, 25–35. <https://doi.org/10.1007/s11164-011-0322-y>
- Li, X.M., Juorio, A. V., Qi, J. and Boulton, A.A. (1998) L-deprenyl potentiates NGF-induced changes in superoxide dismutase mRNA in PC12 cells. *Journal of neuroscience research*, 53, 235–8. [https://doi.org/10.1002/\(SICI\)1097-4547\(19980715\)53:2<235::AID-JNR12>3.0.CO;2-5](https://doi.org/10.1002/(SICI)1097-4547(19980715)53:2<235::AID-JNR12>3.0.CO;2-5)
- Ligneau, X., Morisset, S., Tardivel-Lacombe, J., Gbahou, F., Ganellin, C.R., Stark, H., Schunack, W., Schwartz, J.-C. and Arrang, J.-M. (2000) Distinct pharmacology of rat and human histamine H 3 receptors: role of two amino acids in the third transmembrane domain. *British Journal of Pharmacology*, 131, 1247–1250. <https://doi.org/10.1038/sj.bjp.0703712>
- Lim, H.D., Van Rijn, R.M., Ling, P., Bakker, R.A., Thurmond, R.L. and Leurs, R. (2005) Evaluation of histamine H1-, H2-, and H 3-receptor ligands at the human histamine H4 receptor: Identification of 4-methylhistamine as the first potent and selective H 4 receptor agonist. *Journal of Pharmacology and Experimental Therapeutics*, 314, 1310–1321. <https://doi.org/10.1124/jpet.105.087965>
- Lin, J.-S., Sergeeva, O.A. and Haas, H.L. (2011) Histamine H 3 Receptors and Sleep-Wake Regulation Histamine's Role in Waking. *Journal of Pharmacology and Experimental Therapeutics*, 336, 17–23. <https://doi.org/10.1124/jpet.110.170134.basal>

Reference

- Linney, I.D., Buck, I.M., Harper, E. a, Kalindjian, S.B., Pether, M.J., Shankley, N.P., Watt, G.F. and Wright, P.T. (2000) Design, synthesis, and structure-activity relationships of novel non-imidazole histamine H(3) receptor antagonists. *Journal of medicinal chemistry*, 43, 2362–70.
- Lipinski, C.A., Lombardo, F., Dominy, B.W. and Feeney, P.J. (2012) Experimental and computational approaches to estimate solubility and permeability in drug discovery and development settings. *Advanced Drug Delivery Reviews*, 64, 4–17. <https://doi.org/10.1016/j.addr.2012.09.019>
- Lipton, S.A. (2007) Pathologically activated therapeutics for neuroprotection. *Nature Reviews Neuroscience*, 8, 803–808. <https://doi.org/10.1038/nrn2229>
- Liu, C., Ma, X.J., Jiang, X., Wilson, S.J., Hofstra, C.L., Blevitt, J., Pyati, J., Li, X., Chai, W., Carruthers, N. and Lovenberg, T.W. (2001) Cloning and pharmacological characterization of a fourth histamine receptor (H4) expressed in bone marrow. *Molecular Pharmacology*, 59, 420–426. <https://doi.org/10.1124/mol.59.3.420>
- Long, J.M. and Holtzman, D.M. (2019) Alzheimer Disease: An Update on Pathobiology and Treatment Strategies. *Cell*, 179, 312–339. <https://doi.org/10.1016/j.cell.2019.09.001>
- Löscher, W. and Rogawski, M.A. (2012) How theories evolved concerning the mechanism of action of barbiturates. *Epilepsia*, 53, 12–25. <https://doi.org/10.1111/epi.12025>
- Lovenberg, T.W., Roland, B.L., Wilson, S.J., Jiang, X., Pyati, J., Huvar, A., Jackson, M.R. and Erlander, M.G. (1999) Cloning and functional expression of the human histamine H3 receptor. *Molecular Pharmacology*, 55, 1101–1107. <https://doi.org/10.1124/mol.55.6.1101>
- Lutsenko, K., Hagenow, S., Affini, A., Reiner, D. and Stark, H. (2019) Rasagiline derivatives combined with histamine H3 receptor properties. *Bioorganic & Medicinal Chemistry Letters*, 29, 126612. <https://doi.org/10.1016/j.bmcl.2019.08.016>
- Macdonald, R.L. and Olsen, R.W. (1994) GABA A Receptor Channels. *Annual Review of Neuroscience*, 17, 569–602. <https://doi.org/10.1146/annurev.ne.17.030194.003033>
- Mahapatra, S., Albrecht, M., Behrens, B., Jirno, A., Behrens, G., Hartwig, C., Neumann, D., Raap, U., Bähre, H., Herrick, C. and Dittrich, A.M. (2014) Delineating the role of histamine-1- And -4-receptors in a mouse model of Th2-dependent antigen-specific skin inflammation. *PLoS ONE*, 9. <https://doi.org/10.1371/journal.pone.0087296>
- Maintz, L. and Novak, N. (2007) Histamine and histamine intolerance. *The American Journal of Clinical Nutrition*, 85, 1185–1196. <https://doi.org/10.1093/ajcn/85.5.1185>
- Malek, R., Arribas, R.L., Palomino-Antolin, A., Totolon, P., Demougeot, C., Koblíva, T., Soukup, O., Iriepa, I., Moraleda, I., Díez-Iriepa, D., Godyń, J., Panek, D., Malawska, B., Głuch-Lutwin, M., Mordyl, B., Siwek, A., Chabchoub, F., Marco-Contelles, J., Kiec-Kononowicz, K., Egea, J., de los Ríos, C. and Ismaili, L. (2019) New Dual Small Molecules for Alzheimer's Disease Therapy Combining Histamine H 3 Receptor (H3R) Antagonism and Calcium Channels Blockade with Additional Cholinesterase Inhibition. *Journal of Medicinal Chemistry*, 62, 11416–11422. <https://doi.org/10.1021/acs.jmedchem.9b00937>
- Malmilöf, K., Zaragoza, F., Golozoubova, V., Refsgaard, H.H.F., Cremers, T., Raun, K., Wulff, B.S., Johansen, P.B., Westerink, B. and Rimvall, K. (2005) Influence of a selective histamine H3 receptor antagonist on hypothalamic neural activity, food intake and body weight. *International Journal of Obesity*, 29, 1402–1412. <https://doi.org/10.1038/sj.ijo.0803036>
- Malspeis, L. and Gold, D. (1964) Stability of cycloserine in buffered aqueous solutions. *Journal of Pharmaceutical Sciences*, 53, 1173–1180. <https://doi.org/10.1002/jps.2600531009>
- Manzoor, S. and Hoda, N. (2020) A comprehensive review of monoamine oxidase inhibitors as Anti-Alzheimer's disease agents: A review. *European Journal of Medicinal Chemistry*, 206, 112787.
- Márquez-Gómez, R., Robins, M.T., Gutiérrez-Rodelo, C., Arias, J.-M.M., Olivares-Reyes, J.-A.A., van Rijn, R.M. and Arias-Montaño, J.-A.A. (2018) Functional histamine H3 and adenosine A2A receptor heteromers in recombinant cells and rat striatum. *Pharmacological Research*, 129, 515–525. <https://doi.org/10.1016/j.phrs.2017.11.036>
- Marras, C., Gruneir, A., Rochon, P., Wang, X., Anderson, G., Brotchie, J., Bell, C.M., Fox, S. and Austin, P.C. (2012) Dihydropyridine calcium channel blockers and the progression of parkinsonism. *Annals of Neurology*, 71, 362–369. <https://doi.org/10.1002/ana.22616>
- Masood, N., Fatima, K. and Luqman, S. (2014) A Modified Method for Studying Behavioral Paradox of Antioxidants and Their Disproportionate Competitive Kinetic Effect to Scavenge the Peroxyl Radical Formation. *The Scientific World Journal*, 2014, 1–12. <https://doi.org/10.1155/2014/931581>
- Matsubara, T., Moskowitz, M.A. and Huang, Z. (1992) UK-14,304, R(-)- α -methyl-histamine and SMS 201-995 block

Reference

- plasma protein leakage within dura mater by prejunctional mechanisms. *European Journal of Pharmacology*, 224, 145–150. [https://doi.org/10.1016/0014-2999\(92\)90798-9](https://doi.org/10.1016/0014-2999(92)90798-9)
- McCormick, D.A., Pape, H.-C. and Williamson, A. (1991) Actions of norepinephrine in the cerebral cortex and thalamus: implications for function of the central noradrenergic system. In *Progress in Brain Research*, pp. 293–305, Elsevier.
- Meanwell, N.A. (2018) Fluorine and Fluorinated Motifs in the Design and Application of Bioisosteres for Drug Design. *Journal of Medicinal Chemistry*, 61, 5822–5880. <https://doi.org/10.1021/acs.jmedchem.7b01788>
- Medhurst, S.J., Collins, S.D., Billinton, A., Bingham, S., Dalziel, R.G., Brass, A., Roberts, J.C., Medhurst, A.D. and Chessell, I.P. (2008) Novel histamine H3 receptor antagonists GSK189254 and GSK334429 are efficacious in surgically-induced and virally-induced rat models of neuropathic pain. *Pain*, 138, 61–69. <https://doi.org/10.1016/j.pain.2007.11.006>
- Meier, G., Apelt, J., Reichert, U., Graßmann, S., Ligneau, X., Elz, S., Leurquin, F., Ganellin, C.R., Schwartz, J.C., Schunack, W. and Stark, H. (2001) Influence of imidazole replacement in different structural classes of histamine H3-receptor antagonists. *European Journal of Pharmaceutical Sciences*, 13, 249–259. [https://doi.org/10.1016/S0928-0987\(01\)00106-3](https://doi.org/10.1016/S0928-0987(01)00106-3)
- Mendgen, T., Steuer, C. and Klein, C.D. (2012) Privileged Scaffolds or Promiscuous Binders: A Comparative Study on Rhodanines and Related Heterocycles in Medicinal Chemistry. *Journal of Medicinal Chemistry*, 55, 743–753. <https://doi.org/10.1021/jm201243p>
- Menniti, F.S., Pagnozzi, M.J., Butler, P., Chenard, B.L., Jaw-Tsai, S.S. and Frost White, W. (2000) CP-101,606, an NR2B subunit selective NMDA receptor antagonist, inhibits NMDA and injury induced c-fos expression and cortical spreading depression in rodents. *Neuropharmacology*, 39, 1147–1155. [https://doi.org/10.1016/S0028-3908\(99\)00211-7](https://doi.org/10.1016/S0028-3908(99)00211-7)
- Meunier, B. (2008) Hybrid Molecules with a Dual Mode of Action: Dream or Reality? †. *Accounts of Chemical Research*, 41, 69–77. <https://doi.org/10.1021/ar7000843>
- Meyer, S.D. and Schreiber, S.L. (1994) Acceleration of the Dess-Martin Oxidation by Water. *The Journal of Organic Chemistry*, 59, 7549–7552. <https://doi.org/10.1021/jo00103a067>
- Micheli, F., Andreotti, D., Braggio, S. and Checchia, A. (2010) A specific and direct comparison of the trifluoromethyl and pentafluoro sulfonyl groups on the selective dopamine D3 antagonist 3-(3-{{4-methyl-5-(4-methyl-1,3-oxazol-5-yl)-4H-1,2,4-triazol-3-yl}}thio}propyl)-1-phenyl-3-azabicyclo[3.1.0]hexane template. *Bioorganic & Medicinal Chemistry Letters*, 20, 4566–4568. <https://doi.org/10.1016/j.bmcl.2010.06.018>
- Mikkelsen, G.K., Langgård, M., Schrøder, T.J., Kreilgaard, M., Jørgensen, E.B., Brandt, G., Griffon, Y., Boffey, R. and Bang-Andersen, B. (2015) Synthesis and SAR studies of analogues of 4-(3,3-dimethyl-butyrylamino)-3,5-difluoro-N-thiazol-2-yl-benzamide (Lu AA41063) as adenosine A2A receptor ligands with improved aqueous solubility. *Bioorganic & Medicinal Chemistry Letters*, 25, 1212–1216. <https://doi.org/10.1016/j.bmcl.2015.01.062>
- Milite, C., Feoli, A., Sasaki, K., La Pietra, V., Balzano, A.L., Marinelli, L., Mai, A., Novellino, E., Castellano, S., Tosco, A. and Sbardella, G. (2015) A novel cell-permeable, selective, and noncompetitive inhibitor of KAT3 histone acetyltransferases from a combined molecular pruning/classical isosterism approach. *Journal of Medicinal Chemistry*, 58, 2779–2798. <https://doi.org/10.1021/jm5019687>
- Mitsunobu, O., Obata, T. and Mukaiyama, T.T. (1967) Preparation of Esters of Phosphoric Acid via Quaternary Phosphonium Salts. *The Journal of Organic Chemistry*, 30, 1071–1073. <https://doi.org/10.1021/jo01015a027>
- Mizuta, I., Ohta, M., Ohta, K., Nishimura, M., Mizuta, E., Hayashi, K. and Kuno, S. (2000) Selegiline and desmethylselegiline stimulate NGF, BDNF, and GDNF synthesis in cultured mouse astrocytes. *Biochemical and Biophysical Research Communications*, 279, 751–755. <https://doi.org/10.1006/bbrc.2000.4037>
- Mochizuki, T., Yamatodani, A., Okakura, K., Horii, A., Inagaki, N. and Wada, H. (1992) Circadian rhythm of histamine release from the hypothalamus of freely moving rats. *Physiology and Behavior*, 51, 391–394. [https://doi.org/10.1016/0031-9384\(92\)90157-W](https://doi.org/10.1016/0031-9384(92)90157-W)
- Molderings, G.J., Weißborn, G., Schlicker, E., Likungu, J. and Göthert, M. (1992) Inhibition of noradrenaline release from the sympathetic nerves of the human saphenous vein by presynaptic histamine H3 receptors. *Naunyn-Schmiedeberg's Archives of Pharmacology*, 346, 46–50. <https://doi.org/10.1007/BF00167569>
- Monczor, F., Fernández, N., Legnazzi, B.L., Riveiro, M.E., Baldi, A., Shayo, C. and Davio, C. (2003) Tiotidine, a histamine H2 receptor inverse agonist that binds with high affinity to an inactive G-protein-coupled form of the receptor. Experimental support for the cubic ternary complex model. *Molecular Pharmacology*, 64, 512–520. <https://doi.org/10.1124/mol.64.2.512>
- Moraski, G.C., Bristol, R., Seeger, N., Boshoff, H.I., Tsang, P.S.Y. and Miller, M.J. (2017) Preparation and

Reference

- Evaluation of Potent Pentafluorosulfanyl-Substituted Anti-Tuberculosis Compounds. *ChemMedChem*, 12, 1108–1115. <https://doi.org/10.1002/cmdc.201700170>
- Moreno, E., Hoffmann, H., Gonzalez-Sepúlveda, M., Navarro, G., Casadó, V., Cortés, A., Mallol, J., Vignes, M., McCormick, P.J., Canela, E.I., Lluís, C., Moratalla, R., Ferré, S., Ortiz, J. and Franco, R. (2011) Dopamine D₁-histamine H₃ Receptor Heteromers Provide a Selective Link to MAPK Signaling in GABAergic Neurons of the Direct Striatal Pathway. *Journal of Biological Chemistry*, 286, 5846–5854. <https://doi.org/10.1074/jbc.M110.161489>
- Morisset, S., Rouleau, A., Ligneau, X., Gbahou, F., Tardivel-Lacombe, J., Stark, H., Schunack, W., Ganellin, C.R. and Arrang, J.M. (2000) High constitutive activity of native H₃ receptors regulates histamine neurons in brain. *Nature*, 408, 860–864. <https://doi.org/10.1038/35048583>
- Morphy, R., Kay, C. and Rankovic, Z. (2004) From magic bullets to designed multiple ligands. *Drug Discovery Today*, 9, 641–651. [https://doi.org/10.1016/S1359-6446\(04\)03163-0](https://doi.org/10.1016/S1359-6446(04)03163-0)
- Morphy, R. and Rankovic, Z. (2006) The physicochemical challenges of designing multiple ligands. *Journal of Medicinal Chemistry*, 49, 4961–4970. <https://doi.org/10.1021/jm0603015>
- Morse, K., Behan, J., Laz, T., West, R.J., Greenfeder, S., Anthes, J., Umland, S., Wan, Y., Hipkin, R., Gonsiorek, W., Shin, N., Gustafson, E., Qiao, X., Wang, S., Hedrick, J., Greene, J., Bayne, M. and Monsma, F.J. (2001) Cloning and characterization of a novel human histamine receptor. *J Pharmacol Exp Ther*, 296, 1058–66.
- Nakamura, T., Itadani, H., Hidaka, Y., Ohta, M. and Tanaka, K. (2000) Molecular cloning and characterization of a new human histamine receptor, HH4R. *Biochemical and Biophysical Research Communications*, 279, 615–620. <https://doi.org/10.1006/bbrc.2000.4008>
- Naylor, D.E. (2010) Glutamate and GABA in the balance: Convergent pathways sustain seizures during status epilepticus. *Epilepsia*, 51, 106–109. <https://doi.org/10.1111/j.1528-1167.2010.02622.x>
- Neuhaus, F.C. and Lynch, J.L. (1964) The Enzymatic Synthesis of d-Alanyl-d-alanine. III. On the Inhibition of d-Alanyl-d-alanine Synthetase by the Antibiotic d-Cycloserine. *Biochemistry*, 3, 471–480. <https://doi.org/10.1021/bi00892a001>
- Nguyen, T., Shapiro, D.A., George, S.R., Setola, V., Lee, D.K., Cheng, R., Rauser, L., Lee, S.P., Lynch, K.R., Roth, B.L. and O'Dowd, B.F. (2001) Discovery of a novel member of the histamine receptor family. *Molecular Pharmacology*, 59, 427–433. <https://doi.org/10.1124/mol.59.3.427>
- Nicklas, W.J., Youngster, S.K., Kindt, M.V. and Heikkila, R.E. (1987) IV. MPTP, MPP+ and mitochondrial function. *Life Sciences*, 40, 721–729. [https://doi.org/10.1016/0024-3205\(87\)90299-2](https://doi.org/10.1016/0024-3205(87)90299-2)
- Nimmrich, V. and Eckert, A. (2013) Calcium channel blockers and dementia. *British Journal of Pharmacology*, 169, 1203–1210. <https://doi.org/10.1111/bph.12240>
- Norinder, U. and Haeberlein, M. (2002) Computational approaches to the prediction of the blood-brain distribution. *Advanced Drug Delivery Reviews*, 54, 291–313. [https://doi.org/10.1016/S0169-409X\(02\)00005-4](https://doi.org/10.1016/S0169-409X(02)00005-4)
- Nuutinen, S., Karlstedt, K., Aitta-Aho, T., Korpi, E.R. and Panula, P. (2010) Histamine and H₃ receptor-dependent mechanisms regulate ethanol stimulation and conditioned place preference in mice. *Psychopharmacology*, 208, 75–86. <https://doi.org/10.1007/s00213-009-1710-5>
- O'Brien, J., Wilson, I., Orton, T. and Pognan, F. (2000) Investigation of the Alamar Blue (resazurin) fluorescent dye for the assessment of mammalian cell cytotoxicity. *European Journal of Biochemistry*, 267, 5421–5426. <https://doi.org/10.1046/j.1432-1327.2000.01606.x>
- Obara, I., Telezhkin, V., Alrashdi, I. and Chazot, P.L. (2020) Histamine, histamine receptors, and neuropathic pain relief. *British Journal of Pharmacology*, 177, 580–599. <https://doi.org/10.1111/bph.14696>
- Oda, T., Morikawa, N., Saito, Y., Masuho, Y. and Matsumoto, S.I. (2000) Molecular cloning and characterization of a novel type of histamine receptor preferentially expressed in leukocytes. *Journal of Biological Chemistry*, 275, 36781–36786. <https://doi.org/10.1074/jbc.M006480200>
- Ogawa, M., Shigeto, H., Yamamoto, T., Oya, Y., Wada, K., Nishikawa, T. and Kawai, M. (2003) D-cycloserine for the treatment of ataxia in spinocerebellar degeneration. *Journal of the neurological sciences*, 210, 53–6. [https://doi.org/10.1016/s0022-510x\(03\)00009-1](https://doi.org/10.1016/s0022-510x(03)00009-1)
- Ohkubo, T. and Shibata, M. (1995) ATP-sensitive K⁺ channels mediate regulation of substance P release via the prejunctional histamine H₃ receptor. *European Journal of Pharmacology*, 277, 45–49. [https://doi.org/10.1016/0014-2999\(95\)00057-R](https://doi.org/10.1016/0014-2999(95)00057-R)
- Omura, K. and Swern, D. (1978) Oxidation of alcohols by “activated” dimethyl sulfoxide. a preparative, steric and mechanistic study. *Tetrahedron*, 34, 1651–1660. [https://doi.org/10.1016/0040-4020\(78\)80197-5](https://doi.org/10.1016/0040-4020(78)80197-5)

Reference

- Ookuma, K., Sakata, T., Fukagawa, K., Yoshimatsu, H., Kurokawa, M., Machidori, H. and Fujimoto, K. (1993) Neuronal histamine in the hypothalamus suppresses food intake in rats. *Brain Research*, 628, 235–242. [https://doi.org/10.1016/0006-8993\(93\)90960-U](https://doi.org/10.1016/0006-8993(93)90960-U)
- Ortner, N.J., Bock, G., Vandael, D.H.F., Mauersberger, R., Draheim, H.J., Gust, R., Carbone, E., Tuluc, P. and Striessnig, J. (2014) Pyrimidine-2,4,6-triones are a new class of voltage-gated L-type Ca²⁺ channel activators. *Nature Communications*, 5, 3897. <https://doi.org/10.1038/ncomms4897>
- Ortner, N.J. and Striessnig, J. (2016) L-type calcium channels as drug targets in CNS disorders. *Channels*, 10, 7–13. <https://doi.org/10.1080/19336950.2015.1048936>
- Oset-Gasque, M.J. and Marco-Contelles, J. (2018) Alzheimer's Disease, the "one-Molecule, One-Target" Paradigm, and the Multitarget Directed Ligand Approach. *ACS Chemical Neuroscience*, 9, 401–403. <https://doi.org/10.1021/acscemneuro.8b00069>
- Ou, B., Hampsch-Woodill, M. and Prior, R.L. (2001) Development and Validation of an Improved Oxygen Radical Absorbance Capacity Assay Using Fluorescein as the Fluorescent Probe. *Journal of Agricultural and Food Chemistry*, 49, 4619–4626. <https://doi.org/10.1021/jf010586o>
- Paiva, T.B., Tominaga, M. and Paiva, A.C.M.M. (1970) Ionization of histamine, N-acetylhistamine, and their iodinated derivatives. *Journal of Medicinal Chemistry*, 13, 689–692. <https://doi.org/10.1021/jm00298a025>
- Palop, J.J. and Mucke, L. (2010) Amyloid-beta-induced neuronal dysfunction in Alzheimer's disease: from synapses toward neural networks. *Nature neuroscience*, 13, 812–8. <https://doi.org/10.1038/nn.2583>
- Panula, P. (2020) Histamine, histamine H₃ receptor, and alcohol use disorder. *British Journal of Pharmacology*, 177, 634–641. <https://doi.org/10.1111/bph.14634>
- Panula, P., Chazot, P.L., Cowart, M., Gutzmer, R., Leurs, R., Liu, W.L.S.S., Stark, H., Thurmond, R.L. and Haas, H.L. (2015) International union of basic and clinical pharmacology. XCVIII. histamine receptors.(ed EH Ohlstein) *Pharmacological Reviews*, 67, 601–655. <https://doi.org/10.1124/pr.114.010249>
- Parmentier, R., Anaclet, C., Guhenec, C., Brousseau, E., Bricout, D., Giboulot, T., Bozyczko-Coyne, D., Spiegel, K., Ohtsu, H., Williams, M. and Lin, J.S. (2007) The brain H₃-receptor as a novel therapeutic target for vigilance and sleep-wake disorders. *Biochemical Pharmacology*, 73, 1157–1171. <https://doi.org/10.1016/j.bcp.2007.01.002>
- Parmentier, R., Ohtsu, H., Djebbara-Hannas, Z., Valatx, J.-L., Watanabe, T. and Lin, J.-S. (2002) Anatomical, Physiological, and Pharmacological Characteristics of Histidine Decarboxylase Knock-Out Mice: Evidence for the Role of Brain Histamine in Behavioral and Sleep-Wake Control. *The Journal of Neuroscience*, 22, 7695–7711. <https://doi.org/10.1523/JNEUROSCI.22-17-07695.2002>
- Parsons, C.G., Stöffler, A. and Danysz, W. (2007) Memantine: a NMDA receptor antagonist that improves memory by restoration of homeostasis in the glutamatergic system - too little activation is bad, too much is even worse. *Neuropharmacology*, 53, 699–723. <https://doi.org/10.1016/j.neuropharm.2007.07.013>
- Passani, M.B., Blandina, P. and Torrealba, F. (2011) The histamine H₃ receptor and eating behavior. *Journal of Pharmacology and Experimental Therapeutics*, 336, 24–29. <https://doi.org/10.1124/jpet.110.171306>
- Pasternak, B., Svanström, H., Nielsen, N.M., Fugger, L., Melbye, M. and Hviid, A. (2012) Use of calcium channel blockers and Parkinson's disease. *American Journal of Epidemiology*, 175, 627–635. <https://doi.org/10.1093/aje/kwr362>
- Patnaik, R., Sharma, A., Skaper, S.D., Muresanu, D.F., Lafuente, J.V., Castellani, R.J., Nozari, A. and Sharma, H.S. (2018) Histamine H₃ inverse agonist BF 2649 or antagonist with partial h₄ agonist activity clobenpropit reduces amyloid beta peptide-induced brain pathology in alzheimer's disease. *Molecular Neurobiology*, 55, 312–321. <https://doi.org/10.1007/s12035-017-0743-8>
- Pauling, L. (1960) *The Nature of the Chemical Bond.*, 3rd ed. Cornell university press, Ithaca, NY.
- Pchitskaya, E., Popugaeva, E. and Bezprozvanny, I. (2018) Calcium signaling and molecular mechanisms underlying neurodegenerative diseases. *Cell Calcium*, 70, 87–94. <https://doi.org/10.1016/j.ceca.2017.06.008>
- Penger, A., Von Hahmann, C.N., Filatov, A.S. and Welch, J.T. (2013) Diastereoselectivity in the Staudinger reaction of pentafluorosulfanylaldimines and ketimines. *Beilstein Journal of Organic Chemistry*, 9, 2675–2680. <https://doi.org/10.3762/bjoc.9.303>
- Pereira, C., Agostinho, P., Moreira, P.I., Cardoso, S.M. and Oliveira, C.R. (2005) Alzheimer's disease-associated neurotoxic mechanisms and neuroprotective strategies. *Current Drug Targets: CNS and Neurological Disorders*, 4, 383–403.
- Petroianu, G., Arafat, K., Sasse, B.C. and Stark, H. (2006) Multiple enzyme inhibitions by histamine H₃ receptor antagonists as potential procognitive agents. *Pharmazie*, 61, 179–182.

Reference

- Pfleger, K.D.G. and Eidne, K.A. (2005) Monitoring the formation of dynamic G-protein-coupled receptor-protein complexes in living cells. *The Biochemical journal*, 385, 625–37. <https://doi.org/10.1042/BJ20041361>
- Pillot, C., Heron, A., Cochois, V., Tardivel-Lacombe, J., Ligneau, X., Schwartz, J.C. and Arrang, J.M. (2002) A detailed mapping of the histamine H3 receptor and its gene transcripts in rat brain. *Neuroscience*, 114, 173–193. [https://doi.org/10.1016/S0306-4522\(02\)00135-5](https://doi.org/10.1016/S0306-4522(02)00135-5)
- Poewe, W., Hauser, R.A. and Lang, A. (2015) Effects of rasagiline on the progression of nonmotor scores of the MDS-UPDRS. *Movement Disorders*, 30, 589–592. <https://doi.org/10.1002/mds.26124>
- Poewe, W., Seppi, K., Tanner, C.M., Halliday, G.M., Brundin, P., Volkman, J., Schrag, A.E. and Lang, A.E. (2017) Parkinson disease. *Nature Reviews Disease Primers*, 3, 1–21. <https://doi.org/10.1038/nrdp.2017.13>
- Popielek-Barczyk, K., Łażewska, D., Latacz, G., Olejarz, A., Makuch, W., Stark, H., Kieć-Kononowicz, K. and Mika, J. (2018) Antinociceptive effects of novel histamine H3 and H4 receptor antagonists and their influence on morphine analgesia of neuropathic pain in the mouse. *British Journal of Pharmacology*, 175, 2897–2910. <https://doi.org/10.1111/bph.14185>
- Posey, D.J., Kem, D.L., Swiezy, N.B., Sweeten, T.L., Wiegand, R.E. and McDougale, C.J. (2004) A pilot study of D-cycloserine in subjects with autistic disorder. *American Journal of Psychiatry*, 161, 2115–2117. <https://doi.org/10.1176/appi.ajp.161.11.2115>
- Powers, J.P., Piper, D.E., Li, Y., Mayorga, V., Anzola, J., Chen, J.M., Jaen, J.C., Lee, G., Liu, J., Peterson, M.G., Tonn, G.R., Ye, Q., Walker, N.P.C. and Wang, Z. (2006) SAR and mode of action of novel non-nucleoside inhibitors of hepatitis C NS5b RNA polymerase. *Journal of Medicinal Chemistry*, 49, 1034–1046. <https://doi.org/10.1021/jm050859x>
- Prell, G.D., Green, J.P., Kaufmann, C.A., Khandelwal, J.K., Morrishow, A.M., Kirch, D.G., Linnoila, M. and Wyatt, R.J. (1995) Histamine metabolites in cerebrospinal fluid of patients with chronic schizophrenia: their relationships to levels of other aminergic transmitters and ratings of symptoms. *Schizophrenia Research*, 14, 93–104. [https://doi.org/10.1016/0920-9964\(94\)00034-6](https://doi.org/10.1016/0920-9964(94)00034-6)
- Prell, G.D., Martinelli, G.P., Holstein, G.R., Matulić-Adamić, J., Watanabe, K.A., Chan, S.L.F., Morgan, N.G., Haxhiu, M.A. and Ernsberger, P. (2004) Imidazoleacetic acid-ribotide: An endogenous ligand that stimulates imidazol(in)e receptors. *Proceedings of the National Academy of Sciences of the United States of America*, 101, 13677–13682. <https://doi.org/10.1073/pnas.0404846101>
- Proschak, E., Stark, H. and Merk, D. (2019) Polypharmacology by Design: A Medicinal Chemist's Perspective on Multitargeting Compounds. *Journal of medicinal chemistry*, 62, 420–444. <https://doi.org/10.1021/acs.jmedchem.8b00760>
- Pulido, D., Casadó-Anguera, V., Pérez-Benito, L., Moreno, E., Cordoní, A., López, L., Cortés, A., Ferré, S., Pardo, L., Casadó, V. and Royo, M. (2018) Design of a True Bivalent Ligand with Picomolar Binding Affinity for a G Protein-Coupled Receptor Homodimer. *Journal of Medicinal Chemistry*, 61, 9335–9346. <https://doi.org/10.1021/acs.jmedchem.8b01249>
- Purser, S., Moore, P.R., Swallow, S. and Gouverneur, V. (2008) Fluorine in medicinal chemistry. *Chemical Society Reviews*, 37, 320–330. <https://doi.org/10.1039/b610213c>
- Ranaldi, G., Islam, K. and Sambuy, Y. (1994) D-cycloserine uses an active transport mechanism in the human intestinal cell line Caco 2. *Antimicrobial Agents and Chemotherapy*, 38, 1239–1245. <https://doi.org/10.1128/AAC.38.6.1239>
- Rao, A.U., Shao, N., Aslanian, R.G., Chan, T.Y., Degrado, S.J., Wang, L., McKittrick, B., Senior, M., West, R.E., Williams, S.M., Wu, R.L., Hwa, J., Patel, B., Zheng, S., Sondey, C. and Palani, A. (2012) Discovery of a potent thiazole class of histamine H3 receptor antagonist for the treatment of diabetes. *ACS Medicinal Chemistry Letters*, 3, 198–202. <https://doi.org/10.1021/ml200250t>
- Rapanelli, M. and Pittenger, C. (2016) Histamine and histamine receptors in Tourette syndrome and other neuropsychiatric conditions. *Neuropharmacology*, 106, 85–90. <https://doi.org/10.1016/j.neuropharm.2015.08.019>
- Rascol, O., Fitzer-Attas, C.J., Hauser, R., Jankovic, J., Lang, A., Langston, J.W., Melamed, E., Poewe, W., Stocchi, F., Tolosa, E., Eyal, E., Weiss, Y.M. and Olanow, C.W. (2011) A double-blind, delayed-start trial of rasagiline in Parkinson's disease (the ADAGIO study): prespecified and post-hoc analyses of the need for additional therapies, changes in UPDRS scores, and non-motor outcomes. *The Lancet. Neurology*, 10, 415–23. [https://doi.org/10.1016/S1474-4422\(11\)70073-4](https://doi.org/10.1016/S1474-4422(11)70073-4)
- Reddy, C.V., Mahesh, M., Raju, P.V.K., Babu, T.R. and Reddy, V.V.N. (2002) Zirconium(IV) chloride catalyzed one-pot synthesis of 3,4-dihydropyrimidin-2(1H)-ones. *Tetrahedron Letters*, 43, 2657–2659. [https://doi.org/10.1016/S0040-4039\(02\)00280-0](https://doi.org/10.1016/S0040-4039(02)00280-0)

Reference

- Rempel, V., Atzler, K., Behrenswerth, A., Karcz, T., Schoeder, C., Hinz, S., Kaleta, M., Thimm, D., Kiec-Kononowicz, K. and Müller, C.E. (2014) Bicyclic imidazole-4-one derivatives: a new class of antagonists for the orphan G protein-coupled receptors GPR18 and GPR55. *Med. Chem. Commun.*, 5, 632–649. <https://doi.org/10.1039/C3MD00394A>
- Richelson, E. (1978) Histamine H1 receptor-mediated guanosine 3',5'-monophosphate formation by cultured mouse neuroblastoma cells. *Science*, 201, 69–71. <https://doi.org/10.1126/science.26974>
- Rickle, A., Bogdanovic, N., Volkman, I., Winblad, B., Ravid, R. and Cowburn, R.F. (2004) Akt activity in Alzheimer's disease and other neurodegenerative disorders. *NeuroReport*, 15, 955–959. <https://doi.org/10.1097/00001756-200404290-00005>
- van Rijn, R.M., van Marle, A., Chazot, P.L., Langemeijer, E., Qin, Y., Shenton, F.C., Lim, H.D., Zuiderveld, O.P., Sansuk, K., Dy, M., Smit, M.J., Tensen, C.P., Bakker, R.A. and Leurs, R. (2008) Cloning and characterization of dominant negative splice variants of the human histamine H4 receptor. *Biochemical Journal*, 414, 121–131. <https://doi.org/10.1042/BJ20071583>
- Ritz, B., Rhodes, S.L., Qian, L., Schernhammer, E., Olsen, J.H. and Friis, S. (2010) L-type calcium channel blockers and parkinson disease in Denmark. *Annals of Neurology*, 67, 600–606. <https://doi.org/10.1002/ana.21937>
- Rodriguez, J.R., Agejas, J. and Bueno, A.B. (2006) Practical synthesis of aromatic ethers by SNAr of fluorobenzenes with alkoxides. *Tetrahedron Letters*, 47, 5661–5663. <https://doi.org/10.1016/j.tetlet.2006.06.029>
- Rodriguez, J.A. and Hrbek, J. (1999) Interaction of sulfur with well-defined metal and oxide surfaces: Unraveling the mysteries behind catalyst poisoning and desulfurization. *Accounts of Chemical Research*, 32, 719–728. <https://doi.org/10.1021/ar9801191>
- Rodríguez Sarmiento, R.M., Nettekoven, M.H., Taylor, S., Plancher, J.M., Richter, H. and Roche, O. (2009) Selective naphthalene H3 receptor inverse agonists with reduced potential to induce phospholipidosis and their quinoline analogs. *Bioorganic and Medicinal Chemistry Letters*, 19, 4495–4500. <https://doi.org/10.1016/j.bmcl.2009.03.100>
- Ross, S.B. (1976) Long-term effects of N-2-chlorethyl-N-ethyl-2-bromobenzylamine hydrochloride on noradrenergic neurones in the rat brain and heart. *British journal of pharmacology*, 58, 521–7. <https://doi.org/10.1111/j.1476-5381.1976.tb08619.x>
- Rouleau, A., Ligneau, X., Tardivel-Lacombe, J., Morisset, S., Gbahou, F., Schwartz, J.C. and Arrang, J.M. (2002) Histamine H3-receptor-mediated [³⁵S]GTPγ[S] binding: Evidence for constitutive activity of the recombinant and native rat and human H3 receptors. *British Journal of Pharmacology*, 135, 383–392. <https://doi.org/10.1038/sj.bjp.0704490>
- Rovnyak, G.C., Atwal, K.S., Kimball, S.D., O'Reilly, B.C., Schwartz, J., Hedberg, A., Moreland, S., Gougoutas, J.Z. and Malley, M.F. (1992) Dihydropyrimidine Calcium Channel Blockers. 4. Basic 3-Substituted-4-aryl-1,4-dihydropyrimidine-5-Carboxylic Acid Esters. Potent Antihypertensive Agents. *Journal of Medicinal Chemistry*, 35, 3254–3263. <https://doi.org/10.1021/jm00095a023>
- Rovnyak, G.C., Kimball, S.D., Beyer, B., Cucinotta, G., DiMarco, J.D., Gougoutas, J., Hedberg, A., Malley, M., McCarthy, J.P., Zhang, R. and Moreland, S. (1995) Calcium Entry Blockers and Activators: Conformational and Structural Determinants of Dihydropyrimidine Calcium Channel Modulators. *Journal of Medicinal Chemistry*, 38, 119–129. <https://doi.org/10.1021/jm00001a017>
- Ryu, J.H., Yanai, K. and Watanabe, T. (1994) Marked increase in histamine H3 receptors in the striatum and substantia nigra after 6-hydroxydopamine-induced denervation of dopaminergic neurons: An autoradiographic study. *Neuroscience Letters*, 178, 19–22. [https://doi.org/10.1016/0304-3940\(94\)90279-8](https://doi.org/10.1016/0304-3940(94)90279-8)
- Sadek, B., Saad, A., Latacz, G., Kuder, K., Olejarz, A., Karcz, T., Stark, H. and Kiec-Kononowicz, K. (2016a) Non-imidazole-based histamine H3 receptor antagonists with anticonvulsant activity in different seizure models in male adult rats. *Drug Design, Development and Therapy*, Volume 10, 3879–3898. <https://doi.org/10.2147/DDDT.S116192>
- Sadek, B., Saad, A., Sadeq, A., Jalal, F. and Stark, H. (2016b) Histamine H3 receptor as a potential target for cognitive symptoms in neuropsychiatric diseases. *Behavioural brain research*, 312, 415–430. <https://doi.org/10.1016/j.bbr.2016.06.051>
- Sadek, B., Saad, A., Subramanian, D., Shafiullah, M., Łazewska, D. and Kieć-Kononowicz, K. (2016c) Anticonvulsant and procognitive properties of the non-imidazole histamine H3 receptor antagonist DL77 in male adult rats. *Neuropharmacology*, 106, 46–55. <https://doi.org/10.1016/j.neuropharm.2015.10.023>
- Sadek, B. and Stark, H. (2016) Cherry-picked ligands at histamine receptor subtypes. *Neuropharmacology*, 106, 56–73. <https://doi.org/10.1016/j.neuropharm.2015.11.005>

Reference

- Sagara, Y., Ishige, K., Tsai, C. and Maher, P. (2002) Tyrphostins Protect Neuronal Cells from Oxidative Stress. *Journal of Biological Chemistry*, 277, 36204–36215. <https://doi.org/10.1074/jbc.M203895200>
- Sams, A.G., Mikkelsen, G.K., Larsen, M., Langgård, M., Howell, M.E., Schröder, T.J., Brennum, L.T., Torup, L., Jørgensen, E.B., Bundgaard, C., Kreilgård, M. and Bang-Andersen, B. (2011) Discovery of phosphoric acid mono-{2-[(E/Z)-4-(3,3-dimethyl-butylamino)-3,5-difluorobenzoylimino]-thiazol-3-ylmethyl} Ester (Lu AA47070): A phosphonoxyethylene prodrug of a potent and selective hA 2A receptor antagonist. *Journal of Medicinal Chemistry*, 54, 751–764. <https://doi.org/10.1021/jm1008659>
- Sanad, S.M.H., Kassab, R.M., Abdelhamid, I.A. and Elwahy, A.H.M. (2016) Microwave assisted multi-component synthesis of novel bis(1,4-dihydropyridines) based arenes or heteroarenes. *Heterocycles*, 92, 910–924. <https://doi.org/10.3987/COM-16-13441>
- Sánchez-Lemus, E. and Arias-Montaño, J.A. (2004) Histamine H3 receptor activation inhibits dopamine D1 receptor-induced cAMP accumulation in rat striatal slices. *Neuroscience Letters*, 364, 179–184. <https://doi.org/10.1016/j.neulet.2004.04.045>
- Sander, K., von Coburg, Y., Camelin, J.-C., Ligneau, X., Rau, O., Schubert-Zsilavec, M., Schwartz, J.-C. and Stark, H. (2010a) Acidic elements in histamine H(3) receptor antagonists. *Bioorganic & medicinal chemistry letters*, 20, 1581–4. <https://doi.org/10.1016/j.bmcl.2010.01.089>
- Sander, K., Kottke, T., Hoffend, C., Walter, M., Weizel, L., Camelin, J.-C., Ligneau, X., Schneider, E.H., Seifert, R., Schwartz, J.-C. and Stark, H. (2010b) First Metal-Containing Histamine H 3 Receptor Ligands †. *Organic Letters*, 12, 2578–2581. <https://doi.org/10.1021/ol100419y>
- Sander, K., Kottke, T. and Stark, H. (2008) Histamine H3 receptor antagonists go to clinics. *Biological and Pharmaceutical Bulletin*, 31, 2163–2181. <https://doi.org/10.1248/bpb.31.2163>
- Sander, K., Kottke, T., Tanrikulu, Y., Proschak, E., Weizel, L., Schneider, E.H., Seifert, R., Schneider, G. and Stark, H. (2009) 2,4-Diaminopyrimidines as histamine H4 receptor ligands-Scaffold optimization and pharmacological characterization. *Bioorganic and Medicinal Chemistry*, 17, 7186–7196. <https://doi.org/10.1016/j.bmc.2009.08.059>
- Sander, K., Kottke, T., Weizel, L. and Stark, H. (2010c) Kojic Acid Derivatives as Histamine H3 Receptor Ligands. *CHEMICAL & PHARMACEUTICAL BULLETIN*, 58, 1353–1361. <https://doi.org/10.1248/cpb.58.1353>
- Savoie, P.R. and Welch, J.T. (2015) Preparation and utility of organic pentafluorosulfanyl-containing compounds. *Chemical Reviews*, 115, 1130–1190. <https://doi.org/10.1021/cr500336u>
- Scammell, T.E. (2015) Narcolepsy.(ed EW Campion) *New England Journal of Medicine*, 373, 2654–2662. <https://doi.org/10.1056/NEJMra1500587>
- Schampel, A. and Kuerten, S. (2017) Danger: High Voltage—The Role of Voltage-Gated Calcium Channels in Central Nervous System Pathology. *Cells*, 6, 43. <https://doi.org/10.3390/cells6040043>
- Schiffmann, S.N., Libert, F., Vassart, G., Dumont, J.E. and Vanderhaeghen, J.J. (1990) A cloned G protein-coupled protein with a distribution restricted to striatal medium-sized neurons. Possible relationship with D1 dopamine receptor. *Brain Research*, 519, 333–337. [https://doi.org/10.1016/0006-8993\(90\)90097-U](https://doi.org/10.1016/0006-8993(90)90097-U)
- Schiffilliti, D., Grasso, G., Conti, A. and Fodale, V. (2010) Anaesthetic-Related Neuroprotection. *CNS Drugs*, 24, 1. <https://doi.org/10.2165/11584760-000000000-00000>
- Schlegel, B., Laggner, C., Meier, R., Langer, T., Schnell, D., Seifert, R., Stark, H., Höltje, H.D. and Sippl, W. (2007) Generation of a homology model of the human histamine H3 receptor for ligand docking and pharmacophore-based screening. *Journal of Computer-Aided Molecular Design*, 21, 437–453. <https://doi.org/10.1007/s10822-007-9127-x>
- Schlicker, E., Malinowska, B., Kathmann, M. and Göthert, M. (1994) Modulation of neurotransmitter release via histamine H 3 heteroreceptors. *Fundamental & Clinical Pharmacology*, 8, 128–137. <https://doi.org/10.1111/j.1472-8206.1994.tb00789.x>
- Schneider, E.H., Schnell, D., Papa, D. and Seifert, R. (2009) High constitutive activity and a G-protein-independent high-affinity state of the human histamine H 4-receptor. *Biochemistry*, 48, 1424–1438. <https://doi.org/10.1021/bi802050d>
- Schreiber, J.A., Schepmann, D., Frehland, B., Thum, S., Datunashvili, M., Budde, T., Hollmann, M., Strutz-Seebohm, N., Wünsch, B. and Seebohm, G. (2019) A common mechanism allows selective targeting of GluN2B subunit-containing N-methyl-D-aspartate receptors. *Communications Biology*, 2, 1–14. <https://doi.org/10.1038/s42003-019-0645-6>
- Schwartz, J. (2011) The histamine H3 receptor: From discovery to clinical trials with pitolisant. *British Journal of Pharmacology*, 163, 713–721. <https://doi.org/10.1111/j.1476-5381.2011.01286.x>

Reference

- Schwartz, J.C., Arrang, J.M., Garbarg, M., Lecomte, J.M., Ligneau, X., Schunack, W., Stark, H., Ganellin, C.R., Leurquin, F. and Sigurd, E. (2000) Non-imidazole alkylamines as histamine H₃-receptor ligands and their therapeutic applications. Publication Numer: WO0006254 (A2)
- Schwartz, B.L., Hashtroudi, S., Herting, R.L., Schwartz, P. and Deutsch, S.I. (1996) d-Cycloserine enhances implicit memory in Alzheimer patients. *Neurology*, 46, 420–424. <https://doi.org/10.1212/WNL.46.2.420>
- Schwartz, J.-C. and Lecomte, J.-M. (2006) Treatment of parkinson's disease obstructive sleep apnea, dementia with lewy bodies, vascular dementia with non-imidazole alkylamines histamine H₃ receptor ligands. Publication Numer: EP1707203A1
- Schwartzbach, C.J., Grove, R.A., Brown, R., Tompson, D., Then Bergh, F. and Arnold, D.L. (2017) Lesion remyelinating activity of GSK239512 versus placebo in patients with relapsing-remitting multiple sclerosis: a randomised, single-blind, phase II study. *Journal of Neurology*, 264, 304–315. <https://doi.org/10.1007/s00415-016-8341-7>
- Schweiger, A. (1993) Concepts for the measurement of hyperfine structure in EPR spectroscopy. *Applied Magnetic Resonance*, 5, 229–264. <https://doi.org/10.1007/BF03162524>
- Seelig, A. and Landwojtowicz, E. (2000) Structure-activity relationship of P-glycoprotein substrates and modifiers. *European Journal of Pharmaceutical Sciences*, 12, 31–40. [https://doi.org/10.1016/S0928-0987\(00\)00177-9](https://doi.org/10.1016/S0928-0987(00)00177-9)
- Seifert, R. and Wenzel-Seifert, K. (2002) Constitutive activity of G-proteins-coupled receptors: Cause of disease and common property of wild-type receptors. *Naunyn-Schmiedeberg's Archives of Pharmacology*, 366, 381–416. <https://doi.org/10.1007/s00210-002-0588-0>
- Selkoe, D.J. and Hardy, J. (2016) The amyloid hypothesis of Alzheimer's disease at 25 years. *EMBO Molecular Medicine*, 8, 595–608. <https://doi.org/10.15252/emmm.201606210>
- Setlik, J., Bond, G.R. and Ho, M. (2009) Adolescent prescription ADHD medication abuse is rising along with prescriptions for these medications. *Pediatrics*, 124, 875–880. <https://doi.org/10.1542/peds.2008-0931>
- Setnik, B., McDonnell, M., Mills, C., Scart-Grès, C., Robert, P., Dayno, J.M. and Schwartz, J.-C. (2020) Evaluation of the abuse potential of pitolisant, a selective H₃-receptor antagonist/inverse agonist, for the treatment of adult patients with narcolepsy with or without cataplexy. *Sleep*, 43. <https://doi.org/10.1093/sleep/zsz252>
- Sheinin, A., Shavit, S. and Benveniste, M. (2001) Subunit specificity and mechanism of action of NMDA partial agonist D-cycloserine. *Neuropharmacology*, 41, 151–8. [https://doi.org/10.1016/s0028-3908\(01\)00073-9](https://doi.org/10.1016/s0028-3908(01)00073-9)
- Shenton, F.C., Hann, V. and Chazot, P.L. (2005) Evidence for native and cloned H₃ Histamine receptor higher oligomers. *Inflammation Research*, 54, S48–S49. <https://doi.org/10.1007/s00011-004-0422-x>
- Sheppard, W.A. (1960) Arylsulfur trifluorides and pentafluorides. *Journal of the American Chemical Society*, 82, 4751–4752. <https://doi.org/10.1021/ja01502a083>
- Sheppard, W.A. (1962) The Electrical Effect of the Sulfur Pentafluoride Group. *Journal of the American Chemical Society*, 84, 3072–3076. <https://doi.org/10.1021/ja00875a007>
- Shimamura, T., Shiroishi, M., Weyand, S., Tsujimoto, H., Winter, G., Katritch, V., Abagyan, R., Cherezov, V., Liu, W., Han, G.W., Kobayashi, T., Stevens, R.C. and Iwata, S. (2011) Structure of the human histamine H₁ receptor complex with doxepin. *Nature*, 475, 65–70. <https://doi.org/10.1038/nature10236>
- Silver, R.B., Mackins, C.J., Smith, N.C.E., Koritchneva, I.L., Lefkowitz, K., Lovenberg, T.W. and Levi, R. (2001) Coupling of histamine H₃ receptors to neuronal Na⁺/H⁺ exchange: A novel protective mechanism in myocardial ischemia. *Proceedings of the National Academy of Sciences of the United States of America*, 98, 2855–2859. <https://doi.org/10.1073/pnas.051599198>
- Silver, R.B., Poonwasi, K.S., Seyedi, N., Wilson, S.J., Lovenberg, T.W. and Levi, R. (2002) Decreased intracellular calcium mediates the histamine H₃-receptor-induced attenuation of norepinephrine exocytosis from cardiac sympathetic nerve endings. *Proceedings of the National Academy of Sciences of the United States of America*, 99, 501–506. <https://doi.org/10.1073/pnas.012506099>
- Simms, B.A. and Zamponi, G.W. (2014) Neuronal voltage-gated calcium channels: Structure, function, and dysfunction. *Neuron*, 82, 24–45. <https://doi.org/10.1016/j.neuron.2014.03.016>
- Simonoff, E., Pickles, A., Charman, T., Chandler, S., Loucas, T. and Baird, G. (2008) Psychiatric disorders in children with autism spectrum disorders: prevalence, comorbidity, and associated factors in a population-derived sample. *Journal of the American Academy of Child and Adolescent Psychiatry*, 47, 921–9. <https://doi.org/10.1097/CHI.0b013e318179964f>
- Singh, I. (2008) Beyond polemics: Science and ethics of ADHD. *Nature Reviews Neuroscience*, 9, 957–964. <https://doi.org/10.1038/nrn2514>

Reference

- Singh, M. and Jadhav, H.R. (2013) Histamine H3 receptor function and ligands: recent developments. *Mini reviews in medicinal chemistry*, 13, 47–57. <https://doi.org/10.2174/138955713804484695>
- Singh, R.K., Mandal, T., Balsubramanian, N., Viaeane, T., Leedahl, T., Sule, N., Cook, G. and Srivastava, D.K. (2011) Histone deacetylase activators: N-acetylthioureas serve as highly potent and isozyme selective activators for human histone deacetylase-8 on a fluorescent substrate. *Bioorganic and Medicinal Chemistry Letters*, 21, 5920–5923. <https://doi.org/10.1016/j.bmcl.2011.07.080>
- Smit, M., Leurs, R., Alewijnse, A.E., Blauw, J., Van Nieuw Amerongen, G.P., Van De Vrede, Y., Roovers, E. and Timmerman, H. (1996a) Inverse agonism of histamine H2 antagonists accounts for upregulation of spontaneously active histamine H2 receptors. *Proceedings of the National Academy of Sciences of the United States of America*, 93, 6802–6807. <https://doi.org/10.1073/pnas.93.13.6802>
- Smit, M., Timmerman, H., Hijzelendoorn, J.C., Fukui, H. and Leurs, R. (1996b) Regulation of the human histamine H1 receptor stably expressed in Chinese hamster ovary cells. *Br J Pharmacol*, 117, 1071–1080. <https://doi.org/10.1111/j.1476-5381.1996.tb16699.x>
- Snider, R.M., McKinney, M., Forray, C. and Richelson, E. (1984) Neurotransmitter receptors mediate cyclic GMP formation by involvement of arachidonic acid and lipoxygenase. *Proceedings of the National Academy of Sciences of the United States of America*, 81, 3905–3909. <https://doi.org/10.1073/pnas.81.12.3905>
- Soltoff, S.P. (2004) Evidence that Tyrphostins AG10 and AG18 Are Mitochondrial Uncouplers that Alter Phosphorylation-dependent Cell Signaling. *Journal of Biological Chemistry*, 279, 10910–10918. <https://doi.org/10.1074/jbc.M305396200>
- Spicuzza, L., Caruso, D. and Maria, G. (2015) Obstructive sleep apnoea syndrome and its management. *Therapeutic Advances in Chronic Disease*, 6, 273–285.
- Stammer, C.H., Kartha, C.C., Chaturvedi, N.C. and McKinney, J.D. (1970) Cycloserine derivatives. *Journal of Medicinal Chemistry*, 13, 1013–1015. <https://doi.org/10.1021/jm00299a063>
- Stanika, R.I., Villanueva, I., Kazanina, G., Andrews, S.B. and Pivovarova, N.B. (2012) Comparative Impact of Voltage-Gated Calcium Channels and NMDA Receptors on Mitochondria-Mediated Neuronal Injury. *Journal of Neuroscience*, 32, 6642–6650. <https://doi.org/10.1523/JNEUROSCI.6008-11.2012>
- Stark, H., Hüls, A., Ligneau, X., Purand, K., Pertz, H., Arrang, J.M., Schwartz, J.C. and Schunack, W. (1998) Development of FUB 181, a selective histamine H3-receptor antagonist of high oral in vivo potency with 4-(ω -(arylalkyloxy)alkyl)-1H-imidazole structure. *Archiv der Pharmazie*, 331, 211–218.
- Stark, H., Krause, M., Arrang, J.-M., Ligneau, X., Schwartz, J.-C. and Schunack, W. (1994) Unsymmetrically substituted guanidines as potent histamine H3-receptor antagonists. *Bioorganic & Medicinal Chemistry Letters*, 4, 2907–2912. [https://doi.org/10.1016/S0960-894X\(01\)80838-6](https://doi.org/10.1016/S0960-894X(01)80838-6)
- Stephens, M.D., Yodsanit, N. and Melander, C. (2016) Evaluation of ethyl N-(2-phenethyl) carbamate analogues as biofilm inhibitors of methicillin resistant *Staphylococcus aureus*. *Organic & Biomolecular Chemistry*, 14, 6853–6856. <https://doi.org/10.1039/C6OB00706F>
- Stevens, D.R., Eriksson, K.S., Brown, R.E. and Haas, H.L. (2001) The mechanism of spontaneous firing in histamine neurons. *Behavioural Brain Research*, 124, 105–112. [https://doi.org/10.1016/S0166-4328\(01\)00219-4](https://doi.org/10.1016/S0166-4328(01)00219-4)
- Stölting, F. (2020) *Structural Motifs of Potential Multitargeting Ligands for Neurodegenerative Diseases (Bachelor's Thesis at the Institute for Pharmaceutical and Medicinal Chemistry)*. Heinrich Heine University.
- De Strooper, B. and Karran, E. (2016) The Cellular Phase of Alzheimer's Disease. *Cell*, 164, 603–615. <https://doi.org/10.1016/j.cell.2015.12.056>
- Sugiura, M., Kumahara, M. and Nakajima, M. (2009) Asymmetric synthesis of 4H-1,3-oxazines: Enantioselective reductive cyclization of N-acylated β -amino enones with trichlorosilane catalyzed by chiral Lewis bases. *Chemical Communications*, 3585–3587. <https://doi.org/10.1039/b905102c>
- Sun, P., Takatori, S., Jin, X., Koyama, T., Tangsucharit, P., Li, S., Zamami, Y., Kitamura, Y. and Kawasaki, H. (2011) Histamine H3 receptor-mediated modulation of perivascular nerve transmission in rat mesenteric arteries. *European Journal of Pharmacology*, 655, 67–73. <https://doi.org/10.1016/j.ejphar.2011.01.020>
- Svenningsson, P., Le Moine, C., Fisone, G. and Fredholm, B.B. (1999) Distribution, biochemistry and function of striatal adenosine A(2A) receptors. *Progress in Neurobiology*, 59, 355–396. [https://doi.org/10.1016/S0301-0082\(99\)00011-8](https://doi.org/10.1016/S0301-0082(99)00011-8)
- Svensson, M.-L.L. and Gatenbeck, S. (1982) The pathway of D-cycloserine biosynthesis in *Streptomyces garyphalus*. *Archives of Microbiology*, 131, 129–131. <https://doi.org/10.1007/BF01053994>
- Swanson, D.M., Shah, C.R., Lord, B., Morton, K., Dvorak, L.K., Mazur, C., Apodaca, R., Xiao, W., Boggs, J.D. and

Reference

- Feinstein, M. (2009) Heterocyclic replacement of the central phenyl core of diamine-based histamine H3 receptor antagonists. *European Journal of Medicinal Chemistry*, 44, 4413–4425. <https://doi.org/10.1016/j.ejmech.2009.06.007>
- Szökő, É., Tábi, T., Riederer, P., Vécsei, L. and Magyar, K. (2018) Pharmacological aspects of the neuroprotective effects of irreversible MAO-B inhibitors, selegiline and rasagiline, in Parkinson's disease. *Journal of Neural Transmission*, 125, 1735–1749. <https://doi.org/10.1007/s00702-018-1853-9>
- Takemura, M., Kishino, J., Yamatodani, A. and Hiroshi, W. (1989) Inhibition of histamine release from rat hypothalamic slices by ω -conotoxin GVIA, but not by nilvadipine, a dihydropyridine derivative. *Brain Research*, 496, 351–356. [https://doi.org/10.1016/0006-8993\(89\)91087-1](https://doi.org/10.1016/0006-8993(89)91087-1)
- Takehita, Y., Watanabe, T., Sakata, T., Munakata, M., Ishibashi, H. and Akaike, N. (1998) Histamine modulates high-voltage-activated calcium channels in neurons dissociated from the rat tuberomammillary nucleus. *Neuroscience*, 87, 797–805. [https://doi.org/10.1016/S0306-4522\(98\)00152-3](https://doi.org/10.1016/S0306-4522(98)00152-3)
- Tamaddon, F., Razmi, Z. and Jafari, A.A. (2010) Synthesis of 3,4-dihydropyrimidin-2(1H)-ones and 1,4-dihydropyridines using ammonium carbonate in water. *Tetrahedron Letters*, 51, 1187–1189. <https://doi.org/10.1016/j.tetlet.2009.12.098>
- Tao, M., Aimone, L.D., Huang, Z., Mathiasen, J., Raddatz, R., Lyons, J. and Hudkins, R.L. (2012) Optimization of 5-pyridazin-3-one phenoxypropylamines as potent, selective histamine H3 receptor antagonists with potent cognition enhancing activity. *Journal of Medicinal Chemistry*, 55, 414–423. <https://doi.org/10.1021/jm201295j>
- Tao, M., Raddatz, R., Aimone, L.D. and Hudkins, R.L. (2011) Synthesis and structure-activity relationships of 4,5-fused pyridazinones as histamine H3 receptor antagonists. *Bioorg. Med. Chem. Lett.*, 21, 6126–6130. <https://doi.org/10.1016/j.bmcl.2011.08.045>
- Tardivel-Lacombe, J., Morisset, S., Gbahou, F., Schwartz, J.C. and Arrang, J.M. (2001) Chromosomal mapping and organization of the human histamine H3 receptor gene. *NeuroReport*, 12, 321–324. <https://doi.org/10.1097/00001756-200102120-00028>
- Tatton, W.G. and Greenwood, C.E. (1991) Rescue of dying neurons: A new action for deprenyl in MPTP parkinsonism. *Journal of Neuroscience Research*, 30, 666–672. <https://doi.org/10.1002/jnr.490300410>
- Teleb, M., Zhang, F.-X., Farghaly, A.M., Aboul Wafa, O.M., Fronczek, F.R., Zamponi, G.W. and Fahmy, H. (2017a) Synthesis of new N3- substituted dihydropyrimidine derivatives as L-/T- type calcium channel blockers. *European Journal of Medicinal Chemistry*, 134, 52–61. <https://doi.org/10.1016/j.ejmech.2017.03.080>
- Teleb, M., Zhang, F.-X., Huang, J., Gadotti, V.M., Farghaly, A.M., AboulWafa, O.M., Zamponi, G.W. and Fahmy, H. (2017b) Synthesis and biological evaluation of novel N3- substituted dihydropyrimidine derivatives as T-type calcium channel blockers and their efficacy as analgesics in mouse models of inflammatory pain. *Bioorganic & Medicinal Chemistry*, 25, 1926–1938. <https://doi.org/10.1016/j.bmc.2017.02.015>
- Temme, L., Schepmann, D., Schreiber, J.A., Frehland, B. and Wünsch, B. (2018) Comparative Pharmacological Study of Common NMDA Receptor Open Channel Blockers Regarding Their Affinity and Functional Activity toward GluN2A and GluN2B NMDA Receptors. *ChemMedChem*, 13, 446–452. <https://doi.org/10.1002/cmdc.201700810>
- Teuscher, C., Subramanian, M., Noubade, R., Jian, F.G., Offner, H., Zachary, J.F. and Blankenhorn, E.P. (2007) Central histamine H3 receptor signaling negatively regulates susceptibility to autoimmune inflammatory disease of the CNS. *Proceedings of the National Academy of Sciences of the United States of America*, 104, 10146–10151. <https://doi.org/10.1073/pnas.0702291104>
- Thangam, E.B., Jemima, E.A., Singh, H., Baig, M.S., Khan, M., Mathias, C.B., Church, M.K. and Saluja, R. (2018) The role of histamine and histamine receptors in mast cell-mediated allergy and inflammation: The hunt for new therapeutic targets. *Frontiers in Immunology*, 9, 1–9. <https://doi.org/10.3389/fimmu.2018.01873>
- Thanigaimalai, P., Le Hoang, T.A., Lee, K.C., Bang, S.C., Sharma, V.K., Yun, C.Y., Roh, E., Hwang, B.Y., Kim, Y. and Jung, S.H. (2010) Structural requirement(s) of N-phenylthioureas and benzaldehyde thiosemicarbazones as inhibitors of melanogenesis in melanoma B 16 cells. *Bioorganic and Medicinal Chemistry Letters*, 20, 2991–2993. <https://doi.org/10.1016/j.bmcl.2010.02.067>
- Tomasch, M., Schwed, J.S., Paulke, A. and Stark, H. (2013) Bodilisant—A Novel Fluorescent, Highly Affine Histamine H3 Receptor Ligand. *ACS Medicinal Chemistry Letters*, 4, 269–273. <https://doi.org/10.1021/ml300383n>
- Tong, J., Rathitharan, G., Meyer, J.H., Furukawa, Y., Ang, L.C., Boileau, I., Guttman, M., Hornykiewicz, O. and Kish, S.J. (2017) Brain monoamine oxidase B and A in human parkinsonian dopamine deficiency disorders. *Brain*, 140, 2460–2474. <https://doi.org/10.1093/brain/awx172>
- Torrent, A., Moreno-Delgado, D., Gómez-Ramírez, J., Rodríguez-Agudo, D., Rodríguez-Caso, C., Sánchez-

Reference

- Jiménez, F., Blanco, I. and Ortiz, J. (2005) H3 autoreceptors modulate histamine synthesis through calcium/calmodulin- and cAMP-dependent protein kinase pathways. *Molecular Pharmacology*, 67, 195–203. <https://doi.org/10.1124/mol.104.005652>
- Traiffort, E., Ruat, M., Arrang, J.M., Leurs, R., Piomelli, D. and Schwartz, J.C. (1992) Expression of a cloned rat histamine H2 receptor mediating inhibition of arachidonate release and activation of cAMP accumulation. *Proceedings of the National Academy of Sciences of the United States of America*, 89, 2649–2653. <https://doi.org/10.1073/pnas.89.7.2649>
- Traiffort, E., Vizuete, M.L., Tardivellacombe, J., Souil, E., Schwartz, J.C. and Ruat, M. (1995) The Guinea Pig Histamine H2 Receptor: Gene Cloning, Tissue Expression and Chromosomal Localization of Its Human Counterpart. *Biochemical and Biophysical Research Communications*, 211, 570–577. <https://doi.org/10.1006/bbrc.1995.1851>
- Tsai, G.E., Falk, W.E., Gunther, J. and Coyle, J.T. (1999) Improved cognition in Alzheimer's disease with short-term D-cycloserine treatment. *The American Journal of Psychiatry*, 156, 467–469. <https://doi.org/10.1176/ajp.156.3.467>
- Tunnicliff, G. (1998) Pharmacology and function of imidazole 4-acetic acid in brain. *General Pharmacology*, 31, 503–509. [https://doi.org/10.1016/S0306-3623\(98\)00079-2](https://doi.org/10.1016/S0306-3623(98)00079-2)
- Tuomisto, L., Lozeva, V., Valjakka, A. and Lecklin, A. (2001) Modifying effects of histamine on circadian rhythms and neuronal excitability. *Behavioural Brain Research*, 124, 129–135. [https://doi.org/10.1016/S0166-4328\(01\)00222-4](https://doi.org/10.1016/S0166-4328(01)00222-4)
- Tuomisto, L. and Tacke, U. (1986) Is histamine an anticonvulsive inhibitory transmitter? *Neuropharmacology*, 25, 955–958. [https://doi.org/10.1016/0028-3908\(86\)90029-8](https://doi.org/10.1016/0028-3908(86)90029-8)
- Tuomisto, L. and Tuomisto, J. (1982) Diurnal variations in brain and pituitary histamine and histamine-N-methyltransferase in the rat and guinea pig. *Medical Biology*, 60, 204–209.
- Turnbull, K., Caslake, R., Macleod, A., Ives, N., Stowe, R. and Counsell, C. (2005) Monoamine oxidase B inhibitors for early Parkinson's disease. *Cochrane Database of Systematic Reviews*. <https://doi.org/10.1002/14651858.cd004898.pub2>
- Turpaev, K., Ermolenko, M., Cresteil, T. and Drapier, J.C. (2011) Benzylidenemalononitrile compounds as activators of cell resistance to oxidative stress and modulators of multiple signaling pathways. A structure–activity relationship study. *Biochemical Pharmacology*, 82, 535–547. <https://doi.org/10.1016/j.bcp.2011.05.028>
- Turpaev, K. and Welsh, N. (2016) Aromatic malononitriles stimulate the resistance of insulin-producing beta-cells to oxidants and inflammatory cytokines. *European Journal of Pharmacology*, 784, 69–80. <https://doi.org/10.1016/j.ejphar.2016.05.010>
- Twohig, D. and Nielsen, H.M. (2019) α -synuclein in the pathophysiology of Alzheimer's disease. *Molecular neurodegeneration*, 14, 23. <https://doi.org/10.1186/s13024-019-0320-x>
- Uchida, S., Yamada, S., Nagai, K., Deguchi, Y. and Kimura, R. (1997) Brain pharmacokinetics and in vivo receptor binding of 1,4-dihydropyridine calcium channel antagonists. *Life Sciences*, 61, 2083–2090. [https://doi.org/10.1016/S0024-3205\(97\)00881-3](https://doi.org/10.1016/S0024-3205(97)00881-3)
- Upadhyaya, D.J., Barge, A., Stefania, R. and Cravotto, G. (2007) Efficient, solventless N-Boc protection of amines carried out at room temperature using sulfamic acid as recyclable catalyst. *Tetrahedron Letters*, 48, 8318–8322. <https://doi.org/10.1016/j.tetlet.2007.09.126>
- Vanover, K.E., Weiner, D.M., Makhay, M., Veinbergs, I., Gardell, L.R., Lameh, J., Del Tredici, A.L., Piu, F., Schiffer, H.H., Ott, T.R., Burstein, E.S., Uldam, A.K., Thygesen, M.B., Schlienger, N., Andersson, C.M., Son, T.Y., Harvey, S.C., Powell, S.B., Geyer, M.A., Tolf, B.-R., Brann, M.R. and Davis, R.E. (2006) Pharmacological and Behavioral Profile of N-(4-Fluorophenylmethyl)-N-(1-methylpiperidin-4-yl)-N'-(4-(2-methylpropyloxy)phenylmethyl) Carbamide (2R,3R)-Dihydroxybutanedioate (2:1) (ACP-103), a Novel 5-Hydroxytryptamine 2A Receptor Inverse Agonist. *Journal of Pharmacology and Experimental Therapeutics*, 317, 910–918. <https://doi.org/10.1124/jpet.105.097006>
- Vaquero, J.J., Fuentes, L., Del Castillo, J.C., Pérez, M.I., García, J.L. and Soto, J.L. (1987) The Reactions of Benzylmalononitriles with Hydrazine and Hydroxylamine. Synthesis of Pyrazoles, Isoxazoles, and Pyrazolo[1,5-a]-pyrimidine Derivatives. *Synthesis*, 1987, 33–35. <https://doi.org/10.1055/s-1987-27831>
- Varty, L.A.M., Gustafson, E., Laverty, M. and Hey, J.A. (2004) Activation of histamine H3 receptors in human nasal mucosa inhibits sympathetic vasoconstriction. *European Journal of Pharmacology*, 484, 83–89. <https://doi.org/10.1016/j.ejphar.2003.10.051>
- Vater, M., Möckl, L., Gormanns, V., Schultz Fademrecht, C., Mallmann, A.M., Ziegart-Sadowska, K., Zaba, M.,

Reference

- Frevert, M.L., Bräuchle, C., Holsboer, F., Rein, T., Schmidt, U. and Kirmeier, T. (2017) New insights into the intracellular distribution pattern of cationic amphiphilic drugs. *Scientific Reports*, 7, 1–12. <https://doi.org/10.1038/srep44277>
- Venkatachalam, K., Eissa, N., Awad, M. Al, Jayaprakash, P., Zhong, S., Stölting, F., Stark, H. and Sadek, B. (2021) The histamine H3R and dopamine D2R/D3R antagonist ST-713 ameliorates autism-like behavioral features in BTBR T+tf/J mice by multiple actions. *Biomedicine & Pharmacotherapy*, 138, 111517. <https://doi.org/10.1016/j.biopha.2021.111517>
- Verweij, E.W.E., Al Araaj, B., Prabhata, W.R., Prihandoko, R., Nijmeijer, S., Tobin, A.B., Leurs, R. and Vischer, H.F. (2020) Differential Role of Serines and Threonines in Intracellular Loop 3 and C-Terminal Tail of the Histamine H4 Receptor in β -Arrestin and G Protein-Coupled Receptor Kinase Interaction, Internalization, and Signaling. *ACS Pharmacology and Translational Science*, 3, 321–333. <https://doi.org/10.1021/acsptsci.0c00008>
- Wang, N., Ma, J., Liu, J., Wang, J., Liu, C., Wang, H., Liu, Y., Yan, H. and Jiang, S. (2020) Histamine H3 receptor antagonist enhances neurogenesis and improves chronic cerebral hypoperfusion-induced cognitive impairments. *Frontiers in Pharmacology*, 10, 1–14. <https://doi.org/10.3389/fphar.2019.01583>
- Wargel, R.J., Shadur, C.A. and Neuhaus, F.C. (1970) Mechanism of D-cycloserine action: transport systems for D-alanine, D-cycloserine, L-alanine, and glycine. *Journal of Bacteriology*, 103, 778–788. <https://doi.org/10.1128/JB.103.3.778-788.1970>
- Watson, G.B., Bolanowski, M.A., Baganoff, M.P., Deppeler, C.L. and Lanthorn, T.H. (1990) d-Cycloserine acts as a partial agonist at the glycine modulatory site of the NMDA receptor expressed in *Xenopus* oocytes. *Brain Research*, 510, 158–160. [https://doi.org/10.1016/0006-8993\(90\)90745-W](https://doi.org/10.1016/0006-8993(90)90745-W)
- Weisler, R.H., Pandina, G.J., Daly, E.J., Cooper, K. and Gassmann-Mayer, C. (2012) Randomized clinical study of a histamine H3 receptor antagonist for the treatment of adults with attention-deficit hyperactivity disorder. *CNS Drugs*, 26, 421–434. <https://doi.org/10.2165/11631990-000000000-00000>
- Welch, J.T. and Lim, D.S. (2007) The synthesis and biological activity of pentafluorosulfanyl analogs of fluoxetine, fenfluramine, and norfenfluramine. *Bioorganic and Medicinal Chemistry*, 15, 6659–6666. <https://doi.org/10.1016/j.bmc.2007.08.012>
- WHO. (2015) *WHO Model List of Essential Medicines 19th List (April 2015)*.
- Williamson, A. (1851) Ueber die Theorie der Aetherbildung. *Annalen der Chemie und Pharmacie*, 77, 37–49. <https://doi.org/10.1002/jlac.18510770104>
- Wilson, D.M., Apps, J., Bailey, N., Bamford, M.J., Beresford, I.J., Brackenborough, K., Briggs, M.A., Brough, S., Calver, A.R., Crook, B., Davis, R.K., Davis, R.P., Davis, S., Dean, D.K., Harris, L., Heslop, T., Holland, V., Jeffrey, P., Panchal, T.A., Parr, C.A., Quashie, N., Schogger, J., Sehmi, S.S., Stean, T.O., Steadman, J.G.A., Trail, B., Wald, J., Worby, A., Takle, A.K., Witherington, J. and Medhurst, A.D. (2013) Identification of clinical candidates from the benzazepine class of histamine H3 receptor antagonists. *Bioorganic and Medicinal Chemistry Letters*, 23, 6890–6896. <https://doi.org/10.1016/j.bmcl.2013.09.090>
- Wingen, K. and Stark, H. (2013) Scaffold variations in amine warhead of histamine H3 receptor antagonists. *Drug Discovery Today: Technologies*, 10, 1–7. <https://doi.org/10.1016/j.ddtec.2013.07.001>
- World-Health-Organization. (2017) Obesity - Overview, Complications, Prevention and Control. URL https://www.who.int/health-topics/obesity#tab=tab_1 (Accessed 30 December 2020)
- World-Health-Organization. (2019) Autism spectrum disorders. URL <https://www.who.int/news-room/fact-sheets/detail/autism-spectrum-disorders> (Accessed 31 December 2020)
- Wright, C., Shin, J.H., Rajpurohit, A., Deep-Soboslay, A., Collado-Torres, L., Brandon, N.J., Hyde, T.M., Kleinman, J.E., Jaffe, A.E., Cross, A.J. and Weinberger, D.R. (2017) Altered expression of histamine signaling genes in autism spectrum disorder. *Translational Psychiatry*, 7. <https://doi.org/10.1038/tp.2017.87>
- Xia, P., Chen, H.S.V., Zhang, D. and Lipton, S.A. (2010) Memantine preferentially blocks extrasynaptic over synaptic NMDA receptor currents in hippocampal autapses. *Journal of Neuroscience*, 30, 11246–11250. <https://doi.org/10.1523/JNEUROSCI.2488-10.2010>
- Xiamuxi, H., Wang, Z., Li, J., Wang, Y., Wu, C., Yang, F., Jiang, X., Liu, Y., Zhao, Q., Chen, W., Zhang, J., Xie, Y., Hu, T., Xu, M., Guo, S., Akber Aisa, H., He, Y. and Shen, J. (2017) Synthesis and biological investigation of tetrahydropyridopyrimidinone derivatives as potential multireceptor atypical antipsychotics. *Bioorganic and Medicinal Chemistry*, 25, 4904–4916. <https://doi.org/10.1016/j.bmc.2017.07.040>
- El Yacoubi, M., Ledent, C., Parmentier, M., Bertorelli, R., Ongini, E., Costentin, J. and Vaugeois, J.M. (2001) Adenosine A2A receptor antagonists are potential antidepressants: Evidence based on pharmacology and A2A receptor knockout mice. *British Journal of Pharmacology*, 134, 68–77. <https://doi.org/10.1038/sj.bjp.0704240>

Reference

- Yamasaki, T., Tamai, I. and Matsumura, Y. (2001) Activation of histamine H₃ receptors inhibits renal noradrenergic neurotransmission in anesthetized dogs. *American Journal of Physiology-Regulatory, Integrative and Comparative Physiology*, 280, R1450–R1456. <https://doi.org/10.1152/ajpregu.2001.280.5.R1450>
- Yan, C., Theodorescu, D., Miller, B., Kumar, A., Kumar, V., Ross, D. and Wempe, M.F. (2016) Synthesis of novel Ral inhibitors: An in vitro and in vivo study. *Bioorganic and Medicinal Chemistry Letters*, 26, 5815–5818. <https://doi.org/10.1016/j.bmcl.2016.10.021>
- Yan, H., Zhang, X., Hu, W., Ma, J., Hou, W., Zhang, X., Wang, X., Gao, J., Shen, Y., Lv, J., Ohtsu, H., Han, F., Wang, G. and Chen, Z. (2014) Histamine H₃ receptors aggravate cerebral ischaemic injury by histamine-independent mechanisms. *Nature Communications*, 5. <https://doi.org/10.1038/ncomms4334>
- Yang, R., Hey, J.A., Aslanian, R. and Rizzo, C.A. (2002) Coordination of Histamine H₃ Receptor Antagonists with Human Adrenal Cytochrome P450 Enzymes. *Pharmacology*, 66, 128–135. <https://doi.org/10.1159/000063794>
- Yang, F., Jiang, X., Li, J., Wang, Y., Liu, Y., Bi, M., Wu, C., Zhao, Q., Chen, W., Yin, J., Zhang, J., Xie, Y., Hu, T., Xu, M., Guo, S., Wang, Z., He, Y. and Shen, J. (2016) Synthesis, structure-activity relationships, and biological evaluation of a series of benzamides as potential multireceptor antipsychotics. *Bioorganic and Medicinal Chemistry Letters*, 26, 3141–3147. <https://doi.org/10.1016/j.bmcl.2016.04.087>
- Yao, B., Hutchins, C., Carr, T., Cassar, S., Masters, J., Bennani, Y., Esbenshade, T. and Hancock, A. (2003) Molecular modeling and pharmacological analysis of species-related histamine H₃ receptor heterogeneity. *Neuropharmacology*, 44, 773–786. [https://doi.org/10.1016/S0028-3908\(03\)00056-X](https://doi.org/10.1016/S0028-3908(03)00056-X)
- Yao, X., Liu, H., Zhang, R., Liu, M., Hu, Z., Panaye, A., Doucet, J.P. and Fan, B. (2005) QSAR and classification study of 1,4-dihydropyridine calcium channel antagonists based on least squares support vector machines. *Molecular Pharmaceutics*, 2, 348–356. <https://doi.org/10.1021/mp050027v>
- Yarım, M., Saraç, S., Ertan, M., (Sarnıç) Batu, Ö. and Erol, K. (1999) Synthesis, structural elucidation and pharmacological properties of some 5-acetyl-3,4-dihydro-6-methyl-4-(substituted phenyl)-2(1H)-pyrimidinones. *Il Farmaco*, 54, 359–363. [https://doi.org/10.1016/S0014-827X\(99\)00042-7](https://doi.org/10.1016/S0014-827X(99)00042-7)
- Yoshimoto, R., Miyamoto, Y., Shimamura, K., Ishihara, A., Takahashi, K., Kotani, H., Chen, A.S., Chen, H.Y., MacNeil, D.J., Kanatani, A. and Tokita, S. (2006) Therapeutic potential of histamine H₃ receptor agonist for the treatment of obesity and diabetes mellitus. *Proceedings of the National Academy of Sciences of the United States of America*, 103, 13866–13871. <https://doi.org/10.1073/pnas.0506104103>
- Yoshioka, E., Kohtani, S., Tanaka, E., Hata, Y. and Miyabe, H. (2015) Carbon radical addition-cyclization reaction induced by ruthenium-photocatalyst under visible light irradiation. *Tetrahedron*, 71, 773–781. <https://doi.org/10.1016/j.tet.2014.12.068>
- Youdim, M.B.H., Edmondson, D. and Tipton, K.F. (2006) The therapeutic potential of monoamine oxidase inhibitors. *Nature Reviews Neuroscience*, 7, 295–309. <https://doi.org/10.1038/nrn1883>
- Young, T., Palta, M., Dempsey, J., Skatrud, J., Weber, S. and Badr, S. (1993) The Occurrence of Sleep-Disordered Breathing among Middle-Aged Adults. *New England Journal of Medicine*, 328, 1230–1235. <https://doi.org/10.1056/nejm199304293281704>
- Yung-Chi, C. and Prusoff, W.H. (1973) Relationship between the inhibition constant (K_i) and the concentration of inhibitor which causes 50 per cent inhibition (I₅₀) of an enzymatic reaction. *Biochemical Pharmacology*, 22, 3099–3108. [https://doi.org/10.1016/0006-2952\(73\)90196-2](https://doi.org/10.1016/0006-2952(73)90196-2)
- Zamponi, G.W. (2016) Targeting voltage-gated calcium channels in neurological and psychiatric diseases. *Nature Reviews Drug Discovery*, 15, 19–34. <https://doi.org/10.1038/nrd.2015.5>
- Zamponi, G.W. (2017) A Crash Course in Calcium Channels. *ACS Chemical Neuroscience*, 8, 2583–2585. <https://doi.org/10.1021/acschemneuro.7b00415>
- Zamponi, G.W., Striessnig, J., Koschak, A. and Dolphin, A.C. (2015) The Physiology, Pathology, and Pharmacology of Voltage-Gated Calcium Channels and Their Future Therapeutic Potential. (ed DR Sibley) *Pharmacological Reviews*, 67, 821–870. <https://doi.org/10.1124/pr.114.009654>
- Zhang, D.D., Sisignano, M., Schuh, C.D., Sander, K., Stark, H. and Scholich, K. (2012) Overdose of the histamine H₃ inverse agonist pitolisant increases thermal pain thresholds. *Inflammation Research*, 61, 1283–1291. <https://doi.org/10.1007/s00011-012-0528-5>
- Zhu, Y., Michalovich, D., Wu, H.L., Tan, K.B., Dytko, G.M., Mannan, I.J., Boyce, R., Alston, J., Tierney, L.A., Li, X., Herrity, N.C., Vawter, L., Sarau, H.M., Ames, R.S., Davenport, C.M., Hieble, J.P., Wilson, S., Bergsma, D.J. and Fitzgerald, L.R. (2001) Cloning, expression, and pharmacological characterization of a novel human histamine receptor. *Molecular Pharmacology*, 59, 434–441. <https://doi.org/10.1124/mol.59.3.434>

Reference

- Zimmermann, A.S., Burhenne, H., Kaefer, V., Seifert, R. and Neumann, D. (2011) Systematic analysis of histamine and N-methylhistamine concentrations in organs from two common laboratory mouse strains: C57Bl/6 and Balb/c. *Inflammation Research*, 60, 1153–1159. <https://doi.org/10.1007/s00011-011-0379-5>
- Zimmermann, D., Krogsgaard-Larsen, P., Ehrhardt, J.-D., Madsen, U. and Janin, Y.L. (1998) Unambiguous synthesis of 1-methyl-3-hydroxypyrazoles. *Tetrahedron*, 54, 9393–9400. [https://doi.org/10.1016/S0040-4020\(98\)00579-1](https://doi.org/10.1016/S0040-4020(98)00579-1)
- Zlokovic, B. V. (2011) Neurovascular pathways to neurodegeneration in Alzheimer's disease and other disorders. *Nature reviews. Neuroscience*, 12, 723–38. <https://doi.org/10.1038/nrn3114>
- Zvilichovsky, G. and David, M. (1983) Molecular rearrangements. Synthesis, stability, and rearrangements of 2-imino-2H-isoxazolo[2,3-a]pyrimidines and 2-aminoisoxazolo[2,3-a]pyrimidinium salts. *The Journal of Organic Chemistry*, 48, 575–579. <https://doi.org/10.1021/jo00152a032>

8 Annex

8.1 List of Abbreviations

$^1\text{H-NMR}$	Proton nuclear magnetic resonance spectroscopy
5-HT	5-Hydroxytryptamine (serotonin)
$^{13}\text{C-NMR}$	Carbon nuclear magnetic resonance spectroscopy
A _{2A} R	Adenosine A _{2A} receptor
AAPH	2,2'-Azobis(2-amidinopropane dihydrochloride)
abs.	Absolute
Ac ₂ O	Acetic acid anhydride
AChE	Acetylcholinesterase
AcOH	Acetic acid
AD	Alzheimer's disease
ADH	Aldehyde dehydrogenase
ADHD	Attention deficit hyperactivity disorder syndrome
Asp	Aspartic acid
BBB	Blood-brain-barrier
Boc	<i>tert</i> -Butyloxycarbonyl
br	Broad singlet (multiplicity of NMR signals)
BuChE	Butyrylcholinesterase
CAD	Cationic amphiphilic drug
calc.	Calculated
cAMP	Cyclic adenosine monophosphate
CCB	Calcium channel blocker
c-hexane	Cyclohexane
CHN	Elemental analysis
CHO (cells)	Chinese hamster ovary
CNS	Central nervous system
CREB	cAMP response element-binding
cryo-EM	Cryogenic electron microscopy
d	Doublet (multiplicity of signal in NMR)
δ	Chemical shift (ppm)
dd	Doublet of doublet (multiplicity of signal in NMR)
D ₁ R	Dopamine D ₁ receptor
D ₂ R	Dopamine D ₂ receptor

Annex

Da	Dalton
DAC	1,2-Diacylglycerol
DAO	Diamine oxidase
DCE	Dichloroethane
DCM	Dichloromethane = Methylene chloride
DCS	D-Cycloserine
DHP	Dihydropyridine
DHPM	Dihydropyrimidine
DIAD	Diisopropyl azodicarboxylate
DIBAH	Diisobutyl aluminum hydride
di-Boc	Di- <i>tert</i> -butyl dicarbonate
DIHD	Diisopropyl hydrazine dicarboxylate
DMAP	4-Dimethyl aminopyridine
DMF	<i>N,N</i> -Dimethylformamide
DMSO	Dimethyl sulfoxide
DOPA	3,4-Dihydroxyphenylalanine
DSP-4	<i>N</i> -(2-Chloroethyl)- <i>N</i> -ethyl-2-bromobenzylamine
ECL	Extracellular Loop
EDS	Excessive daytime sleepiness
EMA	European Medicines Agency
EPR	Electron paramagnetic resonance
ERK	Extracellular-signal regulated Kinase
ESI	Electrospray ionization
EtOAc	Ethyl acetate
EtOEt	Diethyl ether
EtOH	Ethanol
FA	Formic acid
FDA	The U.S. Food and Drug Administration
GABA	γ -Aminobutyric acid
GABA _A	GABA receptor subtype A
Glu	Glutamic acid
GPCR	Guanine nucleotide-binding protein-coupled receptor
GSK-3 β	Glycogen synthase kinase 3 isoform β
h	Human, in the combination of receptors
H ₁ R	Histamine H ₁ receptor
H ₂ R	Histamine H ₂ receptor

Annex

H ₃ R	Histamine H ₃ receptor
H ₄ R	Histamine H ₄ receptor
H _{ax}	Proton in the axial position in a cyclohexane-like ring system
HCl	Hydrogen chloride
HDC	Histidine decarboxylase
HEK (cells)	Human embryonic kidney
H _{eq}	Proton in equatorial position in a cyclohexane-like ring system
hERG	human ether-a-go-go related gene
HMT	Histamine <i>N</i> -methyltransferase
IC ₅₀	Half maximal inhibitory concentration
ICL	Intracellular loop
IMA	Imidazole acetic acid
IP ₃	Inositol-1,4,5-triphosphate
<i>J</i>	Coupling constant
<i>K_i</i>	Dissociation constant of the ligand-receptor complex
LC-MS	Liquid chromatography coupled with mass spectrometry
LTCC	L-Type calcium channel
LTP	Long-term potentiation
<i>m</i>	Multiplet (descriptor of signal in NMR)
<i>M</i>	Mol pro liter
MAO-A	Monoamine oxidase isoenzyme A
MAO-B	Monoamine oxidase isoenzyme B
MAPK	Mitogen-activated protein kinase
MeCN	Acetonitrile
MeOH	Methanol
MIMA	<i>N</i> ^ε -Methyl imidazole acetic acid
MPP ⁺	1-Methyl-4-phenyl-pyridinium
MPTP	1-Methyl-4-phenyl-1,2,3,6-tetrahydropyridine
MS	Mass spectrometry
MW	Microwave reactor
NAMH	<i>N</i> ^α -Methylhistamine
NF-κB	Nuclear factor -κB
NMDA	<i>N</i> -Methyl-D-aspartate
NMR	Nuclear magnetic resonance
ORAC	Oxygen-radical absorbance capacity
OSA	Obstructive sleep apnea

Annex

p	quintet (A multiplicity of signal in NMR)
PAINS	Pan-assay interference compounds
PBS	Phosphate buffered saline
PD	Parkinson's disease
P-gp	P-glycoprotein
Ph	Phenyl
PI3K	Phosphatidylinositol 3-kinase
Pipera	Piperazine
Piperi	Piperidine
PKA	Protein kinase A
PKB	Protein kinase B
PKC	Protein kinase C
PLC	Phospholipase C
PPh ₃	Triphenylphosphine
q	Quartet (multiplicity of signal in NMR)
RAMH	(<i>R</i>)- α -Methylhistamine
R _f	Retardation factor
ROS	Reactive oxygen species
rpm	Rounds per minute
r.t.	Room temperature, ambient temperature
s	Singlet (multiplicity of signal in NMR)
SAR	Structure-activity relationship
SD	Standard deviation
SEM	Standard error of the mean
Sf	<i>Spodoptera frugiperda</i>
SN	Substantia nigra
t	Triplet (multiplicity of signal in NMR)
<i>t</i> -BuOOH	<i>tert</i> -Butyl hydroperoxide
TEA	Triethylamine
TEMPO	2,2,6,6-Tetramethyl piperidinyloxy free radical
THF	Tetrahydrofuran
TLC	Thin-layer chromatography
TM	Transmembrane domain
Trolox	6-Hydroxy-2,5,7,8-tetramethylchroman-2-carboxylic acid
VGCC	Voltage-gated calcium channels
VMAT	Vesicular monoamine transporter

8.2 Curriculum vitae

Personal Data:

Name	Sicheng Zhong
Sex	Male
Adress	Einsiedelstr. 5 40597 Düsseldorf
Place and date of birth	02.11.1986 in Guiyang, China
Nationality	Chinese
Mobile	0152-53479278
Email	zsc.stephen@gmail.com

Work Experience

Since 05.2021	Dom-Apotheke in Cologne (Pharmacist)
01.2016-01.2021	Heinrich-Heine-University Düsseldorf Research associate: Planning, design, synthesis, purification, and analysis of organic molecules Teaching assistant: Preparation and supervision of Laboratory course for inorganic chemistry
05.2014-09.2015	Schloss-Apotheke in Bad Köstritz, Pharmacist
05.2013-04.2014	Bahnhof-Apotheke in Weimar, Internship
11.2012-04.2013	Pharmacy of university hospital Jena, Internship

Education

Since 01.2016	Doctoral research at the pharmaceutical and medicinal chemistry institute of Heinrich-Heine-University Düsseldorf in the research group of Prof. Dr. Dr. h.c. Holger Stark
01.2014	Approbation for pharmacist
10.2010-09.2012	Pharmacy study at Friedrich-Schiller-University in Jena (Staatsexamen)
09.2005-08.2009	Pharmacy study at China Pharmaceutical University in Nanjing (Bachelor of Science with focus on traditional Chinese herbal medicine)

Additional Skills

Computer	Good skills in using MS Word, Excel, and PowerPoint Good knowledge of computer hardware
Language	Chinese: Mother language German: C1 level English: Good knowledge of writing and speaking

8.3 Publications

Venkatachalam, K., Eissa, N., Awad, M. Al, Jayaprakash, P., **Zhong, S.**, Stölting, F., Stark, H. and Sadek, B. (2021) The histamine H3R and dopamine D2R/D3R antagonist ST-713 ameliorates autism-like behavioral features in BTBR T+tf/J mice by multiple actions. *Biomedicine and Pharmacotherapy*, 138, 111517.

<https://doi.org/10.1016/j.biopha.2021.111517>

Zhong, S., Stark, H. (2020) Wie war das noch? Beratungswissen zu Z-Substanzen und Benzodiazepinen. *Deutsche Apothekerzeitung*, 51, 56-65

Brückmann, H., **Zhong, S.**, Stark, H. (2018a) Juckreiz, Schuppen, Rötung - Pathogenese und leitliniengerechte Therapie der atopischen Dermatitis. *Deutsche Apothekerzeitung*, 31, 42-45.

Brückmann, H., **Zhong, S.**, Stark, H. (2018b) Blick in die Zukunft – Neue Wirkstoffe gegen atopische Dermatitis im Markt und in der Pipeline. *Deutsche Apothekerzeitung*, 31, 46-52.

Tröger, T., Langenberg, M., **Zhong, S.**, Ambrosini, D. and Enzensperger, C. (2014) Fishing for accessory binding sites at GPCRs with “loop-hooks” - an approach towards selectivity? Part I. *Chemistry & biodiversity*, 11, 197–208.

<https://doi.org/10.1002/cbdv.201300292>

8.4 Eidesstattliche Erklärung

Ich versichere an Eides statt, dass die vorliegende Dissertation von mir selbstständig und ohne unzulässige fremde Hilfe unter Beachtung der „Grundsätze zur Sicherung guter wissenschaftlicher Praxis an der Heinrich-Heine-Universität Düsseldorf“ erstellt wurde. Die Dissertation wurde in der vorliegenden oder in ähnlicher Form bei keiner anderen Fakultät eingereicht.

Düsseldorf, September 2021

Sicheng Zhong